IAHR 2017

37th IAHR WORLD CONGRESS

13-18 August, 2017

Kuala Lumpur, Malaysia

THEME 1: RIVER AND SEDIMENT MANAGEMENT

Editor: Aminuddin Ab. Ghani

IAHR 2017

37th IAHR
WORLD CONGRESS
13-18 August, 2017
Kuala Lumpur, Malaysia

Supported by Spain Water and IWHR, China

RIVER CONSERVATION AND RESTORATION

SENSITIVITY ANALYSIS OF THE HYDROMORPHOLOGICAL INDEX OF DIVERSITY USING NUMERICAL GENERATED DATA

SEVERIN STÄHLY[(1)], PIERRE BOURQUI[(2)], CHRISTOPHER T. ROBINSON[(3)] & ANTON J. SCHLEISS[(4)]

[(1)] Laboratory of Hydraulic Constructions, Ecole Polytechnique Fédérale de Lausanne, Lausanne, Switzerland, severin.staehly@epfl.ch
[(2)] Laboratory of Hydraulic Constructions, Ecole Polytechnique Fédérale de Lausanne, Lausanne, Switzerland, pierre.bourqui@epfl.ch
[(3)] Federal Institute on Aquatic Science and Technology, Dübendorf, Switzerland, christopher.robinson@eawag.ch
[(4)] Laboratory of Hydraulic Constructions, Ecole Polytechnique Fédérale de Lausanne, Lausanne, Switzerland, anton.schleiss@epfl.ch

ABSTRACT

River restoration has become a priority goal in many countries. The interest in rivers as valuable habitats for floral and faunal diversity and as an ecosystem with important functions has increased. For evaluating the structural changes from a river restoration project, quantitative methods are needed to support engineers and resource managers in decision making. The Hydromorphological Index of Diversity (HMID) is a metric using the statistical values of flow depths and flow velocities measured at several points at multiple cross-sections of a river reach. For restoration project planning, however, numerical models often are applied offering a rapid calculation of flow depth and flow velocity for multiple variants of a study reach.This is a case study of a 2-km meandering residual flow stretch in the Sarine River in Switzerland downstream of a dam with a constant discharge of 2.5 m^3/s. In this river, flow depths and flow velocities are measured at 27 cross-sections. Further, a numerical model is created to generate flow depths and flow velocities using BASEMENT.The roughness of the numerical model is first estimated based on grain characteristics. The model is then calibrated. Analyses show that HMID changes substantially between the values generated with the physically feasible roughness and the calibrated roughness value. It turns out to be less profound for higher discharges. Analysis of the influence of extreme values then shows a strong dependence of the HMID on them. Therefore, extreme values from numerical models may have significantly lesser weight due to the large sample size compared to field measured data, where only the values of 27 cross-sections are taken into account.

Keywords: Morphology; indices; restoration; numerical modelling; habitat diversity.

1 INTRODUCTION

In Europe, river training is an essential measure mainly for flood protection, navigation and agricultural land gain purposes. Rivers are used as energy sources, with high-head power plants in the Alps and run-of-the-river power plants in lowland areas. Overall, rivers contribute much to the development of Europe and its welfare. River constructions, on the other side, also have negative effects on the environment. Therefore, authorities launched projects to enhance ecological conditions for in-stream organisms in the last decades. In the densely populated Switzerland, for example, hydropower accounts for 56% of the total electricity production (SFOE, 2015). According to the Swiss federal office of Environment, more than 15,000 km of the river network is categorized as strongly modified or artificial. In order to classify the natural state of a river, a solid method is needed. Commonly used methods, such as the Rapid Bio assessment Protocol based on visual observations, are sensitive to the person responsible for the survey. Especially in large countries, where each province has its responsible people for rivers, an objective tool is needed in order to compare classifications and reveal where priority for a restoration project should be given. The Hydromorphological Index of Diversity (Gostner et al., 2013) could serve as such a tool and will be the focus of the analysis in this conference paper.

1.1 Site description

This study was carried out on the Sarine River in Switzerland. The Sarine has its origin in the western Swiss Alps and drains into the Aare, a tributary of the Rhine. Due to its steep slope of 1.4%, it is subjected to multiple hydropower plants. Its regime is highly modified due to artificial lakes, dams and power houses. The study site is situated downstream of Gruyère lake and consists of a ca. 2-km long residual flow reach. It is a meandering river with a constant residual discharge of 2.5 m^3/s in winter and 3.5 m^3/s in summer. The study site has a bed-rock alluvial river bed and a large variety of river channel structures, such as multiple gravel bars, islands and riffle-pool sequences. Due to its large canyon-like incision – it is more than 100 m lower than the local surroundings – it is less affected by human built structures and at some areas the alluvial forest is flooded during high flows. An illustration of the study site is given in Figure 1, flow direction from south to north.

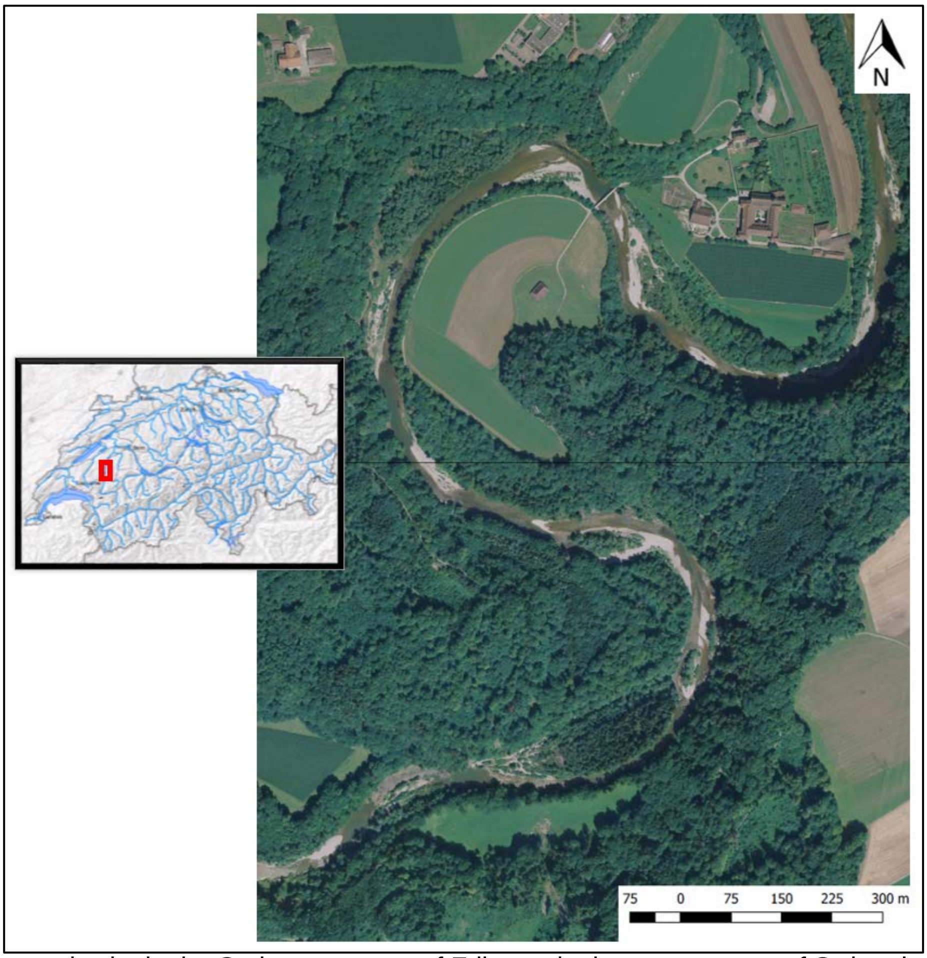

Figure 1: The study site in the Sarine upstream of Fribourg in the western part of Switzerland. The flow direction is from south to north

2 METHODS

2.1 The hydromorphological index of diversity (HMID)

The HMID is an index used to classify the habitat diversity in a river reach and was developed by Gostner et al. (2013). It is based on the coefficient of variation (CV) of the flow velocity and flow depth measured in a series of cross-sections in the river reach of interest, see Eq. [1]. The scale varies from: a channelized or heavily altered site, with uniform cross-sections and minor geomorphic patches (HMID < 5) to a reference site with fully developed spatial dynamics and full range of hydraulic habitats (HMID > 9). If the HMID lies between these two values (5 < HMID < 9), the study site shows limited variability to near natural morphology. Patterns of intact natural state are not developed in this class.

$$HMID_{Site}=\prod_i (1+CV_i)^2 = \left(1+\frac{\sigma_h}{\mu_h}\right)^2 \cdot \left(1+\frac{\sigma_v}{\mu_v}\right)^2 \qquad [1]$$

where,

CV=coefficient of variation [-]
μ=mean value[m] or [m/s]
σ=standard deviation [m] or [m/s]

Gostner et al. (2013) also showed that the CV of different other variables, e.g. CV of substrate or Thalweg diversity, correlate with the CV of flow velocity. Therefore, flow depth and flow velocity variation can be considered to represent the main factors that define the shape of a river accurately. In order to keep the objectivity and the representability of the method, the distances between cross-sections measured in the river need to be constant as well as the distance between the measurement points in a cross-section, as illustrated in Figure 2.

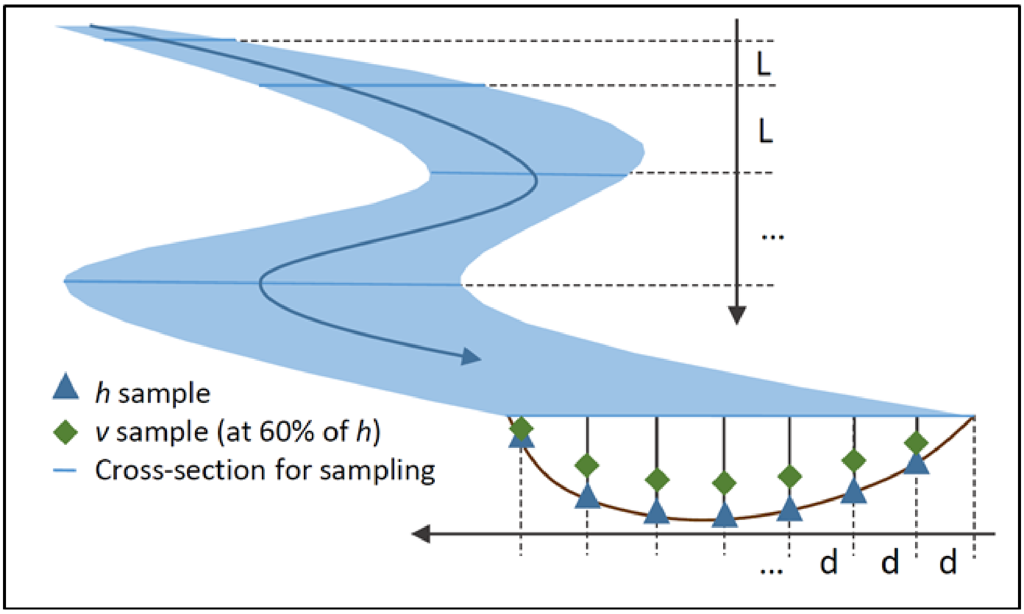

Figure 2: Sampling procedure for the variables *h* (flow depth) and *v* (flow velocity) used to calculate the HMID. It is important that the distances *L* and *d* remain constant

2.2 Measurement instruments

Flow depth was measured with a simple double meter attached to a global navigation satellite system (GPS). The GPS was a TOPCONHiPer Lite connected to the local mobile phone network using a SIM card for higher precision, resulting in a spatial precision, both vertically and horizontally,less than 2 cm. The positioning data obtained was then used for the Numerical model construction (see chapter 2.3). Flow velocity was obtained with a handheld velocimeter (SonTek FLOWTRACKER®). Where the water was too deep, an acoustic Doppler current profiler (ADCP, SonTek RIVERSURVEYOR®) was used to measure both flow depth and flow velocity. Figure 3 shows the tools used to determine flow velocity.

Figure 3: Tools used to measure flow velocity: on the left side SonTek RIVERSURVEYOR®, and on the right side the SonTek FLOWTRACKER®. Images were taken in the Sarine River, Switzerland.

2.3 Numerical model description

The use of numerical models has facilitated river restoration planning substantially. The HMID can be easily applied using a numerical model wherefore the influence of a restoration measure on habitat diversity can be quantified. A numerical 2D model of the study site was built in BASEMENT (Faeh et al., 2006) in order to simulate flow depth and flow velocity. The digital elevation model for the simulation consisted of data from two different sources. The terrestrial elevation came from a LiDAR flight and the in-river data came from 27 cross-sections that were measured at regular distances of 80 m, as described in section 2.1 using a GNSS. A linear interpolation between the cross-sections was done, before the DEM was generated, using the software SMS from AQUAVEO. The minimum distance between nodes was 2 m.

2.4 Grain size distribution (GSD)

Grain size properties were determined with 18 line-samplings (Fehr, 1987). In addition, two photos were analyzed using BASEGRAIN (Detert &Weitbrecht, 2012). The d_{90} varied from 9.1 to 13.0 cm, with an average of 11.3 cm. According to the Manning-Strickler velocity law (Eq. [2]), flow velocity and flow depth depend on the roughness.

$$v=K\cdot\sqrt{J}\cdot R_h^{2/3} \qquad [2]$$

where,

K=Strickler roughness value $[m^{1/3}/s]$
K is the inverse of the Manning roughness n
J=energy slope[-]
R_h=hydraulic radius [m]

The roughness, on the other hand, depends on grain properties, and in alpine gravel-bed rivers can be calculated using Eq. [3] (Strickler, 1923).

$$K=\frac{21.1}{\sqrt[6]{d_{90}}} \qquad [3]$$

where,

K=Strickler roughness value $[m^{1/3}/s]$
K is the inverse of the Manning roughness n
d_m=mean diameter[m]

Based on Eq. [3], a Strickler value of 30.4 $m^{1/3}/s$ is obtained.

2.5 Analyses

With the data available, the influence of roughness on the HMID was calculated. For computational reasons, only the Manning-Strickler velocity law was applied.

- In the first step, the numerical model was calibrated. Therefore, the Strickler value was changed until the sum of the absolute differences in flow depth in the cross-sections was minimal (difference between $h_{simulated}$ and $h_{measured}$).
- Further, the HMIDs were calculated for the values between the physically reasonable roughness and the roughness value determined through the calibration. For comparison, the same procedure was also done for a higher discharge.
- Since there is a difference between the HMID determined by the model and the field data, the influence of extreme values (flow depth and flow velocity) was analyzed. Therefore, the same amount of extreme values (max and min) from both variables was removed and the performance of the HMID was observed. For example, for 4% of the removed extreme values, the highest and lowest 1% of the values from flow depth and flow velocity were removed from the data series.

3 RESULTS

3.1 Calibration result of the numerical model

For calibration, the difference between the simulated and the measured flow depths in the 27 cross-sections were measured. The resulting maximum and mean of the absolute differences in flow depth for the different scenarios are displayed in Table 1.

Table 1. The maximum and mean difference of the absolute differences in flow depth measured with the different Strickler values at a discharge of 2.5 m^3/s.

K [$m^{1/3}/s$]	MAX DIFFERENCE [m]	MEAN DIFFERENCE [m]
30.4	0.45	0.20
28	0.45	0.19
16	0.41	0.12
14	0.39	0.11
12	0.38	0.09
10	0.35	0.09

3.2 HMID dependence on the Strickler value

The influence of the different calibration values on the HMID was calculated: first on the measured discharge of 2.5m^3/s and for comparison also for a higher discharge of 100 m^3/s. For the 100 m^3/s floods, only the gravel banks but not the floodplain were assessed. Bankfull discharge was estimated around 150 m^3/s. Figure 4 shows that HMID highly depends on the roughness applied in the numerical model. With a Strickler value of 30.4 $m^{1/3}/s$, the HMID achieves a value of more than 12 for a discharge of 2.5 m^3/s,which corresponds to a hydromorphological reference site. The best fitting result from the calibration, HMID = 8.4, indicates a limited variability. To compare, the HMID calculated with the data from the field survey, resulted in HMID = 9.4. At 100 m^3/s, the influence on the HMID was significantly less.

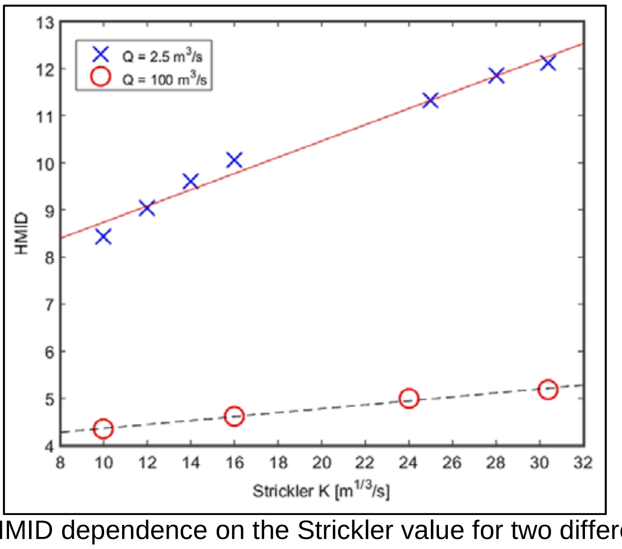

Figure 4: The HMID dependence on the Strickler value for two different discharges

3.3 Influence of extreme values on the HMID

For a Strickler value K = 10 $m^{1/3}/s$ and a discharge Q = 2.5 m^3/s, extreme values were continuously removed. Figure 5 shows that HMID decreases exponentially when extreme values are removed. The 5% highest extreme values made the HMID drop by almost 25%.

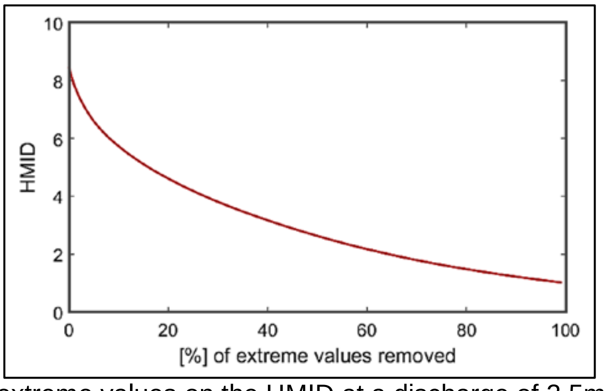

Figure 5: The influence of extreme values on the HMID at a discharge of 2.5m^3/s and a Strickler value of 10 $m^{1/3}/s$.

4 CONCLUSIONS

The results clearly show that an accurate calibration of a numerical 2D model in order to calculate the HMID is necessary. A Strickler value of 10 $m^{1/3}/s$ shows the best results of the tested Strickler values. However, this value does not represent the physical conditions found in the river reach. This low representation may be explained with the research done by Millar (1999), who indicated that bed forms such as pool-riffles sequences, pebble clustering and bars – bedforms found in the Sarine - may significantly influence the roughness of the river bed. The low submergence ratio with a discharge of 2.5 m^3/s brings out this effect even more and macro-roughness may cause its influence. Berchtold (2015) concluded that the calibration of a 2D model results in half or more than the physically expected Strickler values while doing experiments with BASEMENT. Therefore, the flow law of Chézy might be more appropriate for a 2D flow simulation, but if this is also true for the HMID needs to be proven. The importance of extreme values on the HMID is evident. This might therefore be the driving factor why the field measured HMID is higher than the model generated value (9.4 from the field data and 8.4 from the numerical flow data). Since the numerical model has almost 23,000 nodes while the field data consists of only about 700 data points, a reduced impact of extreme values may result. Different mesh resolutions and cell selection methods in future investigations may help in minimizing this difference.

ACKNOWLEDGMENTS

This research is founded by the Swiss National Science Foundation (SNF) in the framework of the national research program 70 (NRP 70): Energy turnaround. We thank Diego Tonolla, Zurich University of Applied Science (ZHAW) as well as our colleagues Elena Battisacco and Jonas Durand-Gasselin for their valuable support in the field.

REFERENCES

Berchtold, T. (2015). *Numerische Modellierung von Flussaufweitungen*. VAW Report 231, ETH Zürich.

Detert, M. & Weitbrecht, V. (2012). Automatic Object Detection to Analyze the Geometry of Gravel Grains–A Free Stand-Alone Tool. *River flow*, 595-600.

Faeh, R., Mueller, R., Rousselot, P., Veprek, R., Vetsch, D., Volz, C. & Farshi, D. (2006). BASEMENT—Basic Simulation Environment for Computation of Environmental Flow and Natural Hazard Simulation. *VAW*, ETH Zürich.

Fehr, R. (1987), Einfache Bestimmung der Korngrössenverteilung von Geschiebematerial, *Schweizer Ingenieur Architekt*, 105(38), 1004–1109.

Gostner, W., Alp, M., Schleiss, A.J. & Robinson, C.T. (2013). The Hydro-Morphological Index of Diversity: A Tool for Describing Habitat Heterogeneity in River Engineering Projects. *Hydrobiologia*, 712(1), 43-60.

Millar, R.G. (1999). Grain and formresistance in gravel-bedrivers Résistances de grain et de forme dans les rivières à graviers. *Journal of Hydraulic Research*, 37(3), 303-312.

SFOE. (2015). *SchweizerischeElektrizitätsstatistik 2015*. Swiss Federal Office of Energy, Swiss confederation, 52.

Strickler, A. (1923). *Beiträge zur Frage der Geschwindigkeitsformel und der Rauhigkeitszahlen für Ströme, Kanäle und geschlossene Leitungen*. Bern: Eidg. AmtfürWasserwirtschaft.

INFLUENCE OF LATERAL RECTANGULAR EMBAYMENTS ON THE TRANSPORT OF SUSPENDED SEDIMENTS IN A FLUME

CARMELO JUEZ[(1)], IRIA BUEHLMANN[(2)], GAETAN MAECHLER[(3)], ANTON J. SCHLEISS[(4)] & MÁRIO J. FRANCA[(5)]

[(1,2,3,4,5)] École Polytechnique Fédéral de Lausanne (EPFL), Lausanne, Switzerland
carmelo.juez@epfl.ch

ABSTRACT

Systematic experimental investigations have been performed under uniform flow conditions in a channel whose banks are equipped with large scale rectangular roughness elements. The practical motivation of this project is to see how restoration of banks, such as lateral cavities, has an influence on the transport of fine sediments. The implementation of lateral cavities may affect the sediment and morphological equilibrium of the river since these may trap sediments. This work aims to study the influence of the lateral cavities on the transport of fine sediments in the main channel. A set of laboratory experiments are done which covers a wide range of rectangular cavity configurations and includes aspect ratios (lateral cavity depth divided by cavity length) between 0.2 and 0.8. Key parameters such as the flow discharge and the initial sediment concentration are tested. Surface PIV, sediment samples and turbidity temporal records are collected during the experiments. The trapping efficiency of the cavities and the associated flow patterns are calculated and discussed. The resulting conclusions provide useful information for the future design of river restoration projects.

Keywords: Fine sediments; river restoration; ateral embayments; surface PIV; shallow flows.

1 INTRODUCTION

River restoration is nowadays a major issue in the field of hydraulics. The natural course and geometry of the rivers have been artificially changed by human activities for different purposes (land gaining, flood protection, agriculture, hydropower production). However, this man intervention has caused an alteration in the continuity of the sediment transport (Allan and Castillo, 2007; Schleiss et al., 2016). This way, the quasi-natural equilibrium between the in-coming and outgoing fluxes of sediments is broken (McCartney, 2009), leading to: (i) a deficit situation or (ii) an excess situation downstream the reaches with a deficit situation. The aforementioned unbalanced sediment equilibrium causes a twofold local morphological response: bed-erosion and instability of river-banks in areas where there is a sediment deficit and strong deposition and clogging in areas with a sediment excess (Kondolf, 1997). Also, from an ecological point of view, the disruption of the sediment cycle has important consequences for the riparian habitats: fine suspended sediments behave as transporting vectors of nutrients that help in algae growth (Von Bertrab et al., 2013) and also, they contribute to the creation of areas with differentiated velocity values that have a potential for fish and plants (Wood and Armitage, 1997; Kemp et al., 2011).

Furthermore, rivers channelized by man activity often display a straight path and monotonous river banks. One way to restore rivers consists of transforming the artificial banks by adding macro-roughness elements in the lateral river banks. However, these lateral cavities may be also responsible for the change of the river morphology, since they may trap the fine sediments travelling within the water.

The impact of these lateral embayments on the hydraulics of the rivers have already been thoroughly analyzed in several studies where different objectives have been targeted: (i) exchange process between the main flow and the cavity in relation to the turbulence motions in groyne fields and lateral cavities: experimental (Uijttewaal et al., 2001; Kolyshkin and Ghidaoui, 2002; Le Coz et al., 2006; Weitbrecht et al., 2001 Rivière et al., 2010; Uijttewaal, 2014; Akutina, 2015; Mignot et al., 2016) and numerical works (Hinterberger et al., 2007; McCoy et al., 2008), (ii) determination of the flow resistance effect owed to the lateral embayments created in the river banks Meile et al. (2011) and Sukhodolov (2014) and (iii) role of the sediment siltation in groynes fields for the sediment budget of rivers (Abad et al., 2008; Ten Brinke et al., 2004; Yossef and de Vriend, 2010; Henning and Hentschel, 2013). Despite the effort devoted by previous authors, laboratory experiments related to lateral embayments and morphodynamics are scarce and difficult to carry out (Henning and Hentschel, 2013) since sedimentation processes are related with: the variability of discharge, the geometrical configuration of the river banks and the sediment concentration transported in the flow. Thus far, only minimal details about measured sedimentation in laboratory channels can be found in Sukhodolov et al. (2002). Common practice, in the literature mentioned earlier, consists of deriving sedimentation patterns based on groyne field, flow patterns measured in the channels and observed in the field. However, the accuracy of the sedimentation-erosion forecasts is hampered by the fact that the morphological response of the lateral embayment is assumed negligible in relation with the flow patterns. The fine material trapped in the embayment may modify the velocity field, enabling the alteration of the location and magnitude of the eddies and consequently, the pick-up and settling ratio of the fine particles inside the cavity.

In order to address which is the morphological answer of these lateral embayments, systematic experimental investigations in a channel have been carried out with a large number of different geometrical bank configurations. The practical questions answered in this study are: (i) which is the impact of the lateral embayments on the hydraulics patterns, (ii) which type of lateral embayment will be filled up fast with fine sediments and should be avoided in restoration projects and (iii) which type of lateral embayment will be filled up partially having zones with high and low velocities and potential for various habitat.

2 EXPERIMENTAL SETUP

2.1 Flume description

Experiments had been performed in a hydraulic system which worked in a closed circuit with different components, this included: (i) an upstream tank of 2 m long, 1 m wide and 1 m high that served as a mixing tank where suspended sediments had been mixed, (ii) a rectangular open channel which was 7.5 m long, 1.0 m wide and 1.0 m high with 0.1 % slope (typical slope for the subcritical flows in the Alpine valleys) and (iii) a downstream tank of 3.5 m long, 1 m wide and 1 m high that collected the circulating flow. The water was then pumped from down-stream to the upstream tank. A sketch of the experimental set up is shown in Figure 1.

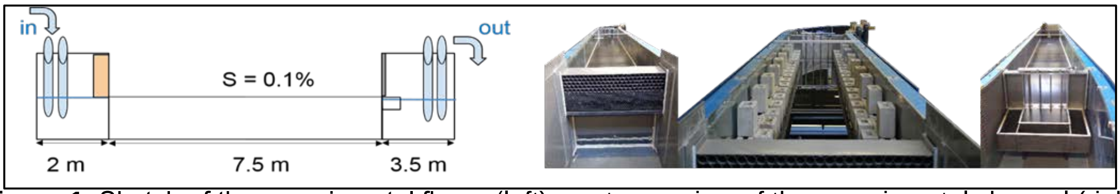

Figure 1. Sketch of the experimental flume (left); upstream view of the experimental channel (right-a); rectangular channel with the macro-roughness elements (right-b); downstream view of the experimental channel (right-c) Initial conditions.

2.2 Macro roughness configurations

The large-scale depressions, namely the rectangular cavities at the sidewalls were formed by concrete bricks (0.25 m long, 0.10 m wide, and 0.19 m high). A base channel width based on the prismatic elements, configurations 1.0, 2.0 and 3.0, had been set as a reference for all tests. They were inspired by Meile et al. (2011) who studied macro-rough flows and they were considered as large-scale depression roughness (Morris, 1955). They were characterized by the length of the cavity l, the distance between two cavities L and the lateral depth of the cavities W. These geometrical parameters had been systematically varied among them and also, in relation with the base width b of the channel as shown in Figure 2. Furthermore, the combination of the characteristics lengths of the lateral embayments led to the definition of several geometrical ratios: aspect ratio, AR= W/l, roughness ratio, RR= W/L, and expansion ratio, ER= (b+2W)/b.

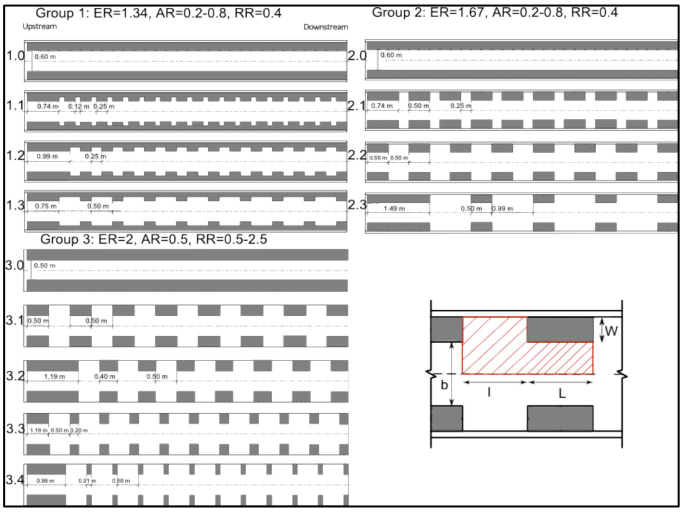

Figure 2. Geometric configurations tested and detail of the definition of the geometric lengths of the macro-roughness configurations.

The combination of these three different ratios with three different discharges had resulted in 30 different vertical axis-symmetric geometrical configurations that had been studied in this work, see Table 1.

Table 1. Summary of test ranges of the geometrical parameters of the configurations. Listed are the expansion ratio (ER), the aspect ratio (AR) and the roughness ratio (RR).

Group	Configuration	ER [-]	AR [-]	RR [-]
1	1.1	1.34	0.80	0.40
	1.2	1.34	0.40	0.40
	1.3	1.34	0.20	0.40
2	2.1	1.67	0.80	0.40
	2.2	1.67	0.40	0.40
	2.3	1.67	0.20	0.40
3	3.1	2.00	0.50	0.50
	3.2	2.00	0.50	0.60
	3.3	2.00	0.50	1.20
	3.4	2.00	0.50	2.50

2.3 Initial conditions

Three different discharges (representatives of a low, medium and peak discharge) with their corresponding maximum capacity sediment concentration had been considered in this study (Table 2). These discharges are defined by the shallowness relation b/h between the water depth, h, and the channel width, b. The influence of the water depth is well known as a key parameter: shallow flows lead to quasi-2D turbulence structures which are the net contributors for the mass exchange between the main flow and the lateral embayments (Uijttewaal et al., 2001; Uijttewaal, 2014). Conditions for the low and medium discharges allow to have shallow flows whereas the peak discharge situation is in the border of the shallowness condition.

Table 2. Summary of initial conditions for each discharge tested.

Discharge [ls^{-1}]	Q_1= 4.8	Q_2= 8.5	Q_3= 15.0
Water depth [m]	0.035	0.050	0.070
Shallowness ratio *b/h* [-]	0.26	11.50	8.20
Velocity [ms^{-1}]	0.26	0.32	0.40
Froude number [-]	0.442	0.458	0.484
Reynolds number [-]	4835	8334	13966
Concentration [gl^{-1}]	0.50	1.00	1.50
Experiment duration [h]	3.00	4.00	5.00

Characteristic values of Froude number, Reynolds number and the mean flow velocities can be seen in Table 2. These values showed that the experiments had been conducted under subcritical and turbulent conditions.

Polyurethane artificial sediments had been considered in all the experiments. The properties of this material are: a grain size of d_{50} = 0.2 mm, a density equal to 1160 kgm^{-1} and a uniformity equal to 0.47. The mean diameter of the particles was chosen to be in the range of non-cohesive fine sediment, 0.062-0.5 mm, according to Van Rijn (2007).

Sediment concentration had been chosen in order to fulfill the maximum suspended capacity of the flow. Experiments were performed until reaching a quasi-equilibrium concentration state. The channel had its own inertia regarding the sediment decay: some of the particles were trapped in the small gaps between bricks and walls. Nonetheless, the sediment concentration decay was compared with the reference situations, thus making it possible to compare it with the outcomes of all the experiments.

3 EXPERIMENTAL TECHNIQUES

3.1 2D surface PIV

The study of the flow pattern inside the cavity had been performed using a 2D-surface PIV technique as it had been previously done in (Uijttewaal et al., 2001; Weitbrecht and Jirka, 2001; Uijttewaal, 2014). Systematic photo sequences had been taken on the same cavity for the three discharges and for all the configurations. It was assumed that the position of the cavity, in the center of the channel, was representative of the flow pattern for all the cavities, as there was no influence of the channel extremities. Water-level fluctuations were also checked by means of ultrasonic probes. The accuracy of the water level measurements was at least ± 0.002 m.

The PIV technique had been applied by seeding the channel with polystyrene particles with a diameter of 3 mm and a density slightly under the one of water (0.946 gl^{-1}). The acquisition of the photos had been done with a SUMIX SMX-160 camera, which was placed above the cavity. The recording process was performed at the beginning of the experiment at a rate of 3 frames/s (30 Hz). Photos sequences were subsequently post-processed using Matlab and the package PIVLab (Thielicke and Stamhuis, 2014): a technique of window deformation was considered to track particles in the photo sequence. The picture was divided in small interrogation areas and a cross correlation algorithm derived the most probable particle displacement. This generated an instantaneous velocity field for each time step. Next, this information was time averaged in order to analyze the stationary flow patterns present in the embayment.

The measures obtained with the surface PIV only provided information concerning the motion of the free surface. Nevertheless, the shallowness of the configurations allowed to consider that the velocity field in the embayment was mainly 2D (Tuna et al., 2013) and consequently, these results can be used as a proxy for a better comprehension of the phenomena occurring.

3.2 Suspended sediment monitoring

The temporal evolution of the suspended sediment concentration was recorded in two locations in the channel: upstream and downstream. However, a transitional length was left (close to the tranquilizer and the gate) to avoid any perturbation in the measurements.

The data acquisition was carried out by two turbidimeters Cosmos-25. The signal was sampled with a frequency of 100 ms. Subsequently, the data was averaged for every 25 time steps before storing the values of the concentration. Information provided by the turbidimeters was punctual and it corresponded to a value in the vertical concentration profile.

3.3 Sediment deposition pattern

The study of the influence of the sedimentation on the cavity was performed following a twofold protocol: (i) plan view photos of the sedimentation patterns were taken in the same cavity where the PIV technique was applied. These photos were treated for extracting the surface occupied by the sediments in order to cross-correlate their location with the information provided by the PIV technique. (ii) The total mass of sediment mass trapped inside the lateral embayments was collected. Later, the sediment samples were dried in an oven to eliminate the water content and weighted. This mass was divided by the total area occupied by the embayments in order to compute the trapping efficiency.

4 RESULTS

4.1 Flow patterns

2D surface PIV results of the lateral cavities are presented for configurations 2.2 (See Figure 3). Thanks to this technique, instantaneous (u',v') and mean velocity vectors ($\bar{u}$,$\bar{v}$) are obtained, being u and v the longitudinal and streamwise velocities respectively. Results are available for the cavity and the area of the main channel close to it. A dimensionless scale is used to characterize the cavity, x=l denotes the longitudinal direction while y=l the transversal direction. l is the length of the cavity. In addition to the velocity field, statistics on the turbulence were also performed. Mean Reynolds shear stress $\overline{u'v'}$ and mean vorticity, were computed.

Depending on the aspect ratios of the lateral embayments, the flow was characterized by the formation of one or more large-scale vortical structures that can fit the whole embayment or can occupy it partially.

For every discharge, a single clockwise recirculating system is observed. This vortex is located in the downstream part of the cavity and its center is after the 0.5 x=l position. It therefore confirms the influence of the downstream cavity wall in the reflection of the eddies: the flow hits the opposite cavity wall and the recirculating zone starts at this boundary. While the discharge is increasing, the vortex tends to be longer in the x=l direction. Regarding the velocities, a velocity plume appears when the flow leaves the cavity and it reenters in the main flow. Velocity vectors indicate that outside of the lateral embayment the flow is unidimensional following the main direction of the channel. Results indicate a clear strengthening of the vortex velocity with discharge and it is illustrated that for the highest discharge a secondary eddy appears in bottom-left corner of the cavity.

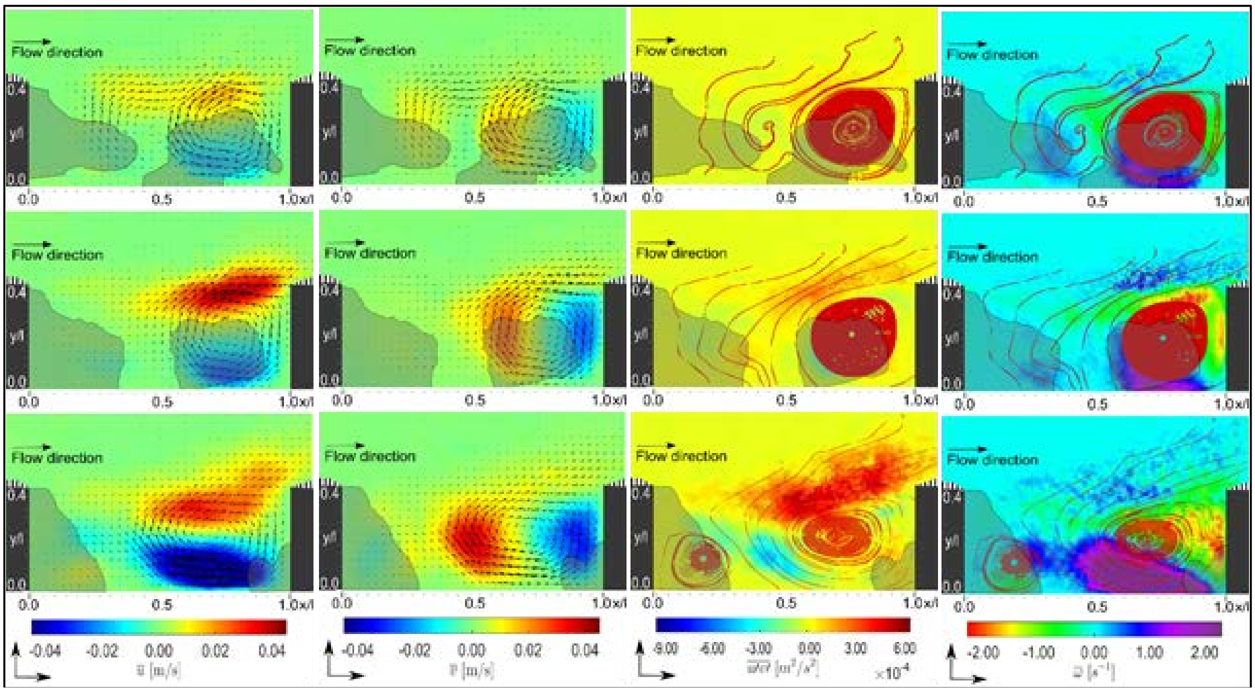

Figure 3. Geometric configuration 2.2. Mean longitudinal velocity field along with the velocity vectors (top-left); mean streamwise velocity field along with the velocity vectors (top-right); mean Reynolds shear stress field along with a few streamlines (bottom-left) and mean vorticity field along with a few streamlines (bottom-right). The results for the three different discharges are plotted from top to bottom and from 4.8 ls^{-1} to 15.0 ls^{-1}. The shaded area indicates the region where the sediments settled down at the end of the experiment. In the dashed area, the information was not available for performing the PIV computations.

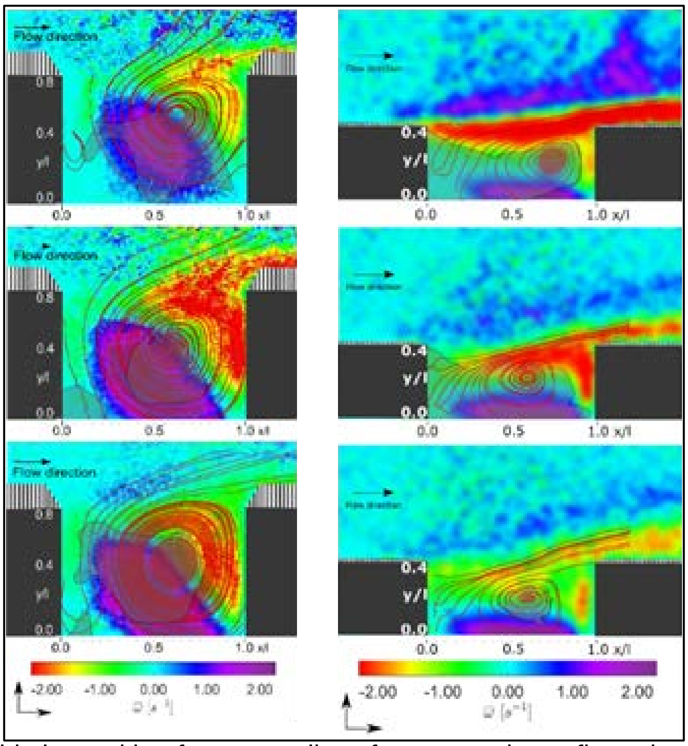

Figure 4. Mean vorticity field along with a few streamlines for geometric configuration 2.1 (left) and geometric configuration 1.3 (right). The results for the three different discharges are plotted from top to bottom and from 4.8 ls-1 to 15.0 ls-1. The shaded area indicates the region where the sediments settled down at the end of the experiment. In the dashed area, the information was not available for performing the PIV computations.

Regarding the shear stress and vorticity: two trends are observed when comparing among configurations: (i) For geometric configurations with high aspect and expansion ratios, it is stated that by increasing the discharge, the magnitude of the shear stress also increases. Thus, the vorticity also increases with higher discharges. The effect of the wall is observed in the magnitude of the vorticity which is larger in the bottom-right corner. See configuration 2.1 in Figure 4(left) as an example. (ii) However, it is observed that for configurations with low expansion and aspect ratio, higher discharges do not imply higher values of shear stress and vorticity (see configuration 1.3 in Figure 4 on the right).

4.2 Time decay of the normalized concentration

During the experiments, the concentration was continuously measured at two positions in the channel. These measurements show the dynamics of the sedimentation and although the results of the three groups show some differences, the main patterns are similar.

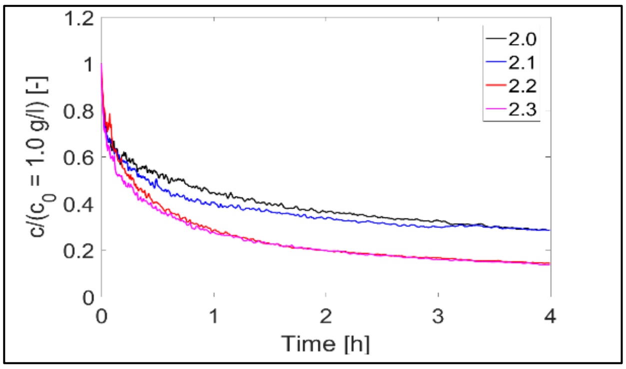

Figure 5. Geometric configurations for group 2. Time decay for the normalized sediment concentration. Results are shown for 4.8 ls-1. The curves are normalized by the initial concentration.

While the concentration of all the configurations drops rapidly in the beginning, it stabilizes and converges to an equilibrium value at the end of the experiment. Regarding the aspect ratio, one can see a correlation focusing on the dynamics. The lower the aspect ratio, the faster the drop in the concentration (see especially configuration 2.3 in Figure 5).

4.3 Trapping efficiency

To obtain the trapping efficiency of the different geometrical configurations, the trapped sediments were collected after each experiment. The total mass is then divided by the area occupied by the embayments in order to obtain the trapping efficiency. In Figure 6, these efficiencies are depicted for all the geometrical groups, starting with group 1.

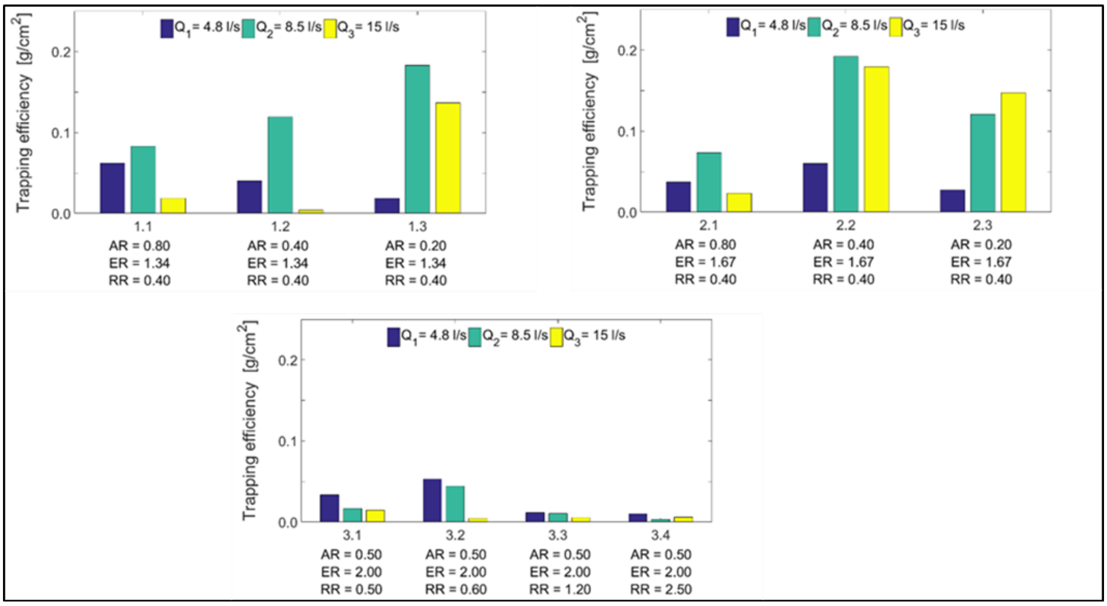

Figure 6. Trapping efficiency for all the geometric configurations. Below the figures, the values for the aspect ratio (AR), the expansion ratio (ER) and the roughness ratio (RR) are given.

 ©2017, IAHR. Used with permission / ISSN 1562-6865 (Online) - ISSN 1063-7710 (Print)

Regarding the AR, it can be seen, that for the highest AR of 0.8, the lowest efficiencies are achieved. This can be observed both in groups 1 and 2. Between the smaller aspect ratios of 0.4 and 0.2, no clear tendencies are observed. There are clear tendencies regarding the discharge. The medium discharge of 8.5 ls-1 obtains the highest efficiency in all the three geometrical groups. For the low discharge, the trapping efficiency shows only small differences when changing the ratios.

5 CONCLUSIONS

The aspect ratio (AR) is the most important parameter to characterize lateral embayments. Both flow patterns and sedimentation processes are highly dependent on the AR. It is an important measure in order to analyze the location and number of eddies inside the cavities. In addition, the smaller the aspect ratio is, the more easily the flow attaches to the sidewall of the cavity. The trapping is faster and more sedimentation is trapped in the cavity.

The consequences for river restoration projects are as follows. The type of lateral embayment that will be filled up the fastest, is characterized by a small AR, a high ER and a low RR. Embayments of a larger AR and RR are providing better conditions for restoration projects, as they are not filled up as fast. This provides a more sustainable solution, as these embayments satisfy their purpose over a longer time period. In order to gain a lateral embayment that provides different zones of varying velocities and the potential for sand/ gravel banks, low AR are needed. Due to the low AR, it will be filled up partially with fine sediment inducing zones with higher and lower velocities. A combination with a rather high RR or low ER may control the sedimentation, in order to prevent completely filled up embayments.

In addition to the ratios of the embayments, the magnitude of the discharge shows a major impact on the sedimentation. The medium discharge achieves the highest trapping efficiency. The amplified gravity waves have a stabilizing effect on the shear instabilities. This causes an increased trapping efficiency for the medium discharge. For the higher discharge, the trapping is reduced, due to the intensified recirculating force of the eddies in the embayment. As the recirculation is stronger, the turbulences in the embayments are higher, which decreases the settling of the particles. Although, the exchange between the embayments and the main channel is increased for high discharges, the particles cannot settle. This can be an indicator to design artificial floods as large as possible in order to keep the small particles in motion and avoid trapping in all the low flow areas downstream.

The flow pattern recorded by the PIV shows a good correlation with the observed sedimentation patterns. The main vortex corresponds generally well to the area of sediment deposition in the embayment. Further, a coherent mixing layer is also found. And, high positive velocities correspond to areas that are free of sedimentation. However, for cavities of higher ER some inconsistencies can be seen. They can be explained by the three-dimensional conditions in this wide shallow embayments.

ACKNOWLEDGEMENTS

This work was funded by the ITN-Programme (Marie Curie Actions) of the European Union's Seventh Framework Programme FP7-PEOPLE-2013-ITN under REA grant agreement 607394-SEDITRANS. The experiments were funded by FOEN (Federal Office for the Environment, Switzerland).

REFERENCES

Abad, J., Rhoads, B., Guneralp, I. & Garcia, M. (2008). Flow Structure at Different Stages in Ameander-Bend with Bendway Weirs. *Journal of Hydraulic Research*, 134(8), 1052-1063.

Akutina, Y. (2015). Experimental Investigation of Flow Structures in a Shallow Embayment using 3D-PTV, *PhD Thesis*. McGill University, Montréal.

Allan, J.D. & Castillo, M.M. (2007). *Stream Ecology: Structure and Function of Running Waters*. Springer, Netherlands.

Henning, M. & Hentschel, B. (2013). Sedimentation and Flow Patterns Induced by Regular and Modified Groynes on the River Elbe, Germany. *Ecohydrology*, 6(4), 598-610.

Hinterberger, C., Frohlich, J. & Rodi, W. (2007). Threedimensional and Depth-Averaged Large Eddy Simulations of Some Shallow Water Flows. *Journal of Hydraulic Engineering*, 133(8), 857-872.

Kemp, P., Sear, D., Collins, A., Naden, P. & Jones, I.(2011). The Impacts of Ne Sediment on Riverine Fish. *Hydrological Processes*, 25, 1800-1821.

Kolyshkin, A.A. & Ghidaoui, M.S. (2002). Gravitational Shear Instabilities in Compound and Composite Channels. *Journal of Hydraulic Engineering*, 128(12), 1076-1086.

Kondolf, G.M. (1997). Hungry Water: Effects of Dams and Gravel Mining on River Channels. *Environnemental Management*, 21(4), 533-551.

Le Coz, J., Brevis, W. & Niño, Y. (2006). Open-Channel Side-Cavities: A Comparison of Field and Flume Experiments. In River Flow 2006, Two Volume Set: *Proceedings of the International Conference on Fluvial Hydraulics, Lisbon*, Portugal, 6-8 September 2006 (145). CRC Press.

McCartney, M. (2009). Living with Dams: Managing the Environmental Impacts. *Water Policy,* 11(S1), 121-139.

Constantinescu, G. & Weber, L.J. (2008). Numerical Investigation of Ow Hydrodynamics in a Channel with a Series of Groynes. *Journal of Hydraulic Engineering*, 134(2), 157-172.
Meile, T., Boillat, J.-L. & Schleiss, A.J. (2011). Flow Resistance Caused by Large-Scale Bank Roughness in a Channel. *Journal of Hydraulic Engineering*, 137(12), 1588-1597.
Mignot, E., Cai, W., Launay, G., Rivière, N. & Escauriaza C. (2016). Coherent Turbulent Structures at the Mixing-Interface of a Square Open-Channel Lateral Cavity. *Physics of Fluids*, 28(4), 045104.
Morris, M.H. (1955). A New Concept of Flow in Rough Conduits. *Transactions American Society of Civil Engineers*, 120, 373-410.
Rivière, N., Garcia, M., Mignot, E. & Travin, G. (2010). Characteristics of the Recirculation Cell Pattern in a Lateral Cavity. *Proc. Int. Conf. Fluvial Hydraul., IAHR*, 673-679.
Schleiss, A.J., Franca, M.J., Juez, C. & De Cesare, G. (2016). Reservoir Sedimentation, *Journal of Hydraulic Research,* 54(6), 595–614.
Sukhodolov, A (2014). Hydrodynamics of Groyne Fields in A Straight River Reach: Insight from Field Experiments. *Journal of Hydraulic Research*, 52(1), 105-120.
Ten Brinke, W.B.M., Schulze, F. & Van Der Veer, P (2004). Sand Exchange between Groyne-Field Beaches and The Navigation Channel of The Dutch Rhine: The Impact of Navigation Versus River Flow. *River Research and Applications*, 20, 899-928.
Thielicke, W. & Stamhuis, E.J. (2014). PIVlab – Towards User-friendly, Affordable and Accurate Digital Particle Image Velocimetry in MATLAB. Journal *Open Research Software*, 2(1), 1-30.
Tuna, B., Tinar, E. & Rockwell, D.(2013). Shallow Ow Past A Cavity: Globally Coupled Oscillations as a Function of Depth. *Experiments and Fluids*, 54(8), 1586.
Uijttewaal, W.S.J. (2014). Hydrodynamics of Shallow Flows: Application to Rivers. *Journal of Hydraulic Research,* 52, 157–172.
Uijttewaal, W.S.J., Lehmann, D.V. & Mazijk, A.V. (2001). Exchange Processes between a River and Its Groyne Fields: Model Experiments. *Journal of Hydraulic Engineering*, 127(11), 928-936.
Von Bertrab, M.G., Krein, A., Stendera, S., Thielen, F. & Hering,D. (2013). Is Fine Sediment Deposition a Main Driver for The Composition of Benthic Macroinvertebrate Assemblages? *Ecological Indicators*, 24, 589-598.
Van Rijn, L.C.(2007). Unified View of Sediment Transport by Currents and Waves. I: Initiation of Motion, Bed Roughness, and Bed-Load Transport. *Journal of Hydraulic Engineering*, 133, 649–667.
Weitbrecht, V. & Jirka, G.H.(2001). Flow Patterns and Exchange Processes in Dead Zones of Rivers, in: *Proceedings of the Congress-International Association for Hydraulic Research*. 439–445.
Wood, P.J. & Armitage, P.D. (1997). Biological Effects of Fine Sediment in the Lotic Environment. *Environnemental Management*, 21, 203–217.
Yossef, M.F.M. & de Vriend, H.J. (2010). Sediment Exchange between A River and its Groyne Fields: Mobile-Bed Experiment. *Journal of Hydraulic Engineering*, 136, 610–625.

SWITCHING OF BIFURCATION TO SINGLE CHANNEL: CASE OF A SAND BED BRAIDED RIVER

SHAMPA [1], YUJI HASEGAWA [2], HAJIME NAKAGAWA [3], HIROSHI TAKEBAYASHI[4] & KENJI KAWAIKE[5]

[1, 2, 3, 4, 5]Kyoto University, Kyoto, Japan,
shampa.25v@st.kyoto-u.ac.jp; hasegawa.yuji.3e@kyoto-u.ac.jp;nakagawa@uh31.dpri.kyoto-u.ac.jp;takebayashi.hiroshi.6s@kyoto-u.ac.jp; kawaike.kenji.5n@kyoto-u.ac.jp

ABSTRACT

Bifurcation plays a major role in shaping the braided river. Switching of bifurcation is a very frequent natural phenomena which has a great impact on the development process of compound bars of sand bed braided rivers. Through this study, such a switching phenomenon of bifurcation has been investigated in the braided river of Brahmaputra-Jamuna by numerical simulation. This study indicates that bifurcation switching phenomenon largely depends on upstream control e.g. incoming discharge. Nevertheless, this phenomenon is highly related with the upstream channel geometry and hydraulic condition. The dimension of downstream mid channel bar, which is the cause of bifurcation may influence the discharge asymmetry greatly but may possess an indirect impact over the switching process.

Keywords: Braided; sand bed; bifurcation; switch; delft 3D.

1 INTRODUCTION

Bifurcation is one of the major “building block” elements of braided river network (Mosley, 1976). Being generated by mid channel bar, bifurcation regulates the flow and sediment transport to the downstream branches and, thus plays a major role in the morphology of the braided network (Ferguson et al., 1992; Bristow and Best., 1993; Schuurman et al., 2015). Insand bed braided river can generally be divided into two types of mid channel bars, one is unit and another is compound. Bifurcation plays a significant role in the development process of these compound bars. Merging with other bars, dissection of bar through cross bar channels during high stage, loosing of connection or local narrowing of adjacent branch channels causes non-uniformity in the growth of these type of bars and these processes are strongly related with the dynamics of bifurcation (Schuurman et al., 2013). Switching of bifurcation is a key process in the development stage of these types of bar as this process allows the bar to be merged with other bars. Therefore, this study focuses on the process of bifurcation switch in a large sand bed river of Brahmaputra-Jamuna.

Previous studies (Wang et al., 1995; Pittaluga et al., 2003; Kleinhans et al., 2006; Bertoldi and Tubino, 2007; Federici and Paola, 2003,) showed the process of bifurcation but most of them were based on nodal point concept rather than the network formation process of the braided river. (Schuurman et al., 2015). In spite of greater simplifications of the real process, these models can predict the major aspects of bifurcation dynamics (Pittaluga et al., 2003; Miori et al., 2006). The laboratory experiment of Bertoldi and Tubino (2007) validated the model of Pittaluga et al. (2003). Most of the work were focused to characterize the symmetrical bifurcation with steady flow condition. But in nature, most of the bifurcations are asymmetrical and experience unsteady flow (Ashmore, 1991). Based on field observation, lab experiment and numerical simulation, it was explained that either the planform of the bifurcation or the hydraulic property of upstream channel plays the major role in case of closing one channel (Klassen et al., 1993; Kleinhans et al., 2006; Federici and Paola, 2003). This study attempts to determine factors that control the switching phenomenon of bifurcation using natural river bathymetry in a small branch of Brahmaputra-Jamuna River as shown Figure 1.

Satellite imagery showed that this 17 km Long Branch showed such switching process from 2011 to 2013 (Figure 1). The dry season satellite image showed that in 2011, a relatively larger channel (channel A compared to channel B) was flowing along the left side of a cluster of bars but in 2013 the right sided channel became larger (Figure 1 b and c). This study tries to replicate this phenomenon by varying the upstream discharge or downstream water level using unsteady flow condition through numerical simulation. The main objective of this study is to determine factors that accelerate the switching phenomenon, upstream control or downstream one in unsteady flow condition. Several cases are considered for this purposes which will be described in the next sections. The relationship of the upstream channel and downstream midchannel bar geometry with the switching phenomenon are also investigated. The effect of bifurcation angle on the switching process has also been studied in this research.

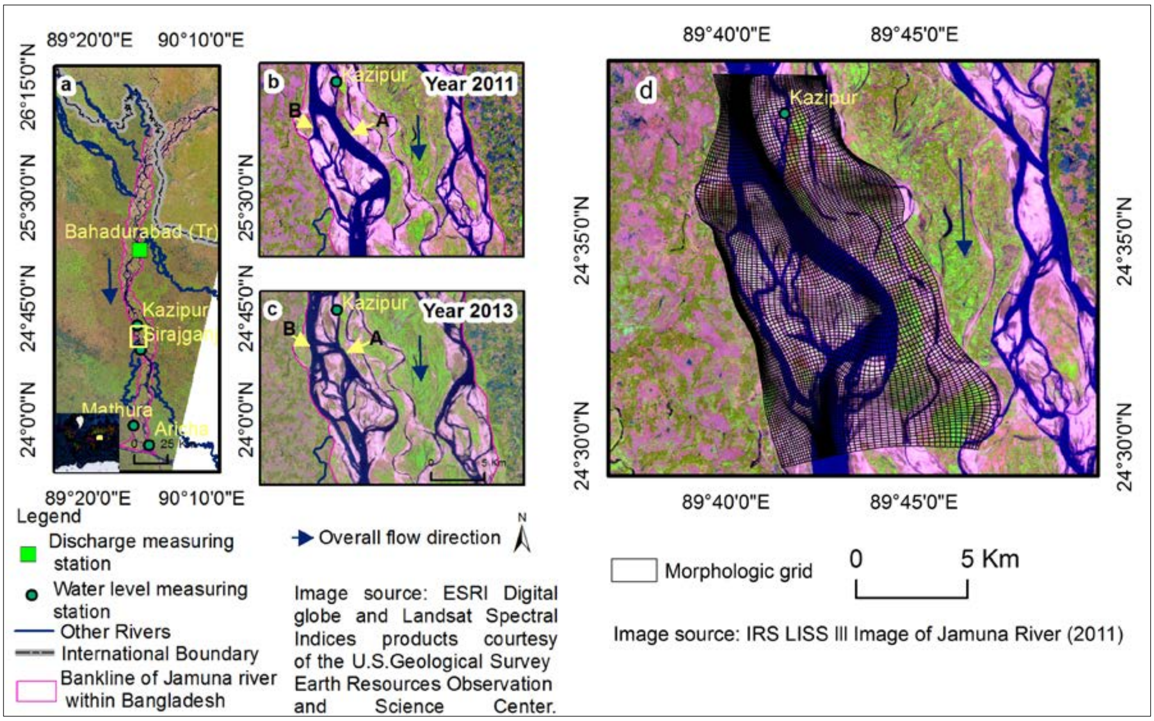

Figure 1. (a) Map showing the study area; (b) and (c) changes of the study area over time (d) Model domain of the numerical simulation.

2 METHODOLOGY

2.1 General approach

In this study, a 2D depth average morphological model was developed using Delft 3D (version 4.00.01) software for a 17km long river reach (Figure 1d). Then several attempt had been made to reproduce bifurcation switching phenomenon by considering several cases shown in Table 1 and Figure 2. The total simulation period was 137 days which reflected only the peak stage of the river. Four cases were considered including the base condition. Base condition was fixed on basis of the hydraulic condition of the year 2011. In Case 1, the discharge was increased 1.5 times of the base condition which was identical to the real river discharge of 2013 but keeping the downstream water level the same as of 2011. In Case 2, the discharge was kept the same as the base condition but the water level was decreased 0.90 times of the base condition to match with the river water level of 2013. The boundary condition of case 3 was almost similar to the river hydraulic condition of 2013.

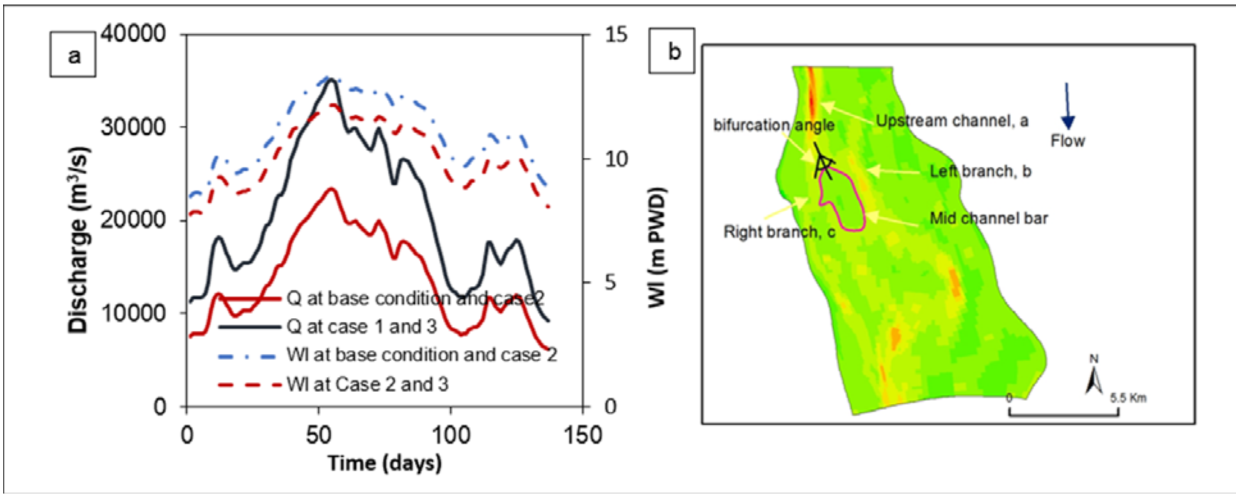

Figure 2. (a) Boundary Condition of the considered cases (b) Definition and terminology used in the model result analysis.

Table 1. Initial and boundary conditions.

PARAMETER	UNIT	BASE CONDITION	CASE 1	CASE 2	CASE 3
PEAK DISCHARGE QP	m^3/s	23388	35082	23388	35082
WATER LEVEL AT QP	m PWD	8.5	8.5	7.73	7.73
D_{50}	µm	277	277	277	277
INITIAL WATER LEVEL	m PWD	10	10	10	10
SEDIMENT TRANSPORT PREDICTOR	-	Van Rijn (1993)	Van Rijn (1993)	Van Rijn (1993)	Van Rijn (1993)
HYDRODYNAMIC TIME STEP	s	60	60	60	60
MORPHO-DYNAMIC TIME STEP	s	180	180	180	180
GRID CELL DIMENSION	m^2	167*88	167*88	167*88	167*88
ROUGHNESS (MANNINGS)	$s/[m^{1/3}]$	0.027	0.027	0.027	0.027
OVER ALL BED SLOPE	-	5.8x10-5	5.8x10-5	5.8x10-5	5.8x10-5

In case of braided river during high stage, the flow generally covers the full width of the river. During that time, it is difficult to define the left and right branches. The channel areas where the sediment transport is higher (more than 25%) than the average channel sediment transport were considered as branches during peak flow. To define other parameters, the definitions of previous researches were followed (Pittaluga et al., 2003; Bertoldi and Tubino, 2007). So, the upstream channel aspect ratio β_a and shields stress ϑ_a are defined by Eq. [1] and [2], respectively

$$\beta_a = \frac{W_a}{2D_a} \qquad [1]$$

$$\vartheta_a = \frac{\tau_a}{(\rho_S - \rho)gD_S} \qquad [2]$$

where W_a is the upstream channel width, D_a is the upstream channel depth τ_a is the average bed share stress, ρ_s and ρ are the sediment and water density, respectively and lastly, g is the gravitational acceleration (Figure 2b shows the location of channels and other definition). Bar aspect ratio, α is defined by the bar length to width ratio. The discharge ratio, r_q is the ratio of discharge of branch b to branch c.

2.2 Description of 2D Model

A two dimensional depth average model was developed using Delft 3D (version 4.00.01) software. The hydrodynamics were modeled by applying conservation of momentum (Eq [3] and [4]) and mass balance Eq. [5] equations, assuming hydrostatic pressure:

Conservation of momentum in x-direction:

$$\frac{\partial u}{\partial t} + u\frac{\partial u}{\partial x} + v\frac{\partial u}{\partial y} + g\frac{\partial \eta}{\partial x} - fv + \frac{gu|U|}{C^2(d+\eta)} - \frac{F_x}{\rho(d+\eta)} - v_t\left(\frac{\partial^2 u}{\partial x^2} + \frac{\partial^2 u}{\partial y^2}\right) = 0 \qquad [3]$$

Conservation of momentum in *y*-direction:

$$\frac{\partial v}{\partial t} + u\frac{\partial v}{\partial x} + v\frac{\partial v}{\partial y} + g\frac{\partial \eta}{\partial y} - fu + \frac{gv|U|}{C^2(d+\eta)} - \frac{F_y}{\rho(d+\eta)} - v_t\left(\frac{\partial^2 v}{\partial x^2} + \frac{\partial^2 v}{\partial y^2}\right) = 0 \qquad [4]$$

Conservation of mass, also known as the continuity equation:

$$\frac{\partial \eta}{\partial t} + \frac{\partial[(d+\eta)u]}{\partial x} + \frac{\partial[(d+\eta)v]}{\partial y} = 0 \qquad [5]$$

Where

η = water level elevation (here in m)

d = water depth (m)
u,v = velocity in the *x*- and *y*-directions, respectively (m/s)
U = magnitude of total depth-averaged velocity (m/s)
$F_{x,y}$ = *x* and *y* components of external forces
f = Coriolis parameter which is equal to 2*Ω* sin *θ*, where *Ω* is the earth's angular velocity and *θ* is the geographic latitude ($rad.s^{1}$)
g = acceleration due to gravity (m/s^{-2})
ρ = water density (kg/m^3)
ν_t = eddy viscosity (m^2/s)
C = Chézy coefficient ($m^{1/2}/s$)

For non-cohesive sediment transport, the equations of Van Rijn(1993) were used. The total load,*qθ* (Eq. [6]) is calculated as the sum of bed load transport *qθb* and suspended-load transport *qθs*:

$$q\theta = q\theta\theta + q\theta\theta \tag{6}$$

The bed load transport rate *qθb* is computed by Eq. [7]

$$q\theta\theta = \begin{cases} 0.053\sqrt{\Delta g D_{50}^{3}}\, D_*^{-0.3}\left(\dfrac{\mu_c \tau - \tau_c}{\tau_c}\right)^{2.1} & \text{if}\left(\dfrac{\mu_c \tau - \tau_c}{\tau_c}\right) < 3.0 \\ 0.1\sqrt{\Delta g D_{50}^{3}}\, D_*^{-0.3}\left(\dfrac{\mu_c \tau - \tau_c}{\tau_c}\right)^{1.5} & \text{if}\left(\dfrac{\mu_c \tau - \tau_c}{\tau_c}\right) \geq 3.0 \end{cases} \tag{7}$$

The dimensionless particle parameter D* is estimated by

$$D_* = D_{50}(\Delta\Delta g/^{2}) \tag{8}$$

where ν is the dynamic viscosity (m^2/s), τ_c = critical bed shear stress, τ = bed shear stress and μ_c is defined by

$$C_{d_{90}} : \mu_c = (C/C_{d_{90}})^2 \tag{9}$$

where, C_{d90} is grain-related bed roughness.

The suspended-load transport *q θs* is defined by

$$q\theta\theta = f_s U d C_a \tag{10}$$

In which
f_s = shape factor for the vertical distribution of suspended sediment
Ca = reference concentration (VanRijn, 1984)

After each time step Δt, the bed level is updated using the modified form of Exner (1925) equation for mass conservation of sediment:

$$\Delta\eta_b \big/ \Delta t = MF\left(\frac{\Delta q_x}{\Delta x} + \frac{\Delta q_y}{\Delta y}\right) \tag{11}$$

Here, MF = Morphological acceleration factor, which reduces the computational time, $\Delta\eta_b$ is change in bed level, Δq_x and Δq_y are changes in the direction deviation of sediment transport from the bed shear stress direction due to the bed slope effect, and q_x and q_y are calculated using the following equations

$$q_x = q\theta\theta(\cos_T - f(\theta(\frac{\partial \eta_b}{\partial x}) \quad [12]$$

$$q_y = q\theta\theta(\sin_T - f(\theta(\frac{\partial \eta_b}{\partial y} \quad [13]$$

$$f(\theta(= \frac{1}{\varepsilon\theta^{\beta}} \quad [14]$$

Here, θ is the shield mobility parameter, ε and β are the calibration parameters and ϕ_τ is the angle between the flow direction and sediment transport vector and is determined by

$$\tan(\varphi_t) = \frac{v}{u} - A\frac{d}{R} \quad [15]$$

where

$$A = \frac{2}{\kappa^2}\left(1 - \frac{\sqrt{g}}{\kappa C}\right) \quad [16]$$

where κ is the Von Karman constant.

3 RESULTS

3.1 Switching of channel

The changes of discharge ratio, r_q between the branch b to c are shown in Figure 3a. This figure indicates that in case of base condition and case 2, no bifurcation switch occurred but during case 1 and case 3 switching happened. The minimum value of r_q was 0.64 which happened in case 3 and the maximum value of 1.79 occurred in case 1. In response to unsteady flow during the peak time, the discharge ratio decreased in all cases but with the decrease of total discharge, this ratio increased.

Figure 3(b) shows the final bed elevation of different cases. This figure indicated that in case 1 and case 3, the changes of planform were higher (more channels were visible) compared to case 2 and base condition. Though the channel width of branch c (right branch) did not vary (average width was 362.83m) largely, but during case 1 and case 3, channel deepening occurred. The lowest elevation happened in case 3 and the value was -1.19m PWD; about 1.25 times lower than the initial value of 3.86m PWD.

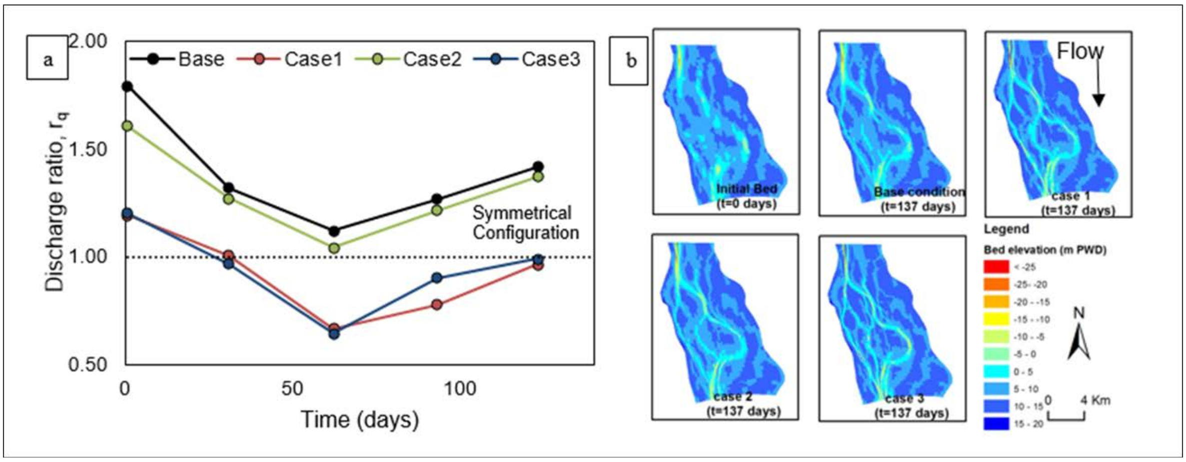

Figure 3. (a) Changes of discharge ratio, r_q over time (b) Final bed elevation of the considered cases.

3.2 Relation between bifurcation switch and upstream channel geometry and hydraulic condition

The relationship between the upstream channel geometry change and the bifurcation switching phenomenon is shown in Figures 4, 5 and 6. In all cases, the upstream channel aspect ratio changed from 27.54 to 50.54. The switching showed a relatively small value of aspect ratio (here was 27.56). This figure also indicated that once switching had happened, the r_q tended to be stable even with high aspect ratio.

Bed share stress is an indicator to predict the morphological evolution of the channel. Figure 5 shows the bed share stress at the day of peak flow and this figure indicated that during case 1 and 3, bed share stress was higher in the right branch (the values were 7.34N/m^2 and 10.11N/m^2 in case 1 and 3, respectively). The relationship between shield stress and discharge ratio is shown in Figure 6. In this particular case, the value of shields stress varied from 0.07 to 0.63 with an average value of 0.22. It indicated that the higher the asymmetry in the discharge ratio was, the lower the value of shields stress. This figure clearly showed the distinction between switching and non-switching bifurcations. It showed switching happened only when the shield stress in the upstream channel was higher than 0.2.

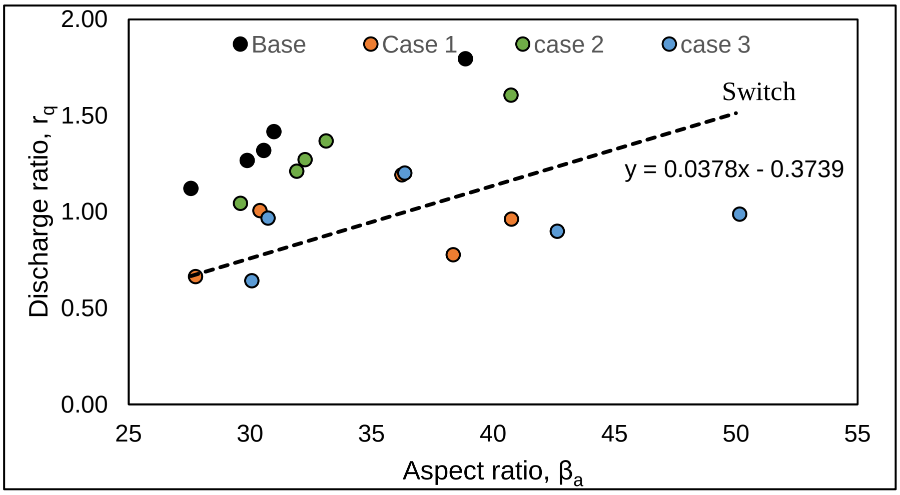

Figure 4. Changes of Discharge ratio, r_q with upstream channel aspect ratio, β_a.

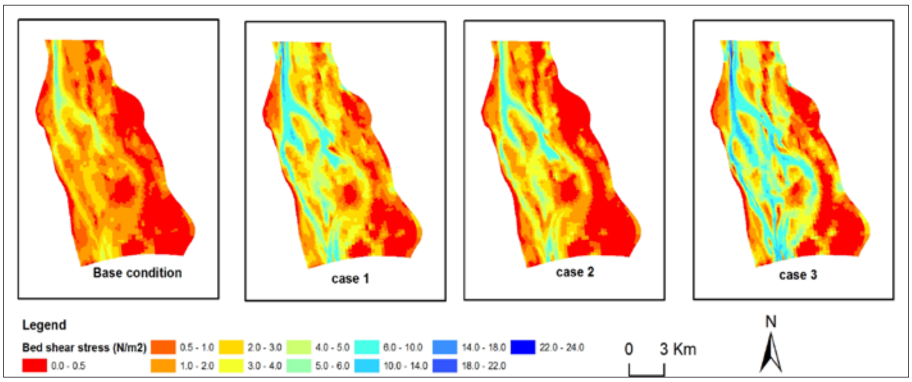

Figure 5. Bed share stress of the considered cases at peak flow.

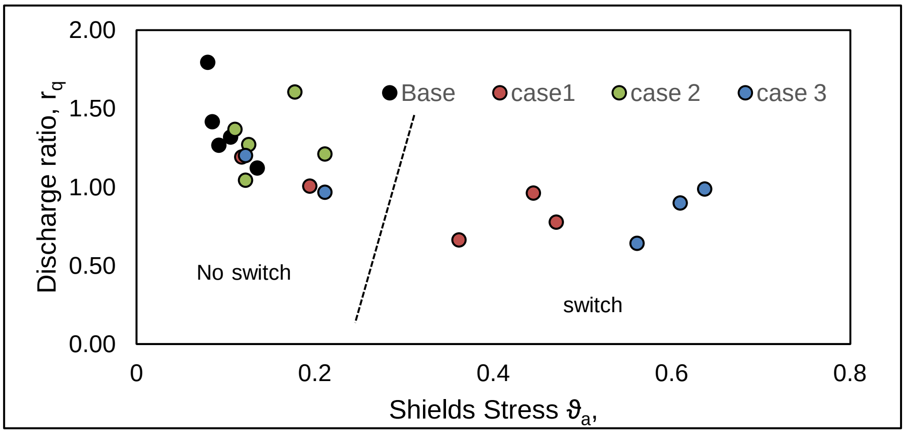

Figure 6. Change of discharge ratio with the change of upstream channel shield stress.

3.3 Bifurcation switch and downstream mid channel bar

The relationship between r_q and angle of bifurcation was estimated from the model results. This relationship is shown in Figure 7(a). This figure indicated that no specific relationship existed between these parameters. Figure 7(b) describes the relationship between r_q and the aspect ratio of downstream midchannel bar. The aspect ratio of bar varied from 1.3 to 3.5 with an average value of 2.4. Though with the increment of aspect ratio of downstream midchannel bar, the r_q tended to decrease but it did not show any particular trend with the switching phenomenon.

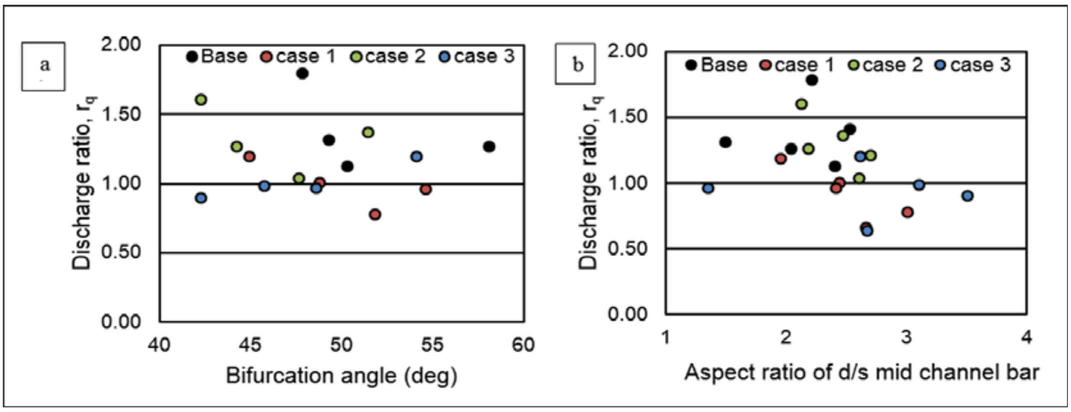

Figure 7. Relationship between (a) r_q and angle of bifurcation (b) r_q and aspect ratio of mid channel bar.

4 DISCUSSION

The numerical simulation is only carried out for one peak period. Morphological update has been accelerated by applying Morphological acceleration factor. But in reality such change may take several years to happen or it can even happen quicker than that of the simulation. In this research, four cases were considered. Assuming one as the base condition, the upstream and downstream boundaries have been changed to assess the response of the process.

The general observation is that the configuration of bifurcation is normally asymmetrical in all cases. Upstream control plays the major role in the switching phenomenon of the channel (Figures 3, 4 and 6) as the switch happens only in case 1 and case 3 when the discharge is higher.

Based on laboratory experiments, Bertoldi and Tubino (2007) found that the higher the aspect ratio of upstream channel, the higher the asymmetry is. However, in this study,this statement is found to be valid up to a threshold near the symmetrical configuration; after that switching happens (Figure 4).The unbalance is higher in very low shields stress which is in agreement to the the lab findings of Federici and Paola (2003); Bertoldi and Tubino (2007) but after switching; the discharge ratio becomes stable even if the shields increase further in the upstream channel (Figure 6).

There is no specific relationship observed between the bifurcation angle and switching phenomenon or discharge asymmetry (Figure 7a). But Fedrerici and Simenara (2003) and Van der Mark and Moselman (2013) indicated that there may be an acceptable relationship between these two. Downstream mid channel bar aspect ratio is not directly related to the switching phenomenon (Figure 7b) but there exists a correlation with the upstream channel aspect ratio and downstream channel mid channel bar (Figure 8).

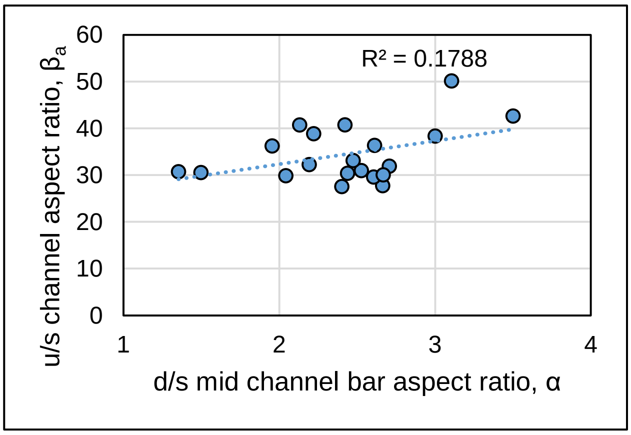

Figure 8. Relation between u/s channel aspect ratio and d/s mid channel bar aspect ratio.

5 CONCLUSIONS

Bifurcation switching/ abandonment is a very basic mechanism in the development process of compound bars of the braided river. Through this research, the bifurcation switching phenomenon is investigated using unsteady flow condition and natural river bathymetry of a large sand bed braided, Brahmaputra-Jamuna. Previous researches emphasized the condition of symmetrical configuration of bifurcation, while this study investigates factors that make the bifurcation more unstable and eventually one big bifurcate shifts to another. Based on the simulations and analyses, the following conclusions can be drawn:

- In case of bifurcation switching, upstream control (discharge) has more effect compared to the downstream control (water level);

- Unbalance in discharge is higher is case of high aspect ratio of upstream channel. It lowers down as it approaches to symmetrical configuration. But as it reaches its threshold, switching happens;
- At lower shields stress, higher asymmetry of discharge distribution is observed. Towards the symmetrical configuration, shields stress becomes higher. After the switch, discharge ratio becomes stable with the fluctuation of shields stress;
- This research demonstrates that there may not be any plausible relationship between bifurcation angle and the switching phenomenon;
- The dimension of the downstream mid channel bar influences the switching phenomenon by affecting the upstream channel aspect ratio and not directly influencing the discharge distribution.

ACKNOWLEDGEMENTS

The authors would like to acknowledge JST-JICA funded SATREPS project "Research on Disaster Prevention/Mitigation Measures against Floods and Storm Surges in Bangladesh" for funding this research.

REFERENCES

Ashmore, P.E. (1991). How Do Gravel-Bed Rivers Braid? *Canadian Journal of Earth Sciences*, 28(3), 326-341.

Bertoldi, W. & Tubino, M. (2007). River Bifurcations: Experimental Observations on Equilibrium Configurations. *Water Resources Research*, 43(10), 1-10.

Pittaluga, B.M., Repetto, R. & Tubino, M. (2003). Channel Bifurcation in Braided Rivers: Equilibrium Configurations and Stability. *Water Resources Research*, 39(3), 1046.

Bristow, C.S. & Best, J.L. (1993). Braided Rivers: *Perspectives And Problems.* Geological Society, London, Special Publications, 75(1), 1-11.

Exner, F.M. (1925). On The Interaction between Water and Sediment in Rivers. Akad. Wiss. Wien Math. Naturwiss. Klasse, 134(2a), 165-204.

Federici, B. & Paola, C. (2003). Dynamics of Channel Bifurcations in Noncohesive Sediments. *Water Resources Research*, 39(6), 1162.

Federici, B. & Seminara, G. (2003). On the Convective Nature of Bar Instability. *Journal of Fluid Mech*anics, 487, 125–145.

Ferguson, R.I., Ashmore, P.E., Ashworth, P.J., Paola, C. & Prestegaard, K.L. (1992). Measurements in a Braided River Chute and Lobe. 1. Flow Pattern, Sediment Transport Andchannel Change, *Water Resources Re*search, 28(7), 1877–1886.

Klaassen, G.J., Mosselman, E., Masselink, G., Bruhl, H., Huisink, M., Koomen, E., & Seymonsbergen, A.C. (1993). *Planform Changes in Large Braided Sand-Bed Rivers*. Delft Hydraulics.

Kleinhans, M.G., Ferguson, R.I., Lane, S.N. & Hardy, R.J. (2013). Splitting Rivers At Their Seams: Bifurcations And Avulsion. *Earth Surface Processes and Landforms*, 38(1), 47-61.

Kleinhans, M., Jagers, B., Mosselman, E. & Andsloff, K. (2006). Effect of Upstream Meanders on Bifurcation Stability and Sediment Division in 1D, 2D and 3D Models. *River Flow 2006*, 1355-1362.

Miori, S., Repetto, R. & Tubino, M. (2006). A One-Dimensional Model of Bifurcations in Gravel-Bed Channels with Erodible Banks. *Water Resource Research,* 42, 1-12.

Mosley, M.P. (1983). Response of Braided Rivers to Changing Discharge*. Journal of Hydraulics*, NZ, 22(1), 18–67.

Schuurman, F. & Kleinhans, M.G. (2015). Bar Dynamics And Bifurcation Evolution In A Modelled Braided Sand-Bed River. *Earth Surface Processes and Landforms*, 40(10), 1318-1333.

Schuurman, F., Marra, W.A. & Kleinhans, M.G. (2013). Physics-Based Modeling Of Large Braided Sand-Bed Rivers: Bar Pattern Formation, Dynamics and Sensitivity. *Journal of Geophysical Research: Earth Surface*, 118(4), 2509-2527.

Van Rijn, L.C. (1984). Sediment Transport, Part I: Bed Load Transport. *Journal of Hydraulics Engineering,* 110(10), 1431–1456,

Van Rijn, L.C. (1993). *Principles of Sediment Transport in Rivers, Estuaries and Coastal Seas*. 1006. Amsterdam: Aqua Publications.

Van Der Mark C.F. & Mosselman, E. (2013). Effects of Helical Flow in One-Dimensional Modelling Of Sediment Distribution at River Bifurcations. *Earth Surface Processes and Landforms*, 38(5), 502-511.

Wang, Z.B., De Vries, M., Fokkink, R.J., & Langerak, A. (1995). Stability of River Bifurcations in ID Morphodynamic Models. *Journal of Hydraulic Research*, 33(6), 739-750.

RUNOFF SIMULATIONS OF MIXED LAND USE OF SKUDAI WATERSHED: SENSITIVE PARAMETERS

KHAIRUL ANUAR MOHAMAD(1), NOORBAHARIM HASHIM(2) & ILYA KHAIRANIS OTHMAN(3)

(1)National Hydraulic Research Institute of Malaysia (NAHRIM), Seri Kembangan, Malaysia,
khairulanuar@nahrim.gov.my
(2) Universiti Teknologi Malaysia, Skudai, Malaysia,
drbaharim@yahoo.com
(3) Universiti Teknologi Malaysia, Skudai, Malaysia,
ilya@utm.my

ABSTRACT

The Hydrological Simulation Program-Fortran (HSPF) is used to study runoff simulation of mixed land use of Skudai watershed, the heaviest polluted river in the district of Johor, Malaysia. The aim of this study is to examine the sensitivity of HSPF parameters during runoff simulations for upstream of Skudai watershed. The model is calibrated using data from November 2013-February 2014 and validated with observed data from March-May 2012. Different land use types are shown to be sensitive to HSPF parameters especially to the index of the mean infiltration capacity of the soil followed by the fraction of groundwater inflow which will enter deep (inactive) groundwater, the upper zone nominal storage and the lower zone nominal storage. Statistical analysis comprising the coefficient of determination, Nash-Sutcliffe efficiency and the relative error are used as evaluation indicators between simulated and observed runoff. By examining the sensitivity analysis, it has been concluded the index to the mean infiltration capacity of the soil (INFILT) is most sensitive to runoff followed by the fraction of groundwater inflow which will enter deep (inactive) groundwater (DEEPFR), the upper zone nominal storage (UZSN) and the lower zone nominal storage (LZSN). It is found that the coefficient of determination (R^2) for validation is better than calibration with an average 0.88 compared with 0.83 in daily time steps.Based on this study, HSPF is capable of simulating runoff using hourly time-step for mixed land use in Malaysia.

Keywords: HSPF; Skudai Watershed; the coefficient of determination; HSPF parameters; mixed land use.

1 INTRODUCTION

Nowadays, simulation models of watershed hydrology have become one of the principal aspects towards sustainable water resource development, planning, and management. These models are influenced by various factors such as spatial variability of soils, elevation, land use, weather and human activities. With the rapid development in some watersheds, increasing pollution mainly from urban and agricultural lands has deteriorated the water quality in rivers. Hence, simulation models that combine the use of long-term continuous and storm event are needed in order to adequately manage watersheds and address water quantity and quality problems. Hydrological Simulation Program-Fortran (HSPF) is one of few models that combine the long-term continuous and storm event.

Hydrological Simulation Program-Fortran (HSPF) consists of sets of module that allow users to simulate complex and continuous storm events especially from non-point loadings such as agricultural and urban land activities. In order to achieve Best Management Practice (BMP), careful planning and accurate runoff models are needed to maintain agricultural productivity while minimizing adverse water quality effects. Besides, pollutants can be transported by runoff into the surface waters by infiltration (with deep percolation) into the groundwater. To enhance model predictions, suitable watershed models must be carefully selected. HSPF has been widely used due to its capability to execute a continuous and short period simulation of less than a day prior to a flood event while generating excessive changes in river flow and water quality. Soil and Water Assessment Tool (SWAT) offers the same requirement but often used for rural areas that are dominated by agricultural applications. SWAT requires descriptive vegetative changes data and agricultural practices (Neitsch et al. 2002).

HSPF has been widely used for watershed modelling especially in the hydrological simulation. Detailed simulation of 23 watersheds in the Patuxent River estuary found that annual water discharges from the watersheds increased relative to the proportion of developed land (Jordan et al., 2003). Zariello and Ries (2000) evaluated the effects of water withdrawals on flow in the Ipswich River Basins, Massachusetts. Singh (2004) and Diaz et al.(2011) utilized HSPF to simulate detailed hydrologic processes including pollutant fate and transport, as well as climate and land cover variability using water quality simulation models. Jing et al.(2009) used HSPF to improve the assessment of hydrologic activities in shallow ground water settings and Hayashi et al.(2004) simulated runoff and sediment load over a relatively short time interval for Upper

Changjiang river basin in China. As an analytical tool, HSPF model subdivides watershed into smaller, more uniform pervious and impervious land segments based on land use types in the watershed. To develop User Control Input (UCI), Bicknel et al. (1996) had categorized HSPF model data requirement for users. To create UCI file, users must have three sets of data; spatially distributed data, environmental and meteorological monitoring data and point source data. HSPF model uses both daily and hourly meteorological data to generate outputs for continuous simulation. The present study aims to determine the most sensitive parameters associated with runoff simulation for mixed land use in Skudai watershed.

2 MATERIAL AND METHODS

The Skudai Watershed encompasses 29,370 hectares (293.7 km^2) of land area located at southern of Malaysia, in the state of Johor. The characteristics of the study site are summarized in Table 1. The land use in Skudai watershed are dominated by urban and agricultural activities. Figure 1 shows that Skudai River and its tributaries flow from Sedenak in Kluang District and drains into the Johore Straits in Johore Bahru District. Figure 2 shows a variation of land use at the Skudai Watershed in percent. The Skudai River is subjected to seasonal fluctuation with maximum discharges usually occurs around November until March due to heavy rainfall during the North-East Monsoon.

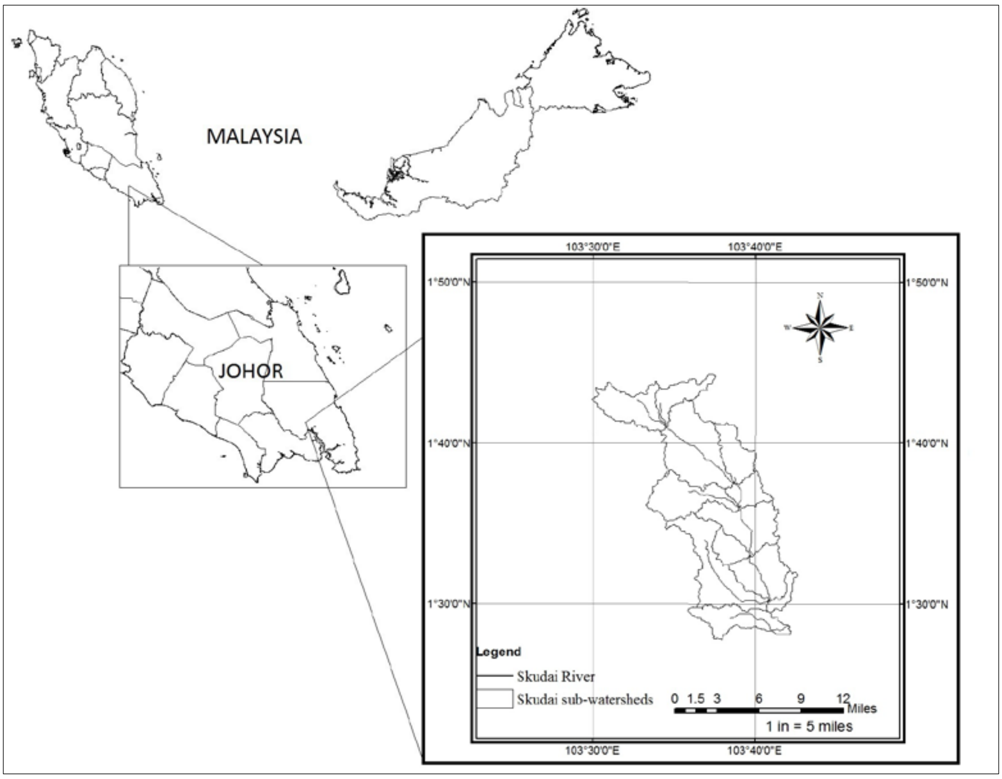

Figure 1. The Skudai river and its tributaries.

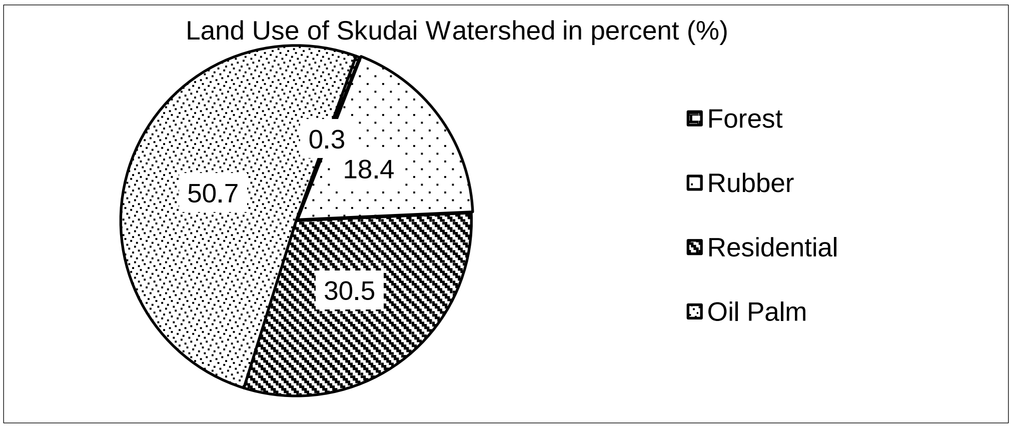

Figure 2. Land Use of Skudai watershed.

Table 1. Characteristics of the study site.

Characteristics	Value
Annual Precipitation 2014 (mm)	2500
Channel Slope	1 : 204
Mean Temperature (^{0}C)	27
Land Elevation (m)	0 to 500 m

Under current usage, Skudai Watershed is divided into pervious and impervious land segments. The impervious land segments consist of forestland (3.83%), agricultural land (39.76%), urban/residential land (52.46%) and barren land (3.96%).

3 THEORY AND CALCULATION

HSPF is a comprehensive water quality model that is able to simulate complex hydrological processes in comparison to the simple method used in Export Coefficient Models. HSPF is designed with three different routines which are Pervious Land Segments (PERLND), Impervious Land Segments (IMPLND) and Reach Segment Operations (RCHRES). In HSPF, PERLND is the module that simulates the water quality and quantity processes which occur on a pervious land segment. The primary module sections in PERLND simulate snow accumulation and melt, water budget, sediment produced by land surface erosion and water quality constituents by various methods. Modules in IMPLND are similar to the PERLND module. However, the IMPLND sections are less complex, since they contain no infiltration function and consequently, no subsurface flows. The operation module used to simulate Channel Reaches (referred to as RCHRES in the HSPF model) contains separate sections of code to simulate hydraulic behavior, pH, temperature and other water quality related processes. HSPF/BASINS used spatial variability of Skudai watershed to divide the basin into many hydrologically homogeneous land segments and simulating runoff for each segment independently. The HSPF needs precipitation, temperature and estimation of potential evapotranspiration input data to perform the hydrologic simulation. Hourly precipitation and temperature input data were collected from Senai International Airport which was 20km from the site location. These data were monitored by the Malaysian Meteorological Department (MMD). Input data for potential evapotranspiration were estimated using maximum and minimum hourly temperature based on Hamon PET equation. These input data were disaggregated into hourly input data since the hydrological simulation was done using hourly time step.

The HSPF model for the Skudai Watershed was calibrated from 5/11/2013 to 5/2/2014 and then validated from1/3/2012 to 15/5/2012. The watershed model was calibrated and validated using river flow data from the Department of Irrigation and Drainage Malaysia (DID) gauge station at Kampung Pertanian, Kulai Johor, and 5km from the site location. The flow data was obtained from rating curve and from Automatic Global (WL16) Water Level Data Logger (Global Water, 2014) at Kampung Pertanian. The Rating Curve for Skudai River was generated by using Automatic Sample Pump ISCO 6712 (Teledyne ISCO, 2012) that collected water level data every week. During high flows, the sample nozzle pump was submerged at the bottom of the river to determine the exact total suspended solids that had been collected. Subsequently, after sufficient data had been collected, linear correlation analysis between flow and total suspended solids were estimated. The statistical analysis of hourly observed and simulated runoff were defined using linear regression (coefficient of determination, R^2), Nash-Sutcliffe efficiency (E_{Ns}) and the relative error (D_v). Nash-Sutcliffe efficiency is given as in Eq. [1].

$$E_{NS} = 1 - \frac{\sum_{i=1}^{N}(O_i - S_i)^2}{\sum_{i=1}^{N}(O_i - O_{Avg})^2} \qquad [1]$$

where N is the number of observations during the simulated period, Oi and Si are the observed and simulated values at each difference point i and O_{Avg} is the mean of the observed values. E_{NS} ranges from negative to infinity, with 1 denotes a perfect agreement with observed data. Nash-Sutcliffe efficiency has been used in many researches to determine model evaluation and considered as one of the best statistics for evaluation of continuous hydrograph simulation programs (ASCE, 1993).The coefficient of determination, denoted as R^2 , is a number that indicates how well data fit a statistical model. It ranges from zero to 1, with 1 is the perfect agreement between simulated and observed data. R^2 is given by Eq. [2].

$$R^2 = \left\{\frac{\sum_{j=1}^{n}(O_j - \bar{O})(S_j - \bar{S})}{\left[\sum_{j=1}^{n}(O_j - \bar{O})^2\right]^{0.5}\left[\sum_{j=1}^{n}(S_j - \bar{S})^2\right]^{0.5}}\right\}^2 \qquad [2]$$

Where O_j is the observed flow at time step j, $\overline{O}$ is the average observed flow during the simulation period, S_j is the model-simulated flow at time step j and $\bar{S}$ is the average simulated flow at time step j.
The relative error (D_v) is calculated as:

$$D_v(\%) = \frac{X_m - X_s}{X_m} \times 100 \qquad [3]$$

Where X_m is the observed total runoff volume and X_s is the model-simulated total runoff. Smaller number of D_v gives better result for simulation and observation data. For a perfect model, D_v would be equal to zero.

4 RESULTS

The HSPF uses several parameters to select sensitivity analysis for hydrologic simulation which can be defined in EPA BASINS Technical Note 6 (USEPA, 2000). The time step of simulation used was 1 hour and was carried out within less than 3 months. Modelled parameters affect both water balance and flow by distributing capacity of water between surface runoff, interflow, baseflow and deep groundwater. Table 2 summarizes the final values of hydrologic pervious land parameters and Table 3 summarizes values of hydrologic impervious land parameters that were adjusted during calibration and validation process. These values fall within the range of values as stated at the typical range below.

Table 2. Parameter values for hydrologic simulation for the Skudai river watershed (Pervious Land).

	Parameter	Calibrated Value	Typical Range
LZSN	The lower zone nominal storage	6.2	3.0-8.0
INFILT	The index to the mean infiltration capacity of the soil	0.24	0.01-0.25
LSUR	The length of the assumed overland flow plane	600	200-500
SLSUR	The slope of the overland flow plane	0.078-0.09	0.01-0.15
KVARY	The parameter which affects the behavior of groundwater recession flow	1	0.0-3.0
AGWRC	The basic groundwater recession rate if KVARY is zero and there is no inflow to groundwater	0.93-0.99	0.92-0.99
INFEXP	The exponent in the infiltration equation	2	2
INFILD	The ratio between the maximum and mean infiltration capacities over the pervious land segments	2	2
DEEPFR	The fraction of groundwater inflow which will enter deep (inactive) groundwater	0.2	0.0-0.2
BASETP	The fraction of remaining potential E-T	0.05	0.0-0.05
AGWETP	The fraction of remaining potential E-T	0.05	0.0-0.05
CEPSC	The interception storage capacity	0.25	0.03-0.2
UZSN	The upper zone nominal storage	0.55	0.1-1.0
NSUR	The Manning's n for the overland flow plane	0.33	0.15-0.35
INTFW	The interflow inflow parameter	3	1.0-3.0
IRC	The interflow recession parameter	0.5	0.3-0.85
LZETP	The lower zone E-T parameter	0.5	0.5-0.7
CEPS	The initial interception storage	4	0.0-100.0
SURS	The initial surface (overland flow) storage	5	0.0-100.0
UZS	The initial upper zone storage	0.1	0.0-100.0
IFWS	The initial interflow storage	0.01	0.0-100.0
LZS	The initial lower zone storage	1	0.0-100.0
AGWS	The initial active groundwater storage	0.01	0.0-100.0
GWVS	The initial index to groundwater slope	0.01	0.0-100.0
LSUR*	The length of the assumed overland flow plane*	250	50.0-250.0
SLSUR*	The slope of the assumed overland flow plane*	0.001	0.001-0.15
NSUR*	The Manning's n for the overland flow plane*	0.15	0.01-0.15
RETSC*	The retention (interception) storage capacity of the surface*	0.13	0.01-0.3

Note: *Parameter values of hydrologic simulation for Impervious Land

5 DISCUSSIONS

5.1 Sensitivity Analysis

The sensitivity analysis was carried out by comparing monthly observed and simulated flow. The most sensitive factors governing simulated river flow for Skudai river were LZSN, UZSN, DEEPFR and INFILT. These indicate that base flow component is very significant for the river flow. LZSN have a major effect in the routing of the flow in Skudai river and frequently adjusted when calibrating HSPF. In the present study, after the initial calibration, LZSN was set at 0.16 m and held constant for all land uses. The upper zone nominal storage UZSN, a user specified parameter was set according to EPA BASINS Technical Note 6 (USEPA, 2000). Donigian et al. (1978) assumed UZSN as 0.06 of LZSN for steep slopes, limited vegetation, low depression storage; 0.08 of LZSN for moderate slopes, moderate vegetation, and moderate depression storage; 0.14 of LZSN for heavy vegetal or forest cover, soils subject to cracking, high depression storage and very mild slopes and final value was set to be 0.55 inch. For Skudai Watershed, 0.08 of LZSN was used since it had a moderate slope (0.5%) and moderate vegetation and depression storage. Since surface runoff and base flow indicated the direct contribution of water quality simulation, the fraction of groundwater inflow DEEPFR was set at 0.2 to ensure model stability. For the mean soil infiltration rate parameter, INFILT possible value was set to be 0.24 in/hr and may decrease to produce more upper zone and interflow storage water. The excessive value of INFILT can lead to a greater overland flow and interflow in Skudai river. To have a better picture of these four parameters sensitivity, Table 4 summarizes the detailed analysis of this assessment.

Table 4. Parameters sensitivity analysis for Skudai river.

Parameters		Runoff in (%)
INFILT (inch/hr)	Increased 0.05	Increased 6.78
DEEPFR (inch)	Increased 0.1	Decreased 14.96
UZSN (inch)	Increased 0.3	Decreased 20.52
LZSN (inch)	Decreased 1.0	Increased 5.94

Based on the sensitivity analysis performed, it is concluded that runoff volume is highly sensitive to INFILT compared to DEEPFR, UZSN and LZSN. High INFILT causes less water to flow out as runoff and low DEEPFR increases runoff, resulting in reduced fraction of groundwater inflow.

5.2 Model calibration

Calibration of the model was conducted between simulated and observed flow monitoring data from Kampung Pertanian station. During the calibration process, each of parameter was adjusted to match the observed and simulated flows. Initial value parameters were adjusted one by one within typical range and keeping others constant. The simulated output values were then compared with the initial values to check its sensitivity with total runoff volumes. A time-series plot of the observed and simulated hourly flows (cfs) in Figure 3 showed simulated monthly yields generally was within 10.09% of recorded values, although there were some imbalances between the first and third months.

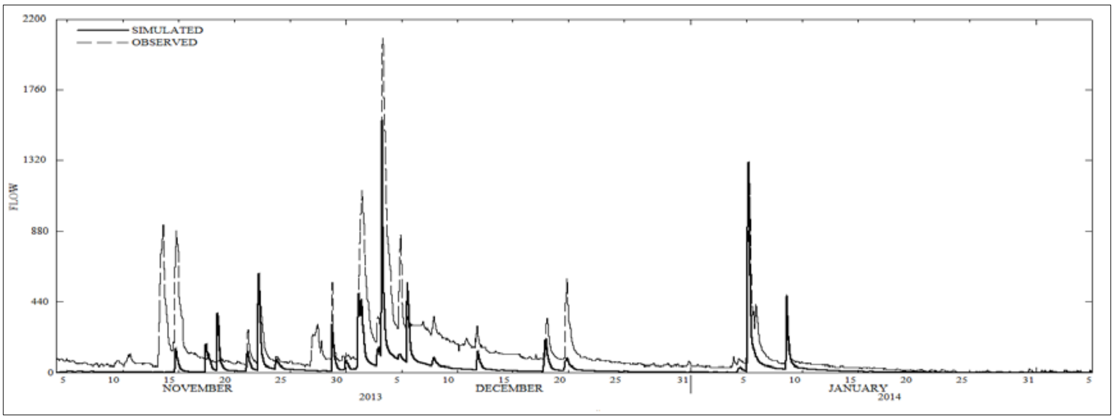

Figure 3. Observed and calibrated hourly streamflow at Kampung Pertanian, Kulai.

As shown in Table 5, simulated runoff volumes of November are consistently underestimated compared to observed runoff volumes likely attributed to low rainfall at Kampung Pertanian gauging station. The coefficient of determination (R^2) indicated that the model gave almost 74% of total variability in the observed data at an hourly level which was considered as fair. At the daily level, the model correlated well with a coefficient of determination of 83%. NS values for calibration were 0.3 for hourly and 0.26 for the daily interval. Comparison from the observed river flow data at Kampung Pertanian suggests that HSPF underestimates hourly and daily flows by 77% (relative error). It can be seen that the error in Table 6 may also be attributed to less detailed hydrological survey at this area (Tetratech, 2009).

Table 5. Observed and simulated hourly flow and percentages.

Month	Observed (Acre-ft)	Simulated (Acre-ft)	Percentage (%)
November	10463.42	4863	-115.16
December	8093.69	10700	24.36
January	65.55	5149	98.73
Total	18622.66	20712	10.09

Table 6. Summary of HSPF statistical analysis model results for calibration period.

Statistical	Hourly	Daily
R^2	0.74	0.83
E_{NS}	0.3	0.26
Relative Error (%)	76.82	77.09

5.3 Model validation

The calibrated HSPF model was validated from March 2012 to April 2012 and the idea behind the selection of these time periods for validation was to test during lower rainfall months. The results of model validation for hourly runoff are presented in Figure 4. Although these periods were relatively wet as compared to the calibration period, the simulated runoff volume showed a moderate response when attained close to observed runoff pattern. However, the model underestimates runoff in the initial phase owing to drier soil and more infiltration but the model response changes during April when continuous rainfall is recorded. During April, the validated runoff values match well with those observed and this could be attributed to unpredictable rainfall recorded in Kampung Pertanian gauging station. The observed and simulated runoff volumes (cfs) for validation are summarized in Table 7. The differences between observed and simulated runoff in both months may be due to the location of rainfall gauge at Kampung Pertanian. In general, R^2 and Ns values are fair for hourly intervals and good to very good for daily intervals as described in Table 8. The statistical test showed R^2 of 0.83 and 0.88 for hourly and daily, respectively whereas NS values indicated 0.63 and 0.61 for hourly and daily, respectively.

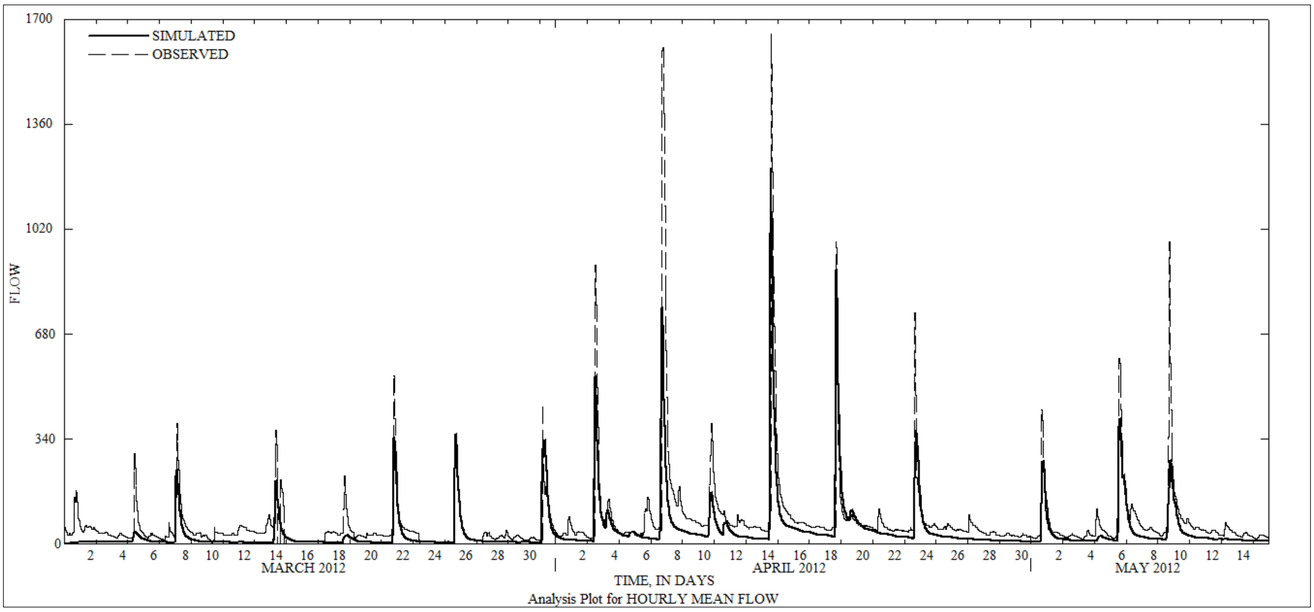

Figure 4. Observed and validated hourly streamflow at Kampung Pertanian, Kulai.

Table 7. Observed and simulated hourly streamflow and percentages.

Month	Observed (Acre-ft)	Simulated (Acre-ft)	Percentage (%)
March	2432.81	4870	50.04
April	5990	13510	55.66
Total	8422.81	18380	54.17

Table 8. Summary of HSPF statistical analysis model results for validation period.

Statistical	Hourly	Daily
R^2	0.83	0.88
E_{NS}	0.63	0.61
Relative Error (%)	28.03	29.98

6 CONCLUSIONS

The HSPF model predictions compare fairly close to observed measurements during wet and dry months and produce a working best-fit set of model parameters within acceptable ranges given from EPA technical note for runoff simulation. By examining the sensitivity analysis, it has been concluded that INFILT is the most sensitive to runoff followed by DEEPFR, UZSN and LZSN. Approximation sensitivity parameters from this study would be used in future applications of the model under similar types of watershed studies. The study demonstrates that the HSPF model is capable of evaluating hydrology processes in the tropical region of Malaysia on an hourly time basis.

ACKNOWLEDGEMENTS

The authors would like to acknowledge the technicians and support groups from the Faculty of Civil Engineering, Universiti Teknologi Malaysia for their support and co-operation and Dr.Noor Baharim Hashim for his research grant.

REFERENCES

ASCE (1993). Criteria for Evaluation of Watershed Models. *Journal of Irrigation Drainage Engineering,* 119(3), 429-442.

Bicknell, B. R., Imhoff, J. C., Kittle, J. L., Jr., Donigian, A. S., Jr. & Johanson, R.C. (1996*).“Hydrological Simulation Program - Fortran User's Manual for Release 11,”* Environmental Research Laboratory, Office of Research and Development, U.S. Environmental Protection Agency, Athens, GA.

Diaz, R. J., McAnally, W. H. & Martin,J. L. (2011). Analysis of Hydrological Processes Applying the HSPF Model in Selected Watersheds in Alabama, Mississippi, and Puerto Rico. *American Society of Agricultural and Biological Engineers*, 27(6), 937 - 954.

Donigian, A.S.Jr. & Davis, H.H.Jr. (1978). *User's Manual for Agricultural Runoff Management (ARM) Model*, U.S. Environmental Protection Agency, EPA 600/3.78.080.

Global Water. (2014). A xylem brand. Retrieved 19 May 2011, from *http://www.globalw.com/downloads/WL16/WL16B.pdf.*

Hayashi, S., Murakami, S., Watanabe, M. & Bao, H.X. (2004). HSPF Simulation of Runoff and Sediment Loads in the Upper Changjiang River Basin, China. *Journal of Environment Engineering*, 130(7), 801–815.

Jing,Z., Ross, M.A., Trout, K. & Zhou, D.M. (2009). Calibration of the HSPF Model with a New Coupled FTABLE Generation Method. *Progress in Natural Science,* 19, 1747-1755.

Jordan, T.E., Weller, D.E. & Correll, D.L. (2003). Sources of Nutrient Inputs to the Patuxent River Estuary. *Estuaries,* 26(2a), 226–243.

Neitsch, S.L., Arnold, J.G., Kiniry, J.R., Williams, J.R. & King, K.W. (2002). Soil and Water Assessment Tool Theoretical Documentation, Version 2000. Available at *http://www.brc.tamus.edu/swat/downloads/doc/swat2000theory.pdf*.Accessed in May 2005.

Singh, J. (2004). Hydrologic Modeling of a Large Agricultural Watershed in Illinois using BASINS-HSPF. Critical Transitions in Water and Environmental Resources Management. *World Water and Environmental Resources Congress 2004*, 1-9.

Teledyne ISCO (2012). ISCO 6712 Full-Size Portable Sampler. Retrieved 20 August 2012, from *http://www.isco.com/WebProductFiles/Product_Literature/201/Portable_Samplers/FullSize_Portable_Samplers/6712_Fullsize_Portable_Sampler.pdf.*

Tetratech. (2009). *Baseline Model Calibration and Validation Report: Ventura River Watershed Hydrology Model,* Ventura County Watershed Protection District Ventura, 187.

USEPA (2000). *BASINS Technical Note 6: Estimating Hydrology and Hydraulic Parameters for HSPF*, EPA-823-R00-012. Washington D.C, U.S. EPA, Office of Water.

Zariello, P.J. & Ries, K.G. (2000). *A Precipitation-Runoff Model for Analysis of the Effects of Water Withdrawals on Streamflow, Ipswich River Basin, Massachusetts*, U.S. Geological Survey Water-Resources Investigation Report 00-4029, Massachusetts.

DRIVING FORCE ANALYSIS OF FISH COMMUNITIES AND HABITATS EVOLUTION IN THE LOWER YELLOW RIVER

MIAO WU(1), ANG CHEN(2), PENGYUAN WANG(3) & CHEN SHEN(4)

(1) College of Hydrology and Water Resources, Hohai University, Nanjing, China
3water@hhu.edu.cn
(2, 3) Institute of Hydropower and Environment Research, China Three Gorges Corporation, Beijing, China
chen_ang@ctg.com.cn; wang_pengyuan@ctg.com.cn
(2, 4)School of Civil Engineering, Tsinghua University, Beijing, China
chen_ang@ctg.com.cn; schristiana@126.com; chen_ang@ctg.com.cn

ABSTRACT

This paper presents a detailed study on fish survey and habitat assessment, which focuses on driving force of fish community and fish habitats evolution in the downstream of Xiaolangdi Dam. Firstly, six typical hydrological stations are chosen as fish survey sections and two fish resources reserved sites as important fish habitats. Four times survey has been finished. Secondly, both fish species and their abundance are compared with survey results in the past, and fish habitats parameters in the two important habitats are analyzed. Not only fish community and habitats in the past, but also differences before and after water-sediment regulation are compared. Thirdly, driving forces are analyzed based on hydrological alteration analysis. Five groups of IHA parameters are used to compare different hydrological regimes. Relationship between water-sediment regulation and downstream fish community and habitats are discussed. Finally, driving forces of fish community and habitats evolution are analyzed, and the results reveal that: (1) fish species and resources decrease heavily compared to those in 1980s, flow and sediment significantly decrease in the last sixty years, and flow recovers after Xiaolangdi Dam operation, (2) downstream fishes decrease in water-sediment regulation period which probably affected by the high velocity flow and decreased DO, but fish resources recover in 15~30 days after regulation, (3) hydrological alteration might be the driving force of aquatic ecosystem in the lower Yellow River, habitats do not suit the fishes because the flow and sediment increase, while DO decrease in the regulation period, but it is still under discussion whether fish habitats inundation and erosion which would lead to death of eggs, juvenile fishes and even adult fishes are resulted from water-sediment regulation (4) long-term aquatic monitoring is needed for establishing the relationship between hydrological alteration and fish community and habitats, and more reasonable operation mode should be proposed to consider more on downstream aquatic ecosystem.

Keywords: Driving forc; xiaolangdi; water-sediment regulation; the Yellow River; fish habitat.

1 INTRODUCTION

Hydropower development is rapidly increasing in the last ten decades in China, and impacts on the downstream aquatic ecosystem are not fully assessed due to the lack of aquatic monitoring data and some of the influences do not appear until after several years of operation. Though the post project environment impact assessment was an effective method for hydropower projects, the regulation was carried out in the late 2015 (Chen et al., 2014; Chen et al., 2014). Flow regimes have become a fundamental part of ecological informatics to reveal the complex interactional mechanism lying between flow regimes and ecological system (Yang, Yan and Liu, 2012). Runoff and sediment load in the lower Yellow River display a gradually decreasing trend over the past 60 years (Liu et al., 2012; Peng, Chen and Dong, 2010). Due to the construction and operation of the dams, the migration fishes were threatened in large rivers like the Yangzte River and the Yellow River in China (Yi, Yang and Zhang, 2010). The flow restoration methods have been used to calculate environmental flow for fish in the lower Yellow River, and the Yellow River Conservancy Commission (YRCC) has also finished environmental flow research of the Yellow River for multiple targets, not only for the fish protection, but also for maintaining water quality, birds, wetlands, etc. (Jiang, Angela and Liu, 2009; Liu et al., 2008). With fish species being protected targets in the Yellow River and one of the many sensitive indices, impacts of dam operation on downstream fish communities and habitats became one of the most critical problems. Suitable flow regimes were the key driven force for maintaining the ecological integrity in the lower Yellow River, especially for maintaining the connectivity of fish habitats. The hydrologic regime has been improved effectively due to the integrated water regulation and water-sediment regulation, but the flood pulse process disappeared and the hydrologic process became flat. The hydrological processes are incapable of meeting the ecological flows and short of the flow pulsing for fish reproduction during April to June (Zhang et al., 2013). Because of the sediment in the river, the amount of fish species in the lower Yellow River was low. Through calculating the key index number of the various species, researchers found that the hair tail, Yellow

River carp and piebald carp were the key species of aquatic ecosystem of the main Yellow River (Jiang et al., 2005). Three indices which contained the environmental flow, water quality and aquatic environment were proposed to protect the representative fishes, but the indices were still relatively sketchy. In order to quantify the impacts of Xiaolangdi Dam on the Yellow River carp, the habitat and flow requirements were estimated through River 2D hydraulic model (Jiang, Zhao and Zhang, 2010). Therefore, it is meaningful to analyze the impact of Xiaolangdi Dam operation and water-sediment regulation on the downstream fish communities, and distinguish the key indices that affect the fish habitat and life history.

In order to identify the driving force of fish communities and habitats in the lower Yellow River, we took four times fish survey from 2012 to 2013 as comparison with fish resources in 1980s and 2000s, and two times survey in water-sediment regulation period in 2010 and 2011. The Indicators of Hydrological Alterations (IHA) and Range of Variability Approach (RVA) are adapted to optimize the water released strategies which can be helpful to understand the changes of the eco-hydrological status and provide suitable flow regime for fish species. Water depth, flow velocity and DO density of the habitats in water-sediment regulation period are discussed to understand the quality of fish habitat. The goals of this paper are: (1) to analyze the driving force of fish changes over the last three decades, and (2) to analyze the recovery of flow regime and driven force of fish habitat evolution. All of these will be helpful to provide technical support for fish protection and habitat restoration, and provide proper regulation for maintaining the ecosystem health in the lower Yellow River.

2 MATERIALS AND METHODS

2.1 Study area

The study area in this paper was the downstream from Xiaolangdi Dam to the estuary in the lower Yellow River (Figure 1). And we focused on the two important national germplasm resources protection area as fish habitats. One was called the Zhengzhou Yellow River Carp Germplasm Resources Reserve (ZZYRCGRR), and the other one was Lu & Yu Junction Germplasm Resources Reserve (LYJGRR). Xiaolangdi Dam is located on the lower end of the middle reaches of the Yellow River, downstream of the major water and sediment source areas of the basin. Xiaolangdi Dam is a multipurpose project which occupies a critical position in controlling both water and sediment of the Yellow River, and there are no other dam projects in the downstream of Xiaolangdi. At this point, the catchment area is 92.3% of the basin total, runoff is 91.5% of the basin total, and sediment load is 98% of the basin total. Xiaolangdi Reservoir has a total capacity of 12.6×10^9 m^3 and a capacity to trap 7.5×10^9 m^3 of sediment, and the development mission was flood control, ice prevention, sedimentation reduction, irrigation, power generation and comprehensive utilization. After the operation of Xiaolangdi Dam, the two protected area was affected by the direct hydrological alteration and other indirect factors.

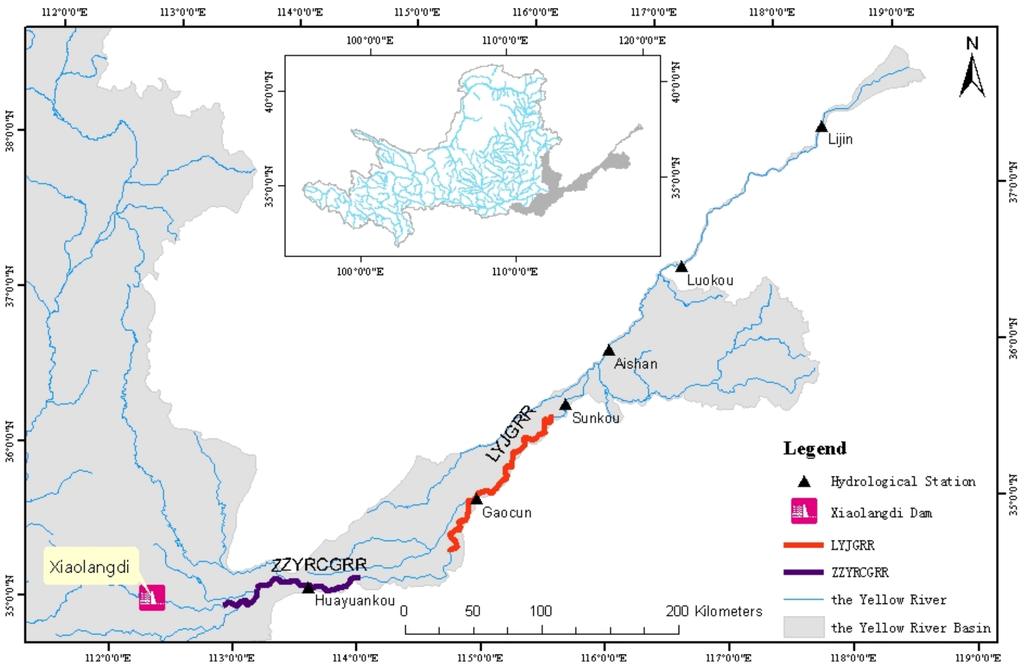

Figure 1. Study sites.

(1) Zhengzhou Yellow River Carp Germplasm Resources Reserve

Zhengzhou Yellow River Carp Germplasm Resources Reserve (ZZYRCGRR) is located 70 kilometers away from the Xiaolangdi Dam which was named by the Ministry of Agriculture China in 2007. The area of

ZZYRCGRR is 24651 hm^2, the latitude and longitude ranges are N34°46′00"~N34°59′54" and E112°56′49"~E114°04′37", respectively. The mainly protected targets are the Yellow River carp and their spawning sites, feeding grounds and wintering grounds. The aquatic and terrestrial ecosystem are also protected and the special protected period of the core region are from April 1st to June 30th.

(2) Lu & Yu Junction Germplasm Resources Reserve

Lu & Yu Junction Germplasm Resources Reserve (LYJGRR) is located at the boundary of Shandong and Henan provinces along the Yellow River which is 120km away from the Xiaolangdi Dam. The area of LYJGRR is 10005.32km^2, the latitude and longitude ranges are N35°00′22″~N35°50′58″ and E114°50′06″~E115°50′54″, respectively. There is a hydrologic station (Gaocun station) in the LYJGRR, and the protected fishes are the Yellow River carp, catfish, Squaliobarbus, culter, snakehead, loach, high phosphorus bream, bream, like eupogon, Trionyx sinensis, etc.

2.2 Fish survey method

In this research, we took two times survey in downstream habitats in water-sediment regulation period in 2010 and 2011, and 4 times fish survey from 2012 to 2013. The survey time was in July 2012, Oct. 2012, Jan. 2013 and May 2013 representing summer, autumn, winter and spring seasons, respectively. And we set 8 survey sections from Xiaolangdi dam to Lijin station (Figure 1). The survey sections from upper stream to downstream were separately (1) below Xiaolangdi Dam (XLD), (2) Luoyang yellow river bridge (LYYRB), (3) Huayuankou station (HYK), (4) Gaocun station (GC), (5) Aishan station (AS), (6) Luokou station (LK), and (7) Lijin station (LJ).

This survey contained several types of contents, including basic aquatic environment condition and fish resources condition. The basic aquatic environment survey concludes the longitude and latitude, the elevation of the sections, the water temperature, transparence, flow velocity, bottom materials, etc. Fish resources survey contained four types of contents including fish fauna, fish resources, fish propagation characteristics and important fish habitats. The fish fauna identification concludes species names, composition and distribution. Fish resources status survey concludes fish population and composition, fish catches statistics and fishery status survey. Fish propagation characteristic survey concludes the seasons, types, time, scale and the environmental condition of spawning. Important fish habitat survey concludes the spawning sites, feeding grounds and wintering grounds survey and the eco-hydrological parameters identification.

Fish sample collection, qualitative and quantitative analysis were based on “Neilu shuiyu yuye ziran ziyuan diaocha shou ce” and “Investigation method for freshwater biological resources” by the Chinese Academy of Sciences (Zheng et al., 2014). The survey was combined with fishing, visiting and data access, and the fishing nets were in different specifications from 1.2cm to 4.5cm with monolayer and three layers. The trapping cages were shrimp cage with the pole length of 1.5m to 2.5m and the fish fry species were surveyed with T type net. After fishing, we took all the by-catch into classification by counting and weighting them. The less injured fishes were chosen as identification specimens. Firstly, we placed them into 10% formaldehyde solution and stewing for 24 hours, and then the specimens were transferred into 4% formaldehyde solution for long time storage and species identification.

3 RESULTS AND DISCUSSION

3.1 Fish community’s evolution

3.1.1 Fish community in history

(1) Fish survey result in 1980s

There was a fishery resources survey conducted in the Yellow River from 1981 to 1982. .There was a total of 18 sections from upstream to downstream, and 15 representative lakes and reservoirs. Fish survey was completed separately according to a distributed plan, and fish sampling and laboratory tests were performed in “Neilu shuiyu yuye ziyuan diaocha gui fan”. Due to high sediment concentration, water transparency of the Yellow River was low, and water transparency was high in non-flood season. Water temperature in the main stream increased gradually from upstream to downstream, while dissolved oxygen saturation was high and the rate changed from 85% to 115%.

According to the survey results, there were 191 kinds of fishes and subspecies in total, which belonged to 15 orders, 32 families and 116 genera. The carps were 87 species accounted for 45.5% of the Yellow River fish; loaches were 27 species accounted for 14.1% of the Yellow River fish, Gobiidae, Salangidae were 15, and the remaining 28 families were limited number of species. There were 125 kinds of fishes and subspecies in the main stream of the Yellow River, which belonged to 13 orders, 24 families and 85 genera. The population was mainly carps totalling 80 species and accounted for 64% of the total fish. There were 136 species comprising mainly of Carps in the lower Yellow River. And fish fauna composition varied widely from 1960 to 1980 with some species such as Dabry’s sturgeon (Acipenser dabryanus) and white sturgeon (Acipenser transmontanus) disappeared. Otherwise, the distribution area of crucian and carp would have expanded. Overall, fish production declined sharply in the 1970s, population structure and composition of fish catches had changed, and catch carps in the proportion general declined. For example, the proportion of captured carps in the 1950s accounted for 50% to 70% of the total production, and the proportion declined to 15% in the 1960s, then further declined to 7.1% in the 1980s. Research results showed that the main reason of fish population reduction was hydrological alteration, water quality deterioration and hydropower projects construction activities. There were ten years cutoff in non-flood season from 1972 to 1981 which resulted in the increase of sediment concentration that led to fish suffocation to death when sediment concentration was higher than 200kg/m^3 (He, 1987).

(2) Fish survey result in 2000s

Based on the survey results conducted by the Institute of the Yellow River Fisheries Research from 2002 to 2008, there were 82 kinds of indigenous fishes in the Yellow River which belonged to 13 orders and 23 families, and there were 48 genus of fish species in the lower Yellow River (Han, 2009). Based on the survey results of Institute of Hydrobiology, Chinese Academy of Sciences during spring (May to June) and autumn (September to November) of 2008, there were 54 fish species which belonged to 7 orders, 13 families and 43 genera and there were four endemic fish species. The composition was mainly Teleostei which accounted for 68.5% of the total. There were 41 fish species in the lower Yellow River, the richest section was in huayuankou which accounted for 31 kinds of fishes (Ru et al., 2010). Part of the caught fish had been found in the historical fish survey, while PseudOlaubuca engraulis had been caught in 2011 in Henan, and Misgurnus mizolepis, oryzias latipe, barracuda, and Mastacembelus aculeatus occurred respectively in 2010 and 2011 in Shandong. Most of the fishes caught were only one, and the population had already reduced drastically. National protected Songjiang perch in the lower reaches and estuary disappeared many years, but it appeared again in Kenli. Although results of this fish survey showed that it still existed in the lower Yellow River, it is difficult to catch it when the population had severe recession.

3.1.2 Current fish survey results

(1) Aquatic conditions in each survey

In the process of fish survey, we recorded the hydrological condition in each survey section. The main flow parameters were flow velocity (*v*), dissolved oxygen (DO) and water temperature (T). The elevation of surveyed sections was also recorded in Table 1. The *Cyprinidae* was 18, 20, 17 and 21 in the four times survey. In July 2012, the survey result was relatively poor because of the water-sediment regulation. In the other three survey periods, the results were all relatively objective with minor influence of regulation.

Table 1. Hydrological condition in different survey period from 2012 to 2013.

Date	Sections Elevation (m)	XLD 123	LYYRB 113	HYK 96	GC 59	AS 37	LK 25	LJ 10
Jul.2012	v (m/s)	1.4	0.3	0.4	0.8	0.5	4.1	1.5
	DO (mg/L)	1.505	3.94	3.3	5.65	5.39	5.65	5.34
	T (℃)	26.1	25.8	25.8	28.2	26.1	27.3	27.4
	TD(cm)	12	8	2	1.5	1.5	1	1.5
Oct.2012	v (m/s)	0.6	0.3	0.3	0.4	0.6	0.5	0.4
	DO (mg/L)	6.77	8.28	7.71	8.76	9.25	8.45	9.28
	T (℃)	19.9	20.3	18.3	16.4	15.8	17.3	16.7
	TD(cm)	250	152	9.2	12.5	8.5	11.5	12
Jan.2013	v (m/s)	0.4	0.35	0.295	0.1	0.2	0.015	0.06
	DO (mg/L)	11.52	11.56	11.73	11.78	11.65	12.01	11.99
	T (℃)	6.2	6.2	4.7	1.2	1.1	0.2	0
	TD(cm)	284	150	10	8	10	8	7
May.2013	v (m/s)	0.44	0.38	0.56	1.13	0.97	1.11	0.92
	DO (mg/L)	10.12	9.64	8.93	8.45	8.24	6.55	5.56
	T (℃)	10.8	11.2	11.1	13.6	15.5	18.5	21
	TD(cm)	245	220	28	17	15	13	14

(2) Fish survey results

From Xiaolangdi Dam to Lijin station, we obtained a total of 38 species which belonged to 5 orders and 10 families. We caught 18, 31, 24 and 27 species in summer, autumn, winter and spring seasons, respectively. The carp family was the main species which accounted for 26 species of them. Compared with the fish survey results in 1960s and 1980s, the percentage of Yellow River carp decreased. In 1960s, the percentage was about 50% to 70%, and it decreased to 20% in the 1980s. In our survey, the percentage decreased to 10%. We not only recorded the species, but also recorded the catch fresh weight and amount of each fish species. The total weight percentage and total amount percentage of each fish species in each season were shown in Figure 2. In July 2012, the total caught fish species was 18, the dominant species was Cyprinus arassius Linnaeus and the caught number was 172. In the following three time survey, the total caught number was 1118, 533 and 1190, respectively.

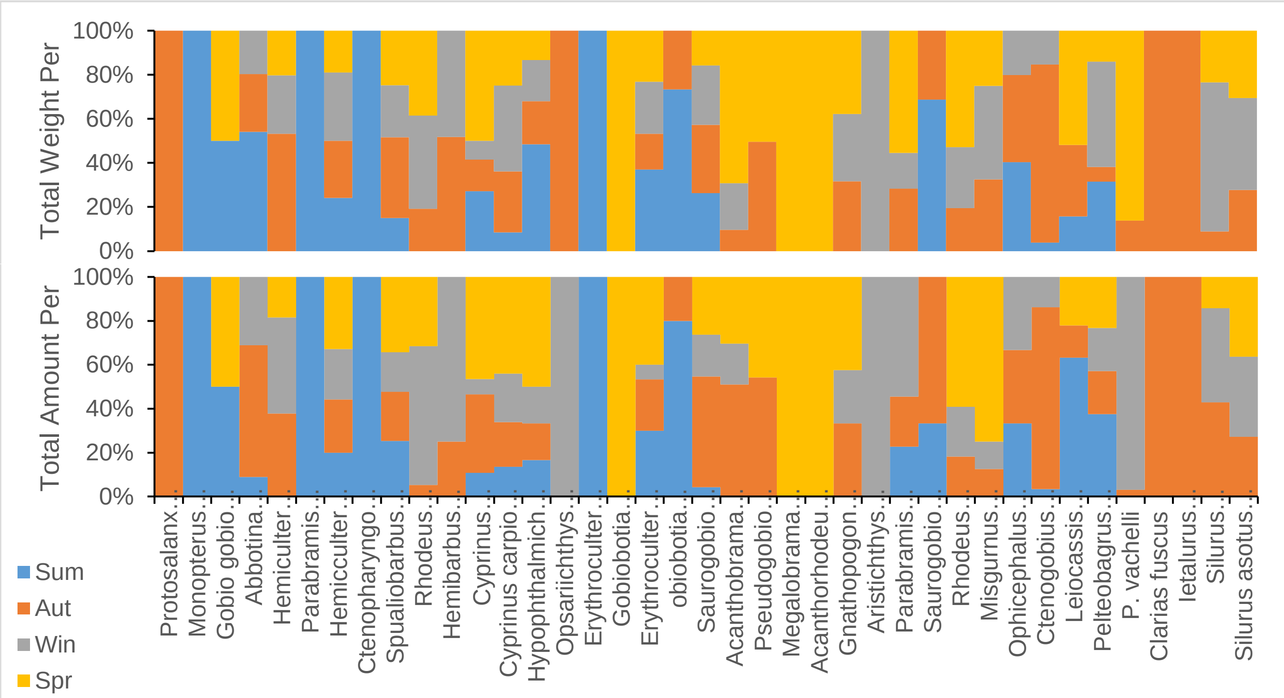

Figure 2. Total weight percentage and total amount percentage of catches in each season.

3.1.3 Comparison of fish communities in different periods

Compared with the survey results in 1980s, there was a reduction of 35 fish species in this survey which belonged to 8 orders and 10 families. The caught fishes were mainly Carps accounted for 62.86%, and local fishermen had reported to catch two black carps in Luoyang in the downstream of Xiaolangdi Dam. The proportion of the catch had greatly changed as the fish species decreased. Representative catches were small fishes such as Pelteobagrus, crucian and gobioninae despite some differences in this survey. The main economic fish production decreased and miniaturized, and the proportion accounted for less than 10%. Compared with fish species composition in 1980s, it had undergone significant changes in fish species composition in the lower Yellow River. Except for the reduced fish species, there were also some increases in new fishery species such as Protosalanx chinensis, pond smelt, clarias leather and channel catfish. Invasion of fish species had a certain impact on the Lower Yellow River fish ecosystem.

3.2 Fish habitat evolution

3.2.1 Water and sediment alteration

According to the main reserved area, we chose HYK and GC as representative hydrological sections. The monthly average flow (MAF) data was divided into four periods to analyze the flow regime alteration (Figure 3).

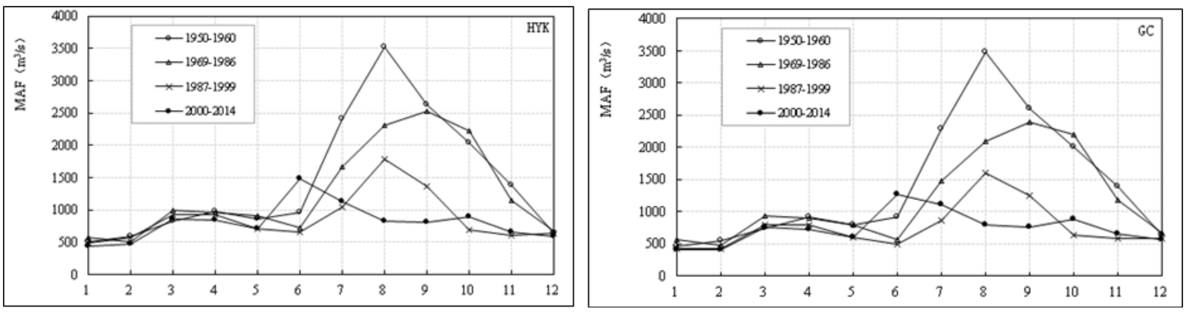

Figure 3. Monthly average flow variation in different period.

According to the sensitive periods in the reserve zones, its spawning period was from April to June, growth period was from July to March in the following year, and water and regulation period was from June to July. Combined with the eco-hydrological response, we analyzed the impacts of flow, flow velocity and water depth variation on Yellow River carp in the two habitats. Flow in GC decreased by 77% and 73% in August and September, respectively as compared with the natural flow. And the flow slightly decreased in July, October and November. From December to March in the following year, the flow was relatively the same with the natural flow. The flow in April and May of 2000~2014 decreased 24% and 44%, respectively compared with 1950~1960 in HYK. But at the same time, the flow in June increased heavily which was nearly 10% compared to the natural flow. We conclude that the flow alteration was mainly due to the water regulation of the cascade reservoirs. For GC station, the flow decreased year by year in April. The decreased percentage was 20% in 2000~2014 compared with 1950~1960, and the natural flow had changed. The flow in May slightly increased, but in June it significantly increased by 7%, which was affected by the water-sediment regulation.

When the construction of Xiaolangdi Dam had completed, the sediment in the flow was relatively lower than before except during the water-sediment regulation period. So, we mainly analyzed the relationship between sediment regulation impacts in this section. The first three years of water and regulation experiment were 2002~2004. We also collected the data in 2010 for comparison (Figure 4). And the period was mainly in July. The maximum sediment concentration was 87.23 kg/m^3 in HYK and 86.36kg/m^3 in GC in 2010.

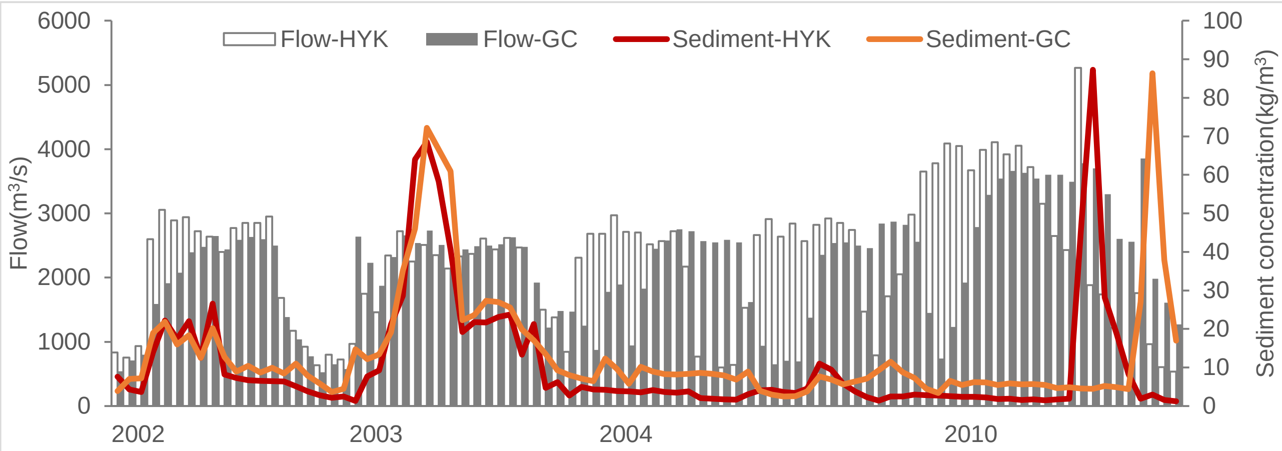

Figure 4. Flow sediment concentration variation in water and regulation period.

3.2.2 Flow velocity and water depth

The flow in the late of spawning period had changed drastically in June, which resulted in variation of flow velocity and water depth. When the water-sediment regulation began, the flow suddenly increased and decreased significantly when the regulation ended. At the same time, the flow velocity and water depth increased as flow increased. The flow velocity and water depth variation had negative effects on the spawning and growth of Yellow River carps by washing out the fish habitats. And the fishes spawning in which the fish that had demersal egg and viscid egg would also be affected.

3.3 Driving force analysis

3.3.1 Driving force of fish communities

The annual average runoff of Xiaolangdi station was shown in Figure 5. The multi-year average volume from 2000 to 2014 was 235.33×10^9m, which was heavily decreased compared with the period from 1950 to 1960. And the average runoff from 1987 to 1999 started to decrease and reached the lowest point in 1997. The multi-year average volume of runoff decreased about 122×$10^9$$m^3$ from the 1950s to 2000s, and decreased about 17×$10^9$$m^3$ from 1990s to 2000s, although the flow began to recover after the operation of Xiaolangdi reservoir.

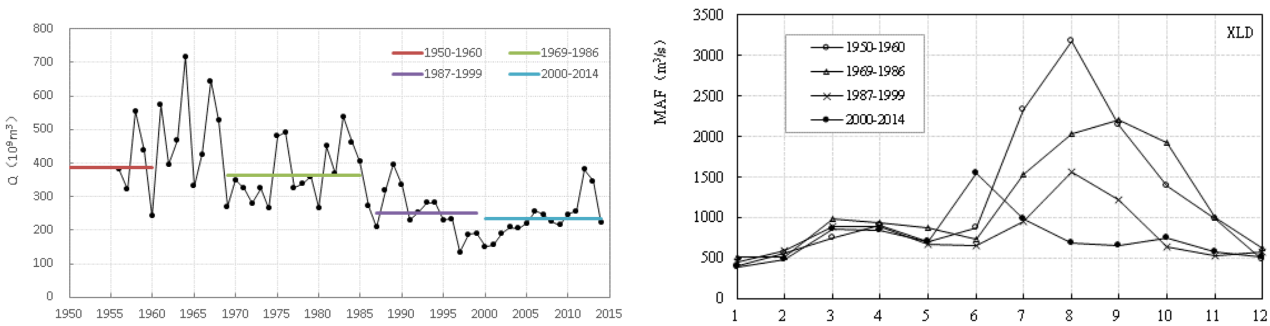

Figure 5. Annual and monthly average flow variation of Xiaolangdi from 1956 to 2011.

  / ISSN 1562-6865 (Online) - ISSN 1063-7710 (Print)

We calculated the monthly average flow variation of Xiaolangdi station from 1956 to 2011. From the figure, we can conclude that the multi-year monthly average flow decreased from the 1950s to 2000s. The percentage of decreased flow from July to September in 2000~2014 were 74% compared with the period 1950~1999. And the flow slightly increased at the end of the flood season because of the cascade operation. The flow almost remained the same from December to March in different period. The monthly average flow changes were less from December to May in the following year. Compared with the period 1987-1999, the flow decreased heavily from July to November. Then, we observed that the monthly flow was mainly reduced in the flood season. After the operation of Xiaolangdi Dam, monthly flow from June to August changed. The maximum flow month changed from August to June due to the impacts of water-sediment regulation. So, we focused on the flow in June to analyze the relationship between the water-sediment regulation and its impacts on downstream fish communities.

We divided the indicators into five groups and compared the daily flow series between the pre-impact and post-impact period using IHA tools. The result showed that Xiaolangdi Dam had significantly changed the natural flow regime downstream. The monthly mean flow in the post-impact period was almost lower than the pre-impact period except in June. The monthly mean flow in June was 1516 m^3/s in post-impact period which was about double than the pre-impact period. The 1, 3, 7, 30, 90 day minimum and maximum flows were decreased than the pre-impact period, and the base flow index increased from 0.172 to 0.2644. The difference was that the date of minimum flow delayed from the 82nd day to 153rd day, and the date of maximum flow shifted from the 228th day to 192nd day. The low and high pulse parameters in group#4 changed much. The low pulse count increased from 1.476 to 8.3 and the low pulse duration decreased from 8.843 to 1.905. Meanwhile, high pulse count decreased from 5.048 to 2.7, but high pulse duration did not change much.

Table 2**.** IHA Parametric RVA Scorecard of Xiaolangdi station.

	Parameters	Pre-impact	Post-impact		Parameters	Pre-impact	Post-impact
Group #1	January	486.7	329	Group #2	1-day minimum	141.1	115.4
	February	535.5	372.8		3-day minimum	166.9	159.4
	March	979.1	689.1		7-day minimum	186.7	183.6
	April	973.4	680.9		30-day minimum	304.4	236.5
	May	898.4	584.8		90-day minimum	598.2	373.6
	June	791.1	1516		1-day maximum	4935	3572
	July	1572	810.1		3-day maximum	4322	3498
	August	2207	591.5		7-day maximum	3791	3386
	September	2142	600.1		30-day maximum	2959	1981
	October	1722	781.2		90-day maximum	2225	1181
	November	1012	593.7		Number of zero days	0	0
	December	655.2	486.2		Base flow index	0.172	0.2644
Group #3	Date of minimum	82	153	Group #4	Low pulse count	1.476	8.3
	Date of maximum	228	192		Low pulse duration	8.843	1.905
Group #5	Rise rate	155.1	159.5		High pulse count	5.048	2.7
	Fall rate	-131.1	-160		High pulse duration	9.574	9.168
	Number of reversals	144.9	218.6				

3.3.2 Driving force of fish habitat

We analyzed the fish species and its abundance variation before and after water-sediment regulation in order to quantize the impacts on fish species (Table 3).

Table 3. Comparison of fish species before and after water-sediment regulation.

Species	WSR in 2010		WSR in 2011		
	Before	After	Before	After 15 days	After 30 days
Cyprinus carpio Linnaeus	1	1	2		
Cyprinusarassius Linnaeus	15		8	5	4
Pelteobagrus fulvidraco	2				4
Hemicculter Leuciclus Basilewaky	142	100	18	6	10
Spualiobarbus Curriculus Richardson	3	1			
Erythroculter ilishaeformis Bleeker	35				
Saurogobio dumerili Bleeker	18		10	5	7
Erythroculter dabryi	65				
Parabramis pekinensis Basilewsky	6				
Acanthobrama imony B1eeker			10	8	8
Pseudorasbora parua Tmminck et Schlegel	1				
Silurus asotus Linnaeus			3	1	1
Pseudolaubuca sinensis			43	54	66

Before WSR in 2010, the species were as many as 10. But it was only 3 species after the regulation. Hemicculter Leuciclus Basilewaky took the absolute advantage of the species, and the proportion were respectively 46% and 98% before and after the regulation. The situation was different in 2011, species before and after the regulation were approximately the same. But the dominant species changed from Hemicculter Leuciclus Basilewaky to Pseudolaubuca sinensis. Although both in 2010 and 2011, fish species mostly decreased after the regulation, fishes recovered to the level before regulation after 30 days for some species. And it had almost recovered to half the level before the regulation for other species like Cyprinusarassius Linnaeus and Saurogobio dumerili Bleeker.

Fish abundance comparison before and after water-sediment regulation was shown in Table 4. As seen from the above analysis, fish species were mainly affected by the flow, sediment and DO in spawning season due to water-sediment regulation. The density of DO was about 5.69~8.15mg/L and 5.59~7.47mg/L before and after water-sediment regulation, respectively. During the regulation, the maximum density was 0.41 mg/L, and had not been detected in ZZYRCGRR which was far below the DO criterion. Since the water-sediment regulation period was relatively short of about half a month, there was no historically monitoring dissolve DO data available in LYJGRR during water-sediment regulation. We chose the water quantity monitoring data in fish survey in 2012~2013 to quantify the impacts. The DO densities were 5.65mg/L, 8.76 mg/L, 11.78mg/L and 8.45mg/L in the four times survey. The minimum DO density was 5.65mg/L in Jul.10th 2012 because the regulation had just finished. As a result, the fish survey amount and weight were both relatively low in this period. In 2010, caught weight of fish abundance decreased from 11780g and 2025g to 5891g and 928g after the regulation. The rates of resources density observed were about 50% and 54% loss in ZZYRCGRR and LYJGRR, respectively. For the two reserved areas, fish recourses were heavily affected in the regulation period. But one month later after the regulation, fish resources began to recover. As shown in 2011, the rate of resources loss reduced from 61 to 47% in LYJGRR, although it was not obvious in ZZYRCGRR. We estimated that fish resources were extremely affected because of the regulation and recovered slowly after the regulation.

Table 4. Comparison of fish abundance before and after water-sediment regulation.

Period		Fish abundance	ZZYRCGRR	LYJGRR
WSR in 2010	Before	Caught weight (g)	11780	2025
		Resources density obversion (kg/km^2)	2552	439
	After	Caught weight (g)	5891	928
		Resources density obversion (kg/km^2)	1276	201
		Rate of resources loss (%)	50	54
WSR in 2011	Before	Caught weight (g)	18838	1246
		Resources density obversion (kg/km^2)	4082	270
	After 15 days	Caught weight (g)	2397.3	485
		Resources density obversion (kg/km^2)	519	105
		Rate of resources loss (%)	87	61
	After 30 days	Caught weight (g)	2877	660
		Resources density obversion (kg/km^2)	623	143
		Rate of resources loss (%)	85	47

Due to Xiaolangdi Dam operation, monthly average flow in July, August and September from the four periods decreased, and the flood pulse in flood season decreased heavily in HYK and GC. From the sediment concentration monitoring data, it was nearly positive correlation between flow and sediment concentration. The main growth season of Yellow River carp was from July to March in the following year, and the spawning period was from April to June. There have been many researches about the biological relationship between sediment concentration and fish species growth. It is undoubted that there are abundant of nutrients carried in sediments. But with the sediments increasing, amount of fishes decreases as sediments increase will result in the DO decrease, and the sediment grain will block fish gills. Results showed that a more than 50% decrease in fish resources presented after water-sediment regulation, and fish population diversities declined sharply. The proportion of main economic fish, such as common carp, crucian carp and catfish, decreased from 87.75% to 81.79% (Qing et al., 2012). There is a direct correlation between DO and sediment concentration in downstream of the reservoir during sediment release period, which means that DO would decrease with the increase of sediment concentration. Most fishes would be dead when DO density decreased below 2mg/L (Baiyin et al., 2012). As recorded, fishes largely died in July 2010 which maybe resulted from high concentrated sediments flow. Both the large individuals like carps, big-head carps and small individuals like silverfish were affected. The totally affected fishes were 11 species which belonged to 5 orders and 5 families. Dead fishes are often found during the period of reservoir sediment flushing. Field surveys in 2010 showed that DO decreased rapidly with the increase in suspended sediment concentration and that dead fishes and the high sediment concentration (average value of 90788 mg/l) and DO reduction (<2 mg/l) contributed to the deaths of fishes (Baiyin et al., 2016). The rapid flowing water with high sediment concentration might be one of the dominant reasons for “flowing fish” during the sediment scouring process (Sun et al., 2012). Sediment deposition with contaminants and water scouring altered the distribution of demersal fishes. While sediment content was lower than 60kg/m^3, by survey and experience, there were no deaths of fish in downstream river reach.

The flow components identified in the unregulated river regime are closely correlated with the known ecological habitat requirements of the Yellow River Carp. The Xiaolangdi Dam operation significantly altered the pattern of flow pulses, small floods and large floods. Elimination or reduction in the frequency of flow pulses compromised the availability of spawning habitat for the Yellow River Carp (Jiang, Zhao and Zhang, 2010). The correlation between fishes and DO had not been established (Li et al., 2015). Although the sediment transport coefficient is a useful index for efficiently guiding the operation of the dams in a way that would minimize channel changes downstream (Ma et al., 2012), it is not an efficient index for assessment the impact on fish habitats. Previous findings showed that there is a direct correlation between DO and sediment concentration downstream of the reservoir during sediment release period, which means that DO would decrease with the increase of sediment concentrations (Baiyin et al., 2012). Compared with previous research results, water-sediment regulation mode including storing the fresh water in none flood seasons and sluicing the muddy water in the flood season was suggested (Chen, Zhou and Han, 2015). The flow and sediment increase, while DO decreases in the downstream. And at the same time, it may result in fish habitats inundation and erosion which would lead to death of eggs, juvenile fishes and even adult fishes. Kong (2015) found that the runoff and sediment load, the sediment grain size, and the river channel of the lower Yellow River have all altered dramatically since the implementation of the regulation (Kong et al., 2015). And flow velocity and water depth were also the key factors which affected the spawning and growth of fishes. The DO and water quality were also affected by the flow alteration. The research showed that the two main factors affecting the fish life are the reduction of oxygen intake function by micro sediment particles clogging the gills and the declination of dissolved oxygen concentration in water (Baiyin and Chen, 2012). The environmental risk of contaminants might increase in the downstream of Xiaolangdi Dam during that regulation period. Dong (2015) suggested that the effect of water-sediment regulation on the bioavailability and environmental risk should be considered in the operation and management in the future (Dong et al., 2015).

Above all, natural flow regime was changed and flow increased after Xiaolangdi Dam operation. Fish species decreased heavily in this survey compared with 1980s. Although sediment might be one of the many reasons for fish reduction, it is still under discussion whether it resulted from water-sediment regulation. And it is also difficult to distinguish the natural reduction and impacts of dam operation. We concluded that the fish habitats are affected by many habitat parameters. Flow regime, sediment concentration, flow velocity and water depth are all the factors which control the habitat quality. Meanwhile, the interaction between the various factors and water-sediment regulation needs to be given further attention. And sediment concentration could be better controlled by implementing a more stringent regulation to protect the fish habitats.

4 CONCLUSIONS

After fish survey and complete analysis of hydrological alteration before and after the Xiaolangdi dam operation are carried out, we separately establish the relationship between upstream regulation and response of downstream flow regime, sediment, water quality, fish communities and fish habitats. The results reveal that:

(1) The flow tends to decrease from 1956 to 2011, and downstream flow and sediment significantly change after Xiaolangdi Dam operation. The flow tends to increase from 2001 and begins to recover. As for the operation results, the discharged flow tends to be more uniform in inter annul and intra annul scales. And the high flood pulse in water-sediment regulation period is controlled for downstream river channel scouring. The sediment is low throughout the year due to sediment regulation except for water and regulation period in which sediment density in downstream river channel significantly increase.

(2) After the fish survey in the lower Yellow River, we find that fish species decreases heavily compared with 1980s. The percentage of Yellow River carp decreases from 20% to 10%, and the dominant fishes change. Fish species and resources are obviously decreasing after the regulation, and the amount begins to recover after 15 to 30 days of the regulation. Although main stream channel is flushed in water-sediment regulation period, it is still under discussion whether fish communities decrease is resulted from the regulation that really affects the spawning period and fish habitat.

Considering Yellow River carp protection, we suggest that the cascade reservoir operation should consider more on impacts on fish species and habitats especially during water-sediment regulation period. And at the same time, more regulation experiments which aim at fish species and fish habitat restoration could be proposed.

ACKNOWLEDGEMENTS

This research is financially supported by National Natural Science Foundation of China (51420105014), China Postdoctoral Science Foundation (2016M592404), China Institute of Water Resources and Hydropower Research, China Three Gorges Corporation (0799556, 0799564, 0799558).

REFERENCES

Baiyin, B., Feng-Ran, X. & Chen, X.R. (2012). Impact of Sediment Flushing of Xiaolangdi Reservoir on Downstream Fish. *Journal of Hydraulic Engineering*.

Baiyin, B., Xu, F. & Chen, X. (2012). Impact of Sediment Flushing of Xiaolangdi Reservoir on Downstream Fish. *Journal of Hydraulic Engineering*, 1146-53.

Baiyin, B., Xu, F. & Chen, X. (2016). Acute Impacts of Reservoir Sediment Flushing on Fishes in the Yellow River. *Journal of Hydro-Environment Research,* 17, 26-35.

Baiyin, B. & Chen, X. (2012). Research Progress of Impacts of Sediment Flushing on Downstream Fish. *Journal of Sediment Research*, 74-80.

Chen, A., Sui, X. & Wang, D.S. (2014). *A Brief Review on Post-Project Environmental Appraisals of Dam Projects and Recommendations for China*. In Advanced Materials Research, 3451-6.

Chen, A., Sui, X. & Wang, D.S. (2014). *River Ecosystem Health Assessment and Implications for Post-Project Environmental Appraisal in China*. In Applied Mechanics and Materials, 8-12.

Chen, J., Zhou, W. & Han, S. (2015). Ponderations and suggestions on Operation Mode of Xiaolangdi Reservoir in its Second Stage of Sediment Retaining. *Journal of Hydraulic Engineering*, 46(5), 574-83.

Dong, J., Xia, X. & Wang, M. (2015). Effect of Water–Sediment Regulation of the Xiaolangdi Reservoir on the Concentrations, Bioavailability and Fluxes of PAHs in the Middle and Lower reaches of the Yellow River. *Journal of Hydrology,* 527,101-12.

Han, M. (2009). *The Research of Fishery Resource Investigation and the Sustainable Utilization in Yellow River Area*. Graduate School of Chinese Academy of Agricultural Sciences, 57.

He, Z. (1987). Fishery Resource Research on Yellow River System. *Journal of Dalian Fisheries College*, 63-6.

Jiang, X., Angela, A. & Liu, C. (2009). Environmental Flow Requirements by Major Fishes in the Lower reach of the Yellow River Determined by Flow Restoration. *Journal of Beijing Normal University (Natural Science)*, 537-42.

Jiang, X., Liu, X. & Zhang, S., et al. (2005). Distinguishing Key Species of Aquatic Ecosystem of the Main Yellow River. *Yellow River*, 1-3.

Jiang, X., Zhao, W. & Zhang, W. (2010). The Impact of Xiaolangdi Dam Operation on the Habitat of Yellow River Carp. *Acta Ecologica Sinica*, 30(18), 4940-4947.

Kong, D., Miao, C., Wu, J., Duan, Q., Sun, Q., Ye, A., Di, Z. & Gong, W. (2015). The Hydro-Environmental Response on the Lower Yellow River to the Water–Sediment Regulation Scheme. *Ecological Engineering,* 79, 69-79.

Li, B., Li, P. & Tang, Y., et al. (2015). Acoustic Survey of the Fisheries Resources in the Main Channel of Xiaolangdi Reservoir in the Yellow River. *Journal of Fisheries of China*, 1134-43.

Liu, F., Chen, S. & Dong, P. & Peng, J. (2012). Spatial and Temporal Variability of Water Discharge in the Yellow River Basin over the Past 60 years. *Journal of Geographical Sciences,* 22, 1013-33.

Liu, X., Lian, Y. & Huang, J. (2008). Environmental Flows of the Yellow River. *Science and Technology Review*, 24-30.

Ma, Y., Huang, H. Q., Nanson, G.C., Li, Y. & Yao, W. (2012). Channel Adjustments in Response to the Operation of Large Dams: The Upper reach of the Lower Yellow River. *Geomorphology,* 147-148, 35-48.

Peng, J., Chen, S. & Dong, P. (2010). Temporal Variation of Sediment Load in the Yellow River Basin, China, and its Impacts on the Lower reaches and the River Delta. *Catena,* 83, 135-47.

Qing, Z.G., Liang, Z.R., Lei, H.X. & Ping, H.Z. (2012). Impact of Water and Sand Diversion in Xiaolangdi Reservoir on Fish and Ecological Sensitive Area in the Middle Yellow River. *Journal of Hydroecology,* 33, 7-12.

Ru, H., Wang, H. & Zhao, W., Shen, Y., Wang, Y. & Zhang, X. (2010). Fishes in the Mainstream of the Yellow River: Assemblage Characteristics and Historical Changes. *Biodiversity Science*, 18(2), 169-76.

Sun, L., Baoyin, B. & Niu, C. & Li, C. (2012). Acute Stress caused by Sand Discharging on Yellow River Carp (Cyprinus Carpio) in Xiaolangdi Reservoir. *Acta Ecologica Sinica*, 32(7), 2204-11.

Yang, Z., Yan, Y. & Liu, Q. (2012). Assessment of the Flow Regime Alterations in the Lower Yellow River, China. *Ecological Informatics,* 10, 56-64.

Yi, Y., Yang, Z. & Zhang, S. (2010). Ecological Influence of Dam Construction and River-Lake Connectivity on Migration Fish Habitat in the Yangtze River Basin, China. *Procedia Environmental Sciences,* 2, 1942-54.

Zhang, A., Dong, Z. & Zhao, J., et al. (2013). Effects of the Integrated Water Regulation and Water-Sediment Regulation of the Yellow River on the Eco-Hydrology of its Estuary. *Journal of Hydraulic Engineering*, 987-93.

Zheng, L., Lv, Z. & Li, F., et al. (2014). Fish Community Structure in the Yellow River Estuary: Effect of Water and Sediment Discharge Regulations. *Journal of Fishery Sciences of China*, 602-10.

SIMULATING GEOBAG REVETMENT FAILURE PROCESSES

LEILA KHAJENOORI[(1)], GRANT WRIGHT[(2)], & MARTIN CRAPPER[(3)]

[(1)] Institute for Infrastructure and Environment, Heriot Watt University, Edinburgh, UK
Lk117@hw.ac.uk
[(2)] Institute for Infrastructure and Environment, Heriot Watt University, Edinburgh, UK
G.B.Wright@hw.ac.uk
[(3)] Faculty of Engineering and Environment, Northumbria University, Newcastle-upon-Tyne, UK
Martin.Crapper@northumbria.ac.uk

ABSTRACT

An experimental and numerical study has been carried out to help develop design guidelines for the construction of low-cost river bank protection using geobags. Building upon previous work, a 1:10 scale model is tested in a laboratory flume, comparing two different construction methods (running bond and stack bond), subjected to three different water depths. It is found that whilst the failure pattern is highly dependent on water depth, the construction method has no noticeable impact, and it is concluded that the dominating factor is the friction between individual geobags, which itself is dependent on bag overlap rather than specific construction method. A simple Discrete Element Method (DEM) model is constructed using the LIGGGHTS open source software with drag and lift models applied to a multisphere simulation of the laboratory model geobags. It is found that despite its simplicity this DEM model could reproduce the failure pattern of revetments very well, and thus has potential for future use in developing design guidelines aimed at the developing world.

Keywords: Geobag revetment; failure; DEM; LIGGGHTS.

1. INTRODUCTION AND PREVIOUS WORK

Riverbank erosion is a significant problem in rivers which flow through low-lying alluvial plains. Recently, sand filled geotextile bags (geobags) have been applied as a long-term means of riverbank protection in developing countries (JMREM, 2006; Oberhagemann and Hossain, 2011; Akter et al., 2013a, 2013b; NHC, 2006), and also used as sacrificial protection for bridge piers against local scouring phenomena (Korkut et al., 2007; Akib et al., 2014).

The hydraulic stability of geobag structures is affected by a wide range of factors, which can combine to create a number of different failure modes. To date, the vast majority of previous research has been focused on geobag performance in coastal situations (Bezuijenet et al., 2004; Saathoff et al., 2007; Recio and Oumeraci, 2009a, b; Dassanayake and Oumeraci, 2012a, b). However, the perpendicular wave action found in coastal scenarios is not significant in fluvial applications, where the flow direction is generally parallel to riverbank revetments, so the performance and failure mechanisms of geobag revetments in rivers is considerably different from that of coastal structures. One study that did focus on the use of geobags in the fluvial environment was conducted as part of the wider Jamuna–Meghna River erosion protection scheme in Bangladesh (NHC, 2006). This experimental study concluded that the optimum geobag weight for stability was 126 kg and, when traditionally “launched” from the riverside, geobag revetments tend to form 1V:2H slopes. To date, only one study has considered the hydrodynamic forces associated with varying water depth and toe scouring phenomena affecting a fluvial geobag revetment (Akter et al., 2013a, 2013b). This work successfully simulated initial failure of geobag revetments using the Discrete Element Method (DEM) and predicted the active shear stress necessary to initiate bag movement applying a conveyance estimation system (CES) model, thus yielding a good understanding of conditions leading to failure (Akter et al., 2013b).

Failure mechanisms associated with simple geobag riverbank revetments are now relatively well understood, and numerical modeling has advanced to the stage where incipient failure can be well simulated using DEM. Notwithstanding recent advances, a fuller understanding of geobag fluvial revetment performance is still required to understand geobag revetment in different conditions. As part of a more general study aimed at developing robust design guidelines, this paper focuses both on the effect of construction method on revetment performance and the suitability of a very simple DEM modeling approach as a tool to simulate complete revetment failure. In order to achieve these aims, both experimental and numerical investigations have been carried out.

2. EXPERIMENTS

Whilst the work undertaken focused on the development of efficient numerical simulation techniques, it was necessary to undertake a comprehensive programme of small-scale experimental tests in order to improve our understanding of geobag–water flow interactions and gather the data required to calibrate and validate the numerical model.

2.1. Experimental setup

Experiments were conducted in a recirculation flume 23 m long, 0.75 m wide and 0.5 m deep, which contained a 3 m long geobag revetment test section made up of ~600 model geobags on a fixed, non-erodible bed (Figure 1). The full-scale geobags used in the field were scaled down to achieve a laboratory model of geobag size of 103 × 70 mm and a dry mass of 0.126 kg, with approximately an 80% bag filling ratio. Nonwoven geotextiles, identical to that used in the field, and fine sand were used for bag preparation.

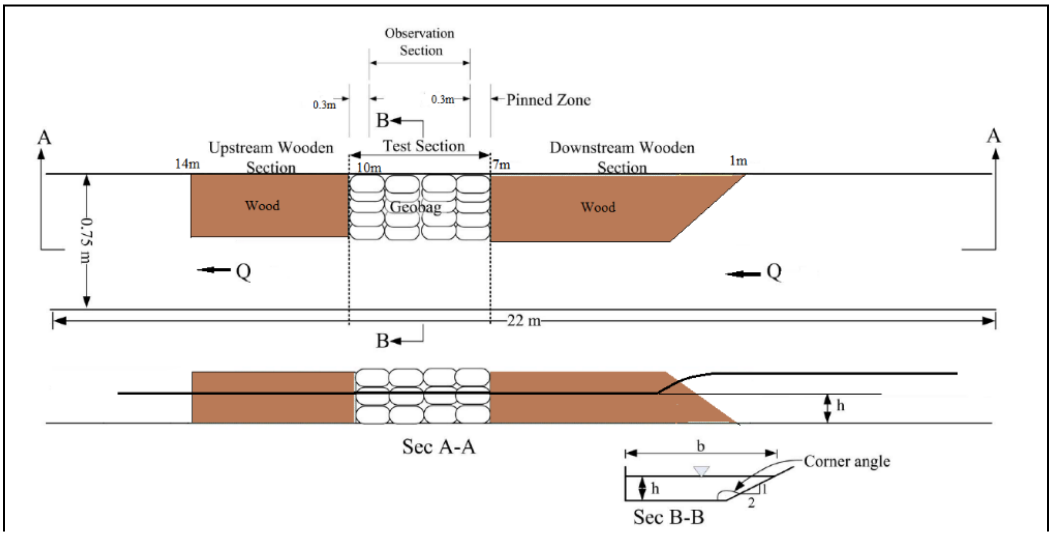

Figure 1: Experimental apparatus

Following previous laboratory work (NHC, 2006; Akter et al., 2013a), a side slope of 1V:2H was selected, resulting in revetment dimensions of 0.375 m width and 0.18 m height. To overcome the influence of the sudden flow contraction and expansion at the upstream and downstream ends of the test section, tapered wooden sections were installed to smooth the transitions. Furthermore, to avoid adverse effects from the interface between the wooden tapers and the geobag structure, the geobags were pinned down a distance 0.3m of the test section at either end.

In order to determine the likely effects of construction method on revetment failure, two different bonds were tested; a running bond, with 50% longitudinal overlap, and a stack bond, with no longitudinal overlap (Figure 2). For both construction bonds, geobags were placed with their longer axis parallel to the flow direction, and with a transverse overlap of 50%.


Figure 2: Revetment construction - stack bond (left), running bond (right)

Experiments ran for approximately seven hours, which was sufficient for the failure processes to stabilise, i.e. there was no significant further change in revetment structure. From previous studies (Akter et al., 2013a), it was observed that specific failure modes tend to occur in different ranges of water-depth. Thus, experiments were run with 3 different water depths, as detailed in Table 1.

Table 1: Flow conditions at different water depths

Condition	Water depth % revetment height	Mean water level (m)	Mean velocity (m/s)	Flow rate (m^3/s)	Froude number	Reynolds number
Low	0-49%	0.07	1.12	0.035	1.52	58623
Medium	50-60%	0.095	1.23	0.055	1.47	82458
High	60-80%	0.115	1.30	0.072	1.44	101605

2.2. Experimental Results and Discussion

Figures 3 and 4 show images taken during and after experiments undertaken with both construction bonds. Experimental observations highlighted a number of different failure modes in the submerged layers of geobags, including pull-out, dislodgement and uplifting. Vertical sliding failure, initiated with the failure of the submerged supporting bags, was also observed in the layers above the water surface.

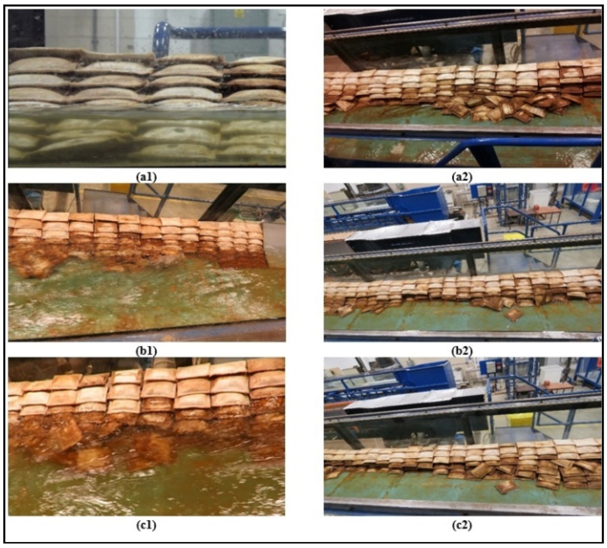

Figure 3: Failure processes for stack bond construction for low (a1, a2); medium (b1, b2); and high water depths (c1, c2)

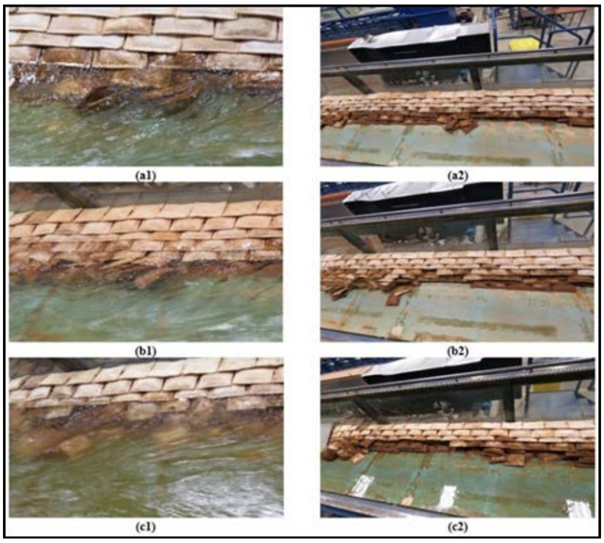

Figure 4: Failure processes for running bond construction for low (a1, a2); medium (b1, b2); and high water depths (c1, c2)

For the low to medium water depths (40-60% of revetment height), and for both different bonds, the failure process created a clump of collapsed bags, which then led to a localised increase in upstream water depth. Whilst this phenomenon exposed the upper layers of geobags to the flow, it also decreased local flow velocities, which seemed to help prevent more upstream bags from being washed away.

Figure 5 illustrates the number of geobags dislodged and washed away at the end of each test, for different bonds and water depths. As can be seen, whilst the extent of failure depends severely on water depth, it is generally independent of the construction method. Laboratory observations showed that once the first bags started moving and pulling out from the revetment, the failure process occurred quickly. Since there are no mortar-like bonds between individual geobags, it is likely that the integrity of a revetment is dependent on the contact area between individual geobags, which can be considered a proxy for frictional resistance, rather than specific construction method. This finding has potentially important implications for revetment construction methods which often depend on the dropping of bags by unskilled manual labourers. However, further tests with different levels of bag overlap in the transverse direction will be required to fully investigate this.

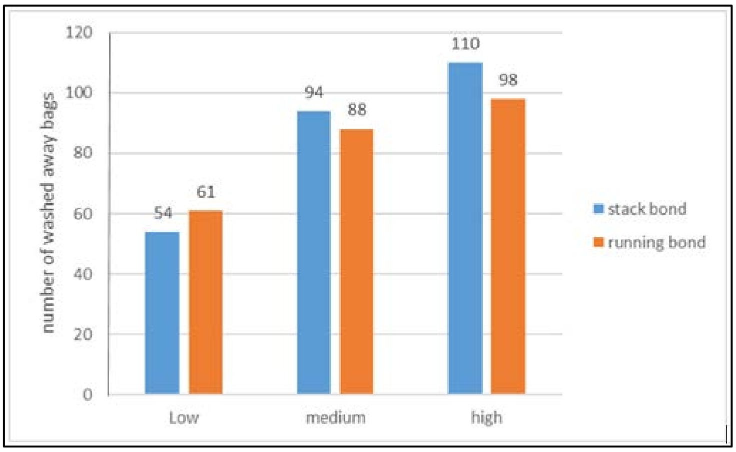

Figure 5: Number of bags which were washed away from revetment at the end of each test for two different bonds.

3. NUMERICAL MODELLING

In order to work towards the primary aim of developing design guidelines for geobag revetments in rivers, numerical simulations were attempted using the Discrete Element Method (DEM) (Akter et al., 2013b). DEM simulates the movement of each element, in this case each geobag, according to Newton's Laws of Motion, accounting for collisional and frictional forces between elements and between elements and boundaries, and for hydraulic forces, in particular drag, lift and buoyancy.

Hydraulic forces in DEM depend on a formulation to describe them in terms of the surrounding fluid. This can come directly from experimental measurements, from a modeling approach such as CES (Akter et al, 2013b) or from CFD simulations. In the latter case, the link between the DEM and the CFD can be one-way, in which the discrete elements (geobags) have no impact on the flow field, or fully-coupled, in which the momentum and volume of the geobags are source terms in the CFD simulation and are updated at every computational time step. The latter is theoretically more accurate, but requires vastly more computational resource to transfer data between the DEM and CFD aspects of the simulation.

The approach followed herein was to use a one-way coupled approach for initial model runs, with additional comparisons to a full-coupled approach to determine whether the additional computational expense was warranted.

3.1. REPRESENTING GEOBAGS AS DISCRETE ELEMENTS

In order to represent the characteristic shape of geobags in a DEM framework, a multisphere approach was adopted, in which a rigid body representing a geobag was built by combining spheres of different sizes. This method was extensively used for approximating complex particle shapes in DEM simulations (see for example Ferellec and McDowell, 2010). For this work, a model of 178 spheres, using four different sizes, was employed (Figure 6).

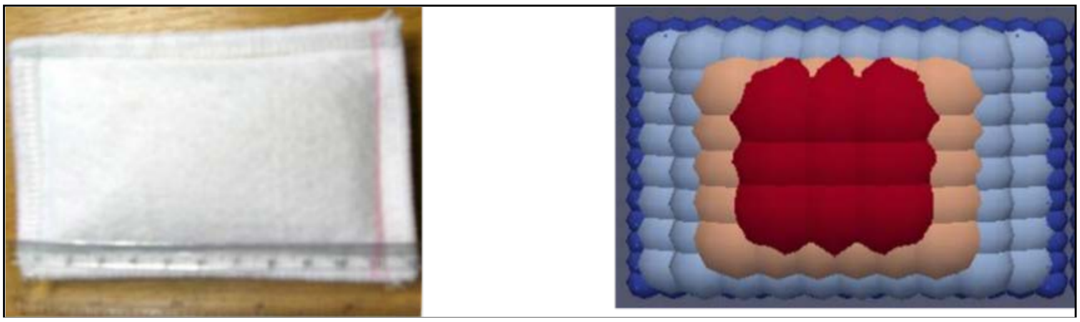

Figure 6: Laboratory (left) and DEM representation (right) of a geobag

3.2. Simulation Setup

A 3D DEM model of the laboratory experiment was created using the LIGGGHTS open source, C++, MPI parallel DEM code (Kloss, 2016). In addition to hydraulic forces, the LIGGGHTS model accounted for geobag self-weight under gravity, sliding friction and tangential and normal forces in collisions using a Hertz-Mindlin soft-sphere collision model (Kloss, 2016). Figure 7 shows the two different construction bonds as in the numerical model (refer to Figure 2 for the experimental equivalent).

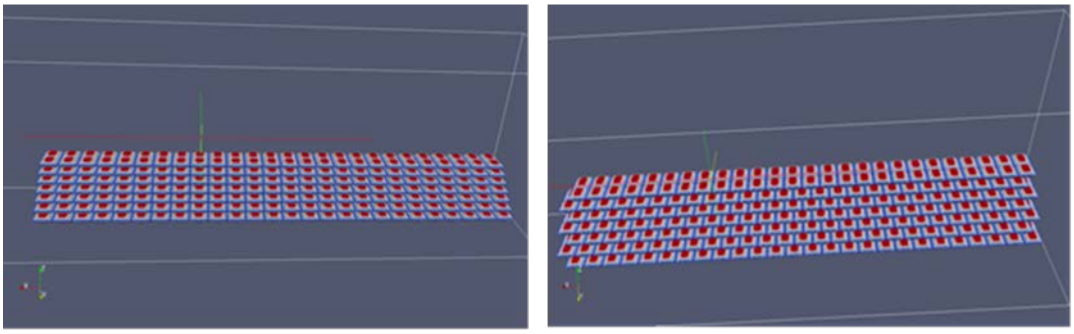

Figure 7: Simulated revetment with stack bond (left) and running bond (right)

3.3. Hydrodynamic forces on geobags: one-way coupling

One-way coupling is in essence a very simple method of simulation. Constant drag and lift forces were applied using traditional simple formulations as in equations 1 and 2:

$$F_D = 0.5 C_D \rho_W A_S u^2 \quad [1]$$

$$F_L = 0.5 C_L \rho_W A_T u^2 \quad [2]$$

Here, ρ_W is the density of water, C_D and C_L are drag and lift coefficients, u is the velocity of the geobag relative to the water, A_S is the cross-sectional area normal to the flow and A_T the cross-sectional area tangential to the flow.

The buoyancy force was also included in the calculations, and forces were calculated and applied individually for each sphere in the multisphere geobag model. A constant drag coefficient of 0.47, appropriate to spheres (Bird et. al, 2002; White, 2006) was used and a constant lift coefficient of 0.88 was calibrated using data from low water depth conditions and validated using the other water depth condition data sets.

3.4. Simulation results and discussion

Visual comparison is the most common, and often the only available technique for validating DEM models (Yang et al., 2008). In this study, the laboratory results had been visually compared with the LIGGGHTS simulations.

Comparing the simulation results with experimental observations (Figures 8 and 9) shows that the basic modeling approach replicates failures very well, especially some important failure modes such as uplifting, vertical sliding and dislodgement. Comparisons also show that the model is capable of predicting the position of failure in the revetment in different water depths.

4. CONCLUSIONS AND RECOMMENDATION

An experimental and numerical study has been conducted with an aim to ultimately produce design guidelines for low-cost river bank protection using geobags. Two construction bonds are tested. Experimental results indicate that although failure mechanisms strongly depend on water depth and flow conditions, construction method does not noticeably impact the progress of failure.

The numerical results show that a simple, one-way coupled CFD-DEM simulation with basic drag and lift formulations is capable of reproducing the experimental results very well, including the location and pattern of failure.

Further work will extend the study to a variety of different construction methods and revetment geometries, resulting in useable design guidelines for construction.

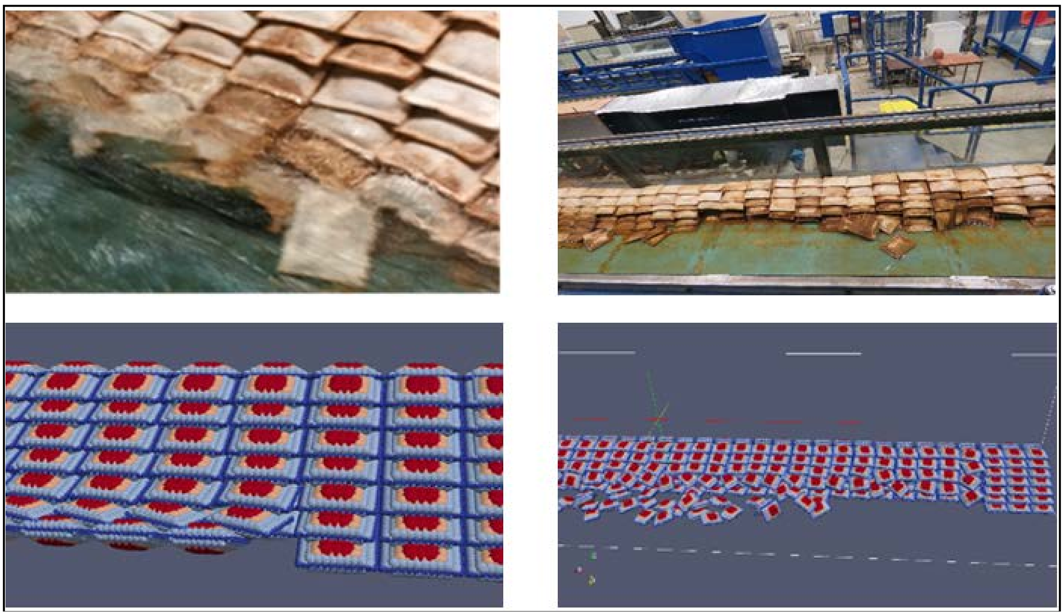

Figure 8: Experimental and numerical results for revetment failure processes (stack bond construction, low depth)

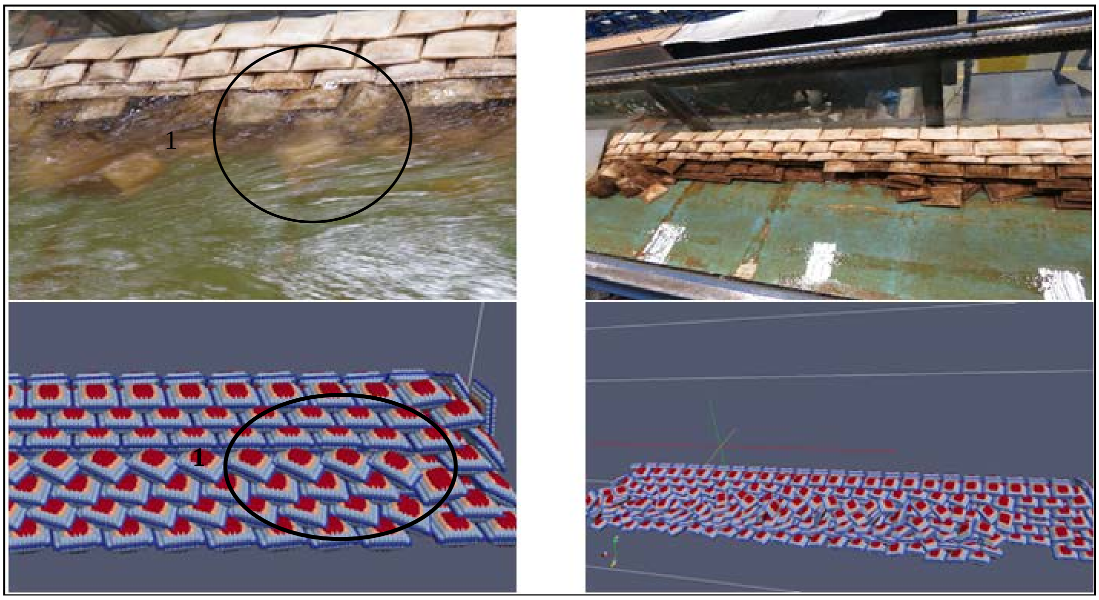

Figure 9: Experimental and numerical results for revetment failure processes (running bond construction, high depth)

ACKNOWLEDGMENTS

This study has been funded by the Institute for Infrastructure and Environment at Heriot-Watt University, with additional support provided by Alexander Podlozhnyuk and NAUE Gmbh& Co. Their support is gratefully acknowledged.

REFERENCES

Akib, S., Mamat, N.L., Basser, H. & Jahangirzadeh, A. (2014). Reducing Local Scouring at Bridge Piles using Collars and Geobags.*The Scientific World Journal*, 2014, 1-7.

Akter, A., Crapper, M., Pender, G., Wright, G. & Wong, W.S. (2012). Modelling the Failure Modes in Geobag Revetments. *Journal of Water Science & Technology*, 65(3), 418-425.

Akter, A., Pender, G., Wright, G. & Crapper, M. (2013a). The Performance of a Geobag Revetment, I: Quasi–Physical Modelling*. Journal of Hydraulic Engineering*, 139(8), 865–876.

Akter, A., Crapper, M., Pender, G., Wright, G. & Wong, W.S. (2013b). The Performance of a Geobag Revetment, II: Numerical Modelling*. Journal of Hydraulic Engineering*, 139(8), 877–885.

Bezuijen, A., Groot, M.B., Breteler, M.K. & Berendsen, E. (2004). Placing Accuracy and Stability of Geocontainers. *Proceedings 3rd Geosynthetics Conference*, Munich, Technische Universität München, Cent, Geotech, 1, 123-128.

Bird, R.B., Stewart,W. & Lightfoot,E. (2002). *Friction Factors for Flow around Spheres*.Transport Phenomena. 2nd edition, John Wiley & Sons: New York, Book, Chapter 6.

Darshana, T., Dassanayake, D.T. & Oumeraci, H. (2012b). Hydraulic Stability of Coastal Structures Made of Geotextile Sand Container (GSCS): Effect of Engineering Properties of GSCS. *33rd Conference on Coastal Engineering,* Santander, Spain.

Dassanayake, D.T. & Oumeraci, H. (2012a*).* Important Engineering Properties of Geotextile Sand Containers and Their Effect on The Hydraulic Stability of GSC-structures. *Terra et Aqua Journal*, 12, 3-11.

Ferellec, J.F. & McDowell, G.R. (2010). A Method to Model Realistic Particle Shape and inertia in DEM. *Granular Matter,* 12, 459-67.

JMREM, (2006). Jamuna-Meghna River Erosion Mitigation Project Part B*. Special Report* 17, Geobag Revetments. Government of the People's Republic of Bangladesh, Asian Development Bank and Bangladesh Water Development Board.

Kloss,C. (2016), LIGGGHTS(R)-PUBLIC Documentation, Version 3.X.;CFDEM®project,LIGGGHTS®PUBLIC, (2016). https://www.cfdem.com/media/DEM/docu/Manual.html [Accesed on 30 November 2016]

Korkut, R., Martinez, E.J., Morales, R., Ettema, R. & Barkdoll, B. (2007). Geobag Performance as Scour Countermeasure for Bridge Abutments*. Journal of Hydraulic Engineering*, *ASCE*, 133 (4), 431-439.

Northwest Hydraulics Consultants (NHC). (2006). Jamuna-Meghna River Erosion Mitigation Project Part B. *Special Report* 11, Physical Model Study (Vancouver, Canada), Final Report*,* Government of the People's Republic of Bangladesh, Asian Development Bank and Bangladesh Water Development Board.

Oberhagemann, K. & Hossain, M.M. (2011). Geotextile Bag Revetments for Large Rivers in Bangladesh. *Geotextiles and Geomembranes,* 29 (4), 402–414.

Oumeraci, H., Hinz, M., Bleck, M. & Kortenhaus, A. (2003). Sand-Filled Geotextile Containers for Shore Protection. *Proceedings 'Coastal Structures* 2003', Portland, Oregon, *USA*.

Recio, J. & Oumeraci, H. (2009). Process Based Stability Formulae for Coastal Structures Made of Geotextile Sand Containers. *Coastal Engineering*, 56, 632-658.

Recio, J. & Oumeraci, H. (2009). Processes Affecting The Hydraulic Stability of Coastal Revetments Made of Geotextile Sand Containers. *Coastal Engineering*, 56, 260-284.

Saathoff, F., Oumeraci, H. & Restall, S. (2007). Australian and German Experiences on the Use of Geotextile Containers. *Geotextiles and Geomembranes*, 25 (4-5), 251-263.

White, F. M. (2006). *Flow past Immersed Bodies*. Fluid Mechanics. 6th edition, McGraw-Hill, Inc.: New York, Book, Chapter 7.

Yang, S.Q., Shu, Y.M. & Yang, X.C. (2008). Flume Experiment and Numerical Analysis for Bank Reinforcement with Geocontainer. *Proceedings of the 4th Asian Regional Conference on Geosynthetics*, Shanghai, China, 630-636.

Proceedings of the 37th IAHR World Congress
August 13 – 18, 2017, Kuala Lumpur, Malaysia

DEVELOPING A NEW STATISTICAL MODEL TO ESTIMATE THE RIVER QUALITY PERSPECTIVE FROM MACRO PARAMETERS IN RIVER BASINS, CASE STUDY: SIMINEHROOD RIVER BASIN, IRAN

FARSHID BOSTANMANESHRAD[(1)], SADEGH PARTANI[(2)] & ROOHOLLAH NOORI[(3)]

[(1,2)]Civil Engineering Department, Faculty of Engineering, Islamic Azad University, Central Tehran Branch (IAUCTB), Tehran, IRAN
[(3)]Graduate Faculty of Environment, University of Tehran, Tehran, IRAN
S_Partani@ut.ac.ir

ABSTRACT

Prediction of micro chemicals through the macro parameters in river basin has led this research to find an estimation model to depict the micro water quality variables. The macro parameters include land use/land cover (LU/LC), erosion, geology and density which are significant factors that directly affect the river water quality. This research is carried out on one of the large rivers in Iran which terminates in Uremia Lake. 15 stations and three sampling periods for 9 National Sanitation Foundation (NSF) micro water quality variations are investigated. Four different statistical analyses that are carried out support both macro parameters and micro water quality variations of the study, where they have close conceptual and statistical relation with regard to primary screening. Then, a MLR model is applied to the micro water quality variables and macro parameters as dependent and independent variables, respectively. The results have demonstrated the significant relationship between land use and phosphorus, total solids, turbidity, erosion levels, electricity conductivity and solids. Discriminate analysis is applied to group ranging categories for prediction. Simple weighting is applied to groups of micro variables to calibrate the extracted model. Physical micro variables and phosphorus components are significantly related as dependent variables to LU/LC, erosion and geology. Biological Oxygen Demand and nitrate fluctuation are slightly affected by urban land use and population. The input data for extracted model is the macro parameters layer, while output data is the water quality prediction in downstream of the terminal of each reach where the discharge spot of submarine drain is located. New weighting and distance system employed in the model increase the outcome accuracy of the prediction. This model can be employed in river quality monitoring system. Online integrated estimation of water quality due to macro parameters monitoring as input data is recorded in the organization data bank. This study suggests that the inspection and monitoring, water operation administrators, etc. to focus more on polluted potential zones to make use of advanced data recoding sensors in new pattern of time step.

Keywords: Macro parameters; water quality; micro variable; river basin.

1 INTRODUCTION

Population growth and industries are developing near rivers because they are one of the most important available water resources. Since surface water has immediate contact with its open environment, the influence of land use, land cover, geology, etc. on water quality has been a concern which could be representative of significant factors on water quality.

Most recently, with the rapid development of geographical information systems' techniques, relationship between physical and chemical properties of surrounding media like land use, geology, erosion etc. as macro scale parameters (MSP_S), and water quality variations as micro scale variations (MSVs), have begun to be applied in such studies.

Several factors have direct or indirect effects on MSV_S (land use, erosion, geology, population density). Many qualitative studies have been done to identify the various factors affecting surface water quality by using different methods of Land use/Land cover changes modeling (Wan et al., 2014; Li et al., 2012) and multivariate statistical analysis (Li et al., 2009; Zhang et al., 2012) . Using Bayesian hierarchical modeling approach by Wan and Yang (2014) in the Xitiaoxi River Watershed in China showed that urban land use and agriculture are the main sources of TP and TN.

Research by Li and Liu (2012) on the relationship between land use/land cover and water quality in Liao river basins using statistical analysis showed that BOD_5, COD, Sediment, hardness, nitrate Nitrogen, Total Dissolved Solid (TDS) were related to forest and agriculture.

Different multivariate statistical techniques by (Li et al., 2009) were used to evaluate variations in surface water quality of the Songhua River Basin. This study showed that the major causes of water quality deterioration were related to inflow of effluent from domestic and industrial wastewater disposal. Research findings by Zhang et al (2012) showed that nitrate-nitrogen was related to chemical fertilizer input intensity, soil loss and rainfall.

  / ISSN 1562-6865 (Online) - ISSN 1063-7710 (Print)

In addition to recognizing the effect types and parameters affecting the river's water quality variables, position and distance parameter can also play a significant role in their severity and effect. Researchers studying the effects of distances, have examined different basins with different physiographical characteristics (Gyawali et al., 2013; Zhao et al., 2015).

Application of buffers along the river banks demonstrated that the urban land use increases the water temperature (TEMP), dissolved solids (TDS), suspended solids (TSS) and reduces pH, while agricultural land causes increased TSS, TDS and reduced TEMP, DO (Gyawali et al., 2013).

Zhao and Yang (2015) studied the effects of each of the MSP_s by using circular buffers in 5 scales. The effects of MSP_s on any scale were found to be different. The closer distance buffers have more influence than the main river. This research is conducted to ascertain the relationship between MSP_s and MSV_s as well as to predict the characteristics of water quality in rivers via macro scale parameters which are available in all global data banks such as satellite recording data.

2 METHODOLOGY

2.1 Study area

The study was carried out at the Siminehrood River Basin. The Siminehrood River is located in north-west of Iran (Figure 1) as one of the important rivers which terminates in Uremia Lake (Ahmadi et al., 2015; Tisseuil et al., 2013). The longitude and latitude of the basin are 45°, 35' through 46°, 25' E and 36°, 10' through 37° A, respectively. Siminehrood catchment area is 3884 Km^2 (Sharifi, 2010) and the length of the river is 200 km (Afshin, 1995). The average elevation of the basin is about 11650 m. Watershed average slope is 1.37 percent and general slope area is from southwest to northeast. The river flow passes through two provinces, Kurdistan and West Azerbaijan.

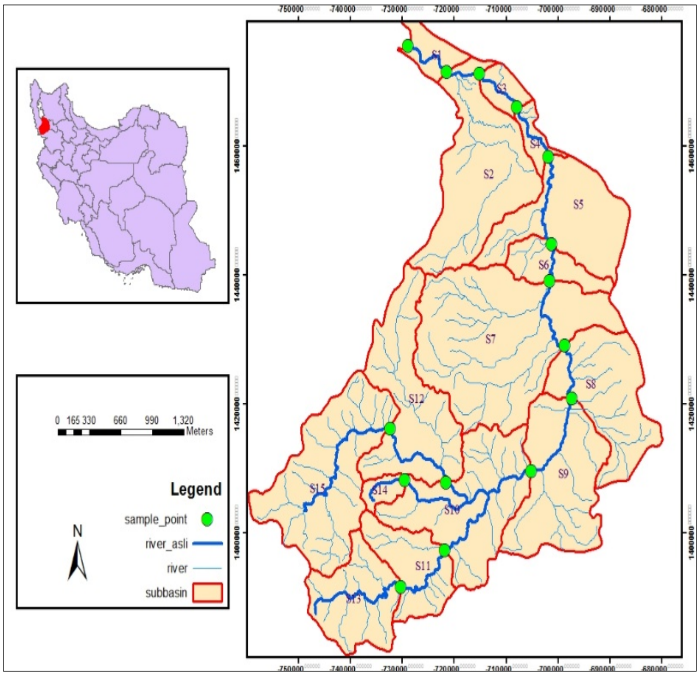

Figure 1. Study area and sampling stations.

2.2 Water quality sampling

The main flow of the river was calculated as cumulative for each sub-basin (Table 1) by using geographic information system. The sampling process was carried out at 15 stations, in three stages that each sub-basin was terminated to the sampling sites. Chemical and physical features of water quality were tested in the Siminehrood river basin. The sampling, preservation, transportation and analysis of the water samples were performed following the standard of Handbook for Sampling and Sample Preservation of Water and Waste Water (US EPA, 1982).

Table 1. Accumulation basin.

Sub basin	Accumulation basin
1	1-2-3-4-5-6-7-8-9-10-11-12-13-14-15
2	2-3-4-5-6-7-8-9-10-11-12-13-14-15
3	3-4-5-6-7-8-9-10-11-12-13-14-15
4	4-5-6-7-8-9-10-11-12-13-14-15
5	5-6-7-8-9-10-11-12-13-14-15
6	6-7-8-9-10-11-12-13-14-15
7	7-8-9-10-11-12-13-14-15
8	8-9-10-11-12-13-14-15
9	9-10-11-12-13-14-15
10	10-11-12-13-14-15
11	11-12
12	12-15
13	13
14	14
15	15

2.3 Micro–scale variables (MSV_S)

MSV_s are defined as water quality index variations. Thirteen variations were chosen to measure in the samples. NSF parameters (Said & Stevens, 2004; Effendi & Wardiatno, 2015) were also included in the variations. Sampling and measurements have been carried out by the Iran Department of Environment (2012). The MSV_s are consist of pH, dissolved oxygen (DO), electrical conductivity (EC), total dissolved solids (TDS), biological oxygen demand (BOD_5), orthophosphate (PO_4), fecal coliforms (FC), total coliform (TC), total solids (TS), turbidity (Tur.), temperature (T) and nitrate **(**NO_3).

DO, pH, EC and T were measured using in-situ devices. The remaining MSV_s were measured in the laboratory using gravimetric (TDS, TS), Nephelometric (Tur.) and Spectrophotometric (COD, PO4, NO3) methods.

2.4 Macro–scale parameters (MSP_S)

Macro scale parameters are defined as physical and chemical properties scheme of surrounding environment which have direct and indirect effects on MSV_s and origin of pollution sources. MSP_s are available through aerial snapshots, geographical information etc. MSP_s investigated in this study included land use, population density, geology and erosion layers (Iran Department of Environment, 2012) which are illustrated in Figures 2 to 6, respectively.

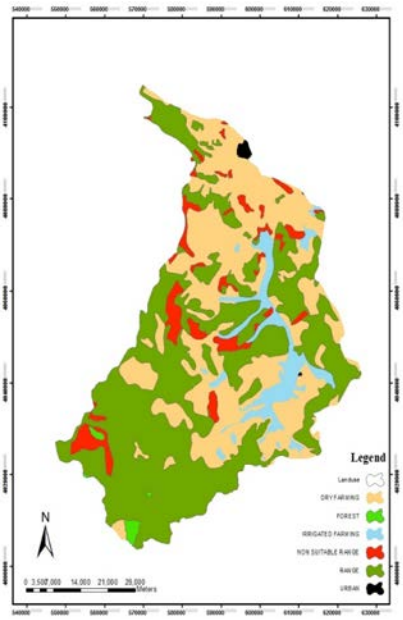

Figure 2. Land use geographical distribution.

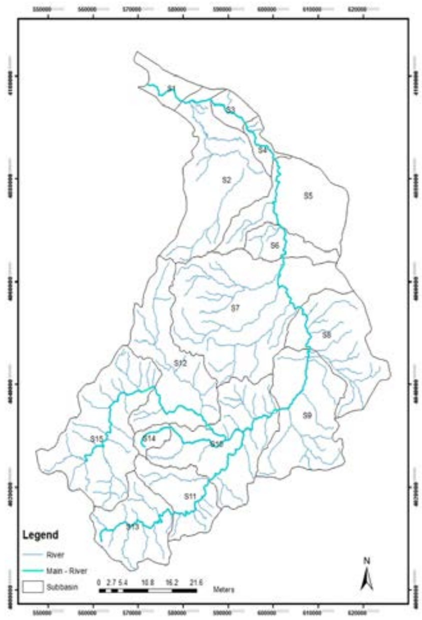

Figure 3. Sub basins boundaries.

  / ISSN 1562-6865 (Online) - ISSN 1063-7710 (Print)

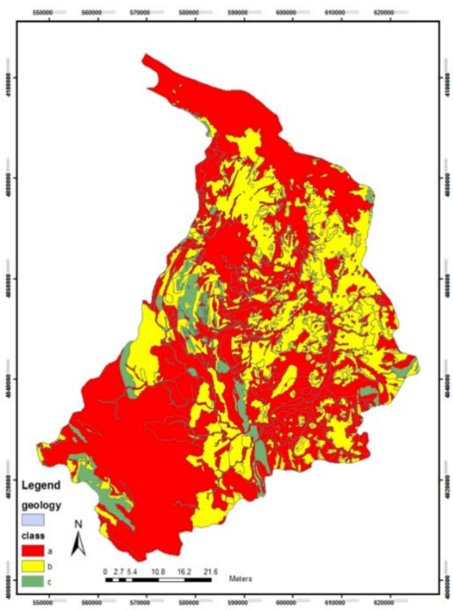

Figure 4. Geology pollution potential indices categories in river basin.

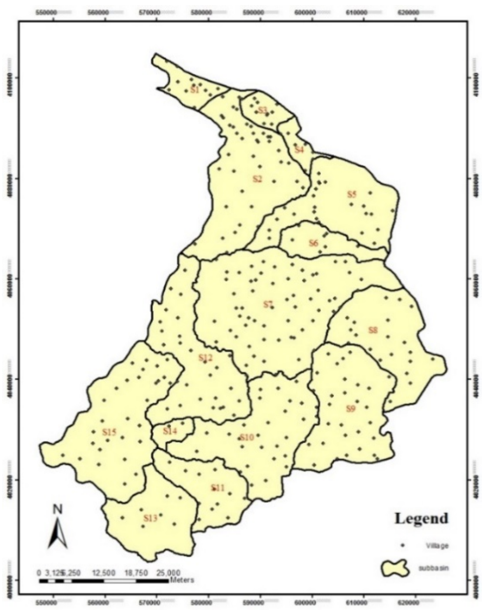

Figure 5. Population density based on rural/urban spots/areas.

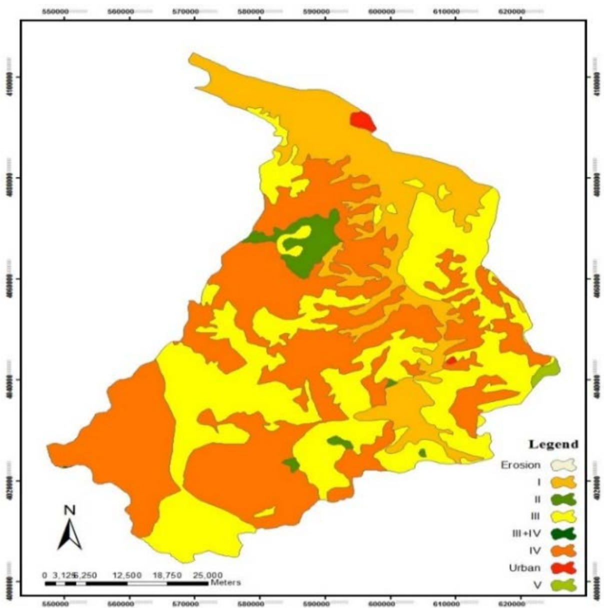

Figure 6. Erosion intensity categories.

2.5 Preliminary data validation tests (QA/QC)

Normality tests were applied to all data and outliers were detected using Cook's distance calculations. Quality control and quality assurance procedures were done in two stages, field sampling (US EPA, 2000) and laboratory measurements (SMWW, 2012).

2.6 Primary statistical analysis

Introduction of used variables has been shown in Table 2. Four pair wise statistical analysis were applied to all normalized data to find out the potential relationship with regard to primary screening. Each analysis was applied to 7 series of data (Figure 7) including three tables on seasonal separately, three tables on two-season collection and one table on all three seasons' data. Couples which appeared in three or more series with high potential of significant relationship (such as correlation factor, similarity index, etc.) were selected for final screening. Physical micro variables such as TDS, TS and EC and chemicals such as PO_4 and BOD_5 were identified in three primary analyses shown in Figure 7 (a, c, d). The reason can be attributed to the main sources of phosphors in crust and erosion as the causes of TSS and TDS in the basin. Due to the final step couples which appeared in 3 or 4, primary pair wise statistical analysis were selected (Table 3).

Table 2. Introduction of variables.

Land Use	Erosion	Density	Geology Potential Pollution
ZD (Dry farming)	I		A (Top)
ZA (Irrigated Farming)	II		
M (Rang)	III		B (Middle)
MN (Non Suitable Rang)	III+IV	Population Density	
J (Forest)	IV		C (down)
SH (City)	URB		
	V		

MPV$_S$	MSV$_S$
ZD	BOD5 - EC - PO4 - TDS - TS - TUR
ZA	EC - PO4 - TDS - TS - TUR
M	EC - PO4 - TDS - TS - TUR
MN	TUR
J	EC - TDS - TS
SH	BOD5 - EC - pH - TDS - TS - TUR
I	BOD5 - EC - PO4 - TDS - TS - TUR
II	BOD5 - DO - EC - PO4 - TDS - TS - TUR
III	TDS - TS - TUR
III+IV	DO
IV	
Urban	BOD5 - DO - EC - TDS - TS - TUR
V	BOD5 - EC - PO4 - TDS - TS
Density	BOD5 - EC - PO4 - TDS - TS - TUR
A	NO3 - T
B	EC - PO4 - TDS - TS - TUR
C	EC - PO4 - TDS - TS

(a) Matrix Plot

MPV$_S$	MSV$_S$
ZD	TUR
ZA	PO4 - TS - T
M	
MN	
J	
SH	TUR
I	DO - TDS
II	EC
III	
III+IV	
IV	
Urban	
V	
Density	
A	
B	
C	

(b) Discriminant Analysis

MPV$_S$	MSV$_S$
ZA	BOD5 - EC - PO4 - TDS - TS - TUR
ZA	BOD5 - EC - PO4 - TDS - TS
M	NO3 - T
MN	FC - TC
J	DO - pH
SH	BOD5 - EC - PO4 - TDS - TS - TUR
I	BOD5 - EC - PO4 - TDS - TS - TUR
II	BOD5 - EC - PO4 - TDS - TS - TUR
III	NO3 - T
III+IV	FC - TS
IV	FC - TS
Urban	BOD5 - EC - PO4 - TDS - TS - TUR
V	BOD5 - EC - PO4 - TDS - TS - TUR
Density	BOD5 - EC - PO4 - TDS - TS - TUR
A	DO - Ph
B	BOD5 - EC - PO4 - TDS - TS - TUR
C	NO3 - T

(c) Dendrogram

MPV$_S$	MSV$_S$
ZA	BOD5 - EC - PO4 - TDS - TS - TUR
ZA	EC - PO4 - TDS - TS - TUR
M	EC - PO4 - TDS - TS - TUR
MN	TUR
J	EC - TDS - TS
SH	BOD5 - EC - pH - TDS - TS - TUR
I	BOD5 - EC - PO4 - TDS - TS - TUR
II	BOD5 - DO - EC - PO4 - TDS - TS - TUR
III	TDS - TS - TUR
III+IV	DO
IV	
Urban	BOD5 - DO - EC - TDS - TS - TUR
V	BOD5 - EC - PO4 - TDS - TS
Density	BOD5 - EC - PO4 - TDS - TS - TUR
A	NO3 - T
B	EC - PO4 - TDS - TS - TUR
C	EC - PO4 - TDS - TS

(d) Pearson's Correlation

Figure 7. Results of primary screening on related MSV$_S$ versus MSP$_{S.}$

  / ISSN 1562-6865 (Online) - ISSN 1063-7710 (Print)

Table 3. Results of final screening**.**

ZD	BOD5 - EC - PO4 - TDS - TS - TUR
ZA	EC - PO4 - TDS - TS
SH	BOD5 - EC - TDS - TS - TUR
I	BOD5 - EC - PO4 -TDS - TS - TUR
II	BOD5 - EC - PO4 - TDS - TS - TUR
III+IV	DO - TC
Urban	BOD5 - EC - TDS - TS - TUR
V	BOD5 - EC - PO4 - TDS - TS - TUR
Density	BOD5 - EC - PO4 - TDS - TS - TUR
B	EC - PO4 - TDS - TS - TUR

2.7 Geographical Data Preparation

Geographical data which are presented as map layers in this step were quantified by allocating the normalized value of MSP_s to each cell. Then, the MSP_s' layers were multiplied by broke sub-weights (by certified experts) and new quantified layers were extracted.

2.8 Distance Effects

Distance effects were studied through three geographical patterns (Parallel Euclidean, radian Euclidean, hydrological) and two weighting methods. The distance weight of MSP_s to the main river was calculated in 5 steps (1/r (r=parallel Euclidean distance), 1/Ln r (r=Parallel Euclidean distance), 1/r (r=radial Euclidean distance), 1/Ln r (r=radial Euclidean distance), 1/r (r=hydrological distance)). Zonal statistics as table applications were employed to calculate the sum of pixel values in 5 steps for each of the MSP_s (Figures 8 to 10).

2.9 Multivariate Statistical Analysis

Multivariate linear regression analysis (MLR) was applied as multivariate statistical analysis on MSP_S and MSV_S as independent and dependent variables, respectively based on the primary screening results. The results which were followed by some multivariate equations can estimate MSV_S. This estimation had some errors and differences as compared to the in-situ measurements. Therefore, another linear equation was developed in combination with the MLR equation and the recent one, as a modification to provide a water quality Statistical Estimation Model for the river base.

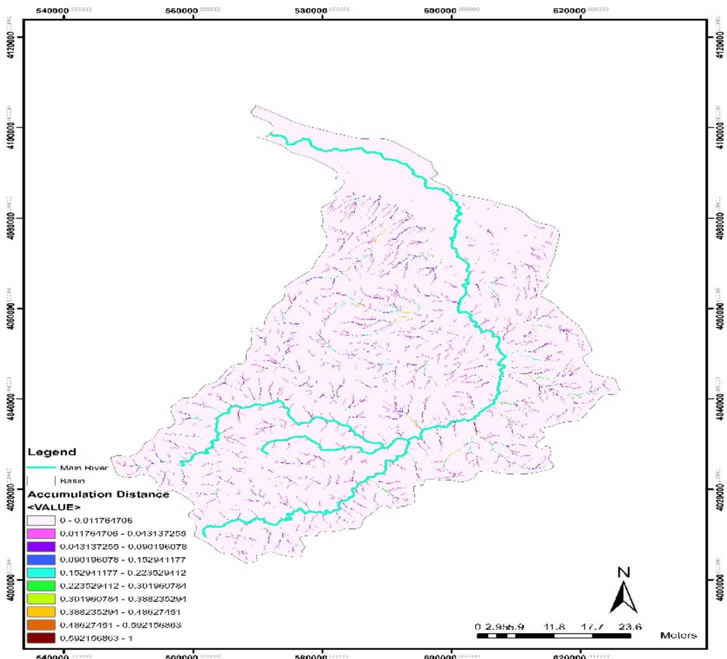

Figure 8. Hydrological distance.

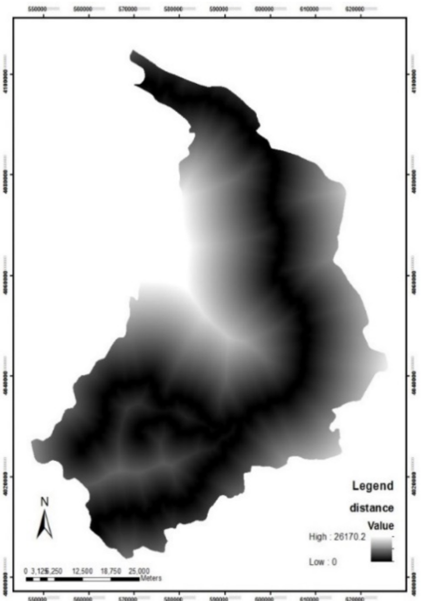

Figure 9. Parallel Euclidean distance weight from river axis

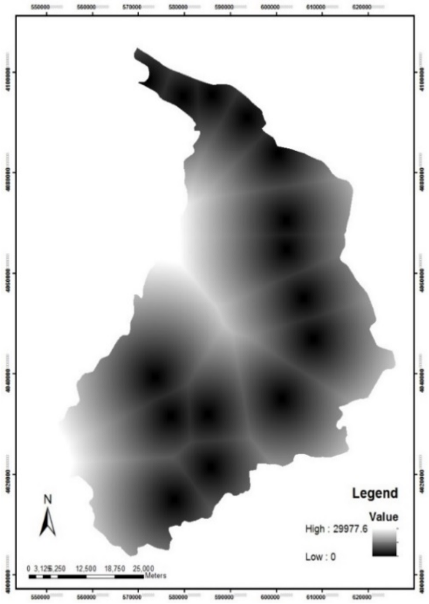

Figure 10. Radial Euclidean distance weight from sampling points

3 RESULTS AND DISCUSSION

The weights of MSP_S had been demonstrated by the expert system in Table 4. Three identifications of distance in two weights were considered for analysis. Four variables were examined using the extracted multi linear regression and modified equations. Each equation was examined by using the standard deviation (STD). Significant variables were remarked if the coefficient of variances from average were less than STD. In order to satisfy appropriate correlations of improved R^2 and estimation model calibration, modified equations were suggested after validation of outputs with the actual field data.

PO_4 in 1/r (R=Hydrological) weight showed the highest R^2 (0.574) in a multivariate regression analysis. In the case of NSF with R^2=0.83 for parallel Euclidean distance (1/r), EC with R^2=0.95 for 1/Ln r (r=Parallel Euclidean distance) and TS with R^2=0.67 for 1/r (r= radial Euclidean distance), they were selected as significant factors (Figure 10). Hydrological, parallel and radial distance coefficients of MSP_S in Figure 10 were examined with the coefficients in Table 4.

Table 4. The weights of MSPs by expert system.

MSP_S	Weight
Land Use	0.298
Density	0.224
Erosion	0.239
Geology	0.2376

Distance Type	Distance Weight	Estimated Variable	Multivariate Regreesion Analysis (MLR) on MSPs	R^2	Modification Equation	R^2	Effective Factors
Hydrological	1/r	NSF	0.286Land Use-0.030Density-0.155Erodion-0.031Geology+75.279	0.84	y* =0.8098x** +13.087	0.837	Erosion/Geology/Density
		TS	3.139Land Use-0.392Density+0.743Erosion-0.658Geology+19.296	0.63	y=0.6209x+12.541	0.625	Density/Erosion/Geology
		EC	1.399Land Use-0.493Density+0.566Erosion-0.191Geology+32.175	0.56	y=0.5642x+27.903	0.563	Erosion/Density/Geology
		PO4	3.067Land Use-0.133Density+1.677Erosion-0.906Geology+11.988	0.57	y=0.5743x+1615	0.574	Erosion/Density/Geology
Parallel	1/r	NSF	0.01Land Use+0.01Erosion+0.001Density-0.005Geology+76.07	0.84	y=1.0037x-1.7422	0.838	Land Use/Erosion/Geology/Densi
		TS	0.070Land Use-0.052Erosion-0.024Density+0.005Erosion+18.176	0.7	y=0.6907x+11.546	0.6659	Erosion/Density/Greology
		EC	0.218Land Use+0.187Erosion+0.005Density-0.079Geology+61.074	0.76	y=0.8114x-44.537	0.754	Land Use/Erosion/Density/Geolo
		PO4	0.033Geology-0.093Erosion-0.012Density-0.038Land Use-7.949	0.56	y=0.5783x+17.571	0.559	Land Use/Density/Geology
	1/Lnr	NSF	1.876Land Use+0.304Erosion-0.416Density-2.677Geology	0.83	y=380513x-3e+07	0.8145	Land Use/Erosion/Density
		TS	7.864Land Use-1.732Erosion-2.9Density-2.664Geology	0.71	y=-58927x-1e+06	0.419	Density/Erosion/Geology
		EC	0.001Land Use+37.646	0.64	y=-39.4x+598.61	0.95	Land Use
		PO4	1.195Land Use-1.753Erosion-0.347Density+1.621Geology	0.56	y=20791x+881564	0.5413	Land Use/Geology/Erosion/Densi
Redial	1/r	NSF	0.0251Land Use+0.006Erosion-0.001Density-0.010Geology+74.636	0.83	y=0.8933x+6.6931	0.829	Geology/Erosion/Density
		TS	0.465Land Use-0.063Erosion-0.111Density-0.035Geology+13.794	0.67	y=0.6824x+11.138	0.673	Erosion/Density/Geology
		EC	0.534Land Use+0.485Erosion-0.066Density-0.184Geology+38.990	0.71	y=0.7227x+18.533	0.712	Land Use/Erosion/Density/Geolo
		PO4	0.123Erosion-0.015Land Use+0.041Density-0.017Geology-0.516	0.55	y=0.5527x+17.265	0.5484	Land Use/Density/Geology
	1/Lnr	NSF	2.346Land Use-0.249Erosion-2.370Density-0.651Geology	0.83	y=316923x-2e+07	0.814	Land Use/Density/Erosion/Geolo
		TS	8.093Land Use-2.027Erosion-2.421Density-3.081Geology	0.73	y=-49703x-1e+06	0.412	Erosion/Density/Geology
		EC	0.001Land Use+37.390	0.63	y=2.892x+71.657	0.301	Land Use
		PO4	1.323Land Use-1.880Erosin+1.705Density-0.433Geology	0.56	y=19284x+791870	0.543	Land Use/Erosion/Density/Geolo

Figure 10. Extraction process of MSV_s statistical estimation model equation.
*Modified Estimated MSV_S (which is calibrated by actual field data)**Estimated MSP_S according to MLR in each row

  / ISSN 1562-6865 (Online) - ISSN 1063-7710 (Print)

4 CONCLUSIONS

The results show that new distance type which is identified as hydrological distance, satisfies MSVs estimation and water quality prediction with a slightly better accuracy. The results are in agreement with those of Gyawali et all (2013) and Zhao et all (2015), who also applied parallel and radial distance weight. It is also shown in the study the inverse effects of MSP_S distance. In the aggregation of NSF as a water quality index in rivers, it has shown better compatibility with all kinds of MSPs and the MLR estimation modified model in terms of all distance weights and all kinds of distance that can satisfy the water quality estimation. Recent research on LU/LC changes modeling has employed these equations shown in Figure 10 to determine the primary characteristics of river water quality based on river basin characteristics and all MSP_s, considering the nearest and furthest MSP_s in the basin. The results also indicate that physical water quality variations have the most relation with MSP_s, thus they would have the most significant effect in the estimation models.

ACKNOWLEDGEMENTS

The authors would like to acknowledge the support given by the Modares Environmental Research center (MERC) of Tarbiat Modares University of Iran in data preparation. The authors also highly appreciate the effort by Professor Ahmad Khodadadi, administrator of MERC and human affairs deputy of Department of Environment (DOE) of Iran for providing accessibility to some previous reports. This research is carried out under the master thesis studies of Mr. Bostanmaneshrad under the supervision of Dr. S. Partani and Dr. R. Noori, assistant professors of Islamic Azad University, Central Tehran Branch (IAUCTB) and University of Tehran, respectively. So, all authors truly appreciate the inspiring support given by the civil engineering department and research deputy of IAUCTB.

REFERENCES

Afshin, Y. (1995). *Rivers of Iran,* Jmab Consulting Engineering Company, Ministry of energy, Iran.

Ahmadi, J., Kahforoushan, D., Fatehifar, E., Zoroufchi, Kh. & Ndjafi, M. (2015). Forecasting Surface Area Fluctuations of Urmia Lake by Image Processing Technique. *Research in Water and Wastewater,* 4,183–187.

Effendi, H. & Wardiatno, Y. (2015). Water Quality Status of Ciambulawung River, Banten Province, based on Pollution Index and NSF-WQI. *Procedia Environmental Sciences,* 24, 228–237.

Gyawali, S., Techato, K. & Yuangyai, C. (2013). Assessment of Relationship between Land Uses of Riparian Zone and Water Quality of River for Sustainable Development of River Basin, A case study of U-Tapao River Basin, Thailand. *Procedia Environmental Sciences,* 17, 291–297.

Iran Department of Environment (2012). Siminehrood River Basin Pollution Study,1.

Li, Y.L., Liu, K., Li, L. & Zo, Z.X. (2012). Relationship of Land Use/Cover on Water Quality in the Liao River Basin, China. *Procedia Environmental Sciences,* 13(2011), 1484–1493.

Li, Y., Xu, L. & Li, S. (2009). Water Quality Analysis of the Songhua River Basin Using Multivariate Techniques. *Scientific Research*, 2, 110–121.

Said, A. & Stevens, D.K. (2004). An Innovative Index for Evaluating Water Quality in Streams. *Environmental Management,* 34(3), 406–414.

Sharifi, H. (2010). The Assessment of Engineering Geological Formations Properties in Siminehrood Watershed, M.Sc thesis, Tarbiat Modares university of Iran.

Tisseuil, C., Rushan, G.H.R., Nasrabadi, T. & Asadpour, G.A. (2013). Statistical Modeling of Future Lake Level under Climatic Conditions, Case study of Urmia Lake (Iran). International Journal of Environmental Research, 7(1), 69–80.

US EPA. (2000)**.** *Environmental Investigations Standard Operating Procedures and Quality Assurance Manual,* Region 4 Science and Ecosystem Support Division (SESD), Athens, GA

US EPA (1982). Handbook for Sampling and Sample Preservation of Water and Wastewater.

Wan, R., Cai, S.H., Li, H., Yang, G. & Li, Z.H. (2014). Inferring Land Use and Land Cover Impact on Stream Water Quality using a Bayesian Hierarchical Modeling Approach in the Xitiaoxi River. *Environmental Management,* 133, 1–11.

Zhang, W., Li, H., Sun, D. & Zhou, L. (2012). A Statistical Assessment of the Impact of Agricultural Land Use Intensity on Regional Surface Water Quality at Multiple Scales. *Environmental Research and Public Health,* 3, 4170–4186.

Zhao, J., Lin, L., Yang, K., Liu, Q. & Qian G. (2015). Influences of Land Use on Water Quality in a Reticular River Network Area : A case Study in Shanghai, China. *Landscape and Urban Planning,* 137, 20–29.

Proceedings of the 37th IAHR World Congress
August 13 – 18, 2017, Kuala Lumpur, Malaysia

COMPARISON OF DIFFERENT METHODS FOR PREDICTING ZONAL DISCHARGE OF STRAIGHT HETEROGENOUSLY ROUGHENED COMPOUND CHANNELS

XIAONAN TANG[(1)]

[(1)]Department of Civil Engineering, Xi'an Jiaotong-Liverpool University, Suzhou, China
xiao.tang@xjtlu.edu.cn

ABSTRACT

Accurate prediction of flow discharge in different parts of a compound river channel is increasingly important in river management, such as flood mitigation, eco-environment design, restoration and sediment transport. This paper compares four most recently developed 1-D methods, namely Interacting Divided Channel Method (IDCM), Energy Concept Method (ECM), Modified Divided Channel Method (MDCM) and Apparent Shear Stress Method (ASSM), against a wide range experimental data in this study and the data available in the literature. The 32 datasets used include heterogeneously roughened symmetric channels (22 datasets) and asymmetric channels (10 datasets) with various aspect ratios [channel total width (*B*) at bankfull / main channel bottom (*b*) =2.6 ~ 15.8], bed slopes (S_o = 4.3x10^{-4} ~1.3x10^{-2}), and ratios of Manning's roughness between floodplain and main channel (1.1 ~ 3.9). It is found that none of the methods performed well against all the datasets. Compared with the traditional Divided Channel Method (DCM), all above methods, in general, predict both the total discharge and main channel discharge reasonably well within 12%, but they have relatively large errors for the prediction of the zonal discharge, particularly for floodplain with large roughness. The ASSM has shown the best overall performance on both the total and zonal discharge prediction.

Keywords: Overbank flow; compound channel flow; heterogeneous compound channel; zonal discharge.

1 INTRODUCTION

Compound channels (or two-stage channels) with roughened floodplains widely exist in most natural rivers; in certain cases compound channels are deliberately constructed in order to increase conveyance capacity in times of floods, or create environmentally friendly space in the floodplain. Traditional one-dimensional (1-D) channel divisional methods, namely the Divided Channel Method (DCM), and the Single Channel Method (SCM), are still widely used in practice because of their simplicity. However, it is well-known these methods either overestimate or underestimate channel discharge, particularly for zonal discharge (i.e. discharge in main channel and its floodplain) (Wormleaton et al.,1982; Knight et al.,1984; Tang & Knight, 2007; Yang et al., 2007). When a floodplain is inundated, the velocity differences between the main channel and floodplain result in a mixing shear layer due to lateral momentum exchange. Early research (Wormleaton et al., 1982; Knight & Demetriou, 1983; Knight & Hamed, 1984; Prinos & Townsend, 1984; Christodoulou, 1992) indicated the importance of considering the main channel / floodplain interaction effects.

Despite the availability of 2-D or 3-D approaches that take into account the interaction between the main channel and floodplain, e.g. Krishnappan and Lau (1986), Shiono and Knight (1991), Cater and Williams (2008), Marjang and Merkley (2009), they are usually complex and require more information and turbulence parameters, which are not available. 1-D approach has still been developing even since due to its simplicity and practical significance.

In river management and water environmental design, it is required precisely to predict not only the overall discharge but also zonal discharge (main channel and floodplain discharge, respectively) in a compound river channel. Recently many newly developed 1-D methods have emerged, for example, the Interacting Divided Channel Method (IDCM) by Huthoff et al. (2008), the Energy Concept Method (ECM) by Yang et al. (2012), and the Modified Divided Channel Method (MDCM) by Khatua et al. (2012), Mohanty & Khatua (2014) and Devi et al. (2016). These methods had taken into account the effect of the lateral momentum exchange in different forms, and they were developed and validated based on their own limited data. Most recently, Tang (2016) compared these methods against a large set of data in homogenous compound channels and concluded that they can predict the total discharge reasonably well within an average error of 5% for symmetric compound channels, but do not for asymmetric channels, particularly in the prediction of zonal discharge. It is worth noting that heterogeneously roughened compound channels widely exist in natural rivers, so it is important to understand how good the above-mentioned methods are compared with each other for a wide range of data in heterogeneously roughened channels, particularly for zonal discharge.

In this paper, we compare four recently developed 1-D methods, namely the IDCM, ECM, MDCM, and the Apparent Shear Stress Method (ASSM) that are based on the force balance with the apparent shear stress proposed by Moreta and Martin-Vide et al. (2010), against a wide range of experimental data in this study and the data available in the literature. 32 datasets of heterogeneously roughened compound channel are used for comparison of the methods. These datasets include cases in both symmetric and asymmetric compound channels with different bed slope and a wide range of roughness ratio between floodplain to main channel. The datasets also cover various channel cross-sections (rectangular or trapezoidal).

2 METHOD

For the convenience of reference in the subsequent context, the sketched cross-sections of symmetric and asymmetric compound channels are shown in Figure 1, where H, h and h_f are the flow depth of main channel, bankfull, and floodplain (subscript f), respectively. b and b_f are the widths of the main channel bottom and floodplain, respectively; S_c and S_f are the side slopes of the main channel and floodplain, respectively.

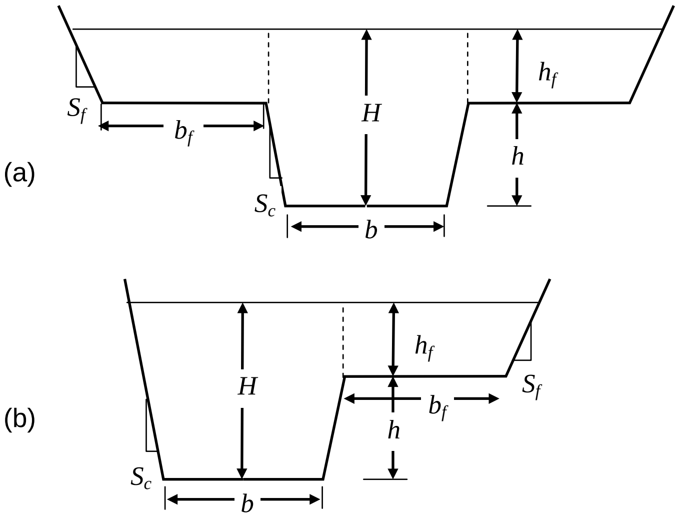

Figure 1. Sketched cross-sections of compound channels: (a) - symmetric cross-section, (b) - asymmetric cross-section.

In this study, the four methods that take into account the momentum transfer of flow between the main channel and the floodplain are summarized as follows:

2.1 Interacting divided channel method (IDCM)

As proposed by Huthoff et al. (2008), the zonal velocities were evaluated by considering the impact of apparent shear stress (τ_a) at the interface between main channel and its floodplain, as expressed by

$$\tau_a = \frac{1}{2}\rho\alpha_m(U_c^2 - U_f^2) \qquad [1]$$

Based on the force balance of each part of channels per unit length (i.e. main channel and floodplain), it follows,

$$\rho g A_c S_o = \rho f_c U_c^2 P_c + N_f \tau_a h_f \qquad [2]$$

$$\rho g A_f S_o = \rho f_f U_f^2 P_f - \tau_a h_f \qquad [3]$$

Then, the zonal velocities are

$$U_c^2 = U_{c,0}^2 - \frac{\frac{1}{2}\alpha_m N_f \epsilon_c (U_{c,0}^2 - U_{f,0}^2)}{1+\frac{1}{2}\alpha_m(N_f\epsilon_c+\epsilon_f)} \qquad [4]$$

$$U_f^2 = U_{f,0}^2 + \frac{\frac{1}{2}\alpha_m \epsilon_f (U_{c,0}^2 - U_{f,0}^2)}{1+\frac{1}{2}\alpha_m(N_f\epsilon_c+\epsilon_f)} \qquad [5]$$

with the coefficients:

$$\epsilon_c = h_f/f_c P_c \quad [6a]$$

$$\epsilon_f = h_f/f_f P_f \quad [6b]$$

Where *U* is the cross-sectional velocity, A is the cross-sectional area, ρ is the density of fluid, S_o is the bed slope of channel, α_m is the interface coefficient, h_f is the depth of flow at the interface (i.e. the flow depth of floodplain), *P* is the wetted perimeter, *f* is the frictional factor, N_f is the number of floodplain, the subscripts *c* & *f* denote the main channel and floodplain respectively, and the subscript (,0) denotes the values based on DCM with vertical interface excluded.

Huthoff et al. (2008) validated their method using 11 sets of laboratory data in homogeneous channels and recommended a constant for the interface coefficient (α_m =0.02). However, the efficiency of the method for predicting zonal discharges was not undertaken by Huthoff et al.

2.2 Modified divided channel method (MDCM)

Many modified division channel methods have been developed to improve the prediction of stage-discharge. Here described is the one recently proposed by Khatua et al. (2012), who quantified the boundary shear stress distribution in a compound channel based on a new parameterization of the interface shear stress between the main channel and floodplain.

$$P_c\tau_c + X_c\tau_c = \rho g A_c S_o \quad [7a]$$

$$P_f\tau_f + X_f\tau_f = \rho g A_f S_o \quad [7b]$$

Where τ is the averaged boundary shear stress, S_o is the bed slope of channel, *A* is the cross-sectional area, and *X* is the interacting length, which is calculated by,

$$X_c = \frac{100P_c}{(100-\%S_f)[1+(\alpha-1)\beta]} - P_c \quad [8a]$$

$$X_f = P_f - \frac{100(\alpha-1)\beta}{\%S_f[1+(\alpha-1)\beta]} P_f \quad [8b]$$

Where the geometrical parameters α and β are *B/b* and *(H-h)/H*, respectively; $\%S_f$ is the percentage of boundary shear force of the floodplain. Through the data analysis, Khatua et al. (2012) found $\%S_f$ can be calculated by,

$$\%S_f = 4.1045\ (\%A_f)^{0.6917} \quad [9]$$

Thus, the zonal discharges are

$$Q_c = \frac{\sqrt{S_o}}{n_c} A_c^{5/3} (P_c + X_c)^{-2/3} \quad [10a]$$

$$Q_f = \frac{\sqrt{S_o}}{n_f} A_f^{5/3} (P_f - X_f)^{-2/3} \quad [10b]$$

Where $\%A_f$ is the percentage of the floodplain area, *n* is the Manning coefficient, and *Q* is the discharge. It is worth noting that Eq. [9] was obtained based on experimental data, which have the width ratio (α) up to 6.67 for smooth, straight and symmetric compound channels. Considering the impact of roughness of floodplain, Mohanty & Khatua (2014) extended Eq.[9] for symmetric compound channels as follows:

$$\%S_f = 3.3254(\%A_f)^{0.7467} \times (1 + 1.02\sqrt{\beta}\log_{10}(\gamma) \quad [11]$$

Where γ is the ratio of Manning coefficient between main channel and floodplain ($=n_f/n_c$).
Most recently, Devi et al. (2016) developed anequation similar to Eq.[9] for asymmetric compound channels as follows:

$$\%S_f = 3.576(\%A_f)^{0.717} \quad [12]$$

2.3 Apparent shear stress method (ASSM)

Due to the velocity difference between the main channel and floodplain, the momentum transfer exists. This can be evaluated by the apparent shear stress (τ_a) at the interface. Unlike the expression of Eq.[1], (τ_a) is directly related to the velocity difference, given by,

$$\tau_a = \frac{1}{2}\rho\alpha_d(U_{c,0} - U_{f,0})^2 \qquad [13]$$

where α_d is the interface coefficient. Based on the force balance similar to Eqs. [2] and [3], we can obtain,

$$U_c^2 = U_{c,0}^2 - \frac{8\, N_f\, h_f\, \tau_a}{\rho\, f_c\, P_c} \qquad [14a]$$

$$U_f^2 = U_{f,0}^2 + \frac{8\, h_f \tau_a}{\rho f_f P_f} \qquad [14b]$$

Various formulae had been proposed to evaluate the coefficient (α_d) in Eq. [13]. In this study, Moreta and Martin-Vide (2010)'s formula was used because their formula was proposed based on a wide range of data, and demonstrated to have better performance against other methods for homogeneous compound channels (Tang, 2016). They related α_d to the geometric parameters and relative roughness, given by

$$\alpha_d = K_1 \frac{B}{B_c}\left(\frac{h}{B_c} Dr\right)^{-1/3} - K_2 Dr^{\frac{1}{3}} \left(\frac{n_f}{n_c} - 1\right)^{-\delta} \qquad [15]$$

Where $Dr = (H\text{-}h)/H$, the same as β in the MDCM method by Khatua et al. (2012), and B_c is the width of main channel at bankfull. Moreta and Martin-Vide (2010) suggested that for symmetric channels: K_1 = 0.004, K_2 = 0.018, δ = 0.2 for small-scale flumes; K_1 = 0.003, K_2 = 0.002, δ = 2 for large-scale flumes; however, for asymmetric channels, the corresponding values of K_1 are 0.005 (small-scale flumes) and 0.004 (large-scale flumes), although there is not any clear criterion for the classification of flume scale. It is also worth noting that Eq.[15] is not validated by rough asymmetric compound channels and limited to B/b< 6.7.

2.4 Energy Concept Method (ECM)

Based on the energy loss and the transition mechanics of fluid in open channels, Yang et al. (2012) proposed a method for estimating the discharge in straight, symmetrical compound channels, as expressed by the following equation,

$$Q_t = Q_{c,0} + Q_{f,0} - \frac{\tau_a\,(H+h_f)(U_{c,0}-U_{f,0})}{4\rho g S_o} \qquad [16]$$

Where *g* is the gravitational acceleration and the subscript (,0) denotes the values using DCM. Yang et al. evaluated Eq. [16] by examining various formulae of the apparent shear stress term (τ_a), including Eqs. [1] and [13]. They recommended Eq. [13] to be used with α_d= 0.01B/b, which is proposed by Christodoulou (1992) due to its simplicity and accuracy in the calculation. Noting that the α_d proposed by Christodoulou was valued only by homogeneous compound channels, so the α_d given by Eq.[15] for the ECM method was used in this study. Furthermore, this method cannot predict the zonal discharge but the total discharge. Therefore, this method was not included in the comparison of zonal discharge.

3 DATA FOR ANALYSIS

To compare the four methods in Section 2, a wide range of different experimental data was used in heterogeneously roughened compound channels. These data were from www.flowdata.bham.ac.uk (created by the author) and the literature. A total of 32 datasets used included 22 datasets of symmetric compound channel and 10 datasets of asymmetric compound channel, with the aspect ratio (*B/b*) being 2.6 ~ 15.8 and the bed slope being S_o = 4.3x10^{-4} ~1.3x10^{-2}. The datasets also covered various channel cross-sections (rectangular or trapezoidal) either symmetric (sym) or asymmetric (asym). The details are shown in Table 1, where N_f is the number of floodplain, *N* is the number of experiment runs, and other notations can be referred to Figure 1. It is worth noting that Manning's coefficient (n_f) of floodplain was the averaged value for the experiments where large elements were used to roughen the floodplain.

Table 1. Details of experimental datasets of heterogeneously roughened compound channels.

Series	N_f	N	n_c	n_f/n_c	b_f(m)	b (m)	B/b	S_c	S_f	Q_t (m^3/s)	Dr
FCF data (1992), S_o= 0.001027, h =0.15 m											
FCF7	2	8	0.01	1.04-3.78	2.25	1.50	4.20	1	1	0.2160-0.5434	0.038-0.504
FCF11	2	7	0.01	1.36-3.78	2.25	1.50	4.40	2	1	0.2601-0.6066	0.096-0.505
University of Birmingham (2001), S_o=0.002024, h=0.05 m											
UB05	2	9	0.0091	1.59-5.51	0.4073	0.398	3.05	0	0	0.0148-0.0501	0.234-0.702
UB01	2	7	0.0091	1.77-2.67	0.4073	0.398	3.05	0	0	0.0149-0.0343	0.197-0.521
Knight and Hamed (1984), S_o=0.000966, h=0.076 m											
DWK4	2	6	0.0097	1.11-1.17	0.229	0.152	4.01	0	0	0.0052-0.0297	0.104-0.511
DWK6	2	6	0.0097	1.38-1.63	0.229	0.152	4.01	0	0	0.0054-0.0264	0.113-0.515
DWK7	2	6	0.0097	1.74-2.41	0.229	0.152	4.01	0	0	0.0051-0.0211	0.113-0.502
DWK9	2	6	0.0097	2.51-4.78	0.229	0.152	4.01	0	0	0.0043-0.0158	0.137-0.505
Prinos and Townsend (1984), S_o=0.0003, h=0.102 m											
PT03	2	5	0.011	1.27	0.381	0.203	5.26	0.5	0	0.0061-0.0180	0.089-0.329
PT04	2	5	0.011	1.64	0.381	0.203	5.26	0.5	0	0.0055-0.0161	0.089-0.329
PT05	2	5	0.011	2.00	0.381	0.203	5.26	0.5	0	0.0048-0.0140	0.089-0.329
PT06	2	5	0.011	1.27	0.381	0.305	3.83	0.5	0	0.0096-0.0245	0.089-0.329
PT07	2	5	0.011	1.64	0.381	0.305	3.83	0.5	0	0.0087-0.0225	0.089-0.329
PT08	2	5	0.011	2.00	0.381	0.305	3.83	0.5	0	0.0082-0.0204	0.089-0.329
Wormleatonet al. (1982), S_o=0.00043, h=0.12 m											
W-B	2	6	0.01	1.40	0.46	0.29	4.17	0	0	0.0170-0.0480	0.205-0.429
W-C	2	8	0.01	1.70	0.46	0.29	4.17	0	0	0.0115-0.0430	0.143-0.429
W-D	2	8	0.01	2.10	0.46	0.29	4.17	0	0	0.0090-0.0380	0.143-0.429
Patra et al. (2012), S_o=0.000311,h=0.08m											
Patra	2	6	0.0098	1.12	0.805	0.12	15.75	1	0	0.0475-0.0908	0.281-0.408
Hu et al. (2010), S_o=0.001, h=0.06 m											
Hu	2	7	0.011	1.18	0.35	0.30	3.33	0	0	0.0091-0.0388	0.134-0.535
Joo et al. (2007), S_o=0.013, h=0.05m											
JS	1	8	0.011	2.00	0.20	0.05	5.00	0	0	0.0030-0.0061	0.207-0.342
James and Brown (1977), S_o=0.001, h=0.069m(sym), 0.508 m (asym)											
JB131	2	7	0.01	1.60	0.502	0.243	5.71	1	1	0.0115-0.0328	0.097-0.385
JB51	1	14	0.01	1.20	0.191	0.178	2.64	1	1	0.0041-0.0138	0.025-0.444
JB61	1	15	0.01	1.20	0.368	0.243	3.64	1	1	0.0041-0.0142	0.123-0.413
JB71	1	12	0.01	1.20	0.572	0.243	4.79	1	1	0.0046-0.0143	0.058-0.378
James and Brown (1977), S_o=0.002, h=0.069 m(sym), 0.508 m (asym)											
JB132	2	6	0.01	1.60	0.502	0.243	5.71	1	1	0.0141-0.0330	0.048-0.337
JB52	1	11	0.011	1.09	0.191	0.178	2.64	1	1	0.0054-0.0142	0.042-0.389
JB62	1	14	0.011	1.09	0.368	0.243	3.64	1	1	0.0061-0.0142	0.079-0.351
JB72	1	9	0.011	1.09	0.572	0.243	4.79	1	1	0.0057-0.0137	0.025-0.291
James and Brown (1977), S_o=0.003, h=0.069 m(sym), 0.508 m (asym)											
JB133	2	5	0.01	1.60	0.502	0.243	5.71	1	1	0.0162-0.0340	0.044-0.296
JB53	1	11	0.011	1.09	0.191	0.178	2.64	1	1	0.0061-0.0157	0.002-0.369
JB63	1	14	0.011	1.09	0.368	0.243	3.64	1	1	0.0060-0.0144	0.048-0.311
JB73	1	8	0.011	1.09	0.572	0.243	4.79	1	1	0.0065-0.0148	0.008-0.282

4 RESULTS AND DISCUSSION

To evaluate the error of each method against the experimental data, the percentage of error in predictive discharge was used as a criterion for the purpose of method evaluation. The percentage of error in predicted discharge of each flow depth is calculated by:

$$\%E_{Q,i} = \frac{|Q_{cal,i} - Q_{exp,i}|}{Q_{exp,i}} \times 100\% \qquad [17]$$

Where $\%E_{Q,i}$ is the percentage error of predicted discharge, and $Q_{cal,i}$ and $Q_{exp,i}$ are the predicted and observed discharge at i^{th} flow depth, respectively. Therefore, the average error of each method for an experiment is obtained by

$$\%E_Q = \frac{1}{N}\sum_{i=1}^{N}(\%E_{Q,i}) \qquad [18]$$

Where N is the total number of runs.

Table 2 shows the average percentage errors of predicted discharge by the four methods for all 32 datasets, where subscriptst, c, f denote the values for the total channel, main channel, and floodplain, respectively. For comparison, the results using the DCM are also given in Table 2. The corresponding results of $\%Q_t$ are given in Figure 2. For convenience, in the subsequent figures, Sym = symmetric channels, Asym=asymmetric channels, Mean = the average for all channels.

Table 2. Summary of averaged percentage errors of methods for predicting discharges.

Series	ECM	IDCM			MDCM			ASSM			DCM		
	$\%Q_t$	$\%Q_c$	$\%Q_f$	$\%Q_t$	$\%Q_c$	$\%Q_f$	$\%Q_t$	$\%Q_c$	$\%Q_f$	$\%Q_t$	$\%Q_c$	$\%Q_f$	$\%Q_t$
FCF7	21.62	15.79	37.48	18.97	2.58	39.84	10.08	4.35	35.18	8.82	33.21	32.30	29.78
FCF11	20.76	16.73	79.18	25.42	2.68	85.01	14.00	3.06	73.93	13.13	38.71	54.92	39.91
BU05	31.38	27.70	34.40	28.21	46.56	49.46	18.07	19.05	32.77	14.61	88.15	24.93	65.28
BU01	20.68	16.31	20.33	17.95	2.43	34.81	7.08	15.36	14.67	14.92	44.26	11.45	34.29
DWK4	5.66	2.56	8.63	2.72	5.02	10.47	2.45	10.79	9.83	4.06	16.49	12.91	6.65
DWK6	4.93	5.23	10.19	4.92	12.61	9.52	7.24	4.37	16.90	3.81	16.09	21.96	3.34
DWK7	6.43	3.24	19.73	5.62	13.30	13.12	10.57	1.50	26.12	7.01	26.84	32.94	6.83
DWK9	3.03	15.00	26.84	8.58	25.34	16.89	17.36	13.28	30.77	12.87	56.42	39.90	24.93
Hu	4.46	22.46	43.79	2.54	28.25	54.30	4.92	15.47	31.36	3.33	11.37	27.10	3.58
JS	5.37	18.23	27.75	21.05	6.92	41.51	13.27	3.91	35.99	14.84	36.36	15.55	27.67
PT03	9.00			11.21			14.46			11.96			19.47
PT04	13.24			18.74			21.34			17.65			30.54
PT05	16.67			26.07			27.18			22.68			40.68
PT06	8.89			10.26			11.22			11.36			17.30
PT07	9.33			13.00			13.46			12.93			22.45
PT08	11.22			15.67			16.16			15.75			28.47
W-B	7.28			5.90			5.42			5.68			14.23
W-C	12.95			17.34			13.81			13.35			30.93
W-D	19.85			24.53			20.60			18.48			43.14
Patra	1.89			2.99			8.02			2.81			6.61
JB131	4.97			3.32			4.15			3.13			10.77
JB132	12.37			8.31			9.25			5.59			17.30
JB133	11.71			9.46			10.01			4.79			17.70
JB51	5.33			2.23			6.00			3.92			5.30
JB52	5.01			3.80			6.51			5.05			6.08
JB53	13.57			5.45			8.09			6.61			7.68
JB61	1.52			1.52			4.18			1.94			4.23
JB62	3.29			0.94			3.19			1.60			3.01
JB63	6.32			5.43			7.44			5.76			7.80
JB71	10.57			2.01			0.89			2.88			1.01
JB72	24.75			6.67			6.44			8.07			5.06
JB73	25.29			1.36			2.93			1.75			2.86

As shown in Table 2, compared with the DCM, all four methods, which take into account the momentum transfer of flow between the main channel and floodplain, show an overall improved prediction of total discharge (Q_t), although the ECM does not performance well for asymmetric channels. This is not surprising because the ECM method was based on symmetric channels, and not validated by compound channels with roughened floodplain. Figure 3 demonstrates that all four methods have the combined average percentage of error less than 12%, whereas the DCM overestimates the discharge with the combined averaged percentage of error larger than 20%. Further analysis in Figure 4 shows that the roughness of floodplain affects the precision of prediction, i.e. all four methods give a better prediction of total discharge for the relative lower ratio of roughness ($\gamma = n_f/n_c < 2$) than that for the higher ratio of roughness (γ>2).

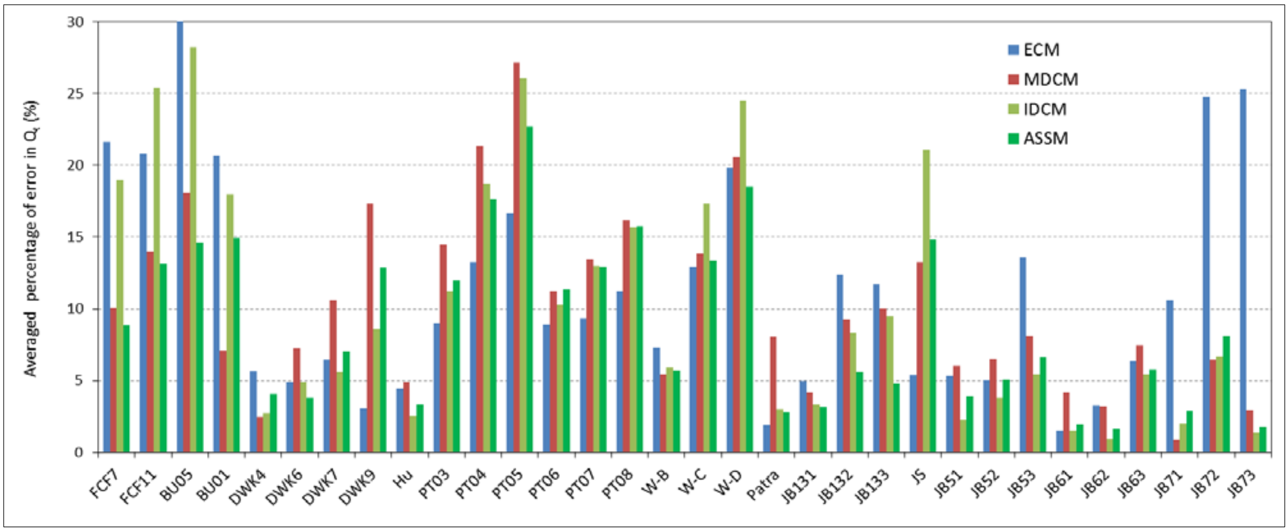

Figure 2. Averaged percentage error of total discharge (%Q_t) by four methods in heterogeneous channels.

This is true for both symmetric and asymmetric channels. Among the four methods, the ASSM gives the best results in the prediction of overall discharges (Q_t), and the other three methods (ECM, MDCM and IDCM) have a similar prediction precision of total discharge. This is not surprising because the ASSM takes various geometric parameters into account, namely the interface coefficient (α_d) of apparent shear stress (τ_a) for predicting the discharge.

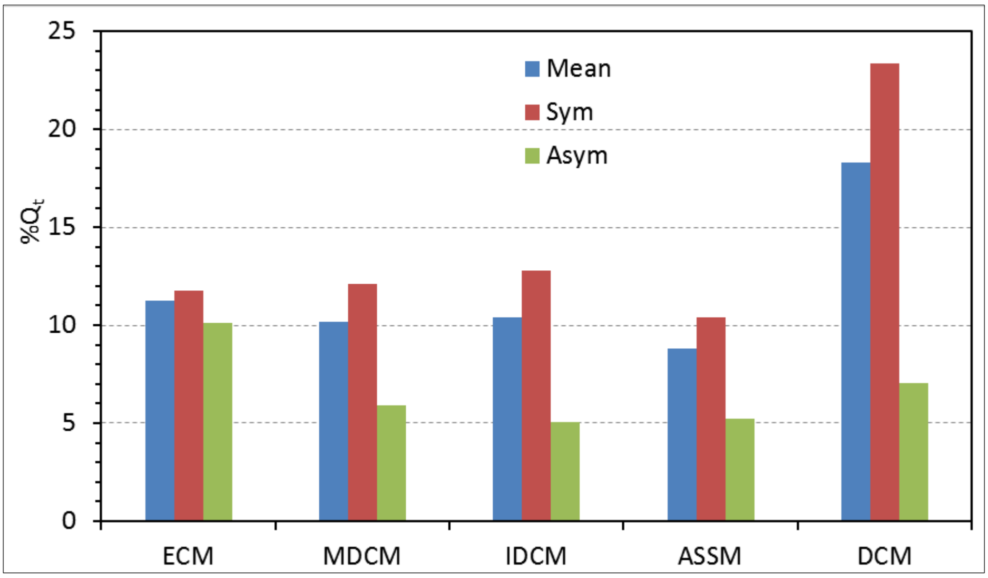

Figure 3. Averaged percentage errors of Q_t.

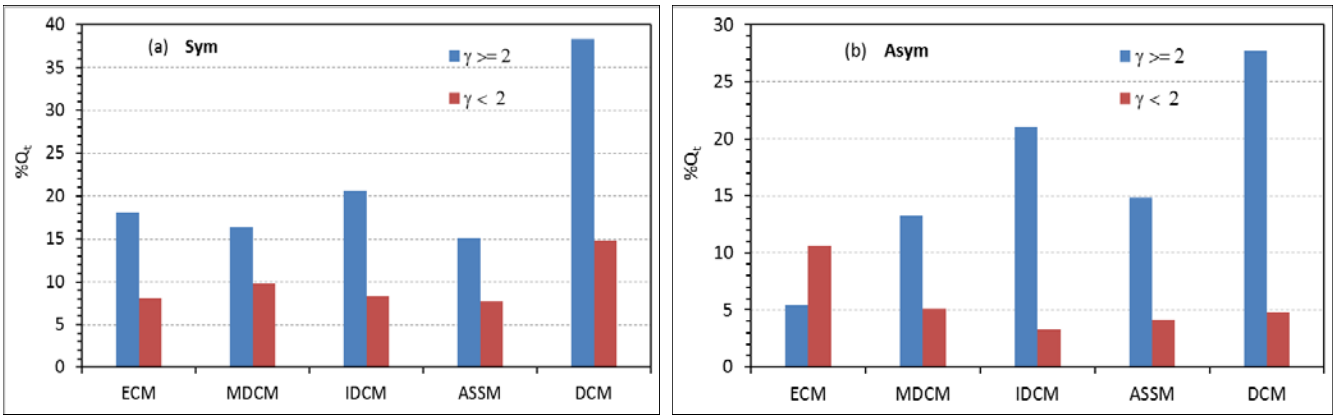

Figure 4. Averaged percentage errors of Q_t for (a)symmetric and (b) asymmetric channels.

For zonal discharge, the ECM is excluded in the analysis due to its incapability. As shown in Figure 5, all the methods significantly improve the prediction of main channel discharge within an averaged error below 15%, particularly the ASSM within an error less than 10%; however, they do not have any improvement for the prediction of floodplain discharge compared with the DCM. Although the ASSM isn't significantly different from the MDCM and IDCM in zonal discharge prediction, the ASSM shows good prediction of zonal discharge percentage (both Q_c/Q_t and Q_f/Q_t). This can be seen in Figure 6 as an example, where both the MDCM and IDCM underestimate the discharge percentage of main channel, but overestimate the discharge percentage of floodplain, particularly in higher relative flow depths of floodplain.

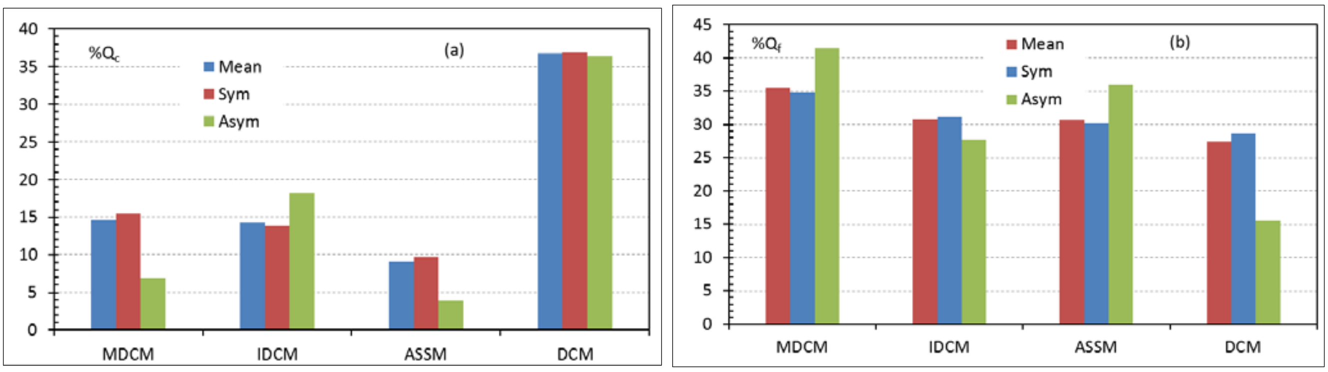

Figure 5. Averaged percentage errors: (a)%Q_c; (b) %Q_f.

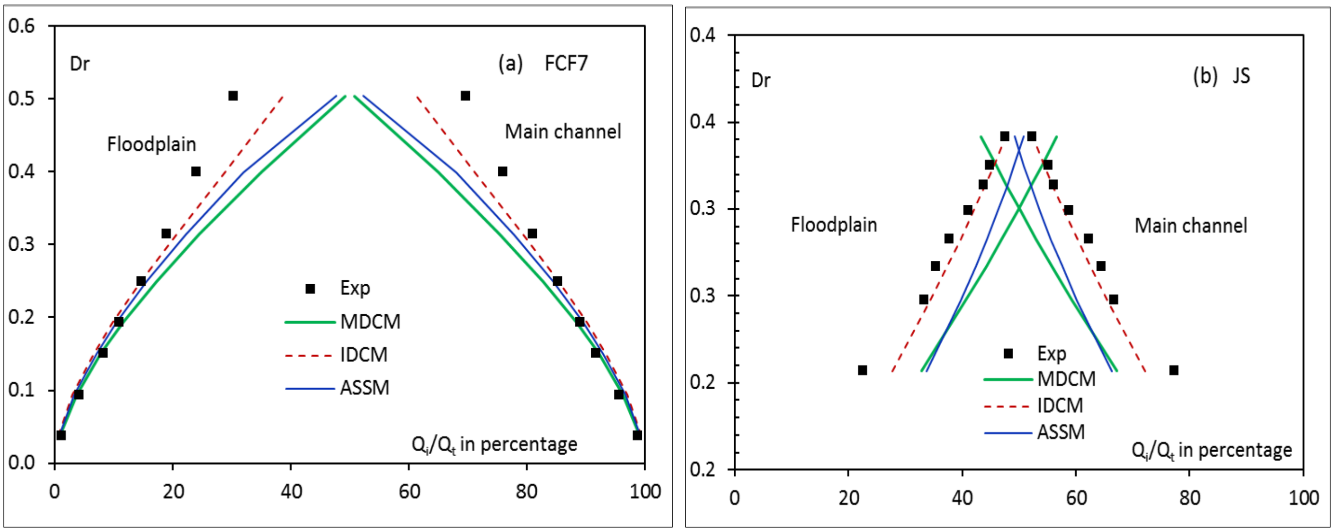

Figure 6. Comparison of zonal discharge percentage for: (a) FCF7, (b) JS.

Finally, it is worth noting that in all four methods except the IDCM, the roughness of floodplain had been taken into account in the prediction of discharge, while a single value of parameter α_m (=0.02) was used in the IDCM for channels with various roughened floodplains. Therefore, it is not surprising that the IDCM has shown relatively higher errors in the prediction of total discharge (see Figure 4).

5 CONCLUSIONS

Through comparison against a wide range of data in heterogeneously roughened compound channels, the four recently developed methods that take into account the impact of momentum transfer between the main channel and floodplain show that:

- Compared with DCM, all four methods improve the prediction of total discharge with the precision within 12% for roughened compound channels and the ASSM gives the best overall results, whereas the DCM has an averaged error over 20%. The four methods improve the prediction of total discharge significantly as the ratio of roughness between floodplain and main channel reduces; for example, the percentage of error in discharge reduces almost half when γ (=n_f/n_c) changes from above 2 to below 2.
- The four methods can also improve the prediction of main channel discharge within an averaged error less than 15% for symmetric channels, but they do not perform well for the prediction of floodplain discharge. Furthermore, except the ASSM, the other methods do not predict zonal discharge percentage well. Typically, they overestimate the discharge percentage of floodplain but underestimate the discharge percentage of main channel, particularly for the higher relative flow depth of floodplain.
- In general, the ASSM can be used to predict total discharge within an average error less than 10%, which can be further improved with decreasing ratio of roughness (γ). However, for zonal discharge prediction, none of these methods predicts well, so further study is needed, especially for asymmetric roughened floodplain compound channels.

NOTATION

%A_f= area percentage of floodplain
%S_f= shear force percentage of floodplain
B= width of main channel at bankfull
b= width of main channel bottom
D_r= relative depth of floodplain,= $(H-h)/H$
f= friction factor
g= acceleration of gravity
h= bankfull height
H= main channel depth
h_f= flow depth of floodplain
n= Manning's coefficient
N_f= number of floodplain
Q= discharge of cross-section
S_o= bed slope of channel
U= mean velocity of cross-section
X= interaction length
α= aspect ratio, = B/b
α_m= interface coefficient (also α_d)
ρ= density of water
γ= ratio of Manning coefficients between main channel and floodplain, =n_f/n_c
τ= averaged shear stress of boundary
τ_a= apparent shear stress at the interface

Subscripts:
,0= reference values based on DCM
c= main channel
f= floodplain
t= total

REFERENCES

Al-Khatib, I.A., Dweik, A.A. & Gogus, M. (2012). Evaluation of Separate Channel Methods for Discharge Computation in Asymmetric Compound Channels. *Flow Measurement and Instrumentation*, 24, 19-25.

Cater, J.E. & Williams, J.J.R. (2008). Large Eddy Simulation of a long Asymmetric Compound Open Channel. *Journal of Hydraulic Research*, 46(4), 445-453.

Christodoulou,G.C.(1992). Apparent Shear Stress in Smooth Compound Channels. *Water Resources Management*, 6(3), 235-247.

Devi,K., Khatua, K.K. & Das,B.S. (2016). *Apparent Shear in an Asymmetric Compound Channel*, *River Flow 2016*,Constantinescu, Garcia & Hanes (Eds), 48-56; July 12-15, St. Louis, USA.

Hu, C., Ju, Z. & Guo,Q. (2010). Flow Movement and Sediment Transport in Compound Channels. *Journal of Hydraulic Research*, 48(1), 23–32.

Huthoff,F., Roos,P.C., Augustijn,D.C.M. & Hulscher,S.J.M.H. (2008). Interacting Divided Channel Method for Compound Channel Flow. *Journal of Hydraulic Engineering*, 134(8), 1158-1165.

James, M. & Brown, B.J. (1977). *Geometric Parameters That Influence Food Plain Flow*. *Research report H-77-I*, U.S. Army. Vicksburg, Missouri, U.S.A: Hydraulic Laboratory.141pp.

Jazizadeh, F. & Zarrati,A.R. (2008). Development of a Three-Dimensional Numerical Model to Solve Shallow-Water Equations in Compound Channels. *Journal of Civil Engineering*, 35(9), 963-974.

Joo, C.B.H. & Seng,D.M.Y. (2007). Study of Flow in a Non-Symmetrical Compound Channel with Rough Flood Plain. *The Institution of Engineers Journal*, 69(2), 18-26.

Khatua, K.K. Patra, K.C. & Mohanty, P.K. (2012). Stage-Discharge Prediction for Straight and Smooth Compound Channels with Wide Flood Plains. *Journal of Hydraulic Engineering*, 138 (1), 93–99.

Knight, D.W. & Demetrious,J.D. (1983). Flood Plain and Main Channel Flow Interaction. *Journal of Hydraulic Division (ASCE)*, 109 (8), 1073-1092.

Knight, D.W. & Hamed, M.E. (1984). Boundary Shear in Symmetrical Compound Channels. *Journal of Hydraulic Engineering*, 110(10), 1412-1430.

Krishnappan, B.G. & Lau, Y.L. (1986). Turbulence Modeling of Flood Plain Flows. *Journal of Hydraulic Engineering*, 112(4), 251-266.

Marjang, N. & Merkley, G.P. (2009). Velocity Profile Modelling in Rectangular and Compound Open-Channel Cross Sections. *Irrigation Science*, 27(6), 471–484.

Mohanty,P.K. & Khatua, K.K. (2014). Estimation of Discharge and its Distribution in Compound Channels. *Journal of Hydrodynamics*, 26(1), 144-154.

Moreta, P.J.M. & Martin-Vid, J.P. (2010). Apparent Friction Coefficient in Straight Compound Channels. *Journal of Hydraulic Research*, 48(2), 169–177.

Myers, W., Knight, D.W., Lyness, J.F., Cassells, J.B. & Brown, F. (1999). Resistance Coefficients for Inbank and Overbank Flows. *Proceeding of Institution of Civil Engineers Water, Maritime & Energy*, 136, 105-115.

Noutsopoulos, G. & Hadjipanos, P. (1983). Discharge Computations in Compound Channels. *Proceeding of 20th IAHR Congress*, Moscow, 5, 173-180.

Patra, K.C, Sahoo, N. & Khatua, K.K. (2012). Distribution of Boundary Shear in Compound Channel with Roughness Flood Plain. *9th international conference on Advances in Fluid Mechanics*, June 28, University of Split,Croatia.

Prinos, P. & Townsend, R.D. (1984). Comparison of Methods for Predicting Discharge in Compound Open Channels. *Advanced Water Resource*s, 7, 180-187.

Shiono, K. & Knight,D.W. (1991). Turbulent Open Channel Flow with Variable Depth across the Channel. *Journal of Fluid Mechanics*, 222, 617-646.

Tang, X. (2016).*Critical Evaluation on Different Methods for Predicting Zonal Discharge of Straight Compound Channels.* River Flow 2016, Constantinescu, Garcia & Hanes (Eds), 57-64; July 12-15, St Louis, USA.

Tang, X. & Knight,D.W. (2007).An Improved Discharge Prediction Method for Overbank Flows. *Proceeding of 2nd Congress of IAHR*, July 1-6, Venice, Italy.

University of Birmingham (2001). *Flow database* [online]. Retrieved from: www.flowdata.bham.ac.uk.

Wormleaton, P.R., Allen, J. and Hadjipanos,P. (1982). Discharge assessment in compound channel flow. *Journal of Hydraulic Division (ASCE)*, 108 (9), 975-994.

Yang, K., Cao, S. & Liu,X. (2007). Flow Resistance and Its Prediction Methods in Compound Channels. *Acta Mechanica Sin*ica, 23(1), 23-31.

Yang, Z., Gao,W. & Huai, W. (2012). Estimation of Discharge in Compound Channels Based on Energy Concept. *Journal of Hydraulic Research*, 50(1), 105-113.

Proceedings of the 37th IAHR World Congress
August 13 – 18, 2017, Kuala Lumpur, Malaysia

IMPROVED DISCHARGE PREDICTION OF STRAIGHT COMPOUND CHANNELS BASED ON ENERGY TRANSITION

XIAONAN TANG[1]

[1] Department of Civil Engineering, Xi'an Jiaotong-Liverpool University, Suzhou, China
xiao.tang@xjtlu.edu.cn

ABSTRACT

Accurate estimation of flow discharge in a compound river channel is increasingly important in river management and eco-environment design. In this paper, a new model is proposed to improve the prediction of flow based on Energy Concept Method (ECM) and Weighted Divided Channel Method (WDCM) along with the apparent shear stress at the interface between main channel and floodplain. The new model is compared with a wide range of our experimental data and the data available in the literature. The 26 datasets used include homogenously roughened symmetric channels (22 datasets) and asymmetric channels (4 datasets) with various aspect ratios [channel total width (B) at bankfull / main channel bottom (b) =1.5 ~ 15.8] and bed slopes (S_o = 4.3x10^{-4} ~1.3x10^{-2}). It is found that the new model has significantly improved the accuracy of flow prediction compared with the ECM and DCM methods against all the datasets, particularly for relatively low flow depths of floodplain where the flow discharge is most difficult to predict correctly. The new model predicts the total discharge well for both symmetric and asymmetric channels, within an averaged relative error of 5%.

Keywords: Overbank flow; compound channel flow; energy transition; zonal discharge; symmetric and asymmetric channel.

1 INTRODUCTION

Many natural rivers and man-made channels have a compound cross-section, which consists of one deep main channel bounded with one or two shallow floodplains. Such a compound channel will increase conveyance capacity of channel in times of floods when the flow is above the bankfull stage, or provide environmental friendly space in the floodplain where no flow exists in dry seasons. Conventional one-dimensional (1-D) channel divisional methods, namely the Single Channel Method (SCM) and the Divided Channel Method (DCM), are still widely used to predict discharge in practice because of their simplicity. However, it is well-known that these methods either under-estimate or over-estimate channel discharge (Wormleaton et al., 1982; Knight et al., 1984; Tang & Knight, 2007; Yang et al., 2007). When a floodplain is inundated, the velocity differences between the main channel and floodplain result in a mixing shear layer due to lateral momentum exchange. Sellin (1964) carried out experimental study on the mechanism of momentum transfer in a compound channel; afterward many other researches indicated the importance of taking into account the main channel / floodplain interaction effects in the prediction of compound channel discharge (Wormleaton et al., 1982; Knight & Demetriou, 1983; Knight & Hamed, 1984; Prinos & Townsend, 1984; Christodoulou, 1992).

Despite the availability of 2-D or 3-D approaches that takes into account the interaction between the main channel and floodplain, e.g. Krishnappan and Lau (1986), Shiono and Knight (1991), Cater and Williams (2008), Marjang and Merkley (2009), they are usually very complex and require more information and turbulence coefficients, which are not available. 1-D approach has still been developing ever since due to its simplicity and practical significance.

In the river management and environmental assessment, it is required precisely to predict not only the overall discharge but also zonal discharge (i.e. both main channel and floodplain discharge) in a compound river channel. Various 1-D methods have recently been developed to improve the prediction of flow discharge. These recently developed methods, for example, include the Weighted Divided Channel Method (WDCM) by Lambert & Myers (1998), the Interacting Divided Channel Method by Huthoff et al. (2008), the Energy Concept Method (ECM) by Yang et al. (2012), the Apparent Shear Stress Method (ASSM) (Wormleaton & Merrett, 1990; Christodoulou, 1992; Moreta & Martin-Vide, 2010), and the Modified Divided Channel Method (Khatua et al., 2012; Mohanty & Khatua, 2014; Devi et al., 2016). These methods have taken into account the effect of the lateral momentum exchange either directly or indirectly, and they were developed and validated based on their own limit data. Most recently, Tang (2016) compared these methods against a large set of data in homogenous compound channels and concluded that they predict the total discharge reasonably well within an averaged error of 8% for symmetric compound channels, but do not for asymmetric channels, particularly in the prediction of zonal discharge. Moreover, none of these recently developed methods can predict discharge well in relatively low flow depths of floodplain.

In this paper, we develop a new model to improve the prediction of flow discharge against a wide range of 26 datasets, based on the ECM and WDCM along with the apparent shear stress at the interface between the main channel and floodplain. These datasets include data of both symmetric and asymmetric compound channels with different bed slopes. The new model has significantly improved the accuracy of flow prediction compared with the ECM against all the datasets, particularly for relatively low flow depths of floodplain where the flows are most difficult to predict correctly.

2 METHOD

For the convenience of reference in the subsequent sections, Figure 1 shows the sketched cross-sections of symmetric and asymmetric compound channels, where H, h and h_f are the flow depths of main channel, bankfull, and floodplain (subscript *f*), respectively; b and b_f are the widths of main channel bottom and floodplain, respectively; S_c and S_f are the side slopes of main channel and floodplain, respectively.

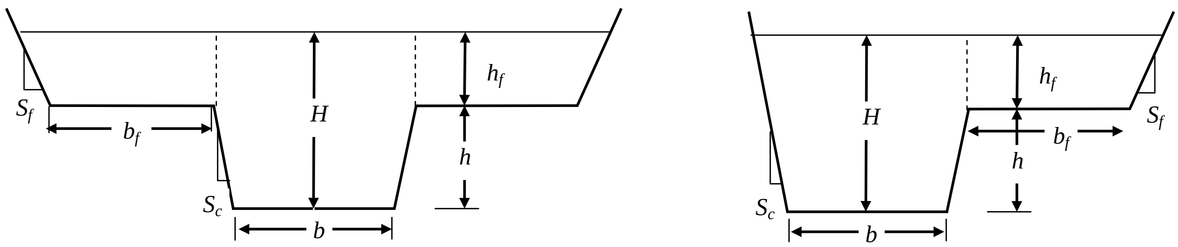

(a) (b)

Figure 1. Sketched cross-sections of compound channels: (a) symmetric, (b) asymmetric cross-section.

In the present paper, the new developed model is based on the Energy Concept Method (ECM) proposed by Yang (2012), and the basic discharge is assessed based on the Weighted Divided Channel Method (WDCM) proposed by Lambert & Myers (1998). In the following section, it is necessary to briefly introduce the ECM, followed by the new model.

2.1 Energy concept method (ECM)

Consider a water body of unit length in an open channel, the total energy E_t per unit time can be described by

$$E_t = \rho g S_f Q_t \quad [1]$$

where ρ is the density of water, g is the gravitational acceleration, S_f is the energy slope, and Q_t is the total discharge.

In a compound channel, the energy loss and transition take place along both the vertical (z-direction) and transverse (y-direction) directions due to the existence of velocity difference, as illustrated in Figure 2. Based on energy conservation, E_t has to be equal to the energy loss and transition along both directions, resulting in

$$E_t = E_{LV}^t + E_{TV}^t + E_{LT}^t + E_{TT}^t \quad [2]$$

where E_{LV}^t and E_{TV}^t are the total energy loss and transition along the vertical direction, respectively; E_{LT}^t and E_{TT}^t are the total energy loss and transition along the transverse direction, respectively. Replacing E_t of Eq. [1] by Eq. [2] generates

$$Q_t = \frac{1}{\rho g S_f}(E_{LV}^t + E_{TV}^t + E_{LT}^t + E_{TT}^t) \quad [3]$$

Referring to Figure 2, the energy loss and transition in Eq. [3] can be described as follows:

- In the vertical direction (see Figure 2a):

$$E_{LV} = \tau \frac{du}{dz} \; ; \quad E_{TV} = -\frac{d(\tau u)}{dz} \quad [4]$$

where the shear stress (τ) of steady uniform flow can be described as (Chow 1959)

$$\tau = \rho g(H - z)S_f \quad [5]$$

Inserting Eq. [5] into Eq. [4], the total energy loss and transition become

$$E_{LV}^t = \int_0^H \int_0^B \tau du\, dy = \int_0^H \int_0^B \rho g(H - z)S_f du\, dy = \rho g S_f Q \quad [6]$$

$$E_{TV}^t = -\int_0^H \int_0^B d(\tau u)\, dy = -B\int_0^H d(\tau u) = 0 \quad [7]$$

where H is the flow depth, and B is the width of channel.

- In the transverse direction (see Figure 2b):

$$E_{LT} = \tau_a \frac{du_d}{dy}\ ; \quad E_{TT} = \frac{d(\tau_a u_d)}{dy} \quad [8]$$

where u_d is the depth-averaged velocity, and u_d is the apparent shear stress.

By considering the mixing zone from B_l to B_r in the lateral direction with H_i being the average depth of the zone, the total energy loss and transition can be expressed as

$$E_{LT}^t = \int_0^{H_i} \int_{B_l}^{B_r} E_{LT}\, dydz = \int_0^{H_i} \int_{B_l}^{B_r} \frac{\tau_a du_d}{dy} dydz \quad [9]$$

$$E_{TT}^t = \int_0^{H_i} \int_{B_l}^{B_r} E_{TT}\, dydz = \int_0^{H_i} \int_{B_l}^{B_r} d(\tau_a u_d)\, dz \quad [10]$$

In the mixing zone, it may be assumed that

$$H_i = \frac{H+h_f}{2}\ ; \quad \frac{du_d}{dy} = \frac{V_c - V_f}{B_i} \quad [11]$$

where B_i is the average width of the mixing zone, and V_c and V_f are the average velocities of main channel and floodplain, respectively.

Therefore, inserting Eq. [11] into Eqs. [9] and [10] gives

$$E_{LT}^t = \frac{V_c - V_f}{B_i} \int_0^{H_i} \int_{B_l}^{B_r} \tau_a\, dydz = \left(\frac{V_c - V_f}{B_i}\right) H_i \int_{B_l}^{B_r} \tau_a\, dy \quad [12]$$

$$E_{TT}^t = \int_0^{H_i} \left[(\tau_a u_d)\Big|_{B_l}^{B_r} \right] dz \quad [13]$$

The apparent shear stress (τ_a) can approximately be assumed as a linear variation on either side of the interface (Shiono & Knight, 1991). Therefore, Eqs. [12] and [13] become

$$E_{LT}^t = \frac{1}{4}\left(V_c - V_f\right)\left(H + h_f\right)\tau_a^m \quad [14]$$

$$E_{TT}^t = 0 [15]$$

Thus, inserting Eqs. [6-7], [14-15] into Eq. [3], rearranging the resulting equation yields

$$Q_t = Q \quad - \frac{\tau_a^m (H+h_f)(V_{c,0} - V_{f,0})}{4\rho g S_o} \quad [16]$$

where Q is the discharge without considering the impact of momentum exchange, the subscript (,0) denotes the values using the DCM, and the apparent shear stress (τ_a^m) at the interface may be evaluated by the following formula

$$\tau_a^m = \frac{1}{2}\rho\alpha_m (V_c^2 - V_f^2) \quad [17]$$

or

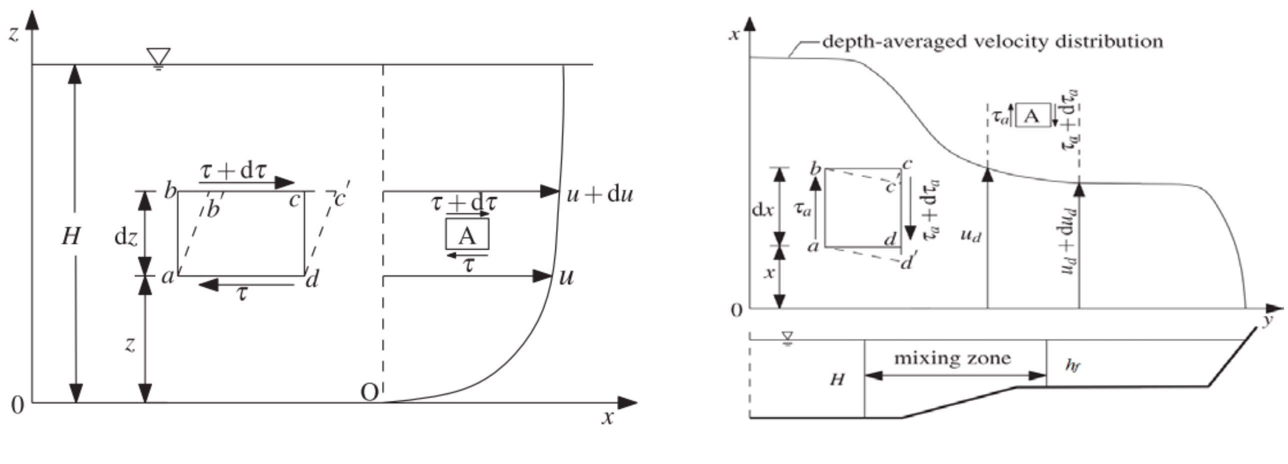

(a) (b)

Figure 2. Shear stress over an element in a compound channel: (a) vertical, (b) lateral direction.

$$\tau_a^m = \frac{1}{2}\rho\alpha_d(V_{c,0} - V_{f,0})^2 \qquad [18]$$

where various values are proposed for the parameters (α_m or α_d). Yang et al. (2012) evaluated Eq. [16] by examining various formulae of τ_a^m, as given by Eqs. [17] and [18]. They recommended to use Eq. [18] with α_d= 0.01B/b, which was proposed by Christodoulou (1992) due to its simplicity and accuracy in the calculation. Furthermore, they also used the DCM to evaluate Q in Eq. [16]. Therefore, Yang et al. [2012] rewrote Eq. [16] as the following expression, called the ECM method in this paper.

$$Q_t = Q_{c,0} + Q_{f,0} - \frac{\tau_a^m(H+h_f)(V_{c,0}-V_{f,0})}{4\rho g S_o} \qquad [19]$$

2.2 New model

In the derivation of Eq. [16], H_{i} was assumed as the averaged depth in the mixing zone, while τ_a^m was taken as the apparent shear stress at the interface between the main channel and floodplain. These two assumptions arguably are not consistent each other. Therefore, it would be appropriate to take H_{i} as the depth (h_{f}) at the interface. Therefore, Eq. [16] can be expressed as

$$Q_t = Q \quad - \frac{\tau_a^m h_f(V_{c,0}-V_{f,0})}{2\rho g S_o} \qquad [20]$$

Furthermore, Yang et al. (2012) also recommended the DCM to calculate Q on the right side of Eq. [16], but it is well known that the DCM method over-estimates discharge. In this paper, we thus recommended the Q to be evaluated by the WDCM method that Lambert & Myers (1998) proposed, since the WDCM has been demonstrated to improve the prediction of total discharge over the DCM (Lambert & Myers, 1998; Atabay & Knight, 2006; Tang & Knight, 2007). To obtain the total discharge (Q), the WDCM method uses the improved velocities for the main channel and its floodplain calculated from both vertical divided method (DCM) and horizontal division method (HDM), respectively, through a weighing factor (ζ), shown as follows:

$$V_C = \xi V_{C-DCM} + (1-\xi)V_{C-HDM} \qquad [21]$$

$$V_f = \xi V_{f-DCM} + (1-\xi)V_{f-HDM} \qquad [22]$$

where ξ ranges from 0 to 1. Lambert & Myers (1998) recommended the ξ value to be 0.5 for homogeneous compound channels, which was well established by Atabay & Knight (2006) and Tang & Knight (2007). Hence, 0.5 was used for ξ in this paper.

Finally, for the consistence of comparison with the ECM, Eq. [18] was used for τ_a^m of Eq. [20] in the proposed new model and the corresponding parameter α_{d} was taken as the same as 0.01B/b proposed by Christodoulou (1992).

3 DATA FOR ANALYSIS

To test the new model in Section 2.2, we used a wide range of different experimental data in homogeneous compound channels. These data are from www.flowdata.bham.ac.uk (created by the author of this paper) and the literature. 26 datasets used includes 22 datasets of symmetric compound channel and 4 datasets of asymmetric compound channel, with the aspect ratio (B/b) being 1.5 ~ 15.8 and the bed slope being S_o = 4.3x10^{-4} ~1.3x10^{-2}. The datasets also cover various channel cross-sections (rectangular or trapezoidal) either symmetric or asymmetric. The details are shown in Table 1, where N_f is the number of floodplain, N is the number of experiment runs, D_r is the relative depth of floodplain (= h_f/H), n is the Manning coefficient, and other notations see Figure 1.

We chose the abovementioned datasets as they are widely used to validate various other methods in the literature. So those datasets were used to test the robustness of the new model proposed in this paper.

Table 1. Details of experimental datasets of homogeneous compound channels.

Series	N_f	N	n	h (m)	b_f (m)	b (m)	B/b	S_c	S_f	Q_t (m^3/s)	D_r
FCF data (1992), S_o= 0.001027											
FCF1	2	8	0.01	0.15	4.10	1.50	6.67	1	0	0.2082-1.0145	0.056-0.400
FCF2	2	10	0.01	0.15	2.25	1.50	4.20	1	1	0.2123-1.1142	0.041-0.479
FCF3	2	10	0.01	0.15	0.75	1.50	2.20	1	1	0.2251-0.8349	0.051-0.500
FCF6	1	8	0.01	0.15	2.25	1.50	2.70	1	1	0.2240-0.9290	0.052-0.503
FCF8	2	8	0.01	0.15	2.25	1.50	4.00	0	1	0.1858-1.1034	0.050-0.499
FCF10	2	9	0.01	0.15	2.25	1.50	4.40	2	1	0.2368-1.0939	0.051-0.464
University of Birmingham (2001), S_o=0.002024											
BU-S	2	11	0.0091	0.05	0.4073	0.398	3.05	0	0	0.0154-0.0552	0.162-0.475
BU-A	1	13	0.0091	0.05	0.4073	0.398	2.02	0	0	0.0150-0.0499	0.184-0.529
Knight and Demetriou (1983), S_o=0.000966											
KD83A	2	6	0.0090	0.076	0.076	0.152	2.00	0	0	0.0052-0.0171	0.108-0.409
KD83B	2	5	0.0093	0.076	0.152	0.152	3.00	0	0	0.0050-0.0234	0.131-0.491
KD83C	2	6	0.0097	0.076	0.229	0.152	4.00	0	0	0.0049-0.0294	0.106-0.506
Bahram (2006), S_o=0.002003											
BD01	2	10	0.0091	0.05	0.10	0.398	5.26	0	0	0.0120-0.0451	0.053-0.536
BD02	2	11	0.0091	0.05	0.20	0.398	5.26	0	0	0.0120-0.0500	0.051-0.522
BD03	2	11	0.0091	0.05	0.30	0.398	5.26	0	0	0.0120-0.0501	0.062-0.487
BD04	2	9	0.0091	0.05	0.40	0.398	3.83	0	0	0.0121-0.0501	0.086-0.468
Khatua et al. (2012), S_o=0.0019											
KH01	2	5	0.0108	0.120	0.16	0.12	3.67	0	0	0.0087-0.0391	0.118-0.461
Mohanty and Khatua (2014), S_o=0.0011											
KH02	2	6	0.01	0.065	1.745	0.330	11.97	1	0	0.0150-0.1062	0.073-0.115
Patra et al. (2012), S_o=0.000311											
Patra	2	7	0.0098	0.08	0.805	0.12	15.75	1	0	0.0494-0.0958	0.111-0.136
Prinos and Townsend (1984), S_o=0.0003											
PT01	2	5	0.011	0.102	0.381	0.203	5.26	0.5	0	0.0066-0.0205	0.089-0.328
PT02	2	5	0.011	0.102	0.381	0.305	3.83	0.5	0	0.0106-0.026	0.089-0.328
Noutsopoulos and Hadjipanos (1983), S_o=0.0015											
NH-A1	2	5	0.01	0.075	0.425	0.15	6.67	0	0	0.0090-0.0450	0.186-0.459
NH-A3	2	6	0.01	0.075	0.325	0.15	5.33	0	0	0.0150-0.0370	0.285-0.468
NH-A4	3	5	0.01	0.075	0.225	0.15	4.00	0	1	0.0100-0.0300	0.248-0.479
Wormleatonet al. (1982), S_o=0.00043											
W-A	2	7	0.01	0.12	0.460	0.29	4.17	0	0	0.0134-0.043	0.115-0.367
Al-Khatib et al. (2012), S_o=0.0025											
AK10-6	1	10	0.015	0.06	0.30	0.10	3.0	0	0	0.003-0.014	0.592-0.818
AK15-6	1	7	0.015	0.06	0.30	0.20	1.5	0	0	0.004-0.014	0.385-0.640

4 RESULTS AND DISCUSSION

To evaluate the error of the method against the experimental data, the percentage of error in predicted discharge was used as a criterion for the purpose of precision. The percentage of error in predicted discharge of each flow depth is calculated by

$$\%E_{Q,i} = \frac{Q_{cal,i} - Q_{exp,i}}{Q_{exp,i}} \times 100\% \quad [23]$$

where $\%E_{Q,i}$ is the relative error percentage of predicted discharge, and $Q_{cal,i}$ and $Q_{exp,i}$ are the predicted and observed discharge at i^{th} flow depth, respectively.

Therefore, the average error of the method for an experiment is calculated by

$$\%E_Q = \frac{1}{N} \sum_{i=1}^{N} (|\%E_{Q,i}|) \quad [24]$$

where N is the total number of runs of an experiment.

Table 2 shows the average percentage errors of predicted discharge by the new model for all 26 datasets, where subscript t denotes the values for the total channel. For the comparison, the results using the other methods, such as the DCM and ECM (used by Yang et al. 2012), are also given in Table 2. The corresponding results of $\%Q_t$ for each experiment are given in Figure 2. For convenience, in the subsequent figures, Sym = symmetric channels, Asym=asymmetric channels, Mean = the average for all channels.

Table 2. Summary of averaged percentage errors of methods for predicting discharges.

Experiments		$\%Q_t$	
	DCM	ECM	New Model
FCF1	11.02	3.72	2.53
FCF2	8.49	3.58	0.48
FCF3	6.33	4.43	0.93
FCF6	7.19	5.72	2.73
FCF8	10.71	5.21	3.13
FCF10	8.17	4.81	1.20
BU-S	6.84	3.90	2.26
BU-A	9.65	8.04	5.22
BD1	5.19	2.57	1.33
BD2	5.04	2.54	1.31
BD3	5.24	2.03	1.81
BD4	9.32	5.28	2.70
KH01	4.15	2.27	1.88
KD83A	9.70	4.58	3.23
KD83B	11.68	5.95	5.68
KD83C	7.60	3.28	3.06
KH02	14.83	8.32	5.68
Patra	7.67	5.27	4.22
PT01	11.01	2.34	4.98
PT02	9.96	2.26	1.52
NH-A1	5.63	4.11	3.38
NH-A2	1.94	2.90	0.80
NH-A4	9.03	3.53	6.29
W-A	3.73	6.81	6.53
AK10-6	4.60	4.53	4.20
AK20-6	8.18	7.55	6.00

As shown in Table 2, compared with the DCM, both the ECM and the New Model showed an overall improved prediction of total discharge (Q_t) for all the datasets, particularly the new model. Figure 3 demonstrated that the new model has the best results with a combined average percentage of error less than 3% in the range of 0.5% – 6%, whereas the ECM had an average percentage of error less than 5%, but with the range of 2.3% -8.3%. However, the DCM over-estimated the discharge with the combined average percentage of error larger than 8%. Furthermore, two methods showed slightly better prediction for symmetric channels than for asymmetric channels, but the DCM had reverse results (Figure 3).

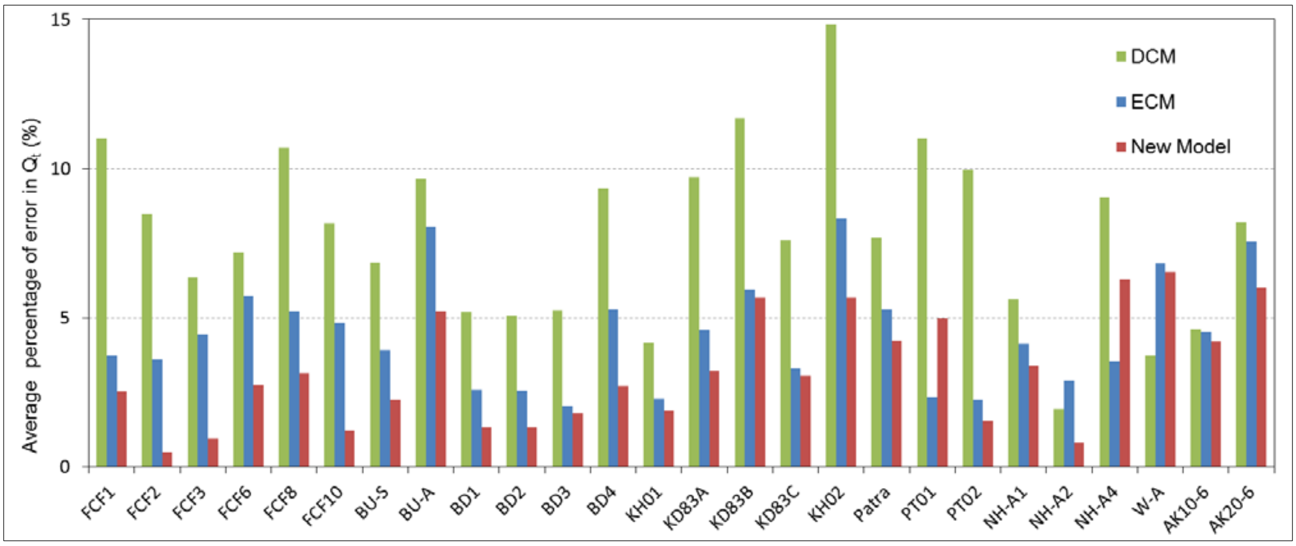

Figure 2. Averaged percentage error of total discharge ($\%Q_t$) by four methods in homogeneous channels.

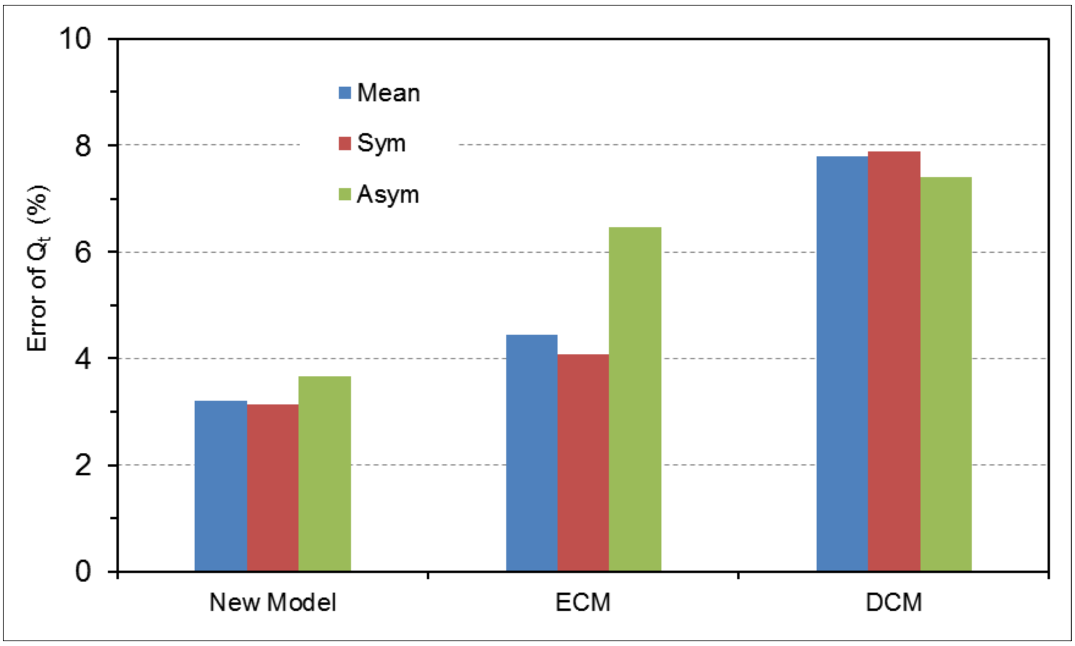

Figure 3. Averaged percentage errors of Q_t.

Although the ECM has shown a relatively small percentage of error within 5% on average for all the datasets, it could not predict well for flow discharge with relatively low flow depths of floodplain, as shown in Figure 4. Moreover, it appears that the ratio of B/b has some impact on the prediction precision of the ECM, whose errors increase as increasing B/b, particularly in the lower depth of floodplain (i.e. smaller D_r), see Figure 4. However, the results of the new model are less affected by B/b. The same conclusion is true for asymmetric channels (see Figure 5).

Finally, although the ECM method predicts the total discharge well with the average percentage error less than 5% for symmetric channels, it should be taken care when this method is used to predict the discharge for flows with relatively low flow depths of floodplain. For example, when D_r< 0.15, in a channel with a wide floodplain (B/b> 6.7), the ECM could have a very large error, as shown Figures 4(c) & 4(d). In these cases, although the average percentage errors by the ECM are small, this method significantly underestimates the discharge at small relative flow depths of floodplain (D_r). Unlike the ECM, the new model is less influenced by B/b and has been shown to have a higher prediction precision of discharge with an overall error of less than 5% over various relative depths, or 7% even in very low relative depths of floodplain (e.g. D_r< 0.15), where the discharge is extremely difficult to predict correctly. The new model predicts discharge well for all the datasets, see Figure 6.

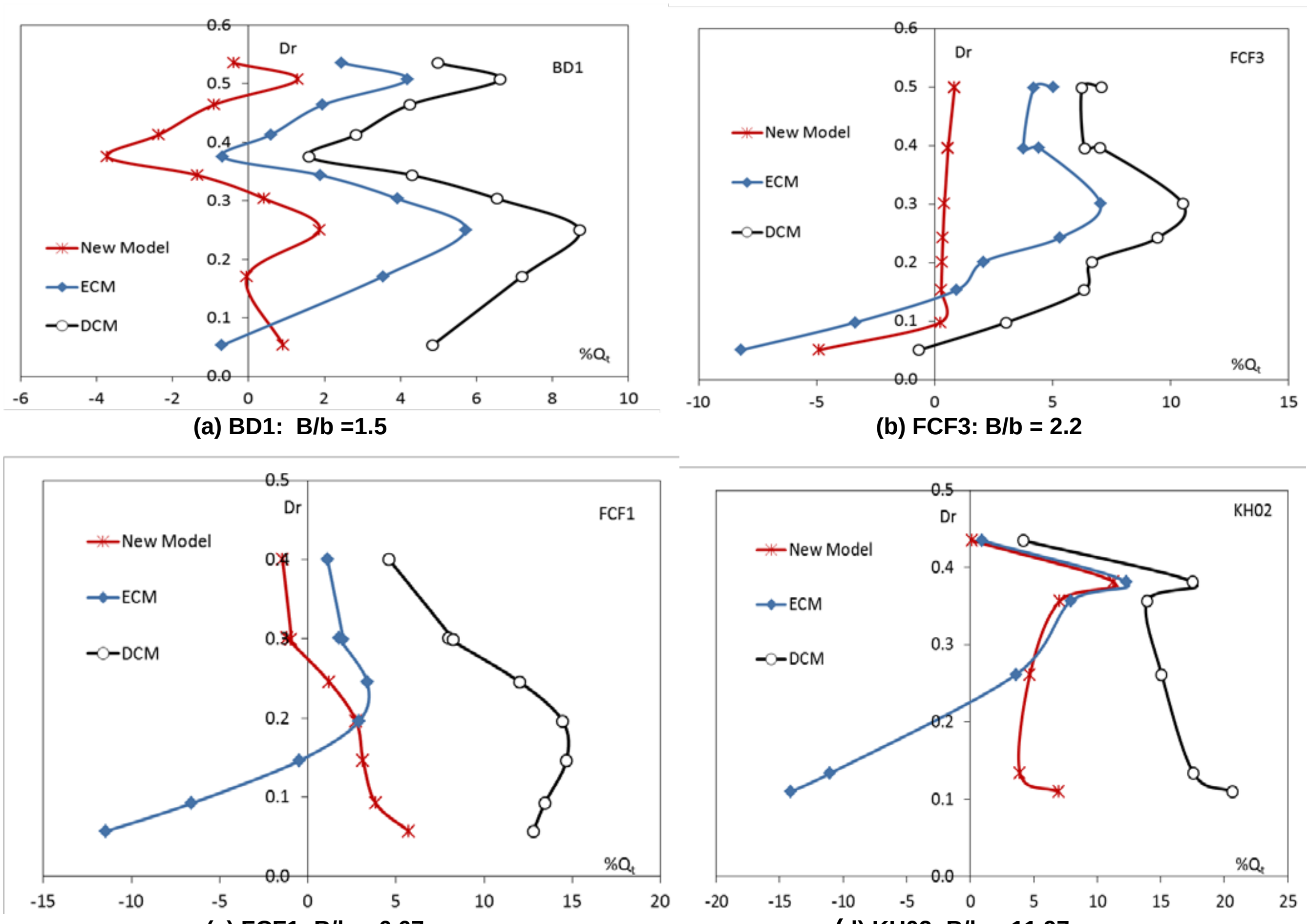

(a) BD1: B/b =1.5

(b) FCF3: B/b = 2.2

(c) FCF1: B/b = 6.67

(d) KH02: B/b = 11.97

Figure 4. Variation of percentage errors of Q_t. with relative depth Dr for symmetric channels.

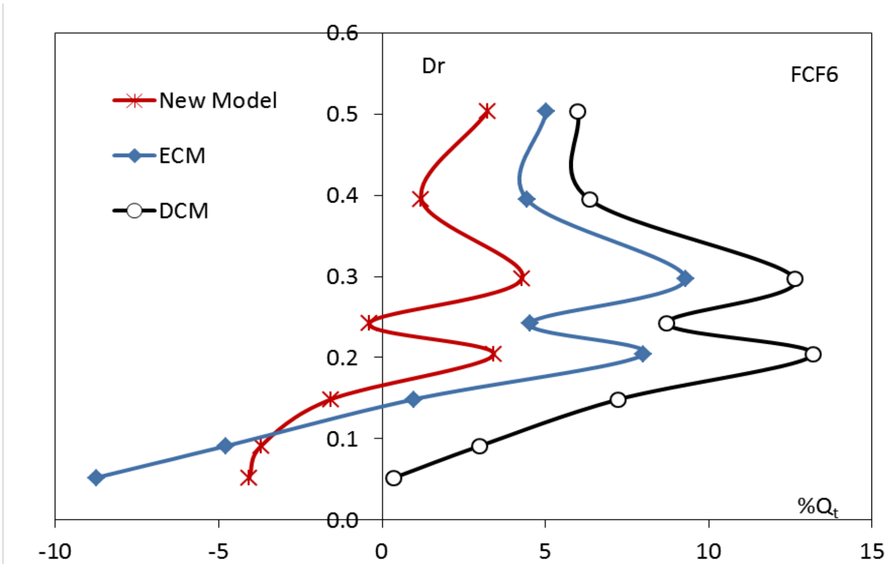

Figure 5. Variation of percentage errors of Q_t with relative depth Dr for asymmetric channel (FCF6).

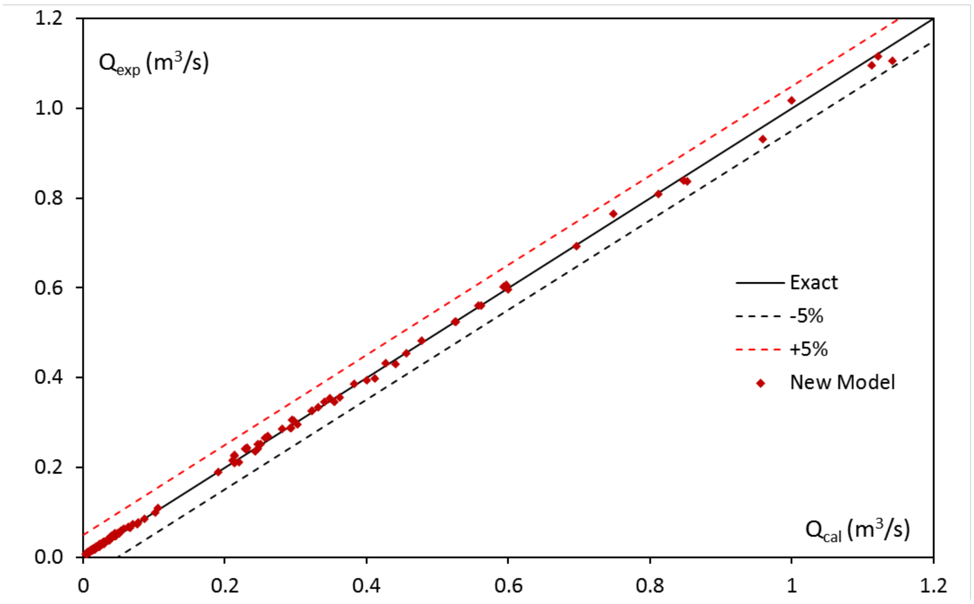

Figure 6. Comparison of the discharge prediction for all datasets.

5 CONCLUSIONS

Through the comparison against a wide range of data in homogeneous compound channels, the new proposed model along with the DCM and ECM shows that:

- Compared with the DCM, the ECM and new model predict the total discharge with the precision within 5% on average for homogeneous compound channels, whereas the DCM has an averaged error over 8%, and the new model gives the best overall results.
- Although the ECM method can predict the discharge reasonably well for channels with small aspect ratios of B/b and high relative depths of floodplain (for example D_r>0.15), both the ECM and DCM methods are not recommended to use for channels with large B/b (e.g. > 6.7) and lower depths of floodplain (e.g. D_r<0.15).
- In general, the new proposed model predicts the discharge well within a combined averaged error of 3% for a wide range of aspect ratio (B/b up to 16). This method significantly improves the prediction of discharge in relative low depths of floodplain, where the discharge prediction with high precision is most difficult to predict.

NOTATION

τ_a^m= apparent shear stress at the interface
B= width of main channel at bankfull
b = width of main channel bottom
D_r= relative depth of floodplain,= $(H\text{-}h)/H$
g = acceleration of gravity
H= main channel depth
h = bankfull height
h_f= flow depth of floodplain
n = Manning's coefficient
N_f= number of floodplain
Q= discharge of cross-section
S_o= bed slope of channel
V= mean velocity of cross-section
α_m= interface coefficient (also α_d)
ρ = density of water
τ = averaged shear stress of boundary
ξ = weighting factor

Subscripts:
,0= reference values based on DCM
c = main channel
f = floodplain
t = total

REFERENCES

Al-Khatib, I.A., Dweik, A.A. & Gogus, M. (2012). Evaluation of Separate Channel Methods for Discharge Computation in Asymmetric Compound Channels. *Flow Measurement and Instrumentation*, 24, 19–25.

Atabay, S. & Knight, D.W. (2006). 1-D Modelling of Conveyance, Boundary Shear and Sediment Transport in Overbank Flow. *Journal of Hydraulic Research*, 44(6), 739-754.

Bahram, R. (2006). Overbank Flow in Compound Channels with Prismatic and Non-Prismatic Floodplains, *PhD Thesis*. University of Birmingham, UK.

Cater, J.E. & Williams, J.J.R. (2008). Large Eddy Simulation of a Long Asymmetric Compound Open Channel. *Journal of Hydraulic Research*, 46(4), 445-453.

Chow, V.T. (1959). *Open Channel Hydraulics*. McGraw Hill, NewYork.

Christodoulou, G.C. (1992). Apparent Shear Stress in Smooth Compound Channels. *Water Resources Management*, 6(3), 235-247.

Devi, K., Khatua, K.K. & Das, B.S. (2016). *Apparent Shear in an Asymmetric Compound Channel, River Flow Constantinescu.* St. Louis, USA, 48-56.

Huthoff, F., Roos, P.C., Augustijn, D.C.M. & Hulscher, S.J.M.H. (2008). Interacting Divided Channel Method for Compound Channel Flow. *Journal of Hydraulic Engineering*, 134(8), 1158-1165.

Khatua, K.K. Patra, K.C. & Mohanty, P.K. (2012). Stage-Discharge Prediction for Straight and Smooth Compound Channels with Wide Floodplains. *Journal of Hydraulic Engineering*, 138(1), 93–99.

Knight, D.W. & Demetrious, J.D. (1983). Flood Plain and Main Channel Flow Interaction. *Journal of Hydraulic Division (ASCE)*, 109(8), 1073-1092.

Knight, D.W. & Hamed, M.E. (1984). Boundary Shear in Symmetrical Compound Channels. *Journal of Hydraulic Engineering*, 110(10), 1412-1430.

Krishnappan, B.G. & Lau, Y.L. (1986). Turbulence Modeling of Flood Plain Flows. *Journal of Hydraulic Engineering*, 112(4), 251–266.

Lambert, M.F. & Myers, W.R.C. (1998). Estimating the Discharge Capacity in Straight Compound Channels. *Proceeding of International Civil Engineers Water, Maritime & Energy*, 130, 84-94.

Marjang, N. & Merkley, G.P. (2009). Velocity Profile Modelling in Rectangular and Compound Open-Channel Cross Sections. *Irrigation Science*, 27(6), 471–484.

Mohanty, P.K. & Khatua, K.K. (2014). Estimation of Discharge and its Distribution in Compound Channels. *Journal of Hydrodynamics*, 26(1), 144-154.

Moreta, P.J.M. & Martin-Vid, J.P. (2010). Apparent Friction Coefficient in Straight Compound Channels. *Journal of Hydraulic Research*, 48(2), 169–177.

Noutsopoulos, G. & Hadjipanos, P. (1983). Discharge Computations in Compound Channels. *Proceeding of 20th IAHR Congress*, Moscow, 5, 173-180.

Patra, K.C., Sahoo, N. & Khatua, K.K. (2012). Distribution of Boundary Shear in Compound Channel with Roughness Floodplain. *9th international conference on Advances in Fluid Mechanics*, June 28, University of Split, Croatia.

Prinos, P. & Townsend, R.D. (1984). Comparison of Methods for Predicting Discharge in Compound Open Channels. *Advanced Water Resource*s, 7, 180-187.

Sellin, R.H.J. (1964). A Laboratory Investigation into the Interaction between Flow in the Channel of a River and that over its Flood Plain. *La Houille Blanche*, 20(7), 793–801.

Shiono, K. & Knight, D.W. (1991). Turbulent Open Channel Flows with Variable Depth across the Channel. *Journal of Fluid Mechanics*, 222, 617-646.

Tang, X. (2016). *Critical Evaluation on Different Methods for Predicting Zonal Discharge of Straight Compound Channels, River Flow 2016, Constantinescu.* St Louis, USA, 57-64.

Tang, X. & Knight, D.W. (2007). An Improved Discharge Prediction Method for Overbank Flows. *Proceeding of 32nd Congress of IAHR*, July 1-6, Venice, Italy.

University of Birmingham (2001). *Flow Database* [online]. Available from: www.flowdata.bham.ac.uk. [Accessed: 3rd December 2016]

Wormleaton, P.R. & Merrett, D.J. (1990). An Improved Method of Calculation for Steady Uniform Flow in Prismatic Main Channel/Flood Plain Sections. *Journal of Hydraulic Research*, 28(2), 157–174.

Wormleaton, P.R., Allen, J. & Hadjipanos, P. (1982). Discharge Assessment in Compound Channel Flow. *Journal of Hydraulic Division (ASCE)*, 108(9), 975–994.

Yang, K., Cao, S. & Liu, X. (2007). Flow Resistance and its Prediction Methods in Compound Channels. *Acta Mech. Sin*., 23(1), 23-31.

Yang, Z., Gao, W. & Huai, W. (2012). Estimation of Discharge in Compound Channels based on Energy Concept. *Journal of Hydraulic Research*, 50(1), 105–113.

DOES INVASIVE RIPARIAN TAMARISK AFFECT WATER AVAILABILITY IN THE LOWER COLORADO RIVER BASIN?

KUMUD ACHARYA[(1)], SACHIKO SUEKI[(2)], JOHN HEALEY[(3)] & YIPING LI[(4)]

[(1,2,3)] Division of Hydrologic Sciences, Desert Research Institute, Las Vegas, NV, USA
Kumud.Acharya@dri.edu
[(4)] College of Environment, Hohai University, Nanjing, China

ABSTRACT

The Virgin River is a tributary of the Colorado River System and flows through the Tri-State area of Arizona, Utah and Nevada. The river's relevance to each state is an important issue as rising population growth results in greater demands on a depleting, limited water supply. One of the ways to manage the water supply of the Colorado River System is vegetation management which includes invasive Tamarisk (Tamarixspp). Tamarisk is the most prolific invasive plant spreading along many riparian corridors of the Southwestern United States. A tamarisk thicket, during a single growth cycle, transpires water at rates that can approach the evaporation rate of an open body of water. Because of the mixed results of traditional control of tamarisk via chemical, mechanical and fire-based methods, biological control using Diorhabdacarinulata (leaf beetle) begins in 2001. The successful release at the banks of Virgin River in St George, UT in 2006 leads to the large-scale establishment of the beetles along the Lower Virgin River. The objective of this study is to determine the effect of beetles' defoliation on tamarisk water consumption based on long-term ET and groundwater data. An eddy covariance tower is installed along the corridor of the Lower Virgin River in 2010. The site is surrounded mostly by tamarisk. Beetles arrive at the site at the end of 2010 and large scale defoliations occurin 2011 and 2012. However, extent of defoliation in subsequent years is not consistent. The ET and groundwater data from 2010 to 2016 suggest that the effect of beetles' defoliationon tamarisk water consumption is short-lived.

Keywords: Eddy covariance; white method; tamarix; saltcedar; leaf beetle.

1 INTRODUCTION

The lower Virgin River is a tributary of the Colorado River system, which is a major component of the water budget of the southwestern United States. The Virgin River is one of the largest free-flowing river basin watersheds in the western United. Currently, the Colorado River and its tributaries support more than 40 million people in Arizona, California, Colorado, Nevada, New Mexico, Utah and Wyoming and provide habitat for a wide range of species including federally endangered animals (U.S. Department of the Interior Bureau of Reclamation, 2016). Demand for Colorado River water has increased with population growth (Cohen, 2011), and with prioritization of maintenance and development of ecological habitats (Follstad Shah et al., 2007). In the Southwestern US (Arizona, California, Nevada, New Mexico, and Utah), combined mean annual runoff and groundwater recharge volume is less than the volume of water consumed each year in the region, leading to extraction of groundwater and ultimately mining of groundwater storage (Ackerman & Stanton, 2011). This issue is compounded by the fact that the Colorado River system is currently facing the worst drought on record (SNWA, 2013). Recent study indicates further dry conditions in the later half of the 21st century in the southwest U.S. (Cook et al. 2015). Several strategies for conserving water have been suggested to address the issue. For example, in 2007 the Southern Nevada Water Authority funded the "Study of the Long-Term Augmentation Options for the Water Supply of the Colorado River System" to examine water resource augmentation options (SNWA, 2009). One of several options was vegetation management, which included tamarisk control. SNWA estimated that 20,000 AFY (24,670,000 m^3/year) of water is potentially available through the control of tamarisk along the Virgin River (SNWA, 2008).

Tamarisk (also known as saltcedar, Tamarix spp.) is an invasive, mostly deciduous, shrubby-tree native to Europe and Asia. Tamarisk first entered the United States as an ornamental plant, which led to further dispersal through nurseries. Dispersal was later encouraged due to beneficial services provided by the plant, such as its suitability as a windbreaker and river bank stabilization, and its authenticity (Robinson, 1965). Extensive establishment of tamarisk along Southwestern riparian zones expanded as anthropogenically induced disturbance and hydrologic regime changed (i.e., reservoir construction, floodplain clearance, fires, and floods) (Graf, 1999) favoring this species. Tamarisk now occupies hundreds of thousands of hectares of North American riparian zones (Nagler et al., 2012). Today, Tamarisk is depicted as a nuisance, responsible for the degradation and consumption of valuable natural resources (Stromberg, 2009) and a target for management to reclaim water (Chew, 2009).

Earlier studies reported estimation of tamarisk ET as high as 3-4 m/yr per plant, which is up to twice that of a reference crop (DiTomaso, 1998). However, other research showed highly variable tamarisk ET and under some circumstances tamarisk actually uses less water than certain natives, like cottonwood and willow (Nagler et al. 2003; Nagler et al. 2010; Owens and Moore, 2007; Shafroth et al. 2005). The Tamarisk Coalition (2009) reported that tamarisk water consumption largely depends on the composition of native communities, stand density, and site conditions.

Despite this newly realized uncertainty, initially perceived opportunity for water savings and the potential for ecological and environmental rehabilitation and protection prompted development of tamarisk removal strategies. Because of mixed results of traditional control of tamarisk via chemical, mechanical, and fire based methods (Shafroth et al., 2005), in the 1970s, tamarisk was considered a suitable candidate for biological control (DeLoach, 1989). Diorhabda elongate (Brullé) sensulato leaf beetles (Coleoptera: Chrysomeliadae) whose larvae and adults feed on leaf foliage and petioles, which results in desiccation and eventual loss of leaves (Pattison et al., 2011) was selected and open field test began in 2001 (DeLoach et al., 2003; DeLoach, 1989). One successful release site is located in St. George, UT on the banks of the Virgin River. The release took place in 2006, leading to the large-scale establishment of the beetles along the Lower Virgin River. Colonies originating in St. George arrived at the Overton arm of Lake Mead in 2011 (Tamarisk Coalition, 2012). However, effect of beetles' herbivory varied and mortality of tamarisk ranged commonly from 20 to 40% after 3-5 years (Dudley and Bean, 2012). Furthermore, the impact of tamarisk defoliation on ET seemed to vary depending upon the growth stage of tamarisk at the time of defoliation (Sueki et al., 2015).

The objective of this study is to determine the effect of beetles' defoliation on tamarisk long term water consumption. This is a follow up to the previous study (Sueki et al., 2015), which reported pre- and post-defoliation ET estimates using an eddy covariance tower installed along the Lower Virgin River. In this study, six years of tamarisk ET after the first defoliation event is reported. The study helps to assess potential water salvage resulting from biocontrol of tamarisk in the Lower Virgin River and has important implications for the Colorado River system.

2 METHODS

ET was estimated using the eddy covariance data. The eddy covariance tower is located approximately 20 km southwest of Mesquite, NV (36°42'09"N, 114°15'29"W) and surrounded mostly by tamarisk, which extends along the river's flood plain for approximately 1.1 km and is about 120 m wide. The lower Virgin River flows along the west side of the study site, and pasture land bounds the tamarisk stands to the east of the study site (Figure 1).The site consists of a groundwater monitoring well and the equipment necessary to apply the eddy covariance technique forestimating turbulent fluxes of ET. Detailed information about the instrument and setups can be found in Sueki et al. (2015).

Data collection occurred monthly during maintenance site visits, at which time, sensors were cleaned and checked, and full memory cards were exchanged with newly formatted cards. Additionally, hand measurements of the groundwater levels were made during site visits and cross checked with pressure transducer measurements.

Turbulent fluxes were processed and corrected using EddyPro, LI-COR Inc. Axis rotations for tilt correction, time lag compensation, turbulent fluctuations with block-averaging and compensation of density fluctuations were applied to the raw data. Raw data were also screened to identify anomalies that may include: spikes, amplitude resolution, drop-outs (gaps), absolute limits, skewness and kurtosis. Spectra were calculated with the Fast Fourier Transform, with Hamming window and low/high frequency range corrections

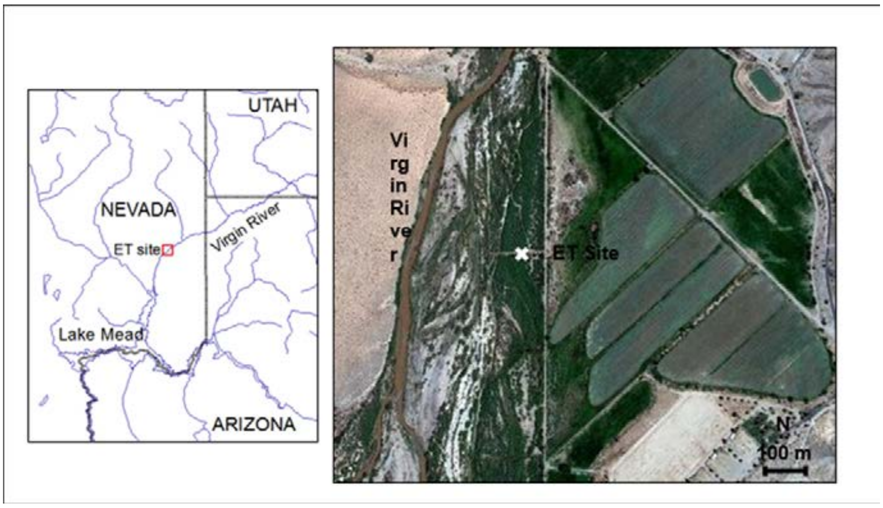

Figure 1. Study area and eddy covariance tower site [Evapotranspiration (ET) site).

applied. Fluxes were also checked for quality based on steady state and weather developed turbulent conditions exist. Flux values deemed to have poor quality were discarded based on the screening mentioned above. Processed and corrected turbulent fluxes were then calculated as 30-minute averages from 10-Hz data. Linear interpolation was used for gap filling if gaps are fewer than four hours. If gaps were more than four hours, and there was no preceding precipitation event within 12 hours, missing data for a respective hour was filled by taking the average value computed from the previous and next day values for that hour. If a precipitation event or change in trend line occurred before the gap, the simple average was calculated using values from two days after the gap. When there were large continuous gaps in the flux data, those gaps were not filled. There were three data gaps not filled. The data gaps, January 25 to February 15 in 2013 and January 20 and February 19 in 2015 were caused by malfunction of the data logger. Data collection ended on November 19, 2016.The footprints were calculated using EddyPro. If peak contribution distance was beyond the tamarisk fetch, that data was excluded and gap filled as mentioned above.

Groundwater water levels were measured at 30-minute intervals. Depth to water hand-measurements were made during the site visit and used to calibrate pressure transducer drift. The corrected water level data was then converted to total head using land surface elevation at the site. Elevation of the site was obtained from National Elevation Dataset, U.S. Geological Survey. Groundwater level time series were used to calculate diurnal fluctuations, and to estimate ET using the White method (White, 1932; Loheideet al., 2005), which assumes that diurnal groundwater fluctuations are caused by phreatophyte water extraction. The White method estimates the ET rate, averaged over a 24-hour period, by multiplying the specific yield by the sum of the daily change in storage and the net inflow rate. The specific yield was estimated to be 0.085 based on a soil texture observed at the site while constructing the well, depth to water, and in the range of what Loheide et al. (2005) suggested. Detail explanation of how the specific yield value was selected can be found in Sueki et al. (2015). The daily change in storage was calculated as the difference between the daily maximum on the day of interest, and the same value on the following day. Similar to Loheide et al. (2005), the net inflow rate was calculated from the slope of the line best fitting the graph of groundwater level data between midnight and 4 a.m., assuming that groundwater consumption by plants is negligible at this time.

3 RESULTS

In the late 2010, beetles arrived at the study site, however beetles did not result in noticeable defoliation of tamarisks which can be easily noticed by changes in the color of the tamarisk field from green to brown. Defoliation events occurred at the site once in 2011 and twice in 2012. After 2012, there was no obvious defoliation event observed even though beetles existed at the site.

Monthly average weather and net radiation measured at the eddy covariance tower from 2013 to 2016 are shown in Figure 2. The study site fetch area is largely energy limited due to the presence of shallow groundwater and riparian vegetation. Average monthly temperature in the summer of 2014 was slightly lower than the other three years. Otherwise, there were no substantial differences in temperature and net radiation throughout the study period. In 2013 and 2014, the highest monthly precipitation occurred in September, whereas the highest monthly precipitation in 2015 and 2016 occurred in February and April, respectively. Annual precipitation was substantially lower in 2015 (about 50 mm) compared to 2013, 2014 and 2016 (more than 100 mm). The seasonality of vaper pressure deficit (VPD) corresponds well with precipitation and temperature. In July of 2014 and 2016, precipitation was low which led to higher VPD. However, as mentioned earlier, temperature was generally lower in 2014. Lower temperature led to a lower VPD in 2014 compared to 2016 even though the precipitation was also lower in July. Average monthly wind speed was consistent at around 1.0 m/s except January and February in 2016 when the site had slightly lower average wind speed. Average wind directions at the site were east-southeast in the winter and southeast-south in the summer months. Fetch analysis indicated that daytime peak contribution point of flux footprint was at 23m± 11m (± one standard deviation) upwind from the tower. Wind direction can vary depending on days. The tamarisk cover around the tower was about 50 m in both east and west directions and over 500 m in the north and south directions.

Figure 3 illustrates groundwater levels measured at 30-minutes intervals in2013 to 2016. The smaller oscillations superimposed on the larger oscillations represent diurnal fluctuations in the water table due to phreatophytic groundwater consumption. Peaks and valleys of the diel fluctuations roughly correspond to daily times of 0600 and 1600 hours, respectively. The summer in 2013 showed slightly higher magnitude of diurnal oscillation compared with that of 2014, 2015 and 2016. In the winter and early spring, diurnal fluctuation was less pronounced since tamarisk is deciduous tree and daytime reduction of groundwater levels was minimal. There is no noticeable change in diurnal groundwater oscillation except seasonal changes from 2013 to 2016.

Daily ET from the eddy covariance data from 2013 to 2016 is shown in Figure 4. Daily ET in 2013 was slightly higher than the other years. On the other hand, daily ET in 2014 was slightly lower than the other years. Daily ET was high in summer months and low in winter months, and there was no substantial drop on daily ET throughout the study years.

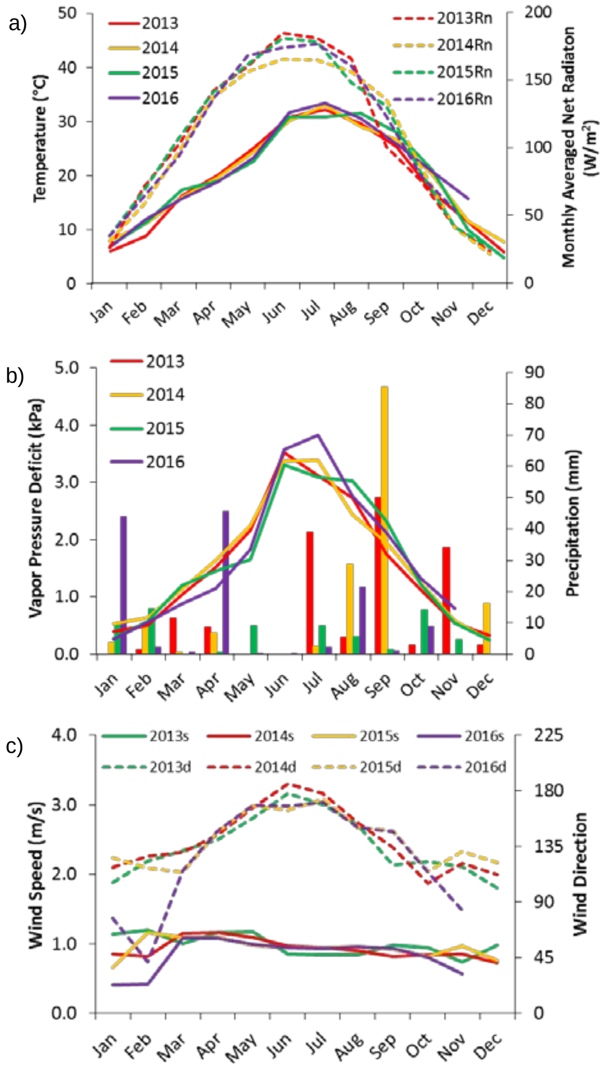

Figure 2. Weather data from the eddy covariance tower during the period of 2013 to 2016: (a) monthly average temperature (solid lines) and net radiation (dotted lines); (b) monthly average vapor pressure deficit (line graph) and monthly total precipitation (bar graph); and (c) monthly average wind speed (solid lines) and direction (dotted lines).

Daily ET estimated using the White method also showed slightly higher daily ET in 2013, whereas daily ET in other years does not show any noticeable difference. The White method resulted in wider ranges of daily ET than that of the eddy covariance data. This is largely attributed to the sensitivity of the White method to changes in specific yield as discussed in Sueki et al. (2015). However, the highest daily ET value was similar in both estimations: about 9 mm/day for eddy covariance data and about 10 mm/day for the White method.

Total ET from April 21 to November 18 were calculated for each year (Figure 5). This time period was chosen for year-to-year comparison of total ET since eddy covariance data was limited to this time period in certain years. In this figure (Figure 5), total ET in 2010, 2011 and 2012, which are reported in Sueki et al. (2015), are also included. Before arrival of beetles, total ET estimated by eddy covariance (ETc) and using the White method (ETw) was 948 and 963 mm, respectively. The lowest total ET was in 2011 when beetles defoliated tamarisk for the first time (789 mm for ETc and 692 mm for ETw). The highest total ET was in 2013 when beetles reduced their herbivory (1,032 mm for ETc and 1,005 mm for ETw). In 2016, total ET estimated by eddy covariance data at the site was almost the same as the pre-defoliation (944 mm) data. Total ET estimated using the White method in 2016 was shown to be slightly lower than that of the pre-defoliation (849 mm) data.

4 DISCUSSIONS

Beetles' defoliation events are clearly observed at the site in 2011 and 2012, indicated by changed color of the tamarisk field from green to brown. Large defoliation events occur in only these two years at the site even though beetles remain throughout the study period. This may be due to the changes in abundance of

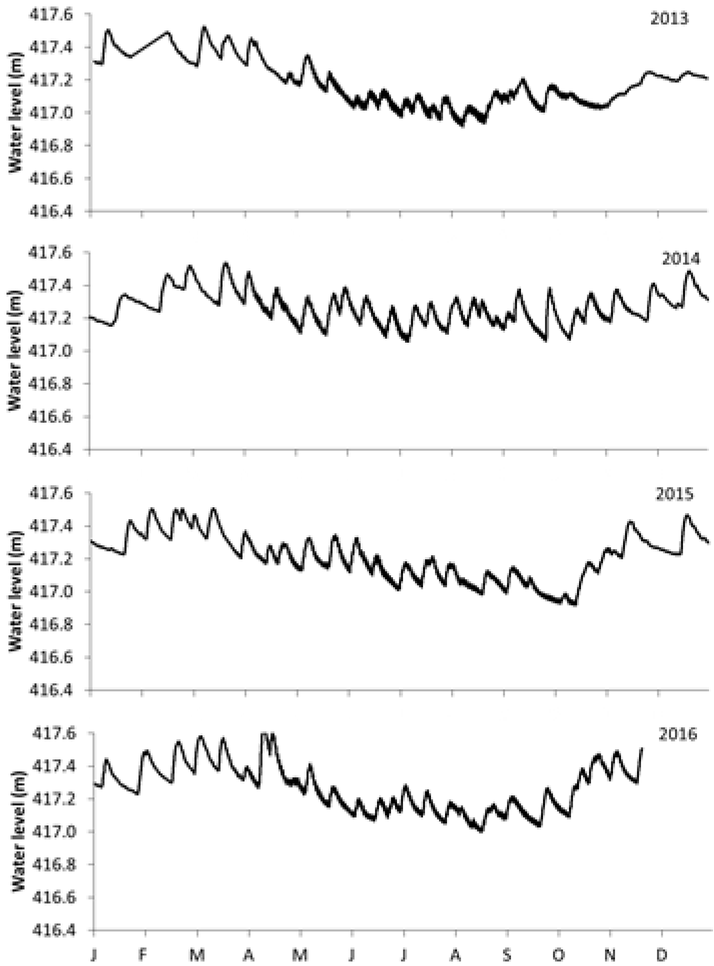

Figure 3. Groundwater level measured at 30-minute intervals from 2013 to 2016.

beetles at the site. Kennard et al. (2016) pointed out that abundance of beetles was highly variable between years. Furthermore, their study sites showed substantial decrease in crown cover and volume in the first two years and little change in crown cover and volume in the next four years. Similar trend is observed in our site as the first two years after beetles' arrival shows obvious defoliation effect at the site but not the rest of our study period.

There are no drastic reductions in ET and damping in diurnal groundwater fluctuation from 2013 to 2016 unlike values reported in Sueki et al. (2015) for 2011 and 2012. This result supports that the beetles' defoliation effect on tamarisk ET is short lived as reported in Snyder et al. (2012), Hultine et al. (2010) and Dennison et al. (2009). Tamarisk ET reduces in our site only in the years when beetles inflict large defoliations. However, tamarisk ET goes back to the pre-beetles infestation rate soon after despite their presence. This is likely due to reduce herbivory in the field. If the beetles' herbivory eventually leads to high percentage of tamarisk dieback, it is possible that tamarisk ET reduces for a longer period. However, in our field site, substantial tamarisk dieback has not yet been observed. Hultineet al. (2015) reported that there was no correlation between number of defoliation events and tamarisk dieback; seven defoliation events caused a few percent canopy diebacks, whereas two defoliation events led to more than 80% canopy diebacks. Therefore, it is difficult to foresee if and when canopy dieback occurs at the site.

5 CONCLUSIONS

This study evaluates the impact of tamarisk defoliation on long-term ET from 2010 to 2016. ET is calculated using eddy covariance data and the White diurnal groundwater fluctuation method. In the years when defoliation events occurr, ET estimates, along with magnitude of diurnal groundwater fluctuations decrease. However, in the subsequent years when large defoliation events do not occur, ET estimates as well as magnitude of diurnal groundwater fluctuations rates return to the pre-infestation days. Six years of beetles' presence at the site has not led to canopy dieback, which may be one of the reasons that ET has not reduced in an extended period. Therefore, it is possible that ET reduction only occurs in sites where canopy dieback caused by beetles' defoliation is reported. Otherwise, effect of beetles' defoliation on tamarisk water consumption is short-lived.

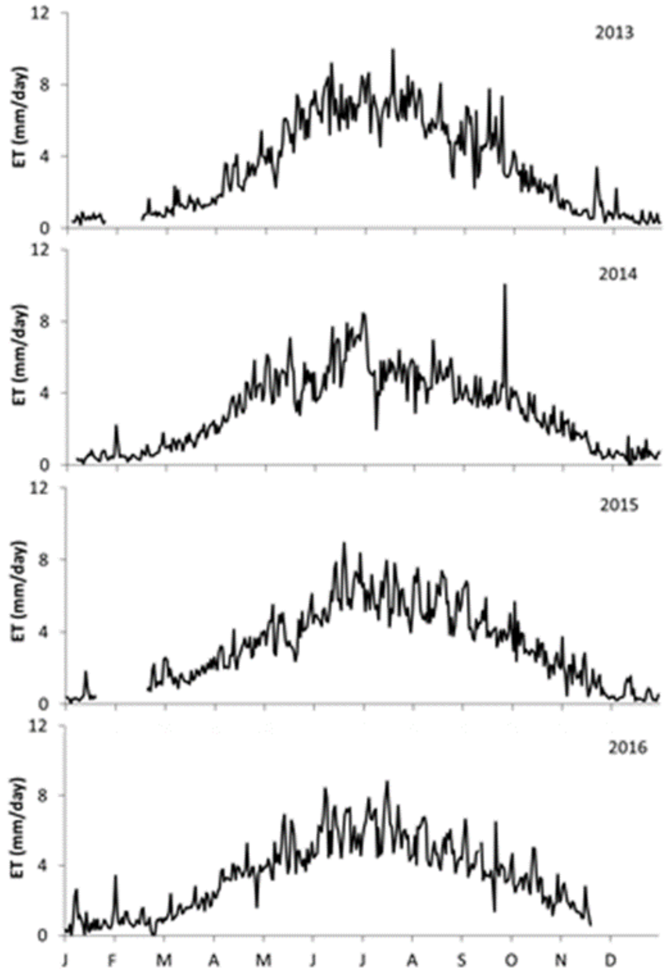

Figure 4. Total daily evapotranspiration (ET) from 2013 to 2016 obtained from eddy covariance data.

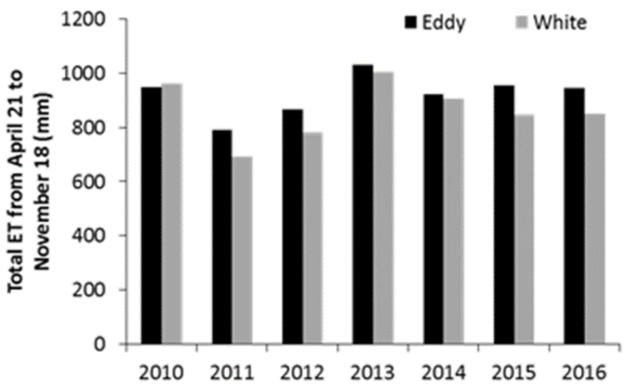

Figure 5. Total evapotranspiration (ET) from 21 April to 18 November calculated using the Eddy covariance method and the White method.

ACKNOWLEDGEMENTS

This project is supported by funds from Maki endowment funding of the Desert Research Institute.

REFERENCES

Ackerman, F. & Stanton, E.A. (2011). The Last Drop: Climate Change and the Southwest Water Crisis. Stockholm Environment Institute - U.S. Center. Retrieved July 9, 2013 at http://sei-us.org/publications/id/371.

Chew, M.K. (2009). The Monstering of Tamarisk: How Scientists made a Plant into a Problem. *Journal of the History of Biology*, 42, 231-266.

Cohen, M.J. (2011). *Municipal Deliveries of Colorado River Basin Water,* Pacific Institute, California.

Cook, B.I., Ault, T.R. & Smerdon, J.E. 2015. Unprecedented 21st century Drought Risk in the American Southwest and Central Plains. *Science Advances*, 1(1), 1-8.

DeLoach, C.J. (1989). Prospects for Biological Control of Saltcedar (Tamarix spp.) in Riparian Habitats of the Southwestern United States. *Proceeding of VII International Symposium Biological Control. Weeds*, 6-11 March 1988, Rome, Italy, 307-314.

DeLoach, C.J., Lewis, P.A., Herr, J.C., Carruthers, R.I., Tracy, J.L. & Johnson, J. (2003). Hot specificity of the leaf beetle, Diorhabda Elongate Deserticola (Coleoptera: Chrysomelidae) from Asia, a Biological Control Agent for Saltcedars (Tamarix: Tamaricaceas) in the Western United States. *Biological Control*, 27, 117-147.

Dennison, P.E., Nagler, P.L., Hultin, K.R., Glenn, E.P. & Ehleringer, J.R. (2009). Remote Monitoring of Tamarisk Defoliation and Evapotranspiration following Saltcedar Leaf Beetle Attack. *Remote Sensing of Environment*, 113, 1462–1472.

DiTomaso, J.M. (1998). Impact, Biology, and Ecology of Saltcedar (Tamarix spp.) in the Southwestern United States. *Weed Technology*, 12, 326-336.

Dudley, T.L. & Bean, D.W. (2012). Tamarisk biocontrol, Endangered Species Effects and Resolution of Conflict through Riparian Restoration. *Biological Control*, 57, 331–347.

Follstat Shah, J.J., Dahm, C.N., Gloss, S.P. & Bernhardt, E.S. (2007). River and Riparian Restoration in the Southwest: Results of the National River Restoration Science Synthesis Project. *Restoration Ecology*, 15, 550-562.

Graf, W.L. (1999). Dam nation: A Geographic Census of American Dams and their Large-Scale Hydrologic Impacts. *Water Resources Research*, 35(4), 1305-1311.

Hultine, K.R., Dudley, T.L., Koepke, D.F., Bean, D.W., Glenn, E.P. & Lambert, A.M. (2015). Patterns of Herbivory-Induced Mortality of a Dominant Non-Native Tree/Shrub (*Tamarix* spp.) in a Southwestern US Watershed. *Biological Invasions*, 17, 1729-1742.

Hultine, K.R., Nagler, P.L., Bush, S.E., Burtch, K.G., Dennison, P.E., Glenn, E.P. & Ehleringer, J.R. (2010). Sap Flux-Scaled Transpiration by Tamarisk (Tamarix spp.) before, during and after Episodic Defoliation by the Saltcedar Leaf Beetle (Diorhabda carinulata). *Agricultural and Forest Meteorology*, 150, 1467-1475.

Kennard, D., Louden, N., Gemoets, D., Ortega, S., González, E., Bean, D., Cunningham, P., Johnson, T., Rosen, K. & Stahlke, A. (2016). *Tamarix* Dieback and Vegetation Patterns following Release of the Northern Tamarisk Beetle (*Diorhabda carinulata*) in Western Colorado. *Biological Control*, 101, 114-122.

Loheide, S.P, II, Butler, J.J. Jr. & Gorelick, S.M. (2005). Estimation of Groundwater Consumption by Phreatophytes using Diurnal Water Table Fluctuations: A saturated-Unsaturated flow Assessment. *Water Resources Research*, 41, 1-14.

Nagler, P.L., Glenn, E.P. & Thompson, T.L. (2003). Comparison of Transpiration Rates among Saltcedar, Cottonwood and Willow Trees by Sap flow and Canopy Temperature Methods. *Agricultural and Forest Meteorology*, 116, 73-89.

Nagler, P.L., Shafroth, P.B., LaBaugh, J.W., Snyder, K.A., Scott, R.L., Merritt, D.M. & Osterberg, J. (2010). *The Potential for Water Savings through the Control of Saltcedar and Russian Olive.* Saltcedar and Russian Olive Control Demonstration Act Science Assessment (33-48). U.S. Geological Survey Scientific Investigations Report 2009-5247.

Nagler, P.L., Brown, T., Hultine, K.R., van Riper, C. III, Bean, D.W., Dennison, P.E., Murray, R.S. & Glenn, E.P. (2012). Regional Scale Impacts of Tamarix Leaf Beetles (Diorhabda Carinulata) on the Water Availability of Western U.S. Rivers as Determined by Multi-Scale Remote Sensing Methods. *Remote Sensing of Environment*, 118, 227-240.

Owens, M.K. & Moor, G.W. (2007). Saltcedar Water Use: Realistic and Unrealistic Expectations. *Rangeland Ecology & Management,* 60, 553-557.

Pattison, R.R., D'Antonio, C.M. & Dudley, T.L. 2011. Biological Control Reduces Growth, and Alters Water Relations of the Saltcedar Tree (Tamarix spp.) in Western Nevada, USA. *Journal of Arid Environments*, 75, 346-352.

Robinson, T.W. (1965). *Introduction, Spread, and Aerial Extent of Saltcedar (Tamarix) in the Western States.* Professional Paper 491-A. US Department of the Interior, Geological Survey: Washington, D.C.

Shafroth, P.B., Cleverly, J,R., Dudley, T.L., Taylor, J.P., van Riper, C. III, Weeks, E.P. & Stuart, J.N. (2005). Control of Tamarix in the Western United States: Implications for Water Salvage, Wildlife use, and Riparian Restoration. *Environmental Management*, 35, 231-246.

Snyder, K.A., Scott, R.L. & McGwire, K. (2012). Multiple Year effects of a Biological Control Agent (Drorhabda carinulata) on Tamarix (saltcedar) Ecosystem Exchanges of Carbon Dioxide and Water. *Agricultural and Forest Meteorology*, 164, 161-169.

SNWA. (2013). Drought. Southern Nevada Water Authority. Accessed on October 10, 2013 at http://www.snwa.com/ws/river_drought.html.

SNWA. (2009). Water Resource Plan 09, Southern Nevada Water Authority. Accessed on July 10, 2013 at http://www.snwa.com/ws/resource_plan.html.

SNWA. (2008). *Study of the Long-Term Augmentation Options for the Water Supply of the Colorado River System,* Prepared for the Colorado River Basin States by Colorado River Water Consultants.

Stromberg, J.C., Chew, M.K., Nagler, P.L. & Glenn, E.P. (2009). Changing Perceptions of Change: The Role of Scientists in Tamarix and River Management. *Restoration Ecology*, 17, 177-186.

Sueki, S., Acharya, K.**,** Huntington, J., Liebert, R., Healey, J., Jasoni, R. & Young, M. (2015). Defoliation Effects of *Diorhabda Carinulata* on Tamarisk Evapotranspiration and Groundwater Levels. *Ecohydrology*, 8(8), 1560-1571.

Tamarisk Coalition. (2009). Independent Peer Review of Tamarisk and Russian Olive Evapotranspiration, Colorado River Basin.Accessed on August, 2013 at http://www.tamariskcoalition.org/PDF/ET%20Report%20FINAL%204-16-09%20%282%29.pdf.

Tamarisk Coalition. (2012). *Yearly Distribution (2007 – 2012) of Tamarisk Leaf Beetle (Diorhabda spp.).* Tamarisk Coalition.

U.S. Department of the Interior Bureau of Reclamation. (2016). *Reclamation Managing Water in the West,* Secure Water Act Section 9503(c), Reclamation Climate Change and Water, Chapter 3: Colorado River Basin. Retrieved from https://www.usbr.gov/climate/secure/docs/2016secure/2016SECUREReport-chapter3.pdf.

White, W.N. (1932). *A Method of Estimating Ground-Water Supplies based on Discharge by Plants and Evaporation from Soil: Results of Investigations in Escalante Valley, Utah. U.S.*, Geological Survey Water Supply Paper 659-A.

Proceedings of the 37th IAHR World Congress
August 13 – 18, 2017, Kuala Lumpur, Malaysia

A COUPLED MODEL OF WATER-SEDIMENT-CONTAMINANT CONTROLLED BY SLUICES

PENGJIE HU[(1)], LINGLING WANG[(2)] & HONGWU TANG[(3)]

[(1,2,3)] State Key Laboratory of Hydrology-Water Resources and Hydraulic Engineering,
College of Water Conservancy and Hydropower Engineering, Hohai University
Nanjing, 210098, China
hpj@hhu.edu.cn; wanglingling@hhu.edu.cn; hwtang@hhu.edu.cn

ABSTRACT

Based on the complex mechanism of water-sediment-contaminant controlled by gates in plain rivers, this paper puts forward an idea of studying it from multiphase transformation in each interface of water, sediment and contaminant. Conclusions based on recent studies of the interface between sand and contaminant are introduced into the two-dimensional shallow water equations. Then six variable values are taken into account, which are the concentration of dissolved phosphorus in water, the concentration of adsorbed phosphorus in water, the concentration of suspended solids in water, the concentration of dissolved phosphorus in sediment, the concentration of dissolved phosphorus in sediment, the concentration of adsorbed phosphorus in sediment and the mass of sediment. The interaction processes between them, such as adsorption and desorption, sedimentation and resuspension, convection and diffusion are also simulated. By using the established mathematical model to study the rule how sediment and contaminant transport under the control of Bengbu gate in Huaihe river, the evolution processes of concentration of total phosphorus and sediment across the studying district under different hydrological conditions and scheduling methods are obtained.

Keywords: Sediment; contaminant; adsorption; diffusion; sedimentation.

1 INTRODUCTION

Sluices are important tools for the exploitation and utilization of water resources. Since 1949, a large number of sluices have been constructed in China. By 2008, China had built more than 7000 large- and medium- sized sluices. Most of these projects have been contributing toward national economic development, flood controlling and water supply. However the hydrological regime and water quality transport processes are greatly influenced by the construction of these sluices. Unlikely general rivers, hydrodynamic factors in the sluice-controlled river reach change quickly and severely, thus having a great influence on the transport process of pollutants (Dou et al., 2014a; Dou et al., 2014b). Meanwhile in the water environmental system, the sediment also affects the transition and transformation process of pollutants, which ultimately affect the ecological environment condition of the river (Yu et al., 2006). Therefore, the transport and transformation rule of phosphorus with the action of water and sediment in the sluice-controlled river reach is difficult. So is how to simulate it by numerical method.

So far, the influence of sluice impacting on river water quality mainly divides into two aspects. One is study of generalized impact on water quality with a single sluice (Xia et al., 2008; Zuo et al., 2010; Dou et al., 2016). The other is study of water quality scheduling ability or scheduling method from the point of river or river network (Zhang et al., 2007; Chen et al., 2014). And the interaction mechanism of water-sediment-contaminant is an important foundation of the study stated above.

Research results of phosphorus adsorption by sediment in the past 20 years explain that the physical and chemical properties, initial concentration of phosphorus in water, sediment concentration, and environmental factors can affect the adsorption amount (Chen et al., 2014). However, most studies are just qualitative analysis. Very few researchers quantitatively analyze the actual adsorption amount by sediment in the natural river (Zhao et al., 2015; House et al., 2000; Huang et al., 1995). With the deep understanding of nature law, the coupling simulation of sediment movement and transport of phosphorus is becoming a new hot issue. Some researchers consider the influence of sediment movement on phosphorus migration by introducing the distribution coefficient K_d (Jalali et al., 2013) of adsorption thermodynamics, or adsorption rate k_1 and desorption rate k_2 (Li et al., 2012) of adsorption kinetics, such as Dobbins (2015); Song et al. (2013). Huang et al. (2014) established a split phase model of hydrodynamic, sediment and phosphorus migration process based on simulation of flow movement and sediment transport. Using the basic chemical reactions, the model can be used to study the migration process of phosphorus in the river.

Overall, most of the studies above are aimed at the coupling process of water quality and water quantity or just water quantity. They are not able to organically relate contaminant and sediment, lack of studies on the complex flow in the sluice-controlled river reach and considering the mechanism of phosphorus conversion in multiphase interface. So, this paper establishes a coupling model of water-sediment-phosphorus in the sluice-controlled river reach to study environmental effect of phosphorus with the coupled action of water and sediment in the sluice-controlled river reach.

2 MATERIALS AND METHODS

Bengbu Lock was constructed in the late 1950s, located in the west of Bengbu, Anhui province, China. It is in the middle reaches of Huaihe River and about 5.5km down from the junction of Guohe River and Huaihe River. This construction has many integrated functions, such as flood control, irrigation, shipping and so on. As is shown in figure1, from left to right side, there are wet land park, 12-gates sluice, 28-gates sluice, hydropower station, old lock, new lock and floodway, respectively.

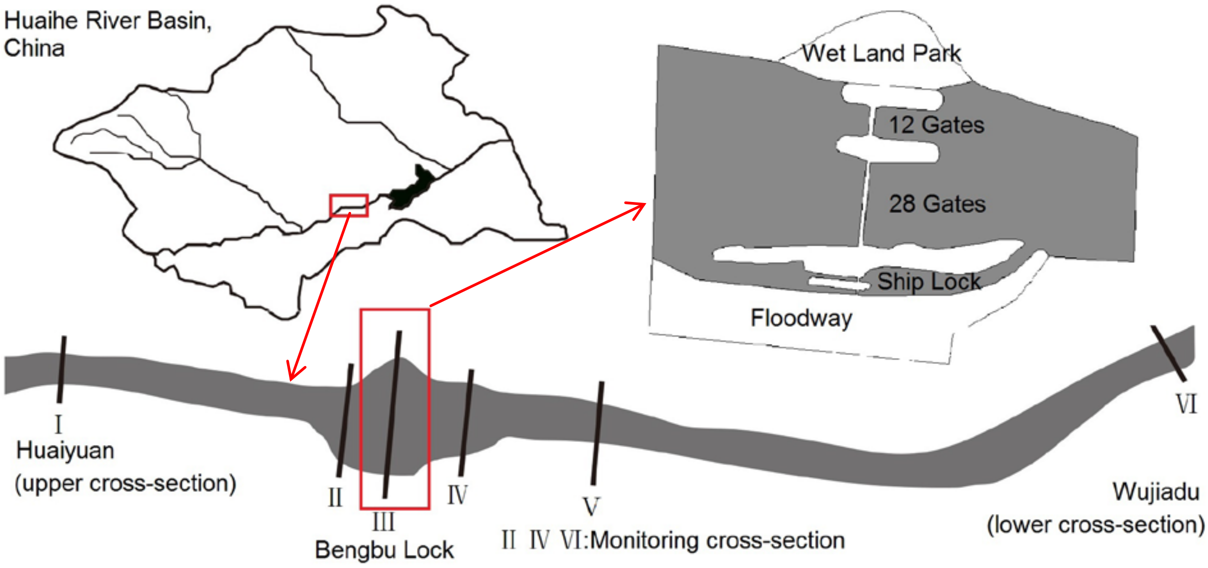

Figure1. Schematic diagram of Huaihe River Basin and study area.

2.1 Hydrodynamic module

Cross-section Ⅰ, named Huaiyuan, was selected as the upper cross-section of the study area, about 4km up from the Bengbu Lock. While cross-section Ⅵ, named Wujiadu hydrologic station, was selected as the lower cross-section, about 9km down from the Bengbu Lock. Other cross-sections Ⅱ, Ⅲ and Ⅴ were monitoring cross-sections.

Based on equation [1], the two-dimensional hydrodynamic mathematical model is built.

$$\begin{cases} \dfrac{\partial Z}{\partial t}+\dfrac{\partial}{\partial x}(Hu)+\dfrac{\partial}{\partial y}(Hv)=0 \\ \dfrac{\partial u}{\partial t}+u\dfrac{\partial u}{\partial x}+v\dfrac{\partial u}{\partial y}+g\dfrac{u\sqrt{u^2+v^2}}{C^2H}+g\dfrac{\partial Z}{\partial x}-\nu_t\nabla^2 u=0 \\ \dfrac{\partial v}{\partial t}+u\dfrac{\partial v}{\partial x}+v\dfrac{\partial v}{\partial y}+g\dfrac{v\sqrt{u^2+v^2}}{C^2H}+g\dfrac{\partial Z}{\partial y}-\nu_t\nabla^2 v=0 \end{cases} \quad [1]$$

where, Z is water level, H is water depth, x and y are coordinate direction, respectively, u and v are depth-averaged velocity of direction x and y, respectively, g is acceleration of gravity, C is Chezy coefficient, v_t is turbulent viscosity coefficient.

After modeling the study area, the grids should be divided into all computational scope. Structured girds, namely rectangular girds (2.4 m x 5 m), were used in the slices area, while unstructured grids were used in the rest of the whole scope (the minimum grid area was 1.7㎡). Local refinement was used near the slices area (as shown in figure 2). The total grid number was 14658. Space discreteness of calculation area was based on the finite volume method of grid center.

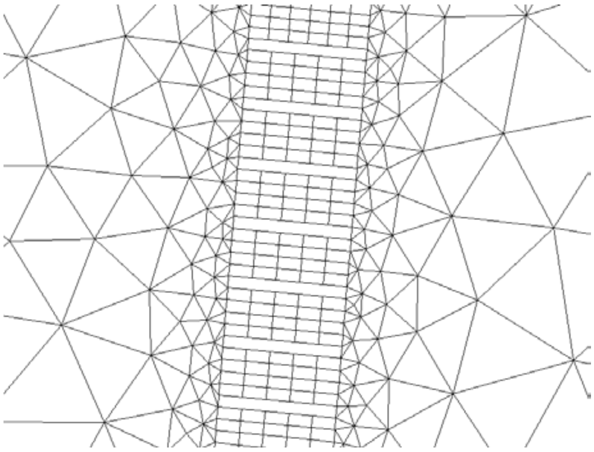

Figure 2. The local grids near the sluices.

2.2 Sediment and phosphorus transport module

Sediment motion and adsorption characteristics are mainly two aspects how sediment affect water quality (Yu et al, 2004). On one hand, sediment particles can adsorb a variety of pollutants. When reaching some kind of dynamic conditions, these pollutants will deposit on the bottom of the riverbed, reducing the amount of pollutants in some period of time. On the other hand, when chemistry, hydrodynamic and other external conditions change, the adsorption of pollutants in sediment particle may change state from the adsorption state (solid) to the dissolved phase (water), or the pollutants deposit in the sediment suspend in the water. Thereby, these changes will alter the chemical composition in overlying water, and even cause secondary pollution of water (Jing et al, 1984).

As shown in figure 3, the model considered six variables which were respectively dissolved phosphorus concentration in the overlying water SP(g/m^3), adsorbed phosphorus concentration in the overlying water XP (g/m^3), suspended sediment concentration XSS(g/m^3), dissolved phosphorus concentration in the bed sediment SPS(g/m^2), adsorbed phosphorus concentration in the bed sediment XPS(g/m^2) and bed sediment concentration XSED(g/m^2). The interaction processes between them, such as adsorption and desorption, sedimentation and resuspension, convection and diffusion were also simulated, which are expressed from [2] to [7]. According to parameters of some water environmental model (such as MIKE ECOLab) and verified parameters of the model in Dou et al.(2016), the adopted parameters are also shown below.

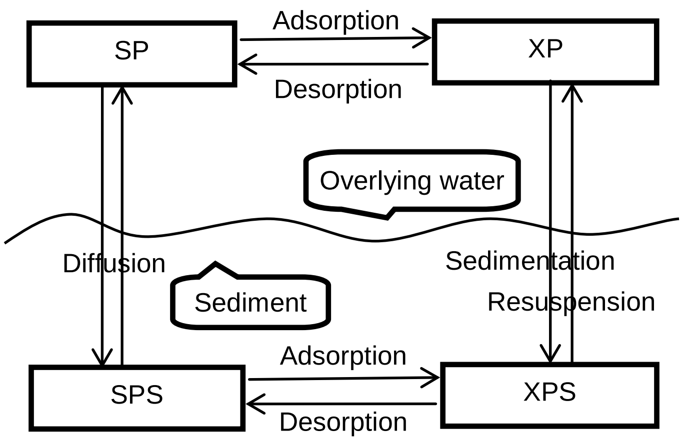

Figure 3. The interaction processes among six variables.

(a) Dissolved phosphorus concentration in the overlying water SP (g/m^3);

$$\frac{dSP}{dt} = -k_w \cdot K_d \cdot SP \cdot XSS + k_w \cdot XP + difw \cdot (\frac{SPS}{por_s \cdot dzs} - SP) \Big/ (dzds \cdot dz) \qquad [2]$$

where k_w is desorption rate in overlying water, equal to 1/d; K_d is partitioning coefficient in water, equal to 0.05 m^3/g ; $difw$ is diffusion coefficient, equal to 0.5 cm^2/s ; por_s is sediment porosity, equal to 0.8; dzs is layer thickness of bed sediment, equal to 0.02m; $dzds$ is thickness of layer diffusion, equal to 0.1m; dz is thickness of computational layer, equal to 2m.

(b) Adsorbed phosphorus concentration in the overlying water XP (g/m^3);

$$\frac{dXP}{dt} = k_w \cdot K_d \cdot SP \cdot XSS - k_w \cdot XP - \frac{vsm \cdot XP}{dz} + resrat \cdot \frac{XPS}{XSED} \Big/ dz \quad [3]$$

where vsm is velocity of sedimentation, equal to 0.1 m/d; $resrat$ is resuspension rate, equal to 1000 $g/m^2/d$.

(c)Suspended sediment concentration XSS (g/m^3);

$$\frac{dXSS}{dt} = -\frac{vsm \cdot XSS}{dz} + \frac{resrat}{dz} (\text{if } cspd > ucrit) \quad [4]$$

where $cspd$ is velocity, equal to $\sqrt{u^2 + v^2}$; $ucrit$ is critical velocity, equal to 0.2m/s.

(d) Dissolved phosphorus concentration in the bed sediment SPS(g/m^2);

$$\frac{dSPS}{dt} = -k_s \cdot K_{ds} \cdot SPS \cdot \frac{XSED}{dzs \cdot por_s} + k_s \cdot XPS + difw \cdot \left(\frac{SPS}{por_s \cdot dzs} - SP\right) \Big/ dzds \quad [5]$$

where k_s is desorption rate in bed sediment, equal to 0.1/d; K_{ds} partitioning coefficient in bed sediment, equal to 0.1 m^3/g.

(e) Adsorbed phosphorus concentration in the bed sediment XPS (g/m^2);

$$\frac{dXPS}{dt} = k_s \cdot K_{ds} \cdot SPS \cdot \frac{XSED}{dzs \cdot por_s} - k_s \cdot XPS + vsm \cdot XP - \frac{resrat \cdot XPS}{XSED} (\text{if } cspd > ucrit) \quad [6]$$

(f) Bed sediment concentration XSED (g/m^2).

$$\frac{dXSED}{dt} = vsm \cdot XSS - resrat(\text{if } cspd > ucrit) \quad [7]$$

The next step is to put these six variables into convection-diffusion equation [8] and couple sediment and phosphorus transport module with hydrodynamic module.

$$\frac{\partial c}{\partial t} + u\frac{\partial c}{\partial x} + v\frac{\partial c}{\partial y} = D_x \frac{\partial^2 c}{\partial z^2} + D_y \frac{\partial^2 c}{\partial z^2} + S_c + P_c \quad [8]$$

where c is one of six variables, u and v are velocity of x and y, respectively, D_x and D_y are diffusion coefficient of direction x and y, S_c is source or sink term, P_c is interaction process of [2]-[7].

3 MODEL CALIBRATION

According to historical hydrologic conditions, the flood process (from 0:00 22/7/2010 to 0:00 1/8/2010) containing flood peak (11:00 27/7/2010) was selected. The boundary condition of upper cross-section was given by flow time series, while the lower cross-section was given by water level time series. The Manning roughness in the scope of 100m up and down from sluices and ship lock Gate 100 m was 0.01, while the rest of the whole area was 0.022. The simulation time step was 30s.

During the simulation time, all sluices were open. So, the water level in the cross-section 500m up from sluices was chosen to be calibrated. As shown in figure 4, the biggest difference was not larger than 0.15m. Thus, the water level of calculation was in good agreement with the measured water level. The model above can be used in the simulation below.

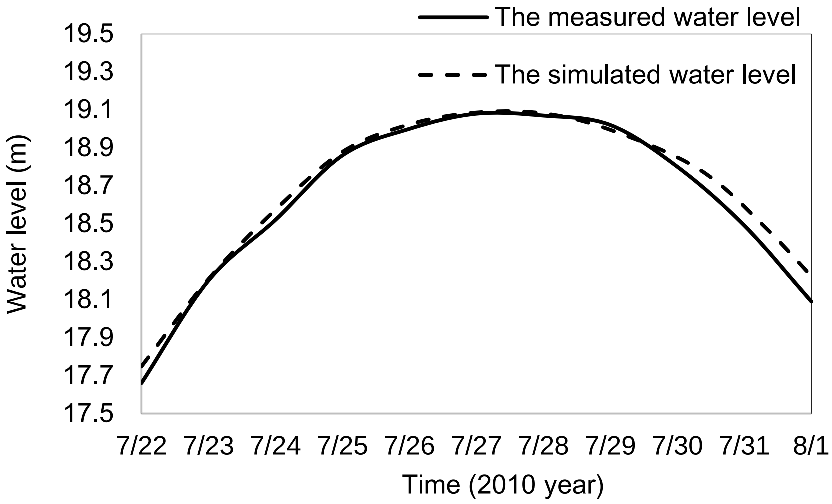

Figure 4. Comparison between measured water level and simulated water level.

4 MODEL APPLICATION

By analyzing the six-times measured results of main station in Huaihe River (such as Huaiyuan, Bengbu Lock, Wujiadu and so on) in 2013, 2014, and 2015, the sediment and phosphorus module was calibrated. Then combining with achievements of transformation in Yuhuan Lin, the initial values of six variables is shown in table 1. And some different conditions were simulated to study how phosphorus transports and evolves along the whole study area.

Table1. Initial values of six variables.

Name	SP	XP	XSS	SPS	XPS	XSED
Initial value	0.1	0.4	500	0.008	0.008	5000
Unit	g/m^3	g/m^3	g/m^3	g/m^2	g/m^2	g/m^2

4.1 Changes of phosphorus along the study area with different inflow

Hydrodynamic boundary conditions were the same as the conditions of model validation. In order to simulate wastewater, the dissolved phosphorus in overlying water SP and pore water in dissolved phosphorus SPS of condition 1 were 5 times as that of table 1, while the rest of four variables were the same. In order to simulate clean water, the dissolved phosphorus in overlying water SP and pore water in dissolved phosphorus SPS of condition 1 were 0, while the rest of four variables were the same. As shown in table 2, all gates of Conditions 1 and 2 are open.

Table 2. Boundary values and initial values of conditions 1 and 2.

	Condition 1			**Condition 2**		
All gates are open	**Initial values**	**Upper boundary values**	**Lower boundary values**	**Initial values**	**Upper boundary values**	**Lower boundary values**
SP(g/m^3)	0.5	0.5	Zero gradient	0	0	Zero gradient
XP(g/m^3)	0.4	0.4	Zero gradient	0.4	0.4	Zero gradient
XSS(g/m^3)	500	500	Zero gradient	500	500	Zero gradient
SPS(g/m^2)	0.04			0		
XPS(g/m^2)	0.008	—		0.008	—	
XSED(g/m^2)	5000			5000		

In order to compare the phosphorus distribution along the whole study area, 3 cross-sections were defined. As is shown in figure 1, they were cross-sections ⅡⅣ and Ⅴ, in which were 500m up from the sluice, 800m down from the sluice and 2km down from the sluice. The changes of phosphorus in overlying water of Conditions 1 and 2 are shown in figure 5.

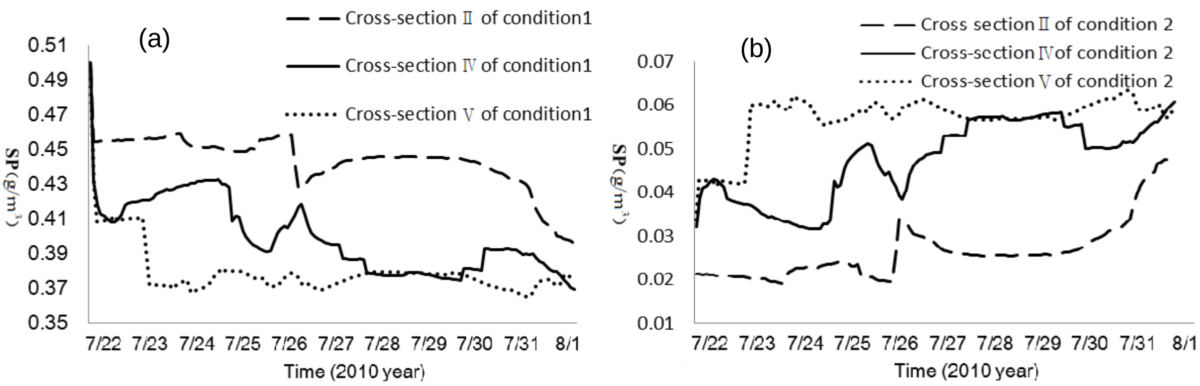

Figure 5. The changes of SP of Conditions 1(a) and 2(b).

Sections ⅡⅣ and Ⅴare three cross-sections from upstream to downstream of the in turn. As shown in figure 5(a), the order of SP from big to small in the whole computation time are the cross-sections Ⅱ, Ⅳand Ⅴ. This indicates that the value of SP is smaller in which the distance is further from the upstream boundary, showing that more adsorption is adsorbed by sediment. It is concluded that adsorption is the main action when there are high concentrations of P in overlying water. On the other hand, as shown in figure 5(b), the order of SP from big to small in the whole computation time are the cross-sections Ⅴ, Ⅳand Ⅱ. This indicates that the value of SP is smaller in which the distance is further from the upstream boundary, showing that more desorption is desorbed by sediment. A result is concluded that desorption is the main action when there are low concentrations of P in overlying water.

4.2 Changes of phosphorus along the study area with different scheduling.

Hydrodynamic boundary conditions were the same as the conditions of model validation. The initial values of Conditions 3, 4, and 5 were the same with the six variables in table 1. And the upstream boundaries XP and XSS were 0.4 g/m^3 and 500 g/m^3 , respectively. The downstream boundary was set to zero gradient. But for simulating a sudden pollution incident, the upstream boundary SP was set to increase uniformly from 0.1 g/m^3 to 0.5 g/m^3, then dropping uniformly to 0.1 g/m^3 during the time 12:00 to 18:00 in 23/7/2010. And in order to simulate the influence of phosphorus transformation by different open case of gates, three different conditions were set up (shown in table 3). 12-gates sluices were located on the left of cross-section III, while 28-gates sluices were located on the right side.

Table 3. The open cases of conditions 3, 4 and 5.

	Condition 3	**Condition 4**	**Condition 5**
12 gates	Open	Closed	Open
28 gates	Open	Closed	Closed

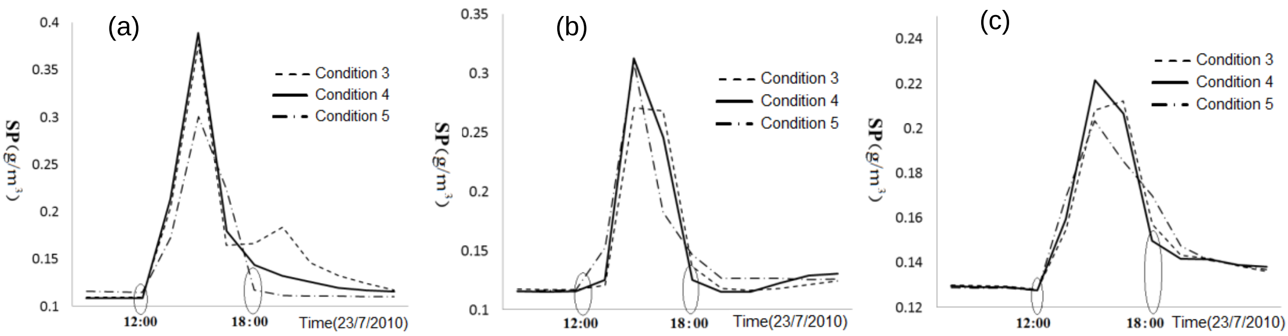

Figure 6. The changes of SP of cross-sections Ⅱ(a) Ⅳ(b) and Ⅴ(c).

Figure 6 illustrates how dissolved phosphorus in overlying water of cross-sections Ⅱ, Ⅳ and Ⅴ changes when there is a sudden pollution incident in the upstream (from 12:00 23/7/2010 to 18:00 23/7/2010). As shown in figure 6(a), the smallest peak value of SP in the right of cross-section Ⅱ was that of condition 5, whose left gates were open and the right were closed. As shown in figure 6(c), the smallest peak value of SP in the right of cross-section Ⅴ was that of condition 5, whose left gates were open and the right were closed. The main reason is that when the gates on the left side of the sluices are open and the right side are closed, phosphorus flow to the left together with the current, thus fewer SP on the right side. As shown in figure 6(b), the smallest peak value of SP in the right of cross-section Ⅳ was that of condition 3, whose both left and right gates were open. The main reason is that when both the left and right side of the sluices are fully open, SP is distributed uniformly in each cross-section. While when some gates are open and some are closed, strong vortexes will happen near the downstream of the gates, thus bringing phosphorus in bed sediment and pore water into the overlying water. And SP increases sharply.

5 CONCLUSIONS

(a) The adsorption effect of sediment.

When the concentration of phosphorus in overlying water is high, the main action is adsorption. While when the concentration of phosphorus in overlying water is low, the main action is desorption. So, it is easy to see that sediment has obvious environmental effect in the Bengbu reach during flood time.

(b)The influence of gates on phosphorus transformation.

Conditions of all gates whether open or closed are studied by this paper. It indicates that the dissolved phosphorus in the overlying water, no matter upstream or downstream, is influenced by the scheduling of sluices. In the future, the influence of gates under different combinations of opening on phosphorus transformation will be studied.

ACKNOWLEDGEMENTS

This paper is mainly funded by the State Key Program of National Natural Science of China (Grant No.51239003), the 111 Project (Grant No.B17015), National Key Research and Development Program of China (2016YFC0401703,2016YFC0401503) and Innovation Research Project for Postgraduate in Jiangsu Province (No.KYLX16_0742).

REFERENCES

Chen, L.G., Shi, Y., Qian, X., Luan, Z.Y. & Jin, Q. (2014). Hydrology, Hydrodynamics and Water Quality Model for Impounded Rivers I—theory. *Advances in Water Science*, 25(04), 534-541.

Chen, Y., Li, Q.Y. & Cao, H.Q. (2014). Research Status and Prospect of Phosphorus Adsorption by River Sediment. *Journal of Yangtze River Scientific Research Institute,* 31(5), 12-16.

Dobbins, W.E. (2015). BOD and Oxygen Relationship in Streams. *Journal of the Sanitary Engineering Division*, Book.

Dou, M., Zheng, B.Q. & Zuo, Q.T. (2014a). Quantitative Relationship of Water Quality Concentration and Operation Mode in the River Reaches Controlled by Sluice. *Journal of Hydroelectric Engineering*, 33(1), 114-119.

Dou, M., Mi, Q.B. & Zuo, Q.T. (2014b). Multi-Phase Transformation Model of Water Quality in the Sluice-Controlled River Reaches. *China Environmental Science*, 35(07), 2041-2051.

Dou, M., Mi, Q.B., Li, G.Q. & Zhang, Y.Y. (2016). Research on Water Quality Transformation Mechanism in Sluice-Controlled River Reaches Development of the Mathematical Model. *Journal of Hydraulic Engineering*, 47(04), 527-536.

House, W.A. & Denison, F.H. (2000). Factors Influencing the Measurement of Equilibrium Phosphate Concentrations in River Sediments. *Water Research*, 34(4), 1187–1200.

Huang, L., Fang, H.W., Wang, J.Y. & He, G.J. (2014). Mathematical Model of Phosphorus Transport with River Sediment. *Journal of Hydraulic Engineering*, 4, 394-402.

Huang, S.L., Huang, Z.H. & Wang, L.X. (1995). Experimental Research on Heavy Metal Desorption for Sediment with Different Grain Size. *Journal of Hydrodynamics (A)*, 10(02), 204-213.

Jalali, M. & Peikam, E.N. (2013). Phosphorus Sorption–Desorption Behavior of River Bed Sediments in the Abshineh River, Hamedan, Iran, related to their Composition. *Environmental Monitoring & Assessment*, 185(1), 537-52.

Jing, X.C. & Lin, G. (1984). The Effect of Heavy Metal Adsorption by Sediment. *Environmental Science & Technology*, (02), 6-11.

Li, Z.J., Yue, Q., Gao, B. & Liu, Q. (2012). Phosphorus release Potential and Pollution Characteristics of Sediment in Downstream Nansi Lake, China. *Frontiers of Environmental Science & Engineering*, 6(2), 162-170.

Song, L.X., Liu, D.F. Xiao, S.B., Guo, H.C., Cui, Y.J. & Chen, L. (2013). Study on Non-Point Nitrogen and Phosphorus Load from Xiangxi River in the Three Gorges Reservoir are based on SWAT. *Acta Scientiae Circumstantiae,* 33(1), 267-275.

Xia, J., Zhao C.S., Liu, M., Wang, G.S., Zhang, Y.Y. & Liu, Y. (2008). Impact Assessment of Dam and Flood Gates Project of Huaihe River on River Ecosystem: A Case Study of the Bengbu Site. *Journal of Natural Resources,* 23(01), 48-60.

Yu, X.Z., Zhong, D.Y., Li, J.X. & Liao, W.G. (2004). Review of Studies on Sediment in Water Environment. *Journal of Sediment Research*, (06), 75-81.

Yu, X.Z., Yang, Z.F., Zhong, D.Y. & Peng, Q.D. (2006). Numerical Model for Interaction between Sediment and Pollutant in River. *Journal of Hydraulic Engineering*, 37(01), 10-15.

Zhang, Y.Y., Xia, J., Wang, G.S., Jiang, Y. & Zhao, C.S. (2007). Research on Influence of Dam's Union dispatch on Water Quality in Huaihe River Basin. *Engineering Journal of Wuhan University*, 40(04), 31-35.

Zhao, H.Q., Tang, H.W., Li, Z.I., Yuan, S.Y., Xiao, Y. & Ji, F. (2015). Review of Effects of flow and Sediment on the Transport and Transformation of Phosphorus in Rivers and Lakes. *South-to-North Water Transfer and Water Science & Technology,* 13(04), 643-649.

Zuo, Q.T., Gao, Y.Y. & Liu, Z.H. (2010). Analysis and Discussion about the Mechanisms of the Impacts of Dams on Water Quality and Quality of Heavily Polluted Rivers. *Resources Science,* 32(02), 261-266.

Proceedings of the 37th IAHR World Congress
August 13 – 18, 2017, Kuala Lumpur, Malaysia

ESTIMATION OF OUTFLOW AND NUTRIENT LOAD BASED ON THE TURBIDITY FUNCTION IN RIVERS IN SANRIKU DISTRICT JAPAN

KUNIHIKOHAMAGAMI[(1)], KEITA ORITO[(2)] & RYU SUGAWARA[(3)]

[(1,2,3)] Faculty of Agriculture, Iwate University, Morioka, Japan,
ham@iwate-u.ac.jp;kei-orito@pref.iwate.jp; sugawara-ry608@pref.miyagi.jp

ABSTRACT

The Sanriku coastal area has suffered serious damage from the Great East Japan Earthquake that occurred on March 11, 2011. Five years have passed since the earthquake, and reconstruction of the aquaculture industry is progressing. In order to achieve sustainable development and promotion, it is necessary to correctly understand the environment of the Sanriku coastline. Sanriku Coast is a type of enclosed coastal sea called a rias coast; hence, substances such as nitrogen and phosphorus from rivers flow out and affect water quality. In this study, in order to consider outflow characteristics and nutrient load in two Sanriku rivers, the outflows, water depths and water qualities were observed of each by periodic field observation. The nutrient loads of the Sanriku River are estimated using the HQ curve and LQ equation. As a result, it reveals that there is no unique relationship between the quantity of outflow and the nutrient load, and consequently the error becomes sometimes large. A hypothesis is deduced that the data variation is not considered that leads to this error. The turbidity is then focused in this study which can be observed continuously.

Keywords: Sanriku coast; nutrient load; outflow; HQ curve; turbidity.

1 INTRODUCTION

The Sanriku coastal area, where there are many coastlines and deep coves, has abundant fishery resources and is used in many ways such as aquaculture and harbor. On the other hand, because of its complicated topography, there are many closed waters like the bay, and flowing substances through the river greatly influence water quality in the water area. In particular, nutrients such as nitrogen and phosphorus are easily accumulated, which lead to eutrophication and deterioration of water quality. Therefore, comprehending the flow condition of the river and the amount of nutrient load is an important factor for water quality control in the closed waters such as the bay.

In general, the nutrient load is expressed by the product of the flow rate and the water quality concentration, and it is most desirable to calculate it by continuous observation at the site in order to grasp the accurate nutrient load. However, it is not realistic to observe all the water quality at each site of the target basin. Therefore, at present, a method of estimating the nutrient load is widely adopted using the relational expression between the quantity of flow Q and the nutrient load L obtained from several observed values (hereinafter referred to as LQ equation). Moreover, although the LQ equation has the convenience of estimating the nutrient load from few numbers of observed data, there are reports that the accuracy is somewhat inferior. In addition, since the nutrient load flowing out during rainfall has hysteresis (Yamamoto et al., 2003; Matsumoto et al., 2012), the variations of the nutrient load cannot be reflected in the LQ equation, and in many cases, a large error is generated with respect to the actual load amount.

Moreover, it is also pointed out that the nutrient load is related to the turbidity (Kashiwadate et al., 2006). Generally, turbidity is calculated by directly measuring the concentration of suspended particles in river water, and its variation is greatly affected by the inflow of suspended matter from surrounding watersheds, accompanying rainfall and flooding. In addition, most of the nutrients at the time of flooding flow out as a suspended state attached to the suspended particles. Makino et.al (2005) reported that most of phosphorus, especially at the time of flooding, is adsorbed by soil particles derived from the surrounding forest and flows out into the river. Therefore, there is a high possibility that it is related to the turbidity and the suspended nutrients, and it is expected to estimate the nutrient load with higher accuracy by reflecting the variation of the suspension state. In this study, for the purpose of improving the estimation accuracy of the nutrient load, LQ equation for the Sanriku coastal river is formulated and its accuracy examined. In addition, the relation between the turbidity, the quantity of flow and the water quality concentration is examined in detail, and the nutrient load by the turbidity is estimated.

2 OUTLINE OF OBSERVATION

The observation site was Kesen River flowing through Sumita-cho and Rikuzentakata-shiin Iwate Prefecture, Japan. The Kesen River is a class B river with a total length of 47 km, originating from Mt.

  / ISSN 1562-6865 (Online) - ISSN 1063-7710 (Print)

Takashimizu in Sumita-cho. It consists of tributaries such as the Oomata River and Sakamoto River, and the basin area is about 520 km^2. In Hirota Bay in the estuary, oyster and other aquaculture businesses are thriving. The observation point is shown in Figure 1. The Kashiwari1-Bridge was set up to grasp the variation of the water quality and the quantity of flow due to the influence of the Oomata River and Komata River basin. The Takenohara-Bridge was set up to ascertain the influence from the Sakamoto River basin, while the set up of Ajimai-Bridge to study the influence from the Yahagi River Basin. Also, in order to grasp the variation of the water quality in the middle Kesen River, Showa-Bridge and Otsubo-Bridge were set up. Mawatate-Bridge was set up as a representative point of the downstream area of Kesen River, and the nutrient load of the Kesen River basin was estimated.

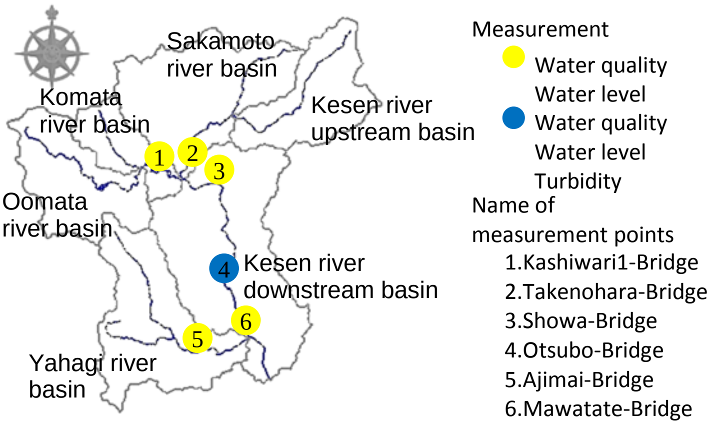

Figure 1. Observation sites.

The survey was conducted from September 2012 until February 2016. The water depth and the water temperature were acquired at 1 hour intervals by pressure type depth meter. The amount of rainfall utilized the data obtained from the Japan Meteorological Agency's rainfall observatory. DO and pH were measured with a glass electrode type of hydrogen ion concentration indicator at monthly intervals. The turbidity was measured at 1 hour intervals by a turbidimeter at continuous observation. As for the turbidity, 10 measurements were taken at 1 second intervals for one measurement, and the average value was taken as the measurement value. Water quality was measured at the intervals of one month.

3 RESULTS

3.1 HQ equation

Figure 2 shows the variation of rainfall and water depth at each measurement point of Kesen River. As the rainfall increases, the water depth is also rising. In addition, large flood water occurred several times a year mainly in the summer, and the maximum hourly rainfall during this period was 63 mm/h at the Sumita Observatory on July 26, 2013. During that period, the Sumita Observatory observed 244 mm/48h, which was a large rainfall corresponding to the 70-year probability rainfall (266.8 mm/48h) which is the flood safety standard of the Kesen River.

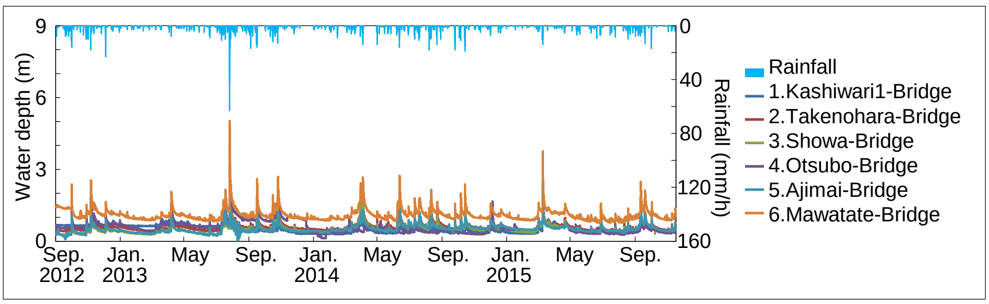

Figure 2. The time variation of rainfall and water depth.

In general, it is difficult to observe the quantity of flow continuously, so the quantity of flow is estimated by the HQ curve showing the relationship between actually measured water depth H and the quantity of flow Q (Kinoshita, 1984). Also in this study, the quantity of flow was estimated from the continuous observation of the water depth by using the HQ curve created at each point. HQ curve was calculated as follows,

$$Q = a(H + b)^2 \quad [1]$$

where *a* and *b* are coeficients. Figure 3 shows the relationship between the quantity of flow and water depth at Showa-Bridge, and Table 1 shows the HQ equation at each observation point.

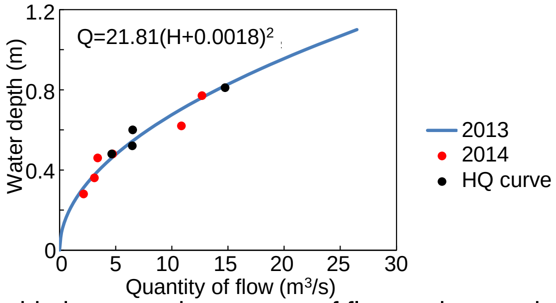

Figure 3. The relationship between the quantity of flow and water depth (Showa-Bridge).

Table 1. HQ equation at each observation point.

Point	HQ equation
1.Kashiwari1-Bridge	$Q = 1.808(H + 0.3842)^2$
2.Takenohara-Bridge	$Q = 18.95(H - 0.1912)^2$
3.Showa-Bridge	$Q = 21.81(H + 0.0018)^2$
4.Otsubo-Bridge	$Q = 3.502(H + 1.003)^2$
5.Ajimai-Bridge	$Q = 7.641(H - 0.1077)^2$
6.Mawatate-Bridge (H<1.4m)	$Q = 25.21(H - 0.4741)^2$
6.Mawatate-Bridge (H>=1.4m)	$Q = 61.49(H - 0.7800)^2$

3.2 Water quality

Figure 4 shows the variation of TN and TP at each measurement point of Kesen River. Although TN was shown from September 2012 to November 2015, TP was measured from July 2015 due to the convenience of analysis equipment. It is revealed that TN has been changing at nearly the same concentration at each point from 2014 to 2015 in the Kesen River.

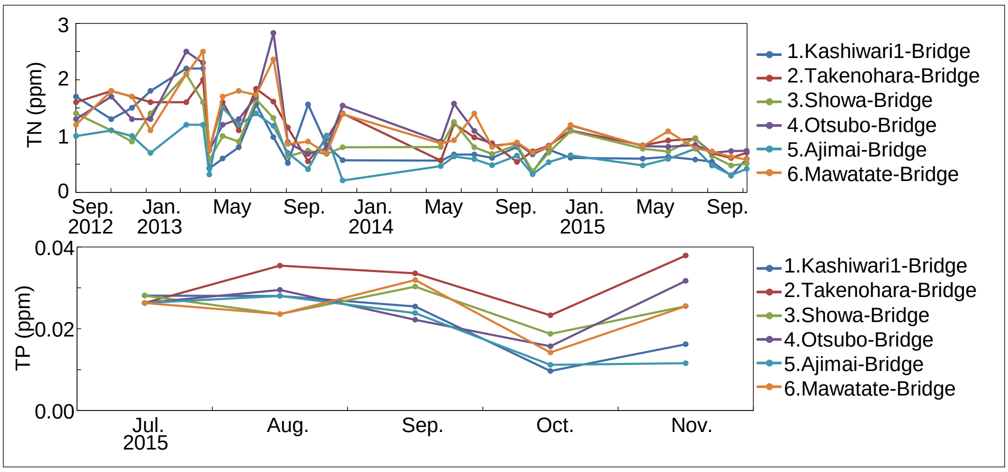

Figure 4. The time variation of nutrients.

Comprehending the flow condition of the river and the amount of nutrient load is an important issue for water quality control in the closed waters such as the bay. However, it is difficult to observe all the water quality at each site of the target basin. Therefore, a method of estimating the nutrient load is widely adopted using LQ equation. LQ equation is calculated as follows,

$$L = cQ^d \quad [2]$$

where, L: the nutrient load, Q: the quantity of flow, c and d: coeficients. As an example, the relationship between the quantity of flow and nutrient load at the Otsubo-Bridge is shown in Figure 5. Table 2 shows the LQ equation and the determination of coefficient R^2 at each measurement point.

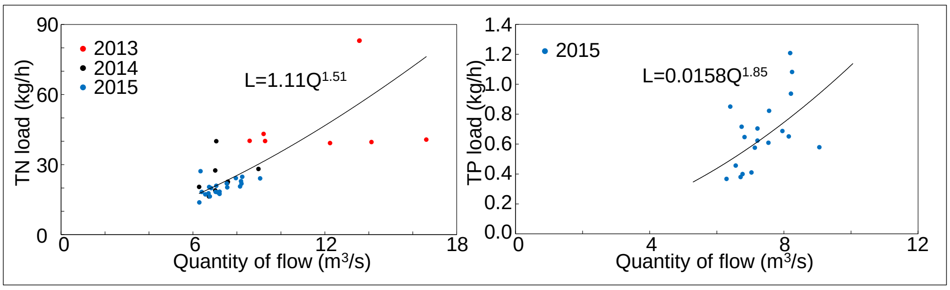

Figure 5. The relationship between the quantity of flow and nutrient load.

Table 2. LQ equations.

Point	TN	TP
1.Kashiwari1-Bridge	$L=1.65Q^{2.05}$ (R^2=0.852)	$L=0.0559Q^{1.42}$ (R^2=0.334)
2.Takenohara-Bridge	$L=3.62Q^{0.933}$ (R^2=0.611)	$L=0.0705Q^{1.41}$ (R^2=0.920)
3.Showa-Bridge	$L=3.53Q^{0.875}$ (R^2=0.592)	$L=0.0491Q^{1.34}$ (R^2=0.910)
4.Otsubo-Bridge	$L=1.11Q^{1.51}$ (R^2=0.629)	$L=0.0158Q^{1.85}$ (R^2=0.300)
5.Ajimai-Bridge	$L=2.15Q^{0.951}$ (R^2=0.563)	$L=0.0523Q^{1.39}$ (R^2=0.629)
6.Mawatate-Bridge	$L=2.12Q^{1.16}$ (R^2=0.676)	$L=0.0310Q^{1.46}$ (R^2=0.889)

The determination of coefficient of TN was 0.6 to 0.7 at most points and showed a relatively high correlation. Therefore, in TN, it can be inferred that simple estimation of the nutrient load by the LQ equation is possible. On the other hand, there was not much correlation with TP at most points. Also, there was a variation in the nutrient load with respect to the same quantity of flow. In particular, the trend was noticeable as the quantity of flow increased. That is, although it is possible to estimate simple nutrient load in the LQ equation, it is not suitable for highly accurate estimation and it can be inferred that the error is large with respect to the actual nutrient load.

3.3 The variation of the nutrient load

The annual nutrient load of the Kesen River was calculated by using the LQ equation of the Mawatate-Bridge which was located downstream of the Kesen River. Figure 6 shows the variation of nutrient load, and Table 3 shows the annual nutrient load of the Kesen River.

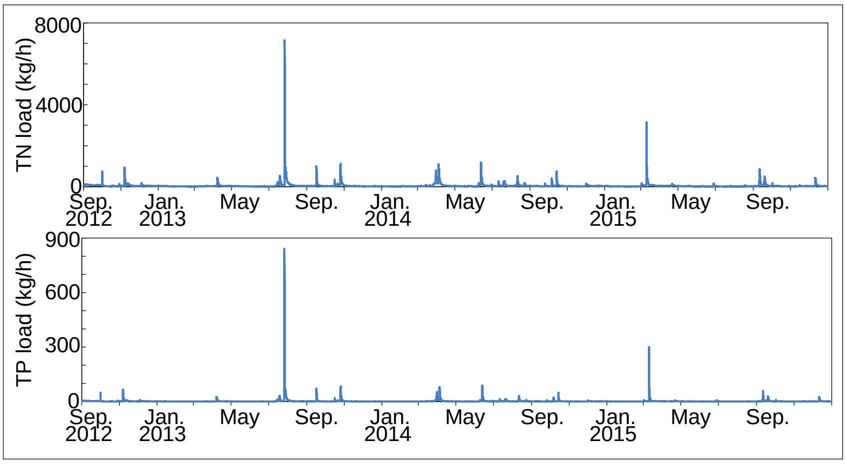

Figure 6. The variation of nutrient load.

Table 3. Nutrient load of the year at Kesen river.

	2013	2014	2015
TN(t/year)	463.0	448.3	345.1
TP(t/year)	23.4	18.8	14.7

Table 3 shows that the trend of the annual nutrient load in the Kesen River is decreasing. In order to manage the water quality of the closed water bodies in the estuary, it is necessary to grasp the trend of the annual nutrient load of the Kesen River basin over a long period of time.

Figure 7 shows the comparison between results of observation and estimation at Otsubo-Bridge. Although the estimated value generally reproduces the actual measurement value, a large error occurs in some data. In particular, the decrease period of the nutrient load cannot be appropriately reflected, and in the LQ equation, the nutrient load is often overestimated. This is due to the fact that the LQ equation cannot adequately reflect the variation of the water quality at the time of flooding.

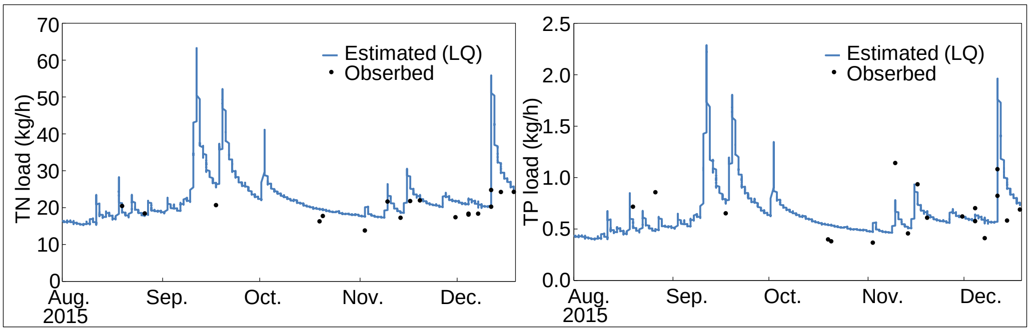

Figure 7. Comparison between results of observation and estimation.

On the other hand, it has been pointed out that the nutrient load is related not only to the quantity of flow but also to turbidity (Aya and Iwasa, 1982). Turbidity varies greatly depending on the influx of pollutant components from the surrounding basin during the flooding. Turbidity is a direct measurement of the concentration of suspended particles in river water, and the nutrient salt flowing into rivers at the time of flooding is mostly in a suspended state attached to the suspended particles. Therefore, there is a high possibility that it is related to the turbidity and the variation of the nutrient salt in the suspension state, and it is presumed that reflecting the variation of the suspended nutrient salt leads to a more accurate grasp of the nutrient load. Therefore, in the next section, for the purpose of improving the accuracy of the nutrient load estimation, the relationship between the turbidity and nutrient load was investigated and the possibility of nutrient load estimation by turbidity examined.

3.4 The relationship between the turbidity and nutrient load

The turbidity was observed from August 2015 at the Otsubo-Bridge, and the relationship between the turbidity, the quantity of flow and water quality concentration was examined. Figure 8 shows the variation of turbidity,the variation of rainfall and the quantity of flow. It can be seen that fluctuation of turbidity is affected by fluctuation of the quantity of flow. In the period from October 19 to November 12, turbidity is missing due to malfunction of the turbidimeter.

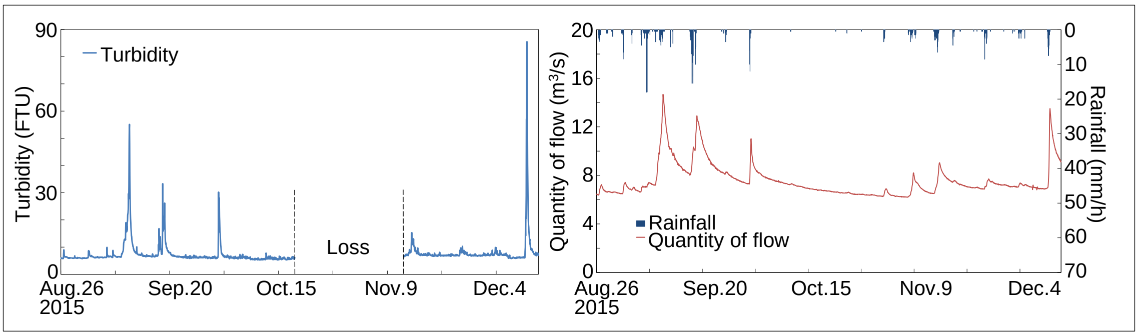

Figure 8. The time variations of the turbidity and the quantity of flow.

As the quantity of flow due to rainfall increases, the turbidity also rises greatly, indicating that the peak of the quantity of flow and the peak of turbidity are roughly similar. However, while the quantity of flow reaches its peak, it gradually decreases, whereas the turbidity decreases sharply and returns to the same value as at the time of flat water. Therefore, although the turbidity is related to the quantity of flow, it is considered that there is a difference in the relation depending on the increase period and the decrease period of the quantity of flow. In order to grasp the relationship between the turbidity and the quantity of flow in more detail, it is compared separately for the increase period and the decrease period of the quantity of flow.

Figure 9 shows the relationship between the quantity of flow and the turbidity. The figure shows that the variation process of the turbidity is different between increasing and decreasing period of the quantity of flow, and that the turbidity has hysteresis with respect to the quantity of flow. Also, there are two hysteresis relationships of the turbidity, and the number 2 in the figure shows the hysteresis relationship in the rain event at December 11, 2015. In this period, although the scale of rainfall was not large, the quantity of flow reached the maximum flow rate in a short time. From this, it is thought that fluctuation of the turbidity is also related to the fluctuation of the quantity of flow.

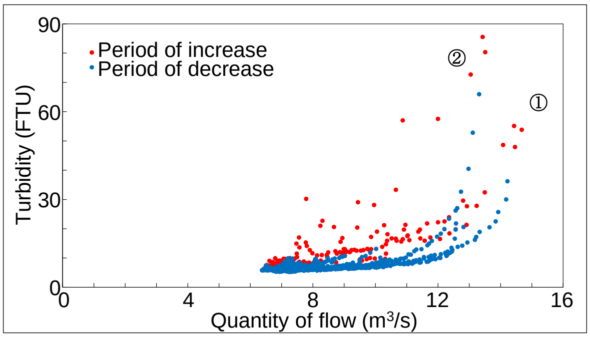

Figure 9. The relationship between the quantity of flow and the turbidity.

On the other hand, Figure 10 shows the relationship between the concentrations of nutrient and the turbidity. These have a very high correlational relationship. The correlation line is decided as follows,

$$C = eT_u + f \quad [3]$$

where, C is the concentrations of nutrient; T_u is the turbidity; e and f are the coefficients. It is found that concentrations of TN and TP increase as the turbidity increases. This is because TN and TP contained suspended nutrients adhering to suspended particles, and the concentration also increased due to the increase in the turbidity. Furthermore, TP has a strong correlation with the turbidity when compared with TN. This is because most of phosphorus flows out into the river from the surrounding waters as a suspended state as the quantity of flow increases during rainfall. Also, since the turbidity has hysteresis, considering the relationship between the turbidity and the concentration of nutrients, there is a difference in nutrient load in the increasing period and the decreasing period despite the same quantity of flow. In other words, it is considered that the error of the nutrient load in the LQ equation is due to failure of adequately reflecting the fluctuation of the nutrient load with only the momentary value of quantity of flow.

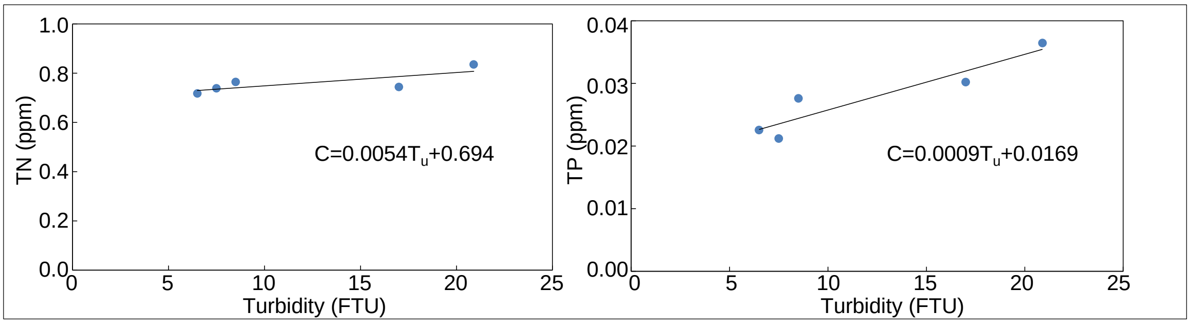

Figure 10. The relationship between the nutrients and turbidity.

3.5 Estimation of the turbidity by the quantity of flow

From the previous section, since there is a relationship between the turbidity and the concentration of nutrients, it is possible to calculate the nutrient load from the turbidity. However, to calculate the nutrient load due to turbidity, it is necessary to acquire the data with a turbidimeter at the site. Therefore, in this study, the turbidity was estimated from the relation between the quantity of flow and the turbidity. The turbidity was estimated with reference to the formula of Watanabe and Yamaguchi (1999).

$$T_u = \left(gQ^h + i\right) + j\frac{dQ}{dt} \quad [4]$$

where t is time, g, h, i and j are the coefficients. The first term on the right-hand side is the averaged correlation between the quantity of outflow and the turbidity. The second term is the correction term. Since the hysteresis relationship between the quantity of flow and the turbidity was different at a certain flow rate, variation rate or greater, the case was divided in $dQ/dt \geqq 1.8\times10^{-4}$. Figure 11 shows the relationship between the quantity of flow and the turbidity and the power approximation from $\left(gQ^h + i\right)$. Then, Figure 12 shows the relationship with the error due to the power approximation for determining the coefficient *j*.

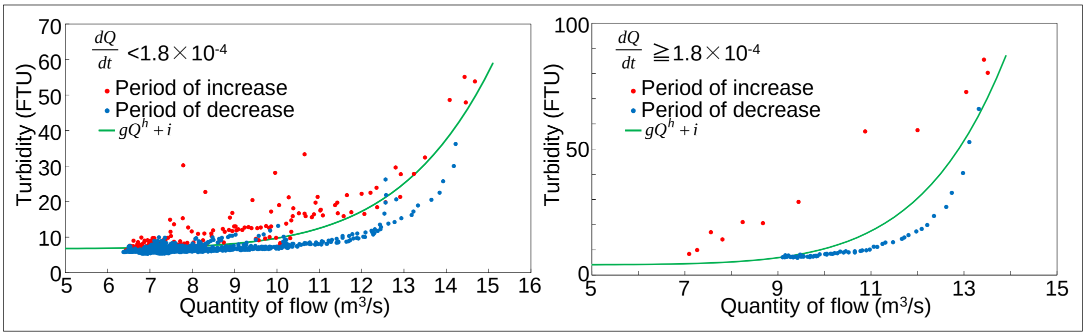

Figure 11. The relationship between the quantity of flow and turbidity.

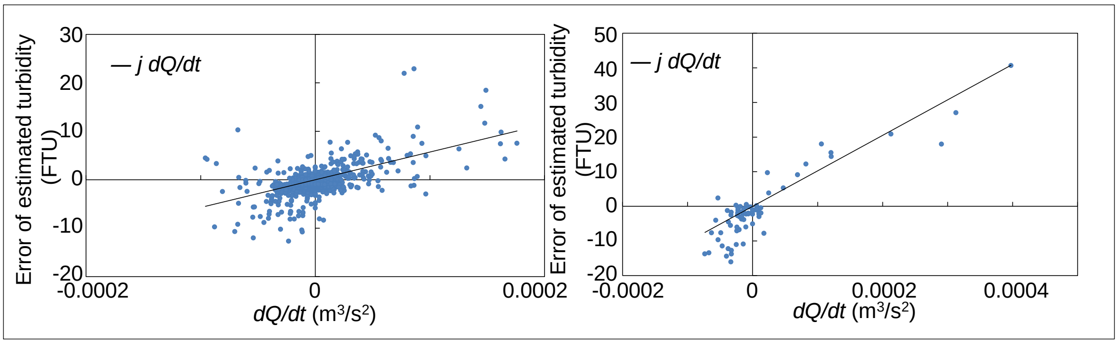

Figure 12. The relationship between dQ/dt and the estimated error of the turbidity.

Estimation equations obtained by examination are shown below.

$$T_u = \left(3.0\times10^{-7} Q^{6.99} + 6.80\right) + 57220\frac{dQ}{dt} \qquad \left(\frac{dQ}{dt} < 1.8\times10^{-4}\right)$$
$$T_u = \left(1.0\times10^{-7} Q^{7.80} + 4.10\right) + 102500\frac{dQ}{dt} \qquad \left(\frac{dQ}{dt} \geqq 1.8\times10^{-4}\right) \qquad [5]$$

From the above fomula, Figure 13 shows the time variations of the observed and estimated turbidity. It reveals that the precision of estimated result is improved by considering the variability of the quantity of flow. However, since hysteresis of the turbidity greatly differs in the case of large fluctuation rate of the quantity of flow, there is a possibility that an error will be generated with respect to the actual turbidity depending on the scale of the flood. Therefore, it is necessary to improve the accuracy of the estimation by grasping the relationship between the quantity of flow and turbidity in detail by longer observation.

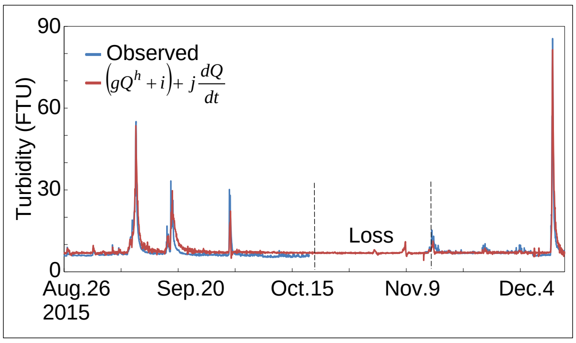

Figure 13. The time variations of the observed and estimated turbidity.

3.6 Estimation of the nutrient load from the turbidity

From 3-4 and 3-5, it became possible to estimate the turbidity by the quantity of flow, and consequently estimate the nutrient load by the turbidity.

Figure 14 shows the comparison of the TN load estimated by the LQ equation and the turbidity. As a result, it reveals that the precision of estimated results of nutrient load is improved by considering the turbidity.

Here, the estimation accuracy for the nutrient load was calculated from the turbidity, the LQ equation, and the result of observation from 2014 to 2015. Figure 14 shows the variation of the nutrient load estimated by each method. From the figure, it reveals that the estimation using turbidity can accurately estimate the variation of the nutrient load as compared with the estimation by the LQ equation. That is, in the case of TN or TP, the turbidity reflects the variation of the suspended nutrient salt attached to the turbidity particles. However, there are future tasks such as underestimation of the increase rate of the nutrient load as compared with the actual measurement value.

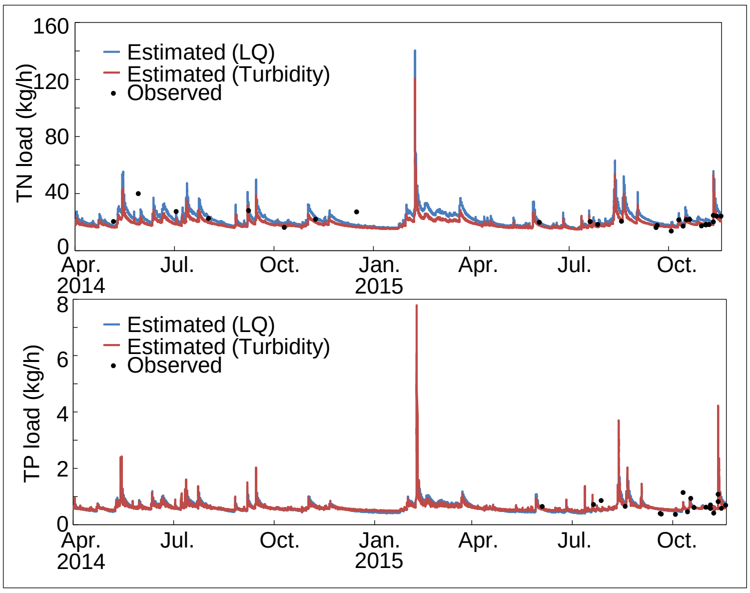

Figure 14. The time variations of the nutrient load estimated by each method.

4 CONCLUSIONS

In this study, the characteristics of the quantity of flow and the nutrient load in the Kesen river flowing in Sanriku District, Iwate Prefecture are investigated. The nutrient load is calculated from HQ equation and the result of water quality observation. The LQ equation is formulated and its accuracy examined. Although the LQ equation can estimate the nutrient load easily, there is no unique relationship between the quantity of flow and the nutrient load, and the error is also large with respect to the actual nutrient load. On the other hand, there is a high correlation between TN, TP and the turbidity. In addition, since the turbidity varies in the process of fluctuation when the quantity of flow is increased or decreased, it is suggested that the nutrient load varies even at the same flow rate. From the relationship between the quantity of flow and the turbidity, the fluctuation of the turbidity can be accurately reproduced by the function of the quantity of flow. The estimation using the turbidity can accurately estimate the variation of the nutrient load as compared with the estimation using the LQ equation. It is imperative to further study the relationship between the turbidity, the water quality and the quantity of flow, and to improve its accuracy.

REFERENCES

Aya, S. & Iwasa Y. (1982).Yield and Dispersion of Turbidity in Some Rivers. *Proceedings of Hydraulic Engineering,* 26, 577-582. (In Japanese).

Kinoshita, T. (1984). Interpretation of the Loop of the Stage Discharge Curve. *Proceedings of Hydraulic Engineering,* 28, 197-200. (In Japanese).

Watanabe, K. & Yamaguchi, H. (1999). Study on the Turbidity Function in Stormflow. *Proceedings of Annual Conference, Japan Society of Civil Engineering, Hokkaido Branch,* 55, 298-301. (In Japanese).

Yamamoto, K., Futamura, T., Sakano, A., Kusakabe, T., Suetsugi, T. & Yokoyama, K. (2003). Estimation of Particulate Nutrients Loads using Turbidity Meter. *Advances in River Engineering,* 9, 515-520. (In Japanese).

Makino, I., Yahagi, Y. & Oi, S. (2005). Analysis Chemistry Consideration of Runoff Component Characteristics at Normal Stage of Water and Flood in River Basin. *Proceedings of Hydraulic Engineering,* 54, 1213-1218. (In Japanese).

Kashiwadate, N., Obadha, O.F., Sato, H., Nomura, M. & Sawamoto, M. (2006). Evaluation of the Amount Loads of the Nutrients from River to Ofunato Bay. *Annual Journal of Civil Engineering in the Ocean,* 22, 787-792. (In Japanese).

Matsumoto, Y., Takaki, T. & Ebata, K. (2012). Runoff Characteristics of Phosphorus during Rainfall Events in an Urban Stream of Toyota City. *Study of Yahagigawa,* 16, 5-10. (In Japanese).

Proceedings of the 37th IAHR World Congress
August 13 – 18, 2017, Kuala Lumpur, Malaysia

ECO-HYDROLOGICAL MODELLING OF A RESTORED RIPARIAN WETLAND

BIRGITTE VON CHRISTIERSON[1], MICHAEL BUTTS[2], LAURA A. NIEUWENHOVEN[3], FLEMMING T. HANSEN[4], JANNICK K. JENSEN[5] & JANE R. POULSEN[6]

[1,2]DHI Denmark, Hoersholm, Denmark, bvc@dhigroup.com, mib@dhigroup.com, fth@dhigroup.com
[3]Atkins, Oxford, United Kingdom, laura.nieuwenhoven@atkinsglobal.com
[4]DTU AQUA, Charlottenlund, Denmark, ftho@aqua.dtu.dk
[5]Capital Region of Denmark, Centre for Regional Development, Hilleroed, Denmark, jannick.kolbjoern.jensen@regionh.dk
[6]Department of Bioscience, Aarhus University, Denmark,jpo@bios.au.dk

ABSTRACT

River channelization and agricultural drains have been widely used across Europe to improve land drainage, increase productive areas and control flooding. However, this has introduced a number of adverse environmental impacts, including the loss of riparian wetlands. It is now widely recognized that riparian wetlands provide beneficial functions to the wider environment through their hydraulic connection to rivers and streams. Through water storage and retention, wetlands support biodiversity, mitigate floods and serve as nutrient buffer zones for the river system. The restoration of rivers and riparian wetlands is increasingly being used to achieve 'good ecological status' of water bodies as required by the EU Water Framework Directive (WFD). In Denmark, wetland restoration is used to improve riparian and channel habitats and to reduce the nutrients loads to Danish streams and fjords. While many studies indicate improved water quality, as a result of wetland restoration, the influence of extensive alterations on the hydraulic interaction between flows in streams, their floodplains and subsurface flows, together with the effect on nutrient processes, has received limited attention. In this study, an integrated eco-hydrological modeling tool is presented representing flow, transport and water quality processes in riparian wetlands that can be used to quantify the impacts of both river restoration and the construction of riparian wetlands. This tool is applied to a restored riparian wetland on the Odense River in Denmark. Results show that the flooding behavior from the stream is critical for nitrate removal, accounting for 85-90% of total nitrate removal. Removing drains is also of significance with respect to restoring natural groundwater flow conditions but less significant in terms of nitrate removal in the subsurface for this particular wetland. The results demonstrate the applicability of this modelling tool for evaluating the benefits of wetland restoration and for use in wetland design.

Keywords: River and wetland restoration; integrated modelling; flooding; hydro-period; water quality.

1 INTRODUCTION

There is an increasing recognition of the ecological and economic values and services of wetlands (Duranel et al., 2007; Acreman and Ferguson, 2010). The environmental benefits of riparian wetlands range from improving the recreational value of rivers, biodiversity and water purification, to flood protection, shoreline stabilization, groundwater recharge, and streamflow maintenance. Riparian zones intercept surface as well as sub-surface flows and function as buffers for river systems, reducing nutrient loadings through processes such as sedimentation and regeneration, de-nitrification/nitrification processes and to a smaller degree plant uptake, decay and mineralization (Fisher and Acreman, 2004; Mayo and Bigambo, 2005). Through water storage and retention, riparian wetlands, not only serve as nutrient buffers but can also mitigate floods and support biodiversity.

Therefore, the restoration of rivers and riparian wetlands is increasingly used as a means in river basin management strategies across Europe for achieving 'good ecological status' of water bodies as required by the EU Water Framework Directive (WFD). In Denmark, restored and constructed wetlands are used to improve the riparian and channel habitats and to reduce the nutrients loads to the Danish stream and fjords as part of the Danish river basin plans.

The dynamics of flooding and the interaction between surface water and groundwater are key factors in determining their effectiveness in reducing nutrient loadings. The influence of physical alterations affecting the hydraulic interaction between streams, their floodplains and subsurface and the effect on nutrient processes is important for assessing the environmental impacts of stream modifications or the potential benefits of river restoration but has received limited attention (Sørensen et al., 1990; Walling and He, 1998). Only a few modelling studies include representations of surface water flooding, unsaturated flow and groundwater flow together with nutrient processes (Restrepo, et al., 1998; Langergraber and Šimůnek, 2005; Rassam, et al., 2008). In this study, a modelling tool is developed capable of representing these processes and the impact of physical alterations of the river and channel system. This tool is based on coupling the integrated hydrological flow and transport model, MIKE SHE (Graham and Butts, 2006) with an ecological modelling tool ECO Lab for water quality and ecological processes (Butts et al. 2012; Loinaz et al., 2013; Loinaz et al., 2014). This tool has, as part of this work, been extended to use ECO Lab in both the surface and subsurface processes. The modelling tool has also been further developed to predict the nitrate reduction processes in the surface and subsurface and this is applied to the analysis of the flooding behavior and the nitrate reduction capacity of a re-constructed wetland that intercepts both surface and groundwater.

2 WETLAND STUDY AREA

The study area is located on the Odense River on the island of Funen, Denmark. The river reach was restored in 2003 by re-introducing meanders in the straightened channel and reducing the flow capacity in the channel by reducing the cross-section area and raising the bed level. More details of the study area and restoration can been found elsewhere (Poulsen et al., 2014; Jensen et al., 2017). The wetland area and the re-meandered river are shown in Figure 1. The catchment area upstream of the wetland is 254 km^2 and the land use is predominantly agriculture (65%).

The catchment and floodplain topography were derived from a digital elevation model with a grid size of 1.6 m model, a vertical resolution of 0.06 from the Danish Geodata Agency (GST). A number of river cross-sections along the restored section were surveyed in 2010, including a detailed cross-section of the wetland site. From previous studies, transect measurements of water depths and velocities had been made in an investigation of the hydraulics and sedimentation in the wetland (Poulsen et al., 2014). A second set of transect measurements of groundwater and nutrient concentrations to investigate nitrate reduction in the groundwater is available from the University of Copenhagen and the Danish Geological Survey (GEUS) (Jensen et al. 2017).

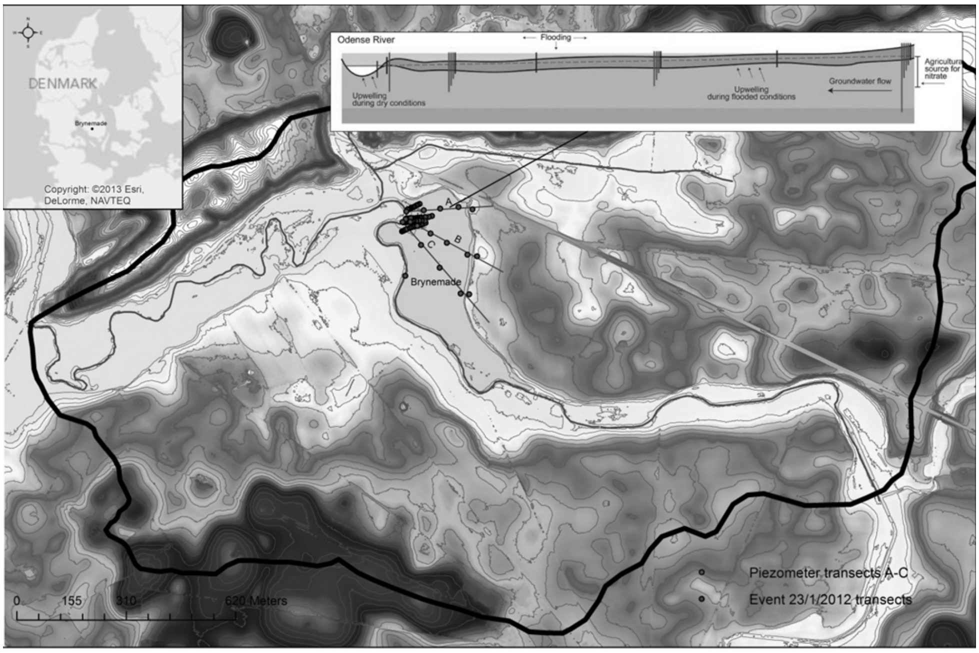

Figure 1. Location of the wetland study area, topography, local model boundary and geological profile.

3 MODELLING TOOLS AND APPROACH

3.1 Water and transport modelling

The integrated hydrological modelling system MIKE SHE (Graham and Butts,2006) simulates the major processes of the terrestrial hydrological cycle; snow accumulation and melting, evapotranspiration, river and channel flows, overland flow, and subsurface flow in the unsaturated and saturated zones, see Figure 2. The different flow processes of MIKE SHE are described either by the governing partial differential equations or by empirical relations and these are then solved by discrete grid-based numerical approximations in space and time.

More recently, the process-based formulation of MIKE SHE has been exploited to develop a more flexible modeling tool, where each of the major processes can be modeled using both conceptual and physics-based representations. There are several advantages in this flexibility, the most important being that the mathematical representation of a particular process can be adapted to the modelling goals and the data available (Butts et al. 2004; Butts and Graham, 2008).

In this study, the two-dimensional diffusive wave approximation in MIKE SHE for overland flow was coupled to the one-dimensional river model, MIKE 11 (Havnø et al., 1995) to describe the floodplain and river channel flows, respectively. In the subsurface, a one-dimensional description of the unsaturated flow and a three dimensional finite difference description of the groundwater flow were used.

The MIKE SHE river and floodplain model domain covered the 3.1 km^2 area of the restored river and flood plain, Figure 1, using a 25m by 25m numerical grid. The domain boundary was delineated based on topographic divide, assuming that the groundwater divide of the underlying shallow sand aquifer and topographic divide coincided. This is typically a reasonable assumption for shallow permeable aquifers (Haitjema and Mitchell-Bruker, 2005). A second model was created covering only the riparian wetland. This MIKE SHE wetland model domain used dynamical boundary conditions from the river and floodplain model, see Figure 1. Within the wetland, a simple geological description was used, consisting of a 1 m layer of peat overlying a 12 m thick sand layer and represented numerically by a single computational layer in the peat and eight computational layers in the sand.

Estimates of the model parameters were taken where possible from previous works (Poulsen et al., 2014; Jensen et al., 2017) or alternatively, typical standard values for Danish catchments were used.

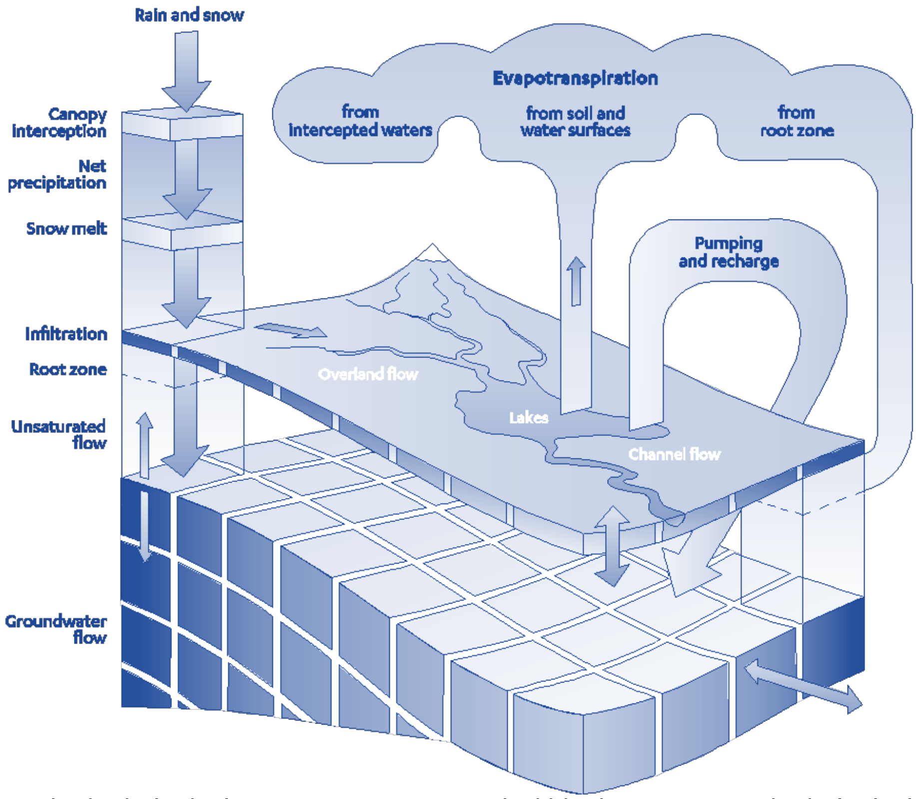

Figure 2. The hydrological processes represented within the MIKE SHE hydrological model.

3.2 Water quality and nitrate modelling

The advection-dispersion processes for conservative transport, in both the surface and subsurface, were represented using the MIKE SHE water quality module (Graham and Butts, 2006).The ecological process model ECO Lab, was used to represent the nitrate processes. ECO Lab is a general process tool that calculates the rate of change of any type of state variable given any number of related variables, processes and forcings (DHI, 2009). The numerical approach is a form of split operator scheme where the conservative transport is first calculated for a given simulation time step. ECO Lab acts as a post-processor solving the full water quality equations by treating these processes as sink/source terms in the complete set of equations (Loinaz et al., 2013).

For this study, a simple representation of the main nitrogen removal processes identified in riparian wetlands was used that included, nitrification, denitrification, plant production and nutrient uptake, plant death, mineralization and adsorption. The processes were assumed to be temperature dependent and the surface and subsurface are shown schematically in Figure 3. Nitrification and denitrification were described by temperature dependent Michalis-Menten or first-order equations (Dørge, 1991). The denitrification rate in saturated peat was assumed to be depth dependent using an exponential decay function presented by Rassam et al. (2008). Plant production and uptake in the wetland were calculated using a simple approach based on light radiation and did not currently depend on nitrate or ammonium concentrations.

The nitrate process parameters had been estimated from values reported in (Jensen et al., 2017) and literature values (Dørge, 1991). It should be noted that denitrification and nitrification rates are site dependent and can vary considerably from wetland to wetland.

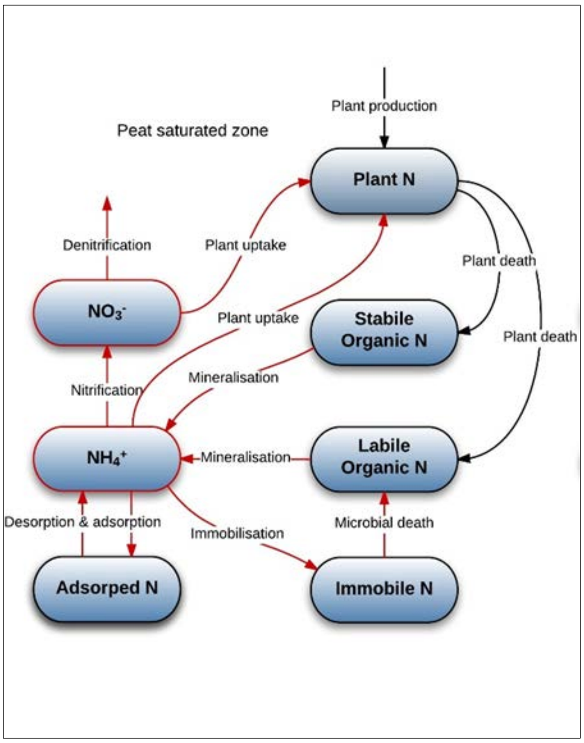

Figure 3. Nitrate processes included in the MIKE SHE-ECO Lab model for the wetland processes.

4 INITIAL MODELLING RESULTS

Calibration of the flow model was performed manually using visual inspection of the groundwater (piezometer) levels in different transects, statistical performance criteria and general experience with calibration. The final simulations appear to reproduce the groundwater levels and their dynamics during flooding quite well, see Figure 4. The pattern of flooding, flood depth and flood extent, are similar to those obtained in previous work using a hydrodynamic modeling approach (Poulsen et al., 2014). Similar discrepancies are found when comparing the observed and simulated flood peak flows (not shown) that may be due to the quality of the data or model structure. These results indicate that the flow model satisfactorily captures the wetland flow behavior.

The dynamic flow boundary conditions from the floodplain model were then used to derive the flow boundary conditions for the smaller wetland model. The nitrate and ammonium boundary conditions in the groundwater were estimated from observed values (Jensen et al., 2017). Initial conditions were set to zero in an initial model run and then replaced by equilibrium conditions at the end of eight years of simulation. In this study simple description, the effect of oxygen was neglected.

Validation of the water quality model was carried out by comparing the simulated concentrations with measurements in the groundwater from Jensen et al. (2017). These first simulation results show that the nitrate plume in the groundwater is not completely attenuated as observed but reaches the stream with very low nitrate concentrations. Assuming this wetland flow and transport model are representative of the actual behavior in the wetland, the total nitrate removal obtained are examined as a result of the restoration as well as the change in flow behavior before and after restoration.

The initial results show that a large percentage of the nitrate entering the wetland model area either through the groundwater or from flooding, is removed. However the nitrate loads entering the wetland via flooding are much higher than those entering from the sub-surface flows. The overall nitrogen balance is summarized in Table 1. A second set of simulations were then carried out in which the model was used to represent the wetland prior to restoration, with a straighter channel, wider cross-sections and active till drains. The flooding behavior is dramatically altered. According to the simulations in this study, little spilling from the river to the wetland occurs prior to restoration and the water levels in the wetland are maintained by groundwater flow. The altered flooding behavior is clearly illustrated in Figure 5, which shows a significant increase in the flooding frequency for this riparian wetland following restoration. While only a relatively small fraction of the mass of nitrate entering the wetland from the stream is removed, this amounts to approximately 130 kg/hectare/year. This is in good agreement with typical retention rates for Danish wetlands found in other studies, which are in the range of 100-200 kg/hectare/year.

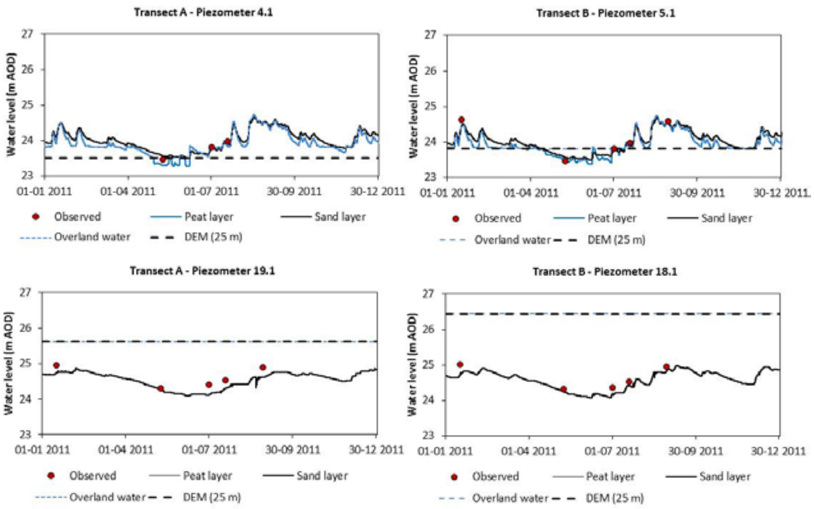

Figure 4. Comparison of the modelled and simulated water levels at selected piezometers. The symbols represent observations and the lines represent the corresponding simulations. Simulated groundwater levels in the peat layer are shown in blue.

Table 1. Modelled nitrogen removal in the wetland, averaged over 2005-2011 (kg/hectare/year).

	RESTORED STATE	PRE-RESTORATION
Total input to the wetland	2644	30
Total nitrogen removed	127	14

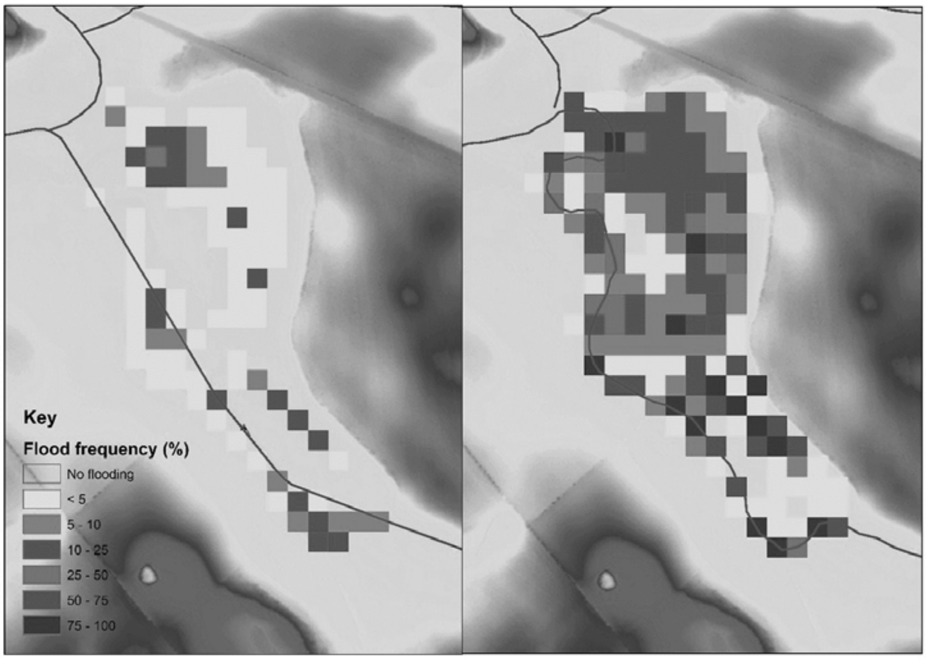

Figure 5. Simulated changes in flood frequency for the wetland in the pre-restoration scenario (left) and following restoration (right).

5 CONCLUSIONS

In this study, an integrated flow and water quality modelling tool are developed capable of representing both flow and nitrate processes in riparian wetlands. This tool is derived by coupling the integrated hydrological model for flow and transport, MIKE SHE with an ecological modelling tool ECO Lab of water quality processes, not only in the surface flows as in previous work but also in the subsurface. This tool has been applied to an assessment of nitrate reduction in a restored riparian wetland on the Odense River, Denmark.

The preliminary simulations presented in this study indicate that this tool is able to capture the observed flows in the groundwater, river and wetland system. Using a relatively simple description of the nitrate processes, it appears that the nitrate reductions estimated are consistent with other studies in Danish wetlands. One of the strengths of this type of tool is that it allows engineers to assess the impact of physical alterations of the river and channel system in terms of flow, water quality and ecology as demonstrated for a pre-restoration scenario. This approach can be used both for assessment of river and wetland restoration and for wetland design. Future work will examine the sensitivity of these results to flow parameters such as dispersion and vertical conductivities in the peat layer as well as the N-process parameters. Simulations at a larger scale for the entire re-meandered reach will be explored.

ACKNOWLEDGEMENTS

We would like to thank Prof. B. Kronvang, Department of Bioscience, Aarhus University and Prof. Peter K. Engesgaard, Department of Geosciences and Natural Resource Management University of Copenhagen for providing data support. Data from Jensen et al. (2017) was obtained as part of the EU FP7 AQUAREHAB project as a collaboration mainly between University of Copenhagen and Geological Survey of Denmark and Greenland.

REFERENCES

Acreman, M.C. & Ferguson, A.J.D. (2010). Environmental Flows and the European Water Framework Directive. *Freshwater Biology*, 55(1), 32-48.

Butts, M.B., Payne, J.T., Kristensen, M. & Madsen, H. (2004). An Evaluation of the Impact of Model Structure on Hydrological Modelling Uncertainty for Streamflow Prediction. *Journal of Hydrology*, 298(1-4), 242-266.

Butts, M.B. & Graham, D.N. (2008). Evolution of an Integrated Surface Water-Groundwater Hydrological Modelling System. *Proceedings of the IAHR International Groundwater Symposium 2008,* 18-20.

DHI. (2009). *ECO Lab: Short Scientific Description,* MIKE.

Duranel, A.J., Acreman, M.C., Stratford, C.J., Thompson, J. R. & Mould, D.J. (2007). Assessing the Hydrological Suitability of Floodplains for Species-Rich Meadow Restoration: A Case Study of the Thames Floodplain, UK. *Hydrology and Earth System Sciences Discussions*, 11(1), 170-179.

Dørge, J. (1991). *Model of Nitrate Transformations in Freshwater Wetlands (In Danish),* DHI Report.

Fisher, J. & Acreman, M.C. (2004) Wetland Nutrient Removal: A Review of the Evidence, *Hydrology and Earth System Sciences,* 8(4), 673-685

Graham, D.N. & Butts M.B. (2006). *Flexible, Integrated Watershed Modelling with MIKE SHE, Watershed Models.* CRC Press, 245-272.

Haitjema, H.M. & Mitchell-Bruker, S. (2005). Are Water Tables a Subdued Replica of the Topography? *Groundwater* 43(6), 781-786.

Havnø, K., Madsen, M.N. & Dørge, J. (1995). *MIKE 11 Ageneralized River Modelling Package. Computer Models of Watershed Hydrology,* Water Resources Publications, Colorado, USA, 733–782.

Jacobsen, T.V. & Graham, D.N. (2009). Integrated Hydrologic Modelling in the Okavango. *32nd Hydrology and Water Resources Symposium, Newcastle: Adapting to Change.* 941-952.

Jensen, J.K., Engesgaard, P. & Nilsson B. (2017). Hydrological Mediated Denitrification in Groundwater below a Seasonal Flooded Restored Riparian Zone. *Water Resources Research,* 53(3), 2074-2094.

Langergraber, G. & Šimůnek, J. (2005). Modeling Variably Saturated Water flow and Multicomponent Reactive Transport in Constructed Wetlands. *Vadose Zone Journal*, 4(4), 924-938.

Loinaz, M., Davidsen, H., Butts, M. & Bauer-Gottwein, P. (2013). Integrated flow and Temperature Modeling at the Catchment Scale. *Journal of Hydrology*, 495, 238-251.

Loinaz, M., Gross, D., Unnasch, R., Butts, M. & Bauer-Gottwein, P. (2014). Modeling Ecohydrological Impacts of Land Management and Water use in the Silver Creek Basin, Idaho. *Journal of Geophysical Research: Biogeosciences*, 119, 487-507

Mayo, A.W. & Bigambo, T. (2005). Nitrogen Transformation in Horizontal Subsurface flow Constructed Wetlands I. *Model development, Physics and Chemistry of the Earth* 30, 658-667.

Poulsen, J.B, Hansen, F., Ovesen, N.B., Larsen,S.E. & Kronvang,B. (2014).Linking Floodplain Hydraulics and Sedimentation Patterns along a Restored River Channel: River Odense, Denmark. *Ecological Engineering* 66, 120-128.

Rassam, D.W., Pagendam, D.E. & Hunter, H.M. (2008). Conceptualisation and Application of Models for Groundwater Surface Water Interactions and Nitrate Attenuation Potential in Riparian Zones. *Environmental Modelling and Software*, 23(7), 859-875.

Restrepo, J.I., Montoya, A.M. & Obeysekera, J. (1998). A Wetland Simulation Module for the MODFLOW Ground Water Model. *Ground Water,* 36(5), 764-770.

Sørensen, H.R., Klucovska, J., Topolska, J., Clausen, T. & Refsgaard, J.C. (1990). *An Engineering Case Study Modelling the Influences of Gabcikovo Hydropower Plant on the Hydrology and Ecology in the Slovakian Part of the River Branch System of Zitny Ostrov.* Distributed Hydrological Modelling, Springer Netherlands, 233-253.

Walling, D.E. & He, Q. (1998). The Spatial Variability of Overbank Sedimentation on River Floodplains. *Geomorphology*, 24(2), 209-223.

Proceedings of the 37th IAHR World Congress
August 13 – 18, 2017, Kuala Lumpur, Malaysia

FLOW STRUCTURE AT CONFLUENT MEANDER BEND CHANNEL

SHEHUA HUANG[1] & BIN SUI[2]

[1]Wuhan, China,Wuhan University
hshh2@126.com
[2] Wuhan, China, Wuhan University
bins@whu.edu.cn

ABSTRACT

The estimated influence of bank roughness on outer bank secondary flow is simulated by two CFD codes solving the N-S equations within a confluent meandering bend channel. The first CFD code is based on Large Eddy Simulation. The other code solves Reynolds-average N-S equation. The numerical results from two codes are tested by comparison to the experimental results, which reveal good agreement between the test and numerical simulation. Results suggest that increasing the outer bank roughness strengthens the outer bank clockwise secondary flow cell and decreases the scale of counter rotating secondary flow. Both LES and RANS simulations can predict the large scale of secondary flow near the outer bank in the confluent meander bend channel, but the RANS model fails to capture the small scale secondary flow cell near the water surface.

Keywords: Confluent meander bend; LES; RANS model; bank roughness; outer-bank; secondary flow.

1 INTRODUCTION

According to researches, confluence rivers are roughly classified into two categories, namely: 1) straight approaching channel and straight-receiving channel (straight channel junction); 2) the straight channel entering into a bend channel at the bend apex on the outer bank. A straight channel junction can either be symmetrical or asymmetrical. The physics of junction flow in meandering river is more complicated, and its flow characteristics have a significant difference with those in a straight channel junction. Due to channel curvature, flow through a bend is subjected to an outward-directed centrifugal force, which is accompanied by a counterbalancing and inward-directed pressure gradient force. The interaction between two forces generates a secondary flow at the cross section of bend. As the tributary stream enters into the main bend channel, the characteristics of the secondary flow are unnecessarily changed for different junction angles and discharge ratios. Meander bend channel helical flow characteristics have a great effect on deposition and erosion in rivers. Secondary flows control river dynamic, flow mixing and sediment transport (BEST, 1987; Best, 1988; Bradbrook, 1998; Rhoads, 2001). Several researches focusing on helical flow have been done in recent years. The outer bank helical flow has been studied by lab experiment and field investigations (Einstein1954, Blanckaert 2012). Most researchers used numerical model to simulate flow structure in meandering bend channel (Stoesser, 2010; Kang, 2011). Two main approaches to calculate the flow in meander bend channel, were based on the LES or RANS turbulence model. (Jin, 1990) and (Thorne, 1995) have researched on the effect of bank roughness in bends channel, but their studies were not detail enough to analyze secondary flow near the outer bank. Many researchers (Keylock, 2005a; Stoesser et al., 2010; Kang, 2011) have investigated the effect on bed roughness in open-channel. Blanckaert 2012 provided detailed analysis the effect of bank roughness on outer bank secondary flow. Only very few researchers put their focus on the influence of the bank roughness. Hence, in this study, based on measurements of flow in lab experimental confluent meandering bend channel and combined with 3D numerical simulation, the influence of the outer bank roughness on secondary flow near the outer bank is investigated and discussed.

2 NUMERICAL MODEL SETUP

Fig 1 shows the numerical model (with the z-direction being positive upwards) that consists of a 1-m-wide main channel and 0.3-m-wide tributary channel. The main channel consisted of a 4-m-long straight inlet, a 180° curved reach, and a 4-m-long straight outlet. The centerline radius of the curved reach was 2 m. The bend inlet and outlet were parallel to each other. The curved segment had a rectangular cross-section. The intersection at the confluence between the tributary and the main channel was located at a 90° cross-section (CS4). The tributary channel was a straight rectangular flume, which was 3.5 m from the confluence. Here, 90° was set as the junction angle between the tributary and the main channel. The gradient of the straight main channel was 1/2000, and the average gradient of the curved segment and the tributary were 1/1250 and 1/1000, respectively.

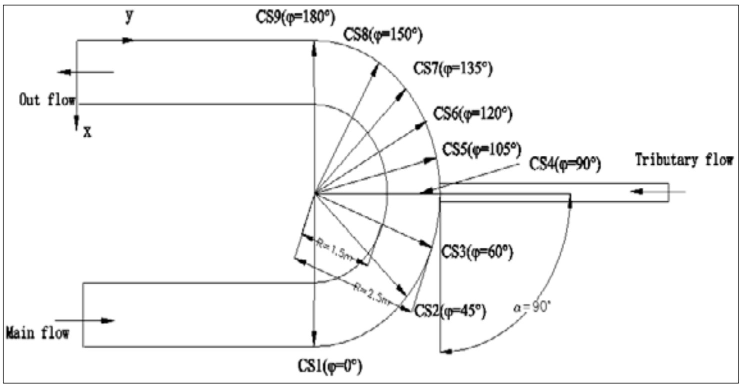

Figure 1. Conceptual model of the confluent meander bend (junction angle is 90°).

The discharge from the main channel was denoted as Q_M (Q_M = 30 L/s) and the discharge from the tributary channel was denoted as Q_T. The simulation was divided into three different roughnesses high ($K_{s1} = 0\text{m}$, $K_{s2} = 0.002\text{m}$ and $K_{s3} = 0.01\text{m}$) for flux ratio ($\lambda = Q_T/Q_M = 0.6$) at junction angle of 90°. The numerical model had the same flow conditions as thephysical model. Simulation of three-dimensional (3D) flow through the meander bend in the numerical model was performed using the Openfoam of large eddy simulation (LES) and RANS turbulence models.

A structured hexahedral mesh was adopted in the model. The grid had a greater density in the junction area, because the hydraulic elements in this region changed relatively faster than those at other locations, and a boundary layer grid was used near the banks. A 3D structured grid system with 6.6 $\times$ 10^6 elements was generated with the grid generator GAMBIT.

2.1 Large eddy simulation

The numerical model employed in this study was based on the 3D LES turbulence model. The LES simulation solved the filtered velocity and pressure field, whereas the influence of filtered small-scale features on larger eddies was modeled through a sub-grid stress (SGS) model. The equations for the LES method are shown as follows:

$$\frac{\partial \overline{u_i}}{\partial x_i} = 0 \qquad [1]$$

$$\frac{\partial \overline{u}_i}{\partial t} + \frac{\partial \overline{u}_i \overline{u}_j}{\partial x_j} = -\frac{1}{\rho}\frac{\partial \overline{p}}{\partial x_i} + \upsilon \frac{\partial^2 \overline{u}_i}{\partial x_j \partial x_j} - \frac{\partial \tau_{ij}}{\partial x_j} \qquad [2]$$

Where $\overline{u_i}$ is the filtered large eddy velocity, and $\tau_{ij}$is the modeled SGS that accounts for the influence of the sub-grid eddies on the large eddies. The SGS model is as follows:

$$\tau_{ij} = \frac{1}{3}\tau_{kk}\delta_{ij} - \upsilon_t \overline{S_{ij}} \qquad [3]$$

$$\upsilon_t = 2(C_s\Delta_f)^2 S \qquad [4]$$

$$S = \sqrt{2\overline{S_{ij}} \cdot \overline{S_{ij}}} \qquad [5]$$

where $\overline{S_{ij}}$is the filtered strain rate tensor, defined by $\overline{S_{ij}} = \frac{1}{2}\left(\frac{\partial \overline{u_i}}{\partial x_j} + \frac{\partial \overline{u_j}}{\partial x_i}\right)$

The inflow condition of velocity and the height of the inlet were provided as obtained by experimental measurements. For the inlet boundary, the flow discharge and velocity of the main channel were specified. The pressure was chosen to have a zero normal gradient for consistency with the velocity condition. The outlet boundary was set to have a zero gradient. The free surface was described by the rigid-lid approximation (using measured water surface data). The finite volume method (FVM) was used for discretion of the Navier–Stokes equations, and the pimple Foam method was used to solve the problem of velocity and pressure coupling. The central difference scheme was accepted for the diffusion terms of the governing equation, and the convection term was solved by a first order upwind scheme.

2.2 RANS model

Continuity equation:

$$\frac{\partial U_i}{\partial x_i} = 0 \qquad [6]$$

with i=1, 2, 3
Reynolds Averaged N-S equation:

$$U_j \frac{\partial U_i}{\partial x_i} = \frac{1}{\rho} \frac{\partial}{\partial x_j} (-P\delta_{ij} - \rho\overline{u_i u_j}) \qquad [7]$$

The simulation was divided into 3 different roughnesses $K_{s1} = 0\, mm\ (smooth)$, $K_{s2} = 2\, mm$, $K_{s3} = 10mm$ on the banks, the roughnesse K_{s1} was selected for comparing with the experiment data, the roughness $K_{s2} = 2\, mm$ was intended to represent the sand bank (K. Blanckaert) and $K_{s3} = 10\, mm$ was intended to represent riprap size. Each roughness corresponds to flux ratio $\lambda = \frac{Q_T}{Q_m} = 0.6$.

3 RESULTS

3.1 Model validation

Correlations between model predictions and measured data were all statistically significant. Physical model experiment data were used to validate the numerical model of confluent meander bend flow. Figures 2 and 3 display the velocity changes with water depth for given radius (radius values R are 1.71 m, 1.88 m, 2.05 m, 2.22 m, and 2.34 m) for cross sections $\varphi = 60^0$ (CS3), $\varphi = 120^0$ (CS6) in the bend channel, where the roughness high $K_{s2} = 2\, mm$, $\lambda = 0.6, \alpha = 90^0$, respectively. As the figures show, the transverse velocity of LES data shows much better agreement with the experimental data than K-Omega data's.

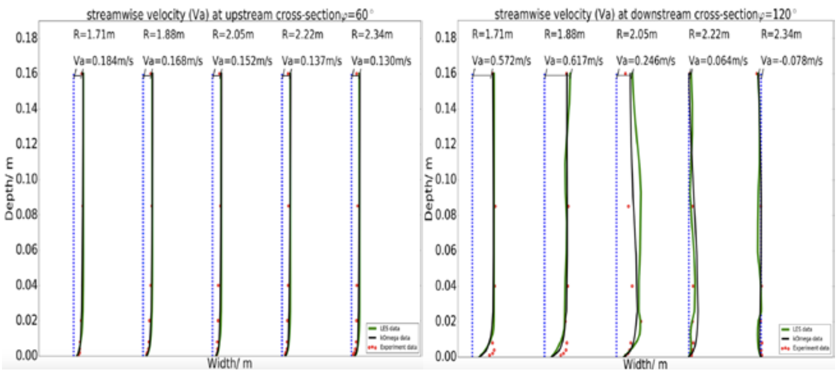

(a) (b)

Figure 2. Comparison of model testing and numerical data for a streamwise velocity distribution in cross sections (a) CS3 (b) CS6 in the bend channel, where the discharge ratio is λ=0.6 and the junction angle is α= 90°. (---axis, ——LES data, ⋯experimental data).

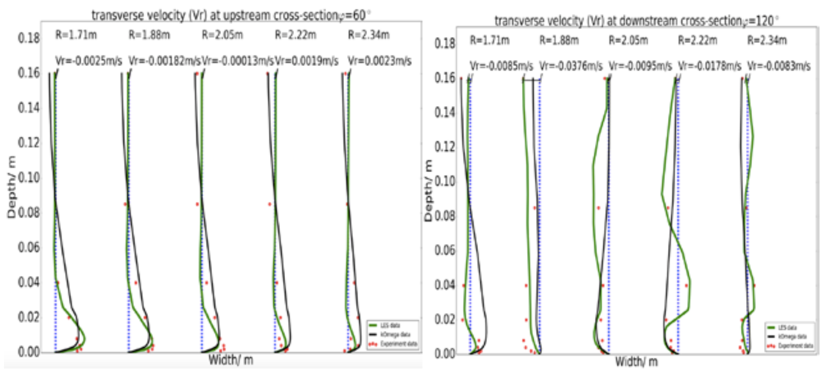

(a) (b)

Figure 3. Comparison of model testing and numerical data for a transvers velocity distribution in cross sections (a) CS3 (b) CS6 in the bend channel, where the discharge ratio is λ=0.6 and the junction angle is α= 90°. (---axis, ——LES data, experimental data).

3.2 Secondary flow

Secondary flow is a special pattern of flow, which is the main cause for erosion of the outer bank and deposition of the inner bank. In the bend flow, vertical and transverse velocities are much smaller than the streamwise velocity. The presence of circulation has a major impact on the bend flow as well as in sediment transport at the channel bottom. In the case of tributary entrance, the confluence of the circulation structure is more complex. Therefore, further numerical model research and analysis are necessary for characterization of circulation structure of junction flow in the meandering river. For constant flux ratio λ =0.6 and junction angle $\alpha = 90^0$, the effects of roughness changes on helical flow of typical cross sections are shown in Figure 4-7, where the roughness high $K_s$are $K_{s1} = 0m$, $K_{s2} = 0.002m$ and $K_{s3} = 0.01m$, respectively. The cross sections were selected as 105^0 (CS5), 120^0 (CS6), 135^0 (CS7) and 150^0 (CS8) at downstream cross-sections. It shows the velocity vector superimposed on the cross-sections of downstream flow contour at two sections.

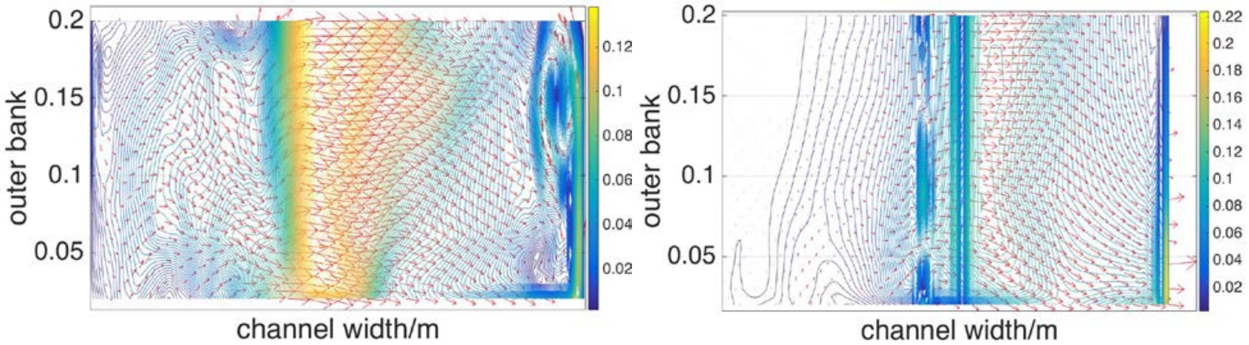

(a) LES $K_{s1} = 0m$ (b) K-omega $K_{s1} = 0m$

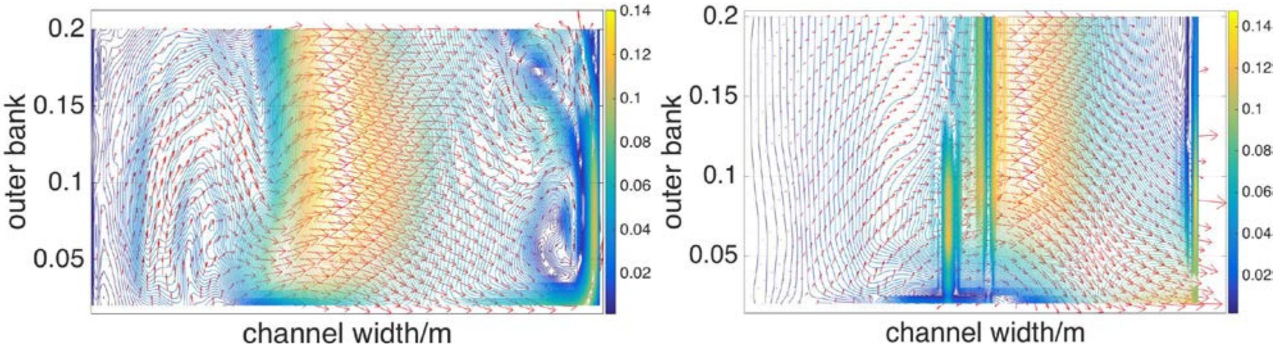

(c) LES $K_{s1} = 0.002m$ (d) K-omega $K_{s1} = 0.002m$

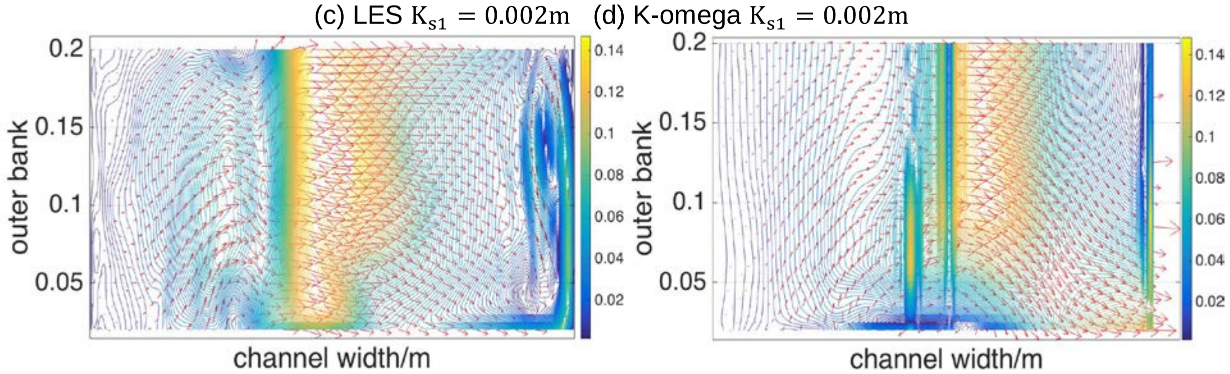

(e) LES $K_{s1} = 0.01m$ (f) K-Omega $K_{s1} = 0.01m$

Figure 4. Velocity vector superimposed on the cross-sections of downstream flow contour at CS5 sections at different roughnesses.

Cross-section CS5 is close to the confluence section, showing a large scale of clockwise secondary flow near the bed and two small scales of counterclockwise secondary flow cells between the outer bank and center line of the channel. These small secondary flows are located near the water surface and on separate sides of the clockwise secondary flow where the outer bank roughness is smooth. The greater the outer bank roughness becomes, the larger the scale of clockwise secondary flow, but the smaller the scale of counter rotating secondary flows. From the K-omega data, in this cross-section, there is only one large scale of clockwise secondary flow close to the bottom. It becomes larger with increasing roughness of the outer bank. But it cannot show any small scale of counter rotating secondary flow, which then can be simulated by LES model.

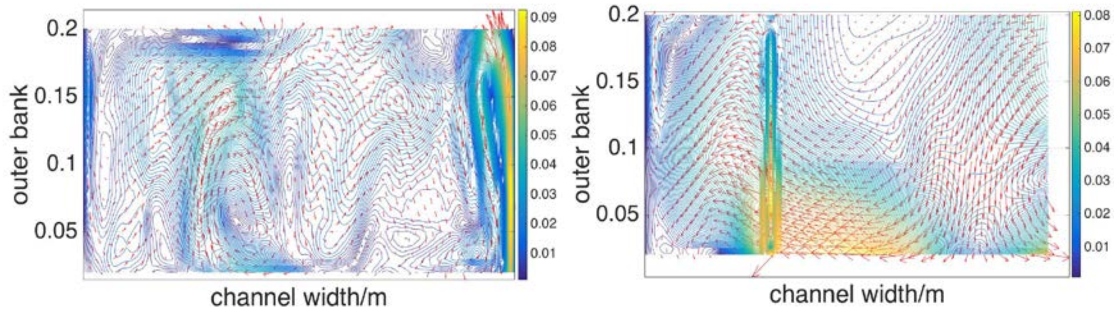

(a) LES $K_{s1} = 0m$ (b) K-omega $K_{s1} = 0m$

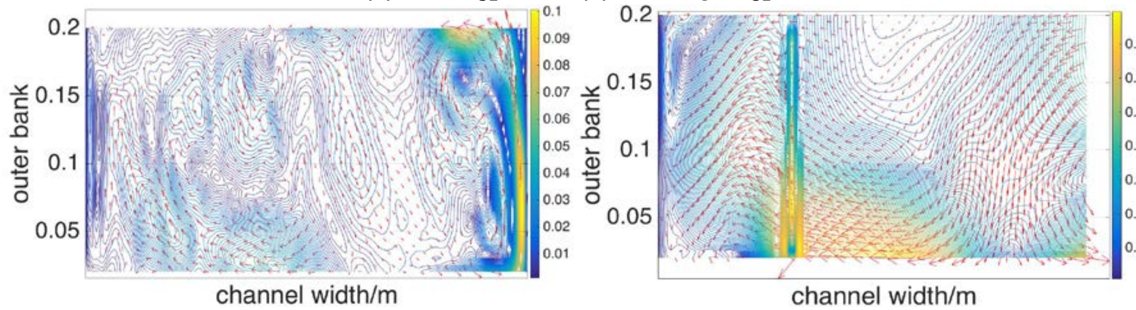

(c) LES $K_{s1} = 0.002m$ (d) K-omega $K_{s1} = 0.002m$

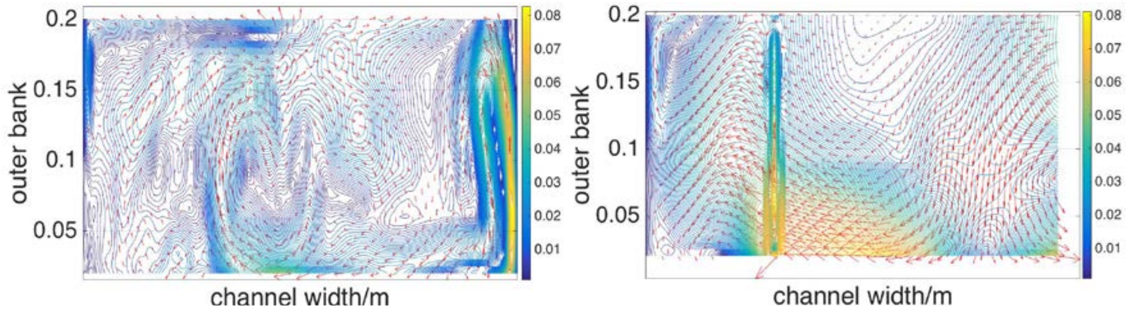

(e) LES $K_{s1} = 0.01m$ (f) K-Omega $K_{s1} = 0.01m$

Figure 5. Velocity vector superimposed on the cross-sections of downstream flow contour at CS6 sections at different roughnesses.

At cross-section $\varphi = 120^0$ (Figure 5), similarly, there is a large clockwise secondary flow near the bottom and two counter rotating secondary flow cells in this section where the outer bank is smooth. The large scale of clockwise secondary flows is generated near the outer bank. Close to the centerline, the small scale of counter rotating secondary flow cell is generated near the water surface. With increasing roughness of the outer bank, the clockwise secondary flow is divided into two clockwise secondary flows. In this cross-section, the greater the outer bank roughness becomes, the larger the scale of two clockwise secondary flows and smaller the scale of counter rotating secondary flows. From the K-omega data, it shows a clockwise secondary flow close to the water surface and a counter rotating secondary flow close to the bottom. The core of clockwise secondary flow moves to the outer bank and becomes larger with increasing roughness of the outer bank, but the smaller the scale of counter rotating secondary flow becomes. In this cross-section, the small scale of secondary flow still cannot be shown by K-omega, which can be simulated by LES model.

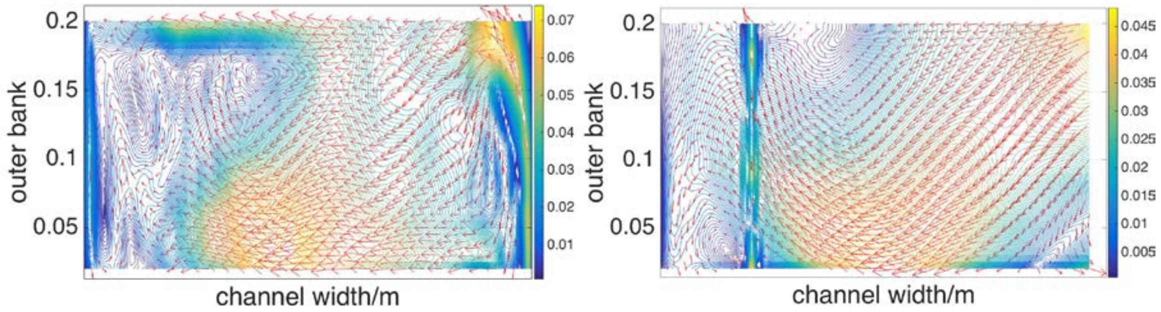

(a) LES $K_{s1} = 0m$ (b) K-omega $K_{s1} = 0m$

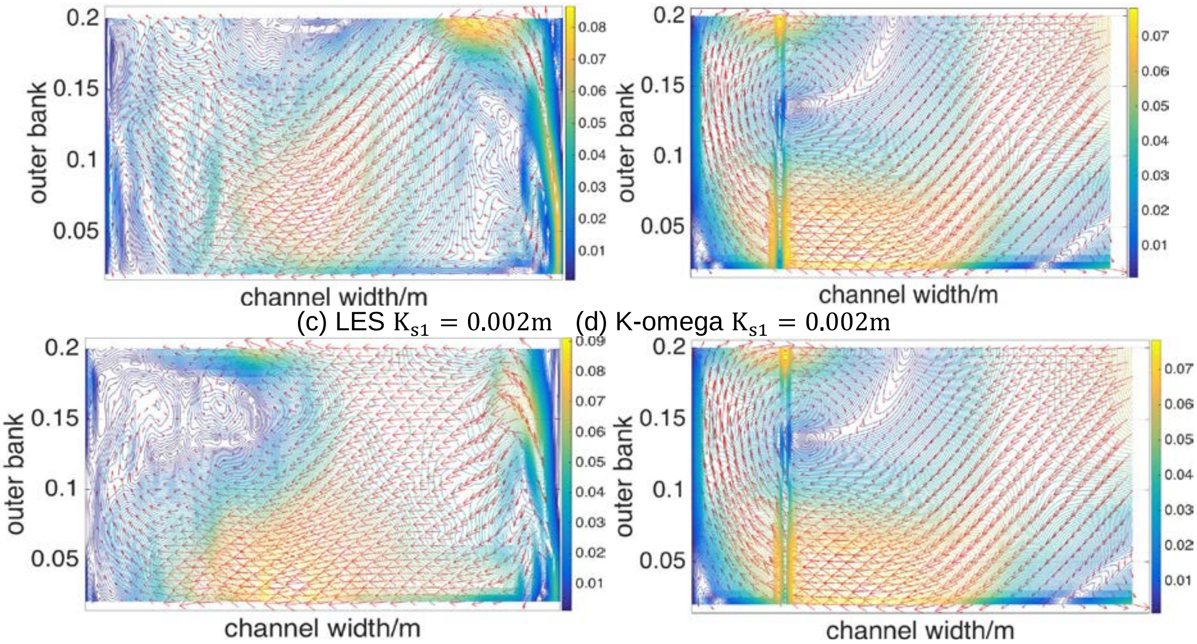

(c) LES $K_{s1} = 0.002m$ (d) K-omega $K_{s1} = 0.002m$

(e) LES $K_{s1} = 0.01m$ (f) K-Omega $K_{s1} = 0.01m$

Figure 6. Velocity vector superimposed on the cross-sections of downstream flow contour at CS7 sections at different roughnesses.

At downstream cross-section CS7, there is a small scale of clockwise secondary flow near the water surface and a counter rotating secondary flow close to the bottom where the outer bank is smooth. When the outer bank roughness is 0.002, there are two large scale of clockwise secondary flows near the water surface, but the secondary flow scale is smaller than those ones where the outer bank roughness is small. When the outer bank roughness is 0.01, the greater the outer bank roughness becomes, the larger the clockwise secondary flow and the smaller the scale of secondary flow. The k-omega data shows a large scale of counter rotating secondary flow and one clockwise secondary flow in this cross-section. The core of clockwise secondary flow moves to the outer bank and the scale of it becomes large with increasing roughness of the outer bank. But the increase in outer bank roughness decreases the scale of counter rotating secondary flow.

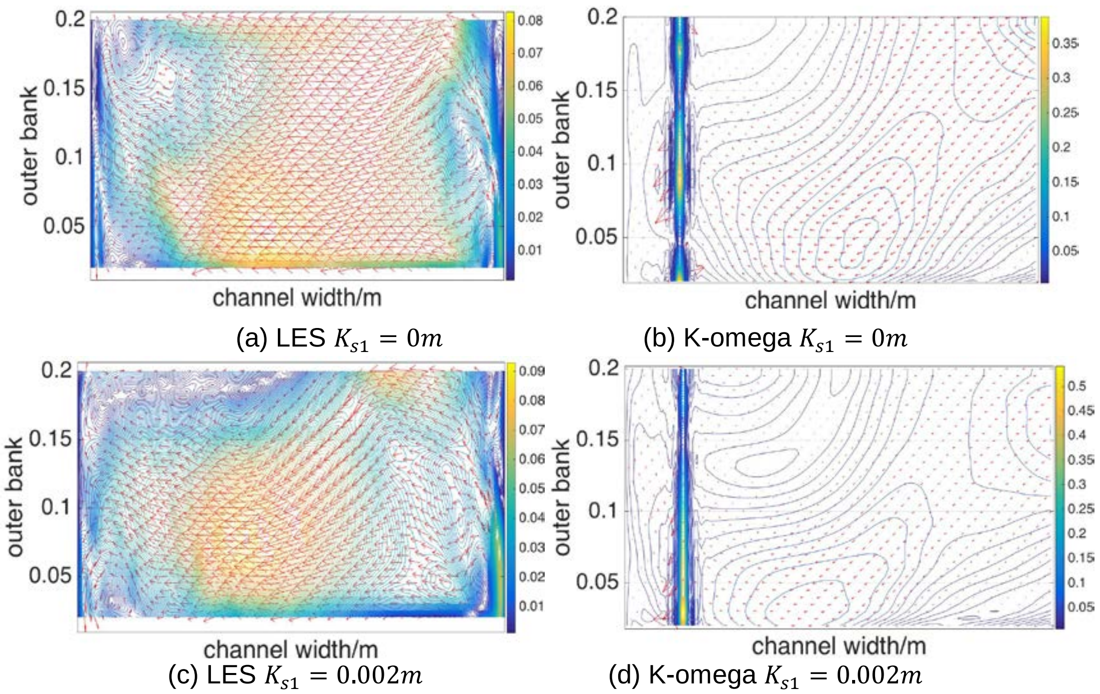

(a) LES $K_{s1} = 0m$ (b) K-omega $K_{s1} = 0m$

(c) LES $K_{s1} = 0.002m$ (d) K-omega $K_{s1} = 0.002m$

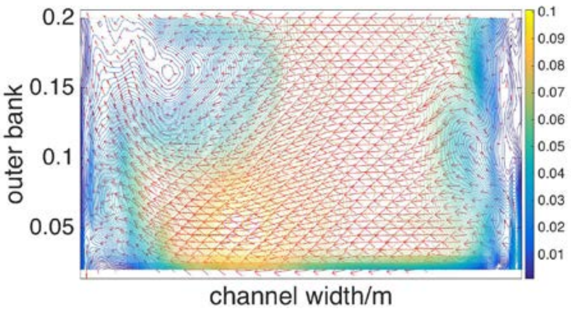

(e) LES $K_{s1} = 0.01m$

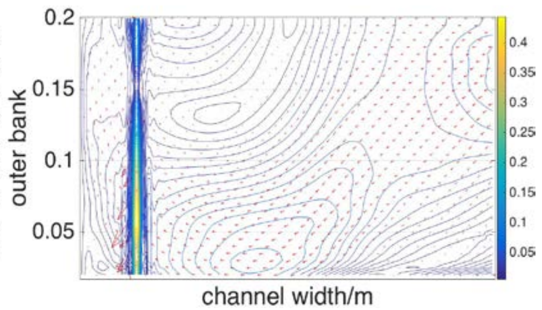

(f) K-Omega $K_{s1} = 0.01m$

Figure 5. Velocity vector superimposed on the cross-sections of downstream flow contour at CS8 sections at different roughnesses.

As Figure 5 (cross- section $\varphi = 150^0$) shows, near the outer bank, there are still two clockwise secondary flows close to the water surface and a counter rotating secondary flow close to the bottom. With increasing roughness of the outer bank, two clockwise secondary flows merge into one clockwise secondary flow. The greater the outer bank roughness becomes, the larger the scale of clockwise secondary flow, but the smaller the scale of counter rotating secondary flow. From K-omega data, it shows a small scale of clockwise secondary flow near the water surface and a counter rotating secondary flow close to the bottom. The greater the outer bank roughness becomes, the larger the scale of clockwise secondary flow, but the smaller the scale of counter rotating secondary flow.

4 CONCLUSIONS

This paper investigates how bank roughness influences the near outer bank circulation structure within a confluent meander bend by numerical simulation. These results suggest that both LES and RANS simulations can predict the large scale of secondary flow near the outer bank in the confluent meander bend channel, but the RANS model fails to capture the small scale secondary flow cell near the water surface. Different bank roughnesses cause changes in the position of large clockwise secondary flow. In addition, increasing the outer bank roughness strengthens the outer bank clockwise secondary flow cell and decreases the scale of counter rotating secondary flow.

REFERENCES

Best, J.L. (1987). Flow Dynamics at River Channel Confluences: Implications for Sediment Transport and Bed Morphology. Recent Dev. Fluvial Sedimentological, (1973), 27–35. URL http://sp.sepmonline.org/lookup/doi/10.2110/pec.87.39.0027

Best, J.L. (1988). Sediment Transport and Bed Morphology at River Channel Confluences, 35, 481–498.

Blanckaert, K., Duarte, A., Chen, Q. & Schleiss, A. J., (2012). Flow Processes near Smooth and Rough (concave) Outer Banks in Curved Open Channels. *Journal of Geophysical Research Earth Surface,* 117(4), 1–17.

Bradbrook, K.F., Biron, P.M., Lane, S.N., Richards, K.S. & Roy, A.G. (1998). Investigation of Controls on Secondary Circulation in a Simple Confluence Geometry using a Three Dimensional Numerical Model. *Hydrological Processes,* 12(8), 1371-1396.

Jin, Y.C. (1990). Roughness Effect on Flow and Shear Stress near Outside Bank of Curved Channel. *Journal of Hydraulic Engineering,* 116(4), 563–577.

Keylock C.J., Hardy R.J. & Parsons, D.R. (2005). The Theoretical Foundations and Potential for Large-Eddy Simulation (LES) in Fluvial Geomorphic and Sedimentological Research. *Earth-Science Reviews,* 71(3–4): 271–304.

Kang, S.K. (2010). Numerical Modeling of Turbulent flows in Arbitrarily Complex Natural Streams, *Dissertations & Theses*, Gradworks.

Rhoads, B.L. & Sukhodolov, N. (2001). Field Investigation of Three Dimensional flow Structure 1. Thermal Mixing and Time Averaged Velocities. *Water Resources Research,* 37(9), 2393–2410.

Stoesser, T. (2010). Physically Realistic Roughness Closure Scheme to Simulate Turbulent Channel Flow over Rough Beds within the Framework of LES. *Journal of Hydraulic Engineering,* 136(10), 812–819.

Stoesser, T., Ruether, N., & Olsen, N.R.B. (2010). Calculation of Primary and Secondary flow and Boundary Shear Stresses in a Meandering Channel. *Advances in Water Resources,* 33(2), 158–170.

Thorne, S.D. & Furbish, D.J. (1995). Influences of Coarse Bank Roughness on Flow within a Sharply Curved River Bend. *Geomorphology*, 12(3), 241–257.

NUMERICAL MODELING OF TURBULENT SECONDARY FLOW IN A HIGH-AMPLITUDE MEANDERING CHANNEL

JOONG CHEOL PAIK[1] & SANG DEOG PARK [2]

[1,2]Gangneung-Wonju National University, Gangneung, Korea
paik@gwnu.ac.kr; sdpark@gwnu.ac.kr

ABSTRACT

The flow structure in the meandering channel is characterized by the helical motion and the shear layer emanating from the inner wall and forming flow separation regions near the bend apex. The production of turbulent kinetic energy is correlated to the recirculation cells of which the generation is related to the local curvature. Mean free surface flow and turbulence characteristics of the secondary flow in a periodic, asymmetric, high-amplitude meandering channel retaining high-order harmonic modes are numerically reproduced by a three-dimensional unsteady numerical solver. The turbulent flow is resolved by the delayed detached-eddy simulation (DDES) to elucidate the dynamic behavior of the turbulent secondary recirculation and flow separation. The variation of instantaneous free surface is captured by aid of a two-phase volume of fluid method. The numerical simulation reproduces the distinct mean flow features including the secondary recirculation cells, flow separation forming shear layers from side walls and free surface gradient in both streamwise and transverse directions that observed in the experiment. Based on the good agreement between computed time-averaged flow fields with the measurement, the present numerical solutions elucidate the rich dynamics of complex, three-dimensional turbulent recirculation cells and shear layers between cells.

Keywords: Meandering channel; turbulent flow; numerical modeling; secondary flow; helical motion.

1 INTRODUCTION

A comprehensive understanding of river meandering mechanism is essential for river management projects involving river restoration, river bank protection and environmental issues. The flow in meandering channels is three-dimensional, where the secondary currents significantly affect the streamwise velocity distribution (Thorne et al. 1985). The flow structure in the bends is considerably complex due to the helical motion that is characterized by surface flow towards the outer bank and the near bed flow towards the inner bank. The orientation of the helical motion is dependent on the vertical distribution of streamwise velocity (Corney et al., 2006). Rivers and streams are dynamic systems as they are consistently changing. The strong secondary current is responsible for higher bed and bank shear stresses near the outer part of the bend. The physical processes underlying the formation of meanders have been the subject of intensive and detailed experimental and numerical researches in the channels consisting of one or two sharp bends (i.e.Blanckaert, 2010; van Balen et al., 2010; Stoesser et al., 2010).

A finite-amplitude equilibrium state at the critical wave number is unstable, and, regardless of magnitude of bend wavelengths, the bend train tends towards the shape of the high-amplitude, so-called Kinoshita curve (Parker and Andrews, 1986). The solution at high amplitude displays a prominent skewing that reveals the direction of flow, while the solution can reduce to the sine-generated curve at low amplitude. Abad and Garcia (2009) confirmed that the high-pressure gradient produced by large superelevation of water surface is responsible for the generation of secondary cells and the production of turbulent kinetic energy is correlated to the recirculation cell which produced the local curvature, through a series of laboratory experiment of turbulent flow in the Kinoshita meandering channel. Abad et al. (2013) carried out 3D RANS computation using the standard two-equation models with wall functions and the rigid-lid approximation for the free surface boundary. The dynamics of the outer-bank, counter-rotating secondary cell evolves from both the centrifugal force and the anisotropy of turbulence (Blanckaert and deVriend, 2004; van Balen et al., 2010). As indicated by Abad et al. (2013), the differences in the velocity distributions between the numerical results and the experimental measurement are related to the applied turbulence model and the advanced high resolution computation is required for more accurate resolving of the detailed characterization of the flow.

A depression in the water surface elevation near inner bank and the interaction of the superelevation of the water surface and the secondary recirculation cell result in the increase in velocity along the inner bank and an adverse water surface gradient (Abad et al., 2009; Blanckaert, 2010). Flow separation and recirculation at the inner bank and counter-rotating cell of secondary flow forming near the surface at the outer bank are important features in terms of energy losses, turbulent energy production and bed and band shear stress distributions (Blanckaert, 2009; Sukhodolov, 2012).

This work aims to carry out a high resolution three-dimensional numerical modeling for reproducing the complex, three-dimensional turbulent secondary flow in the high amplitude meandering channel which was experimentally investigated by Abad et al. (2009). The turbulent flow is resolved by the delayed detached-eddy simulation (DDES), a hybrid LES-RANS approach, and a two-phase volume of fluid method is employed for tracking the free surface.

2 NUMERICAL METHODS

The governing equations for the flow are the unsteady, incompressible Navier-Stokes equations. The interfaces of water, air and debris fluids are captured by means of the multiphase volume of fluid (VOF) method which is capable of modeling flows with complex free surface geometries. The location of the free-surface and interface of fluids are obtained by the volume fraction α in the VOF method. The contribution of the liquid and gas velocities to the evolution of the free surface are proportional to the corresponding phase fraction, and the volume fraction is used to determine the fluid properties.

The governing equations for the mean flow are the unsteady, incompressible Reynolds-averaged Navier-Stokes (RANS) equations:

$$\nabla \cdot (\mathbf{u_f}) = 0 \qquad [1]$$

$$\frac{\partial \rho_f \mathbf{u_f}}{\partial t} + \nabla \cdot (\rho_f \mathbf{u_f} \mathbf{u_f}) = -\nabla p_{rgh} + (\mathbf{g} \cdot \mathbf{x}) \nabla \rho_f + \nabla \cdot (\boldsymbol{\tau}) + \mathbf{F_b} \qquad [2]$$

where the tensor product $\mathbf{u_f}\mathbf{u_f}$ = $u_i u_j e_i e_j$, $\mathbf{g}$ is the gravity vector, $\mathbf{x}$ is the coordinate vector, ρ_f is the density of fluid, and $\mathbf{F_b}$ is the external force term. The only difference from the original RANS equations is that, instead of the pressure p , the piezometric pressure p_{rgh} = $p - \rho_f \mathbf{g} \cdot \mathbf{x}$ is solved. Hence, the term $-\nabla p + \rho_f \mathbf{g}$ in the momentum equation of the vector form of RANS equations is re-written as $-\nabla p_{rgh} - (\mathbf{g} \cdot \mathbf{x}) \nabla \rho_f$.

The free-surface variation is significant at the present high Fr. The interface of water-air fluids is captured by means of the two-phase VOF method which is capable of modeling flows with complex free surface geometries, yet it is remarkably economical in computational terms. The location of the free-surface is obtained by the VOF function F . The contribution of the liquid and gas velocities to the evolution of the free surface is proportional to the corresponding phase fraction, and the velocity of the effective fluid in a VOF model is defined as a weighted average.

$$\mathbf{u_f} = F\mathbf{u_l} + (1 - F)\mathbf{u_g} \qquad [3]$$

where the subscript $\mathbf{l}$ and $\mathbf{g}$ denote the liquid and gas phases, respectively. Consequently, the evolution equation of the volume fraction F can be calculated by solving its transport equation with an artificial surface compression term (Weller 2008).

$$\frac{\partial F}{\partial t} + \nabla \cdot (F\mathbf{u_f}) - \nabla \cdot (F(1 - F)\mathbf{u_{rF}}) = 0 \qquad [4]$$

where $\mathbf{u_{rF}}$ (= $\mathbf{u_l} - \mathbf{u_g}$) is the vector of relative velocity, designated as the compression velocity. This additional convective term in the phase fraction equation is introduced to suppress the smearing of steep gradients induced by the numerical diffusion, contributes significantly to the high resolution of the interface. In this study, the compression coefficient controlling the intensity of the free-surface compression was set to 1.0 which corresponded to the conservative compression.

The delayed detached eddy simulation model (DDES) of Spalart et al. (2006), a hybrid URANS/LES approach was taken into account to resolve the turbulent flow. The hybrid approach preserves the URANS model throughout the boundary layer on the RANS mesh with high aspect ratios, while the flow away from the wall is resolved by the LES mode.

3 COMPUTATIONAL DETAILS

The governing equations were solved numerically by means of the finite volume. Overall, fully second-order-accurate setup both in time and in space was used for the simulations. Pressure implicit with splitting of operator (PISO) pressure-velocity coupling algorithm was used. The generalized second-order-accurate backward, implicit, differencing scheme was used to evaluate the time derivatives. Spatial discretization for the convective term was achieved using the central differencing schemes. To prevent numerical solutions from losing unsteadiness due to the numerical diffusion, this study employed a limiter based blended scheme, so-called "fixedBlended" scheme where the central differencing (CD) and the Gamma scheme were used as the two blending schemes. The Gamma scheme was bounded by blending the second-order central difference and the first-order upwind schemes, and the smooth transition between these two schemes was controlled by the blending coefficient which ranged between 0.1 and 0.5. Smaller value provides a good resolution (less diffusive) solution, while high value is more numerically stable (Jasak et al. 1999). In this study, the coefficient of 0.1, which gives best accurate (least diffusive) solution, was used for the Gamma scheme. Finally, the fixed Blended scheme was specified with the blending factor of 0.9. The least-square gradient method was used for the velocity gradient term, which allows a better representation of the second derivative of the velocity field. Other terms were discretized by using the central difference scheme.

One of the major difficulties in the VOF method is ensuring the transport of sharp interfaces without artificial numerical diffusion or dispersion. In the VOF model, the boundedness of volume faction was maintained by utilizing a bounded central differencing scheme combined with a solution procedure referred to as multi-dimensional universal limiter for explicit solution. The number of sub-cycles for the volume fraction for each physical time-step was set to 4 and the number of correction loops over the volume fraction was set to 2.

Sufficiently refined computational mesh and appropriate boundary conditions are essential to accurately reproduce the dynamics of secondary motions in the bends in the large eddy and detached eddy simulations.The Kinoshita channel was expressed in intrinsic coordinates with the skewness and flatness coefficients, the maximum angular amplitude, the arc wavelength and the streamwise coordinate. Abad and Garcia (2009) employed the 32 m long experimental flume which consisted of three 10 m long bends and two 1 m long reaches upstream and downstream of the meandering channel. The width and depth of the computational channel were 0.6 m and 0.4 m, respectively, which was the same as the experimental one. The experimental channel configurations were exactly generated with the computational mesh, except that the 2 m long upstream reach was used to allow the temporal variation of water surface and velocity distribution at the inlet and the development of the upstream boundary layer at the given discharge and mean water depth. To study the grid sensitivity of numerical solutions, this study used two different meshes: a coarse mesh of 3.5 $\times 10^6$ cells and a fine mesh of 7.2$\times 10^6$ cells. Figure 1 shows the Kinoshita channel numerically generated by the computational mesh consisting of 7.2 million cells.

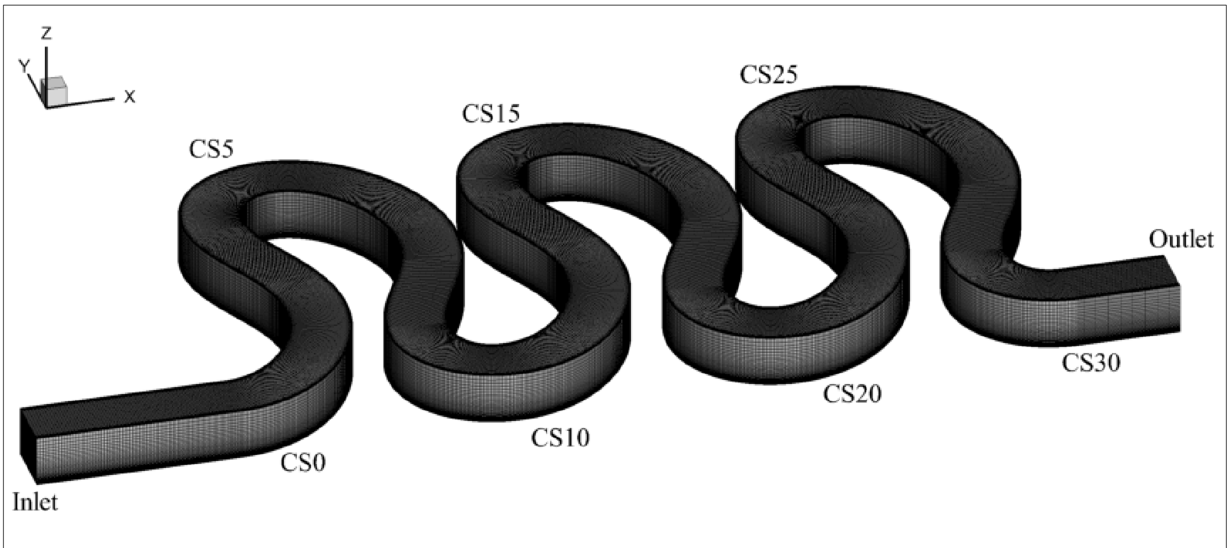

Figure 1. Computational mesh and location of representative cross sections.

Four experiments were conducted by Abad and Garcia (2009) for upstream and downstream valley bend orientations with different flow conditions. This study numerically simulated an experimental case among them which generated with flow conditions of the water discharge Q = 25 L/s, the reference water depth and mean velocity, cross-sectional averaged along the reach, were H = 0.15 m and U_m = 0.28 m/s, respectively. The Froude number, based on the reference water depth and velocity, was Fr = 0.23 and the Reynolds number Re = 4.17× 10^4, respectively. No-slip boundary conditions were applied at the bed and side walls. The computation was carried out using the non-dimensional time step of 2.5× 10^4 for 120 seconds after the flow converges in the whole domain to obtain the time-averaged mean flow and turbulence statistics.

4 NUMERICAL RESULTS

Flow field computed by the DDES was presented in terms of instantaneous and time averaged water surface distributions and instantaneous coherent structures in the entire domain. The instantaneous water surface variation, shown in Figure 1(a), reveals the development of ripples of which wavelength is larger in the upstream part than that developed in the downstream region. Figure 2(b) shows the time-averaged water surface elevation computed in the present flat bed, which clearly reveals the depression of water surface along the inner bank at the bend apex. The transverse slope of water super-elevation, induced by the interaction of the inertial forces and transverse pressure gradient, is responsible for the helical motion. The time-averaged mean water surface slope along the channel is about 4.0×10^{-4}, as shown in Figure 2(b), which is in good agreement with the measured longitudinal water surface slope of about 4.05×10^{-4}. Figure 2(c) shows the coherent vortical structures identified by the iso-surface of Q-criterion, the second invariant of the velocity gradient tensor. The computed vertical structures are colored by the computed instantaneous total pressure so that the blue and red colors depict the near surface and bed structures, respectively. The results reveals that the development of vertical structures initiates along both side walls and channel bed in the first upstream bend. The structures developing along the inner bank is related to the shear layer emanating from the wall, which is stronger than those near the outer bank and channel bed, associated with the boundary layer development. The vortical structures interact with the consecutive bends and become more complicated as they move downstream. The result further shows that the instantaneous vortical structures are controlled by the local curvature – i.e. the flow structures become strong and complex at high local curvature near the bend apex and weaken at low curvature.

Computed time-averaged streamwise velocity contour and secondary velocity vectors were compared with the experimental measurements at three consecutive bend apexes (CS10, CS15 and CS20) in Figure 3. Note that Abad et al. (2009) measured velocity components using down-looking acoustic Doppler velocimeter (ADV) from 5 cm below the free surface and 10 cm away from the side walls. Due to the limitation of ADV usage, unfortunately, this study is not able to compare details of computed flow structures near both free surface and side walls with the experimental measurements. At section CS10, the numerical result reproduces four recirculation cells: a clockwise cell at lower right hand side; a counterclockwise cell at the center and mid-depth; a strong clockwise cell near the lower inner (left) bank associated with the formation of high streamwise velocity distribution; and a relatively small counterclockwise cell near the free surface and the outer (right) bank. The computed first two secondary cells are in very good agreement with the experimental measurement of Abad et al. (2009). However, the latter two cells computed near free surface and inner bank are not visible in the measured data. Recall detailed comparison of flow structures between the experimental and numerical results is not possible due to the limitation of the ADV measurement.

The core of maximum velocity magnitude at the bend apex (CS15) is computed at lower part near the inner bank, which is related to a strong counter-clockwise rotating secondary cell developed near the inner bank. The numerical result reveals that the cell near inner wall pushes high momentum fluid towards lower inner wall and low momentum fluid away for upper inner bank. It is noteworthy that the flow structures computed at two cross-sections, CS10 and CS20, with the same geometrical configurations are slightly different from each other. The experiments were carried out in Kinoshita channel consisting of three consecutive bends, decided based on a preliminary 3D CFD modeling, to generate a fully periodic, three-dimensional mean flow and turbulence structure around the middle of the channel between CS10 and CS 20 (Abad et al. 2009). However, the present numerical result reveals that the reproduced flow is not fully periodic in the longitudinal direction, the maximum streamwise velocity magnitude near the inner bank increases as it moves downstream. The numerical result further shows that the secondary currents become stronger near the inner bank and weaker near the center and outer bank, as they move downstream. It indicates the computed flow field is not fully periodic between CS10 and CS20 and the solution is influenced by the inlet and outlet boundary conditions.Figure 3 confirms that the measured free surface variations (blue line in the measurement) are well reproduced by the present two-phase numerical modeling. The large local superelevation of free surface at the bend apex produces transverse pressure gradient that is responsible for the formation of distinct secondary cells.

Streamlines, colored by the total pressure, in a computed instantaneous flow field are plotted in Figure 4, where blue line part passes below the free surface and red line part is moving along the bed. The streamlines reveal that the magnitude of secondary currents (helical motion) is not much strong relative to the streamwise velocity component. It is visible from the figure that the fluid near the free surface and outer bank moves towards lower inner bank and the fluid near the lower inner bank towards the upper outer banks as they pass through the bends.

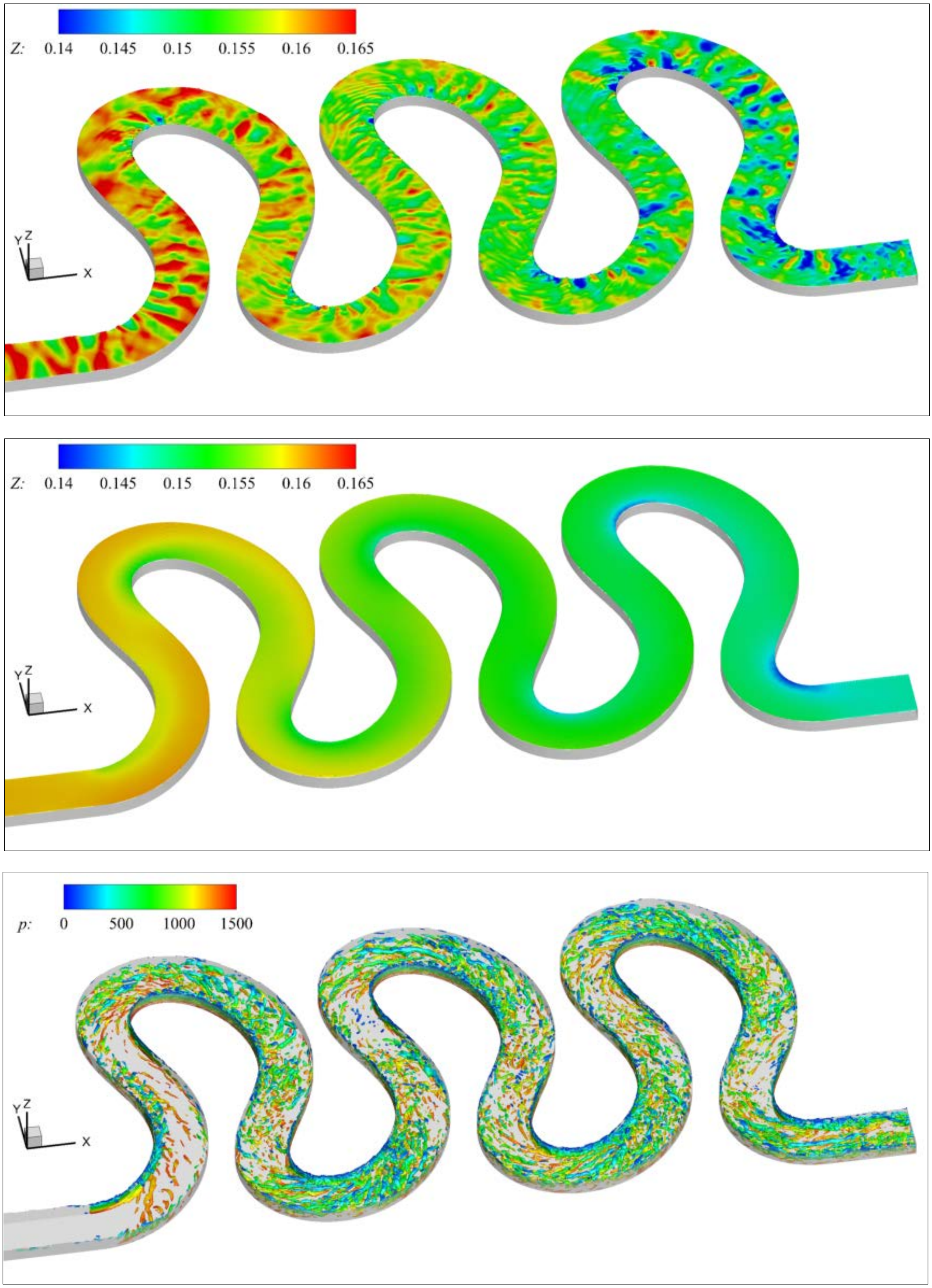

Figure 2. Numerical solutions obtained by the DDES approach: [*upper*] instantaneous free surface distribution colored by elevation contours; [*middle*] time-averaged free surface distribution; and [*lower*] vortical structures visualized by the iso-surface of Q-criterion colored by the total pressure.

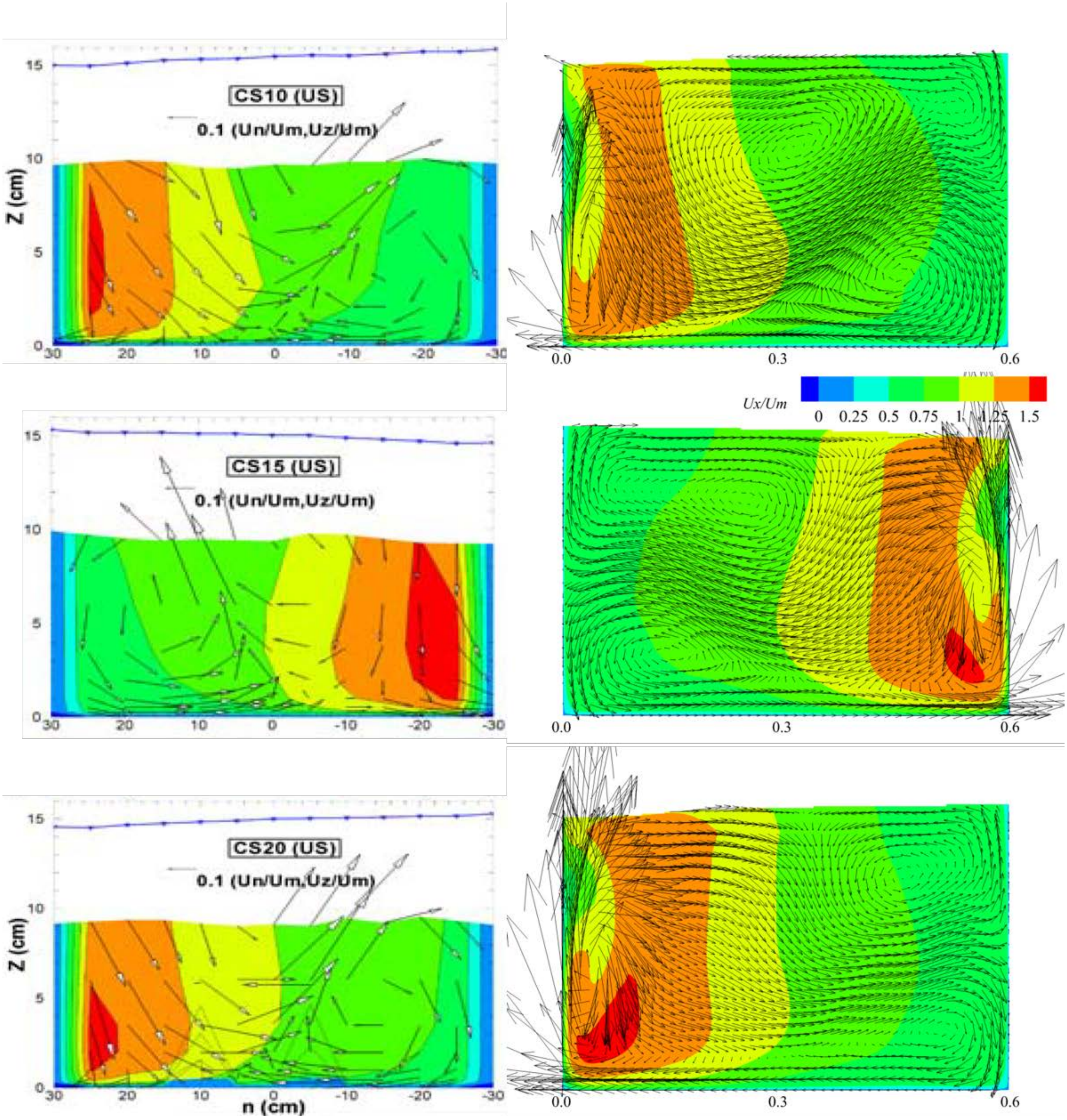

Figure 3. Comparison of time-averaged velocity vectors and streamwise velocity contours at three representative cross sections measured by Abad and Garcia (2009) and computed by the present numerical modeling. All velocity components are normalized by the reference mean velocity.

5 CONCLUSIONS

The secondary flow and the superelevation of the water surface in the high-amplitude Kinoshita channel are reproduced by the DDES approach incorporated with the VOF technique for resolving the variation of water surface elevation. The numerical solution computed by a second-order accurate finite volume method is compared with an existing experimental measurement. The present modeling well predicts the distributions of the cores of maximum velocity magnitude along the inner banks and complex secondary cells in the bend. The secondary recirculation driven by the radial acceleration in the upstream bend affects the flow structure in the downstream bend, which yields a pair of counter-rotating vortices at the bend apex. This complex flow pattern is reasonably well reproduced by both modeling approaches, which includes the prediction of the clockwise-rotating vortex between a pair of counter-rotating vortices which is observed in the experiment. The present computation using the VOF method appears to well reproduce the superelevation and transverse gradient of water surface through the meandering channel.

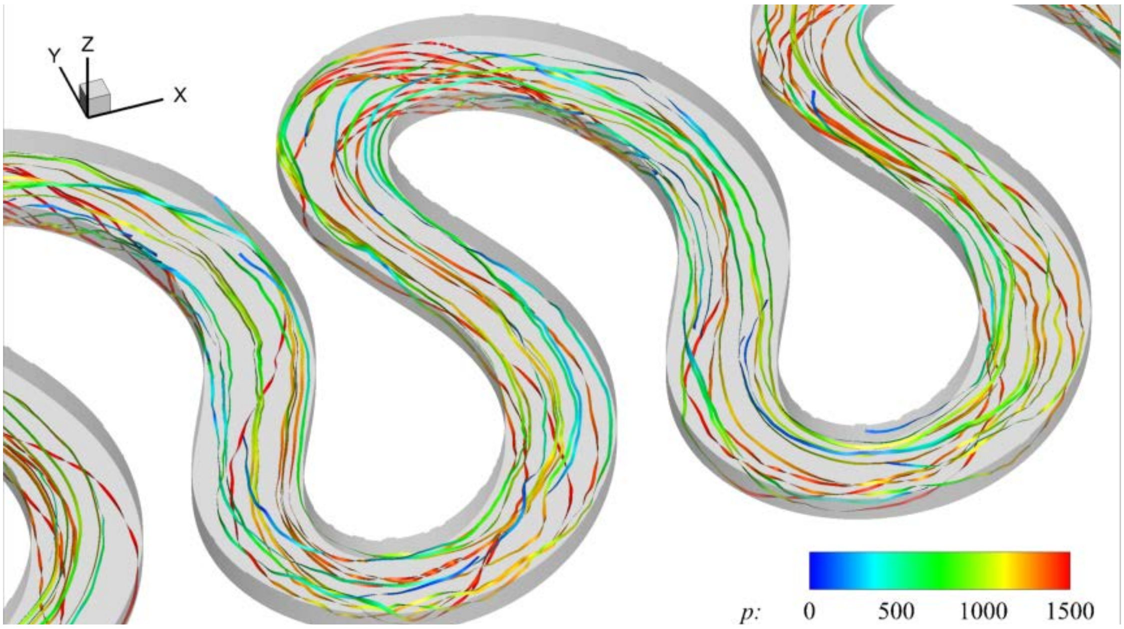

Figure 4. Streamlines colored by the total pressure in a computed instantaneous flow field.

ACKNOWLEDGEMENTS

This work is supported by the National Research Foundation of Korea (NRF) grant funded by the Korean government (MEST). (Grant No. NRF-2015R1D1A1A01060919).

REFERENCES

Abad, J.D. & Garcia, M.H. (2009). Experiments in a High Amplitude Kinoshita Meandering Channel: 1. Implications of Bend Orientation on Mean and Turbulent Flow Structure. *Water Resources Research*, 45(2), 1-19.

Abad, J.D., Frias, C.E., Buscaglia, G.C. & Garcia, M.H. (2013). Modulation of the Flow Structure by Progressive Bedforms in the Kinoshita Meandering Channel. *Earth Surface Processes and Landforms*, 38(13), 1612-1622.

Blanckaert, K. (2009) Saturation of Curvature Induced Secondary Flow, Energy Losses and Turbulence in Sharp Pen Channel Bends: Laboratory Experiments, Analysis and Modeling. *Journal of Geophysical Research*. 114(3), 1-23.

Blanckaert, K. (2010). Topographic Steering, Flow Recirculation, Velocity Redistribution and Bed Topography in Sharp Meander Bends. *Water Resources Research*. 46(9), 1-23.

Blanckaert, K. & Vriend, H.J. (2004). Secondary Flow in Sharp Open Channel Bends. *Journal of Fluid Mechanics*, 498, 353-380.

Corney, R.K.T., Peakall, J., Parsons, D.R., Elliott, L., Amos, K.J., Best, J.L., Keevil, G.M. & Ingham, D.B. (2006). The Orientation of Helical Flow in Curved Channels. *Sedimentology*, 53, 249-257.

Jasak, H. (2009). OpenFOAM: Open Source CFD in Research and Industry. International Journal of Naval Architecture and Ocean Engineering, 1(2), 89-94.

Kinoshita, R. (1961). *Investigation of Channel Deformation in Ishikari River,* Rep. Bureau of Resources, Dept. of Science and Technology, Japan.

Parker, G. & Andrews, E.D. (1986). On the Time Development of Meander Bends. *Journal of Fluid Mechanics*, 162, 139-156.

Spalart, P.R., Deck, S., Shur, M.L., Squires, K.D., Strelets, M.Kh. & Travin, A.K. (2006). A New Version of Detached Eddy Simulation, Resistant to Ambiguous Grid Densities. *Theoretical and Computational Fluid Dynamics*, 20(3), 181-195.

Thorne, C.R., Zevenbergen, L.W., Pitlick, J.C., Rais, S., Bradley, J.B. & Julien, P.Y. (1985). Direct Measurements of Secondary Currents in a Meandering Sand Bed River. *Nature*, 316(6022), 746-747.

Van Balen, W., Uijttewaal W.S.J. & Blanckaert, K. (2010). Large Eddy Simulation of a Curved Open Channel Flow over Topography. *Physics of Fluids*, 22(7), 1-18.

INFORMAL SETTLEMENTS ENCROACHMENT ALONG THE MAJOR RIVERS AND CREEKS: A MAJOR OBSTACLE IN ADDRESSING DRAINAGE PROBLEM AND FLOODING IN THE CENTRAL CLUSTER OF METRO CEBU, PHILIPPINES

JOAN ARCE JAQUE (1), & MA. DOLORES V. LLENOS (2)

(1)Social Development Specialist, Hydronet Consultants Inc., Cebu City, Philippines
joanjaque@hydronet.com.ph
(2)Research Associate, Hydronet Consultants Inc., Cebu City, Philippines llenosmarla@yahoo.com

ABSTRACT

The problem of drainage is commonly viewed as physical and technical concerns. But in reality, the problem is actually complicated by various socio-economic factors. These key factors include: encroachment of settlements and establishments along the water ways; improper solid waste disposal; and unenforced regulations or policies. More than the technical and physical challenges, these issues are more critical and most of the time is more difficult to deal with. Often times these issues become the major hurdle and cause of delay in implementing river improvement projects. The encroachment of informal settlements is a common sight in Metro Cebu's major rivers and creeks. In the central cluster alone, there are about 9,000 informal settlements along or within the three-meter easement of the major rivers and creeks. This number may continue to increase if the Local Government Units (LGU) will not make a definite stand to stop this inappropriate and unlawful encroachment on the waterways. The removal of these informal settlements is imperative. Sooner or later, these houses and structures must be relocated in compliance to the Water Code of Philippines and Urban Development and the Housing Act (RA7279 UDHA) which prohibits the establishment of structures along or within the easements of rivers and creeks or waterways. The relocation or resettlement will not only improve the physical condition of the waterways and its capacity to accommodate the increasing runoff but more importantly, it will uplift the living condition of the affected households, prevent them from possible health and environment hazards and protect lives and properties in case of flooding and other calamities. Humane demolition however does not stop in dismantling these housing structures, it goes toward people's integration to their new living environment. The President Rodrigo Duterte strongly emphasizes in his first State of the Nation address that there shall be *"No Demolition, Without Relocation"*. This paper presents how these social issues will be approached with consideration on the environmental issues and ensuring the social safeguards in carrying out the river improvement programs; which may include people’s participation, comprehensive planning and careful execution to lessen conflicts and negative impacts on people's lives and properties.

Keywords: River management; river encroachment; informal settlements on waterways; issues on river management; hazards on waterways.

1 INTRODUCTION

Metro Cebu has always been plagued with flooding issues that recently worsened because of improper and inadequate drainage system to accommodate the increasing peak flow due to urban development. Rainfall of only 55 millimeters per second can easily cause flooding in the key areas of Cebu City, Mandaue City and Talisay City. The waterways of the central cluster of Metro Cebu are not only narrow but also constricted. Informal settlements and other structures are encroaching the waterways particularly at the downstream section. On a regular basis, dredging of drainage canals are undertaken by the LGUs but due to the encroaching settlements and structures, the waterways are consistently clogged with solid wastes and silts resulting in increasing flood-prone areas. This recurring problem of flooding disrupts the local economy and puts in danger the lives of people living along the waterways. Furthermore, the presence of informal settlements along the waterways not only obstructs the implementation of the drainage program but basically violates the existing laws governing the development and protection of waterways. The Water Code of the Philippines stipulates clearly the required easements in all waterways and their entire lengths and further prohibits construction of any structure within the easements (Article 51, Presidential Decree 1067, dated December 31, 1976). These existing laws are the basis for developing the drainage systems which includes the improvement of the rivers and creeks.

Several drainage masterplans in Metro Cebu were undertaken in 1983, 1995 and 2007. However, these plans were not fully implemented. The plans specifically recommended the improvement of rivers and creeks which included the demolition of structures and relocation of informal settlers that encroached the waterways. However, the relocation of informal settlements is a more complex and tedious process that needs among others people's participation and cooperation, strong political will, sufficient funds and manpower, integrated multi-sectoral support and compassion.

As of this study, the Metro Cebu's Flood Control and Drainage Masterplan and Feasibility Study is on its final stage. The plan includes proposed flood control interventions which includes river and creek improvements. The river improvement projects will entail the clearing and widening of the river and creeks which will directly affect about 9000 structures mostly informal settlements. During the conduct of the study, the issue on relocation of affected structures has been highlighted in several consultation meetings.

This paper will provide an avenue of looking into the complexity of addressing relocation issues and how far this concern can be resolved. The data gathered in this study will initially illustrate the extent of the problem of encroachments along the waterways and will open possible solutions to address the concerns. More specifically, this study will:

1. Describe the extent of the encroachment issues along the waterways in the central cluster of Metro Cebu.
2. Present the proposed solution in addressing the relocation issues in relation to the implementation of the drainage improvement projects.

2 THE STUDY AREA

This study will take into account the issue of encroaching structures in the major rivers and creeks within the Central Cluster of Metro Cebu. The central cluster of Metro Cebu was given the priority because this holds the seat of governance at regional and provincial level and has the location of major commercial and industrial establishments that primarily attract the in-migration.

The study area included three local government units (LGUs), namely: the cities of Mandaue, Cebu and Talisay. They are considered as highly urbanized areas wherein 93% of its total population are situated in its urban barangays, while the remaining 7% are in the rural barangays.

The central cluster of Metro Cebu is traversed by major rivers namely Lahug River, Subangdaku (Mahiga) River, Butuanon River, Kinalumsan River, Bulacao River, Guadalupe River and Mananga River. Contributory to these rivers are several creeks, which include: Hippodromo Creek, Centro-Tipolo Creek, and Basak Creek.

3 DATA COLLECTION

The ocular and profile surveys including informal interviews, drone survey and google earth map were among the sources of information. The surveys revealed the extent and actual location of the structures encroaching the waterways and problems confronting the affected households.

In addition, several consultation meetings with various interest groups and agencies directly involved in handling housing issues and concerns were also conducted to define the encroachment issues and to collect inputs. Through consultation meetings with the housing stakeholders in Metro Cebu, data gaps were identified particularly on the actual number of informal settlements. Current resettlement issues and other related concerns were gathered at the same time. Separate group meetings were also done to have updates on data gaps and to gather inputs that can resolve site-specific issues and concerns.

Inputs from group discussions and consultation meetings were collated to come up with situational analysis and to formulate applicable solutions and options in resolving the issue on encroachment and related concerns in the major rivers and creeks in the central cluster of Metro Cebu.

4 FINDINGS AND ANALYSIS

4.1 Structures encroaching the waterways

Urbanization in Metro Cebu basically started with Cebu City being the oldest city in the Philippines and served as the center of commerce and trade in the Visayas and Mindanao where the socio-economic activities propelled in the past decades. As its urbanization spread to its neighboring areas, Mandaue City became the hub for industries. Talisay City and other Metro Cebu cities and municipalities later became recipients of the spill overs and hosted settlements of the growing populace in Cebu and Mandaue City.

Informal settlements in the central cluster of Metro Cebu can be viewed as an adverse effect of industrialization which became a major concern of the LGUs. Many of the migrants from various places in Cebu Province, Visayas and Mindanao come to Metro Cebu in search for livelihood opportunities. With high standard of living, increasing land value, limited space and unaffordable housing rental, many of these migrants end up settling in areas wherever is possible. Many of them end up living along creeks and rivers which is free most of the time or cheap and near their source of living or workplaces. This scenario eventually became uncontrollable and put a lot of pressure on the LGUs particularly that these houses need to be relocated.

As of this writing, based on the study and secondary data sources, it is estimated that there are about 9,000 structures that are built along the easement or within the waterways of the Metro Cebu Central Cluster, most of which are informal settlements.

Figure 1. Informal settlements encroaching Guadalupe River, Cebu City.

The figure above shows a typical scenario along the major waterways in the central cluster of Metro Cebu. Illegal structures, built through legal or non-legal means, are within the three-meter easement or on the river itself. The table below shows the number of informal settlers along the waterways in each LGU.

Table 1. Number of informal settler families (isfs) along the waterways in the central cluster.

Local Government Units (LGU)	Estimated Number of Informal Settlements
Cebu City	4,326
Mandaue City	3,564
Talisay City	100 - 200

Data Sources: CPDO of LGUs, HUDO for Mandaue City, and DWUP and PCUP for Cebu City

The number remains to be an estimate since the LGUs still need to do an actual headcount or tagging of the structures and profiling of the affected households. It is estimated that there will be about 20% addition to this number as some structures accommodate 2 or more households in one roof. Tagging is essential as there is a tendency for the number of households to grow continuously. In addition, the three meter-easement along the waterways which is declared as non-buildable zone are said to be either government owned, privately owned or currently leased or being occupied illegally by the current settlers.

This situation calls for a definitive action on the part of the LGU to relocate these structures primarily for the people's welfare and to improve the drainage system to minimize flooding events that can cost lives and properties.

4.2 Affected structures by the priority drainage intervention

In response to issues raised by the Metro Cebu Development and Coordinating Board, the Department of Public Works and Highways (DPWH) commissioned the ongoing conduct of the “Flood Control and Drainage Masterplan and Feasibility Study for Metro Cebu”. The masterplan will be used as a basis for implementing drainage improvement projects that will minimize or resolve the recurring flooding in Metro Cebu. This ongoing study initially revealed that the first phase of project implementation will directly affect about 2,000 informal settler families along the waterways that traverse the cities of Cebu and Mandaue. Therefore, the informal settlers along the rivers of Guadalupe, Lahug, Subangdaku, Bulacao and Kinalumsan and those along Tejero Creek need immediate relocation.

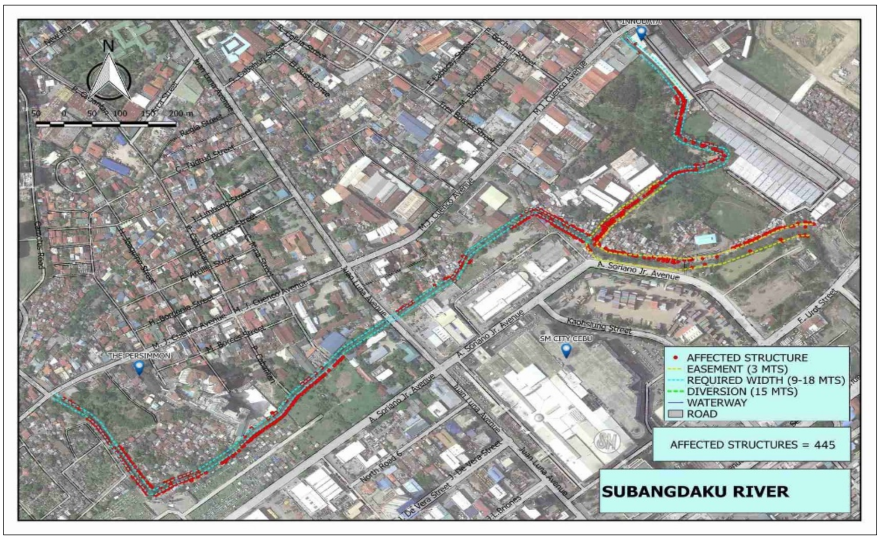

Map 1. Priority affected structures along Subangdaku River.

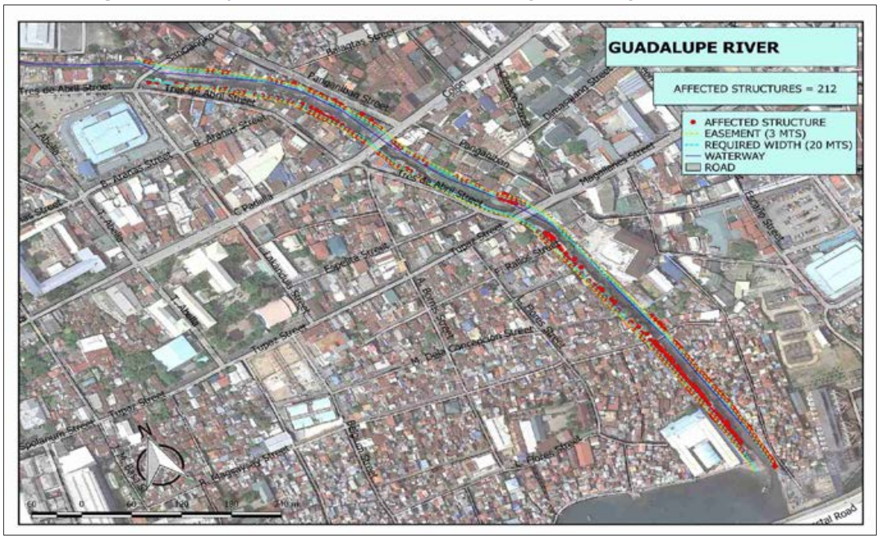

Map 2. Priority affected structures along Guadalupe River.

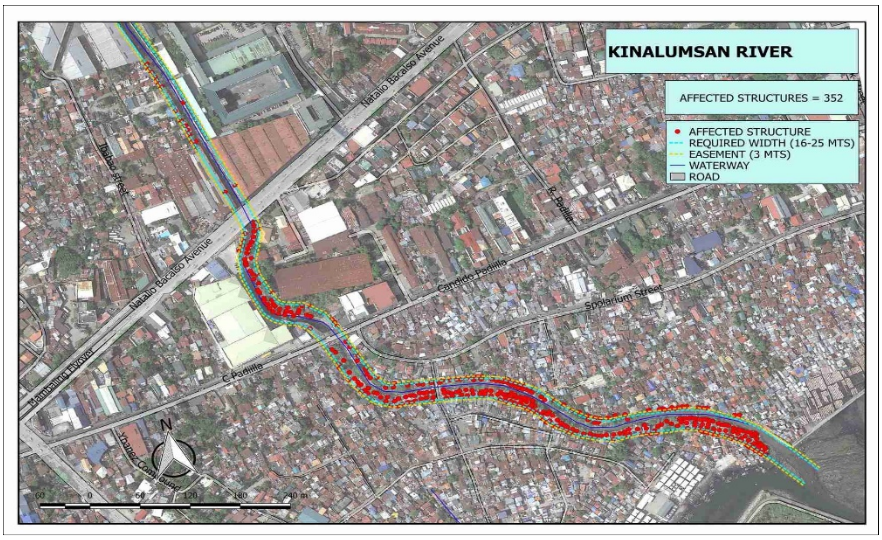

Map 3. Priority Affected Structures along Kinalumsan River.

Map 4. Priority affected structures along Lahug-Tejero Creek.

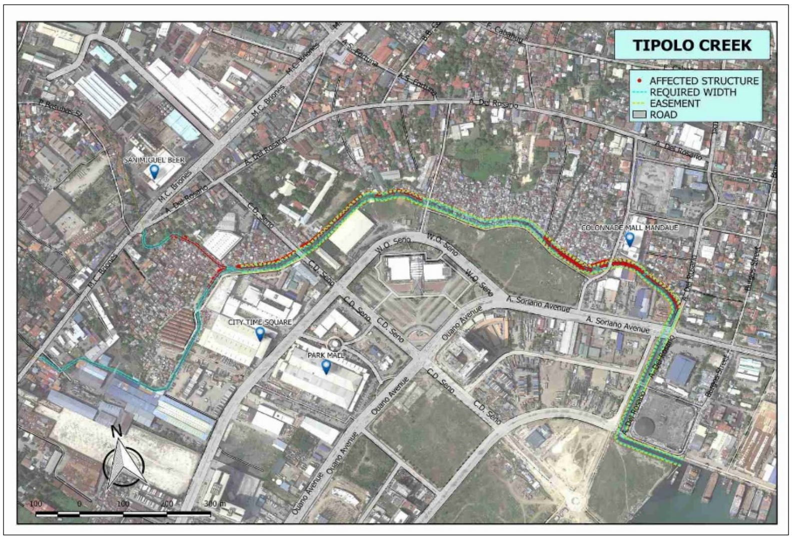

Map 5. Priority affected structures along Tipolo Creek.

4.3 Relocation and resettlement issues and concerns

The responsibility of relocating these affected households and structures encroaching the waterways lies heavily on the Local Government Units. Unfortunately, the LGUs have limited capacity to address this enormous undertaking. The LGUs primarily have limited available funds to finance the relocation and resettlement of these affected households, considering the fact that there are still many informal settlements around the city aside from those along the waterways.

Currently, Mandaue City still needs other resettlement areas to transfer all informal settlers in their recent inventory. The newly established resettlement site of the city has accommodated only about 34% of the total families due for relocation. On the other hand, Cebu City raised the issue of the lack of funds required to relocate the informal settlers along the waterways and other areas including those victims of recent fire. Furthermore, acquired lots for resettlement sites are found to be vulnerable to landslides and very far. The city needs additional funds to purchase lots in other locations. Talisay City also has the pressing problem of resettling the informal settler families within the danger zones. The existing relocation sites of Talisay City are now fully occupied. The city has not yet identified other areas that can be utilized for resettlement of informal settlers within the danger zones or along the waterways.

In addition, despite the presence of many laws which prohibit or disallow the establishment of structures/ housing within or along waterways, many people are still openly violating them. Enforcing these laws and policies is apparently weak and very challenging for the LGUs. Challenges include enormous housing back log, which is becoming difficult to cope with given the lack of resources to establish relocation or resettlement sites. Other challenges are the increasing land value, lack of legal resources, conflicting political agenda, lack of manpower to enforce the law on the ground and increasingly uncooperative people.

During the consultation meeting with the housing sector stakeholder groups, the following issues and concerns in relation to the relocation of their IFS along the waterways are raised:

- Difficulty in buying relocation site;
- Difficulty in acquiring Right of Way (ROW)
- LGU has very limited fund source for relocation projects;
- Local Shelter Plan is still on the process, where relocation program should be included;
- The Housing Board is still newly created or needs to strengthen the existing ones;
- Need for inter-agency coordination and collaboration to assist LGUs in implementing their relocation projects;
- Need to organize the affected communities;
- Need for private sector participation through socialize housing program.

4.4 Funding issues

With 9,000 affected structures needing relocation, the LGUs need an estimated amount of PhP 3.6 Billion Pesos in order to establish a decent resettlement site. Urgently, they need to relocate about 2,000 households who will be affected by the river improvement projects by the DPWH amounting to PhP731 Million Pesos which needs to be implemented this year otherwise the fund will be returned to the national treasury. The cost of the relocation which is about PhP800 Million Pesos, excluding ROW acquisition, is more than the drainage projects.

All the LGUs expressed their concern in relation to the lack of funds in implementing their respective relocation/ resettlement projects. It is then raised during the consultation meetings to include the relocation cost in the drainage improvement budget of the Department of Public Works and Highways. However, the DPWH is not mandated to develop housing settlements, while the National Housing Authority (NHA) who is mandated can only build the resettlement projects if the LGUs will provide the land.

5 PROPOSED SOLUTION

5.1 Implementation of relocation and resettlement projects

First and foremost, the LGU must make a definite stand against encroachment on the waterways and this should be communicated clearly to all constituents of the city. Clear communication can be demonstrated by the actual implementation of the relocation projects. People should see that the government through the LGU is intentional in enforcing the law against encroachment on the waterways by providing the necessary control measures and provision of alternative settlements to qualified beneficiaries. Once the area is cleared, the waterways improvement project should be implemented at once otherwise if the area remains untouched for a period of one to two months, chances are, people will go back.

Meanwhile, in carrying out the relocation or resettlement program, major consideration on environmental and social safeguards must be at the forefront of the project implementation. It also requires comprehensive planning and careful execution to lessen conflicts and negative impacts on people's lives and properties. It is then important for the LGUs to formulate and implement a comprehensive relocation program for the affected households.

Because of the huge number of the affected structures along the whole stretch of the rivers and creeks particularly the informal settlements in Metro Cebu, the relocation resettlement program should be done in three terms, which are:

1. Short Term (within 3 years) – relocation of houses or structures that will be affected by the priority drainage projects and those located at the outfall.
2. Mid Term (in 4 to 6 years) – relocation of houses or structures up to the mid-stream; that is, from the first intersection from the outfall up to mid-stream of the waterway.
3. Long term (in 7 to 10 years) – relocation of all remaining structures along the waterways upstream.

Following the Housing and Urban Development Coordinating Council (HUDCC) LGU guidebook for local housing project, the relocation of the affected households will require three major procedures which come in three phases: pre-relocation, relocation and post-relocation phase.

Pre-relocation phase will include the site selection, land acquisition and fund sourcing. A very crucial element in the pre-relocation phase is the identification of the affected households which is done by tagging, mapping and making inventory of housing structures to be demolished and finalizing the list of beneficiaries. This is to avoid new or disqualified families from claiming residency on cleared lots. The conduct of house to house census will be necessary to determine the household size and other relevant information about the family and their resettlement options including their concerns and apprehensions. The census can also serve as a venue for presenting the concept and value of the relocation projects and how it will benefit them. The LGU will be responsible to undertake these activities through the assistance of community leaders.

As much as possible the involvement of affected households shall be sought to minimize negative impression or resistance towards the relocation project and to instill sense of ownership. Furthermore, there shall be coordination between the LGU through the Housing Department and the Local Housing Board and other concerned agencies such as the NHA, HUDCC, HLURB, NEDA and Subdivision and Housing Developers Association and DPWH. Through the conduct of inter-agency meetings, the details of the actual relocation operation and their respective roles and responsibilities can be defined and committed. The collaboration among these agencies will expand the resource base of the project considering that each entity can contribute in various ways.

Relocation Phase will be done once the resettlement site is already prepared and all the necessary preparations to execute the relocation are put in order. Important activities will also include the confirmation of the actual date of demolition and relocation and the availability of resources and necessary documents. All precautionary measures to facilitate orderly, safe and peaceful relocation will have to be considered. A demolition task force will be formed to spearhead the demolition activities. Agencies such as the PCUP and Commission of Human Rights can also monitor the actual demolition and relocation process. The actual dismantling of structures and movement of families will take place when all the requirements are prepared. It is also encouraged that the affected households voluntarily dismantle their own structures. This will give the affected families the opportunity to recover materials that they can still utilize in their new homes.

Post- relocation Phase is also required because relocating the affected households to the new resettlement site is not the end of the process. Beyond the physical development and movement of families, some efforts will be extended to ensure an orderly integration to the new community and environment. Community welfare programs may have to be introduced to ensure that school-age children are in school, parents have sources of livelihood for the basic needs of their families, health services are accessible, people are morally inclined and not engaged in illegal activities and peace and order is maintained. To effectively do the welfare programs considering the limited resources, the LGU may need to tap other groups aside from the NHA and DSWD. It is recommended to establish partnership with other sectors such as the NGOs, Faith- Based Organizations (FBOs), Civic Clubs, Churches, Academic Institutions and other groups.

5.2 Funding alternatives

In relation to the funding issue, it is believed that the Government of the Philippines will have the fund for the relocation but how to course it through requires some technicalities hence it is proposed to bring the issue at the national level, where at the level of the Department Secretaries (DPWH, Department of Interior and Local Government, NHA, Commission on Audit, National Economic Development Authority and HUDCC) can be resolved or alternative inter-agency solutions can be crafted before involving the Office of the President.

For additional funding, it is proposed to tap and utilize the National Housing Balance Program, where the private developers are mandated to develop or allocate funds equivalent to 20% of their development cost for socialize housing.

5.3 Institutional arrangement

Though the relocation of the affected structures is the primary responsibility of the LGUs, participation and coordination by and between various stakeholder groups are necessary. Addressing the escalating issues on resettlement requires concerted efforts of the local government units and national government line agencies, private sector and representatives of the affected households. An inter-agency committee can be created to assist the LGUs in designing, implementing, monitoring and evaluating their relocation projects. Specific to the drainage projects implementation, the committee shall coordinate with the DPWH to assist and monitor project implementation. Meanwhile, the LGUs will integrate the relocation program into their Shelter Plan. This will ensure the inclusion of the relocation program in the LGUs development agenda for the succeeding years with corresponding budget. In addition, the LGUs will need to strengthen their respective Local Housing Board who will lobby for programs related to housing. Lastly, the active participation of the Local Chief Executive or Mayor will be very crucial in realizing these projects, hence, their involvement should be sought after.

6 CONCLUSION AND RECOMMENDATION

The encroachment of structures along the waterways is the major obstacle in implementing the planned river and creek improvement projects in the Central Cluster of Metro Cebu. If this issue is not resolved, the integrated flood control measures in Metro Cebu will be half baked and the perennial flooding will continue and cause other socio-economic problems that will endanger lives and properties. Hence, the relocation of the structures encroaching the waterways is imperative. As such, the local and national government should make decisive course of action to address this issue with the support of the private sector as proposed.

ACKNOWLEDGMENT

The authors would like to thank the Metro Cebu Drainage Masterplan Study Team for assisting in the conduct of the physical surveys and generation of the maps that provided clear illustration of the extent of the river and creek encroachment problems. Appreciation is also extended to the local government units particularly to DWUP and HUDO who provided data on the number of informal settlement along the waterways.

REFERENCES

Housing and Urban Development Office, Mandaue City. Informal Settlement Inventory. Mandaue City Comprehensive Land Use Plan. (2014).

Cebu City Comprehensive Land Use Plan. 2013

Jaque, J. (2016). *Community Development Program of Metro Cebu Flood Control and Drainage Masterplan Study,* Unpublished Draft Report.

SunStar Publishing, Inc. (2016). *Clogged drainage, constricted river cause Cebu.* Available from <http://www.sunstar.com.ph/cebu/local-news/2017/02/14/clogged-drainage-constricted-river-cause-cebu-flooding-483720#> [January 2017].

Sun Star Publishing, Inc. (2016). Relocate informal settlers widen creeks and rivers now. Available from <http://www.sunstar.com.ph/cebu/local-news/2016/07/12/relocate-informal-settlers-widen-creeks-and-rivers-now-485023> [January 2017].

Proceedings of the 37th IAHR World Congress
August 13 – 18, 2017, Kuala Lumpur, Malaysia

ANECOLOGICAL RESTORATION FRAMEWORK FOR LOWLAND FLOOD CHANNEL IN HONG KONG

YAO WANG[1] & ONYX WING-HONG WAI [2]

[1,2]Department of Civil and Environment Engineering, the Hong Kong Polytechnic University, Hong Kong
wyeureka@gmail.com; onyx.wai@polyu.edu.hk

ABSTRACT

This paper aims to provide a framework for ecological restoration on lowland flood channels for the benefit of inhabited fish. The study area of the present research is located in Tung Chung River in Hong Kong, with a channelized downstream section to be restored. In this study, *Parazaccospilurus* (a widespread endemic fish species) is selected as the target fish as it is sensitive to habitat changes and is commonly found in unpolluted local streams. First of all, taking both physical and fish sampling into equal importance, field survey is conducted in both wet and dry seasons in the study area. A new fish monitoring system specified for lowland flood channel is developed in this study using high resolution underwater camera based on remote underwater video system technology. To establish appropriate fuzzy-sets and fuzzy-rule for modeling the physical habitat of the target fish, the fish daily activities will be monitored and recorded in the laboratory. In addition, the fish swimming velocity and acceleration in an artificial environment with instream structures (e.g. deflectors) will be monitored to investigate the impact of these structures on the fish swimming behavior. The physical habitat model, CASiMiR, will be applied to assess the fish response to changing physical properties based on the fuzzy physical-biota relationships. Finally, in order to attract the target fish back to the lowland channelized section, the water and sediment regime will be modified according to the habitat modeling results. A restoration program focusing on deflector construction will also be proposed to create riffle-pool sequence and meandering based on the effectiveness of deflectors observed in the experiments. It is hoped that the present research could be useful to guide the future development and design of flood channels which are deserved to be protected.

Keywords: River ecological restoration; lowland flood channel; habitat quality index; underwater video system; physical habitat modeling.

1 INTRODUCTION

It is stated in the US National Research Council (1992) that “restoration of an ecosystem aims to return it to a relatively close approximation of its earlier condition which is prior to natural or human disturbances by means of physical reconstruction, chemical cleanup and biological manipulation”.The recognition and practice of river ecological restoration has undergone a long process. In the 1950s, the concept of "Near-natural River Engineering" was developed in Switzerland and Germany, concentrating on comprehensive management of river and emphasizing the connectivity between animals and vegetation, which could be regarded as a milestone of river restoration history. From the late 1960s to the 1970s, the river restoration works mainly stayed on pollution control and water quality improvement, including the "Clean Water Act" brought up in the United States in 1972.

In 1982, the restoration of Itachi River - a straight channel without recreational value, was one of the earliest restoration projects in Japan (Nakamura et al., 2006). In the late 1980s, integrated ecological restoration project on large rivers had been developed. One of the representative projects was the project "Rhine River Salmon 2000" carried out from 1987 to 2000 in order to attract salmon back to the Rhine (Frijters & Leentvaar, 2003). After the project had achieved satisfactory results, the "Rhine Salmon 2020" program was published by the International Commission for the Protection of the Rhine (ICPR). From 1987 to 2002, Denmark also carried out ecological restoration on the local Skjern River to restore the floodplain, which was one of the largest river restoration project implemented in Europe (Pedersen et al., 2007).

During the 1990s, the United States, Japan and some other countries also did ecological restoration of rivers, including the Napa River, the Kissimmee River (Dahm et al., 1995; Toth et al.,1995), the Missouri River (Jacobson et al., 2009) in the United States and the Kushiro River (Nakamura et al., 2006) and Miharu Reservoir (Kantoush & Sumi, 2016) in Japan. In 1990, a Japanese project "Naturally-diverse River Works" was officially initiated to enhance ecosystem with high biodiversity and beautify the landscape of river. The River Bureau in Japan also launched "Nature-oriented River Works" for the purpose of conserving and restoring river biodiversity (Nakamura et al., 2006). In 1999, the Hong Kong government listed the Tai Ho River as a site of special scientific interest for the first time of river conservation (Cheng et al., 2008).

When it comes to the 21st century, river ecological restoration mainly focuses on promoting the continuity of the river and floodplain (Wohl et al., 2015), and more began to emphasize on green ecology and landscape construction. In 2000, the European Union published the "Water Framework Directive (WFD)", and planned to ameliorate the related water bodies ecologically by 2015. The project "Watershed/Urban Regeneration in Accord with Nature" was adopted as national initiative in 2002 in Japan (Yoshikawa, 2003). In 2003, a project aimed to restore the Cheonggyecheon into its original appearance, including demolition of highways, river restoration work and landscape construction was initiated in Seoul, Korea (Hwang, 2004; Cho, 2010). In 2006, the "ABC (Active, Beautiful and Clean) Waters Program" was started in Singapore with the goal of transforming the concrete channel into natural, vibrant, beautiful and clean riversides with functions of recreation (Yap & Koh, 2010). The dynamic combination of Bishan-Ang Mo Kio Park and Kallang River in Singapore (Dreiseitl, 2012) was one of the most inspiring projects of how a city park can function as ecological infrastructure. Hong Kong government also mentioned Water-friendly Culture and Activities in the 2015 policy address: "We will adopt the concept of revitalizing water bodies in large-scale drainage improvement works and planning drainage networks for new development areas so as to build a better environment for the public".

Nowadays, many rivers that pass through urban areas have been channelized into concrete waterways in straight, wide and deep forms (Wohl, 2015) for the purposes of flood prevention, drainage improvement, reduction of bank erosion and river realignment. Channels, after being changed physically, will always strive to readjust themselves to reach equilibrium state again. To avoid instability problems that may be caused by the readjustment, channelized rivers are often heavily protected against erosion by minimizing the existence of sediments, rocks or plants along the channel. However, the transport and dispersion of river sediments plays a fundamental role on the fluvial process. Either sediment excess or sediment deficit in a river system is likely to have some fundamental impact on the process and the form of rivers, leading to the degradation of ecosystems (Wohl et al., 2015). Therefore, a successful river restoration is indispensable from the consideration of sediment regime.Research on physical modeling and numerical simulation of sediment transport is well developed. The first challenge in the context of river restoration is to close the gap by combining the study of sediment transport and river ecological restoration together (Wohl et al., 2015).

It is mentioned in the WFD that preservation and establishment of fish spawning habitats should be considered as one of the major aims in successful river restoration (Hauer et al., 2008). For fish spawning, a suitable mixture of particles (cobbles, pebbles, gravels, sand) is required (Kondolf et al., 2008). If the substrate is too coarse to be moved by fish, the ability of fish to excavate nests will be limited. On the other hand, the accumulation of excess fine sediment may reduce oxygen supply and inhibit the removal of the metabolic waste. And mobilization of bed material can expose and destroy eggs if the bed is scoured below the depth at which the eggs are buried (Cienciala & Hassan, 2013). The state-of-the-art fish spawning suitability studies have made great contribution on the flow and sediment regime simulation of fish habitats. However, the studies lacks effective solution to help increasing the potential fish spawning availability and to reduce the disturbance risk for the preservation and establishment of fish habitats. The second challenge regarding river restoration lies in the integration of fish habitat modeling in the context of river ecological restoration.

According to HK (Hong Kong) River Net, restoration of an artificial river channel is more than a beautification project, and should aim to at least partially restore the river's original mechanisms and functions. An effective ecological restoration for lowland flood channel starts with a comprehensive assessment of river ecosystem to identify the effect of nature or human activities on ecological resources. There are different aspects to assess the health of a river, including the biotic parts (e.g. fish) and the physical characteristics such as water depth, flow velocity, dominant substrate (Noack et al., 2015), bed morphology, floodplain and riparian zone health. If the ecology of river for fish is in an unsatisfactory situation, a goal for restoration should be set after the assessment through discovering a reference site, which can be a historical interval comparable to the present (Wohl,2011), an adjacent river with low human impact, or an upper/lower river with low human impact.

It is the main focus of this paper to combine different topics between river restoration, fish habitat and sediment regime. Using the habitat suitability index as criteria instead of result, solutions will be proposed accordingly to restore the river and to ensure the restored condition meets the habitat suitability criteria so as to bring the target fish back into some specific river reach. As the existing literature concerning river restoration rarely discusses the framework for channelized rivers, this paper aims to provide a framework for ecological restoration on lowland flood channels.

2 STUDY SCOPE

2.1 Tung Chung River

Rivers in Hong Kong are densely distributed since the climate is wet and warm and the precipitation is substantial with approximately 2,200 mm per year. There are more than 200 rivers, streams and nullahs spread in Hong Kong according to the statistics from the baseline survey of Agriculture, Fisheries and

Conservation Department (AFCD) in 2002. Earlier years, for the purposes of enhancing drainage capacity and preventing flooding, Hong Kong witnessed many urban rivers being trained into concrete channels.

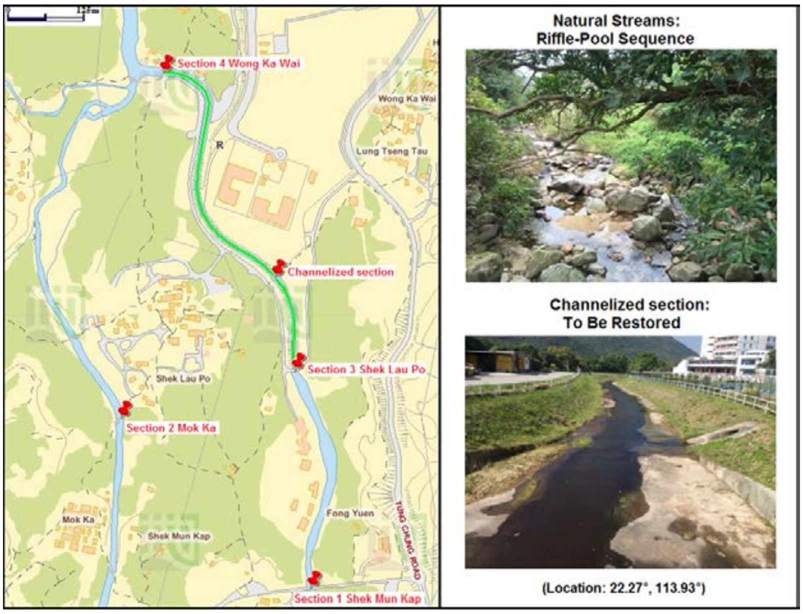

Figure 1. Map of study area (left) and view of the study reaches (right).

The study area of the present research was the Tung Chung River (Figure 1). Originating at an altitude of 880 meters, flowing through northern Lantau Island and reaching the ocean, it is situated on the north-western coast of Hong Kong. The main stream (West stream) flows north through Mok Ka, and merges with a major tributary (East Stream) which flows through Shek Mun Kap and Shek Lau Po before entering Tung Chung Bay. Tung Chung River is short and steep (average gradient is 1:4.90), with a horizontal length of 4.31 kilometers.

With the development of Tung Chung Town, 650 meters downstream part of the East Stream was channelized to prevent flooding from affecting downstream areas, starting from Shek Lau Po east and ending to the northwest of Wong Ka Wai (Green line in Figure 1). The remaining river reaches have been kept in their original natural state. The channelization has brought severe damage to the river ecology, changing the natural shelter for the animals living in this area, decreasing the number and biodiversity of species, isolating the individuals and the environment and causing deterioration of water quality.

Five representative locations (Red pinpoints in Figure 1; Figure 2) were chosen in this research, including two natural river sections (Section 1 Shek Mun Kap and Section 2 Mok Ka), two border river reaches (Section 3 Shek Lau Po and Section 4 Wong Ka Wai) and a typical river section of man-made channel (Section 5). Among the five locations, Section 2 lies in the main stream of Tung Chung River, while the remaining reaches are situated in the tributary flowing north towards Tung Chung Bay.

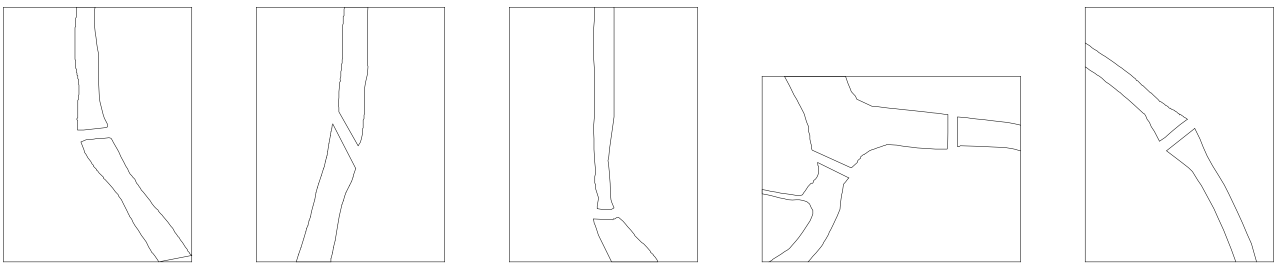

Figure 2. Five river sections in Tung Chung River (section 1 to 5 from left to right).

2.2 Target fish

In this research, one of the commonest local freshwater fish species *Parazaccospilurus* (Figure 3) was selected as the target fish. This species was firstly discovered in mountainous streams in Hong Kong and was scientifically recorded by Günther in 1868. It is one of the rare species that originated from Hong Kong and can be regarded as the representative of local fish.

According to AFCD, it is sensitive to any changes to the habitat and prefers to live in clear and unpolluted streams. The Ichthyological Society of Hong Kong pointed out that this species normally lives in streams with very slight pollution. Therefore, the decline of the quantity of this kind of species can reflect the deterioration of water quality. When their habitat is polluted by domestic water or destroyed by land development, this kind of species will be influenced and will disappear accordingly. Moreover, the construction of dam and reservoir over the entire 1,104 km² of Hong Kong has also changed the habitat of the fish. It is now evaluated as vulnerable in China Red data book according to AFCD database.

Figure 3. Juvenile Parazaccospilurus (left) and adult Parazaccospilurus (right) (Source: AFCD).

3 METHODOLOGY

3.1 Habitat quality assessment

A habitat quality survey was firstly conducted to assess different habitat quality aspects including the substrate, pool-riffle sequence, flow pattern to the fish individuals living in the stream. The results of habitat survey can help yield basic information about the ecological condition of lowland streams. An assessment system was developed by Chan (2001) to evaluate the suitability of river for freshwater fish in Hong Kong using the total value of Habitat Quality Index (HQI). A series of physical habitat types (pollution source, channel planform, channel width, channel substrate type, riparian habitat type, pool-riffle unit, percentage of shade, in stream habitat, other channel features, dominant floodplain and catchment permeability) and the corresponding categories as well as four metrics scores (0,1,3,5) are defined for the Hong Kong streams in particular. The summation of the metrics scores of each physical habitat type gives a final habitat quality index score for each section. The sections with higher total HQI, which means better river habitat quality, maybe used as reference sites for restoring the channelized sections.

3.2 Basic data collection

The measurements of the physical parameters in both inferior river sections - the lowland flood channel and the reference site should be carried out during field surveys. The sampling data of water depth, flow velocity and substrate, which are used to describe the habitat environment, can be used for calibration for the hydromorphological simulation and can be used as the input for physical habitat modeling.

3.3 Fish monitoring

To study how fish are affected by the changing of those physical factors mentioned above, it is required to collect information on the density, diversity, and size of the fish populations (Langlois et al., 2006) in the field. There exist many different kinds of fish survey methods, including underwater visual census, baited remote underwater video (Harvey, 1995; Willis & Babcock, 2000; Cappo et al., 2007; Harvey et al., 2007; Stobart *et al*., 2007; Colton & Swearer, 2010; Bassett & Montgomery, 2011), experimental angling (Willis et al., 2000) and longline survey (Brooks et al., 2011). Langlois (2006) recommended horizontal view baited remote underwater video rather than the downward view since it performed better and recorded more species.

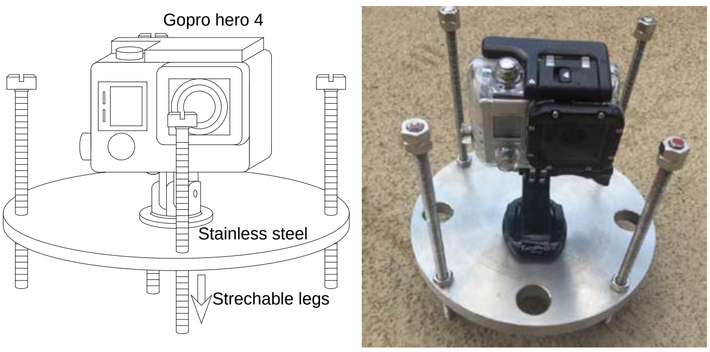

Figure 4. Fish monitoring system prototype (left) and fish monitoring system end product (right).

In this research, fish bait was not employed to avoid man-made interference and to capture the most natural daily activities of fish. A new non-destructive and non-intrusive fish monitoring system (Figure 4) had been modified using a 4K Ultra high resolution underwater camera Gopro hero 4 (41*59mm) on the basis of horizontal remote underwater video system technology which was commonly applied in investigating fish assemblages in marine waters. The stainless steel circular base can serve as both a stand and a ballast to guarantee the stability of the camera even in high-speed flow or on bumpiness bed material. The adjustable four legs of the base can satisfy the needs for fish monitoring in lowland flood channels with relatively lower water depth. The monitoring system was deployed at different locations at daylight hours for more than 5 min to produce a piece of footage in the level of equilibrium. By applying the Anim Get image analysis system, the screenshots can be extracted from the video with the time interval of 10 ms, and the maximum number of fish individuals at one single frame was recorded as the conservative fish density to avoid the repeated counting. The fish number recorded can be compared with the habitat suitability index results from the physical habitat modeling to validate its reliability.

3.4 Fish laboratory experiment

3.4.1 Fish life habit

In order to establish appropriate fuzzy-sets and fuzzy-rule for the target fish *Parazaccospilurus*, their daily activities will be tested and studied in the fish tank in the Eco-hydraulic Laboratory in the Department of Civil and Environmental Engineering in the Hong Kong Polytechnic University. The results can be integrated with expert knowledge to provide background information of the fish species and to generate habitat suitability curves for the later habitat modeling.

3.4.2 Fish behavior with deflectors

The experiments will be conducted in a 9 m long, 1 m wide and 30 cm deep flume in the laboratory. In stream structures (e.g. deflectors) will be introduced in the channel to enhance the creation of pools and riffles to attract fish to enter, pass through, and exit safely with minimum time and energy (Bermúdez et al., 2010; Rodriguez et al., 2010). At the downstream end of the flume, a chamber was designed to introduce the adult fish individuals prior to experimentation. Water temperatures from 21.2 to 22.9^{o}C, pH from 6.9 to 7.9, and dissolved oxygen content from 6.5 to 9.9 mg/L will be maintained throughout the experiment. The channel will be equipped with four fish monitoring systems mentioned above in order to continuously track the fish movements in the pools in a non-intrusive way (Bermúdez et al., 2012). With this monitoring technique, variables such as swimming velocities and accelerations (Morcillo & Castillo, 2014) will be evaluated for the target fish. Besides, the path chosen by fish moving from one pool to another and the resting zones exploited by the fish will be identified accordingly. The final objective of this experiment was to explore the impact of different deflector designs on the enhancement of habitat establishment.

3.5 Physical habitat modeling

Since the 1980s, physical habitat models including PHABSIM (Shoji & Fukui), RHABSIM (Gard & Ballard, 2003), RMA2 (Mussetter et al., 2004), RIVER2D (Schwartz, 2004), ELAM (Goodwin et al., 2006) and CASiMiR (Noack 2012; Noack et al., 2013) have played fundamental roles in river management. Since fixed numerical values and exact functions are normally not capable to express the complexity of natural systems in an accurate way, fuzzy-logic has distinctive advantages compared to classical modeling techniques using “high”, “medium” or “low” to describe physical properties such as flow velocity, water depth and substrate. The Institute for Modeling Hydraulic and Environmental Systems (IWS) of the University of Stuttgart developed a physical habitat model called CASiMiR that incorporated a fuzzy-approach. It will also be applied in this research to assess the biotic responses to altered environmental conditions through the physical-biota relationships. By applying aquatic habitat modeling, the habitat suitability index in the domain of interest can be estimated with the relationship of physical properties and target fish responses.

3.6 River restoration

The state-of-the-art fish spawning suitability studies have made contribution to better understand the flow and sediment regime of fish habitats. However, the understanding does not provide solution to increase the potential fish spawning availability and to reduce the disturbance risk for the preservation and establishment of fish habitats, which is one of the major aims in successful river restoration (Hauer et al., 2008).To restore river corridors with rich biodiversity, solutions will be proposed with a main objective to bring back the target fish into the lowland flood channels. Using the habitat suitability index as criteria, solutions will be proposed accordingly to restore the river and ensure the restored condition meets the habitat suitability criteria. The specific restoration methods included improving the flow and sediment regime using the results from physical habitat modeling and the construction of in stream structure (e.g. deflector) according to the results of the deflector experiments.

4 PRELIMINARY RESULTS AND DISCUSSION

4.1 Results of habitat quality survey

Based on the assessment system developed by Chan (2001), the total value of HQI of each section was calculated through the evaluation of the eleven physical habitat types (see Table 1). It was revealed in the table that natural streams showed better river habitat quality than the channel. Section 1 had its advantages on good habitat quality with more substrate types (sand/gravel: 0.06mm-6.4cm, cobble: 6.4cm-26cm, boulder: >26cm etc.), riparian habitat types (short grass<20cm, low shrub<50cm, native trees etc.), shading (>75% shaded) and other channel features (exposed sand bar, vegetated island, bridge etc.). Section 2 and the two ends of the channelized section (Sections 3 & 4) had equal level on habitat quality from 39 to 32 points. However, the channelized section showed the lowest total HQI of 9 points with poor riparian habitat type of gabions and low percentage of shade (<30%). Therefore, it is highly necessary to improve the ecology situation in the channelized section, like creating riffle-pool sequence, producing meandering and so forth.

Table 1. Habitat quality index (HQI) of the five sections in Tung Chung River.

Physical Habitat Type	Section 1	Section 2	Section 3	Section 4	Channelized Section
Pollution source	5	5	5	5	3
Channel planform	5	5	5	5	0
Channel width	3	3	3	3	0
Channel substrate type	5	3	5	3	0
Riparian habitat type	5	5	5	3	3
Pool-Riffles unit	5	5	5	5	1
Percentage of shade	5	1	1	1	1
Instream habitat	3	5	3	3	0
Other channel features	5	1	3	3	0
Floodplain land use	3	3	3	1	1
Catchment permeability	3	3	0	0	0
Total	47	39	38	32	9

According to the field observations, the target fish is likely to inhabit in the Mok Ka river section as well as the natural river streams adjacent to the channels, while there are barely any fish individuals surviving in the channelized section.

Section 2 Mok Ka, which is the only study stream located in the main stream of Tung Chung River, harbors more target fish than other sections. There is obvious riffle-pool sequence morphology in this section, which provides preferable living space for the target fish since they favor rocky streams with large pools, and they are frequently observed hiding in rock crevices. Therefore, Section 2 can be regarded as a reference site since it performs well on habitat quality and has maximum number of target fish.

The other four sections were located on the main tributary of Tung Chung River from upstream to downstream. Section 1 Shek Mun Kap has plane-bed morphology and rock-dominated bed material. The exposed sediment bar observed in this region on March and April, 2016, has been continuously washed away by flush during wet season. The temporary streams are dry in March, April, and wet in August, September and even in December. Despite the fact that the river reach is a natural river section, there is barely any target fish observed in the main stream, which may be the result of the water level drops caused by the alluvial deposits.

Section 3 Shek Lau Po is the starting point of the channelized section. Right on the border of the natural stream and the channel, there was a meadow, a field habitat vegetated by grass and other non-woody plants, observed here in April, 2016, providing shelter for target fish and some other aquatic biota. The meadow then disappeared after August, combined with the sediment accumulation, causing the natural protective defense for the target fish fading away gradually.

The other end of the channel was situated in Section 4, Wong Ka Wai. On the border of the channel and natural river reach, there is a deep water pool with a large quantity of tadpoles and the target fish in the wet season. Fish is, however not found here in the dry season.

Between Section 3 and Section 4, the channelized section (Section 5) is a wide and concrete lining channel, covered with gabions on the river banks. There are some man-made steps in the middle of the channel built to increase the oxygen content. The water quantity is deficient and the water quality here is deteriorated due to pollution sources in this region. There is no fish observed here probably due to low water volume and pollution.

4.2 Results of fish survey

4.2.1 Fish number

Three locations were selected to conduct the fish monitoring using the newly-developed system in the fish assemblage region in Section 2. Location 1 lies in the halfway of the fish area at the edge of the west river bank. Locations 2 and 3 are the entrance and exit of the fish gathering place in the center of the stream, respectively. It is believed that through observation of the three locations, the fish number of this section can be estimated conservatively. The processed screenshots are shown in Figure 5. In Figure 5(a), 68 target fish was counted based on the image. In Figures 5(b), (c) and (d), there were 175, 211, 67 target fish, respectively. The fish number is also affected by the field of vision and river blockage. Thus, it is important to obtain a good visual field without obstruction. In the future, more data will be collected for the estimation of fish amount.

4.2.2 Fish species identification

On the video footage taken in Section 2, several species other than the target fish were identified to provide supplementary information on the local fish diversity.

There exist a group of Acrossocheilusbeijiangensis, which is one of the rare fish species. The resettling of this kind of precious fish species was once regarded as a symbol of a successful river restoration on Tung Chung River in history. Fish species like Cirrhinusmolitorella, Hemichromisbimaculatus, Hemichromisstellifer, Puntius semifasciolatus, Gambusiaaffinis and Xiphophorushellerii were also found in this section.

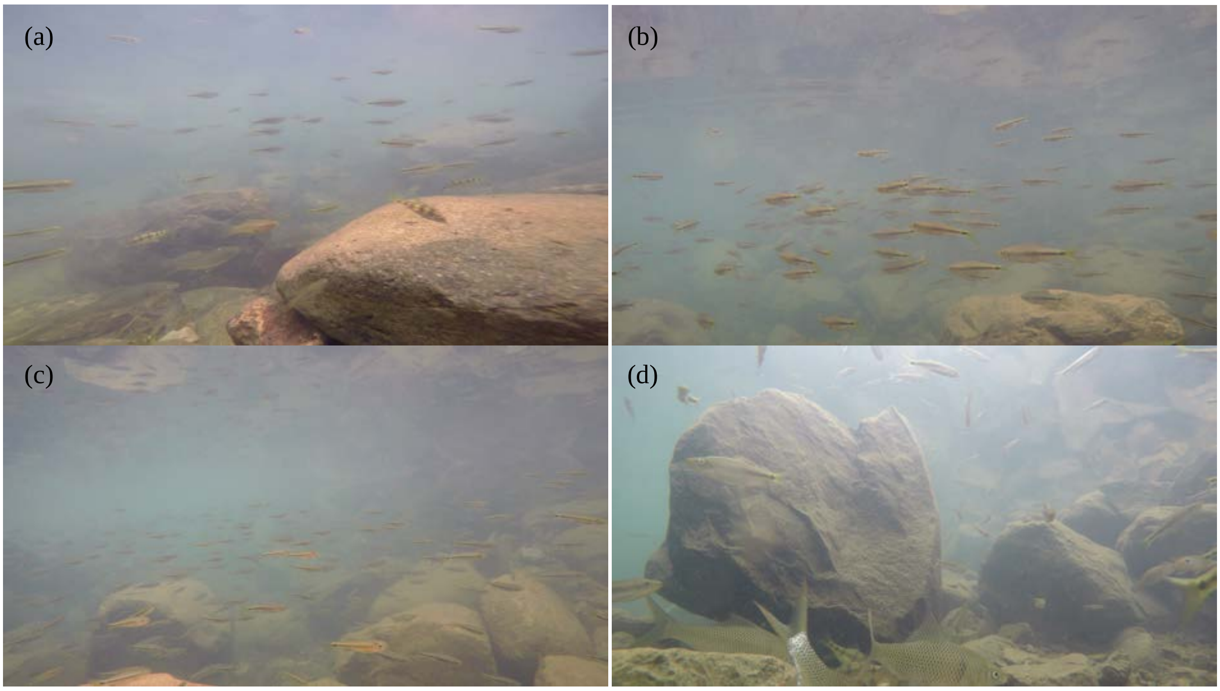

Figure 5. Screenshots with the maximum fish number in one-piece video footage ((a) location 1 in September; (b) location 1 in December; (c) location 2 in December; (d) location 3 in December).

5 CONCLUSIONS

This paper is an attempt to develop a framework for ecological restoration of a lowland flood channel in Hong Kong. The significance of this study lies in its contribution to the future development and design of man-made flood channels. In the study, flow and sediment regime are investigated through field survey and numerical simulation. By applying a new fish monitoring system and fish experimental study in the laboratory, the relationship between the physical environment of lowland channel and the behavior of the target fish can be studied. The preliminary findings of the present research regarding the habitat quality assessment show contrasting behaviors of natural streams and channelized section on multiple aspects. The results of fish monitoring suggest that the reference site is correctly selected to provide good baseline information for the flow and sediment regime paradigm for the ecological restoration of lowland flood channel in Tung Chung River. The field survey of basic data as well as fish monitoring will continue in the wet and dry seasons. Despite much effort, it remains that the fish experimental data and physical habitat modeling data is far from complete and cannot yield results as conclusive as might have otherwise occurred. Additional research will be extended based on the findings of the current study.

ACKNOWLEDGEMENTS

This research is funded by the Environment and Conservation Fund of Hong Kong (Grant 39/2011) and Research Grants Council Funds of Hong Kong (GrantPolyU152161/14E).

REFERENCES

Policy Address. (2015). Retrieved from http://www.policyaddress.gov.hk/2015/eng/p178.html.

Act, C.W. (1972). Clean Water Act of 1972. *Public Law*, 92(1972), 500.

Agriculture, Fisheries and Conservation Department. Hong Kong Biodiverisity Databbase. Retrieved from http://www.afcd.gov.hk/english/conservation/hkbiodiversity/database/popup_record.asp?id=3364.

Bassett, D. K. & Montgomery, J. C. (2011). Investigating Nocturnal Fish Populations in Situ using Baited underwater Video: With Special Reference to their Olfactory Capabilities. *Journal of Experimental Marine Biology and Ecology*, 409(1), 194-199.

Bermúdez, M., Puertas, J., Cea, L., Pena, L. & Balairón, L. (2010). Influence of Pool Geometry on the Biological Efficiency of Vertical slot Fish Ways. *Ecological Engineering*, *36*(10), 1355-1364.

Bermúdez, M., Rodríguez, A., CEA, L., Morcillo, F., Castillo, M. & Aramburu, E. (2012). Implications of Fish Behavior for Vertical slot Fish Ways Design. *9th of ISE,* Vienna.

Brooks, E. J., Sloman, K. A., Sims, D. W. & Danylchuk, A. J. (2011). Validating the Use of Baited Remote underwater Video Surveys for Assessing the Diversity, Distribution and Abundance of Sharks in the Bahamas. *Endangered Species Research*, 13(3), 231-243.

Cappo, M., De'ath, G. & Speare, P. (2007). Inter Reef Vertebrate Communities of the Great Barrier Reef Marine Park Determined by Baited Remote underwater Video Stations. *Marine Ecology Progress Series*, 350, 209-221.

Cheng, L.K., Lui, H. & Yau, H. (2008). *Come from Rivers,* Tung Chung River. Green Power, Hong Kong.

Chan, P.L. (2001). Sustainability and Biodiversity: The Impact, Alternative Design and Prospects of Restoration of Channelized Lowland Streams in Hong Kong. *HKU Theses Online, (HKUTO)*.

Cho, M.R. (2010). The Politics of Urban Nature Restoration: The Case of Cheonggyecheon Restoration in Seoul, Korea. *International Development Planning Review*, 32(2), 145-165.

Cienciala, P. & Hassan, M.A. (2013). Linking Spatial Patterns of Bed Surface Texture, Bed Mobility and Channel Hydraulics in a Mountain Stream to Potential Spawning Substrate for Small Resident Trout. *Geomorphology*, 197, 96-107.

Colton, M.A. & Swearer, S.E. (2010). A Comparison of two Survey Methods: Differences between underwater Visual Census and Baited Remote underwater Video. *Marine Ecology Progress Series*, 400, 19-36.

Dahm, C.N., Cummins, K.W., Valett, H.M. & Coleman, R.L. (1995). An Ecosystem View of the Restoration of the Kissimmee River. *Restoration Ecology*, 3(3), 225-238.

Dreiseitl, A. (2012). Bishan-Ang Mo Kio Park and Kallang River. *GSD Blogs*.

EU. (2000). Establishing a Framework for Community Action in the Field of Water Policy, Directive 2000/60/EC of the European Parliament and of the Council of 23 October 2000, The European Parliament, Brussels.

Frijters, I.D., & Leentvaar, J. (2003). Rhine Case Study. *Unesco.*

Gard, M. & Ballard, E. (2003). Applications of New Technologies to in Stream Flow Studies in Large Rivers. *North American Journal of Fisheries Management*, 23(4), 1114-1125.

Goodwin, R.A., Nestler, J.M., Anderson, J.J., Weber, L.J., & Loucks, D.P. (2006). Forecasting 3-D Fish Movement Behavior using a Eulerian-Lagrangian-Agent Method (ELAM). *Ecological Modelling*, 192(1), 197-223.

Harvey, E., & Shortis, M. (1995). A System for Stereo Video Measurement of Sub-tidal Organisms. *Marine Technology Society Journal*, 29(4), 10-22.

Harvey, E.S., Cappo, M., Butler, J.J., Hall, N. & Kendrick, G.A. (2007). Bait Attraction Affects the Performance of Remote under Water Video Stations in Assessment of Demersal Fish Community Structure. *Marine Ecology Progress Series*, 350, 245-254.

Hauer, C., Unfer, G., Schmutz, S. & Habersack, H. (2008). Morphodynamic effects on the habitat of juvenile cyprinids (Chondrostomanasus) in a restored Austrian Lowland River. *Environmental Management*, 42(2), 279-296.

HK River Net. River Restoration. Retrieved from http://www.greenpower.org.hk/river/eng/tm_restoration.asp.

Hwang, K. Y. (2004). Restoring Cheonggyecheon Stream in the Downtown Seoul. *Seoul: Seoul Development Institute*, 3.

Jacobson, R. B., Blevins, D. W., & Bitner, C. J. (2009). Sediment Regime Constraints on River Restoration - An example from the Lower Missouri River. *Geological Society of America Special Papers*, 451, 1-22.

Kantoush, S.A., & Sumi, T. (2016). *Effects of Sediment Replenishment Methods on Recovering River and Reservoir Functionality.* In River Flow, CRC Press, 2062-2069.

Kondolf, G. M. (2000). Assessing Salmonid Spawning Gravel Quality. *Transactions of the American Fisheries Society*, 129(1), 262-281.

Langlois, T., Chabanet, P., Pelletier, D. & Harvey, E. (2006). Baited under Water Video for Assessing Reef Fish Populations in Marine Reserves. *Fisheries Newsletter South Pacific Commission*, 118, 53.

Morcillo, F. & Castillo, M. (2014). Laboratory Study of the Efficiency for Native Iberian Fish Species of a Vertical Slot Fish Way. *Ecohydraulics*, 4, 1-2.

Mussetter, R.A., Wolff, C.G., Peters, M.R., Thomas, D.B., & Grochowski, D. (2004). Two Dimensional Hydrodynamic Modeling of the Rio Grande to Support Fishery Habitat Investigations. *Proceeding of the 2004 World Water and Environmental Resources Congress, Salt Lake City, Utah,* 27.

Nakamura, K., Tockner, K., & Amano, K. (2006). River and Wetland Restoration: Lessons from Japan. *Bioscience*, 56(5), 419-429.

National Research Council (US), Committee on Restoration of Aquatic Ecosystems-Science, Public Policy, National Research Council (US). Water Science, Technology Board, National Research Council (US), Commission on Geosciences, & Resources. (1992). *Restoration of aquatic ecosystems: Science, Technology and Public Policy*. Haworth Press.

Noack, M. (2012). *Modelling Approach for Interstitial Sediment Dynamics and Reproduction of Gravel Spawning Fish.* Universitat Stuttgart.

Noack, M., Ortlepp, J., & Wieprecht, S. (2015). Simulations of Spawning Habitats for Brown Trout in an Alpine River reach using a two Stage Multivariate Fuzzy Logical Approach. *Journal on Protected Mountain Areas Research*, 7, 41-49.

Noack, M., Schneider, M., & Wieprecht, S. (2013). The Habitat Modelling System CASiMiR: A Multivariate Fuzzy Approach and its Applications. *Ecohydraulics: An Integrated Approach*, 75-91.

Pedersen, M.L., Andersen, J.M., Nielsen, K., & Linnemann, M. (2007). Restoration of Skjern River and its Valley: Project Description and General Ecological Changes in the Project Area. *Ecological Engineering*, 30(2), 131-144

Rodriguez, Á., Bermúdez, M., Rabuñal, J.R., Puertas, J., Dorado, J., Pena, L. & Balairón, L. (2010). Optical Fish Trajectory Measurement in Fish Ways through Computer Vision and Artificial Neural Networks. *Journal of Computing in Civil Engineering*, *25*(4), 291-301.

Schwartz, J.S. (2004). Use of a 2D Hydrodynamic Model for Stream Restoration Design of High Flow Habitat in Low Gradient Midwest Streams. In *Protection and Restoration of Urban and Rural Streams*, ASCE, 242-251.

Shoji, T. & Fukui, Y. Estimating Fresh-Water Fish Habitat Using the Phabsim System.

Stobart, B., García-Charton, J.A., Espejo, C., Rochel, E., Goñi, R., Reñones, O. & Planes, S. (2007). A Baited under Water Video Technique to assess Shallow Water Mediterranean Fish Assemblages: Methodological Evaluation. *Journal of Experimental Marine Biology and Ecology*, 345(2), 158-174.

Toth, L.A., Arrington, D.A., Brady, M.A., & Muszick, D.A. (1995). Conceptual Evaluation of Factors Potentially Affecting Restoration of Habitat Structure within the Channelized Kissimmee River Ecosystem. *Restoration Ecology*, 3(3), 160-180.

Willis, T. J., & Babcock, R.C. (2000). A Baited under Water Video System for the Determination of Relative Density of Carnivorous Reef Fish. *Marine and Freshwater Research*, 51(8), 755-763.

Willis, T.J., Millar, R.B., & Babcock, R.C. (2000). Detection of Spatial Variability in Relative Density of Fishes: Comparison of Visual Census, Angling and Baited under Water Video. *Marine Ecology Progress Series*, 198, 249-260.

Wohl, E. (2011). What should these Rivers Look Like? Historical Range of Variability and Human Impacts in the Colorado Front Range, USA. *Earth Surface Processes and Landforms*, 36(10), 1378-1390.

Wohl, E. (2015). Legacy Effects on Sediments in River Corridors. *Earth Science Reviews*, 147, 30-53.

Wohl, E., Bledsoe, B.P., Jacobson, R.B., Poff, N.L., Rathburn, S.L., Walters, D.M. & Wilcox, A.C. (2015). The Natural Sediment Regime in Rivers: Broadening the Foundation for Ecosystem Management. *Bio Science*, 65(4), 358-371.

Wohl, E., Lane, S.N., & Wilcox, A.C. (2015). The Science and Practice of River Restoration. *Water Resources Research*, 51(8), 5974-5997.

Yap, K.G. & Koh, A. (2010). Creating a City of Gardens and Water–Singapore's Active, Beautiful, Clean Waters Programme. *Proceedings of the Water Environment Federation*, 2, 1-14.

Yoshikawa, K. (2003). Watershed/Urban Regeneration in Accord with Nature. *Civil Engineering, JSCE*, 40, 8-11.

BASIC STUDY ON APPLICABILITY OF SURFACE WAVE METHOD IN UNDERWATER RIVER CHANNELS

TAISHI MORITA[(1)], SHUNZO KAWAJIRI[(2)], YASUHARU WATANABE[(3)] & YUKI TANAKA[(4)]

[(1)] Graduate school of Eng., Kitami Institute of Technology, Hokkaido, Japan
m1652200151@std.kitami-it.ac.jp
[(2)] Dept. of Civil and Environmental Eng., Kitami Institute of Technology, Hokkaido, Japan
skawajiri@mail.kitami-it.ac.jp
[(3)] Dept. of Civil and Environmental Eng., Kitami Institute of Technology, Hokkaido, Japan
y-watanb@mail.kitami-it.ac.jp
[(4)] Graduate school of Eng., Kitami Institute of Technology, Hokkaido, Japan
m1652200105@std.kitami-it.ac.jp

ABSTRACT

This study investigates the applicability of the surface wave method for understanding the geological profile of the area under the riverbed. The profile of the S-wave velocity and the *N*-value are well matched. Therefore, the S-wave velocity near the ground surface in the river zone can be treated as an indicator similar to the *N*-value, because it provides a reasonable estimate of the geological cross-sectional view. In addition, the quasi-three-dimensional distribution of the S-wave velocity is consistent with the local situation. Consequently, with the use of the S-wave velocity distribution obtained from the surface wave method, it is possible to create the three-dimensional hazard map for riverbed degradation and improve the accuracy of the analysis.

Keywords: Surface wave method; S- wave velocity; *N*-value; geological profile; under riverbed.

1 INTRODUCTION

The riverbed degradation of the Muka River in the Tokoro River system is proceeding rapidly due to the excavation of the upstream river channel for renovation, the reduction of the sludge supply from upstream caused by the installation of cross-river structures and narrowing of the low-water channel by the high-water channel (Takahashi et al. 2014). The riverbed degradation accompanied by deteriorating gravel layer, which covers the riverbed, exposes the soft rock and the volcanic ash layer underneath. Once the soft rock or the volcanic ash layer is exposed, riverbed degradation is further accelerated resulting in the loss of riverbank protection functions and reduction of footing depth of bridge piers, which requires immediate implementation of the countermeasures.

It is useful to perform a riverbed variation analysis to examine the countermeasures for the riverbed degradation starting from the current geological structure under the riverbed, which is regarded as the initial value. The riverbed of the Muka River degraded 5 m or more in 32 years from 1979 to 2011 and the degradation is of ongoing nature. To predict the riverbed degradation precisely using riverbed variation analyses, it is necessary to understand the geological structure at least 10 m below the riverbed. The boring method is typically used to investigate the geological structure of the terrestrial area at a specific position; therefore, it is a time- and labor-intensive and costly method when applied to the entire river system. Therefore, the surface wave method to obtain the S-wave velocity, V_S, which indirectly represents the rigidity of the geological structure, has attracted significant attention in recent years.

In this study, the surface wave method is investigated to understand the geological structure underneath the riverbed. Specifically, this study performs surface wave method measurements along multiple survey lines crossing the river where the scour is outstanding in the Muka River. The validity of V_S is verified by comparing the V_S distribution obtained by the surface wave method and the *N*-value obtained by the boring method. V_S of the volcanic ash layer where the scour is outstanding is estimated. By interpolating the V_S distribution obtained for the survey lines crossing the river in the longitudinal direction, the quasi-three-dimensional (3D) distribution of V_S under the riverbed is obtained to understand the spatial distribution of the volcanic ash layer. Jigs are further developed to measure the surface waves within the river channel and the applicability of the surface wave method in the underwater environment is also investigated.

2 SURFACE WAVE METHOD AND TEST SITE

2.2 Surface wave method

The surface wave method is a seismic method used for geophysical site investigation (Park et al. 1999; Hayashi and Suzuki 2004). Figure 1 shows the schematic of the surface wave method. A large wooden hammer was used to impose a vertical force on the ground surface thereby triggering Rayleigh waves in the ground. The surface waves generated high-frequency (short-wavelength) waves propagated in the shallow ground region and low-frequency (long-wavelength) waves propagated in both the shallow and deep parts of the ground, following the characteristics of the Rayleigh waves. The shear wave velocity structure can be estimated by the inverse analysis of the various propagation velocities corresponding to these frequencies.

2.2 Test site and method

Figure 2 shows the investigation area and Figure 3 shows the exposure situation of the volcanic ash layer in KP 5.5 (KP is Kilometer Posts). The investigation area was KP 4.5~7.0 of the Muka River. The survey line length of the surface wave method was 48 m or 72 m. The installation space of the geophone (i.e., seismometer) which measures the surface waves and the space of the shaking point was 2 m.

Figure 4 shows the survey line of the surface wave method performed in the water at KP 5.5. The material, shape, and weight of this jig were determined by a preliminary test using the open channel. The geophones and the jig did not flow out by the water current; thus, the geophones and the jig were formed into an iron cylindrical shape so as not to directly receive noise from the river flow (Figure 5). The open channel experiment confirmed that the flow velocity in the jig was 0.7 m/s at the water depth of 0.3 m. This jig was installed to cover the geophones. In Case 1, similar to a surface wave survey conducted in normal land areas, a dish- shaped metal base portion was attached to the bottom of the geophones (Figure 6, Case 1). The geophones were placed directly on the riverbed under the water and the shaking method was applied that exerted a direct impact to the riverbed under the water surface by a hammer. In Case 2, the base part of the geophones was formed into a metallic needle shape (Figure 6, Case 2). In addition, a geophone was installed on the riverbed by inserting the base part into a hole drilled in the rock bed under the water surface using a hammer drill. Figure 7 shows the surface wave method in the river channel. The shaking was generated using a grounding pipe whose tip was in a pile on the riverbed and hitting the pipe with a hammer from the top.

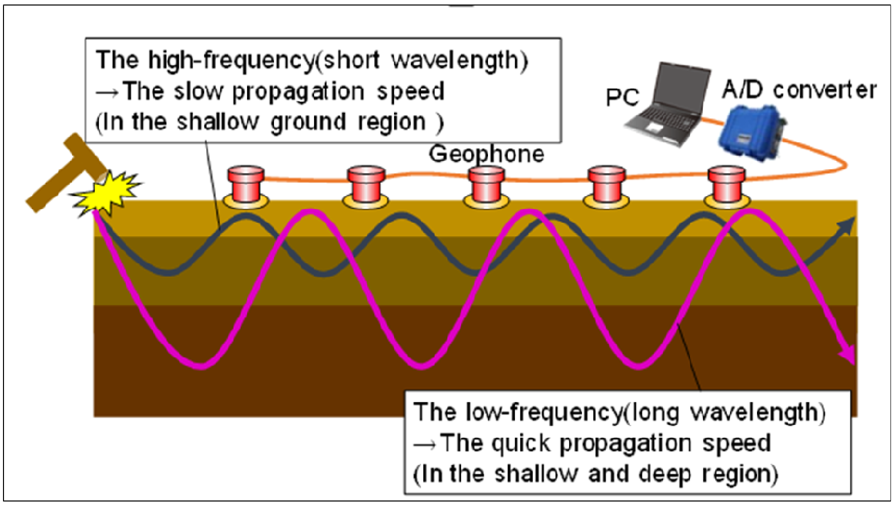

Figure 1. Schema of surface wave method.

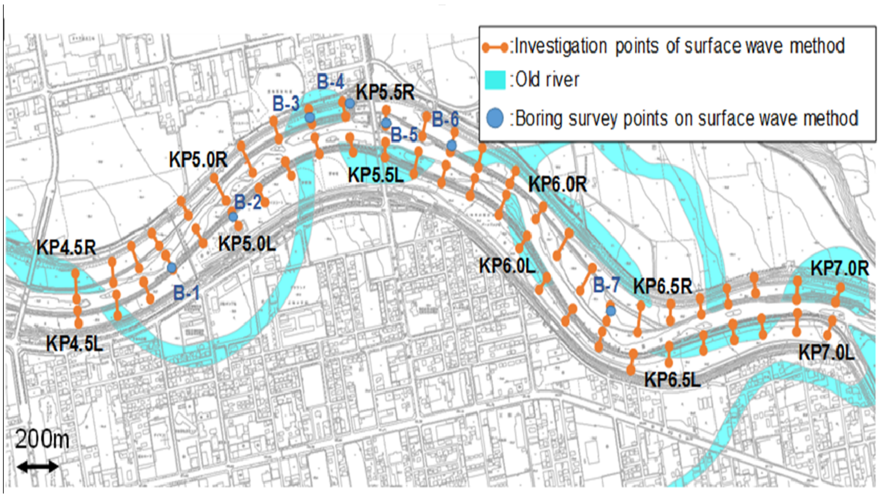

Figure 2. Investigation area of land area.

  / ISSN 1562-6865 (Online) - ISSN 1063-7710 (Print)

Figure 3. Exposure situation of the volcanic ash layer in KP5.5.

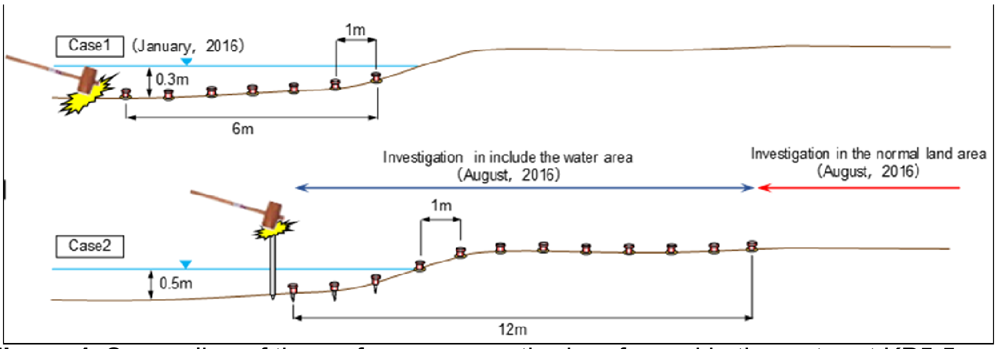

Figure 4. Survey line of the surface wave method performed in the water at KP5.5.

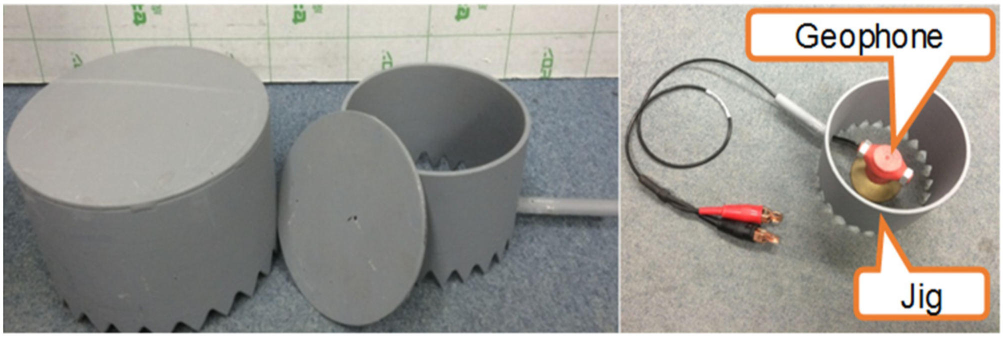

Figure 5. Development jig.

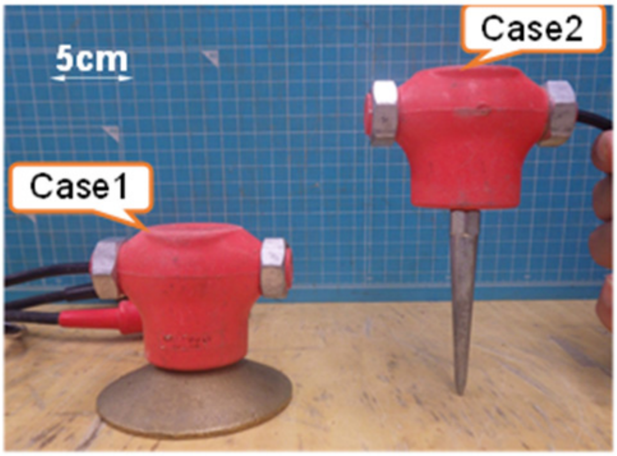

Figure 6. Geophones.

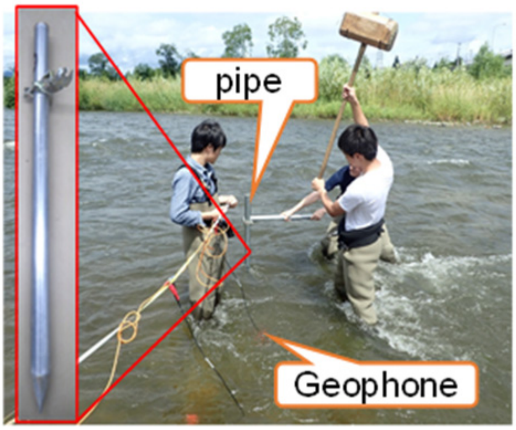

Figure 7. Situation of surface wave figure.

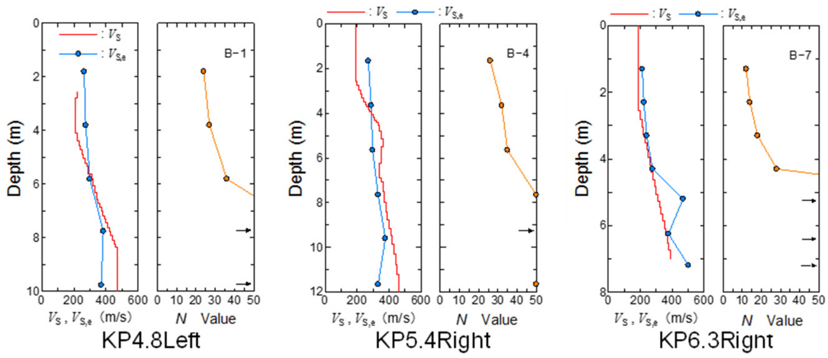

Figure 8. Comparison of VS and N-values at B-1, B-4, B-7.

3 RESULTS AND DISCUSSION

3.1 Relation between V_S and *N*-value

The *N*-value is an index of the ground strength and deformation characteristics and widely used in ordinary ground surveys. However, evaluating the spatial distribution of the *N*-value is difficult because it is in the form of depth data. If the correlation between V_S and the *N*-value from the surface wave method is confirmed, the spatial distribution of the *N*-value can be evaluated by interpolating the boring data with the V_S distribution. The changes in the depth direction of V_S and the *N*-value obtained from the surface wave method were compared. Figure 8 shows the comparison of V_S and *N*-values for B-1, B-4, and B-7 (Figure 2) as the representative results. Note that $V_{S,e}$ in Figure 8 is the V_S estimated from the *N*-value using the empirical equation suggested by Imai and Tonouchi (1982) (Eq. [1]).

$$V_{S,e} = 97.0\, N^{0.314} \qquad [1]$$

V_S and *N*-values tend to increase with depth and are well matched to each other. Therefore, V_S is also an indicator of the ground properties equivalent to the *N*-value in the ground survey of the river area. Furthermore, V_S is consistent with $V_{S,e}$ and it is possible to convert V_S obtained from the surface wave survey to the *N*-value even on the ground of the river area.

Figure 9 shows the relationship between V_S and *N*-value compiled for soil property classifications. Soil property classifications in Figure 9 were determined using the samples collected by the boring survey (Figure 10). Kp 1 and Kp 2 are the lower and the upper layers of the pumice flow deposit (volcanic ash layer), respectively. Kp 1 is the volcanic ash layer, part of which is compacted, with finer grains than Kp 2, while Kp 2 contains more gravel and sand matter than Kp 1. Converted *N*-value calculated using Eq. [2] when the obtained *N*-value exceeds 50.

Converted *N*-value = 50 times × 30 cm / 50 times hitting penetration amount (cm) [2]

The V_S of R(cg) was distributed in the range of 300-500 m/s and the converted *N*-value was in the range of 30-400 (Figure 9), clearly different from the other soils. The V_S of the volcanic ash layer Kp 1 tended to be larger than that of Kp, which was the same value as the V_S of the embankment Bs. On the other hand, both V_S and the converted *N*-value were large for the gravel-soil Ag and it was impossible to confirm a clear magnitude relation with other soils. The average value of V_S at the boundary between Kp 1 and R(cg) was about 310 m/s, which is considered to be the threshold value of V_S between R(cg) and Kp 1.

3.2 Spatial distribution of V_S

The two-dimensional (2D) V_S distribution for each crossing survey line was interpolated longitudinally to obtain the quasi-three-dimensional (3D) distribution of V_S within KP that was subjected to exploration. The commercially available 3D visualization software, Voxler4, was used to convert the 2D distribution data to 3D.

The continuous V_S distribution data was converted to discrete data that consisted of 4,280 points extracted in 2-m intervals in depth-wise and length-wise directions, which was the same as the receiving interval, at each cross section. Water surface level was set to 0 m when drawing the 3D map of the geological structure below the water surface. Figure 11 shows the iso-surface of V_S = 310 m/s, which is the threshold of the conglomerate and other soils with different properties, as a 3D distribution map. In this map, iso-surfaces with V_S = 210 and 260 m/s are also shown as the typical results for V_S smaller than 310 m/s. In Section 3.1, the area with V_S ≤ 310 m/s consisted of a volcanic ash layer where the scour and riverbed degradation proceeded drastically and the area with V_S < 260 m/s, which barely existed on the right bank side of KP 5.5, corresponded to the area where the volcanic ash was exposed (Figure 4). Since outstanding scour and riverbed degradation took place in that area, the low velocity area with V_S < 260 m/s became smaller compared to the other area. At KP 4.5 and KP 6.3, there was an area with V_S < 310 m/s along the river

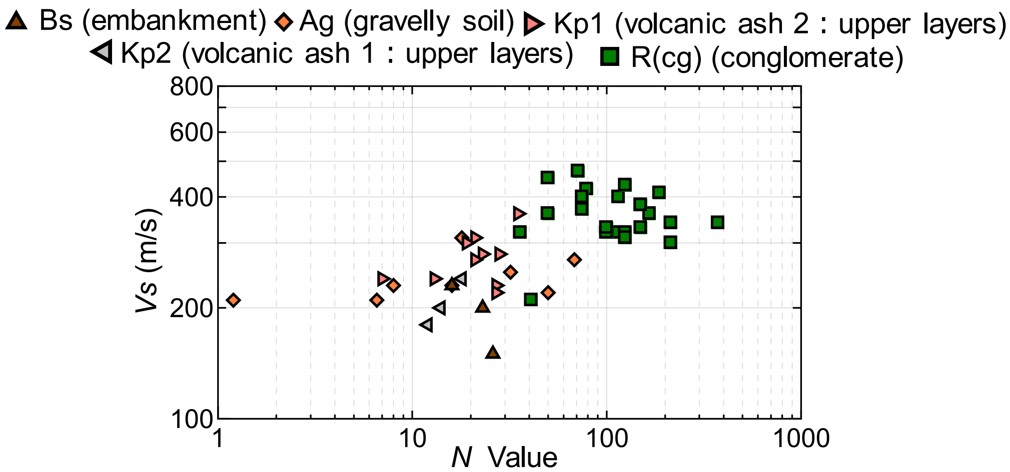

Figure 9. Relationship between V_S and the *N*-value for each soil classification.

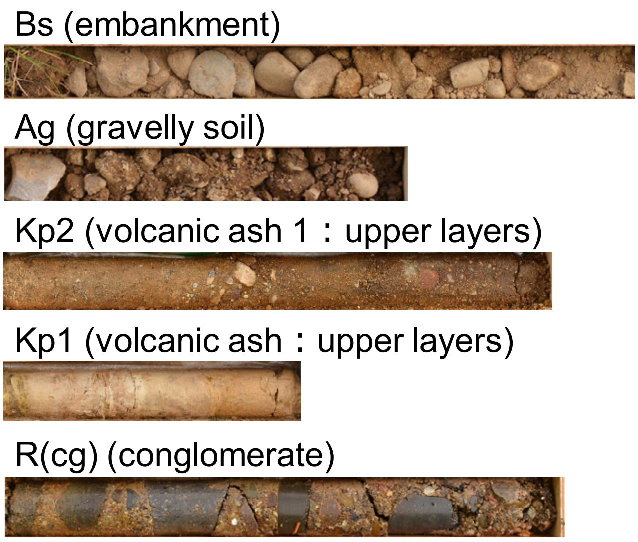

Figure 10. Result of boring survey.

channel and further riverbed degradation may take place there depending on the external force conditions. Thus, a spatial distribution map of V_S related to the soil property classifications works as a 3D hazard map of the scour and/or riverbed degradation and will be useful and practical for the implementation of disaster prevention measures.

3.3 Exploration results for underwater river channel

Earlier studies of underwater surface wave exploration showed that P waves, which propagate in water different from surface waves, were observed in the time domain wave data (P-wave velocity within water V_P = 1,500 m/s). Figure 12 shows an example of the seismograph wave data obtained in this study (wave data of each seismograph at the epicenter−0.5 m in Case 2). The labels of 0 m, 1 m, and 2 m in Figure 12 show the wave data in the water, where P waves are not observed. The jig that reduces the effect of the water flow also reduces the effect of the waves propagating in the water generated by the excitation of the artificial earthquake. Continuously monitoring the wave data of the seismograph after installing the jig in the water did not reveal the effect of the water flow. Therefore, the jig used in this study may be able to reduce the effect of P waves, which propagate in the water and cause noise in surface wave observations, making the measurement of the waves of the underwater riverbed comparatively easy.

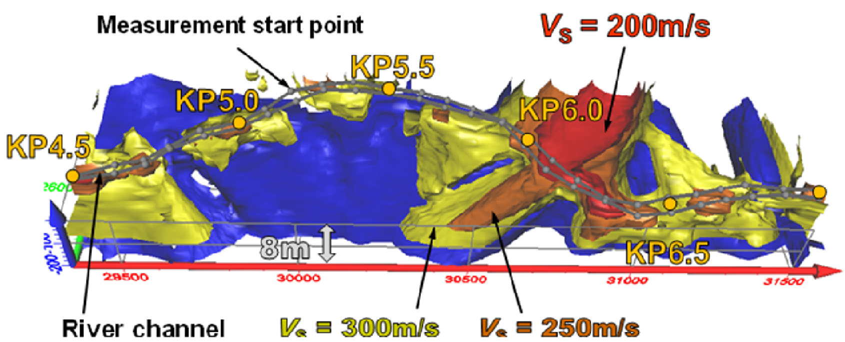

Figure 11. Iso-surface of VS.

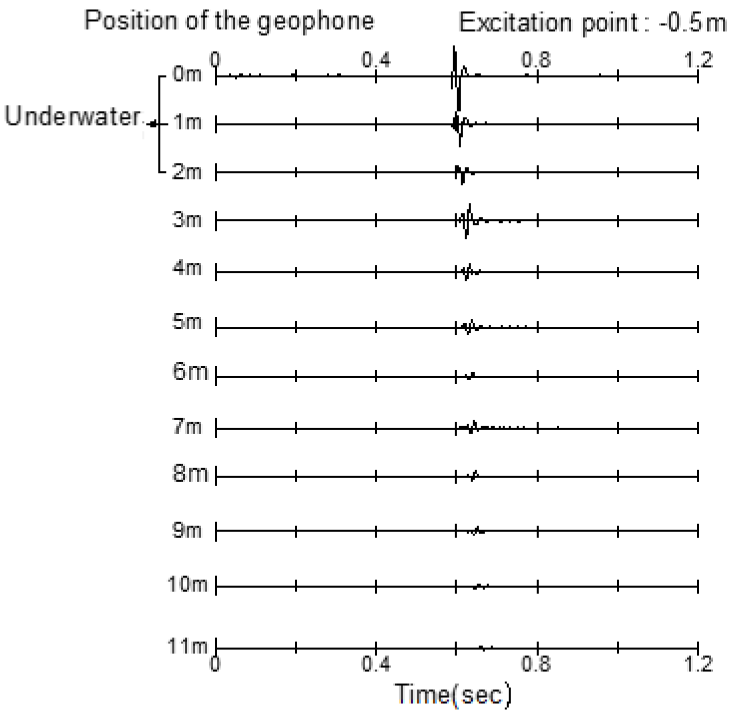

Figure 12. Example of seismograph wave data obtained in this study.

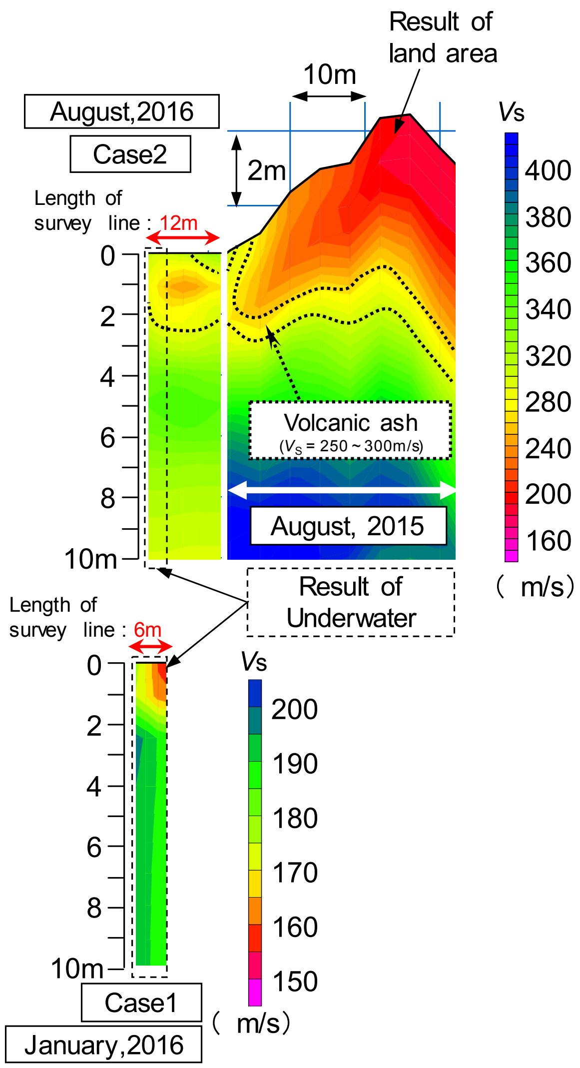

Figure 13. Comparison of V_S on underwater and land area.

Figure 13 shows the S-wave velocity distribution obtained by the surface wave exploration carried out at the right bank of KP 5.5 within the underwater river channel area and the terrestrial area. The S-wave velocity distribution of Case 1 showed that V_S at the riverbed where the underwater volcanic ash layer was exposed was 150 m/s, which was not consistent with the results shown in Figure 10. The underwater S-wave velocity was smaller than the terrestrial area S-wave velocity and the continuity of the S-wave velocity distribution from the underwater area to the terrestrial area was not apparent. This is because the mallet moved through water by the excitation of the artificial earthquake in Case 1 before directly hammering down the riverbed, which made the intensity of the earthquake too low to be detected by the seismograph used in this study. Similarly, the seismograph was set on a shallow bowl-shaped jig on the exposed bedrock, which made the seismograph unstable resulting in a lower surface wave measurement accuracy.

In Case 2, the underwater S-wave velocity distribution was V_S = 250 to 300 m/s at the depth of up to 2 m and V_S = 300 to 350 m/s at the depths from 3 to 6 m. Around the volcanic ash layer, shown by the black dotted line in Figure 13, the volcanic ash layer with low concreteness is exposed as shown in Figure 4 and the S-wave velocity distribution obtained in Case 2 can be considered appropriate. These results showed that the volcanic ash layer of 2 m was deposited even on the underwater riverbed at the explored positions.

The validity of the S-wave velocity distribution obtained by the underwater exploration was examined from the continuity of the S-wave velocity distribution by comparing the distribution in the terrestrial area with that obtained in Case 2. The S-wave velocity distribution matched well up to the depth of 4-5 m, which confirms the continuity of the distribution. Therefore, calculating the velocity distribution from the underwater area to the terrestrial area is possible for depths of up to 4-5 m in the river using the newly developed jig to reduce the effect of the water flow and using the seismograph installation and excitation methods adopted in Case 2. At the depths of 5 m or more, the results obtained for the underwater area and the terrestrial area were different. The terrestrial area consisted of a high-speed layer with V_S ≥ 380 m/s. This high-speed layer was confirmed to be a hard, conglomerate layer with *N*-value ≥ 50 from the boring survey results. Therefore, the reliability of the underwater velocity distribution of S waves at depths ≥ 5 m was low in the current evaluation. As shown in Section 2.1, the lower frequency component of the surface waves reflects a deeper geological structure and surface waves with lower frequency component might not be generated by the excitation method adopted in Case 2. Thus, it is necessary to examine the excitation method to generate the lower frequency component of the surface waves to obtain the S-wave velocity distribution of deeper positions in the underwater river channel.

4 CONCLUSIONS

1) The depth profile of the S-wave velocity obtained by the surface wave method corresponds well with that of the *N*-value. The S-wave velocity can be used as an indicator of ground information in the subsurface exploration of river areas as the *N*-value.
2) With the quasi 3D distribution map made from the 2D S-wave velocity distribution by longitudinal interpolation, the area where the volcanic ash layer is exposed is aligned with the low S-wave velocity area. The volcanic ash layer is degraded at that area with a drastic scour making the low S-wave velocity area smaller compared with others.
3) The S-wave velocity corresponding to the volcanic ash layer of the underwater riverbed is obtained using the seismograph installation method, in which a needle-shaped part is mounted at the bottom and is inserted to the holes drilled in the bedrock beforehand, and the earthquake excitation method, in which a peg-shaped single tube set in the bedrock is hammered down. The results are consistent with the actual state of the bare rocks.
4) As the continuity of the S-wave velocity distribution of the underwater river channel area and the terrestrial area is confirmed for the depths of up to 4-5 m, it is possible to obtain the S-wave velocity distribution from within the water area to the terrestrial area continuously with the method developed in this study. The S-wave velocity obtained for the underwater area is lower than that obtained for the terrestrial area for depths of 5 m or more. Therefore, further examination is necessary for the excitation method to generate surface waves with lower frequency components.

REFERENCES

Hayashi, K. & Suzuki, H. (2004). CMP Cross Correlation Analysis of Multichannel Durface Wave Data. *Exploration Geophysics*, 35(1), 7-13.

Imai, T. & Tonouchi, K. (1982) Correlation of N-value with S-wave Velocity and Shear Modulus. *Proceedings of the 2nd European Symposium of Penetration Testing*, Amsterdam, 67–72.

Park, C.B., Miller, R.D. & Xia, J. (1999). Multichannel Analysis of Surface Waves. *Geophysics*, 64(3), 800–808.

Takahashi, S., Kinoshita, S., Suzuki, T., Koizumi, K., Watanabe, Y. & Nakamura, S. (2014). Filed Trial against Scouring of Soft Rock Riverbed in the Muka River the Tokoro River System and its Efficacy. *Advances in River Engineering,* 20, 229-234. (In Japanese)

THE ROOTS OF RIVER RESTORATION: ROLE OF VEGETATION RECOVER IN BED STABILIZATION

ANDREA ANDREOLI[(1)], GIAN BATTISTA BISCHETTI[(2)], ENRICO CHIARADIA[(3)]ALESSIOCISLAGHI[(4)], & FRANCESCO COMITI[(5)]

[(1, 5)]Faculty of Science and Technology, Free University of Bozen-Bolzano, piazza Università 5, 39100 Bolzano, Italy
andrea.andreoli@unibz.it
[(2, 3, 4)] Department of Agricultural and Environmental Sciences - Production, Landscape, Agroenergy, University of Milano, via Celoria 2, Milano, Italy,
bischetti@unimi.it

ABSTRACT

In-stream and riparian vegetation significantly affect flow discharge and sediment transport in channels with rigid and flexible vegetation under emergent and submerged conditions. Riparian tree cover increases flow resistance inducing sediment deposition and root systems stabilize deposited sediments. So acting vegetation affects stream morphology and sediment transport through soil cohesion exerted by plant root system. In order to estimate the effects of the vegetation root system on sediment retention and stream morphology roots density and strength are measured through the method of trench combined with image analysis in 5 trenches dug in Mareiter River in South Tyrol, hosting one of the largest river restoration interventions carried out so far in Italy. Samples of roots are brought to laboratory for tensile strength testing and root reinforcement are calculated. Moreover, an analysis of vegetation patch difference between pre- and post-restoration is performed in order to extend the effect of root reinforcement at a reach scale. Increased surface occupancy of riparian vegetation and vertical growth is estimated by calculating difference of DEM (DoD) produced with airborne LiDAR and SfM photogrammetry. Results show a decrease in number of patches as result of merging process, while the total covered area by vegetation increases by almost 300%. The minimum size of the patches decreases between pre- and post-restoration attesting a recruitment of new small patches located in little islands in the middle of the channel, whereas the maximum patch surface increases in post-restoration conditions as a result of merging patches. Results from root reinforcement analysis show that roots can exert an additional cohesion from 5 to 30 kPa that underlines the importance to consider the effect of the vegetation role in stabilizing the bed and this consequence on morphology dynamics in gravel-bed rivers.

Keywords: River restoration; vegetation; structure from motion (SfM) photogrammetry; root tensile strength; river morphology.

1 INTRODUCTION

Vegetation is a key element of riverbed corridors that strongly affects the river morphodynamics. Plants interact with fluvial processes, thus altering flow field and sediment transport, while their life cycle is controlled by sequence and magnitude of floods (Greet et al., 2011). Furthermore, vegetation growth and river morphodynamics present similar time scales. Methods to estimate vegetation development and morphological changes at reach scale have undergone a great development in the last few years with the evolution of new low cost technologies such as the Structure from Motion (SfM) photogrammetry. SfM-photogrammetry reconstructs 3D scenes by automatically matching conjugate points between images acquired from different viewpoints (Snavely et al., 2008; 2006). Although SfM has been developed since over a decade ago and particularly applied for computer vision, its use in earth sciences is relatively recent. SfM-photogrammetry can restitute topography from suitable image datasets with minimal input of real-world ground control points. The data are produced as very dense, arbitrarily scaled, 3D point clouds. Ground control and/or camera locations are only required when the user needs to transform the relative, arbitrarily scaled, elevation dataset (either a raster or a point cloud) to map coordinates with correctly scaled elevations. While based on the same fundamental image geometry as traditional photogrammetry, the success of SfM-photogrammetry approaches rests on a new generation of image matching algorithms first developed three decades ago (Lucas and Kanade, 1981), now integrated into readily available software packages as Photo Scan (Agisoft LLC) used in this project. This software package employs a workflow which is very similar to traditional photogrammetry but with certain differences. The key differences from traditional photogrammetry are two. First, the collinearity equations are solved without prior knowledge of camera positions or ground control. Second, SfM-photogrammetry has the ability to match points from imagery of extremely differing scales, view angles and orientations. The approach is relatively inexpensive, and capable of producing elevation datasets with mean errors in the range 0.02–0.15 m, assuming the appropriate use of ground control (Javernick et al., 2014; Fonstad et al., 2013; Verhoeven, 2012; Westoby et al., 2012).

Concerning the bed stabilization, an important factor that directly and indirectly affects several hydro-mechanical processes in hydrology and in earth surface systems is the root reinforcement. Indeed, roots system plays a fundamental role providing additional reinforcement to soil and sediments (Hales et al., 2009; Roering et al., 2003; Schmidt et al., 2001; Wu et al., 1979; Waldron, 1977). The magnitude of fiber reinforcement depends on the diameter distribution of roots, the root tensile strength and the strength of the bond between roots and soil (Cohen et al., 2011; Pollen-Bankhead and Simon, 2010; Wu et al., 1979).Thus, vegetation development and root anchoring capacity represent important factors for river restoration projects.

In the past years, at least 21 restoration projects have been carried out along many rivers and their floodplains in South Tyrol, North Italy (Alverá et al., 2012). The restoration very frequently includes the removal of former regulation measures in order to reestablish the retention areas and habitats. Mostly, the measures comprised the creation of preconditions for natural succession (Alverá et al., 2012).

In this work, different advanced techniques such as SfM-photogrammetry, root image analysis and tensile strength measurement in laboratory are implemented in order to improve the understanding of the vegetation-morphology dynamics in gravel bed rivers, and to emphasize the effects of the roots on them.

2 METHODS

2.1 Field location

The study was carried out in a restored reach of the Mareiter River, in South Tyrol, Italy. The channel drains a catchment area of 212 Km^2, characterized by the presence of glaciers for about 8.24 km^2 of the whole surface (3.9%), and by a typical nivo-glacial regime. The river flows into the Eisack River, near the city of Sterzing (Vipiteno). In the last 150 years, the river was object of various intervention: the two major works consisted of a flow regulation in 1876 and a large sediments extraction to provide material for the construction of the Brennero (Brenner) motorway, in the early 70's. Such activities caused a significant incision and narrowing of the riverbed from the large original braided configuration – up to 300 m width – to a channel 30-40 m wide (Figure 1a & b). The areas of natural retention such as flood plains and riparian areas, have almost completely disappeared making floods more frequent in the Sterzing basin. In the years 2008-2009, river restoration works were carried out by the Civil Protection Agency of the Autonomous Province of Bolzano. Using public lands, the riverbed was enlarged up to twice the width set in the 70's, along a stretch of 2 km (Figure 1c). The excavation material has been deposited in the riverbed, taking care to reproduce forms as natural as possible.

The study reach presented an extension of about 2 km, 1km upstream and 1 km downstream of the confluence with Ratschinger Bach (rio Racines, Figure 1). In this reach, the Mareiter presented a wide ranging from 50 to 80 m wide and a slope changing from 1.7% upstream to 0,6% downstream the confluence with Ratschinger Bach. The river morphology in the study reach was characterized by a braided pattern.

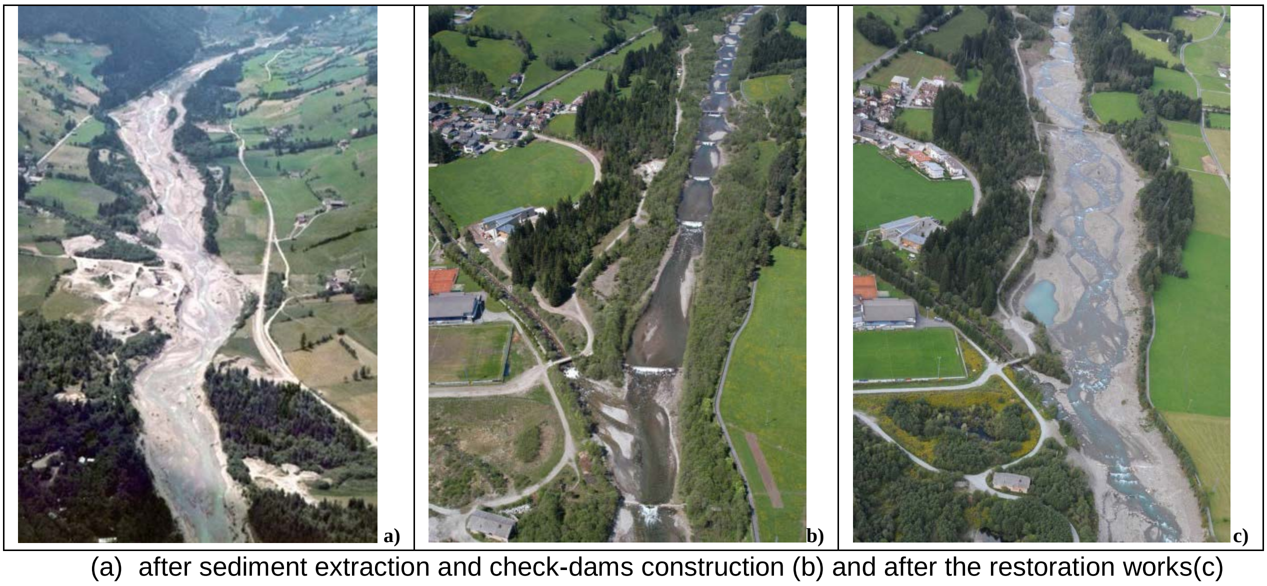

(a) after sediment extraction and check-dams construction (b) and after the restoration works(c) (Vignoli et al., 2011).

Figure 1. The Mareiter River at the confluence with Ratschinger Bachas it appears in the early 70's.

2.2 Aerial photo acquisition

Aerial photographs of Mareiter River were taken on the 22nd of September 2014 by helicopter (Eurocopter AS350B3 Ecureuil) and a Nikon D4S camera with 16, 2 megapixel and an integrated GPS at a mean height of 300m (Figure 2b). This enabled us to produce a series of photographs of very good quality with a resolution of 45 mm/pixel. However, it was difficult to maintain altitude above ground level (AGL) constant due to ground topography diversity (Woodget et al., 2015). The factor determining the image quality was the minimum reachable height by helicopter due to safety factors.

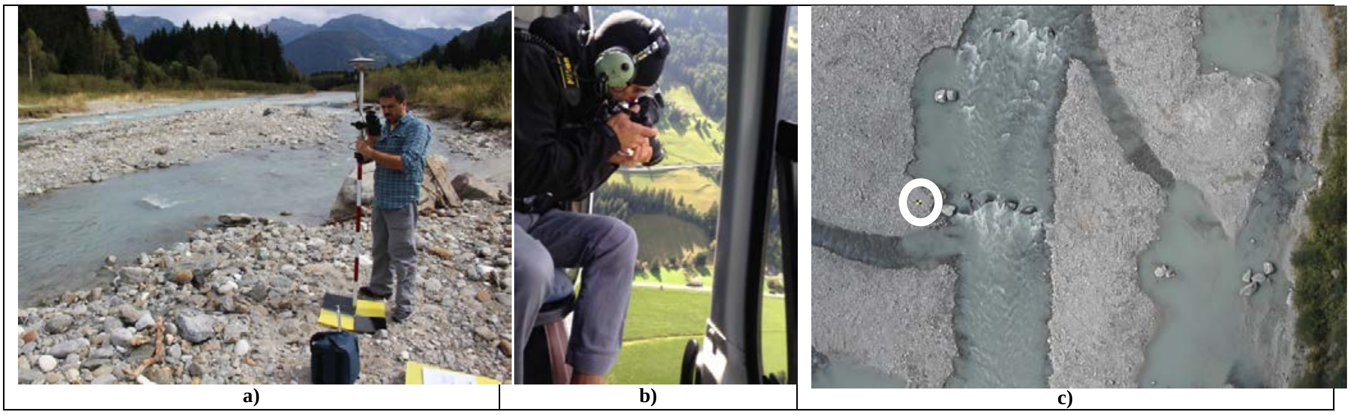

(a) Aerial photo acquisition (b) and particular of the helicopter photo survey (c) Note the GCP in the circle.
Figure 2. Recording of CGPs coordinates with RTK dGPS

2.3 Ground control points (GCP)

The artificial GCPs targets were constructed using 50 cm x 50 cm yellow squares with a thickness of 0,7 cm in PVC and painted two black squares onto each in order to create GCP targets similar to those often used in photogrammetry (Figure 2 a &c). The GPCs were distributed prior to image acquisition and the position of each GPC was recorded using a RTK dGPS device (Ashtech Promark 220, Figure 2a). Figure 3 shows the quantity and the spatial distribution of GCPs on Mareiter River. As suggested by Vericat et al. (2009), efforts were made to ensure GCPs were located in a uniform random pattern, which represented the topographic variation at each site.

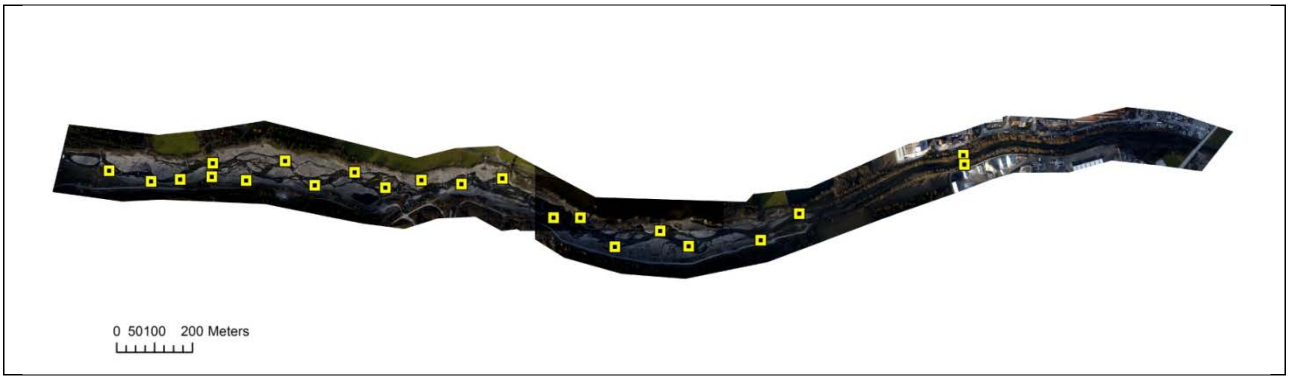

Figure 3. Spatial distribution of GCPs on Mareiter River. A total of 22 targets were installed.

2.4 Structure from Motion (SfM) photogrammetry

Following the workflow depicted in Figure 4a, the Dense Point Cloud of the studied reach of Mareiter river (Figure 4b & c) was computed and then a detailed Digital Elevation Model (DEM). Furthermore, DEM was compared with the LiDAR flight of year 2010. The differences between the two DEMs (DoD, Figure 5) depicted the consequence on channel morphology after the peak flow occurred on the 13th august 2014, characterized by a discharge of 133 m^3/s and a recurrence interval between 10 and 30 years.

2.5 Vegetation patch analysis

Vegetation maps were derived from ortophotos of a LiDAR flight of the study area made in 2010, and the previously mentioned ortophoto of 2014. Differences of patches between the two periods were derived by superimposing the two photo sets.

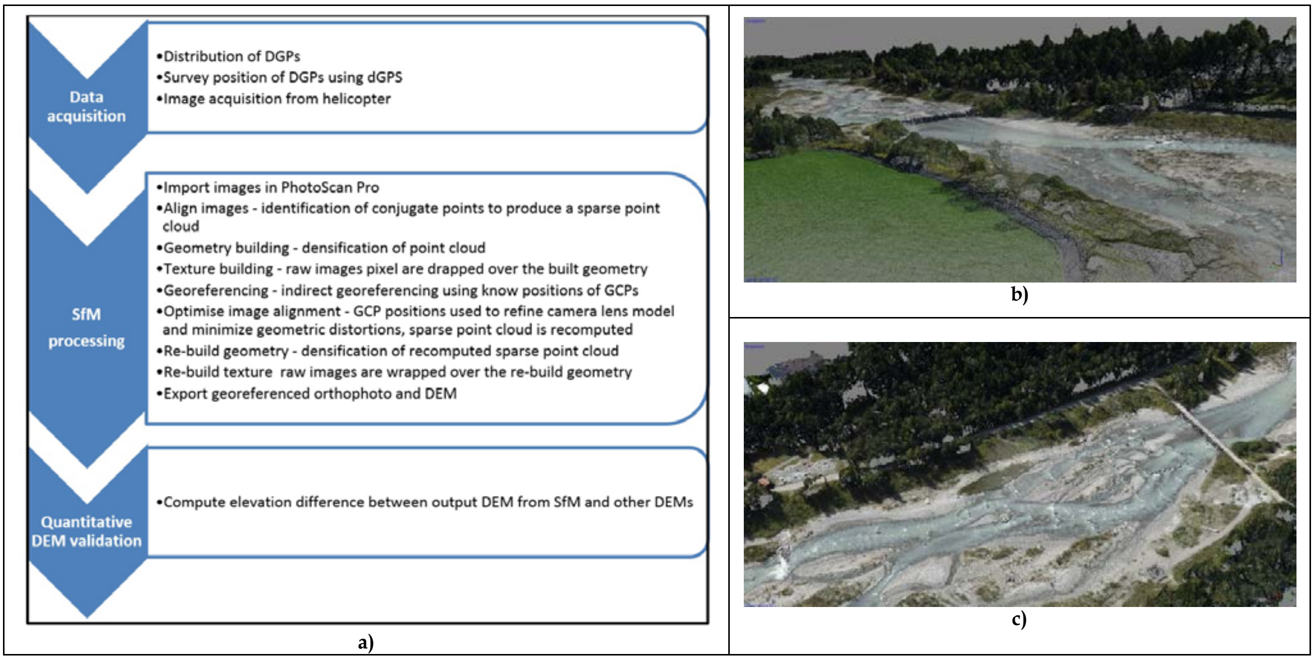

(a) Details of the dense point cloud (DPC), about 22 millions of points at Mareiter River.
Figure 4. Workflow of the SfM process for production and quantitative assessment of fluvial topographic dataset

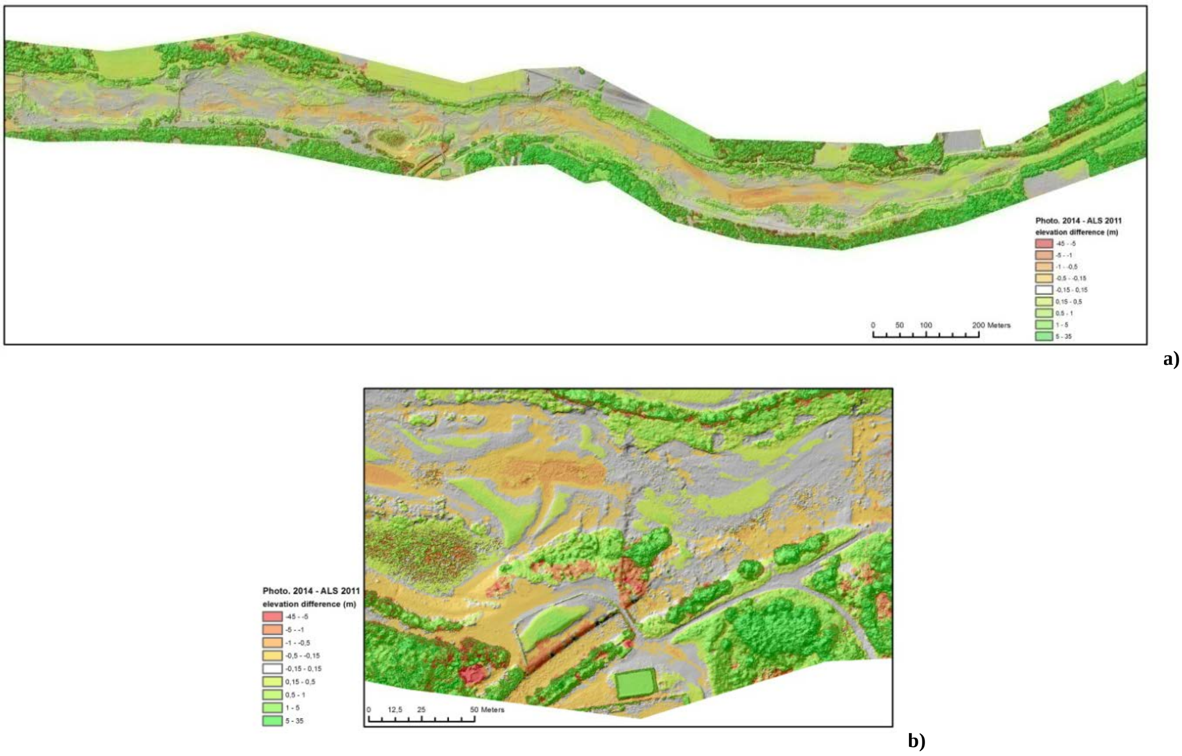

(a) Reach scale (b) details. Red colors indicate scours, while green colors indicate depositions.
Figure 5. Difference of DEM (DoD) at Mareiter river between 2010 LiDAR Flight and 2014 photogrammetric flight:

2.6 Root collection and analysis

Along the study reach, five trenches were dug following the excavation method described by Bohm (1979). The profiles had been smoothed and wetted by water spray to allow a greater contrast between the severed roots and the soil (Figure 6). Thereafter, a grid of 0.5 x 1 meter with 0.1meter interspacing was placed against the wall in order to have, for the post analysis, a reference on the spatial distribution of the roots (Figure 6). Two photographs for each profile (upper-half and lower-half of the grid) were shot taking care to create an overlay margin, and reduce distortions of perspective and curvature of straight lines due to the camera lens and shooting location. Finally, from each trench samples roots were collected, stored in an aqueous solution of 15% in volume of alcohol, sealed and transported to the laboratory for tensile strength testing (Figure 6b). In addition, the main vegetation features (e.g. species, plant height, plant diameter) were analyzed and a particle size analysis of the removed soil for each trench was performed (Table 1).

Table 1. Vegetation and granulometric characteristics of the trenches in the Mareiter River. Height (H) and diameter present standard deviation in brackets.

Trench	Ma	Mb	Mc	Md	Me
Vegetation	Salixeleagnos(28%) S. purpurea(67%) Betulapendula(6%)	Alnus incana (53%) Salix eleagnos (12%) S. purpurea (31%) Betula pendula (2%) Larix decidua (2%)	Alnus incana (86%) S. purpurea (14%)	Alnus incana (16%) Salix eleagnos (2%) S. purpurea (77%) Betula pendula (5%)	Alnus incana (43%) Salix eleagnos (29%) S. purpurea (21%) S.spp. (7%)
H (m)	1,79 (0,58)	2,22 (0,70)	2,20 (0,60)	0,80 (0,37)	2,80 (1,34)
Diameter (mm)	12,65 (5,15)	17,31 (11,80)	23,83 (10,75)	5,43 (3,44)	12,98 (12,78)
Granulometry (mm)	21,28	11,24	17,49	16,36	8,61

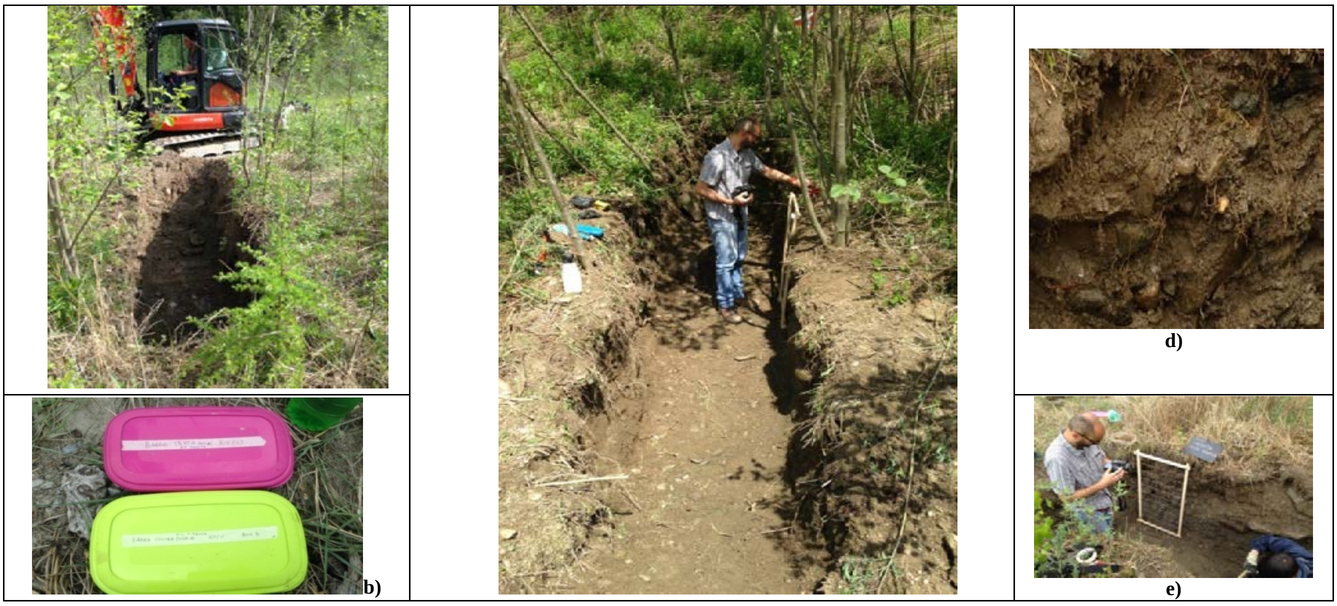

Figure 6. Trench excavation (a), collection of roots samples (b) and image shot (c, d, e) in the Mareiter River.

In the laboratory, the Root Area Ratio (RAR), the ratio between the cross-sectional area of the roots crossing a plane within the soil and the plane area for each soil profile were calculated, rectifying and geo-referencing them with respect to a reference plane tangent to the soil profile using Qgis software (QGIS Development Team, 2011). Each root was then recognized in the profiles and this diameter marked and measured with a line in the shape file (Figure 7). Tensile tests were carried out on collected undamaged roots using a MTS testing machine equipped with a load cell (F.S. 500 N, accuracy 0.1% F.S.).Roots were cut to a portion of 14 cm, and diameter was measured in tree points, and then attached to the specifically developed clamping devices that avoid root damage at the clamping points. The load registered at failure determined the maximum tensile force provided by the root and so called the Tensile Force at Failure (TFF).TFF depends on species and root diameter. The tensile strength-diameter relationship is generally accepted to be represented by the following power law form (Bischetti et al., 2005; Genet et al., 2005; Nilaweera and Nutalaya, 1999; Gray and Sotir, 1996; Abe and Iwamoto, 1986; Burroughs and Thomas, 1977):

$$TFF(d) = ad^b \qquad [1]$$

Where a and b are species-dependent parameters. The suitability of the regressions was evaluated using the coefficient of determination (R^2). In addition, ANCOVA and post-hoc tests were used to compare the different groups of roots collected by different trenches.

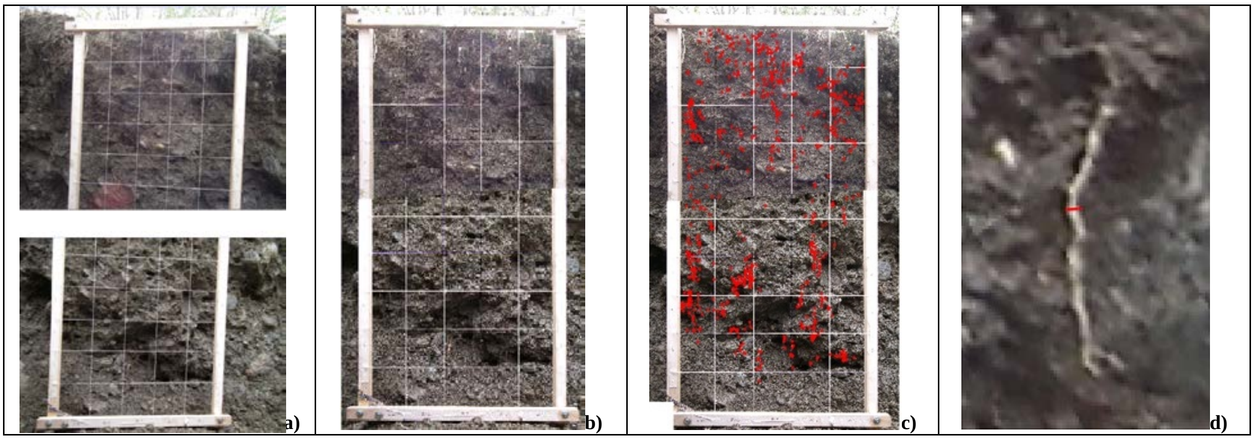

Figure 7. Trench Image analysis to recognize roots and calculate their diameter in Mareiter study site.

2.7 Root reinforcement

Additional root reinforcement (Cr) can be estimated by applying several models and considering (1) the root distribution along the soil profile and (2) the ultimate resisting force obtained before the rupturing of each root (Wu et al., 1979; Waldron, 1977; Pollenand Simon, 2005). One of the most common methods was the Fibre Boundle Model, FBM (Pollen and Simon, 2005) that was chosen in this study because it was simple to implement, required few parameters and was currently considered a reference estimator of the mechanical contribution of plant roots (Bischetti et al., 2009; Hales et al., 2009; Chiaradia et al., 2016).

FBM takes into account the asynchronous break of the roots considering a uniform distribution of stress in the soil and calculating the Cr with a gradual application of a load to a set of roots present in a certain layer of soil for increasing depth classes.

3 RESULTS

3.1 Vegetation patch analysis

Results of vegetation patches analysis show that number of patches decreases by 20 units from 101 in 2010 to 81 in 2014 as a consequence of vegetation merging with a total covered area increase of 57,973m^2 (5.8 ha), from 19,549 m^2 in 2010 to 77,522 m^2 in 2014. The minimum size of the patches decreases between 2010 and 2014, attesting a recruitment of new small patches located in some little island in the middle of the channel, while the maximum patch surface is bigger in 2014 as result of patch merging (Figure 8).

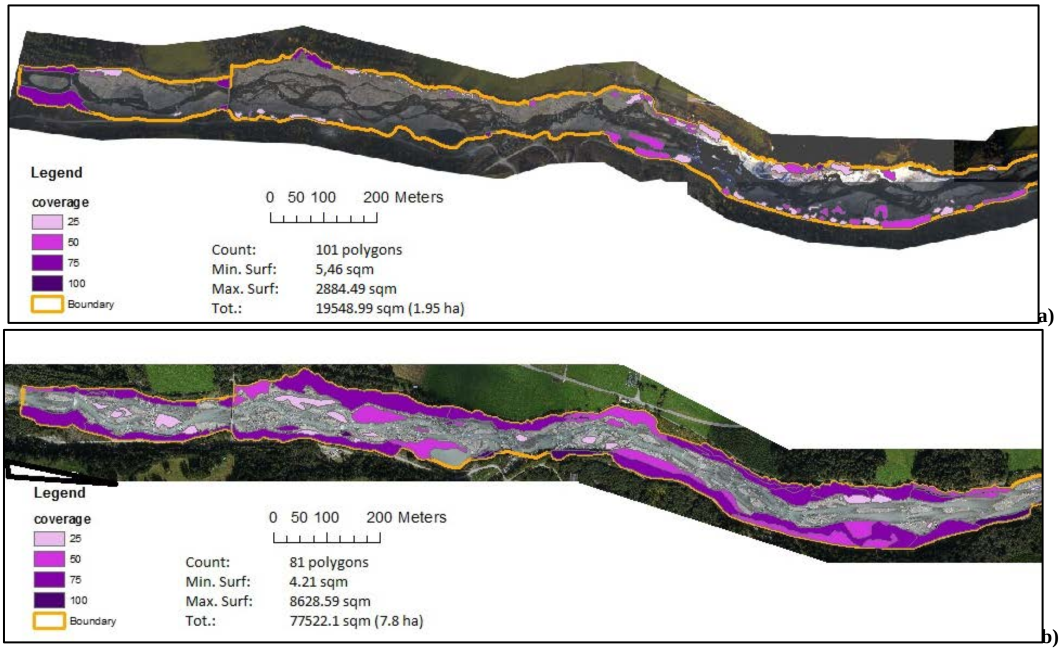

(a) and 2014 (b).

Figure 8. Vegetation patches coverage in 2010.

The mean coverage index of the vegetation in 2014 is 56.17%, distributed mainly in the 75% class (63.7%, Figure 9a) with a medium height of 1.54m mainly concentrated in the 3 meter class, versus a coverage index and a medium height of respectively 39.6%, well distributed in the first three classes (36%, 31% and 33%, respectively in the classes coverage of 25, 50 and 75%), and 2.21 m in 2010. These values confirm an expansion of newly recruited vegetation in the 4 years and a growth in height of the already present vegetation). In 2010, the most representative classes of height of vegetation are 0.3 m (15.55%) and 1 m (33.05%) with 65% of vegetation smaller than 1 meter, while in 2014 the most representative classes of height are 0.5 meter (11.7%) and 3 meter (29.51%) with vegetation smaller than 1 meter reduces to 37% (Figure 8b).

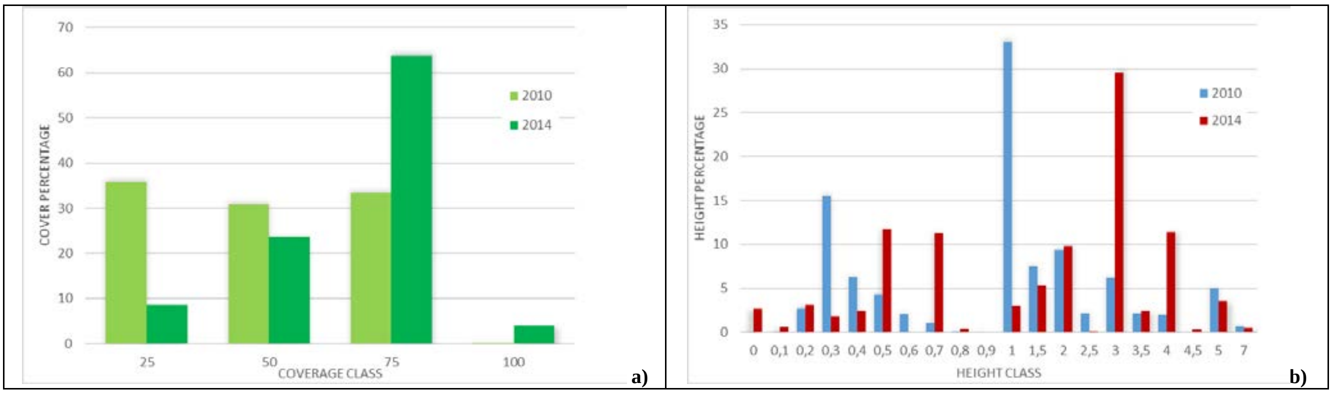

(a) height (b) in 2010 and 2014.
Figure 9. Comparison of vegetation cover percentages.

3.2 Root distribution

A total of 15,496 roots are recognized using image analysis (2,778 in trench A, 4,458 in trench B, 2,989 in trench C, 2,819 in trench D and 2,452 in trench E). As shown in Fig.10, roots of trench A are almost constant along the profile, probably due to the fact that in that portion of ground there are mainly willows (*Salix* spp.) in the initial phase of colonization. Indeed, they have developed roots able to expand up to the bottom due to the shortage of nutrients (Schiechtl, 1996). Trench B presents the highest number of roots in the first 0.20 m of the profile compared with other trenches, with an abrupt change under 0.50 m. This is probably due to a huge presence of white alder (*Alnus incana*, Table 1), with more superficial roots for the presence of sufficient nutrients in the first layers of the profile. In terms of root distribution, trench C follows a similar behavior as trench B, although with much lower concentrations in the first 0.20 m. Such fact is probably due to the different dimension of the plants around the two trenches (e.g. stem diameter and crown density). In trench D, RAR is approximately constant up to the bottom, also in this case due to the initial stage of colonization, characterized by high prevalence of willows able to expand their root systems deeper. Finally, RAR of profile E shows a high presence of roots only in the first 0.30 m because the plants are on a more mature stage of growth and therefore with greater availability of nutrients. These plants do not need a remarkable root development. However, this hypothesis would require a more detailed analysis on the soil nutrients.

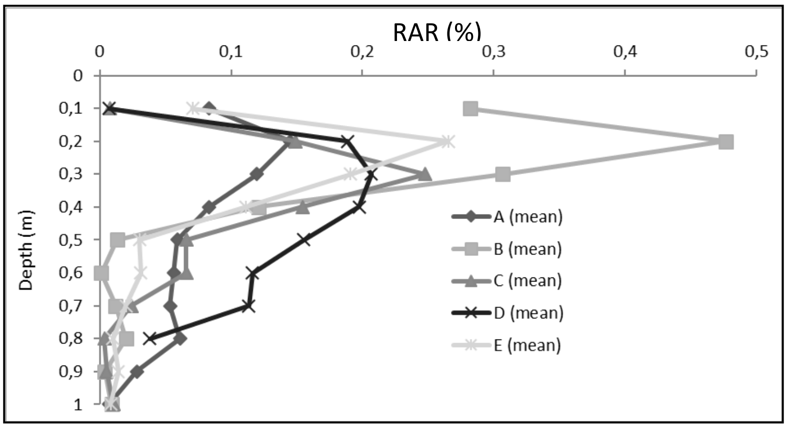

Figure 10. Root area ratio for the five trenches of Mareiter River.

3.3 Root reinforcement

Overall, 200 roots, 40 roots for each trench, were collected in the Mareiter trenches. Tensile strength tests were performed on roots collected taking care to avoid any root damage or stress. In most cases, tensile tests were carried out on fresh roots within 1 week after sampling; in other cases, the roots were preserved for a few weeks using a 15% alcohol solution (Meyer and Gottsche, 1971), which has no influence on the measured parameters (Bischetti et al., 2003). Tests were carried out on roots with typical tortuousness, ranging diameters size between 0.1 to 5.0 mm. (Table 3).

Table 3. Results of tensile strength test carried out on Mareiter samples.

		Diameter (mm)			Force (N)			
Trench	**Num.**	**Min**	**Max**	**Med.**	**Min**	**Max**	**Med.**	**Adj. Med.**
A	40	0,2	2,7	0,9	0,9	96,1	13,1	9,0
B	40	0,3	4,1	1,5	1,0	165,8	26,1	18,4
C	40	0,1	5,0	0,7	0,2	75,2	9,9	7,4
D	40	0,2	1,7	0,6	0,3	24,3	3,4	2,5
E	40	0,2	3,8	1,3	1,6	92,5	20,7	17,1

The tensile strength-diameter relationships were analyzed for the five trenches in Mareitersite. Figure 11 shows the log-transformed regression lines for each trench (A, B, C, D and E). All the regression lines are mostly parallel except for trench D that presents roots less resistant to tensile force. ANCOVA analysis and then a post hoc Tukey test were performed in order to identify which pairs are statistically different. Statistical test shows that the regression line of group D is different from those of other groups, both for slope and intercept (Table 4).

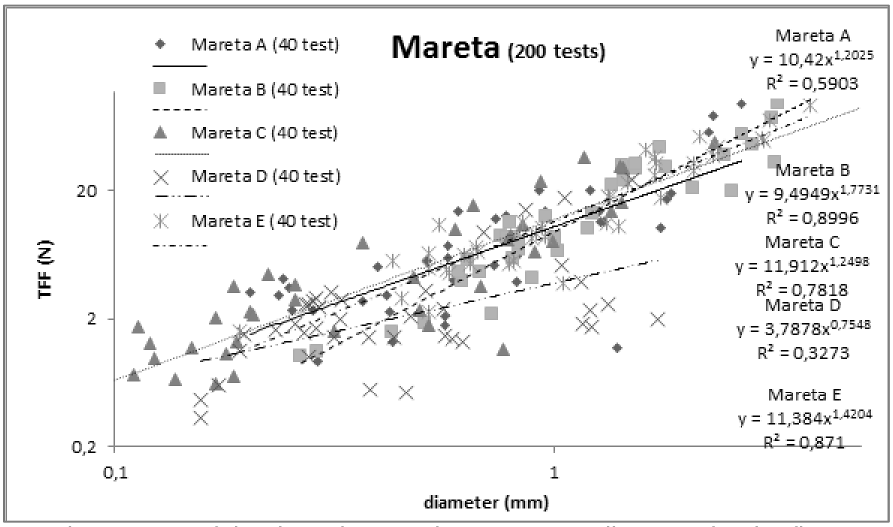

Figure 11. Regression curves of the thread strength versus root diameter for the five trenches of Mareiter study site (logarithmic values in axis).

Table 4. Significance (p) values for TFF difference between Mareiter trenches: results from Tukey HSD test.

All Groups: Tukey HSD test; variable LOG TFF (N). Y (diameter>0.5) Approximate Probabilities for Post Hoc Tests
Error: Between MSE = .07280, degree of freedom df = 129.00

Trench	1	2	3	4	5
	(1.0216)	(1.1791)	(1.0829)	(0.55975)	(1.1580)
Ma		0.142929	0.945588	0.000018	0.267479
Mb	0.142929		0.727307	0.000017	0.997246
Mc	0.945588	0.727307		0.000017	0.869286
Md	0.000018	0.000017	0.000017		0.000017
Me	0.267479	0.997246	0.869286	0.000017	

Results of mean root cohesion calculation are showed in Figure 12. The distribution of Cr and RAR show similar trend due to the fact that the greater the radical presence is, the higher the coefficient of resistance is. The soil is then more stable on superficial layers, while going deeper, and with the decrease of the number of the roots, the reinforcement will be reduced. It is a different case as for D trench, in which the Cr is fairly low at any depth. This probably occurs due to the prevalent presence of herbaceous vegetation in that zone of the bar. Also, note that D trench has not been investigated more than 0.8m due to the presence of water table. Overall, trenches B and C present the most influence on soil stability attributed to a more developed presence of grey alder (Table 1).

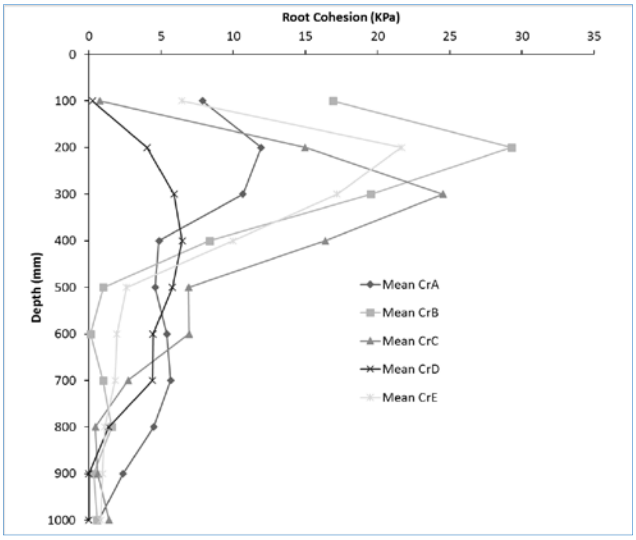

Figure 12. Root cohesion for the five trenches of Mareiter River.

4 CONCLUSIONS

Root cohesion values obtained in this study are high because of a great number of small diameter roots that allow a good vascularization in the soil. This characteristic helps the plants in a dynamic river habitat to consolidate sediments and creates a better condition for vegetation colonization, as demonstrated by analysis of the vegetation evolution. Knowledge of this characteristics and mechanism are important in river management and restoration practices in order to drive and support decision making process, and more research in this area is desirable to know the behavior of different species in different morphological river context. Finally, it is important to consider the effect of the vegetation role in stabilizing the bed and this consequence on morphology dynamics in gravel bed rivers.

ACKNOWLEDGMENTS

The authors would like to thank the Civil Protection Agency of the Autonomous Province of Bolzano for all the support given. The research is granted by the Italian Research Project of Relevant Interest (PRIN2010-2011), project. 20104ALME4, National Network for Monitoring, Modelling, and Sustainable Management of Erosion Processes in Agricultural Land and Hilly-Mountainous Area. Moreover, the authors are grateful to the BSc students, R. Motta, S. Urzì and A. Marabotti for attending the course in Agricultural Sciences and Technologies at the University of Milan for the field support, and to Dr. Joshua Theule of the TerrAlp Research Consulting for help in SfM and DoD elaborations.

Corresponding author is founded by Department of Innovation, Research and University of the Autonomous Province of Bolzano.

REFERENCES

Abe, K. & Iwamoto, M. (1986). An Evaluation of Tree-Root Effect on Slope Stability by Tree-Root Strength. *Journal of the Japanese Forestry Society*, 68(12), 505-510. (In Japan)

Agisoft LLC. (2013). *Agisoft Photo Scan User Manual:* Professional Edition, Version 1.0.0.

Alverá, K., Hecher, P., Zerbe, S. & Gallmetzer, W. (2012). Restoration of Rivers and Floodplains in South Tyrol (Italy)-Synthesis and perspectives. *Naturschutz und Landschaftsplanung*, 44, 165-172.

Bischetti, G., Bonfanti, F. & Greppi, M. (2003). Misura della Resistenza alla Trazione delle Radici: Apparato Sperimentale e Metodologia d'Analisi. *Quaderni di Idronomia Montana*, 21(1), 349-360.

Bischetti, G.B., Chiaradia, E.A., Simonato, T., Speziali, B., Vitali, B., Vullo, P. & Zocco, A. (2005). Root Strength and Root Area Ratio of Forest Species in Lombardy (Northern Italy). *Plant and soil*, 278(1-2), 11-22.

Bohm, W. (1979). *Methods of Studying Root Systems.* Ecological Series. Springer-Verlag, Berlin, Germany.

Burroughs, E.R. & Thomas, B.R. (1977). *Declining Root Strength in Douglas-fir after Felling as a Factor in Slope Stability* U.S. Forest Service, Research Paper INT-190.

Chiaradia, E.A., Vergani, C. & Bischetti, G.B. (2016). Evaluation of the Effects of Three European Forest Types on Slope Stability by Field and Probabilistic Analyses and their Implications for Forest Management. *Forest Ecology and Management*, 370, 114 -129.

Cohen, D., Schwarz, M. & Or, D. (2011). An Analytical Fiber Bundle Model for Pullout Mechanics of Root Bundles. *Journal of Geophysical Research: Earth Surface*, 116, 1-20.

Fonstad, M.A., Dietrich, J.T., Courville, B.C., Jensen, J.L. & Carbonneau, P.E. (2013). Topographic Structure from Motion: A New Development in Photogrammetric Measurement. *Earth Surface Processes Landforms*, 38(4), 421-430.

Genet, M., Stokes, A., Salin, F., Mickovski, S.B., Fourcaud, T., Dumail, J.-F. & van Beek, R. (2005). The Influence of Cellulose Content on Tensile Strength in Tree Roots. *Plant and Soil*, 278(1-2), 1-9.

Gray, D.H. & Sotir, R.B. (1996). *Biotechnical and Soil Bioengineering Slope Stabilization: A Practical Guide for Erosion Control.* John Wiley & Sons.

Greet, J., Angus Webb, J. & Cousens, R. (2011) *The Importance of Seasonal Flow Timing for Riparian Vegetation Dynamics: A Systematic Review Using Causal Criteria Analysis.* Freshwater Biology, 56(7), 1231-1247.

Hales, T.C., Ford, C.R., Hwang, T., Vose, J.M. & Band, L.E. (2009). Topographic and Ecologic Controls on Root Reinforcement. *Journal of Geophysical Research: Earth Surface*, 114, 1-17.

Hales, T., Cole-Hawthorne, C., Lovell, L. & Evans, S.L. (2013). Assessing The Accuracy of Simple Field Based Root Strength Measurements. *Plant and Soil*, 372(1-2), 553-565.

Javernick, L., Brasington, J. & Caruso, B. (2014). Modeling the Topography of Shallow Braided Rivers Using Structure-from-Motion Photogrammetry. *Geomorphology*, 213, 166-182.

Lucas, B.D. & Kanade, T. (1981). *An Iterative Image Registration Technique with an Application to Stereo Vision*, IJCAI, 674-679.

Meyer, F. & Gottsche, D. (1971). *Distribution of Root Tips and Tender Roots of Beech*. Ellenberg, Heinz Integrated Experimental Ecology.

Nilaweera, N. & Nutalaya, P. (1999). Role of Tree Roots in Slope Stabilisation. *Bulletin of Engineering Geology and the Environment*, 57(4), 337-342.

Pollen-Bankhead N. & Simon A. (2010). Hydrologic and Hydraulic Effects of Riparian Root Networks on Streambank Stability: Is mechanical root-reinforcement the whole story? *Geomorphology*, 116, 353-362.

Pollen, N. & Simon, A. (2005). Estimating the Mechanical Effects of Riparian Vegetation on Stream Bank Stability using A Fiber Bundle Model. *Water Resources Research*, 41(7), 1-11.

QGIS Development Team. (2011). *QGIS Geographic Information System ver. 2.14,* Open Source Geospatial Foundation Project.

Roering, J.J., Schmidt, K.M., Stock, J.D., Dietrich, W.E. & Montgomery, D.R. (2003). Shallow Land Sliding, Root Reinforcement, and the Spatial Distribution of Trees in the Oregon Coast Range. *Canadian Geotechnical Journal*, 40, 237-253.

Schiechtl, H. (1996). *I Salici Nell'uso Pratico,* Ed. Arca, Trento.

Schmid, I. & Kazda, M. (2001). Vertical Distribution and Radial Growth of Coarse Roots in Pure and Mixed stands of Fagus Sylvatica and Picea Abies. *Canadian Journal of Forest Research*, 31(3), 539-548.

Schwarz, M., Cohen, D. & Or, D. (2010). Root-Soil Mechanical Interactions during Pullout and Failure of Root Bundles. *Journal of Geophysical Research: Earth Surface*, 115, 1-19.

Snavely, N., Seitz, S.M. & Szeliski, R. (2006). Photo Tourism: Exploring Photo Collections in 3D, ACM Transactions on Graphics (TOG). *ACM*, 835-846.

Snavely, N., Seitz, S.M. & Szeliski, R. (2008). Modeling the World from Internet Photo Collections. *International Journal of Computer Vision*, 80(2), 189-210.

Verhoeven, G. (2012). Getting Computer Vision Airborne–Using Structure from Motion for Accurate Orthophoto Production. *Rspsoc Archaeology Special Interest Group Newsletter*, 4-6.

Vericat, D., Brasington, J., Wheaton, J. & Cowie, M. (2009). Accuracy Assessment of Aerial Photographs acquired using Lighter-than-Air Blimps: Low-Cost Tools for Mapping River Corridors. *River Research and Applications*, 25(8), 985-1000.

Vignoli G., Simoni S. & Todeschini, I. (2011). *Studio di Evoluzione Morfologica e stima del Trasporto Solido per il rio Mareta Presso Stanghe*, Autonome Provinz Bozen, Abteilung 30 Wasserschutzbauten.

Waldron, L. (1977). The Shear Resistance of Root-Permeated Homogeneous and Stratified Soil. *Soil Science Society of America Journal*, 41(5), 843-849.

Westoby, M.J., Brasington, J., Glasser, N.F., Hambrey, M.J. & Reynolds, J.M. (2012). 'Structure-from-Motion' Photogrammetry: A Low-Cost, Effective Tool for Geoscience Applications. *Geomorphology*, 179, 300-314.

Woodget, A.S., Carbonneau, P.E., Visser, F. & Maddock, I.P. (2015). Quantifying Submerged Fluvial Topography Using Hyperspatial Resolution UAS Imagery and Structure from Motion Photogrammetry. *Earth Surface Processes and Landforms*, 40(1), 47-64.

Wu, T.H., McKinnell III, W.P. & Swanston, D.N. (1979). Strength of Tree Roots and Landslides on Prince of Wales Island, Alaska. *Canadian Geotechnical Journal*, 16(1), 19-33.

CHARACTERIZATION OF SURFACE AND HYPORHEIC FLOWS ASSOCIATED WITH A GRAVEL BAR

MOHAMMAD SAEID AHADI [(1)], S.H. SEYED MIRZAEI [(2)] & ANA MARIA FERREIRA DA SILVA [(3)]

[(1,2,3)]Department of Civil Engineering, Queen's University, Kingston, Ontario, Canada,
m.ahadi@queensu.ca; mirzaei.hessam@queensu.ca; amsilva@queensu.ca

ABSTRACT

An experimental and numerical study of the turbulent hyporheic and free surface flows associated with a gravel bar is presented. The hyporheic flow is visualized and quantified with the aid of dye injections; and further resolved with the aid of a numerical model. The mean and turbulence characteristics of the free surface flow are analyzed on the basis of flow velocity measurements using a 2-D ADV. It is found that 14% of the streamflow is entrained into the gravel bar and its substrate. The bar shifts the bulk of the flow towards the upper flow layers, resulting in large velocities towards the free surface for a considerable distance downstream of the bar top, and leading to a region rather protected from the flow action towards the bed after the bar. Two regions of higher turbulence activity are identified downstream of the bar top. In comparison to flow over an impervious gravel bar and bed, differences are found in both the free surface profile and velocities near the bed, especially immediately downstream of the bar top.

Keywords: Gravel bar; hyporheic flow; surface flow; mean flow; turbulence characteristics.

1 INTRODUCTION

As is well-known, in alluvial streams and rivers, pressure gradients caused by the interaction of river flow with topographic elements (e.g., bed forms), changes in depth or changes in direction are sufficient to induce hyporheic flows, i.e. water flows through the permeable sediments (Tonina and Buffington, 2007; Trauth et al., 2013; Fox et al., 2014). These play a significant role in the preservation of the river ecosystem, as they lead to downwelling pore water flows providing dissolved oxygen and organic matter to microbes and invertebrates in the hyporheic zone, and upwelling subsurface flows supplying nutrients to stream organisms (Boulton et al., 1998). Hyporheic flows are essential for the development of fish populations, particularly trout and salmon, which reproduce by depositing eggs in gravel or gravel-dominated bars, usually in the upper stream regions (characterized by relatively steep gradients and fast flows). On the other hand, hyporheic flows can act as an effective mechanism to transport contaminants into the sediment, where they can pose substantial toxicity risk to fish and fish embryos.

It is therefore not surprising that hyporheic flows have received a great deal of attention in the past 20 years or so, with a considerable number of the works produced so far focusing on hyporheic flows induced by dunes (Savant et al., 1987; Elliot and Brooks, 1997a; Elliot and Brooks, 1997b; Packman et al., 2004; Cardenas and Wilson, 2007; Fox et al., 2014; Blois et al., 2014). However, the relatively fast and turbulent hyporheic flows through gravel bars or pool-riffle systems have been the object of only a few isolated experimental and numerical studies (Gariglio et al., 2013; Trauth et al., 2013). This paper is intended as a contribution addressing the existing scarcity of information and data on such flows.

The specific objective of the paper is to present the results of an experimental and numerical study of the turbulent hyporheic and surface flows associated with a gravel bar. This work is to be viewed as an extension of da Silva et al. (2016), who focused strictly on the visualization and numerical modeling of the hyporheic flow induced by a gravel bar. In this work, the same laboratory set-up and flow conditions are utilized, but focus primarily on the surface flow and interaction between the hyporheic and free surface flows.

2 DESCRIPTION OF LABORATORY EXPERIMENT

For the sake of completeness, this section briefly reviewed the experimental set-up and flow conditions in da Silva et al. (2016). The experiment was carried out in an 11 m long, 0.382 m wide, and 0.5 m deep tilting flume, with side walls made of glass (see Figure 1). The substrate underneath a bar was simulated by placing an ≈ 0.20 m deep layer of gravel in the flume, between 5.07 and 7.27 m from the flume entrance.

Table 1. Hydraulic conditions of the flow under investigation.

Q (m^3/s)	D_{50} (m)	S	h (m)	u_{av} (m/s)	Re	Fr
0.022	0.0077	1/750	0.18	0.32	29440	0.24

The floor level was raised both upstream and downstream of this gravel layer by installing raised wooden boards. In order to provide consistent bed roughness along the entire length of the flume, a layer of gravel approximately two grain thick was placed on the wooden boards. The elevation of top surface of this layer matched that of the top of the aforementioned 0.20 m deep layer of gravel in the midst of the flume. A two-dimensional, axi-symmetric gravel bar, 1.4 m long and 0.076 m high, was constructed over the 0.20 m deep gravel layer. The same gravel was used throughout the flume. This consisted of a peastone with grain sizes between 3.4 and 12.5 mm (median grain size D_{50}=7.7 mm; uniformity coefficient D_{60}/D_{10}=1.5).

The hydraulic conditions of the free surface flow were as summarized in Table 1. Here Q is flow rate, S is bed slope, h is undisturbed flow depth (i.e. flow depth sufficiently upstream and downstream of the bar), u_{av} is average flow velocity, Re is flow Reynolds number (= $u_{av}R_h/v$, in which R_h is hydraulic radius and v is fluid kinematic viscosity), and Fr is Froude number (= $u_{av}/(gh_{av})^{1/2}$, in which g is acceleration due to gravity). The bed slope S is the same as the slope of the flume floor (namely 1/750). The flow depth above the crest of the bar was equal to 0.096 m.

Flow depth was measured at several sections along the flume with the aid of a point gauge (resolution ± 0.1 mm).For the purpose of analyzing the mean properties and turbulence characteristics of the streamflow past the gravel bar, measurements of instantaneous local flow velocity were carried out with a 16 MHz 2D Sontek Micro Acoustic Doppler Velocimeter (velocity range = 3, 10, 30, 100, and 250 cm/s; velocity resolution = 0.1 mm/s; sampling volume = a cylinder with the volume 0.09 cm^3 located 5 cm away from the tip sensor; accuracy = 1% of the measured velocity). Such measurements of flow velocity were obtained at the channel centerline of eighteen different cross-sections, as shown in Figure 1. At each measurement vertical, the measurements were collected from 1 cm above the bed surface up to 2 cm below the free surface. In addition, local flow velocity was also measured (with the aid of the 16 MHz Micro ADV) at 3 different verticals at a cross-section located 4 m from the flume entrance (channel centerline and 9.5 cm from the right and left sidewalls). The flow rate reported above was determined on the basis of the just mentioned measurements.

The ADV was operated at a sampling frequency of 20 Hz, with the sensor mounted in an upstream looking configuration. The duration of each individual velocity measurement was 120 s. The mean values of the correlation coefficient (CORR) and signal-to-noise ratio (SNR), calculated on the basis of the 154 velocity signals collected at cross-sections 5.4 to 9.0 m from the flume entrance, were 81% and 18.8 dB, respectively, while their minimum values were 71.2% and 15.3 dB. The present values of CORR and SNR were invariably higher than the minimum values suggested by the manufacturer to ensure the accuracy of the measurements to characterize both mean and turbulence properties of the flow, namely 70% and 15 dB.

The hyporheic flow induced by the gravel bar was visualized using dye injections at 13 different locations, selected so as to enable visualization of the flow in the same as well as the opposite direction of the streamflow. Solutions of blue food dye and water were injected through sections of 3mm-diameter tubing installed in the gravel bed and bar, adjacent to the front glass wall of the flume. The injections at the different locations were performed sequentially using a constant head reservoir set to ≈ 1 cm above the water level. The dye mixture was allowed to flow out of the reservoir until a continuous plume between the injection location and the interface

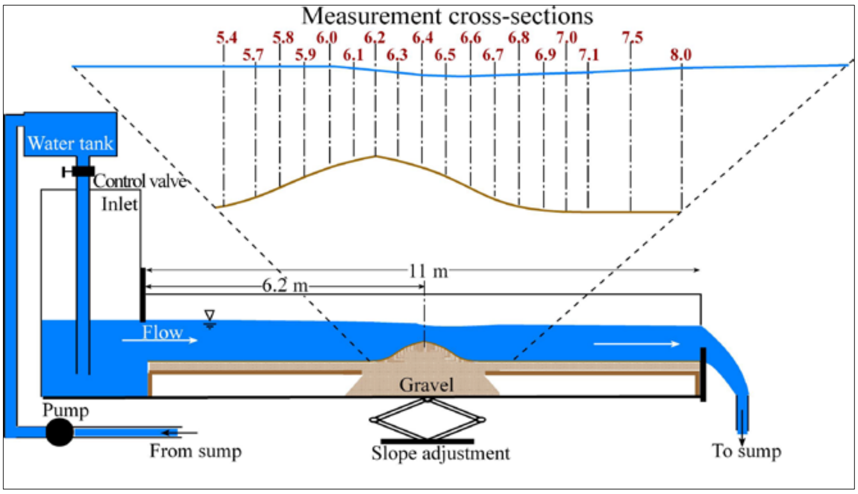

Figure 1. Schematic of the flume and measurement cross-sections (not to scale).

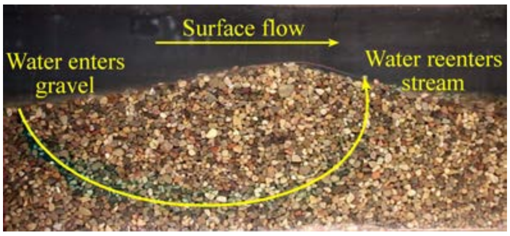

Figure 2. Photo of gravel bar illustrating injection of dye.

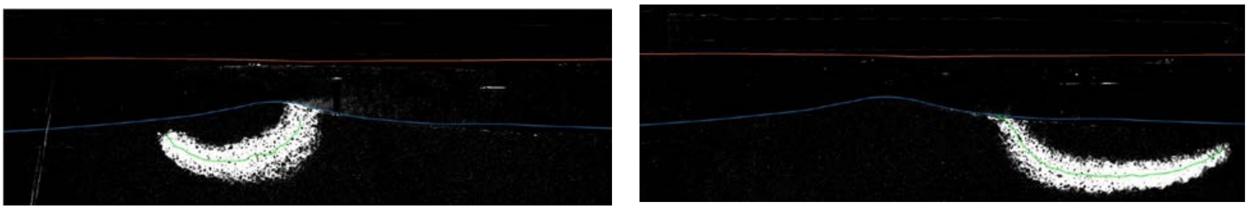

Figure 3. Processed images of hyporheic flow (from da Silva et al., 2016). The free surface of the streamflow is shown in red; the gravel top surface, in blue; hyporheic flow is from the left to the right in the figure at the left; and from the right to the left in figure at the right.

between the gravel and free surface flow was visible (see Figure 2), at which point the flow of dye from the reservoir was stopped.

Images of the dye injection were captured using a digital camera located 2 m from the front flume wall at a frequency of 24 frames per second and a resolution of 108 × 1920 pixels. These were post-processed using MATLAB by converting each image to a greyscale intensity image; and by subtracting a reference greyscale image from each greyscale image. This procedure highlighted dye transport by isolating changes caused by the presence of the dye from variations in pixel intensity caused by differently colored grains of gravel. Two examples of the processed images are shown in Figure 3 for an injection location upstream of the bar (Figure 3, left) and one downstream of the bar (Figure 3, right). Changes in pixel intensity due to the presence of dye are shown in white, the free surface is indicated by the red line, and the interface between the gravel and the free surface flow is indicated by the blue line. Processed images were used to identify streamlines and determine average dye velocities. Streamlines were identified by calculating the first moment of pixel intensity (as a proxy for dye concentration) along multiple transects perpendicular to the dye flow for each dye injection location, and treating the streamline as the pathway between the first moment locations. In Figure 3, the resulting streamlines are indicated by the green lines. Average dye velocities in the hyporheic zone were calculated based on the length of each streamline and the time required for the dye to be transported from the injection location to the gravel-water interface. For further details on the visualization of the hyporheic flow, see Fruetel (2016).

3 RESULTS AND DISCUSSION

3.1 Hyporheic flow

In the following, the hyporheic flow is detailed using both the results of the experiment (Figure 4) and those of a numerical simulation (Figure 5). The CFD package OpenFoam, version 2.2.1, was used in the present simulation, by implementing a fully coupled solution of the surface water and groundwater equations. The flow domain, consisting of the surface water and subsurface, was treated as a continuous medium. The free surface flow was resolved by solving the Reynolds Averaged Navier-Stokes equations and the equation of continuity. The free surface was tracked using a two-phase (water and air) approach based on the volume of fluid method. The shear stress transport (SST) k-ω model was adopted as turbulence closure. The subsurface domain was assumed to be homogeneous and isotropic, with the flow being determined from the conservation of momentum equation for groundwater flow (Vafai and Tien, 1981; Nakayama and Kuwahara, 1999; Pedras and de Lemos, 2000; de Lemos, 2012).

As follows from Figure 4, the average hyporheic flow velocities ranged from 1.1 to 2.4 cm/s on the upstream side of the bar, and were ≈ 0.6 cm/s on its downstream side. The hyporheic flow thus was turbulent. For this reason, the source term in the groundwater flow conservation of momentum equation was defined according to Forchheimer equation. Further details on the numerical model, including the computational grid and boundary conditions, are given elsewhere (da Silva et al., 2016).

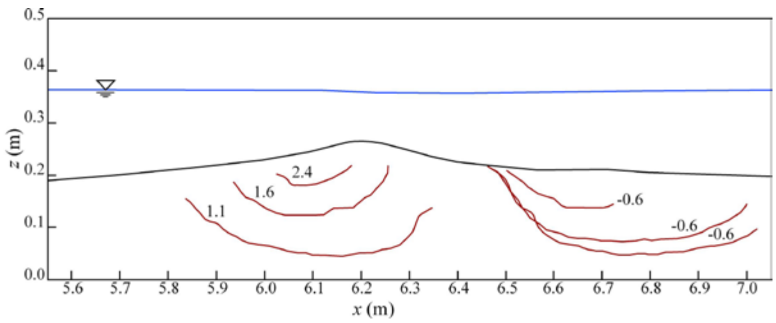

Figure 4. Hyporheic flow lines resulting from the flow visualization experiment; values shown are hyporheic flow velocities in cm/s (from da Silva et al., 2016).

As follows from Figures 4 and 5, the hyporheic flow within and below the bar extended all the way down to the flume bottom. This flow occurred in the direction of the free surface flow, induced from the high pressure regions upstream of the bar to the low pressure regions downstream of the bar top; as well as in the opposite direction sufficiently downstream of the bar top. This hyporheic flow pattern resulted in a flow divide on the downstream side of the bar, ≈ 0.20 m from the bar top (see Figure 5). The location of the flow divide approximately coincided with the point where the free surface acquired its largest depression. The flow rate of the free surface flow is plotted along the flow direction in Figure 6. As follows from this figure, because of water penetrating the gravel in the form of hyporheic flow, the flow rate continuously decreased from a section ≈ 5.4 m from the flume entrance to the bar top, reaching 0.0174 m^3/s at the bar top. That is, overall 14% of the free surface flow was entrained into the subsurface gravel over the distance of the bar.

3.2 Free surface flow

In the following, a brief description of the surface flow is provided, by analyzing its mean properties and turbulence characteristics. It should be emphatically pointed out that, where the flow turbulence characteristics are concerned, this study is limited, as only the longitudinal and transverse components of flow velocity were captured by the present measurements.

The time-averaged flow velocities are reported in Figures 7 and 9, showing the profiles of flow velocity at the different measurement sections and a velocity field contour-plot, respectively. Figure 8 provides a detail of the time-averaged flow velocity from the top of the bar (located 6.2 m from the flume entrance) to a section 0.7 m downstream. As evidenced from Figures 7 and 9, as expected, the flow velocity is the largest over the top of the bar, where the flow depth is the smallest. Downstream of the bar top, the bulk of the flow remains shifted to the upper flow layers for a considerable distance. Thus, even though the bar is axi-symmetric, the velocity profiles immediately downstream of the bar top differ substantially from those immediately upstream. In particular, instead of a sharp velocity gradient near the bed surface, as is the case everywhere else in the flume, the velocity profiles downstream of the bar top exhibit a gradual increase in flow velocity from a near zero value at the bed to a maximum or near maximum value at z ≈ 0.08 to 0.10 m (see Figure 8). Between the section 6.4 and 6.6 m from the flume entrance, the flow near the bed was in the negative x-direction. This suggests that flow separation occurred in that region. On the other hand, such negative values of flow velocity may be merely a manifestation of the re-entrance into the free surface flow of the upstream directed hyporheic flow. Note that the dashed line between section 6.4 and 6.6 m in Figure 9 was determined, from the present velocity measurements as well as flow visualization videos, as the line below which the net flow rate is zero.

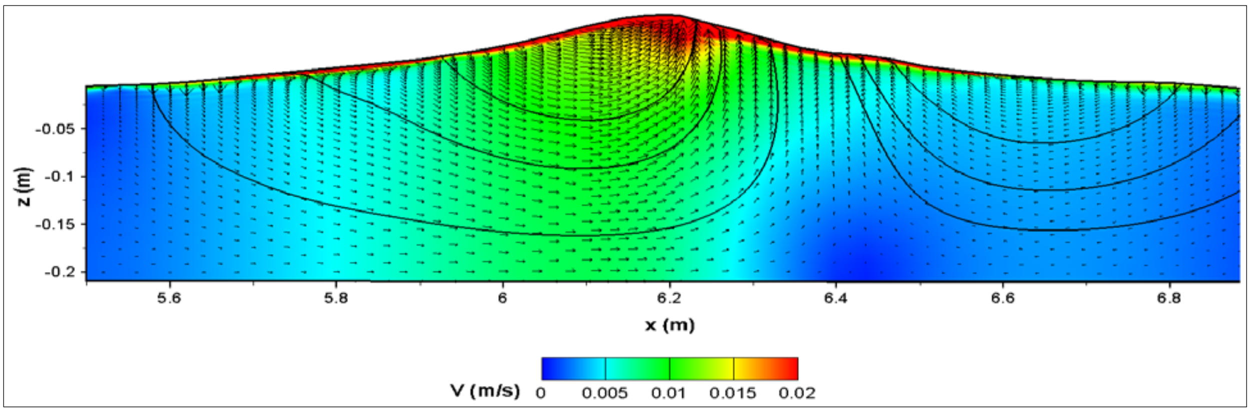

Figure 5. Simulated hyporheic flow field and streamlines.

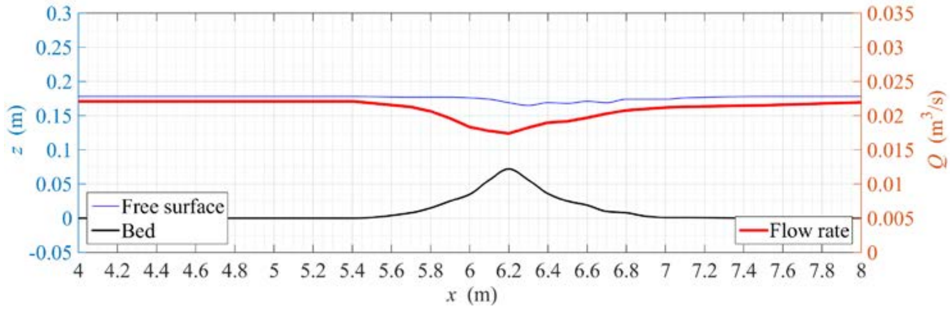

Figure 6. Longitudinal profiles of bed and free surface, and flow rate of the free surface flow along the flume.

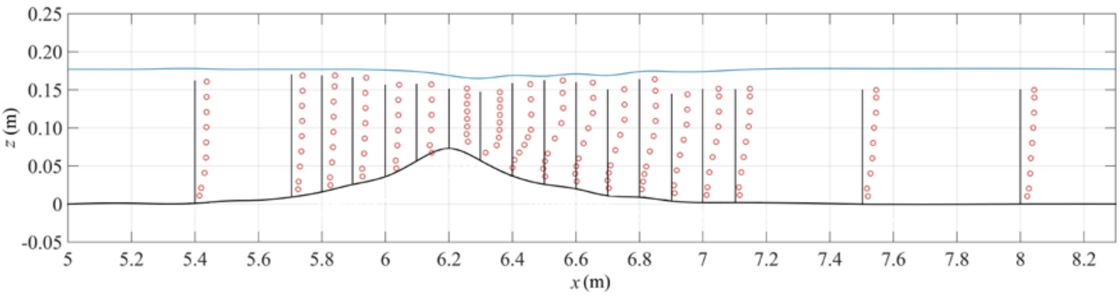

Figure 7. Profiles of time-averaged flow velocity.

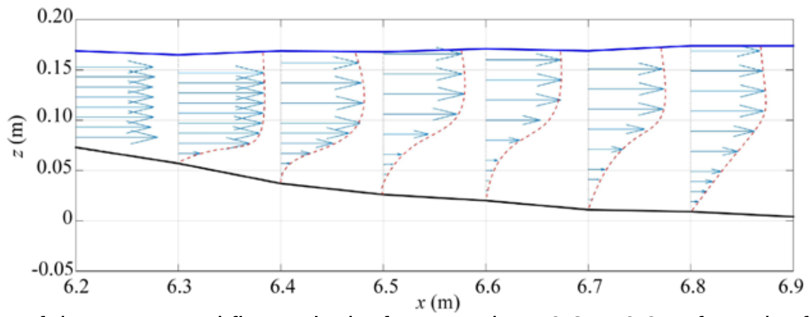

Figure 8. Profiles of time-averaged flow velocity from sections 6.2 to 6.9 m from the flume entrance.

Consider now Figures 10 and 11. Figure 10 shows the plot of downstream turbulence intensity normalized by local vertically-averaged flow velocity, i.e. $(\overline{u'^2})^{1/2}/U$, while Figure 11 shows the contour-plot of $(1/2)(\overline{u'^2}+\overline{v'^2})$. In the absence of measurements of w', this is to be viewed as a surrogate of the turbulence kinetic energy $k=(1/2)(\overline{u'^2}+\overline{v'^2}+\overline{w'^2})$.

Here, u', v' and w' are the fluctuating components of flow velocity in the x, y and z directions, respectively, and U is local vertically-averaged flow velocity. From these plots, it follows that turbulence activity is the most intense at two locations/regions downstream of the bar. The first of such locations is just above the "separation" zone, the second is in the midst of the flow, in the region of the largest velocity gradients in the z-direction. From the observations in this study, both regions appear to be preferential locations for eddy generation.

3.3 Effect of hyporheic flow on the free surface flow

The interaction between the hyporheic and free surface flows was investigated numerically, with the aid of the CFD code described in section 3.1. For the present purposes, and in addition to the simulations previously described, this code was used to simulate also the flow over the gravel bar in the case of an impervious bed. The free surface and velocity profiles of the flow over the porous and impervious bed surfaces are shown in Figure 12. As follows from this figure, the free surface exhibits a deeper depression and occurring further upstream in the case of the impervious bed than it does in the previous case. The difference, however, is small. The main difference occurs in the velocity profiles downstream of the bar top which exhibit considerably larger values of flow velocity close to the bed in the impervious case.

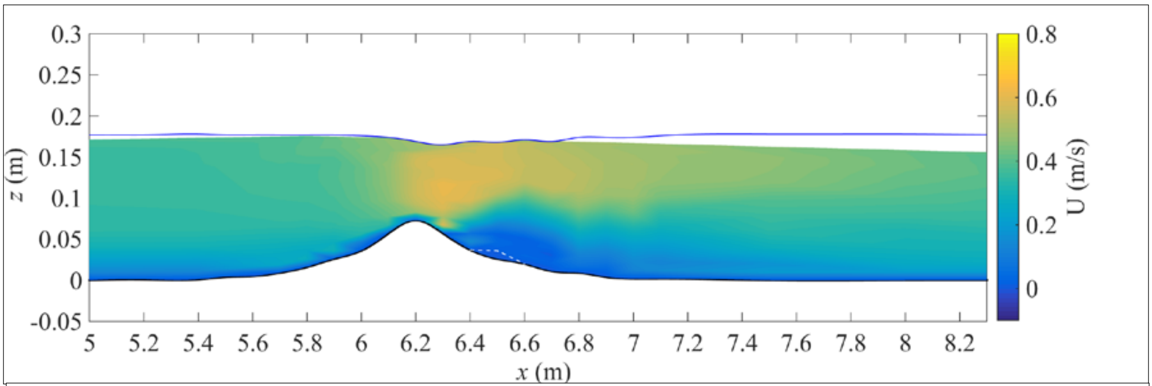

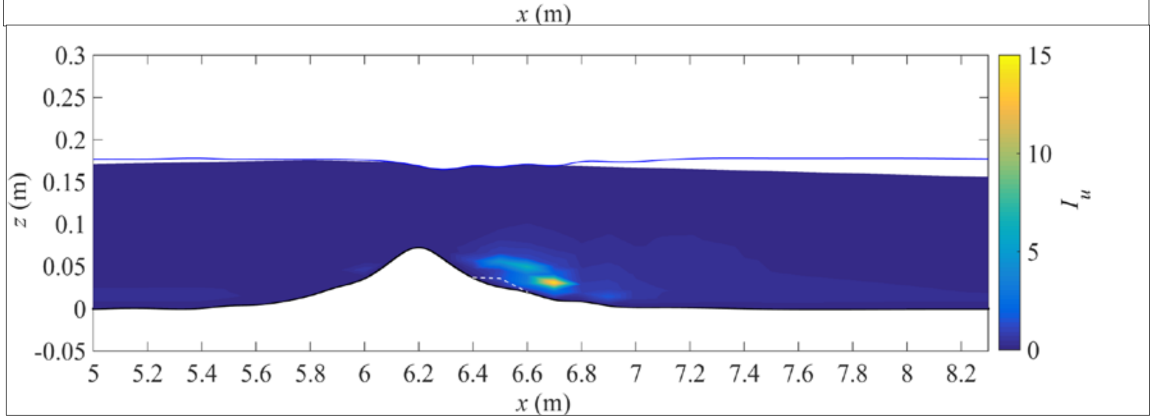

Figure 10. Contour-plot of longitudinal component of normalized turbulence intensity.

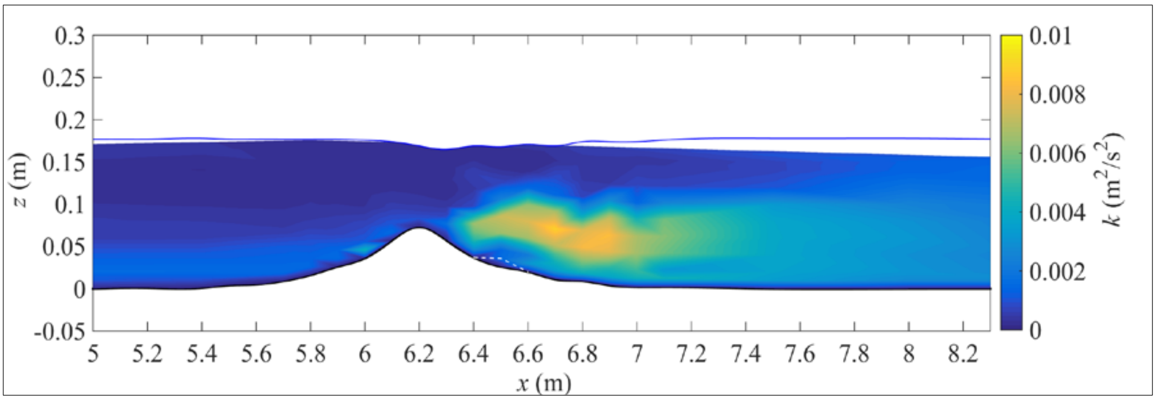

Figure 11. Contour-plot of turbulence kinetic energy.

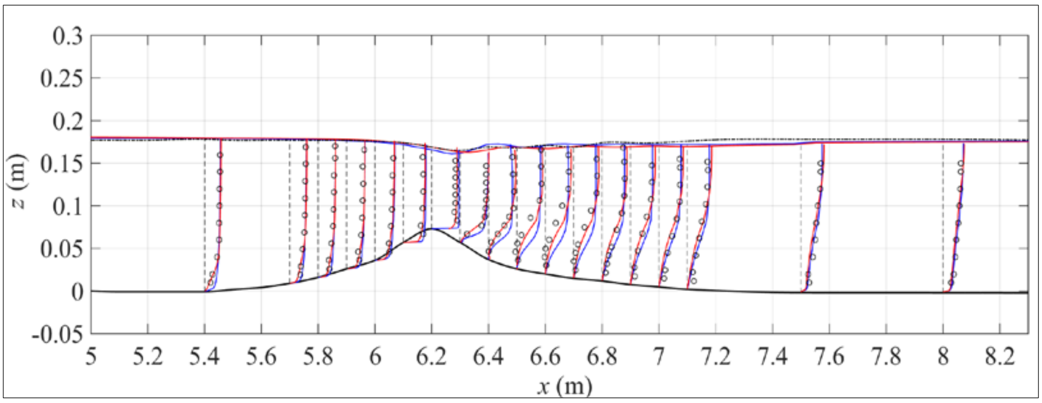

Figure 12. Plot of simulated free surface and velocity profiles. Pervious bed case shown with solid red lines; impervious bed case shown with solid blue lines; measured free surface marked by dashed line; unfilled circles represent measured values of flow velocity.

4 CONCLUSIONS

The present experiment confirms the presence of a turbulent hyporheic flow induced by the gravel bar. A substantial percentage of the free surface flow (≈ 14%) is entrained into the bar. The hyporheic flow consists of two zones, one in which the flow moves in the direction of the streamflow, and another in which it moves in the opposite direction. These two zones are clearly separated by a nearly vertical flow divide. Downstream of the bar top, the bulk of the free surface flow is shifted towards the upper layers, where the largest velocities occur. This pattern is maintained for a considerable distance downstream. A small region with negative flow velocities is observed near the bed downstream of the bar top. Two regions of greater turbulence activity are identified, one immediately above the just mentioned region, and another in the midst of the flow, also downstream of the bar top. When compared to flow over an impervious bed having the same geometry and granular roughness, differences are found in both the free surface profile and the flow velocities especially close to the bed surface downstream of the bar top.

ACKNOWLEDGEMENTS

This research is supported by the Natural Sciences and Engineering Research Council of Canada (NSERC), through the Strategic Project Grant “Contamination of River Beds by Oil Spills and Impact on Fish Habitat”, conducted in partnership with Environment Canada and Northwest Hydraulic Consultants.

REFERENCES

Boulton, A.J., Findlay, S., Marmonier, P., Stanley, E.H. & Valett, H.M. (1998). The Functional Significance of the Hyporheic Zone in Streams and Rivers. *Annual Review of Ecology and Systematics*, 29(1), 59-81.

Blois, G., Best, J.L., Sambrook, S.G.H. & Hardy, R.J. (2014). Effect of Bed Permeability and Hyporheic Flow on Turbulent Flow over Bed Forms. *Geophysical Research Letters*, 41(18), 6435-6442.

Cardenas, M.B. & Wilson, J.L. (2007). Dunes, Turbulent Eddies and Interfacial Exchange with Permeable Sediments. *Water Resources Research*, 43(8), 1-16.

Elliott, A.H. & Brooks, N.H. (1997a). Transfer of Nonsorbing Solutes to a Streambed with Bed Forms: Theory. *Water Resources Research*, 33(1), 123-136.

Elliott, A.H., Brooks, N.H. (1997b). Transfer of Nonsorbing Solutes to a Streambed with Bed Forms: Laboratory Experiments. *Water Resources Research*, 33(1), 137-151.

da Silva, A.M.F., Mumford, K.G., Seyed Mirzaei, S.H., Fruetel, C., Rey, A. (2016). Physical and Numerical Modeling of Hyporheic Flow through a Gravel Bar. *Proceeding of River Flow 2016, 8th International Conference on Fluvial Hydraulics*, St. Louis, USA, 1364-1369.

Fox, A., Boano, F. & Arnon, S. (2014). Impact of Losing and Gaining Streamflow Conditions on Hyporheic Exchange Fluxes Induced by Dune Shaped Bed Forms. *Water Resources Research*, 50(3), 1895-1907.

Gariglio, F.P., Tonina, D. & Luce, C.H. (2013). Spatio Temporal Variability of Hyporheic Exchange through a Pool-Riffle Pool-Sequence. *Water Resources Research*, 49(11), 7185-7204.

Packman, A.I., Salehin, M. & Zaramella, M. (2004). Hyporheic Exchange with Gravel Beds: Basic Hydrodynamic Interactions and Bedform Induced Advective Flows. *Journal of Hydraulic Engineering*, 130(7), 647-656.

Savant, S.A., Reible, D.D. & Thibodeaux, L.J. (1987). Convective Transport within Stable River Sediments. *Water Resources Research*, 23(9), 1763-1768.

Tonina, D. & Buffington, J.M. (2007). Hyporheic Exchange in Gravel Bed Rivers with Pool-Riffle Morphology: Laboratory Experiments and Three Dimensional Modeling. *Water Resources Research,* 43, 1-16.

Trauth, N., Schmidt, C., Maier, U., Vieweg, M. & Fleckenstein, J.H. (2013). Coupled 3-D Stream Flow and Hyporheic Flow Model under Varying Stream and Ambient Groundwater Flow Conditions in a Pool-Riffle System. *Water Resources Research*, 49(9), 5834-5850.

Fruetel, C. (2016). Analysis of Hyporheic Flow Induced by a Bar in a Gravel Stream: An Experimental Study. M.A. *Sc. Thesis,* Dept. Civil Engineering, Queen’s University, Kingston, CA.

Vafai, K. & Tien, C. L. (1981). Boundary and Inertia Effects on Flow and Heat Transfer in Porous Media. *International Journal of Heat and Mass Transfer*, 24(2), 195-203.

Nakayama, A. & Kuwahara, F. (1999). A Macroscopic Turbulence Model for Flow in a Porous Medium. *Transactions-American Society of Mechanical Engineers Journal of Fluids Engineering*, 121, 427-433.

Pedras, M. H. & de Lemos, M.J. (2000). On the Definition of Turbulent Kinetic Energy for Flow in Porous Media*. International Communications in Heat and Mass Transfer*, 27(2), 211-220.

de Lemos, M.J.S. (2012). *Turbulent Impinging Jets into Porous Materials.* Applied Sciences and Technology, Computational Mechanics, Springer, Berlin.

Proceedings of the 37th IAHR World Congress
August 13 – 18, 2017, Kuala Lumpur, Malaysia

COMPARATIVE ANALYSIS OF WATER QUALITY INDICES

SRI PUJI SARASWATI[(1)], SUNJOTO[(2)], B. AGUS KIRONOTO[(3)] & SUWARNO HADISUSANTO[(4)]

[(1,2,3)]Civil and Environmental Engineering Department, Universitas Gadjah Mada, Yogyakarta, Indonesia,
spswatinz@ugm.ac.id,sunysunjoto@ugm.ac,id,kironoto12117@ugm.ac.id
[(4)] Faculty of Biology, Universitas Gadjah Mada, Yogyakarta, Indonesia,
suwarno.h@ugm.ac.id

ABSTRACT

Water Quality Index (WQI) is an important tool in river management. WQI based on conventional water quality parameterization often emphasizes more on anthropocentric views. Water quality analysis using ex-situ and in-situ biomonitoring is considered more objective, more comprehensive representation of the river health status and better approach for river water quality conservation than conventional approach. However, biomonitoring is considered as complicated by engineers and practitioners in water management. Many researchers and practitioners in Indonesia usually use the existing WQI developed in other countries. Three of the most commonly used WQIs are: Storet, Pollution Index and INWQS. The first two are developed in the USA, while INWQS is developed in Malaysia. This research attempts to investigate whether those WQIs developed in countries with different climate and environmental condition are suitable to be used directly in Indonesia. Water quality parameters used as a reference in this study is the biological criteria using ex-situ biomonitoring i.e. AODs (Aquatic Organism environmental Diagnostic) toxicity test using fish and shrimp indicators and in-situ biomonitoring based on EPT (Ephemeroptera, Plecoptera and Trichoptera) diversity index. Water quality parameters are monitored at 5 locations along Gadjah Wong stream, Yogyakarta over 2 years period covering pH, TSS, DO, BOD_5, COD, NH_3. Since Water Qualilty Conservation Standard has not yet been established, water quality as required for level-I water usage in Yogyakarta Governor Regulation is used as the water quality target. Based on this study, WQI results from the three methods are inconsistent with the ex-situ and in-situ biomonitoring results. From the literature review and current study, the three methods are not always applicable in determining the river health status.Tropical climate as well as specific hydrogeobiochemical characteristics of Indonesia necessitate the development of a specific method for WQI determination.

Keywords: Water resources management & conservation; water quality index (WQI); EPT diversity index; AODs toxicity test.

1. INTRODUCTION

Increasing human population and their rapid growth of technology should focus on protecting water resources both in quantity and quality. Historically, the Water Quality Index (WQI) based on physico-chemical variables have been established and used to assess the quality of water resources since 1965 by Horton (Brown et al., 1970; Nemerow and Sumitomo, 1970; Lumb et al., 2006) in the United States. Countries in Europe and Asia (Parparove et al., 2006; Kannel et al., 2007; Sargaonkar and Deshpande, 2003) have also developed their WQI methods. Water quality parameterization often emphasizes more on anthropocentric views, such as water-borne diseases pathogen, self purification and carrying capacity of water resources against pollution load (Saraswati et al., 2011; Thoman and Mueller, 1987) and physico-chemical indicators which dominated by oxygen-demanding waste (Salvato, 1992; Peavy et al., 1986; Metcalf and Eddy, 1979; Novotny, 1996). Water resources are under pressure ranging from sewage effluent and toxic chemical compounds change, erosion due to land use transformation, alteration of stream channel, diversion of flow alteration, over exploitation of biological sources, the spread of toxic chemicals from point and non-point sources (Karr, 1991), making water quality monitoring and management of water resources not sufficient just to be controlled by physico-chemical approach. Water quality analysis using ex-situ and in-situ biomonitoring is considered more objective on ecological implications than conventional, physico-chemical approach (Metcalf and Smith, 1996). However, biomonitoring is considered as complicated by engineers and practitioners in water management. Water quality index (WQI) based on conventional parameters is therefore worth investigating to address this problem.

As different approaches of WQI method have been established in many countries, many researchers and practitioners in Indonesia usually use one of the WQI methods (BLH, 2016; Soesilo and Febriana, 2011; Matahelemual, 2007; Effendi et al., 2015). The question that arises is: does the existing WQI that is developed in different country with different climate and environment suitable to be used directly and does it gives a relevant ecological meaning? This research attempts to answer the question by analyzing several WQI methods that are often used by Indonesian researchers.

2 DATA SET AND METHODS

Three of the well known WQI methods: Storet, Pollution Index (PI), and INWQS (Interim National Water Quality Standard) will be used to calculate the WQI scores based on physico-chemical water quality parameters. The first two were developed in the USA (USEPA, 2011; Nemerow and Sumitomo, 1970) and was adopted in the Guideline for Water Quality Status Determination issued by the Indonesian Ministry of the Environment (No. 115 Year 2003), while INWQS was developed by DOE (Department of Environmental) Malaysia (Al-Mamun and Idris, 2008) which shares similar climate and environment as Indonesia. Water quality parameters used as a reference in this study was the biological criteria which was considered as a more comprehensive representation of the state of the water quality both spatially and temporally (Metcalf and Smith, 1996). The biological criteria was determined using ex-situ biomonitoring i.e. toxicity test examined by AODs (Aquatic Organism Environmental Diagnostic) method (Saraswati, 2015) and in-situ biomonitoring i.e. macrozoobenthic diversity index followed on Lenat method (Lenat, 1988, Lenat, 1993, Roosenberg and Resh, 1993). Water quality parameters were monitored once a month at 5 locations along Gadjah Wong stream, Yogyakarta over 2 years period covering pH, TSS, DO, COD, NH_3N, while BOD_5 parameter was counted based on BOD_5/COD ratio of water quality data measured by BLH (2012). AODs bioassay was conducted using fish and shrimp laboratory test animal (Saraswati, 2015). Macrozoobenthos abundance (EPT Number) and diversity (EPT Taxa) were collected at the same 2 years water quality sampling, and analyzed based on EPT (Ephemeroptera, Plecoptera and Trichoptera) presence, some of the most pollutant sensitive taxons (Lenat, 1988; Lenat, 1993; Roosenberg and Resh, 1993). Water quality as required by Class-I water usage in Yogyakarta Governor Regulation No. 8 Year 2008 was used as the water quality target.

The philosophy underlying the water quality determination of water resources is to integrate a biology criteria into a physico-chemical water quality benchmark in the water resources (Karr, 1991; Metcalf and Smith, 1996; Mason, 1993) so that water quality is measured more comprehensively, reflecting the water quality of water resources and also able to reflect the potential disruption to biological community. Therefore, the river water quality status by all three WQI methods was assessed for compliance according to data from ex-situ biomonitoring methods i.e. AODs toxicity test and in-situ biomonitoring method i.e. Gadjah Wong macrozoobenthos diversity index (Saraswati, 2015).

2.1 Data set

Physico-chemical water quality data, water toxicity data and macrozoobenthos communities were collected in 5 locations in Gadjah Wong stream (Figure 1) that crossed Yogyakarta city which area had a rocky and sandy bottom river.

The selected segments are receiving wastewater effluent from industry, farming and other sources of pollutions. The characteristic of water quality data in Gadjah Wong stream is presented in Table 1. In Figure 2, water toxicity ($AODs_{fish}$ and $AODs_{shrimp}$), water quality status, and also EPT taxa and the status of river water according to Lenat (1988) were presented as X and Y axis, respectively.

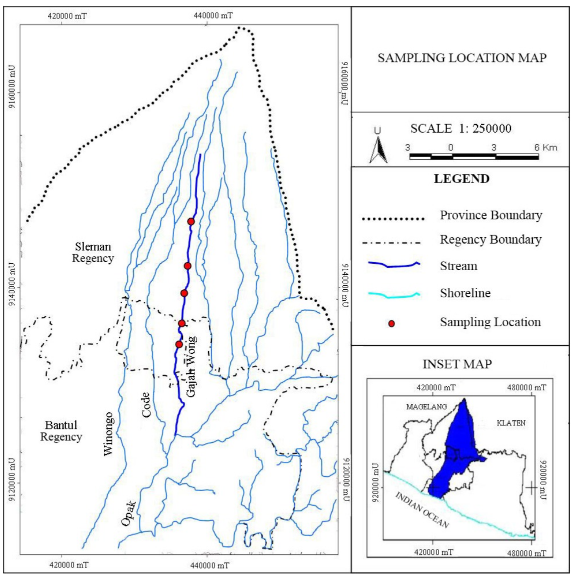

Figure 1. Five locations of water sampling in Gadjah Wong stream.

Table 1. Average, minimum-maximum interval, standard deviation (SD) of some water quality variables in Gadjah Wong stream.

Site		Flow (m^3/sec)	pH	TSS (mg/L)	DO (mg/L)	COD (mg/L)	NH_3-N (mg/L)
1	Min-max	0.034- 0.343	6.54-7.70	2.33-95.00	6.697-7.690	1.619-	0-0.070
	Average	0.107	7.04	13.82	7.287	15.689	0.014
	SD	0.088	0.34	24.60	0.275	15.23	0.021
2	Min-max	0.006-1.479	6.42-7.46	2.00-31.33	5.657-7.461	6.451-	0-0.150
	Average	0.366	7.00	10.77	6.624	19.326	0.028
	SD	0.478	0.35	4.52	0.570	10.01	0.042
3	Min-max	0.012-1.144	6.14-7.78	3.00-28.00	4.175-6.893	3.226-	0-0.460
	Average	0.202	6.81	7.31	5.712	24.460	0.088
	SD	0.297	0.43	6.58	0.909	16.72	0.119
4	Min-max	0.012-1.811	6.00-7.58	2.00-10.00	3.684-7.712	3.226-	0-0.180
	Average	0.590	6.70	5.13	5.880	19.027	0.080
	SD	0.548	0.46	2.54	1.365	19.91	0.058
5	Min-max	0.554-2.835	5.95-7.58	2.00-29.00	3.401-7.161	3.226-	0-0.560
	Average	1,241	6.68	14.13	5.429	24.142	0.286
	SD	0.804	0.47	7.78	1.086	14.49	0.221

Note : Water Quality Class I (YogyakartaGovernor Rgulation No. 20 Year1998), TSS* = 50 mg/l, pH = 6-8,5, BOD_5 = 2 mg/l, COD = 10 mg/l, DO = 6 mg/l, NH_3N= 0,5 mg/l).

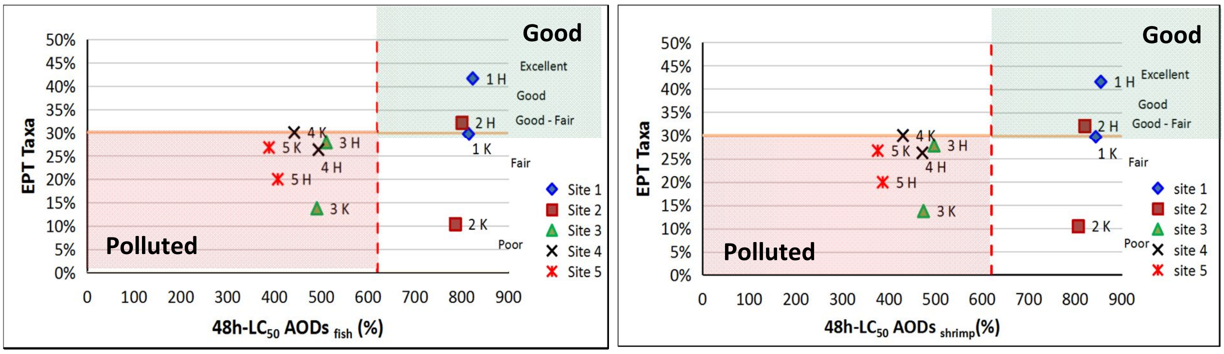

Figure 2. Water quality status at 5 locations, assessed by $AODs_{fish}$ and $AODs_{shrimp}$ toxicity test at X axis and assessed by EPT Taxa index at Y axis.

According to biomonitoring studies, during the rainy season at location 1 written in Figure 2 as (1H) and the dry season at location 1 as (1K), and during the rainy season at location 2 as (2H) lied in the quadrant where water quality was good according to EPT taxa index in which EPT taxa value index was ≥ 30% and AODs toxicity test according to LC50 $AODs_{fish}$ and $AODs_{shrimp}$ score was ≥ 620%. While locations 3, 4 and 5 during the rainy and the dry seasons (3H, 3K, 4H , 4K , 5H , 5K) in the quadrant where, according to AODs toxicity test and index of EPT taxa result, the water was polluted. The anomali condition on water quality was found in location 2 during the dry season (2K) which was good according to AODs toxicity test, but was shown as not good according to EPT taxa index. This might happen because the low stream flow in the dry season is reducing the substrate area as macrozoobenthos habitat. This result underlines that macrozoobenthos is able to be used as a water quality indicator, however there are other factors, beyond water quality, that are able to disrupt macrozoobenthos communities in the river (Karr, 1991).

2.2 Storet, pollution Index and INWQS methods

Basically, there are three important parameters distinguishing WQI formulae, namely, 1) the number and types of water quality variables considered significant to determine the water quality status, 2) a sub-index formula and each variable weight to score the WQI, and 3) formula aggregation of significant variables. Sub-index formula is intended to transform and combine the water quality variables that have different unit dimensions into the WQI formula with the same scale and dimension. Storet, INWQS and Pollution Index are not developed directly by the Delphi technique, a questionnaire based on expert judgment (Abbasi, 2001). Explanation of each method is given below.

2.2.1 Storet

River water quality status by Storet method (USEPA, 2011) is assessed by comparing water quality data to the quality standards appropriate to its purpose. Water quality status by Storet method uses water quality in a series of data monitoring. If the measurement results meet the quality standard then the value is given a score = 0, if the measurement results exceed the quality standards the value is scored according to Table 2. Water quality status are classified into 4 classes i.e. Class A is good, meets quality standards with a score of 0; class B is slightly polluted with a score of -1 to -10; class C is fairly polluted with a score of -11 to -30; class D is heavily polluted with a score of ≤ - 31.

Table 2. The score of each water quality parameters used for storet.

NUMBER OF PARAMETERS	SCORE	PARAMETER		
		PHYSICAL	CHEMICAL	BACTERIOLOGICAL
< 10	Max	- 1	- 2	- 3
	Min	-1	- 2	- 3
	Average	- 3	- 6	- 9
≥ 10	Max	- 2	- 4	- 6
	Min	- 2	- 4	- 6

Source : Indonesian Ministry of the Environment (No. 115/2003).
Note* : number of parameters used to calculate WQI

2.2.2 Pollution Index

The formula is,

$$IP_j = \sqrt{\frac{\left(C_i/L_{ij}\right)^2_M + \left(C_i/L_{ij}\right)^2_R}{2}} \qquad [1]$$

where IP_j is the pollution index for the *j* usage, C_i is water quality parameter i, L_{ij} is water quality concentration of parameter *i* presented in *j* water quality standard of design usage, meanwhile M = maximum, R = average. Water quality index IP for multi-function design water usage, distinguishes some types of water quality parameters, as follows.

i. If the decrease of concentration indicates the decrease of pollution,

$$C_i/L_{ij} \qquad [2]$$

ii. If the decrease of concentration indicates the increase of pollution,

$$\left(C_i/L_{ij}\right)_{new} = \frac{C_{im} - C_{i(measured)}}{C_{im} - L_{ij}} \qquad [3]$$

iii. If the value (C_i/L_{ij}) measurement result is more than 1, therefore

$$\left(C_i/L_{ij}\right)_{new} = 1.0 + P.\log\left(C_i/L_{ij}\right)_{measured} \qquad [4]$$

iv. If the value of water quality standard has a range,

- $C_i<L_{ij}$ average, therefore

$$\left(C_i/L_{ij}\right)_{new} = \frac{\left\{C_i - \left(L_{ij}\right)_{average}\right\}}{\left\{\left(L_{ij}\right)_{minimum} - \left(L_{ij}\right)_{average}\right\}} \qquad [5]$$

- $C_i > L_{ij}$ average, therefore

$$\left(\frac{C_i}{L_{ij}} \right)_{new} = \frac{\left\{ C_i - \left(L_{ij} \right)_{average} \right\}}{\left\{ \left(L_{ij} \right)_{maximum} - \left(L_{ij} \right)_{average} \right\}} \qquad [6]$$

2.2.3 INWQS (Interim National Water Quality Standard)

The formula of INWQS method is

$$WQI = 0.22SIDO + 0.19SIBOD + 0.16SICOD + 0.15SIAN + 0.16SISS + 0.12SIpH \qquad [7]$$

where, SIDO = sub index DO

SIBOD = sub index BOD_5

SICOD = sub index COD

SIAN = sub index Ammonia Nitrogen

SISS = sub index TSS

SIpH = sub index pH

Each with its own sub–index formula (Al-Mamun and Idris, 2008).

2.3 Water Quality Target and The Standard

Another difference between WQI methods is in the water quality design target or water quality standard used. Each country develops WQI index linked to its own water quality standard. Some WQI methods have a flexibility to use standards from different countries, such as the Pollution Index and Storet methods. A healthy river water, generally are natural water quality that has not undergone anthropogenic pollution. Their natural background condition can be determined as the benchmark of water quality condition (Mahida, 1992; Lumb et al., 2006). In this research, the natural water quality condition will be used as an ideal target for river water quality management in the Gadjah Wong stream, which is then called water quality conservation target that can serve as raw water for drinking, agriculture, drainage including ecological water function (Indonesian Water Resources Act, 1975; Karr, 1991). Unfortunately, natural water quality benchmark data for Gadjah Wong stream is not available, therefore as an approximation, the water quality standard Class I of Yogyakarta Governor Regulation No. 20 Year 2008 i.e. river water use of raw water for drinking is used.

INWQS method calculates a WQI score using six water quality parameters, namely pH, TSS, DO, BOD_5, COD and NH_3N. Since this study is comparing the three methods, the WQI calculation for the Storet and PI methods will also use the same parameters. River water quality targets of Gadjah Wong stream for Storet and PI methods, used class I of Yogyakarta Governor Regulation with adjustment by adding TSS water quality parameter with the standard concentration of 50 mg/l. In INWQS–DOE, the water quality standard used was a local “general use” in Malaysia where the value of concentration of the 6 water quality parameters were equivalent to Yogyakarta Class I water quality standard as shown in Table 3.

Table 3. Some water quality parameters in Class I standard (Yogyakarta Governor Regulation No. 20 Year 2008) and General Use of INWQS DOE Malaysia. The score of each water quality parameter used for Storet.

WATER QUALITY PARAMETERS	CLASS I YOGYAKARTA	INWQS DOE **
pH	6-9	6-8.5
TSS (mg/L)	50	50
DO (mg/L)*	6	6
BOD_5 (mg/L)	2	3
COD (mg/L)	10	10
NH_3N (mg/L)	0-5	0.5

Note : * = minimum concentration; ** =WQ parameter standard at INWQS DOE WQI score80 (clean water for *general use*)

3 RESULT AND DISCUSSION

Based on the application of INWQS method, location 1 during rainy (1H) and dry season (1K) and location 2 during rainy season (2H) indicated good water quality condition. These correspond to the water quality assessment standard using the AODs water toxicity test (Figure 2 (a) and 2 (b)) and EPT richness and density index (Figure 3 (a) and 3 (b)). Whereas water qualities at locations 3, 4 and 5 during rainy and dry season (3H; 3K; 4H; 4K; 5H; 5K), using INWQS method, showed varied results of unpolluted category and good quality, respectively. In contrast, according to the water quality assessment using AODs and EPT index, locations 3, 4, and 5 during dry and rainy season (3H; 3K; 4H; 4K; 5H; 5K) were classified as fairly polluted category.

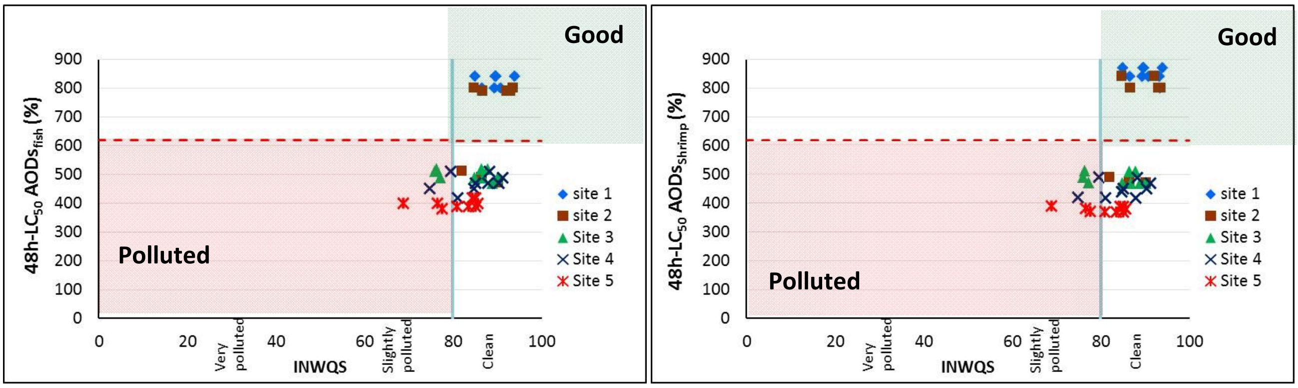

Figure 3. Mapping of water quality status in rainy and dry season at 5 locations in Gadjah Wong stream, scored with INWQS method on the X axis, and assessed by (a) $AODs_{fish}$ toxicity test on the Y axis; (b) $AODs_{shrimp}$ toxicity test on the Y axis.

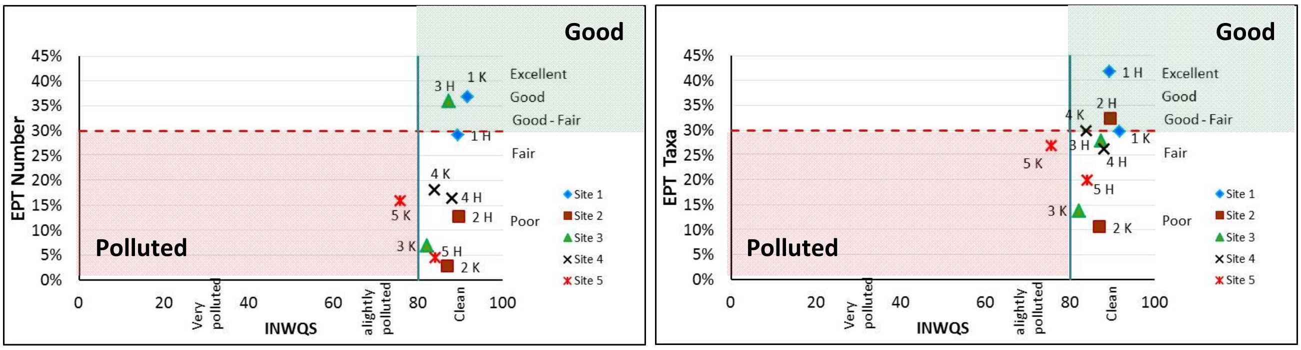

Figure 4. Mapping of water quality status at 5 locations in Gadjah Wong stream, scored with INWQS method on the X axis, and assessed by (a) EPT density (EPT Number) index on the Y axis; (b) EPT Taxa index on the Y axis.

Based on the PI method, locations 1, 2, 3, 4, 5 during rainy and dry seasons, were all classified under polluted category (Figure 5 (a) and 5 (b), Figure 6 (a) and 6 (b)).

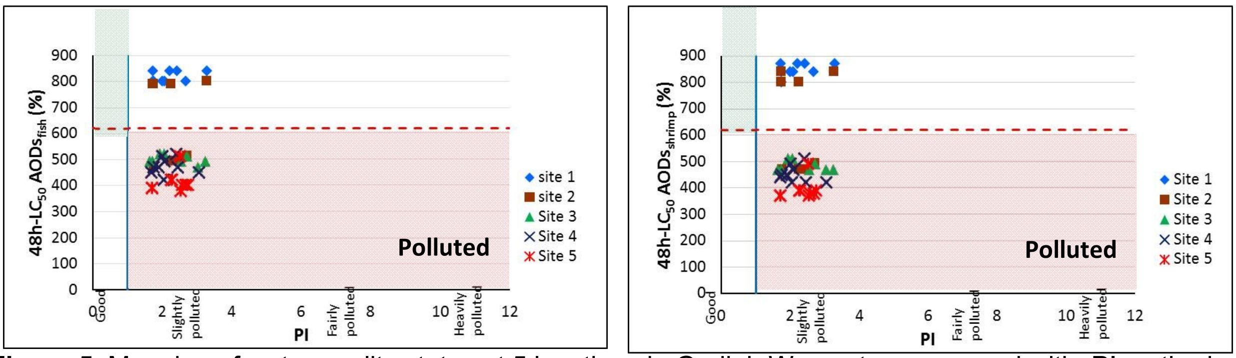

Figure 5. Mapping of water quality status at 5 locations in Gadjah Wong stream, scored with PI method on the X axis, and assessed by (a) $AODs_{fish}$ toxicity test on the Y axis; (b) $AODs_{shrimp}$ toxicity test on the Y axis.

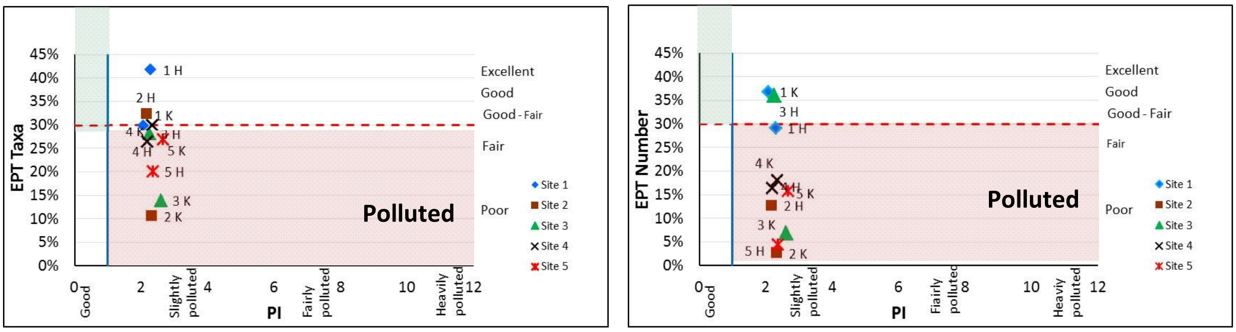

Figure 6. Mapping of water quality at 5 locations in Gadjah Wong stream, scored with PI method on the X axis, and assessed by (a) EPT abundance (EPT Number) index on the Y axis; (b) EPT Taxa index on the Y axis.

These results differed from the AODs toxicity test method (Figure 5 (a) and 5 (b)) and EPT index method (Figure 6 (a) and 6 (b)) results in location 1 during rainy and dry season (1H; 1K) and location 2 during rainy season (2H) showed good water quality, location (2K) showed anomaly, and water quality at locations (3H), (3K), (4H), (4K), (5H), (5K) all categorized as polluted.

According to the Storet method, water quality data at locations (1K), (1H), (2H), showed anomaly at location (2K); locations (3H), (3K), (4H), (4K), (5H), (5K) were polluted (fairly-heavily), see Figure 7 (a) and 7 (b), Figure 8 (a) and 8 (b). The conformity with AODs toxicity test method and EPT index method were found only at locations (1H), (1K), and (2H) which were classified as good, where 48h-LC_{50} $AODs_{fish}$ and 48h-LC_{50} $AODs_{shrimp}$ > 620% and EPT Taxa index > 30%.

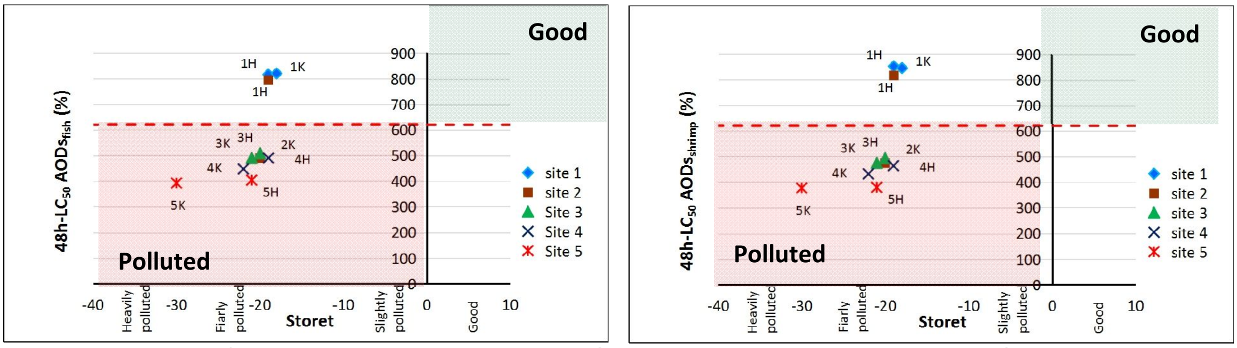

Figure 7. Mapping of water quality at 5 locations in Gadjah Wong stream, scored with Storet method on the X axis, and assessed by (a) $AODs_{fish}$ toxicity test on the Y axis ; (b) $AODs_{shrimp}$ toxicity test on the Y axis.

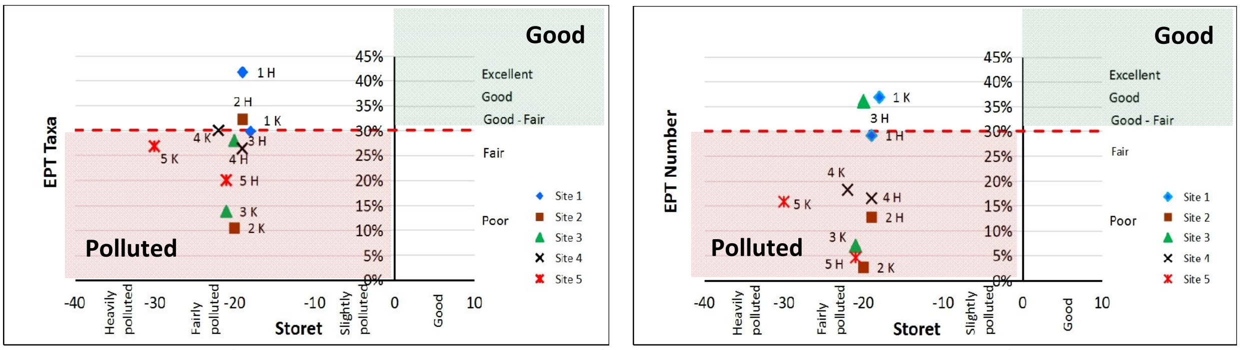

Figure 8. Mapping of water quality at 5 locations in Gadjah Wong stream, scored with Storet method on the X axis, and assessed by (a) EPT abundance (EPT Number) index on the Y axis; (b) EPT Taxa on the Y axis.

The three WQI methods, namely INWQS, PI and Storet, all based on physico-chemical water quality parameters, gave different results on water quality status assessment. INWQS method concluded that water quality at locations (1H), (1K), (2H) was good (anomaly at 2K), similar with AODs toxicity test result and EPT index method. According to PI and Storet methods, locations 1 and 2 water quality were classified as polluted. Whereas locations 3, 4, 5 in rainy and dry season according to INWQS method were partially categorized as polluted and good. These conclusions are different from the biomonitoring results. Water assessment at locations 3, 4, 5 based on PI and Storet method resulted in polluted category, similar with AODs and EPT index results. Conclusions drawn from these three WQI methods differ from quality status assessment by biomonitoring method either ex-situ (at laboratory bioassay) and in-situ (instream bioassay). Storet and PI methods, being an empirical equation developed on certain conditions, are not always suitable for water resource quality evaluation at the observed river in this research. INWQS method developed in Malaysia, despite having similar environmental condition to Indonesia, is also not always suitable to evaluate water quality at Gadjah Wong stream, at which some parts still preserve its natural condition, while water pollution occurs at the other parts that may risk the survivability of aquatic biota. Referring to Metcalf and Smith (1996), Mason (1993) and Karr (1991), river water quality evaluation requires a concept of integrity in the water body that combines physical, chemical and biological dimensions. Comprehensive measurement of water quality index is needed to evaluate water resource condition that satisfies the conservation criteria within ecological and sustainable river management constraint. The dissimilarities among the three WQI methods mentioned above in comparison with water evaluation using biomonitoring method also emphasize what Metcalf and Smith (1996) suggested that ex-situ physico-chemical water quality assessment does not necessarily simulate the actual in-situ condition at the river. Dissimilarities of results from the three methods can also be attributed to improper water quality standard used. There is not always a direct association between water quality criteria based on physico-chemical-bacteriogical water quality variables and aquatic biota condition at the observed water resources. River water quality assessment regulation as prescribed in the policy and technical guidance does not always correspond with the river water conservation efforts. Indonesian Water Resources Act No. 7 Year 2004, emphasizes the importance of preserving natural multi-functionality of water resource including its ecological function. To ensure ecological and sustainable water resource management, the importance of environmental moral-vitalism needs to be emphasized (Nugroho, 1986 in Sunjoto, 2009), a harmony between the water usage for human being and the needs of environmental conservation. Whereas Government Regulation No. 82 Year 2001 and the regulation underneath, which commonly used by water resource management practitioners are more inclined to classify river water quality based on water usage perspective, such as drinking water, irrigation, and industrial use, based on humanistic environment morality, one level below vitalism. On those account, assessment of water quality based on regulation from Indonesian Ministry of the Environmental Decree No. 37 Year 2003 is more appropriate, where water quality index is supposedly not limited in achieving the water physical, chemical, and bacteriology variables but also its conservative objective. By applying comprehensive WQI approach, river water health is focused into a “limit” value for water quality variables with river conservation targets.

Based on the literature study, WQI method which is considered to be the most applicable in Indonesia’s river had yet to be identified. This research has found that the three WQI methods namely Storet, PI and INWQS, are not always suitable. Indonesia with tropical climate, diverse biotic/abiotic environmental condition and diverse hydro-geo-chemical conditions from Aceh to Papua need to have a method for river water health assessment. It is necessary to develop a specific WQI method for Indonesia to serve a variety of purposes such as: primary regulatory tool for water resource protection, and a monitoring tool for water quality evaluation for river water pollution control program (Ott, 1978). River management and water quality monitoring need a comprehensive approach, impartial management among the corresponding board and the monitoring program needs to select the number and type of water quality parameters to be monitored as well as the sampling stations. In so doing, ultimately an efficient and effective procedure to detect water pollution, source and solution can be developed. River water quality quantified by WQI can serve the purpose as an evaluation tool for water resource administrator. By taking water sample at separate time (instant sampling) or continuous time (time series sampling) locally or spatial/ecoregional analysis, WQI can be applied to evaluate operation and flow allocation to restore river water quality to meet ecological and sustainable river management goals (Parparove et al., 2006; Saraswati, 2015). Environmental Agency can benefit from the use of WQI for monitoring and evaluation of river water quality from various sources of pollutant and to correlate them with impact source factor; to set control procedure and restore water quality at its source i.e industry, domestic, and so forth, systematically within the watershed; to allocate resources and evaluate its eco-management (Abbasi et.al., 2006).

4 CONCLUSIONS

From literature reviews and comparative studies of 3 WQI methods, it can be concluded that water quality status determination using Storet, PI and INWQS methods based on physico-chemical indicators at Gadjah Wong stream are inconsistent with the results based on ex-situ and in-situ biomonitoring. River water quality standards of Class I approach do not always imply a good water quality for aquatic organisms. The water quality standards are more inclined toward anthropocentric environmental ethic. Management of water resources in Indonesia needs to establish a WQI method on the basis of conservation which considers the natural peculiarities of diverse river environments.

ACKNOWLEDGEMENTS

The authors would like to acknowledge the financial support from the Civil and Environmental Engineering Department, Faculty of Engineering, GadjahMada University through DPP UGM. The first author is indebted to the Directorate General of Higher Education, Ministry of Education and Culture for the BPPS scholarship that has enabled her to do a major part of this research.

REFERENCES

Abbasi, S.A. (2001). *Water Quality Indeces*: State of the Art. Centre for Pollution Control and Energy Technology Pondicherry University. R. Venkarataman Nagar, Kalapet, Pondicherry-605 014, India.

Abbasi, S.A, Sarkar & Chinmoy. (2006). Qualidex-A New Software for Generating Water Quality Indices. *Journal of Enviromental Monitoring and Assessment*, 119 (2006): 201-231.

Al-Mamun, A. & Idris, A. (2010). Revised Water Quality Indices for The Protection of Rivers in Malaysia. *Twelfth International Water Technology Conference*. IWTC12, Alexandria, Egypt.

Badan Lingkungan Hidup, (BLH). DIY. (2010). *Laporan Analisa Data Kualitas Air Sungai di Provinsi Daerah Istimewa Yogyakarta (Water Quality Analysing Report in Yogyakarta Special Province)*, Yogyakarta.

Brown R.M., McClelland N.I., Deininger R.A. & Tozer R.G. (1970). A Water Quality Index- Do We Dare?. *Journal of Water and Sewage Works*, 339-343.

Effendi H., Romanto & Wardianto Y. (2015). Water Quality Status of Ciambulawung River Banten Province, Based on Pollution Index and NSF-WQI. *The 1st International Symposium on LAPAN-IPB Satelite for Food Security and Environmental Monitoring, Procedia Environmental Science,* 24, 228 - 237.

Kannel, P.R., Lee, S., Lee, Y.S., Kanel, S.R. & Khan, S.P. (2007). Application of Water Quality Indeces and Dissolved Oxygen as Indicators for River Water Classification and Urban Impact Assessment. *Journal of Environmental Monitoring Assessment*, 132, 93-110.

Karr, J.R. (1991). Biological Integrity: A Long-Neglected Aspect of Water Resources Management, *Journal of Ecological Applications*, 1(1), 66-84.

Lenat, D.R. (1988). Water Quality Assessment Using a Qualitative Collection Method for Benthic Macroinvertebrates. *Journal of National of American Benthological Society*, 7, 222-233.

Lenat, D.R. (1993). A Biotic Index for the Southeastern United States: Derivation and List of Tolerance Value, with Criteria for Assigning Water-Quality Ratings. *Journal of the North American Benthology Society*, 12(3), 279-290.

Lumb, A., Halliwell, D. & Sharma, T. (2006). Application of CCME Water Quality Index to Monitor Water Quality: A Case of the Mackenzie River Basin Canada. *Journal of Environment Monitoring and Assessment,* 113, 411-429.

Mahida, U.N.(1982). Pencemaran Air dan Pemanfaatan Limbah Industri (*Water Pollution and Disposal of Waster Water on Land*), translated by Ticoalu G., (1984). CV Rajawali, Jakarta.

Matahelumual, B.C. (2007). “Penentuan Status Mutu Air dengan Sistem STORET di Kecamatan Bantar Gebang“(Water Quality Status Determination using STORET System di Bantar Gebang County). *Journal of Geologi Indonesia*, 2(2), 113-118.

Metcalf & Eddy Inc. (1979). *Wastewater Engineering Treatment/Disposal/Reuse.* Mac Graw Hill, USA 2nd edition, 930.

Metcalf, J.L. & Smith. (1996). *Biological Water Quality Assessment of Rivers: Use of Macro Invertebrate Communities.* River Restoration. Blackwell Science, Oxford.

Nemerow, N.L. & Sumitomo, H. (1970). *Benefits of Water Quality Enhancement, Report No. 16110 DAJ*, U.S. Environmental Protection Agency, Syracuse University, Syracuse, NY.

Novotny V. (1996). Integrated Water Quality Management. *Water Science Technology*, 33(4-5),1-7.

Ott, W.R. (1978). *Water Quality Indeces: A Survey of Indeces used in the United States.* US Environmental Agency, Washington DC, EPA 600\4-78-005.

Parparove, A., Hambright, K.D., Hakanson, L. & Ostapania, A. (2006). Water Quality Quantification: Basic and Implementation. *Journal of Hydrobiologia,* 560, 227-237.

Peavy, H.S., Rowe, D.R. & Tschobanoglous, G. (1986). *Environmental Engineering.* McGraw-Hill Book Co., Singapore.

Roosenberg, D.M. & Resh, V.M. (1993). Introduction to Freshwater Biomonitoring and Benthic Macroinvertebrates. *Freshwater Biomonitoring and Benthic Macroinverte-brates*. Chapman and Hall, New York, USA.

Salvato, J.A. (1982). *Environmental Engineering and Sanitation*. A Wiley-Interscience Publication, New York, USA.

Saraswati, S.P. (2015). Pengembangan Metode Penetapan Kesehatan Perairan Sungai di Daerah Tropis Berbasis Ekohidraulik (Development of New Methods to Determine the Health Status of River Based on Ecohydraulics Approach), *Doctor Dissertation*, UGM.

Saraswati, S.P. & Istiarto, Atiam. (2011). Study on River Water Quality Status of Bedog River Yogyakarta by Using One Dimensional Numerical Simulation. *International Seminar on Environmental Technologies and Management Conference, ITB, Bandung.*

Sargaonkar, A. & Deshpande, V. (2003). Development of an Overall Index of Pollution for Surface Water based on A General Classification Scheme in Indian Context. *Journal of Environmental Monitoring and Assessment*, 89, 43-67.

Susilo, G.E. & Febrina, R. (2011). The Simplification of Doe Water Quality Index Calculation Procedures Using Graphical Analysis. *Australian Journal of Basic and Applied Sciences*, 5(2), 207-214.

Thomann R.V. & Mueller J.A. 1987. *Principles of Surface Water Quality Modelling and Control*. Harperand Row Publishers, New York. New York, 221-227.

United States Environmental Protection Agency (USEPA). (2011). STORET/ WQX Commonly Asked Questions. (http://www.epa.gov/storet/faq.html#101) [accessed in June 2011].

WATER QUALITY ASSESSMENT IN KLANG RIVER BASIN, MALAYSIA

NORHAFEZAH KASMURI[(1)], NORADILA ABDUL HADI[(2)], MEGAWATI OMAR[(3)] & AZRIL HAFIZ AB RAHIM[(4)]

[(1,2,4)]Faculty of Civil Engineering, UniversitiTeknologi MARA, 40450 Shah Alam, Selangor, Malaysia
norhafezahkasmuri@salam.uitm.edu.my; adilameow92@gmail.com
[(3)]Academy of Language Studies, UniversitiTeknologi MARA, 40450Shah Alam, Selangor, Malaysia
megawatiomar@yahoo.com
[(4)]Department of Irrigation and Drainage, Jalan Sultan Salahuddin, 50626 Kuala Lumpur, Malaysia
azrilhafiz@gmail.com

ABSTRACT

Water pollution is viewed crucial which its ill management will cause severe effect to human health, aquatic life and its surroundings. Recently, the amount of waste discharged into the river and its assimilative capacity has affected the quality of river water directly. Hence, this study aims to characterize the water quality of the Klang River using the Water Quality Index (WQI) calculation at three locations along the river. The characterization will be used to assess the River of Life project. The locations are at the upstream of the river commonly known as the Ampang River, the middle river near the Masjid Jamek of Kuala Lumpur and the downstream near the Klang Mosque in Klang. These three water samples are taken between 6thOctober and 31 of October 2015. There are eight times of sampling at each location. This research conducts five in-situ tests and five laboratory tests. The WQI is calculated considering six parameters: the dissolved oxygen (DO), biochemical oxygen demand (BOD), chemical oxygen demand (COD), pH, total suspended solid (TSS) and ammoniacal nitrogen (NH_3-N). The finding shows that the middle part of the Klang River is the highest in terms of quality compared to the other parts. It is recommended that to achieve the Class IIB quality, the two regionals' STPs, which are Bunus and Jinjang, be upgraded.

Keywords: Klang River; Water Quality Index (WQI); River of Life (ROL).

1 INTRODUCTION

Water is an essential natural resource for sustaining life and environment. Following, on June 2012, the Klang River is chosen for the River of Life program due to its location crossing the Kuala Lumpur city center and its present average Class III Water Quality Index (WQI) (PEMANDU, 2014). The aim of the River of Life program is to transform the Klang River into a better river with high economic value and improve its water quality to Class IIB by 2020 (Myrol, 2012). There have been many studies on water pollution and urbanization within the river catchments areas. These studies characterize the water quality by applying the methods of hydrometer or any other suitable methods using chemical, physical and the characteristics of the water (Hossain, Sujaul, & Nasly, 2013).

The objectives of the present study are the following:

(a) To obtain pollutant sources affecting the Klang River water quality (upstream and downstream).
(b) To assess the 'River of Life Project's success (or otherwise) by comparing water quality analysis from three locations.
(c) To know/identify the Klang River water quality in year 2015.

The limitation of this study is that the data are collected between 6th October and 31 of October 2015. This short duration of data collection is essential in order to assess the current condition of the river water and to obtain the current progress needed by the River of Life Project (ROL) with whom the current research is collaborating. The data too, collected from three locations set far apart from each other, need to be analyzed both *in situ* and in laboratory.

This study is very significant to identify the current water quality of Klang River subjected to the ROL's aims of transforming the Klang River into a vibrant and livable water front (Myrol, 2012).

2 PROJECT SITE

The stretch of the Klang River is approximately 10 km long. Its catchment area is 40.4 km^2 covering the Klang Gates Dam, the Ampang confluence and the Klang River (Figure 1). More than 80% of the areas of which the river runs are managed by the Ampang Jaya Municipal Council (MPAJ), while the rest by the Kuala Lumpur City Hall (DBKL). Around 38% of these lands are residential areas, 7% commercial and 5% industrial, respectively. The tributaries of the Klang River are the Gisir River, Kemensah River and Sering River. The estimated population living in the project site is around 146,000.

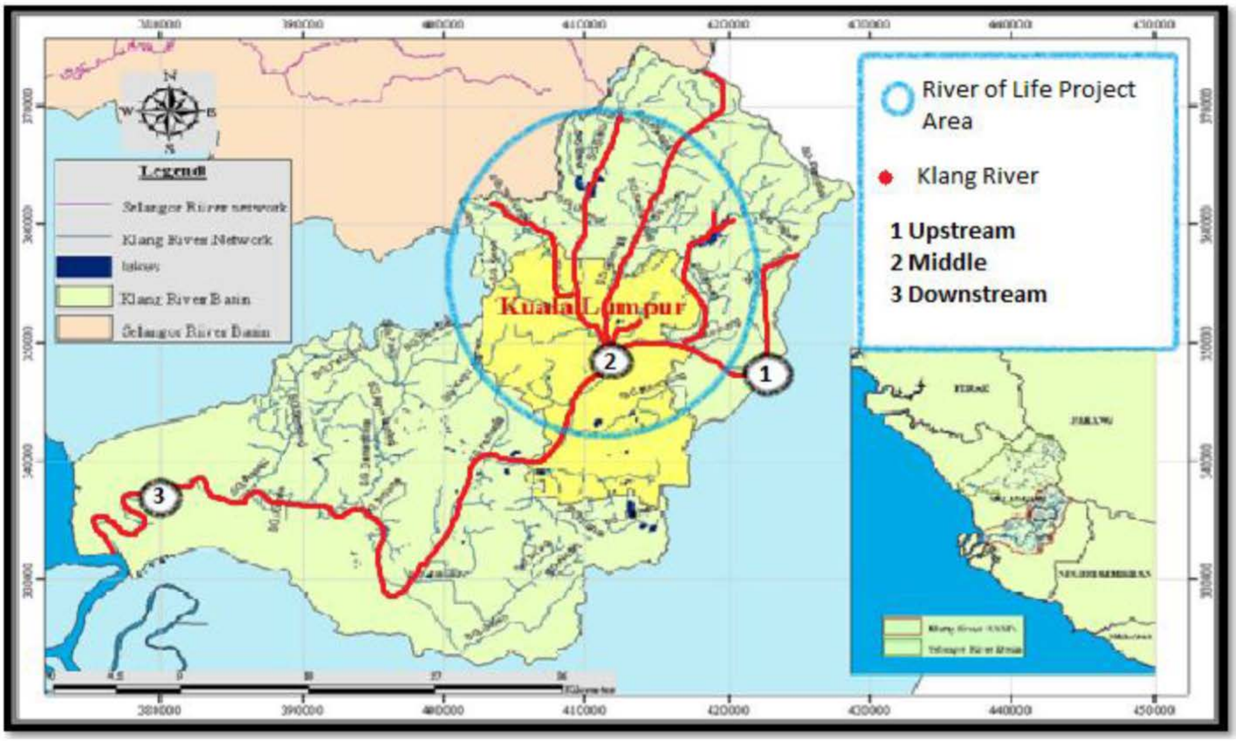

Figure 1. Locations of Water Sampling and the River of Life area withinthe Klang River Basin.

3 DATA COLLECTION

The study selected three sampling stations, which were the Ampang River (the upstream), Masjid Jamek (the middle stream) and Masjid Klang (the downstream). The Water Quality Index (WQI) at the upstream, middle and downstream of the Klang River was calculated based on the data in Tables 1, 2 and 3, using the Department of Environment Water Quality Index. It was calculated to express the overall water quality using the sub-indices (SI) values of the six selected parameters for the three selected locations. The values were the DO, BOD, COD, pH, TSS and ammonia nitrogen (DOE, 2013).

4 RESULTS

The results showed that the major pollutants of the Klang river were biochemical oxygen demand (BOD), ammonia nitrogen (NH_3N) and suspended solid (SS). Table 4 shows the best fit equations used to calculate the SI value for the six parameters and the WQI equation used to determine the WQI.

Table 1. Upstream of the Klang River (known as the Ampang River situated in Ampang).

October 2015		6/10	10/10	13/10	17/10	20/10	24/10	27/10	31/10
In-Situ Test	Temp (°C)	30.99	31.99	30.89	30.99	30.74	30.99	30.87	30.98
	pH	6.05	6.70	6.05	6.05	6.23	6.06	6.08	6.08
	DO (mg/L)	9.80	9.80	8.89	7.67	10.49	9.79	8.76	9.80
	Turbidity (NTU)	46.7	47.8	40.9	53.4	46.6	46.8	46.3	47.2
	TDS (g/L)	0.157	0.159	0.160	0.157	0.158	0.158	0.157	0.157
Laboratory Test	BOD (mg/L)	10.68	9.70	23.68	10.60	9.40	11.28	14.36	11.13
	COD (mg/L)	53	56	50	56	54	53	58	58
	TSS (mg/L)	49	53	59	58	48	49	51	53
	Ammonia (mg/L)	4.48	4.5	4.44	4.48	4.53	4.47	4.40	4.47
	E-Coli (MPN)	>2419.6	>2419.6	>2419.6	>2419.6	>2419.6	>2419.6	>2419.6	>2419.6
	Coliform (MPN)	>2419.6	>2419.6	>2419.6	>2419.6	>2419.6	>2419.6	>2419.6	>2419.6

Table 2: The Middle of the Klang River (near Masjid Jamek in the Centre of Kuala Lumpur).

	October 2015	6/10	10/10	13/10	17/10	20/10	24/10	27/10	31/10
In-Situ Test	Temp (°C)	29.68	30.13	28.36	31.99	29.78	30.18	29.99	30.34
	pH	6.97	4.43	4.56	5.71	6.98	6.79	5.56	6.13
	DO (mg/L)	7.67	14.31	12.26	11.67	10.39	7.49	7.67	8.69
	Turbidity (NTU)	120	126	120	121	127	126	126	120
	TDS (g/L)	0.165	0.165	0.164	0.163	0.168	0.167	0.165	0.166
Laboratory Test	BOD (mg/L)	9.70	9.40	9.38	8.65	9.40	15.64	9.32	10.60
	COD (mg/L)	45	43	43	45	42	45	44	45
	TSS (mg/L)	20	22	21	21	26	28	27	28
	Ammonia (mg/L)	4.5	4.43	4.40	4.45	4.57	4.44	4.55	4.5
	E-Coli (MPN)	59.0	59.0	59.0	59.0	59.0	59.0	59.0	59.0
	Coliform (MPN)	>2419.9	>2419.9	>2419.9	>2419.9	>2419.9	>2419.9	>2419.9	>2419.9

Table 3. Downstream of the Klang River (near the Klang Mosque in Klang).

	October 2015	6/10	10/10	13/10	17/10	20/10	24/10	27/10	31/10
In-Situ Test	Temp (°C)	28.34	28.34	30.15	30.18	30.83	29.0	29.84	28.34
	pH	7.54	7.93	7.94	7.63	7.53	7.54	7.54	7.47
	DO (mg/L)	6.30	10.59	14.67	10.60	7.43	9.13	7.89	10.58
	Turbidity (NTU)	213	214	213	217	220	214	215	213
	TDS (g/L)	0.141	0.141	0.142	0.141	0.141	0.143	0.142	0.141
Laboratory Test	BOD (mg/L)	32.18	7.52	17.89	17.82	11.50	11.20	26.84	24.06
	COD (mg/L)	148	148	146	156	153	149	148	146
	TSS (mg/L)	117	117	123	126	120	118	116	117
	Ammonia (mg/L)	3.54	4.43	4.5	4.56	4.54	4.30	4.53	4.56
	E-Coli (MPN)	>2419.6	>2419.6	>2419.6	>2419.6	>2419.6	>2419.6	>2419.6	>2419.6
	Coliform (MPN)	>2419.6	>2419.6	>2419.6	>2419.6	>2419.6	>2419.6	>2419.6	>2419.6

Table 4. Equations to Estimate the Sub-index Values and the Total WQI Equation (DOE, 2013).

Sub- index	WQI Calculation	Range
SIDO	= 0	For x ≤ 8
	= 100	For x ≥ 92
	= - 0.395 + 0.03 x2 – 0.0002 x3	For 8 < x < 92
SIBOD	= 100.4 – 4.23 x	For x ≤ 5
	= 108 $e^{-0.055x}$ – 0.1 x	For x > 5
SICOD	= - 1.33 x + 99.1	For x ≤ 20
	= 103 $e^{-0.0157x}$ – 0.04 x	For x > 20
SIAN	= 100.5 – 105 x	For x ≤ 0.3
	= 94 $e^{-0.573x}$ – 5 | x – 2 |	For 0.3 < x < 4
	= 0	For x ≥ 4
SISS	= 97.5 $e^{-0.00676x}$ +0.05 x	For x ≤ 100
	= 71 $e^{-0.0061x}$ – 0.015 x	For 100 < x < 1000
	= 0	For x ≥ 1000
pH (SIPH)	= 17.2 – 17.2 x + 5.02 x2	For x < 5.5
	= - 242 + 95.5 x – 6.67 x2	For 5.5 ≤ x < 7
	= - 181 + 82.4 x – 6.05 x2	For 7 ≤ x < 8.75
	= 536 – 77 x + 2.76 x2	For x ≥ 8.75

WQI = 0.15 x SIAN + 0.19 x SIBOD + 0.16 x SICOD + 0.22 x SIDO + 0.16 x SISS + 0.12 x SIPH

Figure 2 shows the trend of the water quality index of the Klang River upstream, middle and downstream. It clearly indicated that the downstream of the Klang River exhibited the lowest WQI value as compared to the other two locations. Based on this WQI, it can be concluded that the upstream was more polluted than the middle.

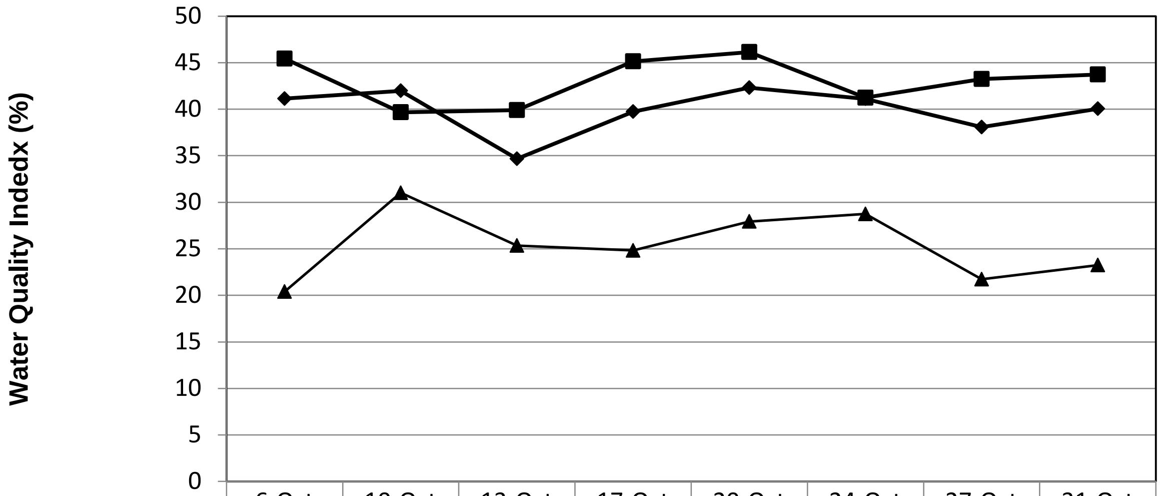

	6-Oct	10-Oct	13-Oct	17-Oct	20-Oct	24-Oct	27-Oct	31-Oct
Upstream	41.13	41.98	34.67	39.74	42.31	41.12	38.07	40.05
Middle	45.43	39.67	39.9	45.14	46.14	41.23	43.24	43.73
Downstream	20.4	31.01	25.35	24.82	27.94	28.74	21.73	23.25

Time (Date)

Figure 2. The Trend of Water Quality Index of the Klang River.

5 CONCLUSIONS

Relating to the current River of Life project implemented in the middle area of Klang River, whose objective is to reduce the pollution and increase the WQI, it can be concluded that the effort is deemed successful.

The key initiatives (KI) involved in the River of Life project are upgrading the existing sewerage facilities and expanding the existing regional sewerage treatment plants; installing wastewater treatment plants (at five wet markets); utilizing retention ponds to remove pollutants from sewage and sludge; relocating squatters to reduce sewage, sludge and rubbish in the river; and implementing drainage and storm water management master plan to upgrade the drainage systems. This on-going KI shows that the WQI could be increased from 54% to 66%, which still maintains the water quality in Class III. To achieve the Class IIB quality, further works are still required by upgrading two regionals' STPs: Bunus and Jinjang. This research recommends the new BOD standard which are 7.5, COD = 50, TSS = 50 & NH_3N = 2. From this, 79.7% of WQI can be achieved.

ACKNOWLEDGMENTS

This research is funded by University Teknologi MARA, Shah Alam, Selangor. The authors would like to thank the technicians and staff for their involvements in this project.

REFERENCES

DOE (2013). *Malaysia Environmental Quality Report.* Department of Environment Malaysia.

Hossain, M.A., Sujaul, I.M. & Nasly, M.A. (2013). Water Quality Index: An Indicator of Surface Water Pollution in Eastern Part of Peninsular Malaysia. *Research Journal of Recent Sciences*, 2(10), 10–17.

Malaysian River of Life, MyROL. (2012). *River of Life - Public Outreach Programme (ROL-POP) - NKEA greater KL/KV*. Available at: http://www.myrol.my/ (Accessed 13 February 2017).

PEMANDU (2014). *ETP Annual Report 2014*. Available at: http://etp.pemandu.gov.my/annualreport2014/ (Accessed 13 February 2017).

Proceedings of the 37th IAHR World Congress
August 13 – 18, 2017, Kuala Lumpur, Malaysia

APPLICATION OF HYDRAULIC ELEVATOR DAM IN WATER ECOLOGICAL CIVILIZATION CONSTRUCTION OF DUNHUA CITY

CHEN YANYU[1], ZHAO YUEFEN[2] , WU HAITAO[3], LIU JIE[4], GENG YEHAN[5] & WANG HONGBO[6]

[1,2,4,5] China Institute of Water Resources and Hydropower Research, Beijing, China,
[3,6] Water Conservancy Bureau of Dunhua City, Jilin, China,
zhao801030@163.com; imex-b@iwhr.com; 26021925@qq.com

ABSTRACT

Based on a moveable weir project in the water ecological civilization construction of Dunhua City in Northeast China Region, this paper compares and analyzes the features, advantages and disadvantages of 4 common types of moveable dams: hydraulic elevator dam, bottom shaft driven steel gate, fix bar locked hydraulic elevator dam and gas shield dam based on the hydrological and geological status of Mudan River. From this study, it is found that the hydraulic elevator dam (HED) is the most preferred dam type. This paper also summarizes major design parameters and the actual construction effect of the project. The project demonstrates that HED is safe on both metal structure and control system after 2 years of overwinter operation, and hence puts forward the new idea that HED is a suitable moveable dam for retaining icy water without deicing treatment and is applicable for the hilly or urban river where the flood rises quickly.

Keywords: Hydraulic elevator dam; icy water retaining; unpowered dam dropping; water ecological civilization construction; landscape.

1 PROJECT OVERVIEW

1.1 Project background

Mudan River Landscape Water Conservancy Weir Project is located in the upstream of Mudan River in Dunhua City in Jilin Province in Northeast China Region (Figure 1). To carry out “Cascade Development Planning of Mudan River” (2007) and “Yanbian water ecological civilization city pilot program” (2014), three moveable weirs/dams, namely Liudingshan, Shuangsheng, Aodong, are proposed to be constructed with icy water retaining functions in the segment from 100m of the upper reaches of No.05 Bridge to Aodong Industrial Park along the river, which, together with existing dams 1 # and 2 # will form 5 continuous year-round lake landscapes to make the urban surroundings more beautiful. Since the project conducts as a pilot ecological civilization construction in Dunhua city of Yanbian antonymous region which is in the National Pilot City List, a modern ecological water conservancy design concept should be implemented including water security, water environment, water landscape, water culture, water economy and water management, to make it as an elite work in water ecological civilization construction works of the city by means of the special organically combined design on functional dam and its shape, artificial waterfall, waterwheel, fish way and other elements.

1.2 Project profile

Its watershed locates in a temperate continental monsoon climate zone in the North Temperate Zone. The temperature difference between winter and summer is large with the icily period lasting up to 4 months (mid-November to late March next year). The extreme low temperature is - 38.3℃ (January 4, 1970). The annual average precipitation is 633.2mm and unevenly distributed during the year, being mainly concentrated in June to September with rainfall accounting for 73.6% of annual precipitation. The average annual wind speed is 3.10m/s with the maximum average wind speed of 16.8m/s. The maximum average wind speed is 11.4m/s in flood season (July to September). 20-year flood peak discharge is 1060m^3/s and 50-year is 1480m^3/s. All the three dams are in the same landform unit with the strata structure being basically the same. Reservoir area siltation and bank collapse problems are not significant, but there are other problems such as certain degrees of immersion and leakage.

According to China Standard of GB50201-94, SL252-2000 and GB50286－2013, Weir project marks in Ⅳ grade, and main structures mark in 4 class. The design flood standard is 20-year flood for error-free operation period, 50-year flood for checked period, and 5-year in construction period. The project includes three moveable dams, namely Liudingshan, Shuangsheng, Aodong, and the width is 188m, 212m and 56m, respectively with the same height of 2m. Each weir is composed of a moveable weir, control room, apron,

  ISSN 1562-6865 (Online) - ISSN 1063-7710 (Print)

embankment, sightseen platform, fish way etc.

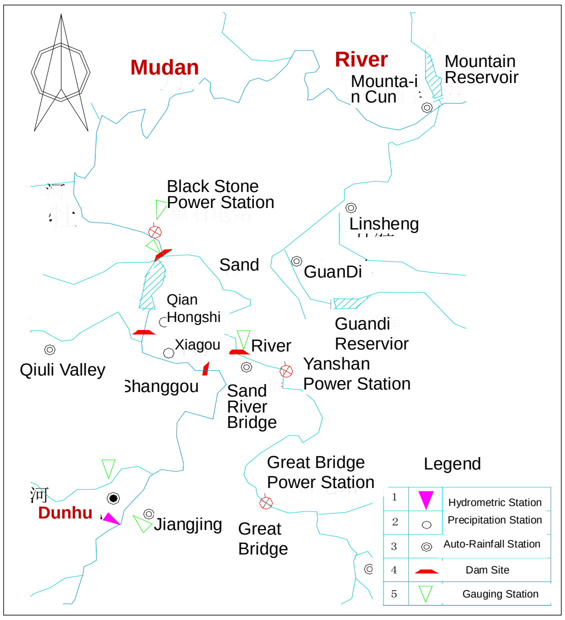

Figure 1. Location map of the proposed Liudingshan, Shuangsheng, Aodong dam site.

2 APPLICABILITY ANALYSES ON DAM TYPE SCHEMES

According to the general requirements and objectives of the construction of water ecological civilization in Dunhua City, 4 common types of moveable dams were considered in the project which was maturely applied at home and abroad: hydraulic elevator dam (HED), bottom shaft driven steel dam (BSD-SD), fix bar locked hydraulic elevator dam (FBL-HED) and gas shield dam (GSD). Typical project photos of the 4 types of moveable dams are shown in Figure 2. After reasonable designs, these 4 types of dams basically meet the project requirements, but have their own performance characteristics in this project. After considering the river nature feature and project construction objectives, technical characteristics in flood safety, landscape and winter operation, operation and maintenance and investment were comprehensively analyzed to optimize a preferred dam type suitable for this project, and as a reference for similar projects design and construction.

Hydraulic elevator dam

Bottom shaft driven steel dam

Fix bar locked hydraulic elevator dam

Gas shield dam

Figure 2. Typical project photos of 4 types of moveable dams.

2.1 Flood safety

Due to the river regulation parts in the Dunhua urban area, the width of the river has been basically defined. For the purpose of not affecting the original river flood safety, the selected dam should not reduce the original river section. The selected 4 types of floodgates are falling down and sticking to the river bed in the flood season, so the gate structure does not affect the river flood. But for BSD-SD, at least three additional engine rooms must lie in the river and each is about 3 meters wide in vertical of water direction and hence, cause potential adverse effects on flood safety and water flow patterns in flood season. The complex operation and maintenance of the in-river engine room should also be carefully considered in design period. The other 3 types of dam may have no middle pier and no wide engine room in the river.

As the flood of urban river is related with the safety of life and property of urban residents, the function of dam dropping safely and quickly in the flood season is preferred and essential. In FBL-HED, two sets of linkage hydraulic system are used in control, and in which the master cylinder provides the support force and the auxiliary cylinder renders assistance in locking and unlocking the fixed rod. Dam-lowering procedures for FBO-HED is complicated and time-consuming, it must push the master cylinder to the maximum stroke to relieve the thrust of fixed support rod on the slot, and then operate the auxiliary hydraulic cylinder below the slot reach out to the top and hold up the fixed support rod out of the slot, and then retract the master cylinder to put down the gate, and the fixed support rod is slid out of the slot and along the slide way. This unlocking procedure might be affected by the crest over flow, high downstream water level, freezing and other factors, therefore the operation process of dam lowering is time-consuming and unlocking reliability is restricted. Unlocking ahead of the flood season can solve the problem, but Mudan River faces spring icy floods, autumn floods and major floods, so it requires frequent operations of dam-lowering and cumbersome management.

HED and GSD combine their own structural characteristics, optimize the design in hydraulic or air charge and discharge system, and possess functions of unpowered dam lowering and one-key dam lowering to effectively protect flood safety and facilitate daily management. Even in case of excessive flood and without power source at the site, the unpowered dam-lowering function can enable the key components in the manually operated hydraulic system to realize a concurrent downing of all the gates and the lowering rate to be adjustable. If the power is guaranteed and the remote control system is configured, one-key lowering of the dam can easily be achieved. This feature of 2 dam type is suitable for urban rivers with the rapid rise and fall of the flood as well as remote mountainous areas with power shortage in addition to this project.

2.2 Ice-period water storage

According to the Standard GBT 50662-2011, for the gate retaining water in icy winter, it should maintain a certain area without frozen between the gates and ice cover; it means the gate should not bear static ice pressure. The project requires water storage in icy winter without de-icing method, while local stable frozen period should be about 131 days, and the average annual river center ice and shore ice thickness are both 0.80m. Static ice pressure is as large as 215kN/m for 0.8m thickness ice thermal expansion referring to the standard, and the pressure causes the deflection and stress increasing fast in partial area of the gate since for the 4 types of dam which own the same feature: the gate rotates around its bottom shaft.

In the event of no de-icing methods in upstream and downstream of the weir for blocking ice cover, these 4 types of dams have the following problems, respectively: In BSD-SD, due to the use of integrated panel structure, ice pressure is quite beyond the capacity of ordinary designed steel dam structure without deicing facilities; and the dam should be unlocked in water storage in icy winter, so to a certain extent this can ease the ice pressure and avoid damaging the panel structure. But for FBL-HED, the master cylinder is slender, and the downstream icing is easy to bend the cylinder and the fixed support rod. The cylinder trapped in the pit is vulnerable to freezing and cannot be operated. There is a problem of floating ice overflowing and directly striking at the piston-rods in ice flood period. GSD combines steel plates and rubber bag and can take full advantage of the flexibility of the airbag to ease the ice pressure, but ice cover may damage airbags and its restraining belt. HED uses a large diameter and short stroke hydraulic cylinder for support with the base floor of low-step structure easing the adverse effect of ice on the cylinder; the hydraulic control system sets the special oil circuit for ice-blocking operation. Through the linkage control of the relief valve and its electrical feedback system, it can release over-pressure caused by ice expansion, and then let the gate slightly back to the top for regular ice breaking automatically to break ice cover near the gate, and to eliminate the potential damage by gradually increased static ice pressure to metal structure. Water leakage or cicles hanging sometimes can be observed from water stop due to it might be partially broken or the gates might be tiny and not stand in a line for HED or FBL-HED in icy water retaining. So it is recommended to use BSD-SD (unlocked) and HED for icy water retaining without deicing facilities. For example, the existing rebuilt 1 # and 2 # HED from rubber dam in Mudan River, ice lakes were formed successfully in winter of 2014 and 2015 for the trial ice cover retaining below the design water level, and its previous rubber dam never works out in winter.

2.3 Landscape upgrading

In order to meet the goal of water ecological city construction in this project, the selected dam type should be unique in dam outline shape, special artificial waterfall, and should be combined with other water conservancy landscape elements organically. In the 4 proposed dam types, HED, BSD-SD and GSD mostly adopt steel panel and have large space in customized design in panel shape and waterfall pattern, thus the rational design can meet the needs of the water conservancy landscape. But for FBL-HED, the panel should upgrade to metal structure in order to get a better landscaping effect, due to it commonly uses reinforced concrete panel which is thin-walled structure and poor to freeze-thawing resistance.

2.4 Floating debris and sediment

This project is located in the upper reaches of Mudan River with the forest coverage rate of 87% and more floating debris in the flood season. During the flood season, all the gates of 4 dam type should be lowered. But for floating debris discharge, both HED and BSD-HED get operation done easily, and partial water discharge can let floating debris drift away. HED is more favorable since it has the benefit for protecting its cylinder compared to BSD-HED due to its structural feature: the floating debris, ice and sediment never fall on the cylinder directly. The floating debris might impact the engine room in river for BSD-SD, hence optimizing the shape of the engine room in the upstream should be taken into consideration. GSD performs better than others since it has airbags at the back as the bumper.

According to sediment observation data in Dunhua Hydrological Station, the annual sediment load is 142,000 tons / year. The problem of siltation in the reservoir area after the flood season is not significant, so it is not the key factor in the dam type analysis.

2.5 Investment comparison

BSD-SD needs to be configured with the engine room in the river and conditionally configured with the repair corridor which features a large amount of civil construction and the floor structure being complex; its investment in metal, mechanical and electrical equipment is higher than the other dams. Civil work is simple with a less investment for GSD, but it has the highest cost of investment in equipment except all of the equipment is localized. From the investment point of view, the total investment of BSD-SD and GSD (imported) are high, while HED and FBL-HED are low. The investment comparison in civil construction and metal, mechanical & electrical equipment is shown in Table 1.

Table 1. Estimate comparison on water conservancy landscape dam project in Mudan River, Dunhua City.

Dam type	Dam construction cost / 10 thousand CNY	Metal structure and mechanical and electrical equipment cost / 10 thousand CNY	Construction temporary project cost / 10 thousand CNY	Independent cost / 10 thousand CNY	Basic reserve fee / 10 thousand CNY	Total / 10 thousand CNY
BSD-SD	998.16	2498.07	318.84	438.73	212.69	4466.49
GSD	650.21	3046.43	203.40	448.50	217.43	4565.96
FBL-HED	780.25	1035.78	219.89	234.13	113.50	2383.56
HED	702.93	1218.57	219.89	242.68	119.21	2503.28

In a word, HED and GSD have better performance in flood safety; BSD-SD and HED are better in water storage in ice period. BSD-SD, HED, and GSD have a larger space in landscape upgrading. HED is the best one in floating debris removal. HED and FBL-HED are better in cost saving. Comprehensive comparison of the key factors leads to the conclusion: the landscape-type HED is selected.

3 PROJECT DESIGN

3.1 General design ideas

Dunhua City Government puts forward the general requirements of the pilot water ecological civilization construction project: Besides paying attention to increasing the urban water area, it should give full consideration to maintaining the river natural properties to display the City's water civilization results so forth. This project should be an elite work to integrate water storage, landscape, ecology, leisure and entertainment as a whole. The overall dam type adopts an organic combination of automatic steel dam, water wheel, fish way and abstract architecture so forth to form a new combination at home and abroad as an innovation. Design innovation points summarized as follow, at the same time as a reference for hydraulic designers to open their mind:

(1) The water spoiler is set at the top of the steel dam weir. While preventing resonance and increasing safety performance, it can generate a water level to create the effect of water spray or waterfall. The viewing platform is set in both sides so as to let the water near the water gate be more beautiful. Retained ice cover make the 3 cascaded ice lakes as huge and long ice rinks or skiing resorts, which explore local tourism resources in winter low season and enhancing the vitality of the city;
(2) Two fish migration channels (0.8m wide and 0.6m high) are set combined with the pier, showing the care of nature and the beauty of harmonious coexistence;
(3) A water wheel of 6m in diameter is installed in the upstream of these two fish channels, respectively. Natural water flow is used to let the water wheel rotate, showing the beauty of primitive water ecology in the City;
(4) In Liudingshan landscape HED, the water conservancy landscape dam adopts the 3-bend type for the following reasons: this dam in principle should be vertical to the river and No.05 Bridge is obliquely intersected with the river. This type can let the dam be partially vertical to the river and parallel to No.05 Bridge so showing the beauty of geometric curves (layout plan Figure 3);
(5) The electromechanical control room adopts a steel structure with its shape being alike an abstract ship, ocean spray and so forth as a symbol on the City's economic and social harmonious development.

3.2 Main architectural designs

The total width of HED should be line with the width of the river in principal to make sure the flood discharge capacity of HED site meet the demand for the original river. After comprehensively consider dam site topographic condition, except the dam axis line of Liudingshan HED adopting the 3 folded-line layout (layout in Figure 3, and cross section in Figure 4), Shuangsheng and Aodong HED are basically similar in layout and main architectures stand in a line.

Take Liudingshan HED as an example to describe main civil works, metal structure, hydraulic and electric control system, while Shuangsheng and Aodong Dam are not described here since others are basically similar in layout and structure. Liudingshan HED is configured from the right bank to the left bank with sequentially the right bank retaining wall and the viewing platform section, the dam section, the left bank retaining wall and the viewing platform section.

It has a total width of 188m and is composed of two piers and three spans; the design water lever is 2m. The span is 56m long on both sides and 72m on the middle; each pier is 2m wide. The open-type broad-crest weir without ramp is used in the base floor and weir crest elevation is 496.0m, and 6m is along the direction of the water flow. The foundation of base floor is placed in the rock bed. A cut-off trench placed 0.5m wide and 0.5m deep in front and back of the base floor. The middle pier uses an independent reinforced concrete structure and is 6.0m long and 2.0m wide. Crest elevation of the middle pier is 498.2m and its base depth is the same as base floor depth. In order to achieve the aesthetic effect and ecological protection requirements, the fish way is set in the pier and the water wheel in the upper. Concrete design code is C25F200W4. Calculation results show no need for a stilling basin. However, in order to ensure safety, the lead wire cage apron is set at the downstream of the base floor, which is 6.0m long and 0.5m thick.

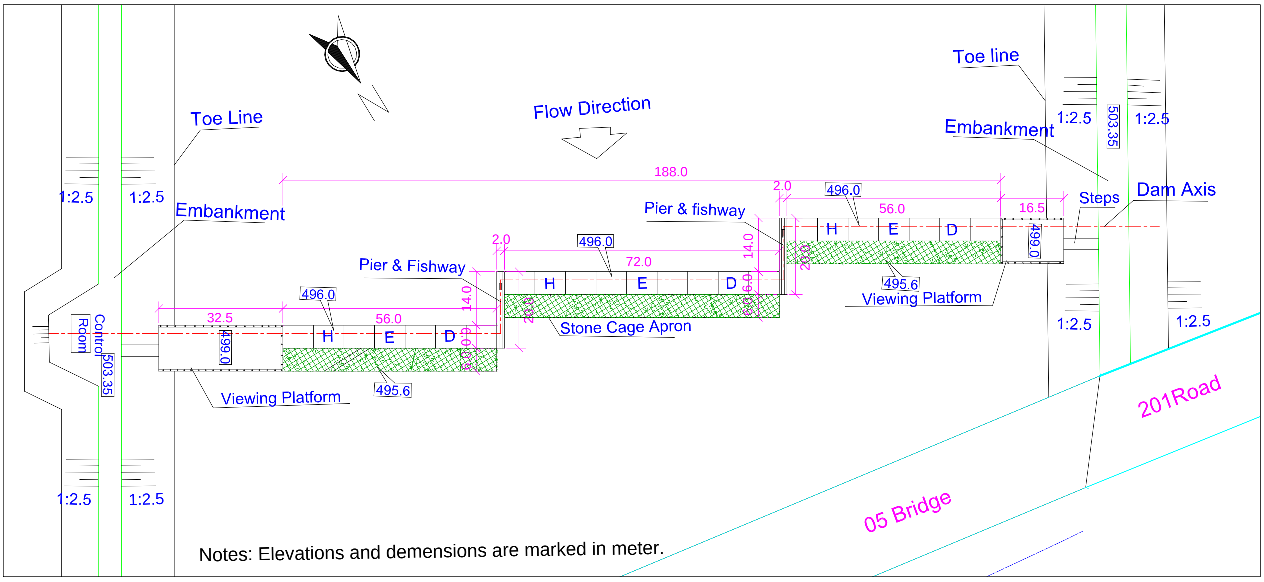

Figure 3. Liudingshan landscape HED layout plan.

 ©2017, IAHR. Used with permission / ISSN 1562-6865 (Online) - ISSN 1063-7710 (Print)

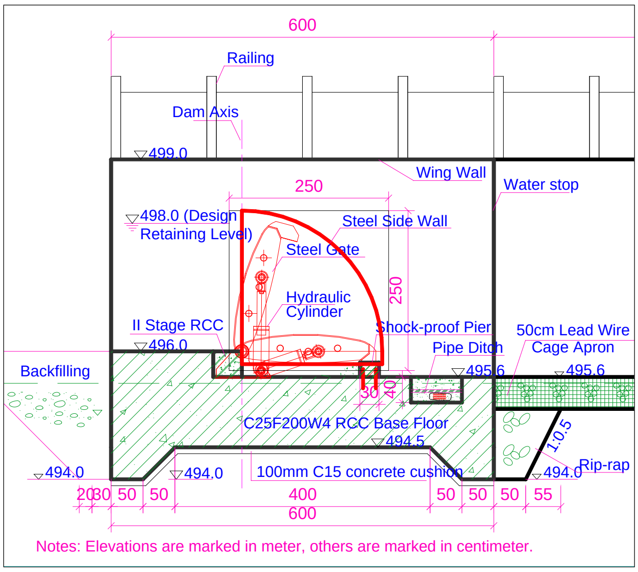

Figure 4. Shuangsheng HED longitudinal profile.

3.3 Metal structure design

Total clear width of Liudingshang HED is 188m, separated into 3 spans, and there are 23 fans with 7 fans at both side and 9 spans in the middle span. The entire HED gate requires hydraulic cylinders operate in hydrodynamic water pressure to adjust the upstream water lever at any height. Each gate size is 8m wide×2m high. Design retaining water level is 2m and maximum design overflow level is 2.3m. It is consisted of Q345C wing-shaped low-temperature manganese steel panels; front plate thickness is 16mm and no back plate. Gates are designed and manufactured in multi-stringer frame structure, and the water side of the panel is configured with the arc-shaped rib slab for the anti-collision, and the top configured with the water spoiler device to ease the negative pressure in the land side and create different waterfall pattern. The hinge adopts self-lubricating cylindrical bearing, and its embedded parts are placed independently and poured with base floor at a time, while some parts like the upstream of the bottom hinge, oil pipe ditch, shock-proof pier, side wall steel plate are poured after HED gates are installed at site. The contact zone of the gate and retaining wall are configured with the steel plate covering as a whole to keep water stop and always play its role even the side gates are opened to any extent.

3.4 Mechanical and electrical design

Hydraulic control system is mainly composed of hydraulic cylinders, oil pipes, assembled hydraulic pump station etc. Each gate is hold by 2 plunger type hydraulic hoists, and each hoist render 500 kN thrust at the working pressure of 16MPa. The diameter of the piston rod is 200mm, operation stroke is around 570mm, rated and maximum working hydraulic pressure is 16 and 25MPa, respectively. Both ends of the hoist are pin-connected to the gate and the hinged support, respectively. There are totally 48 pieces hoists for the project and they share one assembled hydraulic pump station and two sets of valve brackets. Rated displacement of oil pump is 45l/min and matched motor rated power is 30KW for it needs to lift up 5 HED gates (10 hoists) simultaneously, and 2 sets of oil pumps and motors are mutual backups.

Table 2. Main parameters of hydraulic control system.

No.	Item	Parameters	Notes
1	Rated hoist thrust	2×500 kN	Working pressure16Mpa
2	Working operation stroke	0.57m	
3	Maximum operation stroke	0.57m	
4	Rated/max working hydraulic pressure	16/25 Mpa	
5	Piston rod speed of hoist for gate lifting	0.9 m/min	Adjustable
6	Operation conditions	Operate in hydrodynamic water pressure, locking at any opening degree	
7	Type of hoist	Single-action plunger type hydraulic hoist	
8	Rated displacement of oil pump	45 l/min	1 for spare
9	Rated power of motor	30 KW	1 for spare

Four types of alternate operation modes, namely manual operated valves system, PLC control system, local computer control and remote control system, are installed for easily regulating the gate manually or programmed, and mobile phone real time monitor system is developed based on EZVIZ Studio video surveillance software.

4 SUMMARY AND DISCUSSIONS ON PROJECT IMPLEMENTATION EFFECTS

4.1 High integration in landscape HED to ensure flood safety

After the implementation of the project, the cascade landscape HED can realize the following leading functions: any degree of opening for water storage, quick discharge of sand and floating debris, unpowered dam lowering during the flood peak period, water storage without de-icing treatment in the ice period, and artificial waterfall the like. It widens a range of multiple functions, simplifies the operation and management of sluices. Equipped with remote monitoring and control system, it can carry out real-time monitoring, overflow data monitoring, cascaded flood adjustments, off-site gate operation so forth, thereby improving the level of modern water management.

Take Aodong HED as an example (Figure 5), it only takes 2.5 min to lower the 7 gates one by one, and only 40 seconds to put down all the gates simultaneously without any electric power or generator, indicating HED is extremely applicable to the river in the urban or mountainous area where the flood rises or falls quickly, greatly enhancing the safety of emergency control of floods. The maximum overflow depth on top of the gate is about 1.3 m in theory if the hoists work at the maximum operation pressure in the short term, showing HED has the potential to dynamically reduce the risk on the gate, the river and even the surroundings by the steep flood.

Figure 5. Gate lowering of Aodong hydraulic elevator dam.

4.2 Innovative solution for retaining icy water without deicing treatment

The gates retain icy water at the design level of 2m, 1m, and 0m during winter operation without deicing treatment for comparing and testing the effect of ice water storage. After 2~3 years overwinter operation, gate frames and their hoists all withstand the tough winter and ice safely and nearly no obvious damage on the HED parts except little rubber water stops are abraded. It is proven that the new design idea of “giving in to ice and forcing up in time” in hydraulic and electric control system is well performed in the three states mentioned above. And from the site observation, there is a huge and obvious cracked ice strip about 2~4m wide in front of the gates retaining at 1m high. It is probably because the half-drop gates form a small inclination angle, which is conducive to ice crawling along the gate, and the formation of the ice block breaking zone reduces the ice expansion pressure at the gate. For the river management department who encounter the problems in the icy water storage without deicing in the ice period, or a huge ice flood occurs, it is recommended to implement the ice-control program based on reduction of dam height, thus decreasing the operation risk of the project.

4.3 Significant landscape environment effects and economic benefits

The cascade landscaping dam organically combines the modern sluice, waterwheel, fish way, waterscape and abstract buildings as a whole to form a water ecological elite work which integrates water / ice storage, landscape, ecology, recreation and entertainment. After the implementation of the project, combined with existing 1 # and 2 # dam, Mudan River in the urban section can produce continuous water surface and form a larger area of artificial lake so achieving the following results: beautifying the environment, developing the tourism, improving the urban microclimate and the groundwater level the like. Moreover, in the winter, it can form a vast ice rink and snow pack, which plays a promotional role in winter tourism development and economic prosperity in Dunhua City.

After 2 years of overwinter operation, it has proven that HED operates safely and is reliable and no additional cost is required for ice storage, thus greatly reducing the management expenses in the ice period. A broad ice/snow area of about 900,000m^2 is formed, and it may be used as ice rinks in winter and for the development of snow recreation projects. As far as the site is concerned, the average annual rental benefits will be no less than RMB 500,000 (see Figure 6).

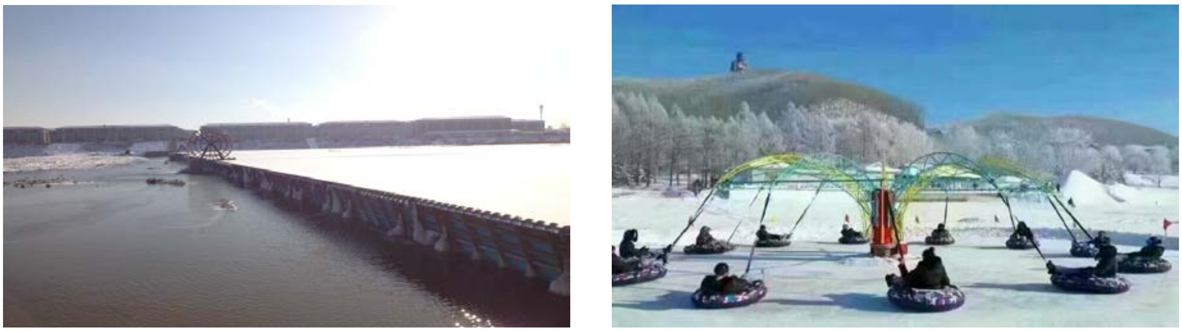

Figure 6. Shuangsheng HED retaining icy water without deicing treatment and typical ice recreation photos.

5 CONCLUSIONS

Hydraulic elevator dam has outstanding safety insurance, unique ice water retaining and various landscape effects; hence it has been promoted and applied at home and abroad quickly in recent years. As there are a lot of problems in water storage of rivers in winter in the north of China, the authors provide a new idea for the design of moveable dam and its winter control concept on icy water retaining of this kind of river, and analyzes the applicability of hydraulic elevator dam, bottom shafted driven steel dam, fixed bar locked hydraulic elevator dam and gas shield dam on the basis of the features of Mudan River. According to the design and practice in the past two years, it shows that hydraulic elevator dam has given full play to the advantages of the technology, especially reflected on the technical effects like operation without de-icing in the ice period and non-power dam lowering in the project.

REFERENCES

Chen, Y. (2015). Condition Analysis on Pilot Water Ecological Civilization Construction of Yanbian Autonomous Region. *Heilongjiang Science & Technology Information*, 11, 216.

PRC Ministry of Construction (1994). Flood Control Standard [S]. GB50201-94.

PRC Minister of Water Resources (2000). Standard for Classification and Flood Control of Water Resources and Hydroelectric Project [S]. SL252-2000.

PRC Ministry of Construction (2013). Code for Design of Levee Project [S]. GB50286-2013.

Wang, Y.H. & Huang, W. (2010). Application of the Fix Bar Lock Hydraulic Elevator Dam in the comprehensive Treatment of the Course of Shalihe River. *Northeast Water Resources and Hydropower,* 3, 38.

Qu, Z.M. (2016). Application of the Hydraulic Elevator Dam in Project Treatment for the Urban Section of Jiangshui River. *Shandong Water Resources*, 5, 40.

Rao, H.P. & Zhu, S.S. (2015). Comparative Study of the Fix Bar Locked Hydraulic Dam and the Traditional Moveable Dam. *Northwest Water Resources and Hydropower*, 36(12), 23-26.

Wang, Z.Y. (2013). Application of the Hydraulic Elevator Dam in the Urban Landscape Construction. *Northeast Water Resources and Hydropower*, 6, 4-6.

Zhu, S.S. (2015). An Arch Landscape Hydraulic Elevator Dam: China, 204080755U[P]. 2015-01-07.

Beijing IWHR Corporation (2013). Integrated Hydraulic Elevator Dam: China, 201320070453.2[P].2013-08-14.

PRC Ministry of Construction (2011). Code for Design of Hydraulic Structures against Ice and Freezing Action[S]. GBT 50662-2011.

Beijing IWHR Corporation (2015). Hydraulic Control System of Hydraulic Elevator Dam Functioned with Ice Pressure Releasing: China, 201520888004.8[P]. 2016-04-13.

Proceedings of the 37th IAHR World Congress
August 13 – 18, 2017, Kuala Lumpur, Malaysia

IMPACT OF INNER-BANK VEGETATION ON THE MEAN FLOW AND TURBULENCE STATISTICS IN A CURVED CHANNEL

SEONMIN LEE(1) & SUNG-UK CHOI(2)

(1,2) School of Civil and Environmental Engineering, Yonsei University, Republic of Korea
lee.sm@yonsei.ac.kr; schoi@yonsei.ac.kr

ABSTRACT

Flows in a curved-channel are highly complicated. In general, due to the centrifugal force, a converging flow occurs along the outer part of the bend with strengthened secondary flows. On the other hand, sediment deposition takes place on the inner part of the bend. This provides a higher chance of presence of vegetation in the inner part of the channel bend. This study investigates numerically the impact of inner-bank vegetation on the mean flow and turbulence statistics in a curved channel. For this purpose, the Reynolds-Averaged Navier-Stokes (RANS) equations are solved with the k-ω SST model. The proposed model is applied to a flat-bed laboratory experiment with a 60° curved channel by Tominaga et al. (1998). Simulation results reveal that the inner bank vegetation changes the mean flow significantly. That is, it is found that the inner bank vegetation in a curved channel moves the maximum velocity towards the outer bank and restricts the region of secondary flows. Turbulence statistics are also found to be affected by the presence of the inner-bank vegetation.

Keywords: Vegetation; channel bend; mean flow; turbulence statistics; k-ω SST model.

1 INTRODUCTION

The flow in a curved channel is generally complicated. The centrifugal force makes the flow accelerate along the outer bank and strengthens the secondary flows. For such flows, the channel curvature is a key factor for the flow establishment.

This feature of the flow results in the morphological change in the curved channel, i.e., bed erosion and sediment deposition along the outer and inner banks of the bend, respectively. The morphological change provides a higher chance that vegetation may intrude on the inner side of the curved channel. The intrusion of vegetation on the inner part tends to modify the flow structure in the curved channel. Then, the pattern of sediment transport and channel morphology will change accordingly. The channel conveyance will also be affected. However, understanding of the interaction between flow, vegetation, sediment transport and morphological change in the curved channel is quite limited.

This study attempts to investigate numerically the impact of inner-bank vegetation on the mean flow and turbulence statistics in a curved channel. For this, the Reynolds-Averaged Navier-Stokes (RANS) equations are solved with the k-ω SST model. The finite volume method is used to solve the RANS equations in the curvilinear coordinate system. For the velocity-pressure coupling, projection method is used.

The proposed numerical model is applied to a flat bed laboratory experiment with a 60° curved channel by Tominaga et al. (1998). Simulation results reveal that the inner bank vegetation changes the mean flow significantly. That is, it is found that the inner bank vegetation in a curved channel moves the maximum velocity towards the outer bank and restricts the region of secondary flows. Turbulence statistics are also found to be affected by the presence of the inner-bank vegetation.

2 GOVERNING EQUATIONS

For computations of vegetated open-channel flows, the RANS equations were solved numerically. The continuity and momentum equations for the vegetated flow are given by, respectively,

$$\frac{\partial \bar{u}_i}{\partial x_i} = 0 \qquad [1]$$

$$\bar{u}_j \frac{\partial \bar{u}_i}{\partial x_j} = -\frac{1}{\rho}\frac{\partial \bar{p}}{\partial x_i} + \frac{\partial}{\partial x_j}\left(\nu \frac{\partial \bar{u}_i}{\partial x_j} - \overline{u_i' u_j'}\right) + g_i - \frac{1}{\rho} f_i \qquad [2]$$

where $\bar{u}_i$ is the mean velocity in the i-direction, ρ is the water density, $\bar{p}$ is the mean pressure, ν is the kinematic viscosity, g_i is the gravitational acceleration, f_i is the drag force per mass due to vegetation, and

$-\overline{u_i' u_j'}$ is the Reynolds stress. In the present study, the k-ω SST model proposed by Menter (1993) was used for the turbulence closure. The k-ω SST model computes the Reynolds stress with the help of the relation such as

$$-\overline{u_i' u_j'} = \nu_t \left(\frac{\partial \bar{u}_i}{\partial x_j} + \frac{\partial \bar{u}_j}{\partial x_i} \right) - \frac{2}{3}\delta_{ij} k \qquad [3]$$

where k is the turbulent kinetic energy and ν_t is the eddy viscosity. In Eq. [2], the drag force per mass due to vegetation (f_i) is expressed as

$$f_i = \frac{1}{2} C_D a \rho \bar{u}_i \sqrt{\bar{u}_j \bar{u}_j} \qquad [4]$$

where C_D is the bulk drag coefficient and a is the vegetation density [L^{-1}]. The drag coefficient is estimated by the following relationship reported by Dunn (1996):

$$\frac{C_D}{\bar{C}_{DA}} = 0.74 + 3.51\left(\frac{z}{h}\right) - 6.41\left(\frac{z}{h}\right)^2 + 2.72\left(\frac{z}{h}\right)^3 \qquad [5]$$

where $\bar{C}_{DA}$ is the depth-averaged value of the drag coefficient. Dunn (1996) proposed $\bar{C}_{DA}$= 1.13 based on laboratory experiments.

3 TURBULENCE MODEL AND NUMERICAL SOLUTION

For the turbulence kinetic energy k and its specific dissipation rate ωin Eq.[3], the following k and ω transport equations are solved, respectively:

$$\bar{u}_j \frac{\partial k}{\partial x_j} = \frac{\partial}{\partial x_j}\left(\frac{\nu_t}{\sigma_k} \frac{\partial k}{\partial x_j} \right) + P - \beta^* \omega k \qquad [6]$$

$$\bar{u}_j \frac{\partial \omega}{\partial x_j} = \frac{\partial}{\partial x_j}\left(\frac{\nu_t}{\sigma_\omega} \frac{\partial \omega}{\partial x_j} \right) + \alpha S^2 - \beta \omega^2 + 2\left(1 - F_1\right)\sigma_{\omega 2} \frac{1}{\omega} \frac{\partial k}{\partial x_i} \frac{\partial \omega}{\partial x_i} \qquad [7]$$

where ν_t is eddy viscosity, P is the production of k, and α, β, β^*, σ_k, σ_ω, $\sigma_{\omega 2}$, and F_1 are the model parameters proposed by Menter (1993).

The finite volume method was used to discretize the RANS equations in the non-staggered curvilinear coordinate system. In the present study, the hybrid scheme was used for differencing the convection and diffusion terms. For the velocity-pressure coupling, projection method was used. The momentum interpolation method proposed by Rhie and Chow (1983) was used to eliminate numerical oscillations, known as checkerboard oscillations, caused by the use of the non-staggered grid. The strongly implicit procedure (SIP) by Stone (1968) was used to solve the discretized equations.

For the numerical solution, four types of boundary conditions are necessary. At the inlet, a fully-developed velocity profile from 2d numerical model was used. At the outlet, velocity and turbulence quantities were extrapolated from the interior. The rigid-lid approximation was used at the free surface. At the solid boundary, the wall-function approach was used.

4 CURVED-CHANNEL FLOW WITH INNER BANK VEGETATION

Figure 1 shows a 60° curved channel with inner-bank vegetation, used in the experiments of Tominaga et al. (1998).The total length of the channel was 17.2 m, consisting of 10.8 m and 3.6 m long straight channels before and after the bend. The radius of curvature of the curved part of the channel was 2.7 m. The inner-bank vegetation was a patch-type emergent vegetation, whose width was 1/4 of the total width of the channel. 3D velocity components were measured at four cross sections denoted in the figure. The flow condition and vegetation density are given in Table 1.

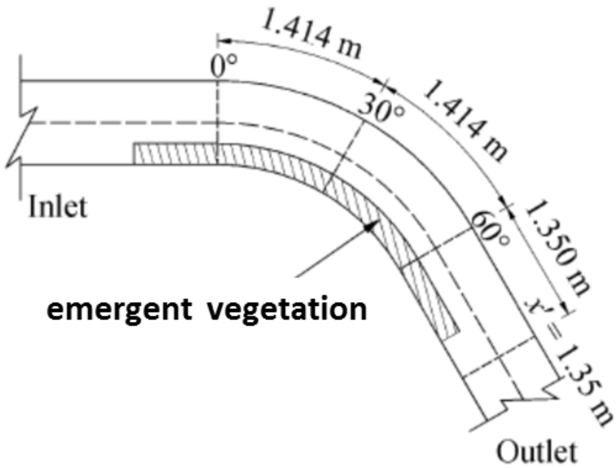

Figure 1. Curved channel with inner-bank vegetation of Tominaga et al.'s experiment.

Table 1. Conditions for Tominaga et al.'s (1998) experiment.

	Radius of curvature (m)	Channel width (m)	Discharge (m^3/s)	Depth (m)	Vegetation density (m^{-1})	Re	Fr
V-2	2.7	0.9	0.04	0.15	2.0	33,000	0.24

5 SIMULATION RESULTS

Figure 2 shows the lateral distribution of the depth-averaged streamwise velocity at two cross sections. The computed profile was compared with measured data in the figure. It can be seen that the distribution of the computed velocity is in good agreement with measured data. The streamwise velocity appears to be reduced significantly by the vegetation patch. That is, the abrupt change in the streamwise velocity indicates the presence of the shear layer near the interface between the vegetated and non-vegetated zones. The velocity difference is more pronounced at 60° section, where the curved part ends in the channel. At that cross section, the flow is observed to accelerate along the outer part of the bend due to the centrifugal force. However, near the interface, the velocity gradient in the lateral direction decreases at the 60° section.

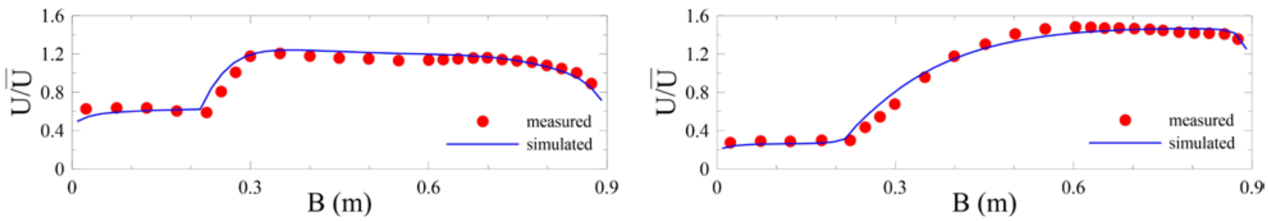

(a) at 0° cross section (b) at 60° cross section

Figure 2. Depth-averaged streamwise velocity.

Figure 3 shows the comparison of computed and measured streamwise velocity at 60° section. In general, the computed velocity agrees well with measured data. Interestingly, both contours show vertical isovels in the vicinity of the shear layer, indicating that the velocity only changes in the lateral direction. However, in the computed result, the velocity dip, which is seen in the measured data, is not observed and the velocity maximum is located in a region quite close to the sidewall. In contrast, the measured data show the velocity maximum is slightly away from the outer part of the bend.

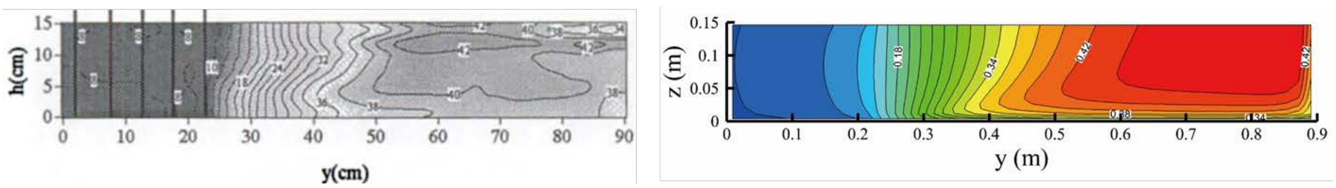

(a) measured velocity (b) computed velocity

Figure 3. Contour map of streamwise velocity at 60° section.

The secondary flows at 60° section are depicted in Figure 4, where measured and computed velocity vectors were compared. Both measured data and computed velocity vectors indicate that a vortex rotating in the clockwise direction is dominant in the non-vegetated region. A close look at the measured data reveals that an outer-bank cell, rotating in the counter-clockwise direction, is present in the region close to the outer part of the bend. However, the numerical model seems to fail to reproduce this outer-bank cell. This outer-bank cell is thought to contribute to determining the location of the velocity maximum as in Figure 3(a).

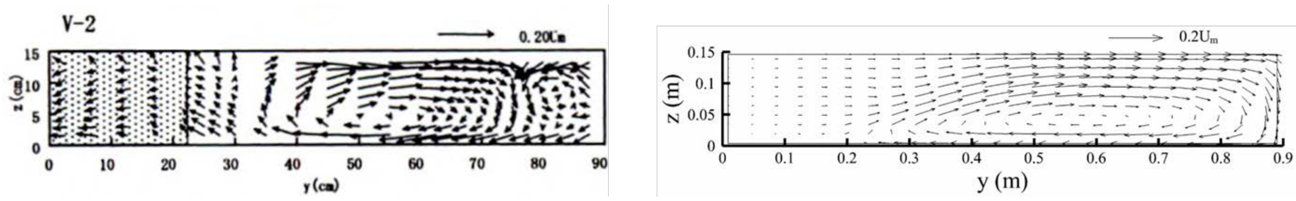

(a) measured velocity (b) computed velocity

Figure 4. Secondary flows at 60° section.

Figure 5 shows the lateral distribution of the depth-averaged streamwise velocity at two cross sections. The velocity distributions with and without inner-bank vegetation were compared in the figure. Without inner bank vegetation, the maximum velocity occurs in a region close to the inner bank in a 30° section. As the flow turns around the bend, this velocity maximum moves towards the outer bank as seen in 60° section. A similar trend is observed in the velocity with inner bank vegetation except for that the velocity maximum occurs in the non-vegetated zone.

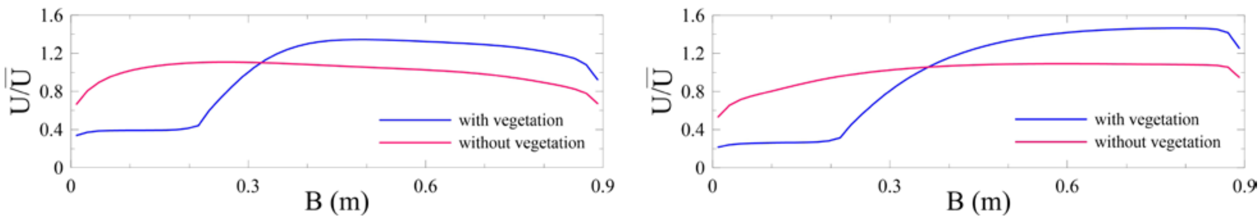

(a) at 30° cross section (b) at 60° cross section

Figure 5. Depth-averaged streamwise velocity with and without inner-bank vegetation.

Figure 6 shows the secondary flows (up) and y-component Reynolds stress (down) in 60° section. The computed results with and without inner-bank vegetation were compared in the figure. Regarding the secondary flows, both figures indicate a vortex rotating in the clockwise direction. However, the secondary flow with inner-bank vegetation is limited to the non-vegetated region. The inner-bank vegetation does not seem to affect seriously the intensity of the secondary flows. The distribution of y-component Reynolds stress shows a maximum near the interface for the flow with inner-bank vegetation, whereas the Reynolds stress does not change greatly for the flow without inner-bank vegetation. It is noticeable that the pattern of the Reynolds stress with inner bank vegetation can easily be told by the distribution of the streamwise mean velocity, see Figure 3.

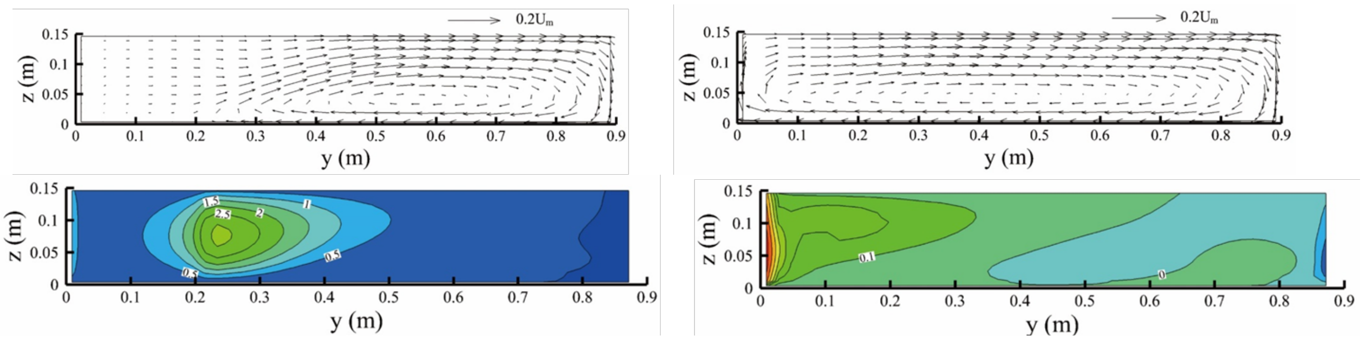

(a) with inner-bank vegetation (b) without inner-bank vegetation

Figure 6. Secondary flows and Reynolds stress with and without inner-bank vegetation.

6 CONCLUSIONS

This study investigates numerically the impact of inner-bank vegetation on the open-channel flow in a curved channel. The RANS equations are solved with the k-ω SST model. The numerical model is applied to Tominaga et al.'s (1998) experiments. The experiments use a 60° curved-channel with patch-type emergent vegetation whose width is 1/4 of the channel width.

The lateral profile of depth-averaged streamwise velocity indicates that the velocity decreases significantly due to the presence of inner-bank vegetation. Thus, a strong shear layer is generated near the interface between vegetated and non-vegetated zones. This is confirmed by the isovels from the distribution of the streamwise velocity. The comparisons between the computed results and measured data suggest that the numerical model successfully simulates the mean flow with inner-bank vegetation in a curved channel. However, the numerical model is not able to reproduce the location of the velocity maximum clearly and outer-bank cell, rotating in the counter-clockwise direction.

The two flows with and without inner-bank vegetation are compared. The comparisons indicate that a vortex, similar to the one generated in the plain open channel, is generated but the dominant region is quite limited to the non-vegetated zone. The lateral component of Reynolds stress is found to be high near the interface, indicating that the shear layer is responsible for the exchange between the two flow zones.

ACKNOWLEDGEMENTS

This work is supported by the National Research Foundation of Korea (NRF) grant funded by the Korean Government [NRF-2014R1A2A1A11054236].

REFERENCES

Dunn, C.J. (1996). Experimental Determination of Drag Coefficients in Open Channel with Simulated Vegetation, *M. Thesis*. University of Illinois, Urbana-Champaign, Urbana, IL.

Menter, F. (1993). Zonal Two Equation kw Turbulence Models for Aerodynamic Flows. *23rd Fluid Dynamics, Plasmadynamics and Lasers Conference*, 2906.

Rhie, C.M. & Chow, W.L. (1983). Numerical Study of the Turbulent Flow past an Airfoil with Trailing Edge Separation. *AIAA Journal*, 21(11), 1525-1532.

Stone, H.L. (1968). Iterative Solution of Implicit Approximations of Multidimensional Partial Differential Equations. *SIAM Journal on Numerical Analysis*, 5(3), 530-558.

Tominaga, A., Nagao, M. & Nezu, I. (1998). Effects of Vegetation on Flow Structures and Bed Profiles in Curved Open Channels. *Proceeding of 2nd International Symposium on Environmental Hydraulics*, Hon Kong, Balkema, 329-334.

Proceedings of the 37th IAHR World Congress
August 13 – 18, 2017, Kuala Lumpur, Malaysia

STUDY ON HYDRAULIC CHARACTERISTICS OF NON - UNIFORM FLOW IN THREE GORGES RESERVOIR

PENG ZHANG(1), SHENGFA YANG(2), JIANG HU(3), MI TIAN(4), SHUAISHUAI ZHANG(5), SICHEN TONG(6), XUELIAN LIU(7), YING SHEN(8) &TAO WANG(9)

(1,4,5)School of River & Ocean Engineering, Chongqing Jiaotong University,Chongqing, China,
zhangpengcquc@139.com;tm0519@163.com;zhangkang2002@126.com
(2,3,6,7,8) National Engineering Research Center for Inland Waterway Regulation (NERCIWR), Chongqing, China,
e-mailysf777@163.com;hujiang77@163.com; tongsichen@163.com;lxlian050@163.com; shenying@tju.edu.cn
(9) Changjiang Chongqing Waterway Engineering Bureau (CCWEB), Chongqing, China,
wangtao5234@163.com

ABSTRACT

Non-uniform flows are often encountered in Three Gorges Reservoir (TGR). When the storage level is at flood control level of 145m, the permanent backwater region is gradually decelerating flow, with the length of 524 km. Field measurements are conducted in the permanent backwater region in Three Gorges Reservoir. The flow instantaneous velocities are measured by using ADCP. Based on the theoretical and experimental analysis methods, this study investigates friction velocity, mean velocity distribution in non-uniform flows in permanent backwater region. Equations of friction velocity are derived by one dimensional open channel Saint - Venant equations. The theoretical results show that influence by the variation of water surface in non-uniform flows has resulted in relationship between friction velocity and the flow depth gradient. The theoretical results are in good agreement with field measurements data. The mean velocity profile in non-uniform flows flat with the increasing of $H/H0$ (where H0, as the uniform flow depth, which meets the Chezy Manning formula uniform flow, in the case of a certain discharge per unit width, roughness and slope of river bed condition).The relationship between slopes of log-law velocity profiles and $H/H0$ show a power function.

Keywords: Non-uniform flows; Three Gorges Reservoir (TGR); Saint-Venantequations; friction velocity; mean velocity profile.

1 INTRODUCTION

Known as the largest hydroelectric project in the world, the Three Gorges Dam (TGD) was constructed at Yichang with the height of 185 m and length of 2335 m (Zhao et al., 2000). When the storage level is at normal water level of 175m with five-year flood (61400m^3/s) in the Three Gorges Reservoir, terminal of backwater is located in Jiangjin district, Chongqing, 663 km away from the TGR. When the storage level is at flood control level of 145m, terminal of backwater is located in Changshou district, Chongqing, 524 km away from the TGR. Therefore, the permanent backwater region is gradually decelerating flow, with the length of 524 km. Knowledge of the flow structure is important for determining sediment transport, pollution control and flow resistance.

Over the past decades, the velocity distributions in steady and uniform flows were extensively investigated. However, only few studied experimentally the effect of backwater extents on velocity distributions, turbulence intensity and friction velocity. Cardoso et al. (1991) conducted laboratory experiments on the structure of spatially accelerating flows in a smooth open channel using a one-component hot-wire anemometer. The velocity distributions cannot be represented by the universal log-law and the turbulence intensity was decreased affected by accelerating flows. Kironoto and Graf (1995) measured velocity distributions in accelerating and decelerating non-uniform open-channel flows over a rough bed. Compared with the ones in uniform flow, the turbulence intensities increase in decelerating flow. They applied Coles' wake-law to describe the velocity in the outer region, whose wake strength depends on the pressure gradient parameter. However,the constant of integration in velocity profile is clearly independent of the pressure-gradient parameter (Song and Chiew, 2001). The von Kármán constant associated with non-uniform flows has an average of κ =0.26, which is lower than the classical value of 0.4 (Emadzadeh et al., 2010).

Only few investigated the bed shear stress and Reynolds-shear stress profiles of non-uniform flows.Song and Chiew (2001) measured the mean and turbulence characteristics in non-uniform flows using ADV. The Reynolds stress increase in decelerating flow, when compared with those in uniform flow. The Reynolds stress distribution is not linear in a decelerating flow. Yang (2009) illustrated the existence of an upward velocity component in decelerating flows and that the classical log-law is applicable if and only if the wall-normal velocity is zero and the existence of an upward velocity component in decelerating flows which is caused by the wake-function. Zhang et al. (2016) suggested a new approach for calculating bed shear stress in non-uniform flow.

The objectives of the present study are to present mean velocity profiles and friction velocity in non-uniform flows and todiscuss the hydraulic characteristics of non-uniform flow in three gorges reservoir.

2 FIELD SITES AND INSTRUMENTS

It is therefore necessary to study the effect of backwater extents on the profiles of velocity (Figure 1). The deposited sediments, occurring at the wide reaches and river bends in the permanent backwater region, were mostly fine sediments with the median diameters less than 0.01 mm, which was not forecasted by previous studies (Li and Wang, 2015).This study selected two typical silt sections in the backwater area of the Three Gorges Reservoir: one was the Huanghuacheng section of Zhongxianreach, which was approximately 350 km away from the TGRand was a meandering and bifurcation reach, and the other was the Qutang Gorge of Fengjiereach, which was 160 km away from the TGRand was a narrow-wide-narrow reach. The reaches of Zhongxian and Fengjie belong to permanent backwater region in the TGR.In the Zhongxian reach (Figure 2), 8 cross sections were selected, and 3 or 4 vertical lines were arranged. In the Fengjie reach (Figure 3), 5 cross sections were selected, and a total of 14 vertical lines were measured.In the Chongqing reach, one point under water level 0.5m was arranged.

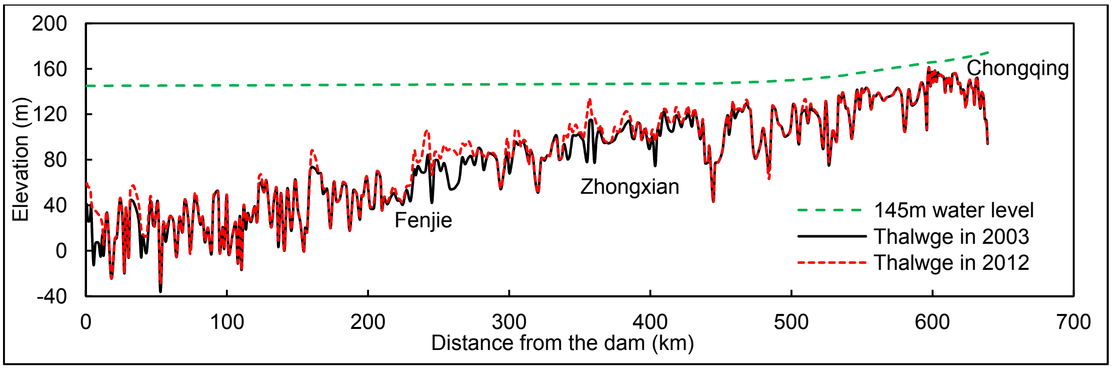

Figure 1.Field measurements locations.

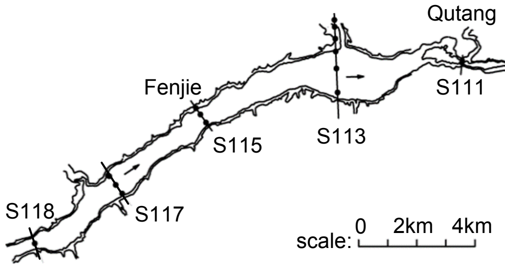

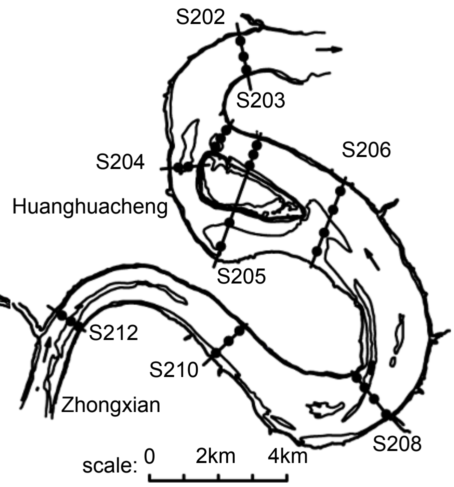

Figure 2.Field measurements in Fengjie reach. **Figure 3**.Field measurements in Zhongxian reach.

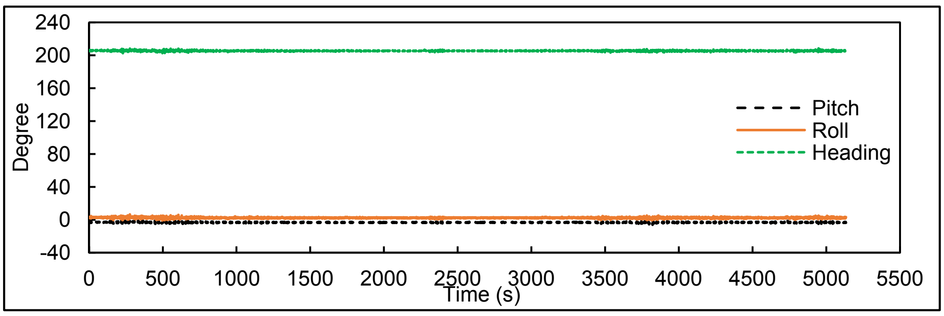

Figure 4. The azimuth Angle recorded by ADCP.

The flow velocities were measured by using ADCP. The sampling frequency of ADCP was 1 Hz. According to the data measured by the ADCP gyroscope, it can be seen that the pitch and roll angles were stable over a long period of time, and the heading angle represented a slight wobble in the horizontal plane (Figure 4). Therefore, the ship had a reliable stability. The fundamental quantities for the field measurements are stated in Table 1.

Table 1. Parameters for field measurements.

Sites	**Time**	No. of **Sample**	**frequency**	**Depth** ***H* (m)**	**Aspect ratios** ***B/H***	**Mean velocity** ***U* (m/s)**	**Surface slope** ***J***	**d*H*/dx**	***Fr***
CQ1	20130423	8065	1Hz	8.3	58	1.55	0.000001	0.000259	0.172
CQ2	20131008	5314	1Hz	13.7	35	0.95	0.000003	0.000257	0.082
S208L4	20130811	21158	1 Hz	16.9	65	0.40	0.000020	0.000240	0.031
S206L4	20130812	16643	1 Hz	28.6	66	0.90	0.000020	0.000240	0.053
S205L5	20130813	16306	1 Hz	33.2	26	0.90	0.000040	0.000220	0.050
S205L1	20130815	13775	1 Hz	9.4	110	0.26	0.000005	0.000255	0.027
S202L1	20130814	13810	1 Hz	35.0	24	0.98	0.000060	0.000200	0.053
S115L3	20120730	53	1 Hz	92.0	13	1.06	0.000012	0.000248	0.035
S115L2	20120730	52	1 Hz	80.2	15	0.84	0.000012	0.000248	0.030

3 MEAN FLOW VELOCITY AND TURBULENCE INTENSITIES

Figure 5a shows the vertical profiles of mean-velocity. Here the mean velocity is normalized by local mean velocity *U*, and the distance from the wall *y* is normalized by flow depth *H*. It is illustrated in Fig. 5a that with increasing backwater extents, the free surface velocity gradually decreases and the distributions of velocity profiles become more concave. Compared with the results of uniform flow tests (J=0.0015,H=33.5mm, Yang et al. (2016)), for the decelerating non-uniform flow, such as CQ1, S206L4 and S205L5, the velocity at surface region is larger than the uniform flow, and the bottom velocity is smaller than the uniform flow, relatively. The same tendency was observed for non-uniform flow by Kironoto and Graf (1995).

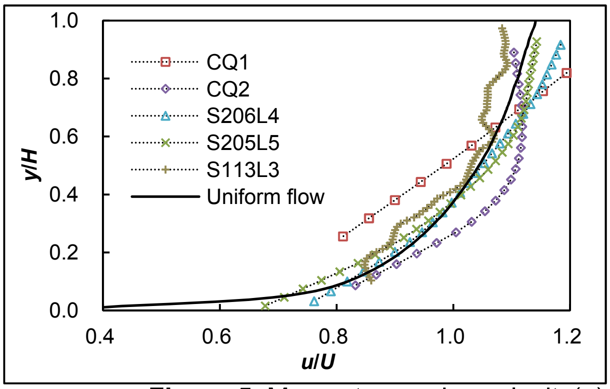

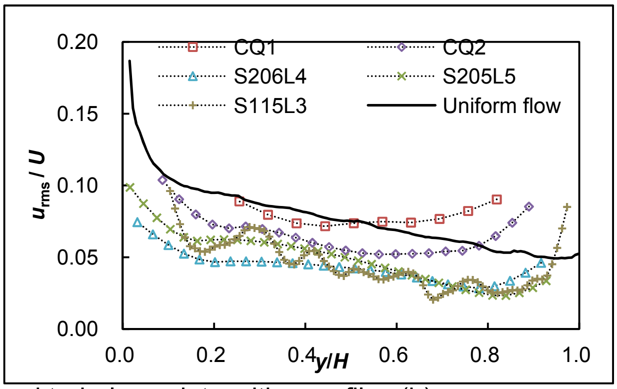

Figure 5. Mean streamwise velocity(a) and turbulence intensities profiles (b).

The turbulence intensities of streamwise velocity is scaled with *U* and plotted against *y*/*H* in figure 5b. The turbulence intensities depend on backwater extents, approximatively. The turbulence intensities distribution of near the wall and water surface is larger than the middle flow. Due to natural climate and human activities, the surface area of the river has greater turbulence intensity. Compared with the experimental results of uniform channel flow, the turbulence intensity of the longitudinal velocity of permanent backwater region is generally weaker than that of the uniform flow channel. According to the continuity equation, the mean flow velocity and kinetic energy are decreasing along with the increasing cross-sectional area. The turbulence intensity decreases further with the increasing of the backwater level. With the increasing of the backwater extent, the region with weak turbulence intensity on the profile gradually approaches the water surface. The region with weak turbulence on CQ1, CQ2 S206L4 and S205L5 profiles are near 0.5*H*, 0.6*H* and 0.8*H*, respectively. With the increasing of backwater conditions, the influence of the water area on the lower water is weakened.

4 FRICTION VELOCITY

4.1 Theoretical consideration

The governing equations for an unsteady one-dimensional gradually varied open channel flow, known as the Saint–Venant equation, can be written as follows:

$$\frac{\partial \mathrm{H}}{\partial \mathrm{t}}+\frac{\partial \mathrm{q}}{\partial \mathrm{x}}=0 \qquad [1]$$

$$\frac{\partial q}{\partial t}+\frac{\partial H\,UU}{\partial x}=-gH\frac{\partial (H+Z_{\mathrm{b}})}{\partial x}-\frac{1}{\rho}\tau_0 \qquad [2]$$

where, $H(x)$ is water depth, q is discharge per unit width, U is mean profile velocity, Z_{b} is bed elevation, τ_0 is bed shear stress, ρ is water density.

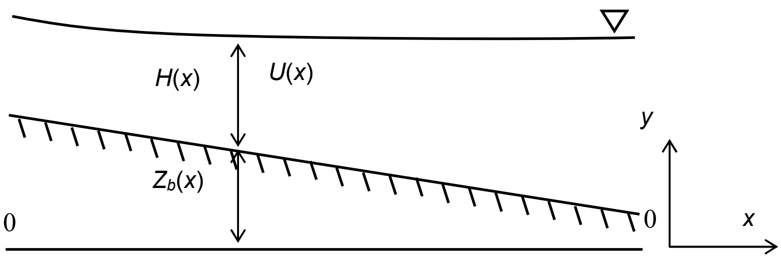

Figure 6. Coordinate system diagram.

According to $q=HU$, the second term on the left side of Eq. [2] can be rewritten as follows:

$$\frac{\partial \mathrm{HUU}}{\partial \mathrm{x}}=\mathrm{U}\left(-\frac{\partial \mathrm{H}}{\partial \mathrm{t}}\right)+\mathrm{q}\frac{\partial \mathrm{U}}{\partial \mathrm{x}}$$

According to $\frac{\partial Z_{\mathrm{b}}}{\partial x}=-s$, where s is bed slope, the first term on the left side of Eq. [2] can be rewritten as follows:

$$-\mathrm{gH}\frac{\partial(\mathrm{H}+Z_b)}{\partial \mathrm{x}}=-\mathrm{gH}\frac{\partial \mathrm{H}}{\partial \mathrm{x}}+\mathrm{gH\,s}$$

Eq. [2] can be rewritten as follows:

$$\frac{\tau_0}{\rho}=gH\,s-\frac{\partial q}{\partial t}+U\frac{\partial H}{\partial t}-q\frac{\partial U}{\partial x}-gH\frac{\partial H}{\partial x} \qquad [3]$$

According to Eq. [1], the four terms on the right side of Eq. [3] can be rewritten as follows:

$$\frac{\partial U}{\partial x}=\frac{\partial (q/H)}{\partial x}=-\frac{q}{H^2}\frac{\partial H}{\partial x}-\frac{1}{H}\frac{\partial H}{\partial t}$$

For steady non-uniform flow, $\frac{\partial}{\partial t}=0$, the second and three terms on the right side of Eq. [3] equal to 0, Eq. [3] can be rewritten as follows:

$$\frac{\tau_0}{\rho}=gH\,s-\left(gH-U^2\right)\frac{\partial H}{\partial x} \qquad [4]$$

According to $\frac{\tau_0}{\rho}=u_*^2$, Eq. [4] is dimensionless by U^2, and can be rewritten as follows:

$$\frac{u_*^2}{U^2} = \frac{s}{Fr^2} - \frac{1-Fr^2}{Fr^2}\frac{\partial H}{\partial x} \qquad [5]$$

4.2 Discussions

According to Eq. [5], when water surface is a horizontal plane, $\frac{\partial H}{\partial x} \to s$, $\frac{u_*^2}{U^2} \to s$; When the flow is uniform flow, $\frac{\partial H}{\partial x} \to 0$, $\frac{u_*^2}{U^2} \to \frac{s}{Fr^2}$.

Citing the experimental data from Kironoto and Graf (1995), Equation [5] is validated. A flume, 16.8 m in length, 0.6 m in width and 0.8 m in height, was used in his experiment. The measuring reach was situated between *x* = 9.89 m and *x* = 12.21 m (measured from the flume entrance), being sufficiently in the reach of fully developed flow. For decelerating flows, five different series (flows) were investigated, including two series(DPA and DPB). The relationship between u_*^2/U^2 and $\partial H/\partial x$ is plotted in Figure 7. According to the field measured data in the TGR, the relationship between u_*^2/U^2 and $\partial H/\partial x$ is plotted in Figure 8. Therefore, Eq. (5) can be applied for the calculation of the friction flow velocity in the decelerating flow.

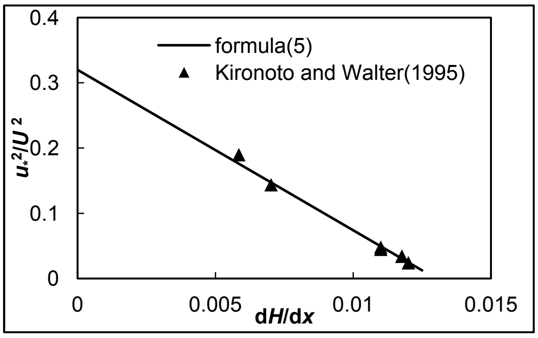

Figure 7. The law of friction velocity in flume.

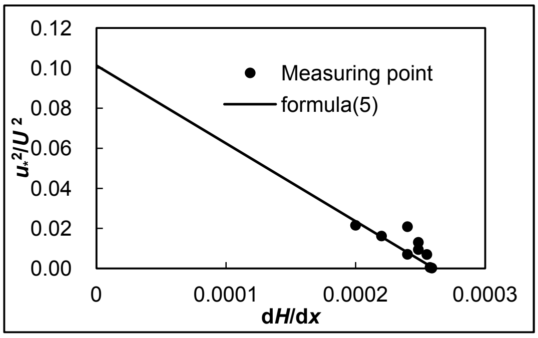

Figure 8. The law of friction velocity in the TGR.

5 MEAN FLOW VELOCITY DISTRUBUTION INFLUENCED BY BACKWATER

The mean velocity profiles of streamwise velocity is scaled with u_* and plotted against y/K_s in figure 9a. In the outer region (0.2*H*<y<0.6*H*), the velocity profiles follow a log-law, equation [6]. In this paper, the equivalent roughness height *K*s is 0.1m.

$$U^+ = A\log\left(\frac{y}{K_s}\right) + B \qquad [6]$$

where, U^+ is dimensionless velocity profile, A and B are different coefficients, Ks is equivalent roughness height.

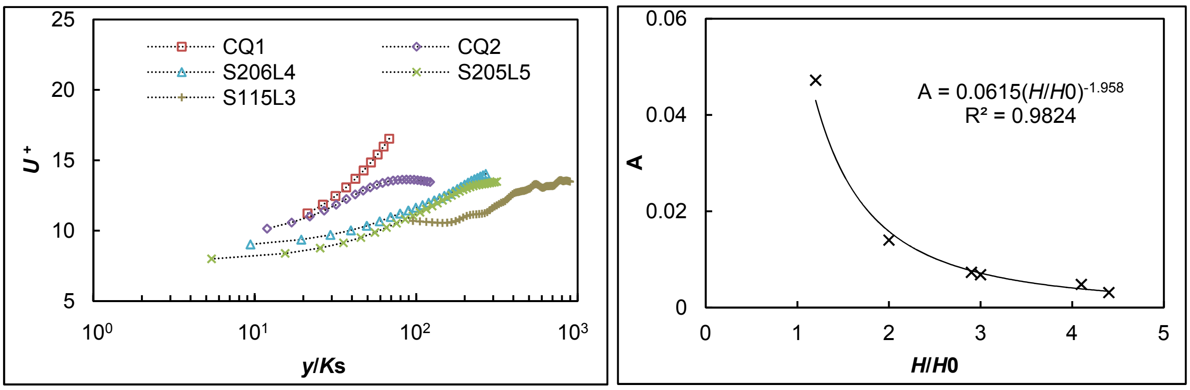

Figure 9. (a) mean velocity profiles, (b) Relationship between *H*/*H*0 and A.

Previous research results on decelerating flows' velocity profile in the inner region (y< 0.2*H*) is applicable to the logarithm law, and the Karman's constant is close to 0.4. For the outer region, the wake function is still applicable to the decelerating flows, and the wake parameter changes accordingly. Due to the prototype measurement in this paper, there is not enough flow field measurement data in the bed region. It is impossible to analyse the velocity distribution of the bed region more finely. For the velocity distribution in the outer region, as shown in Figure 9a, with the increasing of backwater, the trend of velocity distribution is getting flat. In the region of $0.2H<y<0.6H$, the velocity is better in logarithmic distribution and the slope is shown in Figure9b. As the degree of backwater increases, the slope gradually decreases. By fitting measured data, the slope, A, is plotted against $H/H0$ in figure 9b (where, H0, as the uniform flow depth, which meets the Chezy Manning formula uniform flow, in the case of a certain discharge per unit width, roughness and slope of river bed condition). The relationship between A and $H/H0$ is approximately a power function.

6 CONCLUSIONS

Based on the theoretical and experimental analysis methods, this study investigates friction velocity and mean velocity distribution in non-uniform flows in permanent backwater region in TGR. Equations of friction velocity are derived by one dimensional open channel Saint-Venant equations. The following conclusions can be drawn:

1. With increasing $H/H0$, compared with the uniform-flow profiles, the distributions of mean velocity profiles and turbulence intensities show a more concave tendency at around $0.6H$ and waning, respectively.
2. The mean velocity profile in non-uniform flows flat with the increasing of $H/H0$. The relationship between slopes of log-law velocity profiles and $H/H0$ show a power function.
3. The friction velocity in non-uniform flows is influenced by the flow depth gradient.

ACKNOWLEDGEMENTS

This work is financially supported by the National Natural Science Foundation of China (51679020) and National Key Research and Development Program of China (2016YFC0402103).

REFERENCES

Cardoso, A.H., Graf, W.H. & Gust, G.R. (1991). Steady Gradually Accelerating Flow in a Smooth Open Channel. *Journal of Hydraulic Research*, 29(4), 525-543.

Emadzadeh, A., Chiew, Y.M. & Afzalimehr, H. (2010). Effect of Accelerating and Decelerating Flows on Incipient Motion in Sand Bed Streams. *Advances in Water Resources*, 33(9), 1094-1104.

Kironoto B.A. & Graf W.H. (1995). Turbulence Characteristics in Rough Non-Uniform Open-Channel Flow. *Proceedings of the ICE - Water Maritime and Energy*, 112(4), 336–348.

Li, W.J., Wang, J., Yang, S.F. & Zhang, P. (2014). Determining the Existence of the Fine Sediment Flocculation in the Three Gorges Reservoir. *Journal of Hydraulic Engineering*, 141(2).

Song, T. & Chiew, Y. (2001). Turbulence Measurement in Nonuniform Open-Channel Flow Using Acoustic Doppler Velocimeter (ADV). *Journal of Engineering Mechanics*, 127(3), 219-232.

Yang S.F., Zhang, P., Hu J., Li W.J. & Chen Y. (2016). Distribution and Motion Characteristics of Q-events for Open-Channel Uniform Flow. *Advances in Water Science*, 27, 430-438 (In Chinese).

Yang, S.Q. (2009). Velocity Distribution and Wake-Law in Gradually Decelerating Flows. *Journal of Hydraulic Research*, 47(2), 177-184.

Zhang, X.F., Yang, W.T., Xia. & J.Q. (2016). Bed shear stress in non-uniform flow. *Environmental Fluid Mechanics*, 16(4), 777-792.

Zhao, C.H., Zhu, Z.H. & Zhou, D.Z., (2000). *Worldwide Rivers and Dams*. China Water Conservancy and Hydroelectric press, Beijing (In Chinese).

ICHTHYOPLANKTON STRUCTURE IN A DOWNSTREAM REACH AFFECTED BY THE THREE GORGES RESERVOIR ECOLOGICAL OPERATION, YANGTZE RIVER, CHINA

WEI XU[1,2], XIAOJUAN CHEN[1,2], JIANGPING TAO[1,2], XIAOMING ZHANG[1,2] & JIANBO CHANG[1,2,3]

[1,2]Key Laboratory of Ecological Impacts of Hydraulic Projects and Restoration of Aquatic Ecosystem of the Ministry of Water Resources, Institute of Hydroecology, Ministry of Water Resources & Chinese Academy of Sciences, Wuhan, China,
betty3115@126.com
[3]Hubei Provincial Collaborative Innovation Center for Water Resources Security, Wuhan, China,
zhangxiang@whu.edu.cn

ABSTRACT

The structure of ichthyoplankton community is studied in the Shashi reach during the experimental ecological operation of the Three Gorges Reservoir in the middle mainstream of the Yangtze River, China, from 2012 to 2014. A total of 44 fish species are identified as belonging to 5 orders, 9 families and 36 genera. The dominant species by individual number proportion are *Squalidus argentatus, Xenocypris microlepis, Hemiculter bleekeri, Parabramis pekinensis, Pseudolaubuca sinensis* and *Culter alburnus*. The peak of fish spawning season is in May and June, with eggs decreasing and larvae increasing, both markedly in early July. The mean daily drift density of eggs is 95.93 ind./1,000m^3 in 2012, 620.31 ind./1,000m^3 in 2013, and 250.98 ind./1,000m^3 in 2014, with significant differences existing among the years (χ^2=49.52, $p<0.05$); and of larvae is 880.44 ind./1,000m^3 in 2012, 178.37 ind./1,000m^3 in 2013, and 561.75 ind./1,000m^3 in 2014, with no significant difference existing among the years (χ^2=0.26, $p>0.05$). Egg and larva relative abundance show opposite fluctuation trends with the drift density of eggs highest and of larvae lowest both in 2013. The absolute abundance of ichthyoplankton increases year by year, from about 69 billion to 78 billion. Community biodiversity analysis shows both eggs and larvae go through a slight decline during the three years, but it remains smooth for the ichthyoplankton. Preliminary analysis which indicates different patterns in hydrological regime along with water temperature might be mainly attributed to the dynamics of ichthyoplankton community. The man-made flood process created by the ecological operation of TGR has a positive effect on ichthyoplankton recruitment by enlarging the reservoir discharge, but its future development is still a matter of concern. Fundamental research should be strengthened by seeking quantitative relations between ichthyoplankton and key environmental factors to promote the TGR's adaptive management with regard to fish recruitment restoration.

Keywords: Eggs; larvae; abundance; three gorges reservoir; ecological operation.

1 INTRODUCTION

Eggs and larvae are two important early life stages with high mortality and resource fluctuation (Trippel and Chambers, 1997). This is because they are more vulnerable to environmental changes, such as flow and thermal regimes in rivers (Julian and Robert, 2010; Wang et al., 2014). Accordingly, fish species can exhibit different responses to coping with these environmental changes by avoiding, adjusting, adopting and utilizing (Sih et al., 2011), finally leading to the shift of spawning time and location, larval abundance decline and even species extinction (Freeman et al., 2004; Duan et al., 2009; Wang et al., 2014). Many studies have found fish density in the early life stages hindered quantifiable relationships with hydrology (Baumgartner et al., 1997; Merigoux and Ponton, 1999; Tang et al., 2010; Li et al., 2013), and considered it could provide a sensitive tool for monitoring the effect of flow regulation by anthropogenic alterations (Humphries & Lake, 2000; Tan et al., 2010). Through the responding changes in the distribution and abundance of fish during the spawning and recruitment stages within a river system, this research might finally aid the identification of critical management requirements for fish conservation in regulated rivers (Gilligan and Schiller, 2003; King et al., 2010; Rolls et al., 2013).

The Three Gorges Project in China is one of the biggest hydro-power engineering projects worldwide. Regarding its great capacity for regulating water resources, the hydrologic regime in downstream of the Three Gorges Reservoir (TGR) has changed distinctly from the pre-impoundment period, especially in flooding seasons suitable for fish spawning and recruitment. One typical example is the threat to two important native fish species, the four major Chinese carps and the Chinese sturgeon, and it has been verified that the degradation of their spawning has a close association with the changes in hydrological and thermal conditions caused by the TGR (Duan et al., 2008; Guo et al., 2011; Ban and Li, 2007). One compensatory measure is to create a hydrological process similar to the natural state with regard to the survival requirements of the fish by reservoir re-regulation. For example, regulation of the experimental flow of large dams for restoration purposes is often done with the goal of providing conditions that stimulate spawning and recruitment of target fish species in Murray River (King et al., 2009). In recent years, with a large amount of basic research on the ecological requirements for the reproduction of the four major Chinese carps and the feasibility study on the TGR's ecological operation, a man-made flood pulse experiment by TGR which called an 'ecological operation' was carried out for the first time in June 2011, with a concurrent ecological monitoring program on ichthyoplankon using the drift-net method to find out the spawning response by the four carps and other fish species. This kind of experiment and program was integrally implemented over the next three consecutive years, from 2012 to 2014.

The objectives of this study are the following:

- (i) to understand the ichthyoplankton (eggs and larvae) in different levels, species composition, population abundance and community biodiversity;
- (ii) to analyze the annual variation of the ichthyoplankton community and the probable environmental correlates, especially flow and water temperature;
- (iii) to evaluate the current status and reasons for ichthyoplankton variation, and discuss the underlying effects of the TGR's ecological operation on fish conservation.

2 MATERIALS AND METHODS

2.1 Studying area

Fish sampling was designed at a regular site at the Shashi cross-section in the middle mainstream of the Yangzte River (Fig.1). It was located in the Jingjiang hydrologic wharf near Shashi gauge station in Jingzhou City, Hubei Province, about 150 km downstream from Gezhouba dam and 188 km from the Three Gorges dam. The upper adjacent Zhicheng gauge station was about 85 km above the Shashi cross-section, and the Yichang gauge station was 6 km below Gezhouba dam and about 60 km above Zhicheng gauge station. The surveyed area from the Yichang to Jingzhou river reach contained different forms of riverbed, such as straight, sinuous, sandbank, central bar and rock spur, forming different flow conditions for fish spawning and downstream drift during flooding season.

Figure 1. Location map of the surveyed area and sampling site from Yichang to Shashi reach in the middle mainstream of the Yangtze River.

2.2 Sampling process

Egg and larva samples were collected day to day in early summer, respectively from May 18th to July 16th in 2012, from May 8th to July 11th in 2013, and from May 19th to July 17th in 2014, lasting about two months each year. A D-frame net was used for regular site sampling, with a 1.01m semicircular mouth diameter, 2m net body length and 0.64 mm mesh size, as well as a cuboid collecting box (40 cm×30 cm×30 cm) made of the same material of thin silk as the net, and kept floating on the surface of the water by being fixed with wood. A conical net was used for cross-section sampling, with a 0.70m net mouth diameter, 2m net body length and 0.64mm mesh size, and a removable filtering cube at the end of the net. The river temperature in the surface layer, net velocity (a flow meter was fixed in the middle of the net mouth) and water transparency by Secchi disk were measured simultaneously during each sampling session. The data sets of daily runoff and water levels were obtained from the Yichang and Shashi hydrological stations.

The regular sampling site was located at the river bank on the main channel side. Sampling was conducted three times a day, in the morning (6:00-7:00am), midday (12:00-13:00pm) and evening (18:00-19:00pm). A D-frame net was deployed just under the water surface and kept there for about 10 to 30minutes, depending on the net clogging conditions. The cross-section sampling along the river including the regular site was conducted at the flood peak of eggs and/or larvae. The purpose of the cross-section sampling was to obtain the section runoff coefficient of eggs and larvae so as to estimate the total number of eggs and larvae per unit time drifting through the river cross-section. The sampling was set three to five points from the right bank, mid-channel and left bank, and every point vertically collected three samples at the surface (one fifth of water depth), middle (one half of water depth) and bottom layer (four fifths of water depth).

After sampling, all individuals of each sample were counted and separated, and the development stages recorded in the field. The egg samples were cultured in different tanks filled with river water or aerated water for about 5 to 7 days, until they hatched into larvae at the swim bladder gas stage. Larva samples (which always died) were preserved directly in 7% buffered formalin. The water temperature for cultivation was maintained between 22℃ to 24℃. After cultivation, the hatched larvae were fixed in 7% buffered formalin, labeled and preserved for further identification. Species identification was carried out with a binocular dissection microscope (Leica EZ4HD), and the distinct characteristics of each larva were observed and identified to the level of species or genera with reference to national published literature (Cao et al., 2007; Yi et al., 1988).

3 DATA ANALYSIS

3.1 Abundance estimation method

The drift density and daily abundance of the eggs/larvae were calculated in different time periods. The drift density was calculated as the number of eggs/larvae per 1,000m^3 of filtered water through the net during the sampling duration time. The daily abundance calculation consisted of two parts: the estimated number in sampling time and the estimated number in non-sampling time by the interpolation method. Kruskal-Wallis and Mann-Whitney tests were used to test significance in different years with SPSS 17.0. The formulas are as follows:

$$d_i = \frac{m_i}{s \times v_i \times t_i} \qquad [1]$$

$$c_i = \frac{(\sum_{i=1}^{n} d_i/n)}{d_i} \qquad [2]$$

$$M_i = Q_i d_i c_i t_i \qquad [3]$$

$$M_{i,i+1} = \left(\frac{M_i}{t_i} + \frac{M_{i+1}}{t_{i+1}} \right) \frac{t_{i,i+1}}{2} \qquad [4]$$

$$A = \sum M_i + \sum M_{i+1} \qquad [5]$$

Where;

d_i	is drift density in the ‘i’th sampling (ind./m^3);
m_i	is egg/larval number collected from the ‘i’th sampling (ind.);
s	is the net mouth area (m^2);
v_i	is the water velocity at the net mouth in the ‘i’th sampling(m/s);
t_i	is sampling duration time in the ‘i’th sampling(s);
M_i	is egg/larval abundance through the river transect in the ‘i’th sampling period;
Q_i	is transect water discharge in the ‘i’th sampling period;
C_i	is the section egg/larva runoff coefficient in the ‘i’th sampling;
n	is the number of sampling points in cross-section sampling
M_{i+1}	is egg/larval abundance in the time interval between the adjacent ‘i’th sampling and ‘i+1’th sampling;
t_{i+1}	is sampling duration time in the ‘i+1’th sampling;
$t_{i,i+1}$	is the time interval between the adjacent ‘i’th sampling and ‘i+1’th sampling(s);
A	is egg/larval abundance in the whole sampling period.

3.2 Community biodiversity analysis

Four biodiversity indexes were commonly used for analyzing fish community biodiversity, they were Margalef index (*R*), Shannon-Wiener index (H), Simpson index (D) and Pielou index (E).The Margalef index was used to reflect the species richness of the community, the Shannon-Wiener index reflected the species diversity based on species number, the Simpson index reflected the species dominance of the community, and the Pielou index reflected the evenness of the community.

In the formulas, *S* is the number of species, *N* is the total number of collected individuals and P_i is the individual number proportion of the '*i*'th species.

$$R = (S-1)\ln N \quad [6]$$

$$H = -\sum_{i=1}^{S} P_i(\ln P_i) \quad [7]$$

$$D = 1-\sum_{i=1}^{S} (P_i)^2 \quad [8]$$

$$E = H/\ln S \quad [9]$$

4 RESULTS

4.1 The man-made flood pattern of the TGR's ecological operation

In the schedule of the ecological operation experiment, the pattern of man-made floods was different each year in timing, frequency, magnitude and duration (Table 1), and it depended largely on the forecast of precipitation in the upstream and discrepancy in the natural hydrological regime within different years. The ecological operation was launched a total of 4 times, with 2 times in 2012 and 1 time each in 2013 and 2014. The starting period of the ecological operation was mainly in late May and early June (with an exception in 2013), which depended on two factors: the water temperature for fish spawning usually reached 18°c and the corresponding time was in late May in the middle of the Yangtze River, and to comply with the operation regulation of the TGR that the water level in the TGR must be dropped down to 145m before June 10th.

4.2 Water environment and hydrological regime at sampling site

During the sampling period, the water environment and hydrological regime were monitored at the regular site. The range, mean and standard deviation value of the water temperature, water transparency and cross-section runoff were listed in Table 2. The daily variation of water temperature showed a uniform climbing trend over three years, while the curve was obviously higher in 2013 compared with 2012 and 2014 (Fig.2-left). The daily variation of water transparency showed a similar decreasing trend over three years, but the curve showed a sharper fluctuation in 2013 compared with 2012 and 2014 (Fig.2-right). The daily variation of river runoff was totally different among three years, with all three statistical values being lowest in 2014 and highest in 2012. As for the frequency of flood pulse, it occurred six times in 2012, five times in 2013 and four times in 2014, suggesting that the variation curve of the flow seemed smoother in 2014 compared with 2012 and 2013 (Fig.3).

Table1. The flood pattern of different ecological operations from 2012 to 2014.

Time period of ecological operation		Frequency of ecological operation	Average increase of daily flow (m^3/s/d)	Duration in days of water rise (d)
Year	**Date**			
2012	May 25-May 31	2	2,608	4
	June 20-June 27		1,546	4
2013	May 07-May 15	1	1,097	9
2014	June 04-June 07	1	1,450	3

Table2. Statistical value of river temperature, transparency and runoff in Shashi during sampling period from 2012 to 2014.

Year	Water temperature (°C)		Water transparency (cm)		River runoff ($m^3 s^{-1}$)	
	Range	**Mean ± SD**	**Range**	**Mean ± SD**	**Range**	**Mean ± SD**
2012	19.2-24.7	22.4±1.45	5-157	62.1±40.43	12,600-41,600	21,598±8,935
2013	18.4-27.6	23.3±2.60	13-106	54.5±26.56	7,789-30,716	18,987±6,219
2014	19.8-23.9	22.1±1.27	15-174	79.4±41.30	10,585-30,541	17,410±5,479

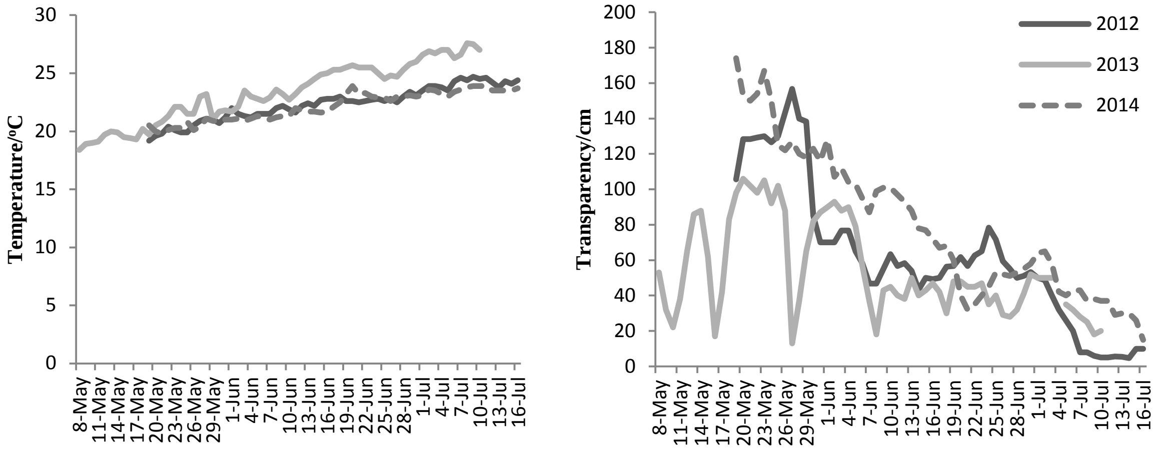

Figure 2. Daily variation of river temperature and transparency in Shashi from 2012 to 2014.

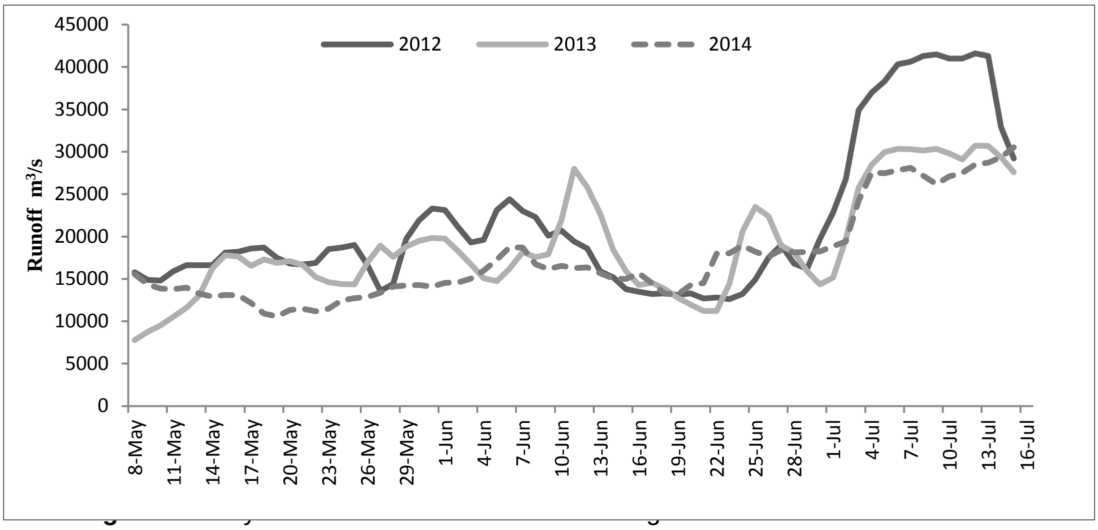

4.3 Species composition of ichthyoplankton

In 747 samples from180 days of sampling, 17,382 fish eggs and 80,957 larvae were finally identified. Eggs were identified to the species, and larvae could at least be identified to the genus. A total of 44 fish species were identified, belonging to 5 orders, 9 families and 36 genera, of which 22 species propagated pelagic eggs. The species number was 35 taxa in 2012, 40 taxa in 2013, and 43 taxa in 2014. The dominant family was Cyprinidae of Cypriniformes, containing 28 taxa accounting for 62.22% of total number; the rest of the families only contained 1 to 4 taxa. Another 12 species were scarce, with individual number proportions less than 0.1%. The species composition, individual number and proportion of eggs and larvae varied among the years. Regularly, *Squalidus argentatus* and *Plagiognathops microlepis* were the dominant species in eggs in three years, respectively accounting for 45.31%, 47.34% and 66.95% of all eggs; *Hemiculter bleekeri*, *Plagiognathops microlepis* were the dominant species in larvae in 2012 accounting for 52.35% of all larvae, and *Pseudolaubuca sinensis*, *Plagiognathops microlepis* were the dominant species in larvae both in 2013 and 2014, respectively accounting for 78.79% and 87.62% of all larvae.

4.4 Density and abundance of ichthyoplankton

The range and mean value of the daily drift density of eggs and larvae are shown in Table 3. A reverse trend in the annual variation of eggs and larvae abundance was observed, with the mean daily drift density of eggs being highest and of larvae being lowest, both in 2013. As for daily variation within one year, the same trend was observed in which several egg peaks occurred mainly in May and June, and larvae peaks only occurred after July along with the sharp descent of eggs. Through statistical analysis, a significant difference in the mean daily drift density of eggs was observed among three years (Kruskal-Wallis test: χ^2=49.524, p$<$0.05), while no significant difference existed in the mean daily drift density of larvae among three years (Kruskal-Wallis test: χ^2=0.26, p$>$0.05).

During the sampling period, the total abundance (the sum of daily abundance in each sampling date) drifting through Shashi cross-section was 11.0 billion in 2012, 63.7 billion in 2013 and 24.7 billion in 2014 for eggs; was 57.9 billion in 2012, 7.5 billion in 2013 and 53.3 billion in 2014 for larvae; and was 68.9 billion in 2012, 71.2 billion in 2013 and 78.0 billion in 2014 for ichthyoplankton. Although the abundance of eggs and larvae both fluctuating over the three years, the total abundance of ichthyoplankton increased year by year.

4.5 Community biodiversity index of ichthyoplankton

Biodiversity indexes of eggs, larvae and ichthyoplankton were calculated and compared over three years (Table 4). For eggs, all indexes showed a declining trend year by year; for larvae, only index *R* gradually increased, while indexes *H*, *D*, and *E* decreased year by year, suggesting that the community biodiversity of eggs/larvae went through a slight decline in the three years, except for the species richness of larvae. As for ichthyoplankton, index *R* increased slightly from 2012 to 2013 and remained nearly stable from 2013 to 2014, while the other three indexes decreased gradually from 2012 to 2014, with a degree of decline slighter than those of the eggs/larvae. The decrease of *D* and *E* gave the explanation that species dominance was increasing and species evenness decreasing year by year.

Table3. The range and mean value of the daily drift density of eggs and larvae from 2012 to 2014

Year	Density of eggs(ind.1000m^{-3})		Density of larvae(ind.1000m^{-3})	
	Range	Mean ± SD	Range	Mean ± SD
2012	0-486.56	95.93±109.42	0-8,441.91	880.44±2,096.58
2013	22.17-4,716.28	620.31±991.43	0-2,863.24	178.37±551.48
2014	20.70-1,446.95	250.98±227.13	0-7,631.13	561.75±1,495.27

Table4. Community biodiversity indexes for eggs, larvae and ichthyoplankton from 2012 to 2014

Biodiversity index	2012			2013			2014		
	Egg	Larva	Ichthyo.	Egg	Larva	Ichthyo.	Egg	Larva	Ichthyo.
R	3.27	2.55	3.56	3.31	2.82	3.95	2.86	3.23	3.81
H	2.37	2.01	2.12	2.26	1.44	1.82	1.81	1.24	1.66
D	0.86	0.81	0.83	0.85	0.66	0.74	0.75	0.61	0.71
E	0.71	0.6	0.58	0.67	0.43	0.49	0.55	0.35	0.45

5 DISCUSSION

5.1 Current status and reasons for ichthyoplankton variation in surveyed area

This study focused on the annual variation of ichthyoplankton in diversity and abundance below the TGR in the Shashi river section for the three years from 2012 to 2014. Fish composition and population were dominated by Cultrinae, Gobioninae, Leuciscinae and Xenocyprinae. The dominant species by individual number proportion were *Squalidus argentatus, Xenocypris microlepis, Hemiculter bleekeri, Parabramis pekinensis, Pseudolaubuca sinensis* and *Culter alburnus*. Similar species composition but higher species richness was found in the surveyed area compared with related research in the Jiangjin section (Jiang, 2009), Jianli section (Duan et al., 2008) and Wuxue section (Li et al., 2010), all located in the mainstream of the Yangtze River. A total of about 69 to 78 billion of ichthyoplankton flowed into the downstream through the Shashi cross-section yearly, and the amount showed an ascending trend year by year. This recruitment scale was greater than that at the upper end reach of the Three Gorges Reservoir in the Luoqi cross-section (12.4 billion, Mu et al., 2014), but only half the amount of that at the downstream reach in the Wuxue cross-section (137 billion, Li et al., 2010).

Flow regime and temperature were always primary restraining factors for the spawning and recruitment of riverine fishes (Bye, 1984; Humphries et al., 1999; Gorski et al., 2011). In this study, the mean drift density of eggs and larvae fluctuated yearly, in particular showing a distinctive but opposite change (inflexion point) both in 2013. To explore the possible correlated factors, a significant difference in water temperature was observed between 2013 and 2012 (Mann-Whitney test: $p<0.05$), and the same between 2013 and 2014 (Mann-Whitney test: $p<0.05$), but no significant difference existed between 2012 and 2014 (Mann-Whitney test: $p>0.05$). The daily average water temperature in 2013 was about 1℃ higher than that in 2012 and 2014, and this coincided with the highest occurrence of egg abundance in 2013, probably resulting from the water temperature effect on the sexual maturation and breeding of adult fish; another significant difference in river runoff was also observed between 2012 and 2013 (Mann-Whitney test: $p<0.05$), and the same between 2012 and 2014 (Mann-Whitney test: $p<0.05$), but no significant difference existed between 2013 and 2014 (Mann-Whitney test: $p>0.05$). As for the daily average river runoff being highest in 2012, this might have some association with the highest larvae abundance occurring that year, probably due to the poor swimming ability of larvae against the current flow, and it might also be a demonstration of how a larger scale of flood can induce a greater abundance of larvae in some fish species (Qiu et al., 2002).

For community biodiversity, a slight decline was observed both for eggs and larvae among the three years (Table 3), this might be largely attributed to the intra-specific dynamics of egg and larvae population in different species. On the whole, the biodiversity indexes of ichthyoplankton seemed to be steady over the three years, likely suggesting that the community structure was in a gradually stable condition. A comparison of four biodiversity indexes among three years reflected a highly stable and diverse egg/larva community structure in 2012 according to its higher richness and evenness, but a lower dominance in species. The reasons for fish population dynamics are complicated, as different levels of complex interactions exist among the environment, aquatic biota and anthropogenic activity.

5.2 Ecological operation effect of the TGR on fish resource recruitment

The flood recruitment model, which was greatly influenced by the flood pulse concept (Junk et al., 1989), maintains that flooding is beneficial to fish populations because it allows access to food resources and different habitats, especially in highly productive and structurally complex aquatic-terrestrial zones (Scharbert and Borcherding, 2013). Also, variations in the magnitude and frequency of flow events affect the hydrogeomorphic complexity of suitable habitats for fish, and could have a pivotal role in population dynamics and community structure (Moore and Thorp, 2008). A conclusion can be drawn that suitable flood conditions could produce successful spawning events, and the occasion and pattern of the flood process might result in different spawning responses of fish (Xu et al., 2015).

In this paper, the 'ecological operation' by the TGR meant an operation of enlarging the reservoir discharge to create a man-made flood for several days each year, for the purpose of inducing the reproduction of the four major Chinese carps, meanwhile maintaining the population of other fish species (Xu et al., 2014). During the part of the sampling period including the ecological operation, an increasing trend in the total abundance and species number of ichthyoplankton was found from 2012 to 2014, with the egg and larva community structure most diverse and stable in 2012. Another result in the same monitoring work uncovered that the egg abundance of the four carps produced during the ecological operation flood was greater than during any other conventional operation flood, and the estimated spawning scale of the four carps was also greatest in 2012 (Xu et al., 2013). A major explanation for the above-mentioned findings is probably that the higher river runoff in 2012 that created a higher flood pulse frequency and a larger degree inflow variation compared to the other two years (Fig.3, Table 2). These results might constitute valuable evidence for the importance of flooding to fish biodiversity maintenance, and the man-made flood process created by the TGR's ecological operation has a positive effect on ichthyoplankton recruitment, but its future development is still a matter of concern.

6 PROBLEMS AND OUTLOOK

The weak point of this study is the insufficient observation data collected for only three years, making the reasons for some findings mostly deductive from the related documents. In other words, quantitative findings on ichthyoplankton with key correlated environmental factors should be explored through continued research. In the next step, experiment of the TGR's ecological operation should be routinized and allocated in different patterns to create multiple flood-pulse process, and the concurrent monitoring of ichthyoplankton should be further specialized and optimized so as to provide valuable information for attaining a deep knowledge of how the flow regime affects the fish population, aquatic community and even their habitat. This is fundamental research for the TGR's adaptive management in terms of downstream fish recruitment restoration in the middle of the Yangtze River.

ACKNOWLEDGEMENT

We are most grateful to the Jingjiang Hydrology and Water Resources Surveying Bureau and Changjiang Water Resources Commission Bureau for the provision of workboats and their crews during field sampling. The research reported herein is funded by the China Three Gorges Corporation, Hubei Provincial Collaborative Innovation Center for Water Resources Security (HB-SAQBZ-01), and National key Research and Development plan Project (2016YFC0402204).

REFERENCE

Ban, X. & Li, D.M. (2007). Ecological Hydrological Influence of Large Water Conservancy Projects on *Acipenser Sinensis* in Yangtze River. *Engineering Journal of Wuhan University*, 40, 10-13.

Baumgartner, G., Nakatani, K., Cavicchioli, M. & Baumgartner, M.S.T. (1997). Some Aspects of the Ecology of Fishes Larvae in the Floodplain of the High Parana River, Brazil. *Revista Brasileira de Zoologia*, 14, 551-563.

Bye, V.C. (1984). *The Role of Environmental Factors in the Timing of Reproductive Cycles, In Fish Reproduction: Strategies and Tactics.* Chichester, Wiley, 187-206.

Cao, W.X., Chang, J.B., Qiao, Y. & Duan, Z.H. (2007). *Fish Resources of Early Life History Stages in Yangtze River*. China Water Power Press, Beijing, 1-252. (In Chinese)

Duan, X.B., Chen, D.Q., Li, Z.H., Wang, K., Huan, M.G. & Liu, S.P. (2008). Current Status of Spawning Grounds of Fishes with Pelagic Eggs in the Middle reaches of the Yangtze River after Impoundment of the Three Gorges Reservoir (In Chinese). *Journal of Fishery Sciences of China*, 15, 523-532.

Duan, X.B., Liu, S.P., Huang, M.G., Qiu, S.L., Li, Z.H., Wang, K. & Chen D.Q. (2009). Changes in Abundance of Larvae of the Four Domestic Chinese Carps in the Middle reach of the Yangtze River, China, before and after Closing of the Three Gorges Dam. *Environmental Biology of Fishery*, 86, 13-22.

Freeman, M.C., Irwin, E.R., Burkhead, N.M., Freeman, B.J. & Bart, H.L.J. (2004). Status and Conservation of the Fish Fauna of the Alabama River system. *American Fisheries Society Symposium,* 45, 557-585.

Gilligan, D., Schiller, C. (2003). *Downstream Transport of Larval and Juvenile Fish in the Murray River.* NSW Fisheries Final Report, 50, 1440-3544.

Gorski, K., De Leeuw, J.J., Winter, H.V., Vekhov, D.A., Minin, A.E. & Buijse A.D. (2011). Fish Recruitment in a Large, Temperate Floodplain: The Importance of Annual Flooding, Temperature and Habitat Complexity. *Freshwater Biology*, 56, 2210-2225.

Guo, W.X., Wang, H.X., Xu, J.X. & Xia Z.Q. (2011). Effects of Three Gorges Reservoir on the Downstream Eco-Hydrological Regimes during the Spawning of Important Fishes. *Journal of Hydroelectric Engineering*, 30, 22-26.

Humphries, P., King, A.J. & Koehn, J.D. (1999). Fish, Flows and Flood Plains: Links between Freshwater Fishes and their Environment in the Murray-Darling River System, Australia. *Environmental Biology of Fishery,* 56, 129-151.

Humphries, P. & Lake, P.S. (2000). Fish Larvae and the Management of Regulated Rivers. *Regulated Rivers: Research and Management*, 16, 421-432.

Jiang, W. (2009). Studies on Fish Early Resources in the Main Stream of State Level Natural Protection Area for Rare and Endemic Fishes in the Upper Yangtze River (In Chinese). *Ph.D. Dissertation*, Institute of Hydrobiology, Chinese Academy of Sciences, Wuhan, 1-150.

Julian, D.O. & Robert, J.N. (2010). Incorporating Thermal Regimes into Environmental Flows Assessments: Modifying Dam Operations to restore Freshwater Ecosystem Integrity. *Freshwater Biology*, 55, 86-107.

Junk, W.J., Bayley, P.B. & Sparks R.E. (1989). *The Flood Pulse Concept in River Floodplain Systems.* Canadian Special Publication in Fisheries and Aquatic Sciences, 106, 110-127.

King, A.J., Tonkin, Z. & Mahoney, J. (2009). Environmental Flow enhances Native Fish Spawning and Recruitment in the Murray River, Australia. *River Research and Applications*, 25, 1205–1218.

King, A.J., Ward, K.A., O'Connor, P., Green, D., Tonkin, Z. & Mahoney, J. (2010). Adaptive Management of an Environmental Watering Event to enhance Native Fish Spawning and Recruitment. *Freshwater Biology*, 55, 17-31.

Li, M.Z., Gao, X., Yang, S.R., Duan, Z.H., Cao, W.X. & Liu, H.Z. (2013). Effects of Environmental Factors on Natural Reproduction of the Four Major Chinese Carps in the Yangtze River, China. *Zoological Sciences*, 30, 296-303.

Li, M.Z., Jiang, W., Gao, X., Duan, Z.H. & Liu, H.Z. (2010). Status Quo of Early Lift History Stages at Wuxue Cross Section of the Yangtze River. *Acta Hydrobiologica Sinica*, 34, 1211-1217. (In Chinese)

Merigoux, S. & Ponton D. (1999). Spatio Temporal Distribution of Young Fish in Tributaries of Natural and Flow Regulated Sections of a Neotropical River in French Guiana. *Freshwater Biology*, 42, 177-198.

Moore, S.L. & Thorp, J.H. (2008). Coping with Hydrogeomorphic Variations in a Prairie River: Resiliency in Young of the Year Fishes. *River Research Applications*, 24, 267-278.

Mu, H.X., Li, M.Z., Liu, H.Z. & Cao W.X. (2014). Analysis of Fish Eggs and Larvae Flowing into the Three Gorges Reservoir on the Yangtze River, China. *Fishery Sciences*, 80, 505-515.

Qiu, S. L., Liu, S. P., Huang, M. G., Chen, D. Q. & Duan, X. B. (2002). Monitoring of Spawning Sites of Four Major Chinese Carps in the Middle Section of Yangtze River. *Acta Hydrobiologica Sinica*, 26, 716-718. (In Chinese).

Rolls, R.J., Growns, I.O., Khan, T.A., Wilson, G.G., Ellison, T.L., Prior, A. & Waring C.C. (2013). Fish Recruitment in Rivers with Modified Discharge depends on the Interacting Effects of Flow and Thermal Regimes. *Freshwater Biology*, 58, 1804-1819.

Scharbert, A. & Borcherding, J. (2013). Relationships of Hydrology and Life History Strategies on the Spatio Temporal Habitat Utilization of Fish in European Temperate River Floodplains. *Ecological Indicators*, 29, 348-360.

Sih, A., Ferrari, M.C.O. & Harris D.J. (2011). Evolution and Behavioral Responses to Human Induced Rapid Environmental Change. *Evolutionary Applications*, 4, 367-387.

Tan, X.C., Li, X.H., Lek, S., Li, Y.F., Wang, C., Li, J. & Luo J.R. (2010). Annual Dynamics of the Abundance of Fish Larvae and its Relationship with Hydrological Variation in the Pearl River. *Environmental Biology of Fishes*, 88, 217-225.

Tang, X.L., Chen, D.Q., Wang, K., Liu, S.P., Luo, H.W. & Duan X.B. (2010). Spatial and Temporal Distribution

  / ISSN 1562-6865 (Online) - ISSN 1063-7710 (Print)

of Larval Resources of Fishes in the Upper reaches of Yangtze River. *Freshwater Fishes*, 40, 27-31. (In Chinese)

Trippel, E.A. & Chambers, R.C. (1997). *The Early Life History of Fishes and its Role in Recruitment Processes, in Early Life History and Recruitment in Fish Populations.* Chapman & Hall, London, 21-32 .

Wang, J.N., Li, C., Duan, X.B., Chen, D.Q., Feng, S.X., Luo, H.H., Peng, Q.D. & Liao W.G. (2014). Variation in the Significant Environmental Factors Affecting Larval abundance of Four Major Chinese Carp Species: Fish Spawning response to the Three Gorges Dam. *Freshwater Biology*, 59, 1343-1360.

Wang, J.N., Li, C., Duan, X.B., Luo, H.H., Feng, S.X., Peng, Q.D. & Liao, W.G. (2014). The Relationship between Thermal Regime Alteration and Spawning Delay of the Four Major Chinese Carps in the Yangtze River below the Three Gorges Dam. *River Research Applications*, 30, 987-1001.

Xu, W., Qiao, Y., Chen, X.J., Cai, Y.P., Yang, Z. & Liu H.G. (2015). Spawning Activity of the Four Major Chinese Carps, in the Middle Mainstream of the Yangtze River, during the Three Gorges Reservoir Operation Period. *Journal of Applied Ichthyology*, 31, 846-854.

Xu, W., Liu, H.G., Tang, H.Y., Zhu, D., Yang, Z. & Qiao Y. (2014). Effects of Ecological Operation of Three Gorges Reservoir on Fish Eggs and Larvae in Shashi Section of the Yangtze River. *Journal of Hydroecology*, 35, 1-8. (In Chinese).

Xu, W., Yang, Q.H., Tang, H.Y. & Liu, H.G. (2013). Natural Reproduction of the Four Major Chinese Carps in Mainstream of Yangtze River Responding to Ecological Operation of Three Gorges Reservoir. *The 3rd Biennial Symposium of the International Society for River Science*, Conference Proceedings, 704-711.

Yi, B.L., Yu, Z.T., Liang, Z.S., Sheng, S.J., Xu, Y.X. & Chen, J.X. (1988). *The Distribution, Natural Conditions, and Breeding Production of the Spawning Ground of Four Famous Freshwater Fishes on the Mainstream of the Yangtze River, Gezhouba Water Control Project and Four Famous Fishes in the Yangtze River*. Hubei Science and Technology Press, China, 1-4. (In Chinese)